Lecture Notes in Civil Engineering

Bibhuti Bhusan Das
Sreejith V. Nanukuttan
Anil K. Patnaik
Neena Shekhar Panandikar *Editors*

Recent Trends in Civil Engineering

Select Proceedings of TMSF 2019

Springer

Lecture Notes in Civil Engineering

Volume 105

Lecture Notes in Civil Engineering (LNCE) publishes the latest developments in Civil Engineering - quickly, informally and in top quality. Though original research reported in proceedings and post-proceedings represents the core of LNCE, edited volumes of exceptionally high quality and interest may also be considered for publication. Volumes published in LNCE embrace all aspects and subfields of, as well as new challenges in, Civil Engineering. Topics in the series include:

- Construction and Structural Mechanics
- Building Materials
- Concrete, Steel and Timber Structures
- Geotechnical Engineering
- Earthquake Engineering
- Coastal Engineering
- Ocean and Offshore Engineering; Ships and Floating Structures
- Hydraulics, Hydrology and Water Resources Engineering
- Environmental Engineering and Sustainability
- Structural Health and Monitoring
- Surveying and Geographical Information Systems
- Indoor Environments
- Transportation and Traffic
- Risk Analysis
- Safety and Security

To submit a proposal or request further information, please contact the appropriate Springer Editor:

– Mr. Pierpaolo Riva at pierpaolo.riva@springer.com (Europe and Americas);
– Ms. Swati Meherishi at swati.meherishi@springer.com (Asia - except China, and Australia, New Zealand);
– Dr. Mengchu Huang at mengchu.huang@springer.com (China).

All books in the series now indexed by Scopus and EI Compendex database!

More information about this series at http://www.springer.com/series/15087

Bibhuti Bhusan Das · Sreejith V. Nanukuttan ·
Anil K. Patnaik · Neena Shekhar Panandikar
Editors

Recent Trends in Civil Engineering

Select Proceedings of TMSF 2019

Springer

Editors
Bibhuti Bhusan Das
Department of Civil Engineering
National Institute of Technology Karnataka
Mangalore, Karnataka, India

Sreejith V. Nanukuttan
Civil Engineering
Queen's University Belfast
Belfast, UK

Anil K. Patnaik
Civil Egineering
University of Akron
Akron, OH, USA

Neena Shekhar Panandikar
Civil Engineering
Don Bosco College of Engineering
Fatorda, Goa, India

ISSN 2366-2557 ISSN 2366-2565 (electronic)
Lecture Notes in Civil Engineering
ISBN 978-981-15-8292-9 ISBN 978-981-15-8293-6 (eBook)
https://doi.org/10.1007/978-981-15-8293-6

This Springer imprint is published by the registered company Springer Nature Singapore Pte Ltd.
The registered company address is: 152 Beach Road, #21-01/04 Gateway East, Singapore 189721, Singapore

Preface

One of the oldest and classical professions is Civil Engineering; however, the same is poised to undergo trending moments in upcoming years, and advancement in research and technology is the steering force behind the innovativeness which construction industry is going to witness. Sustainability, energy efficiency, high-rise buildings, smart structures, intelligent built environment, 3D printing, augmented reality, building information modelling, etc. are equivalently gaining prominence. Keeping all this in mind, this conference aimed to explore innovative applications and recent trends of research in the areas of Structural and Concrete Engineering, Geotechnical Engineering, Transportation Engineering, Environmental Engineering and Construction Technology and Management. "International Conference on Trending Moments and Steer Forces (TMSF-2019)" was organised during 31 October—1 November 2019 at Don Bosco College of Engineering (DBCE), Goa, in association with National Institute of Technology Karnataka (NITK), Surathkal. Selected and peer-reviewed papers from the conference are being published in this book, and the papers are categorised under five different themes: Recent Trends in Structural Engineering, Recent Trends in Geotechnical Engineering, Recent Trends in Construction Technology and Management, Recent Trends in Environmental Engineering and Recent Trends in Transportation Engineering.

I thank Springer Editorial Management Team, Co-editors, Reviewers, Student Volunteers, DBCE Management, Faculty and Staff for their full support and cooperation at all the stages of this event. Special thanks to Dr. Shivaprasad K. N., Assistant Professor, JSSST University, Mysuru and my research scholar Ms. Snehal Kusumadhar for helping me in the editorial activities starting from the beginning till the end. I do hope that this book will be beneficial to students, researchers and practitioners working in the field of Civil Engineering.

Mangalore, India — Bibhuti Bhusan Das

Contents

About the Editors

Dr. Bibhuti Bhusan Das is currently serving as an Associate Professor at National Institute of Technology, Karnataka, Surathkal, India. His research interests include design and development of sustainable construction and building materials, microstructure and durability of concrete, construction planning and practices. Dr. Das has handled a number of research projects sponsored from Department of Science and Technology (DST), Govt. of India; Royal Academy of Engineering (RAEng), UK; Kudremukh Iron Ore Company Limited (KIOCL); Mangalore Refinery and Petro Chemicals Limited (MRPL). The fund generation and research contributions have led to the development of Sustainable Construction and Building Materials Laboratory at NITK Surathkal, a specialized lab that practices the theme of sustainability. He has published over 100 papers in Journals and conferences, and has given several key-note presentations across the world. He has guided four doctoral students and more than sixty master's thesis. Currently, he has eight students who are doing their doctoral thesis and around fifteen students having their master's degree. He has been serving as a Post-Doctoral Research Associate from Centre for Innovative Materials Research (CIMR), Lawrence Technological University, Southfield, Michaigan, USA and has obtained Doctorate of Philosophy from Indian Institute of Technology (IIT) Bombay, India. He is a Master's degree holder in Construction Engineering and Management from Indian Institute of Technology (IIT) Delhi, India. He has won a number of awards one of the prestigious being the Outstanding Reviewer award from Construction and Building Materials Journal, Elsevier. He has edited number of books entitled Sustainable Construction and Building Materials-Select Proceedings of ICSCBM 2018, Recent Developments in Sustainable Infrastructure-Select Proceedings of ICRDSI 2019, Smart Technologies for Sustainable Development-Select Proceedings of SMTS 2019 and also guest edited the June-2019 edition of the Indian Concrete Journal and is on the editorial panel of some of the reputed Construction Engineering and Material journals.

Dr. Sreejith V. Nanukuttan is currently a senior lecturer in the School of Natural and Built Environment, Queen's University Belfast. He graduated from Queen's University Belfast with a Ph.D. in civil engineering in 2007 on development of a non-destructive test for concrete in chloride environments. In 2008, he joined the School

of Natural and Built Environment as a lecturer and was instrumental in developing MSc in durability of structures and course on whole life management of structures. In 2013–14 he took Royal Academy supported industrial secondment with Roads Service Northern Ireland where he was responsible for structural assessment and subsequent rehabilitation of two transport bridges, projects of over £2m. The in-situ test he developed through his Ph.D. for assessing chloride transport through concrete and the instrument is commercialized through Amphora Non-Destructive Ltd., His recently completed EPSRC funded project developed retrofit decision tool for converging energy efficiency measures, this simplified coding is licensed to Energenius for integration with their smart energy management system for social landlords. Through his research he maintains a balance between material technology, building performance and structural efficiency and to date has managed research income of over £1.9m. He has supervised 4 complete Ph.D.s, 6 PDRAs and 2 RAs. He is the immediate past president of Civil Engineering Research Association of Ireland and is a member of RILEM technical committees 230-PSC, 247-DTA and newly formed CIM. He has authored over 75 technical articles including 20 in refereed international journals.

Dr. Anil K. Patnaik is a professor of structural engineering at The University of Akron in Ohio, USA. He earned his Ph.D. from the University of Calgary, and master's degree in structural engineering from the Indian Institute of Technology in Kanpur, and a bachelor's degree in civil engineering from National Institute of Technology, Rourkela in India. He has over twenty years of experience in academic positions at South Dakota School of Mines and Technology (SDSM&T) in Rapid City, Curtin University in Perth (Australia), the University of Western Australia, and presently is working at the University of Akron in Ohio. His current and recently funded research projects are on corrosion of reinforced concrete and steel structures, reinforced concrete members subjected in impact loads, synthetic and basalt fiber reinforced concrete (FRC), fiber reinforced polymer (FRP) materials for structural concrete applications, repair and strengthening of existing structures, construction and long term performance monitoring of bridge decks, structural slab bridges, prestressed concrete adjacent box-beam bridges, and carbon footprint assessment and life cycle analysis (LCA). He is the author or co-author of over 100 technical papers, and over 100 research and design reports. He edited a book on high volume fly ash concrete and co-edited a book on high performance high strength concrete. He has several years of experience as a practicing engineer in design and construction of large industrial, commercial and offshore structures, and tall buildings. He taught and continues to teach several courses on structural engineering including reinforced and pre-stressed concrete design, FRP reinforced concrete design, senior design, tall building design, steel design and structural analysis at the undergraduate and graduate levels at several universities.

Dr. Neena Shekhar Panandikar is principal of Don Bosco College of Engineering, Fatorda Goa, entitled to be the first lady Principal of a technical institution in the state of Goa. She has published twenty research papers in various international

journals, national and international conferences. As a part of social responsibility, she served as a member and developed curriculum for Rural Health Education Project, a joint project of Agnel Technical Education Complex in association with Algonquin College, Canada sponsored by CIDA (Canadian International Development Agency). She was appointed as an expert member as a part of Affiliation Committee by the Goa University to sanction postgraduate program in structural engineering at Goa College of Engineering. She is a life member of ISTE, Association of Structural Engineers and Indian Concrete Institute. She is a Chartered Engineer and has been conferred with IEI fellow membership. She was among 100 leaders selected from across the country to attend a workshop on leadership under AICTE-UKIERI, jointly organized by AICTE in association with Dudley College, UK and has received CMI certification in management and leadership. She is also on the academic council of Goa University and at present serving as a member of Goa State Innovation Council.

Recent Trends in Structural Engineering

Assessment of Pushover Response Parameters Using Response Surface Methodology

Neena Panandikar and K. S. Babu Narayan

Abstract Pushover analysis is a non-linear static method used for the seismic assessment of structures. The simplicity, efficiency in modelling and less computational time make this method popular. Lot of researchers has worked on conventional pushover analysis and after knowing deficiencies of the method have made efforts to improve it. From the literature, it is evident that actual experimental test results carried out so as to verify the analytically obtained pushover results are hardly available. Stress–strain models adopted for modelling of concrete and reinforcement greatly influences both the ultimate load and ultimate displacement for the structure under pushover loads. This paper focuses on assessment of pushover response parameters using response surface methodology (RSM). A three-storied RCC framed structure is tested and the experimental pushover results are available. Uncertain parameters considered include the concrete strength, steel strength, reinforcement cover and hinge location, which are randomly generated by performing stochastic analysis and their effect on responses, which include base shear and displacement is studied. Using Monte Carlo simulation in Sap-2000 design matrix is generated. Modelling and analysis of response parameters are carried out using RSM so as to obtain the characteristics of the pushover curve. The effect of material strength variation, hinge locations and hinge lengths, geometric modelling have been studied, incorporating confined model for concrete. The coefficients and equations that can be used to predict the responses are carried out by performing multiple regression analysis. The validation results demonstrated that the confined model is better than the unconfined.

Keywords Base shear · Displacement · Pushover analysis · Monte carlo · Response surface methodology

N. Panandikar (✉)
Don Bosco College of Engineering, Margao, Goa 403602, India
e-mail: neena110@rediffmail.com

K. S. B. Narayan
National Institute of Technology, Surathkal, Mangalore, Karnataka 575025, India

B. B. Das et al. (eds.), *Recent Trends in Civil Engineering*, Lecture Notes in Civil Engineering 105, https://doi.org/10.1007/978-981-15-8293-6_1

1 Introduction

Pushover analysis is a non-linear static method and is considered as an effective tool for seismic performance evaluation of structures. In this method, increasing loads are applied monotonically to the structure. Lot of researchers has worked on conventional pushover analysis and has made efforts to improve it. However, actual experimental test results to verify analytically obtained pushover results are hardly available as there is lot of expenditure when it comes to experimental investigation. SAP2000 has been used by many researchers to carry out research for seismic evaluation of the existing structures with subsequent suggestions for retrofitting techniques. Certain approximation and simplification are involved in the development of the capacity curve that amount to some variation in seismic demand prediction of pushover analysis. This simple yet powerful technique has scope for further improvement that would result in increase in its reliability as the primary tool for practical seismic analysis [1]. To quantify the effect of modelling uncertainties on the calculated collapse fragilities, they concluded that Monte Carlo method in conjunction with the RSM is proposed as the preferred method to quantify the effects of modelling uncertainties on structural response.

Because the results are sensitive to the geometric model adopted, material properties, hinge properties, hinge location, and stress–strain models of concrete (confined and unconfined) and steel, it has been observed that same model can give different results. In the earlier work carried out by the authors, they had considered a three storied ($G + 2$), reinforced cement concrete framed structure as shown in Fig. 1 and investigated the sensitivity of the pushover curve to modelling. Stochastic analysis was carried out by considering confinement in concrete and uncertain parameters as the concrete strength, steel strength, reinforcement cover, and hinge location, which were randomly generated and incorporated into the analysis. The comparison of the results was done with the unconfined model. User-defined hinges are preferred to

(a) Photograph of the actual test structure

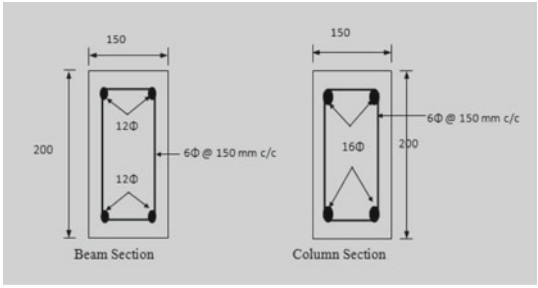

(b) Section properties

Fig. 1 Details of the tested RC framed structure

default hinges in reflecting non-linear behaviour. Hence the authors adopted this option, which requires determination of moment–curvature values. Mander's stress–strain model for confined concrete and British code-recommended (CP 110–1972)—strain curve for steel were adopted. Hinge lengths were determined by using various formulations that are available in literature. Experimental results available were then compared with simulated results.

2 Structural Details

The structure is a three storied, RC framed structure. The photograph of actual tested structure is shown in Fig. 1a.

The beam and column sections are shown in Fig. 1b. Two-legged, 6Φ stirrups/ties @150 mm c/c provide the transverse reinforcement for both beams and columns. The slab is 50 mm thick.

Actual material properties of the tested structure are as follows:

Average value of concrete strength = 35 MPa
Average value of reinforcement yield stress = 478 MPa.

3 Experimental Details: Pushover Analysis Results

Testing of the reinforced concrete frame model was carried out at SERC, Chennai (Fig. 1a), with section details as shown in Fig. 1b.During testing monotonically increasing pushover loads were applied. Based on the formula in Eq. (1) as per FEMA 356, the lateral load is applied across the height of the building. Along the height of the structure the pattern of the load was kept as parabolic with the load ratio of 1:4:9 for first storey: second storey: third storey. The load calculations were done using Eq. (1). The maximum base shear and corresponding roof displacement were found to be 286.5 kN and 0.11 m, respectively ([2]) as per the experimental results. Considering the experimental values of roof displacement and corresponding base shear as the basis, the authors have conducted a simulation of the same structure in SAP2000. In order to maintain consistency of load application in experimental and numerical studies, the lateral load was applied in same ratio to SAP model as done for experimental testing of RC framed structure.

$$F_x = \frac{W_x h_x^k}{\sum_{i=1}^{N} W_i h_i^k} V \tag{1}$$

$$C_{vx} = \frac{W_x h_x^k}{\sum_{i=1}^{N} W_i h_i^k}$$

Preliminary study

When the actual structure is constructed, there is every possibility that there could be variation in the grade of concrete, the grade of steel and reinforcement cover on account of which the experimental results may differ from analytical results. To assess this uncertainty, the authors have earlier carried out stochastic analysis by considering uncertain parameters as the concrete strength, steel strength, reinforcement cover, and hinge location, which were randomly generated and incorporated into the analysis. SAP2000 (version-14) was been used as the general finite element software for modelling and analysis. User-defined hinge properties are incorporated by generating moment curvature data. For this purpose, IS recommended stress–strain model for unconfined concrete, and British code recommended (CP 110–1972) stress–strain curve for steel (Fig. 2) is adopted. Considering lower and upper limit as 15% decrease and 15% increase in reference grade of steel ($f_y = 478$ N/mm^2), reference grade of concrete ($f_{ck} = 35$ N/mm^2), and plus/minus 10 mm variation in cover (20 mm), random numbers were generated and incorporated in the analysis. Randomly generated hinge location was adopted by considering lower and upper limit as 0.0 and 0.2 L, for different hinge length formulations: Sawyer, Mattock, Corley, and Pauley. The programming was carried out in Excel for each hinge length formulation. Simulated results were then compared with experimental results. For considering user-defined hinge lengths following formulations were considered.

1. Corley's formula [3]

$$l_p = 0.5d + 0.2\sqrt{d}\left(\frac{z}{d}\right)$$

2. Mattock's formula [4]

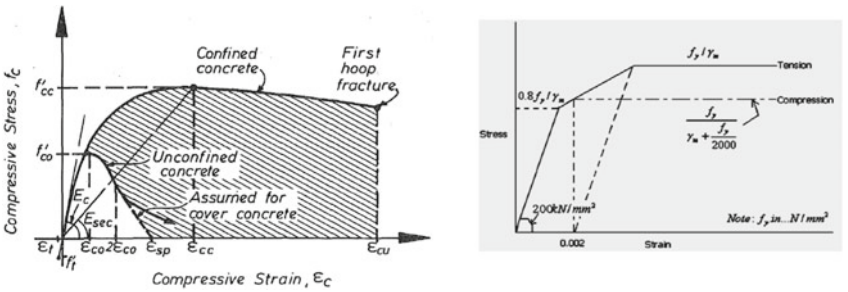

(a) Mander's model for stress-strain relationship for confined concrete

(b) Stress-strain model for steel (British code)

Fig. 2 Material models

$$l_p = 0.5d + 0.05z$$

3. Sawyer's formula [5]

$$l_p = 0.25d + 0.075z$$

4. Pauley-Priestley formula ([6])

$$l_p = 0.08z + 0.022d_b f_y(\text{MPa})$$

db diameter of main reinforcing bars in mm
f_y yield strength of reinforcement bars, in MPa
Z Distance of critical section from point of contraflexure
d effective depth of the member.

Three geometric models were considered, viz; bare frame, rigid and shell frame. Random data generated were incorporated using interactive data base editing feature of SAP 2000 and about 50 iterations were carried out for randomly generated uncertain parameters for each of the above geometric model. From the hypothetical test results carried out, it was evident that Paulay–Priestley's formulation for geometric model with slab as shell assemblage yields closest results to that obtained from experiments. The analytical mean base shear was 0.96 times the experimental base shear (286.5 kN) and the mean analytical displacement was 0.83 times the experimental roof displacement (0.11 m). Panandikar et al. [7]. This model was further investigated for refinement if any with consideration of confinement of concrete by employing Mander's model as shown in Fig. 2a and stress–strain model for steel as shown in Fig. 2b.The design matrix was developed by adopting shell model confined concrete and Pauley priestly hinge length formulation ([8]) as shown in Table 1. Considering Mander's confined model, it is found that though the base shear prediction capabilities of model improve, capability to predict displacement deteriorates slightly. The analytical mean base shear was 0.996 times the experimental base shear and the mean displacement was 0.767 times the experimental displacement. The same design matrix as shown in Table 1 has been used for further progress of the work.

4 Prediction Equations Using RSM

Design of Experiment (DoE) has been frequently often used for analysis in the last two decades and been adapted for many applications in different areas. RSM comprises of mathematical and statistical techniques that are used for optimizing the response of input variables [9].

The data generated in Table 1 have been used to develop predicted equations using RSM for geometric model with slab as an assemblage of shell element, Paulay–Priestley hinge length formulation and Mander's confined model for random material

Table 1 Design matrix (Shell model, confined concrete & Pauley–Priestly hinge length formulation)

Run	Factor1 $f$ck (N/mm^2)	Factor2 f_y (N/mm^2)	Factor3 cv (mm)	Factor4 h.l (m)	Response P (kN)	Response Δ (m)
1	29.11	498.69	14.56	0.049	273.71	0.089
2	35.72	544.46	27.81	0.166	335.7	0.073
3	29.17	409.32	14.68	0.004	231.03	0.094
4	30.33	462.07	13.83	0.085	232.73	0.085
5	39.63	454.16	21.11	0.166	243.52	0.079
6	36.76	537.70	10.62	0.166	351.68	0.069
7	29.71	526.06	11.45	0.069	288.95	0.067
8	30.39	492.98	19.72	0.025	279.12	0.119
9	32.37	435.24	29.86	0.088	235.26	0.079
10	29.51	440.60	17.88	0.182	307.46	0.064
11	29.15	409.34	28.37	0.0007	210.41	0.096
12	37.19	416.90	10.30	0.062	246.16	0.075
13	37.07	467.78	15.63	0.145	297.98	0.067
14	30.66	480.41	18.89	0.0248	273.42	0.079
15	39.94	458.54	10.77	0.096	277.00	0.071
16	29.43	415.22	26.02	0.135	250.889	0.077
17	39.88	515.80	26.52	0.020	270.743	0.108
18	33.44	508.68	12.07	0.033	284.39	0.099
19	36.88	513.60	22.32	0.1176	305.364	0.085
20	39.96	485.43	15.20	0.0479	274.93	0.092
21	37.15	426.21	10.94	0.183	316.68	0.065
22	29.98	537.65	11.80	0.185	381.98	0.076
23	37.27	531.61	14.25	0.005	291.667	0.109
24	32.56	494.08	23.19	0.0271	263.49	0.105
25	29.94	472.79	29.57	0.174	301.468	0.076
26	30.88	535.76	29.81	0.193	356.4	0.080
27	39.94	533.35	13.87	0.109	317.48	0.079
28	38.76	419.81	11.19	0.0986	276.65	0.081
29	39.21	497.91	13.02	0.124	264.42	0.07
30	35.35	471.25	25.94	0.091	274.62	0.089
31	32.45	497.69	10.94	0.082	278.38	0.084
32	29.30	410.01	24.01	0.040	260.24	0.104
33	37.92	435.93	15.30	0.076	243.31	0.08

(continued)

Table 1 (continued)

Run	Factor1 $f$ck (N/mm^2)	Factor2 f_y (N/mm^2)	Factor3 cv (mm)	Factor4 h.l (m)	Response P (kN)	Response Δ (m)
34	35.14	419.98	26.0	0.054	249.73	0.097
35	36.33	502.48	19.29	0.0966	249.015	0.078
36	39.67	499.16	25.97	0.190	346.62	0.072
37	31.67	411.01	14.71	0.109	297.22	0.083
38	34.86	532.52	20.28	0.146	265.58	0.0703
39	34.35	487.51	11.76	0.0722	304.97	0.0917
40	39.69	462.50	24.91	0.127	289.74	0.074
41	36.35	486.44	11.61	0.167	321.61	0.07
42	28.87	519.07	17.15	0.009	265.39	0.112
43	29.92	485.34	10.57	0.030	288.83	0.103
44	33.46	439.72	13.24	0.173	337.72	0.071
45	34.14	507.41	18.27	0.0627	250.53	0.088
46	32.25	437.14	29.35	0.180	327.34	0.077
47	36.84	535.88	26.31	0.018	266.37	0.124
48	40.19	411.01	16.19	0.197	395.4	0.073
49	28.88	422.31	27.44	0.031	286.06	0.08
50	33.20	517.14	14.72	0.058	234.63	0.084

strength, effective cover and hinge location. A multiple regression analysis is carried out to obtain coefficients and the equations that can be used to predict the responses. The software 'Design expert' trial version 8.07.1 of STAT-EASE, USA was used for the analysis. Using the statistically significant model, the correlation between the input parameters and the responses was obtained. The design expert suggested quadratic model for Base shear and linear model for Displacement. For base shear backward regression method was used to eliminate insignificant model terms. The analysis of variance for the reduced quadratic models summarizes the analysis of each response and shows the significant model terms. The analysis of variance results for the base shear and roof displacement are shown in Tables 2 and 3, respectively.

The predicted equations developed are given in Eqs. 2 and 3, respectively. These equations are valid for input variables levels ranging from 406.3 to 549.7 N/mm^2 for f_y, 29.75–40.25 N/mm^2 for f_{ck} and 10–30 mm for cover.

$$\begin{aligned}\text{Base shear}\,(P) = {} & +191.29871 + 0.21610 * f_y - 1.15062 * \text{cv} \\ & - 493.18323 * \text{h.l} + 4635.85524 * h.l^2 \end{aligned} \tag{2}$$

$$\begin{aligned}\text{Displacement}\,(D) = {} & +0.064282 + 3.65449E - 005 * f_{ck} + 5.64298E - 005 * f_y \\ & + 5.03181E - 004 * \text{cv} - 0.18267 * \text{h.l} \end{aligned} \tag{3}$$

Table 2 Analysis of variance for Base shear (confined model)

Source	Sum of squares	df	Mean square	F value	$P > F$	
Model	50,683.64	4	12,670.91	21.63	<0.0001	Significant
B-f_y	0.4303.83	1	4303.83	7.35	0.0095	
C-cv	2607.52	1	2607.52	4.45	0.0405	
D-h.l	35,155.76	1	35,155.76	60.02	<0.0001	
D^2	9636.67	1	9636.67	16.45	0.0002	
Residual	26,358.15	45	585.74			
Cor total	77,041.79	49				
R-square = 0.6579				Adjusted R^2 = 0.6275		
Predicted R-square = 0.5686				Adequate precision = 15.98		

Table 3 Analysis of variance for Displacement (confined model)

Source	Sum of squares	df	Mean square	F value	$P > F$	
Model	6.806E-003	4	1.702E-003	21.88	<0.0001	Significant
A-f_{ck}	8.828E-007	1	8.828E-007	0.011	0.9156	
B-f_y	2.902E-004	1	2.902E-004	3.73	0.0597	
C-cv	5.124E-004	1	5.124E-004	6.59	0.0137	
D-hl	5.783E-003	1	5.783E-003	74.35	<0.0001	
Residual	3.500E-003	45	7.778E-005			
Cor Total	0.010	49				
R-square = 0.6604				Adjusted R^2 = 0.6302		
Predicted R-square = 0.5771				Adequate precision = 16.03		

5 Effect of Parameters on Response (Confined Model)

(a) Base shear

It is evident from results obtained that all the input parameters have significant effect on the base shear. Figure 3 shows a perturbation plot that illustrates the effects of input parameters on base shear. The cover to reinforcement has negative effect on base shear. It is seen that with increase in f_y there is increase in base shear while in case of hinge location, the results demonstrate that increasing the distance of location of hinges from end support until it reaches its central value would result in decreasing the base shear and thereafter the base shear then starts to rise.

(b) Displacement

Figure 3 shows a perturbation plot that illustrates the effects of input parameters on displacement. The hinge location has negative effect on displacement. It is seen that

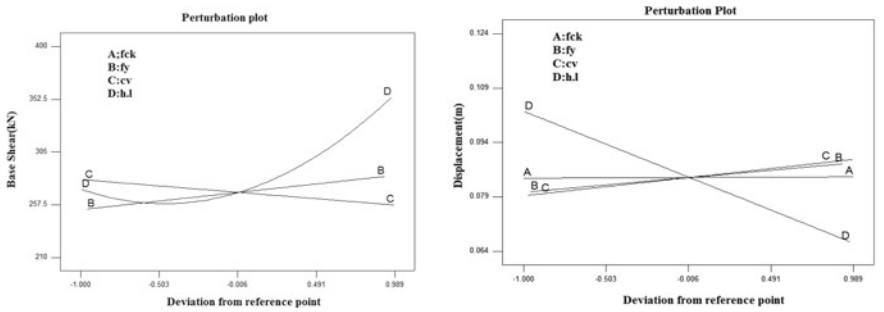

Fig. 3 Perturbation plot showing effect of all factors on Base shear and Displacement (confined model)

Table 4 Comparison of prediction equation for confined model

$f_{ck} = 35$ (N/mm^2)	$f_y = 478$ (N/mm^2)	cv = 20 (mm)		Base shear (P) kN	Displacement (Δ) (m)
Confined model			Actual	286.5	0.11
			Predicted	271.58	0.1026
			Error%	5.49	7.2

with increase in f_y and cv there is increase in displacement. With increase in f_{ck}, there is not much increase in displacement.

6 Validation of the Developed Model

Model validation is a primary means to evaluate accuracy and reliability of computational simulations in engineering design. It is an assessment of how accurately the mathematical model represents the real-world application. The predicted equations developed for confined model are used to find out the responses and results compared with experimental responses. Table 4 summarizes the experimental conditions, the predicted values of responses and the percentage of error.

7 Conclusions

Response surface methodology (RSM) was applied for modelling and analysis of response parameters, viz, base shear and displacement. Multiple regression analysis was carried out to obtain the equations that can be used to predict the responses. Using statistically significant model, the correlation between the parameters and responses was obtained. The difference in the actual and predicted responses exists as the results

are sensitive to stress–strain models of concrete and stress–strain model for steel adopted by analyzer. Modelling of concrete and reinforcement stress–strain curves greatly influences both the ultimate load and ultimate displacement for the structure under pushover loads. The displacement capacity of the structure depends on in which sequence the hinges are formed leading to mechanism. During experimentation, sequence in which the hinges form needs to be noted, which would help in refining the analytical results.

References

1. Elnashai AS (2001) Advanced inelastic static (pushover) analysis for earthquake applications. J Struct Eng Mech. https://doi.org/10.12989/sem.2001.12.1.051
2. Sharma A, Reddy GR, Vaze KK, Khuswaha HS (2008) Experimental and analytical investigation on behavior of scaled down reinforced concrete framed structure under monotonic pushover loads, Bhabha Atomic Research Centre, New Delhi, India
3. CorleyW (1966) Rotational capacity of reinforced concrete beams. J Struct Div, 121–146, ASCE, 92, ST5
4. Mattock AH (1967) Discussion of rotational capacity of reinforced concrete beams. J Struct Div, 519–522, ASCE, 93, ST2
5. Sawyer HA (1964) Design of concrete frames for two failure states. In: Proceedings of the international symposium on the flexural mechanics of reinforced concrete, ASCE- ACI, Miami, pp 405–431
6. Park R, Pauley T (1975) Reinforced concrete structures. John Wiley & Sons, New York
7. Panandikar N, Narayan BKS (2014) Stochastic analysis to assess uncertainty in pushover analysis to modeling methods. In: Second international conference on vulnerability and risk analysis and management, ASCE publication (2014), Liverpool. https://doi.org/10.1061/9780784413609.132
8. Panandikar N (Hede), Babu Narayan KS (2015) Sensitivity of pushover curve to material and geometric modelling—an analytical investigation. Structures 2:91–97
9. Montgomery DC (1984) Design and analysis of experiments. John Wiley & Sons, New York

Application of Proper Orthogonal Decomposition in Concrete Performance Appraisal

A. Manoj and K. S. Babu Narayan

Abstract Mould ability of concrete has made it the most versatile and popular material of construction. Workability, strength and durability of concrete are very important characteristics that depend on a large number of variables like cement and aggregate type, mix proportioning, method of mixing, conveying, placing and curing and environmental conditions of exposure like temperature, humidity, wind velocity and insolation. The degrees to which workability, strength and durability characteristics vary, and also interplay and conflicts make decision on consideration of independent variables that influence concrete performance, make the job of analysts very complex. Proper Orthogonal Decomposition (POD) is a tool that has great usage potential in reorganizing and rationalizing vast data to understand dependence, interdependence and independence of variables that affect the concrete characteristics. This paper presents the utility of Proper Orthogonal Decomposition in concrete performance appraisal.

Keywords Concrete · Variables · Correlation · POD · PCR

1 Introduction

Cement replacement by secondary cementitious materials (SCMs) for production of sustainable concrete has been the trend in construction industry. Geo-polymer concrete is one such attempt where cement is replaced by GGBS, Fly ash and Silica fume to produce eco-friendly concrete.

The replacement of cement by SCMs grossly alters the characteristics of concrete. Quantification of influence of different proportioning of SCMs on wet and set concrete is a challenging task.

POD is of great help in understanding interplay between variables and in manipulation of desired behaviour of concrete [3].

A. Manoj (✉) · K. S. B. Narayan
Department of Civil Engineering, National Institute of Technology Karnataka, Surathkal, Mangalore 575025, India
e-mail: manoja1990@gmail.com

B. B. Das et al. (eds.), *Recent Trends in Civil Engineering*, Lecture Notes in Civil Engineering 105, https://doi.org/10.1007/978-981-15-8293-6_2

2 Proper Orthogonal Decomposition

Proper orthogonal decomposition [2] is a dimensionality reduction technique for understanding high-dimensional datasets.

Subjecting dataset to outlier detection is the first step in any statistical analysis. After the initial check, correlation matrix of data is eigenvalue decomposed to obtain eigenvectors which are orthogonal to each other. Eigenvalues explain amount of variation in the data, and respective eigenvectors give direction of variation. Correlation plots obtained from eigenvectors help in understanding the influence of variables on target characteristic. Vector loadings quantify the influence and help in decision-making of consideration of components for math modelling and refinement.

3 Illustrative Example

Available data set [1] on geo-polymer concrete cured at ambient temperature has been taken up for the study of interaction of concrete variables with its cardinal properties, viz. strength, workability and durability. Data consist of three cases of blends without fibre (FC, FG and GC) and three cases with fibre (FRFC, FRFG and FRGC).

Fine aggregate (630 kg/m^3), coarse aggregate (1800 kg/m^3), NaOH (57.15 kg/m^3), Na_2SiO_3 (142.85 kg/m^3), Gujcon CRF fibres (7 g/m^3) and total fines (400 kg/m^3) quantity are adopted and maintained constant for all combination of concrete mixes.

Cement (OPC), Fly ash, Ground granulated blast furnace slag (GGBS) content, tested slumps (Sl), compressive and split tensile strength at 7 & 28 days (CS7, CS28, STS7 & STS28), modulus of elasticity (E), weight and strength loss due to acid attack (AA_WL, AA_CSL), thermal shock (TS_CSL) and exposure to fire (Fire_CSL) are the data available as variables considered for the study.

POD results of the dataset are presented in the section that follows.

4 Results and Discussions on POD of Data

After an initial inspection of scatter plots, no possible outliers were detected. The normalized dataset correlation matrix was subject to eigenvalue decomposition and results are presented in Tables 1, 2, 3 and 4.

The 12-dimensional dataset can be reduced to two-dimensions as the first two axes account for about 90% of variation.

Tables 2, 3 and 4 give eigenvector information, which are the coordinates of variables in reduced dimensional space. The coefficients reveal orientation of variables to lie in specific dimension.

Table 1 Eigenvalues

Case	Eigenvalue	% variation contribution	Cumulative % variation contribution
FC	7.83 2.87	65.2 23.9	89.1
FRFC	8.70 2.65	72.5 22.1	94.6
FG	10.46 0.90	87.2 7.5	94.7
FRFG	10.38 0.86	86.6 7.2	93.8
GC	7.87 3.86	65.6 32.2	97.8
FRGC	7.23 4.51	60.3 37.6	97.9

Table 2 First two eigenvectors of cement—fly ash mix concrete data without and with fibres

Case	FC		FRFC	
	D1	D2	D1	D2
OPC	0.55	0.80	0.46	−0.88
Fly Ash	−0.55	−0.80	−0.46	0.88
Sl	−0.76	−0.63	−0.55	0.83
CS7	0.98	−0.09	0.98	0.11
CS28	0.95	−0.24	0.97	0.17
STS7	0.95	−0.28	0.98	0.01
STS28	0.96	−0.14	0.96	0.11
E	0.97	−0.13	0.98	0.07
AA_WL	−0.98	−0.14	−0.98	0.10
AA_CSL	−0.77	0.49	−0.86	−0.37
TS_CSL	−0.69	0.43	−0.88	−0.31
Fire_CSL	0.04	0.76	−0.87	−0.35

Correlation plots can be obtained by plotting eigenvectors against each other. Figure 1 shows such correlation plots that are of utility in identifying prime variables influencing targeted concrete characteristics. This exercise immensely helps in discarding variables that do not affect target characteristics. Such elimination vastly reduces time and efforts in modelling and simulations.

It is observable from correlation plots Fig. 1a, b of OPC-Fly ash-based mixes that AA_WL, AA_CSL and TS_CSL are negatively correlated to strength of concrete. In mixes without fibres, Fire_CSL is not well correlated with any other variables considered. With addition of fibres, Fire_CSL is negatively correlated to strength variables. Slump is strongly and positively correlated to fly ash content.

Table 3 First two eigenvectors of fly ash—GGBS mix concrete data without and with fibres

Case	FG		FRFG	
	D1	D2	D1	D2
FlyAsh	−0.98	−0.06	−0.98	0.05
GGBS	0.98	0.06	0.98	−0.05
Sl	−0.92	−0.14	−0.95	−0.22
CS7	0.96	0.16	0.98	−0.02
CS28	0.97	0.14	0.99	−0.03
STS7	0.99	0.09	0.97	0.23
STS28	0.97	0.14	0.95	0.21
E	0.97	0.20	0.96	0.23
AA_WL	−0.94	−0.22	−0.91	−0.22
AA_CSL	−0.82	0.48	−0.85	0.49
TS_CSL	−0.88	0.38	−0.86	0.05
Fire_CSL	−0.79	0.57	−0.77	0.61

Table 4 First two eigenvectors of cement—GGBS mix concrete data without and with fibres

Case	GC		FRGC	
	D1	D2	D1	D2
OPC	0.51	0.86	0.62	0.78
GGBS	−0.51	−0.86	−0.62	−0.78
Sl	0.57	0.82	0.64	0.76
CS7	0.97	0.20	0.99	−0.01
CS28	0.99	0.03	0.97	−0.21
STS7	0.98	0.02	0.99	−0.06
STS28	0.99	−0.07	0.98	−0.21
E	0.99	0.08	1.00	−0.05
AA_WL	−0.46	0.85	−0.66	0.72
AA_CSL	−0.89	0.41	0.41	0.89
TS_CSL	−0.89	0.41	−0.67	0.70
Fire_CSL	−0.61	0.78	−0.39	0.91

In FG and FRFG mixes also, slump increases as fly-ash content increases, as observed in Figs. 1c, d. Strength parameters are positively correlated to GGBS and negatively correlated to fly-ash contents. AA_WL, AA_CSL, TS_CSL and Fire_CSL are more in mixes with higher fly ash quantities. Addition of fibres does not show much change in nature of variables interaction.

Figures 1e, f shows that usage of fibres in cement–GGBS-based mixes has highest influence on AA_CSL. In mixes without fibres, AA_CSL has negative correlation

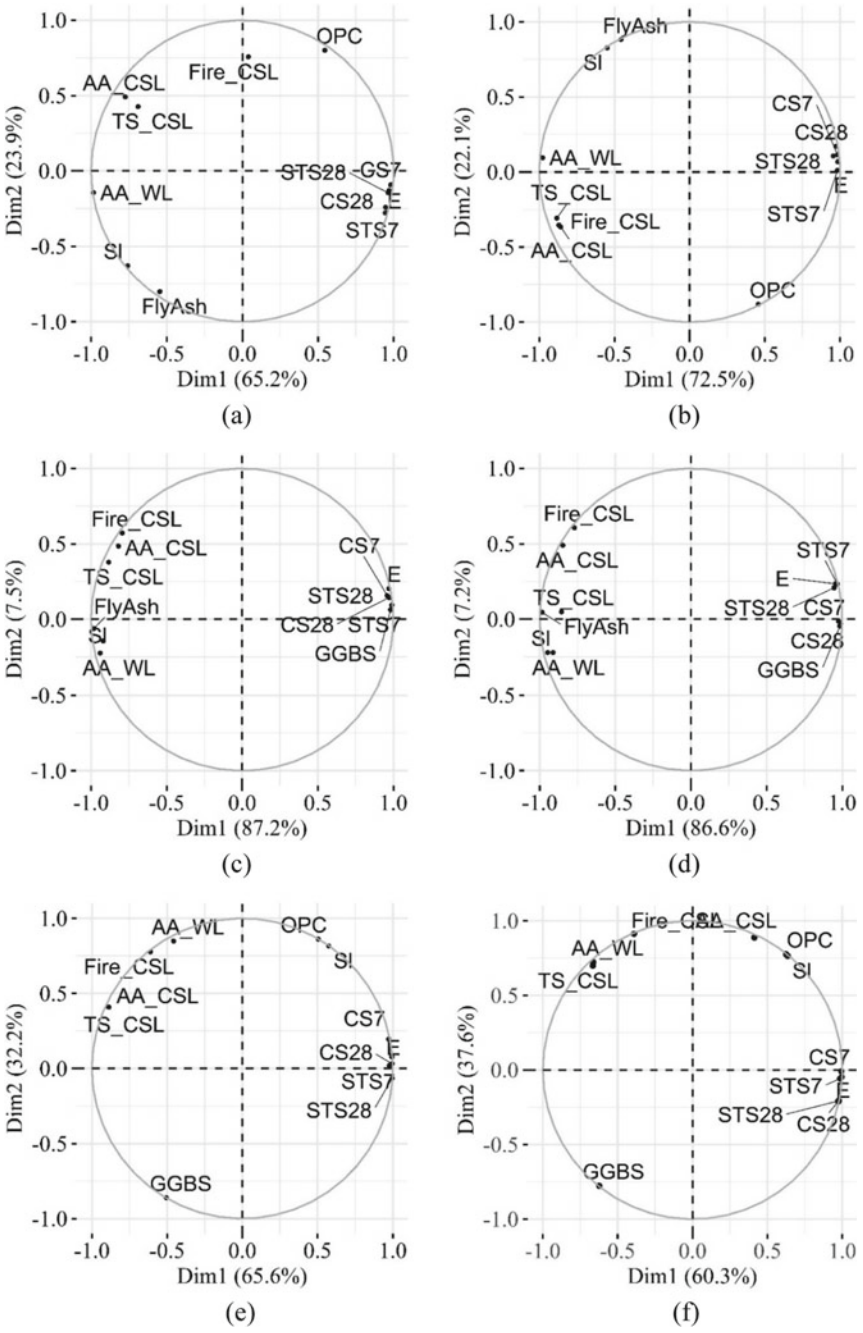

Fig. 1 Correlation plot **a** FC. **b** FRFC. **c** FG. **d** FRFG. **e** GC. **f** FRGC

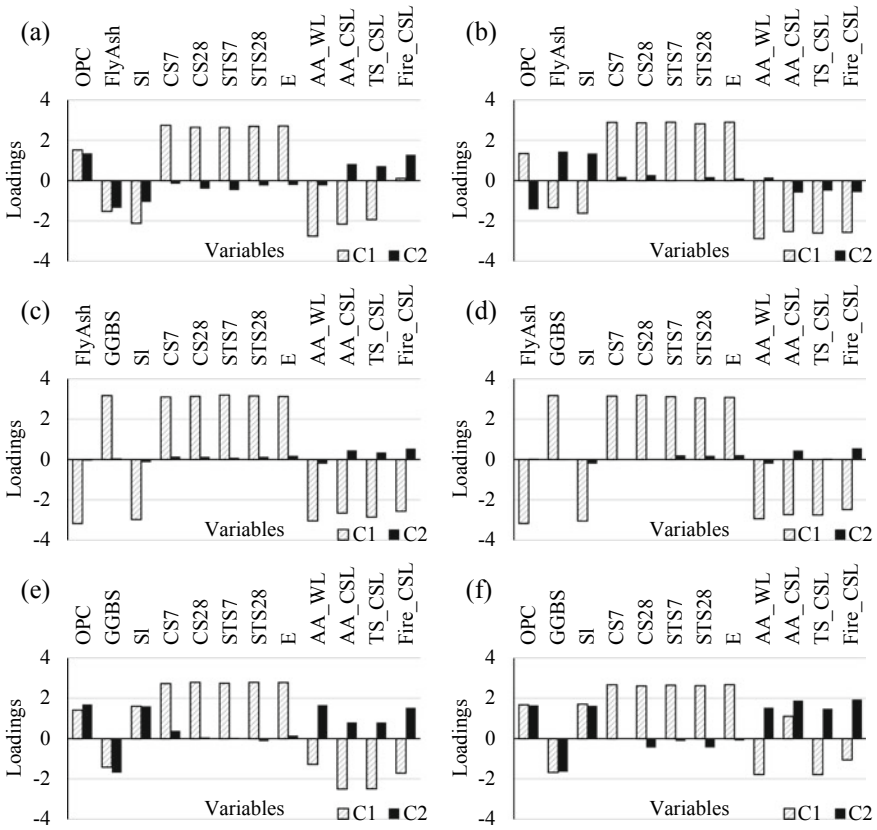

Fig. 2 Vector loadings **a** FC. **b** FRFC. **c** FG. **d** FRFG. **e** GC. **f** FRGC

with strength whereas in mixes with fibres AA_CSL has high positive correlation with cement content. Slump increases with increase in OPC content. Weight loss due to acid exposure and strength loss due to thermal shock and exposure to fire are negatively correlated to 28 days' compressive strength.

Vector loadings are shown in Fig. 2 give an idea of amount of contribution of variables to each dimension and nature of contribution.

5 Principal Component Regression

Principal component regression (PCR) is a method of math modelling for high dimensional concrete data [2]. PCR method is apt when development of multi-linear regression (MLR) models becomes challenging due to high correlation between independent variables and multi-collinearity (high VIFs) issues.

Considering principal components of independent variables to develop models overcome the issue of multi-collinearity. Depending on correlations of dependent variable with the PCs of independent variables considered and contribution of PCs to variation in data, number of PCs to be considered for PCR can be decided. Regression model in its standard form is shown in Eq. (1).

$$y = \beta_0 + \sum_{i=1}^{m} \beta_i z_i + \in \tag{1}$$

where $\beta_i s$ are PCR coefficients corresponding to standardized independent variables (z_i) to predict y and ϵ is the error term.

In dataset considered OPC, fly ash and GGBS contents are varied in such a way that they are perfectly and negatively correlated. This brings the challenge of depicting these variables together, in predictive modelling of slump and 28 days' compressive strength. VIF values are also found to be high.

The computed coefficients of regressors for slump and 28 days' compressive strength are summarized in Tables 5 and 6, respectively. R^2 values of models developed show good predictability of targeted slump and 28 days' compressive strength.

Table 5 Coefficient of principal component regression for slump (mm) prediction

Case	β_o	β_i			R^2
		OPC	Fly Ash	GGBS	
FC	73.10	−4.92	4.92	–	0.87
FRFC	74.50	−5.44	5.44	–	0.93
FG	82.10	–	1.59	−1.59	0.73
FRFG	82.90	–	1.60	−1.06	0.83
GC	51.70	9.48	–	−9.48	0.99
FRGC	52.60	10.84	–	−10.84	0.99

Table 6 PCR coefficients for 28 days' compressive strength (MPa) prediction

Case	β_o	β_i					R^2
		OPC	Fly ash	GGBS	Sl	CS7	
FC	32.40	−1.93	1.93	–	−2.40	12.19	0.97
FRFC	35.60	−0.85	0.85	–	−1.15	12.89	0.95
FG	42.52	–	−3.91	3.91	−3.61	3.88	0.97
FRFG	44.40	–	−4.22	4.22	−4.01	4.17	0.97
GC	74.50	−1.63	–	1.63	0.26	17.23	0.97
FRGC	79.10	−1.23	–	1.23	−0.84	15.66	0.97

Table 7 Mean ($\bar{x}$) of variables used in model development

Case	OPC	Fly Ash	GGBS	Sl	CS7
FC	136	264	–	73.10	23.67
FRFC	136	264	–	74.50	25.79
FG	–	264	136	82.10	25.23
FRFG	–	264	136	82.90	27.58
GC	356	–	44	51.70	57.76
FRGC	356	–	44	52.60	61.36

Table 8 Standard deviation (S) of variables used in model development

Case	OPC	Fly Ash	GGBS	Sl	CS7
FC	139.33	139.33	–	10.52	7.71
FRFC	139.33	139.33	–	11.26	8.08
FG	–	139.33	139.33	3.73	15.03
FRFG	–	139.33	139.33	2.33	16.50
GC	24.22	–	24.22	19.50	12.98
FRGC	24.22	–	24.22	21.77	12.28

Tables 7 and 8 show mean ($\bar{x}$) and standard deviation (S) of independent variables considered in model development. Using $\bar{x}$ and S, predictive equations can be expressed in terms of actual units of variables, if needed.

6 Conclusions

Concrete variables interaction and behavioural aspects can effectively be studied using POD method. The presence of large and highly correlated variables in concrete material makes development of MLR models challenging, due to multi-collinearity issues. Method of PCR has great potential in addressing this problem, as illustrated.

The models developed for slump and 28 days' compressive strength have high R^2 values and can be used as predictors in similar set of conditions.

References

1. Anand Rejilin DR (2018) Strength and durability properties of geopolymer concrete. Anna University
2. Jolliffe IT (2002) Principal component analysis. In: International encyclopedia of education, 2nd edn. Springer, Berlin. https://doi.org/10.1007/b98835
3. Manoj A, Babu Narayan KS (2019) Proper orthogonal decomposition for generation of organized data in concrete technology. In: Ukieri concrete congress, concrete: the global builder. https://ukiericoncretecongress.com/ucc2019/files/Proceedings/pdf/UCC-2019-128.pdf

Effect of Curing Methods on the Artificial Production of Fly Ash Aggregates

K. N. Shivaprasad, B. B. Das, and S. Krishnadas

Abstract The experimental investigation, provides the results on the artificially produced fly ash aggregates through the pelletization process, is presented in this paper. NaOH and Na_2SiO_3 were used as alkali activator as a binder. The composition of alkaline solution is maintained as 5% of Na_2O and SiO_2/Na_2O ratio of 0.3 with respect to weight of fly ash used. The detailed investigation is carried out by varying the water content to identify the optimum dosage of water in the alkaline solution in the fly ash pelletization. Further, different methods of curing were investigated to check for the suitable curing method for the production of fly ash aggregate produced. Optimum water content and suitable curing method will be identified through efficiency of pelletization and aggregate properties. Grey relation analysis is performed on the experimental test results to identify the influence of curing method on the produced aggregates. From these results, it is clearly understood that the curing method has significantly improved produced aggregates.

Keywords Fly ash · Alkaline solution · Water content · Solution curing · Heat curing · Artificial aggregates

1 Introduction

Concrete contains about 70–80% aggregates, 12–14% cement, and 8–10% mixing water by mass. To produce one cubic meter of concrete, approximately two tons of aggregates are required. A recent study reported that the global demand for construction aggregate is about 51.7 billion metric tons in 2018 and it is projected with an annual growth rate of 5.2%. By 2020, in India alone it is predicted, the demand of aggregate will more than five billion metric tons [1]. In this present growth rate,

K. N. Shivaprasad (✉)
Civil Engineering Department, JSS Science and Technology University, Mysuru 570006, India
e-mail: shivaprasadkn@jssstuniv.in; shivaprasad.god@gmail.com

B. B. Das · S. Krishnadas
Civil Engineering Department, National Institute of Technology Karnataka, Surathkal, Mangalore 575025, India

B. B. Das et al. (eds.), *Recent Trends in Civil Engineering*, Lecture Notes in Civil Engineering 105, https://doi.org/10.1007/978-981-15-8293-6_3

natural aggregate consumption has reached a frightening level that leads to serious environmental impacts.

Enough studies were reported on the production of aggregates through artificial process using industrial waste and natural materials through pelletization process [2–4]. The pellets formation in the process of production had better control oversize of the pellet formed in pelletizer of disc type as compared with different types of pelletizer [2]. From the literature, it is observed the production of artificial aggregates with fly ash using several binders are available [3, 5–8]. It is reported by many researchers that the factors influencing the production of aggregates are mainly dependent on the ingredients used such as raw material and binder selected with their chemical and physical properties along with production process involved [3, 5]. Further, it is observed that the different methods are adopted for hardening the pellet producing such as sintering, steam curing, cured in normal water, and autoclaving depending on the binder selected [5, 7–9]. However, the effective curing method for geopolymer as binder in the aggregates production is very much needed.

To study the effect of different methods of curing on geopolymer binder in fly ash aggregates production, through experimental investigation is carried out in two stages. Primarily, to identify the optimum water content required for the pelletization of fly ash aggregates to achieve maximum efficiency. This optimum water content is used in the detailed study to analyse the influence of curing method on engineering properties of artificial produced aggregates. Further, Grey relational analysis is carried with different aggregate types produced with natural aggregates and compared.

2 Materials and Methodology

2.1 Materials

Class F fly ash was used in the present investigation, NaOH flakes of 98% purity and Na_2SiO_3 solution (8.0% Na_2O, 26.5% SiO_2, 65.5% H_2O by mass) were used in alkali solution preparation. In the present study, alkaline solution prepared with the Na_2O content of 5% and SiO_2/Na_2O ratio of 0.3 is kept constant for all the experimental trial runs. However, water content is varied to optimize the maximum efficiency of pelletization. Further, this optimum content is used to study the influence of curing method on the produced aggregate properties. The dosage of Na_2O and water content is expressed in percentage of fly ash in the prepared alkaline solution.

2.2 Aggregates Production

A fabricated pelletizer of disc type is used for the pelletization of fly ash. The pelletization process adopted in these experimental trials is as same as in previous studies [7, 9]. During the pelletization, it is maintained throughout the experiment of 15 min as pelletization duration and 45° as angle of disc. Further, disc rotational speed is maintained at 40 RPM in all experimental trial runs.

2.3 Curing Methods

The artificially produced aggregates in the present investigation were subjected to different curing conditions:

Ambient curing: The produced aggregates in the process were kept in ambient conditions (temperature 28 ± 2 °C and relative humidity of 80%) till they are characterized for their engineering properties.

Heat curing: The produced aggregates in the process were kept under ambient curing condition for 24 h. After that these aggregates were subjected to heat at 80 °C for 24 h and once heating of aggregates is completed, they were kept in ambient curing condition till they are characterized for their engineering properties.

Solution curing: The produced aggregates were allowed for 24 h in ambient conditions. After that aggregates were dipped in Na_2SiO_3 solution for 30 min and removed. Further, these aggregates are kept in an ambient condition till they are characterized for their engineering properties.

Heat-solution curing: In this curing method, the produced aggregates are subjected heat curing first followed by solution curing as explained above.

2.4 Experimental Methodology

In the present investigation, to meet the objectives, experiments are carried out in two stages as follows.

Stage 1: In this stage, the fly ash is pelletized with different dosages in the alkaline solution by varying water content in it. This is to identify the optimum dosage of water content required for the effective pelletization of fly ash.

Stage 2: In this stage, different curing methods as defined in the above section are investigated on the fly ash aggregates production. Further, the Grey relational analysis was analysed to identify the effect of curing method on the produced aggregates properties.

2.5 Testing of Aggregates

Equation 1 is used to evaluate the pelletization efficiency. The produced pellets were analysed for particle size distribution as per the IS 383-2016 [10]. According to IS 2386-1963 Part 3 [11], the produced aggregates are characterized for specific gravity, bulk density, and water absorption properties. Further, aggregate impact value and aggregate crushing value were evaluated as per IS 2386:1963 Part 4 [12].

$$\text{Efficiency of pelletization} = \frac{\text{Weight retained on the IS sieve no 480}}{\text{Total weight of material used}} * 100 \quad (1)$$

The produced aggregates were subjected to crushing strength of individual pellets were determined using Eq. 2 [5]. Cushing strength (σ) of aggregates was evaluated as the average of the batch where sample size of the batch is more than 20 numbers and size of the pellets/aggregates ranges from 6 to 20 mm.

$$\sigma = \frac{2.8 * P}{\pi * x^2} \quad (2)$$

where, P presents the ultimate braking load for each aggregate and aggregates size is measured as x.

2.6 Grey Relational Analysis (GRA)

GRA, is a statistical analysis, was carried out to identify the influencing factor in this experimental study. Many researchers showed the advantage of this analysis [7, 13]. Experimental test results of produced fly ash aggregates were considered as inputs to Grey relation analysis. Sahoo et al. as explained in step by step procedure to analyse, in similar lines, present experimental test results are analysed [13].

3 Experimental Test Results

The pelletization process was carried out by varying the percentage of water in alkaline from 18 to 22%. Using Eq. 1, the production efficiency was evaluated for each trial, runs and results are tabulated in Table 1. Figure 1 presents the particle size distributions for various batches of aggregates obtained by adding various percentage of water.

The produced aggregates are evaluated for specific gravity and bulk density and test results are presented in Table 2. Further, water absorption values of produced aggregates were evaluated and compared with natural aggregates values are presented in Fig. 2.

Table 1 Efficiency values for different dosages of water contents in alkaline solution

Water content in %	Efficiency
18	30.27
19	60.72
20	93.49
21	100
22	100

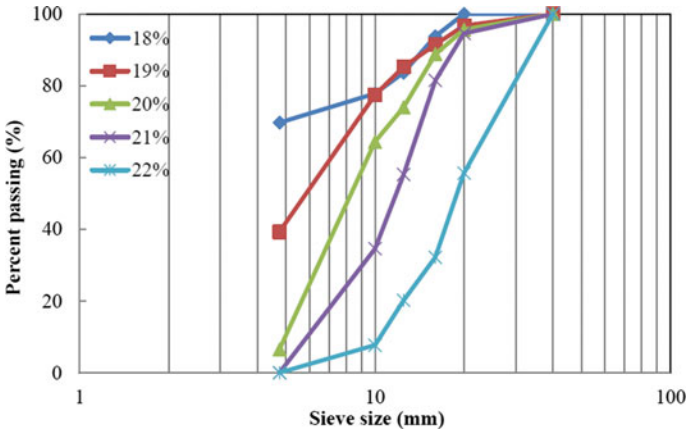

Fig. 1 Particle size distribution for produced aggregates with different water content

Table 2 Specific gravity and bulk density of different types of aggregates

Aggregate type	Specific gravity	Bulk density (kg/m^3)	
		Loose	Compacted
Natural	2.75	1373.7	1558.8
Ambient cured	1.85	1036.0	1134.7
Heat cured	1.76	1033.3	1151.3
Solution cured	1.99	1070.7	1186.7
Heat—solution cured	1.90	1014.0	1131.3

Artificially produced aggregates treated in different curing conditions were assessed for aggregate impact value and aggregate crushing value is evaluated. The experimental test results are compared with natural aggregates are presented in Fig. 3. Further, the crushing strength of individual aggregates of produced aggregates is estimated and test results are presented in Fig. 4.

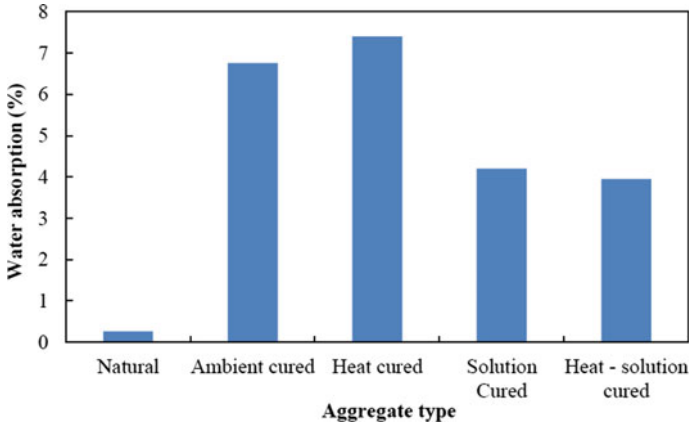

Fig. 2 Water absorption values of different aggregates

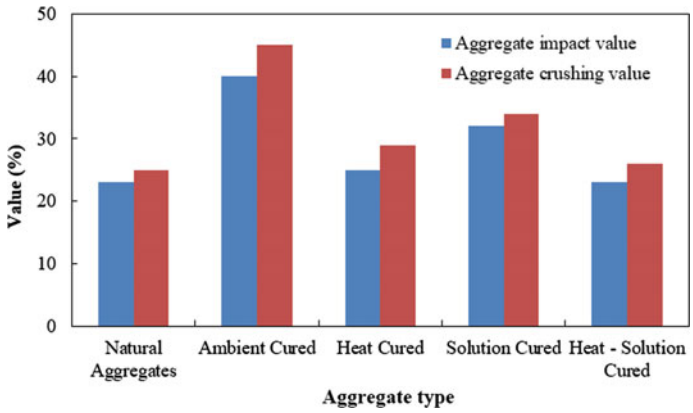

Fig. 3 Aggregate impact values and aggregates crushing values of different aggregates

4 Grey Relational Analysis

GRA was carried out using the experimental test results as responses and Grey relational generations were generated (Table 3). Further, Grey relational coefficients and Grey relational grade (GRG) were estimated for all the produced aggregates cured in different curing conditions and compared with natural aggregates (Table 4).

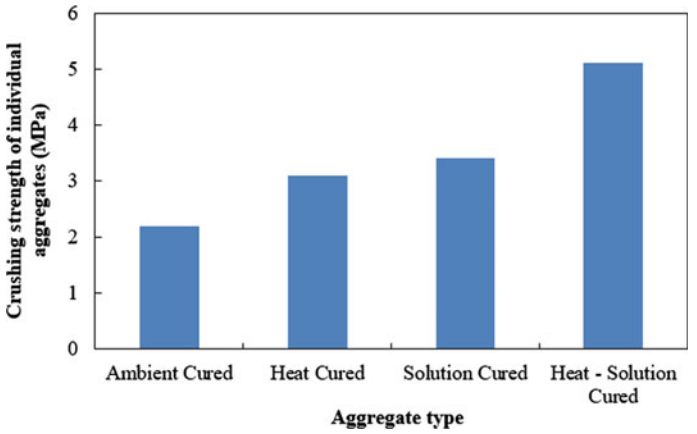

Fig. 4 Individual aggregates crushing strength of different produced aggregates

Table 3 Grey relational generations for engineering properties of produced and natural aggregates

Aggregate type	Grey relational generations				Δ_{0i}			
	Aggregate impact value	Water absorption	Crushing strength of individual aggregates	Aggregate crushing value				
Natural	1.000	1.000	1.000	1.000	0.000	0.000	0.000	0.000
Ambient curing	0.000	0.090	0.000	0.000	1.000	0.910	1.000	1.000
Heat curing	0.882	0.000	0.333	0.800	0.118	1.000	0.667	0.200
Solution curing	0.471	0.448	0.433	0.550	0.529	0.552	0.567	0.450
Heat—solution curing	1.000	0.483	1.000	0.950	0.000	0.517	0.000	0.050

Table 4 Grey relational coefficients and GRG

Aggregate type	Grey relation coefficients				GRG
					γ_i
Natural	1.000	1.000	1.000	1.000	1.000
Ambient curing	0.333	0.355	0.333	0.333	0.339
Heat curing	0.810	0.333	0.429	0.714	0.571
Solution curing	0.486	0.475	0.469	0.526	0.489
Heat—solution curing	1.000	0.492	1.000	0.909	0.850

5 Discussion

From the experimental investigation, the produced aggregates with alkaline solution containing water content of 21% showed 100% efficiency and it has also improved the particle size distribution in the production. It was observed that the particle size distribution from Fig. 1 is well graded when the water content is 21% and it can be noted that more than this water content leads to production larger size particle.

The produced aggregates that are subjected to different curing conditions were estimated for their engineering properties as per standards. It is absorbed that specific gravity of produced aggregates was around 1.76–1.99, which is lesser than the specific gravity natural aggregates. The bulk density of the produced aggregates is found to be in the range of 1014–1186 kg/m^3 is comparatively less when compared natural aggregate bulk density of 1373–1558 kg/m^3. Whereas lowest bulk density values of 1014–1131 kg/m^3 are observed for the heat-solution cured aggregates and highest bulk density values of 1070–1186 kg/m^3 is observed for solution-cured aggregates.

The water absorption of the produced aggregates is found to be high when compared with natural aggregates. Highest water absorption value of 7.4% is observed for heat-cured aggregates and lowest water absorption value of 3.95% is observed for heat-solution cured aggregates. It is noted that solution curing of heat-cured fly ash aggregates water absorption is reduced by 53%. Whereas, the water absorption of heat-solution cured aggregates is 15 times the water absorption of natural aggregates. However, the water absorption of produced aggregates in the present is very less when compared with water absorption values produced in the literature.

Produced aggregates cured under ambient condition are aggregate impact value of 40% and aggregate crushing value of 45%. Further, heat curing of produced aggregates has improved aggregate impact value by 1.6 times and aggregates crushing value by 1.55 times when compared with ambient cured aggregates this may be due to higher degree of geopolymerization under heat curing. Whereas the solution cured fly ash aggregates have improved aggregate impact value and aggregates crushing value by 1.25 and 1.32 times, respectively, when compared with ambient-cured aggregates. However, heat-solution cured aggregates have aggregate impact value of 23% and aggregate crushing value of 25% which very much comparable natural aggregates values of 23% and 25%, respectively.

The produced aggregates subjected to ambient condition have crushing strength of individual aggregates of 2.2 MPa. Further, the heat and solution curing of the produced aggregates have improved to 3.1 and 3.4 MPa, respectively. However, the produced aggregates subjected to heat-solution curing have the highest crushing strength of individual aggregates value of 5.1 MPa this may be due to higher degree of geopolymerization and presence of higher alkaline solution.

From GR, it is observed that, ambient cured aggregates have Grey relational grade (GRG) of 0.339. Whereas the heat and solution curing of produced aggregates has the GRG of 0.571 and 0.489, it clearly indicated that the curing method has high impact on the properties of the produced aggregates. However, the heat-solution

cured method got a GRG of 0.850, which is very much near to the GRG of 1.000 for natural aggregates. It indicated that the artificially produced aggregates subjected to heat-solution curing condition have the better engineering properties and very much comparable to natural aggregates.

6 Conclusions

The following conclusions can be drawn based on the present experimental investigation:

- Water content plays a major part in the production of the fly ash aggregates, with 21% of moisture/water content in the production will be sufficient for the pelletization process for the selected fly ash.
- Specific gravity of the produced fly ash aggregates is found to be in the range of 1.76–1.99 which lesser than natural aggregates. These aggregates can be called as lightweight aggregates.
- The water absorption value is found to be higher in heat-cured fly ash aggregates. It may be due to the refilling of voids created during the heat treatment due to escape of water from the produced aggregates. However, in solution-cured aggregates, the voids are well treated during the curing process, this may led to lower water absorption value.
- From experimental test results, it is clear that properties of aggregates produced and subjected to different curing regime, heat-solution cured aggregates were found to be better in terms of its properties.
- In Grey relational analysis, Grey relational grade clearly indicated that the heat-solution cured aggregates are very much close to natural aggregates when compared with other curing methods.

References

1. Freedonia (2016) World construction aggregates—industry study with forecasts for 2019 and 2024. The Freedonia Group, USA
2. Baykal G, Doven AG (2000) Utilization of fly ash by pelletization process; theory, application areas and research results. Resour Conserv Recycl 30(1):59–77
3. Ramamurthy K, Harikrishnan KI (2006) Influence of binders on properties of sintered fly ash aggregate. Cement Concr Compos 28(1):33–38
4. Gesoglu M, Ozturan T, Guneyisi E (2007) Effects of fly ash properties on characteristics of cold-bonded fly ash lightweight aggregates. Constr Build Mater 21(9), (2007): 1869–1878.
5. Gomathi P, Sivakumar A (2014) Fly ash based lightweight aggregates incorporating clay binders. Indian J Eng Mater Sci 21(2):227–232
6. Priyadharshini P, Ganesh GM, Santhi AS (2011) Experimental study on cold bonded fly ash aggregates. Int J Civ Struct Eng 2(2):493–501

7. Shivaprasad KN, Das BB (2018) Determination of optimized geopolymerization factors on the properties of pelletized fly ash aggregates. Constr Build Mater 163:428–437
8. Manikandan R, Ramamurthy K (2008) Effect of curing method on characteristics of cold bonded fly ash aggregates. Cem Concr Compos 30(9), (2008): 848–853
9. Shivaprasad KN, Das BB, Sharath BP (2020) Pelletization factors on production of fly ashaggregates and its performance in concrete. In: Proceedings of the institution of civil engineers—construction materials
10. BIS (2016) IS 383: Coarse and fine aggregates for concrete—specification, Bureau of Indian Standards, New Delhi
11. BIS (1963) IS 2386—part 3: Methods of test for aggregates for concrete: specific gravity, density, voids, absorption and bulking, Bureau of Indian Standards, New Delhi
12. BIS (1963) IS 2386—part 4: Methods of test for aggregates for concrete: mechanical properties, Bureau of Indian Standards, New Delhi
13. Sahoo S, Das BB, Mustakim S (2016) Acid, alkali, and chlorideresistance of concrete composed of low-carbonated fly ash. J Mater Civ Eng 29(3):04016242, 1–12

Influence of Incorporating Phase Change Materials on Cementitious System—A Review

K. Snehal and Bibhuti Bhusan Das

Abstract Phase change materials (PCMs) are gaining more attention in achieving the sustainability and are being widely adopted as a green building material because of their exclusive ability to store latent heat of thermal energy. PCMs have a capacity to minimize the energy loads and to provide thermal comforts in building infrastructures by its iterative cycle of absorbing and releasing the heat energy. The potential need for manipulating the heating and cooling effect in buildings is significantly increasing especially in temperature fluctuating and varied climatic regions. It is for this one of the significant reasons, PCMs are getting pronounced interest by the research fraternity in the development of a thermally effective PCM-based construction material. In this paper, attempts were made to compile the data reported by the previous researchers on the influence of incorporating PCMs in the engineering properties of cementitious system such as slump, compressive strength, flexural strength, density, porosity, water absorption, shrinkage, durability, heat of hydration, specific heat capacity and thermal conductivity. This paper also discusses the most favorable content of PCM addition and effective methods of incorporating PCMs in the cementitious system.

Keywords Phase change materials · Thermal comforts · Latent heat · Heat of hydration · Durability

1 Introduction

The world's intensity of energy expenditure is increasing swiftly day by day. Buildings and infrastructures are one of the leading energy consumers by the effect of climatic variations particularly in temperature fluctuating regions [1, 2]. Concrete is

K. Snehal (✉) · B. B. Das
Department of Civil Engineering, National Institute of Technology Karnataka, Surathkal, Mangalore 575025, India
e-mail: snehalshine090@gmail.com

B. B. Das
e-mail: bibhutibhusan@gmail.com

B. B. Das et al. (eds.), *Recent Trends in Civil Engineering*, Lecture Notes in Civil Engineering 105, https://doi.org/10.1007/978-981-15-8293-6_4

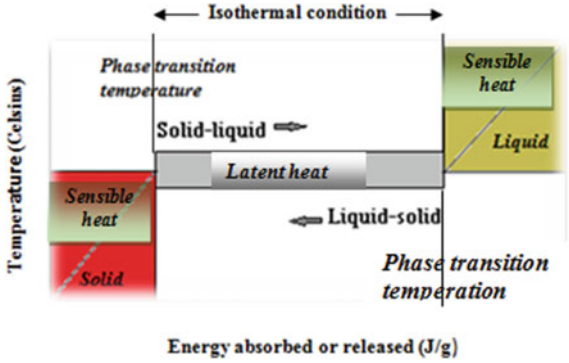

Fig. 1 Representation of idyllic response of PCMs on temperature variation solid to liquid and vice verse phase transition [8]

found to be the chief material of building and construction with high thermal mass storage capacity [2]. However, the capacity to store thermal energy in severe climatic conditions can be tailored by introducing the momentous material in concrete system such as a phase change material [2–4].

Phase change materials (PCMs) are sensible and latent heat storage materials with the potential to accumulate and discard energy in the form of heat, which produces transition in a phase, i.e., solid to liquid, liquid to gas or vice versa [5–7]. The ideal response of PCMs to temperature and heat variation is that it operates as a source of sensible heat storage material with the temperature goes up to the phase transition point and in this high enthalpy phase, conversion occurs either solid to liquid (captures heat and reduces the level of heat in the system) or liquid to solid stage (releases the captured heat and reduces the level of cooling in the system)and therefore acts as an absolute media for latent heat storage either by absorbing or by releasing heat [8, 9]. Figure 1 gives the idyllic response of PCMs on temperature variation solid to liquid and vice versa phase transition.

In this perspective, integrating PCMs in the construction and building elements is identified as a potential means to store thermal energy and found to be very effective way to overcome the energy load essential for heating and cooling in buildings and provide the thermal comfort especially in the recent era buildings and infrastructures [3, 10–12]. Concrete/cementitious composites due to its high volume and surface area as well by its widespread application in construction industry, it acts as idyllic applicants for PCM incorporation [2, 13].

Concrete being a porous material acts as an appropriate media for PCMs [14, 15]. Literature emphasizes that the potential utilization of PCMs in concrete composites is found to be beneficial in terms of refining thermal properties and heat transfer behavior by producing a high performing storage material [16–18]. The presence of PCMs in concrete reduces the effective thermal conductivity by improving its insulating property and enhances the heat storage capacity [19–22]. Researchers reported that PCMs have an ability to control the development of thermal cracks in early age of concrete and minimizes the harmful effects due to freeze and thaw cycles in cold climates [3, 8, 9, 23]. PCMs application in cementitious system reduced

the production of hydration peak temperature, as PCMs engrosses the heat energy developed during the hydration process [3, 24, 25]. Even though inclusion of PCMs in concrete composites performed positively with respect to thermal behavior by sustaining the poise in temperature, on the other hand, researchers noticed that it reduced the mechanical properties by affecting the structural integrity of the concrete probably due to its soft nature and fettering the products of hydration [9, 13, 26].

In the present paper, an attempt has been made to compile the various researcher's data on the impact of integrating PCMs in cementitious system on slump, compressive strength, flexural strength, density, porosity, water absorption, shrinkage, durability, heat of hydration, specific heat/latent heat capacity and thermal conductivity and also the most favorable content of PCM addition and effective methods of incorporating PCMs in the cementitious system.

2 Types of PCMs Exploited by Previous Researchers

The PCMs employed by various researches in investigation of its feasibility in cementitious system are listed in Table 1.

3 Effect of PCMs on Thermal Properties of Cementitious System

3.1 Thermal Conductivity

Data reported by several researchers [2, 7, 19, 21, 24, 29, 30] on the impact of PCM incorporation on thermal conductivity of cement mortar/concrete specimens are plotted and presented in Fig. 2. It can be noted from the figure that there is a decreasing trend of thermal conductivity values with the increase in PCM content in cementitious system.

The study conducted by Cao et al.'s [2] on PCM-based concrete revealed a reduced rate of thermal conductivity with an increase in concentration of microencapsulated PCM. It has been reported that this statistics is mainly owing to the replacement of sand (thermal conductivity range: 1.8–2.5 W/m °C) by microencapsulated PCM (thermal conductivity: 0.2 W/m °C) and also to amplified porosity of specimens. Researchers also noticed that samples with PCM in solid phase showed higher thermal conductivity than in liquid phase and stated that this is due to reason of higher thermal conductivity of PCM in solid phase than liquid phase.

The experimental investigation by Jayalath et al. [7] indicated that there is a drop in thermal conductivity with PCM content in both mortar and concrete specimens and reported that this would be ascribed to the replacement of sand, which contributes

Table 1 List of PCM details used by various researchers for their investigation

Authors [References]	Type of PCM	Form	Transition temperature (°C)	Heat of fusion (kJ/kg)
Bentz and Turpin [3]	PEG-400	Pure and LWA impregnated	−5.6 to 10.6	53.3
	PEG-600		3.6–28	112.6
	PEG-1000		23–44	107.6
	Octadecane		27.7–32.5	208.7
	Paraffin wax		31.6–60.6	150.4
Cao et al. [2]	Paraffin rubitherm RT27	Microencapsulated (shell: polymethyl and ethylvinylacetate)	29.41	199
Choi et al. [27]	$Na_2SO_4 \cdot 10H_2O$	Inorganic pure	32.4	251
	$Na_2HPO_4 \cdot 12H_2O$		35	281
	$Ba(OH)_2 \cdot 8H_2O$		78	266
	$Na_2S_2O_3 \cdot 5H_2O$		48	197
	$CaBr_2 \cdot 6H_2O$		38.2	115
	$Ca(NO_3)_2 \cdot 4H_2O$		47	201
	$Zn(NO_3)_2 \cdot 4H_2O$		36	147
Falzone et al. [26]	Paraffin based—MPCM 24D (Microteck)	Microencapsulated	24	154–164
Fernanded et al. [26]	Paraffin based-Micronal DS 5008X (BASF)	Microencapsulated	23 ± 3	110
Hunger et al. [19]	Paraffin based	Microencapsulated (shell:polymethyl methacrylate)	48.8–35.4	99.7
Jayalath et al. [7]	Paraffin based-Micronal DS 5040X (BASF)	Microencapsulated	23	100
Mankel et al. [11]	Paraffin based-Micronal DS 5008X (BASF)	Microencapsulated	26	110
Sakulichi and Bentz [24]	Paraffin wax-PCM6	LWA (pumice and clay) impregnated	6	162
	Vegetable oil-PTG		4	195
	PEG-400		−7.3 to 3.7	48.7
	PEG-600		0–20	107.9
Yang et al. [28]	PX28 (Rubitherm, Germany)	Microencapsulated	26–29	102

(continued)

Table 1 (continued)

Authors [References]	Type of PCM	Form	Transition temperature (°C)	Heat of fusion (kJ/kg)
Eddhahak et al. [25]	Paraffin based—Micronal DS 5001X (BASF)	Microencapsulated	23	110
Ricklef et al. [21]	Paraffin based—MPCM 24D (Microteck)	Microencapsulated	24	154–164
Zhang et al. [29]	n-Octadecane	Stabilized with graphite	27	207.2
Pisello et al. [30]	Paraffin based	Microencapsulated (17–20 microns)	18	–
		Macroencapsulated (3–5 mm)		
Qiao et al. [31]	n-Octadecane	Pure	28.3	101.1
Cellat et al. [15]	Butyl state	Pure-direct	17–22	134.16
Farnam et al. [32]	Paraffin oil	LWA and embedded tube	2.9	129.4
	Methyl laurate		1.9	160.4
Fenolerra et al. [33]	Paraffin wax	Microencapsulated (shell:polymethyl methacrylate)	23	55
Lucas et al. [34]	Paraffin based—Micronal DS 5008X	Microencapsulated	23	110
Snoeck et al. [23]	Paraffin based—Micronal® DS 5039 X (BASF)	Microencapsulated	23.3	88.1
	Paraffin based—Micronal® DS 5040 X (BASF)		23.3	88.1
	Paraffin based—Mikrathermic D18 (BASF)		18.1	177.2
	Paraffin based—Mikrathermic D24 (BASF)		23.3	134.3
	Paraffin based—Mikrathermic D2 (BASF)		28.3	161.3
Niall et al. [35]	Paraffin wax	Microencapsulated	18–22	–
	Butyl state	LWA impregnated		
Hawes et al. [36]	Potassium fluoride tetrahydrate (a salt hydrate)	Pure	18.5	231

(continued)

Table 1 (continued)

Authors [References]	Type of PCM	Form	Transition temperature (°C)	Heat of fusion (kJ/kg)
	Sodium sulphatedecahydrate (a salt hydrate		32.4	254
	Butyl stearate (an organic PCM)		19	140
	Paraffin (an organic PCM)		20–60	200
Wei et al. [37]	MPCM 6D (Microtech laboratory)	Microencapsulated	4.1	171.4
	MPCM24D (Microtech laboratory)		19.6	160.8
	MPCM43D (Microtech laboratory)		41.2	206.2
	Micronal DS5008X (BASF)		22.8	134.9

**PEG* poly ethelene glycol; *LWA* lightweight aggregate

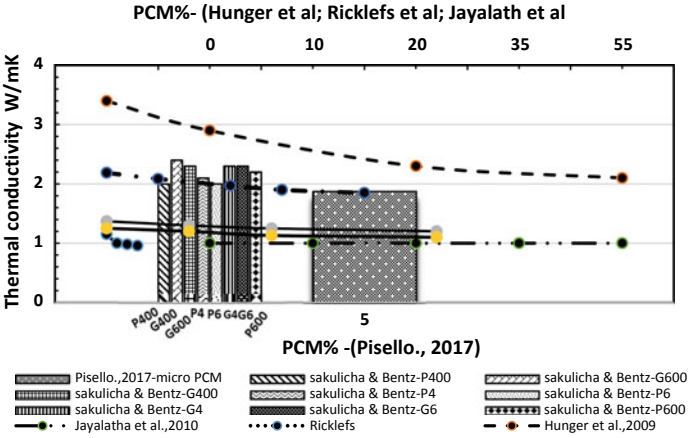

Fig. 2 Plot representing thermal conductivity variation for PCM modified cementitious system [2, 7, 19, 21, 24, 29, 30]

for higher thermal conductivity by PCM particles or may be the reason attributed to the entrapped air.

The experimentation by Hunger et al. [19] revealed that microencapsulated PCM modified concrete mass resulted in declined thermal conductivity and cited that the reason could be due to increased air content.

The study on thermal conductivity of cementitious composites incorporated with microencapsulated PCM by Ricklefs et al. [21] indicated that with the increase in microencapsulated PCM fraction, thermal conductivity declined in a linear trend. Authors described that this could be due to the lower thermal conductivity of both the PCM core and shell compared with that of cement paste. It has also been stated by authors that estimated value (by Felske model, 28) agreed well with the experimental data and deviation was less than 4.5%.

Sakulicha and Bentz [24] reported that control mixes showed higher thermal conductivity compared with that of LWA impregnated PCM specimens. Among all the PCM mixes (paraffin wax, vegetable oil-based PCM, PEG400 & PEG600-400 and 600 molecular mass polyethylene glycol) used in their investigation, pumice/vegetable oil-based PCM indicated the lowermost thermal conductivity, i.e., 2.02 ± 0.06) W/m K and 25.1% lesser than control mix. Authors have specified that test has been carried out at surface dry condition for all the specimens as in wet condition thermal properties are more obvious and thus to avoid the risk of damage.

The experimental study carried out by Pisello et al. [30] reported that microencapsulated PCM added concrete diminished the thermal conductivity and specified that this would be ascribed to the pore filling ability of micron-sized PCMs. It has been reported by the authors that it has increased the thermal wave propagation capacity and presented as a capable thermal energy storage material for cement-based material.

The experimentation conducted by Zhang et al. [29] on measuring the thermal conductivity of cement mortar board specimens assimilated with shape modified PCM composites (n-octadecane/expanded graphite). Authors have reported that experimental results clearly designated a linear drop in thermal conductivity of about 15.5% reduction for 2.5% composite PCM specimens. This has been justified to the fact that enhanced porosity resulted with the presence of PCM, which promoted the thermal insulation of mortar specimens.

The comparative study conducted by Pisello et al. [30] on integrating micro- and macroencapsulated PCM indicated much higher thermal conductivity for macroencapsulated PCM-based specimens with reduced aptitude of insulation and also thermal field transmission ability. Authors also confirmed that the addition of macroencapsulated PCM resulted into the discrepancy in the material morphology. Whereas, drastic reduction in thermal conductivity was observed in case of microencapsulated PCM-based specimens corresponding to its size effect (Fig. 3).

3.2 Thermal Energy Storage

Literature says that sensible heat, specific heat, latent heat, etc., are the methods to measure the thermal energy storage [4, 29, 38, 39], while PCMs are one such material with an ability to store thermal energy. Data reported by several researchers [2, 19, 24] on specific heat capacity of PCM modified mortar/concrete are presented in Fig. 4. It can be noticed from the figure that the quantity of PCM addition is directly responsible to the specific heat capacity.

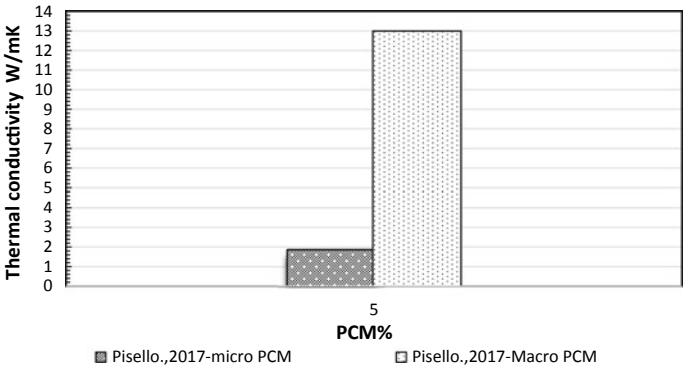

Fig. 3 Plot representing influence of incorporating micro and macroencapsulated PCM in cementitious system on thermal conductivity [30]

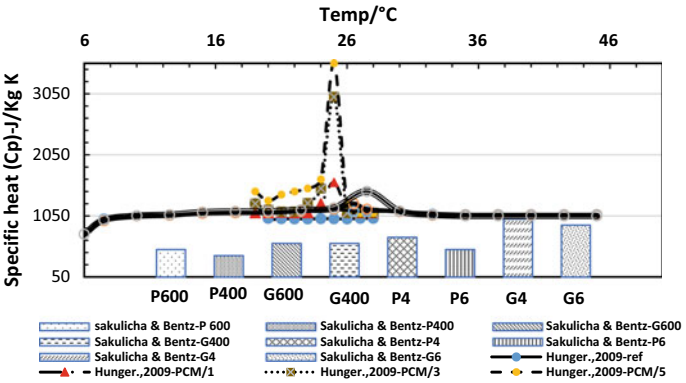

Fig. 4 Plot representing specific heat capacity of PCM modified cementitious system [2, 19, 24]

The research carried out by Cao et al. [2] revealed that specific heat capacity of microencapsulated PCM modified concrete was approximately alike in solid and liquid phase of PCMs, even though the specific heat capacity of microencapsulated PCM is greater in solid phase (3050 J/kg °C) than in its liquid phase (2740 J/kg °C).

Hunger et al. [19] measured the specific heat capacity by means of thermal analysis device with the temperature range of 19–28 °C, while the device temperature maintained at 32 °C. The data recorded from the device, i.e., sample temperature and heat flux, heat capacity were calculated with the following equation:

$$C_p = \frac{Aq}{m\left(\frac{\mathrm{d}T}{\mathrm{d}t}\right)} \text{ and } M_{\text{th}} = mC_p \tag{1}$$

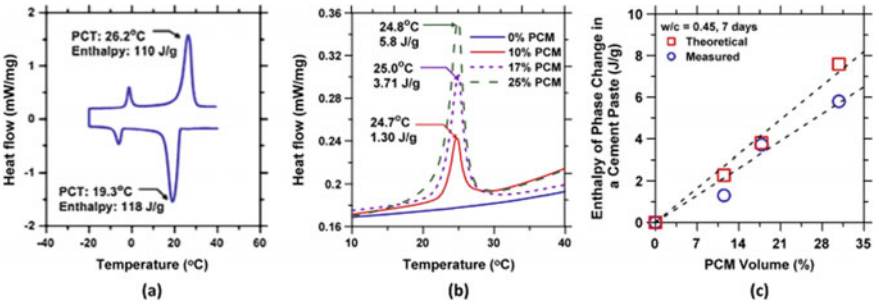

Fig. 5 DSC results for, **a** micro-encapsulated PCM; **b** percentage of PCM incorporated in cement paste; **c** theoretical and experimental enthalpy plot [8]

where, C_p: heat capacity, M_{th}: thermal mass, A: sample heat exchange area, q: heat flux per square meter, m: sample mass, T: sample temperature, and t: time. Experimental results designated the considerable increased rate of specific heat in proportional to the PCM quantity (temperature range of 24–26 °C) and it was about 3.5 times for 5% PCM content. It is also reported that even though the specific heat capacity increased significantly with the increment of PCM concentration, the maximum thermal mass was found to be observed roughly of 6800 J/K on 4–5% PCM content, which would possibly help to enhance the concrete thermal performance. The authors reported that about 12% energy saving can be made with 5% PCM content.

Sakulicha and Bentz [24] reported from their study that control mortar with the absence of PCM content exhibited the minor specific heat by mass while, the mix containing pumice LWA impregnated with vegetable oil PCM showed utmost specific heat by mass in contrast to all other PCM mixes (paraffin wax; vegetable oil-based PCM; PEG400 & PEG600—400 and 600 molecular mass polyethylene glycol).

The Differential Scanning Calorimetry (DSC) results as shown in Fig. 5a, b and c by Fernandes et al. [8] indicated that latent heat capacity of microencapsulated PCM is in the range of 110–118 J/g which is well within the manufacturers value, i.e., 110 J/g. The onset temperature (melting) of the PCM was 21.9 °C and completion temperature was 29 °C with an endothermic peak at 26.2 °C. Authors have observed that endothermic peak temperature (within 21.9–22.7 °C) of microencapsulated PCM integrated cement paste performed relatively same as that of pure PCM irrespective of the PCM dosage as presented in Fig. 5b. However, it has been reported by authors that latent heat capacity of cement paste significantly increased corresponding to the PCM concentration, still the total enthalpy was observed to be lower (approximately 24%) with respect to the theoretical value as presented in Fig. 5c. Authors have justified that it may be due to ruptured capsules or might be due to PCM degradation in caustic ambiance or could be the incorporated PCM was not efficient in thermal storage of the cementitious system.

The experimental study by Jayalath et al. [7] reported that with 20.2 °C as onset temperature for pure microencapsulated PCM (paraffin based) and with the endothermic peak at 24.6 °C, it has been reported that area under the peak (Fig. 6a)

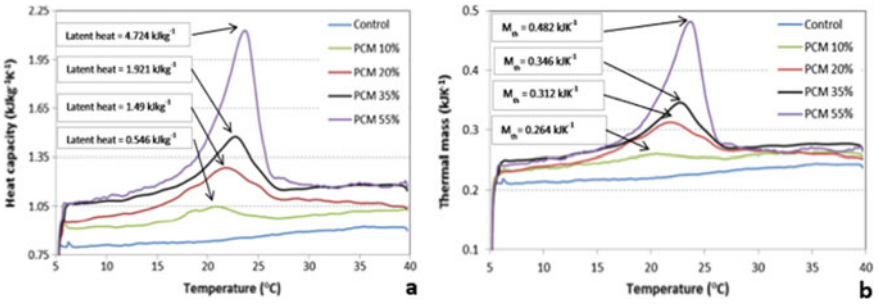

Fig. 6 **a** DSC results, **b** thermal mass of PCM modified mortar for curing age of 28 days [7]

measured an enthalpy of 84.69 $KJKg^{-1}$. Authors have noticed the significant rise in heat capacity with the increase in PCM content, i.e., 55% PCM mixture exhibited three times higher latent heat capacity than 20% PCM mixture as presented in Fig. 6a. On the other hand, authors have also observed that increase in thermal mass of a mixture contains 55% PCM was only 1.8 times to that of a mixture contains 20% PCM (Fig. 6b). The reason could be attributed to the drop in density of the specimens with the replacement of sand by PCM content.

The experimental results by Mankel et al. [11] with respect to temperature evolution v/s time (Fig. 7) of microencapsulated PCM (micronal DS 5008X) incorporated cement composite, measured with the thermocouples revealed that there is a designated fall in temperature distribution as compared with the reference mix. Researchers noticed that in case of higher content of PCM, the dragging influence of PCMs phase change (solid to liquid) tends to be more prominent (Fig. 7a–c). Authors have conveyed in line to the attained experimental results that PCM has a potentiality to manage the energy requirements in building and infrastructures with its ability to store thermal energy. Authors also reported that experimental data simulated with the proposed flow model showed the related temperature evolution promising to the measured values given by Ge et al. [40] (Fig. 8).

The investigation by Bentz and Turpin [3] utilized different PCMs (poly ethylene glycol—PEG—400, 600, 1000; octadecane and paraffin wax) to analyze the thermal property via DSC curves (Fig. 9). Authors have noticed the high-pitched transition (melting and solidification) rate in case of octadecane PCM compared with the other PCMs while for PEG and paraffin wax PCMs transition peaks were observed to be at 30–40 and 50–60 °C, respectively. Authors also recognized that molecular mass of PEG showed great influence on the phase transition temperature (i.e., higher molecular mass is equal to higher transition temperature). The DSC curves (Fig. 9b, c) of PCMs (PEG-1000 and paraffin wax) in lightweight aggregate (LWA) showed a slightly higher shift in peak phase transition temperature in case of LWA/paraffin wax.

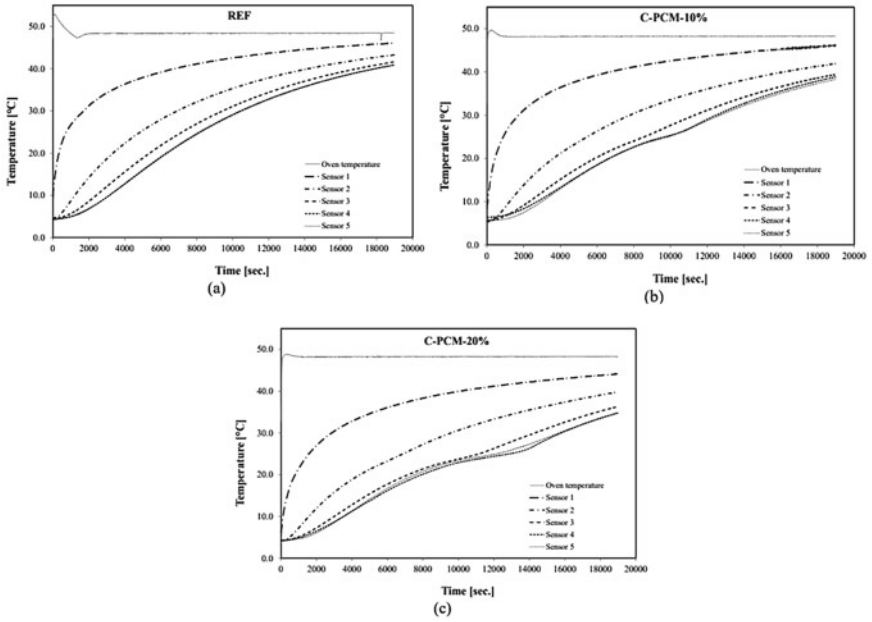

Fig. 7 Time versus temperature evolution data of **a** control mix, **b** mix admixed with 10% PCM and **c** mix admixed with 20% PCM [11]

4 Effect of PCMs on Hydration Properties of Cementitious System

Data reported by several researchers [3, 7, 19, 24, 25] on hydration study were compiled and plotted as shown in Fig. 10a–d.

The experiments carried out by Sakulicha and Bentz [24] examined the influence of incorporating lightweight aggregates—LWA (expanded clay and a naturally porous Greek pumice) impregnated with four different types of PCMs (paraffin wax based, vegetable oil-based, PEG 400, and PEG 600) on cement hydration of mortar samples. Authors have observed from the study that vegetable oil-based PCM impregnated in pumice showed a little higher release in heat compared with that of other PCMs. However, the strength loss was observed to be higher than control in vegetable oil-based PCM and paraffin-based mixes. While, in case of LWA/PEG incorporated samples (P600, P400, G600, and G400; P-pumice and G-clay), almost 40% suppression of hydration peaks were observed irrespective of LWA type and the molecular weight of PEG (Fig. 10a).

Eddhahak et al. [25] observed that mortar specimens with PCM (paraffin based) inclusion set out lower heat of hydration and delayed the hydration kinetics compared with that of control mortar, as well as it is reported that increased dosage of PCM in mix reduced the total rate of hydration heat. Authors have observed that PCMs get

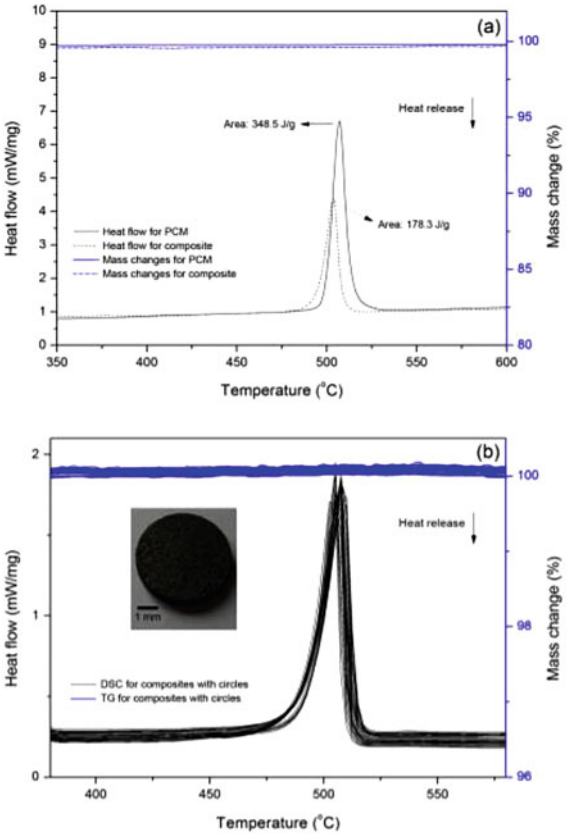

Fig. 8 TG-DSC curve representation for **a** PCM and composites, **b** composites over 28 days thermal cycles [40]

damaged during the mixing process and this resulted to minor deviation in hydration rate of about 4% after 5 days and authors stated that this could be ascribed to the seepage of Paraffin wax distressing the hydration products (Fig. 10a).

The hydration study carried out by Jayalath et al. [7] by means of isothermal calorimetry (Fig. 10 b) showed the delay in heat of hydration peak with the increase in replacement level of sand by microencapsulated PCM particles in comparison to control mortar. Authors reported that 20% and 50% sand replacement with PCM delayed the hydration peak by 1 h and 2.5 h, respectively, with respect to control mix. It has been reported that delay in appearance of maximum hydration peak could be owed to the high latent heat capacity of PCM, even though the smaller particle size of microencapsulated PCM developed the filling effect and positively provoked the hydration rate.

Experimentation conducted by Bentz and Turpin [3] showed that PEG impregnated LWA (impregnated with 6 g) in cement mortar hindered the cement hydration process. Hence, authors have suggested that for its effective employment in fresh concrete, encapsulation through an inert material is essential. The semiadiabatic

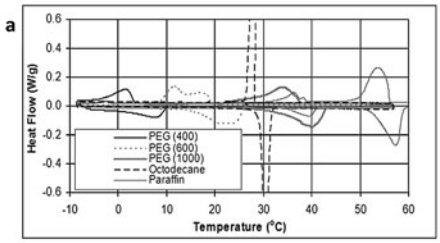

. DSC analysis of phase change materials.

Material	$\Delta H_{cooling}$ (J/g) (solidification)	Temperature range (°C)	$\Delta H_{heating}$ (J/g) (melting)	Temperature range (°C)
PEG: 400 MM	48.7	3.7 to -7.3	53.3	-5.6 to 10.7
PEG: 600 MM	107.9	20 to 0	112.6	3.6 to 28
PEG: 1000 MM	102.2	38.2 to 22.3	107.6	23 to 44
Octodecane	208.7	28.3 to 24.8	208.7	27.7 to 32.5
Paraffin Wax	153.1	56.2 to 31.2	150.4	31.6 to 60.6

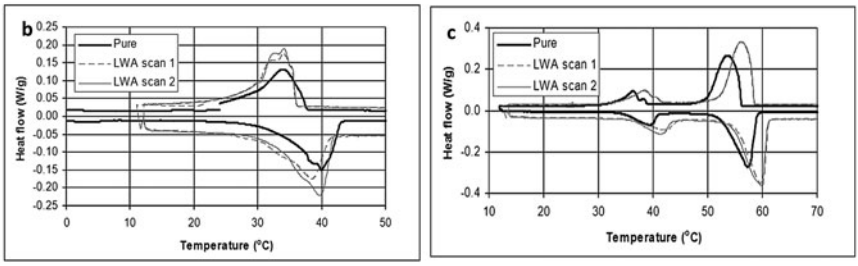

Fig. 9 **a** Heating and cooling DSC curves and data for different phase change materials. Octodecane: the positive peak (1.29 W/g) and negative peak (−1.17 W/g, not displayed on this scale); DSC curve for pure and lightweight aggregate impregnated PCMS, **b** PEG-1000, **c** paraffin wax [3]

temperature v/s time curves (Fig. 10c) for different mixes (control mortar, PEG impregnated LWA mortar and PCM mortar with 27 g of PEG) revealed that PCM modified mixes (both PEG impregnated LWA mortar and PCM mortar with 27 g of PEG) postponed the peak temperature by about 1 h, however, the peak hydration temperature of PCM mortar with 27 g of PEG reduced approximately by 8 °C.

The study by Hunger et al. [19] reported that there is delayed hydration peak (Fig. 10d) and reduced peak height with the increase in PCM dosage. Researchers noticed a small bend at 25 °C (start for the endothermic cycle) in DSC curve for 3 and 5% PCM mixes. Authors have also reported that unpredictable higher rise in temperature was observed in case of 3% PCM mix than 1% mix and stated that this could be attributed to larger rate of damaged PCMs in 3% PCM mix.

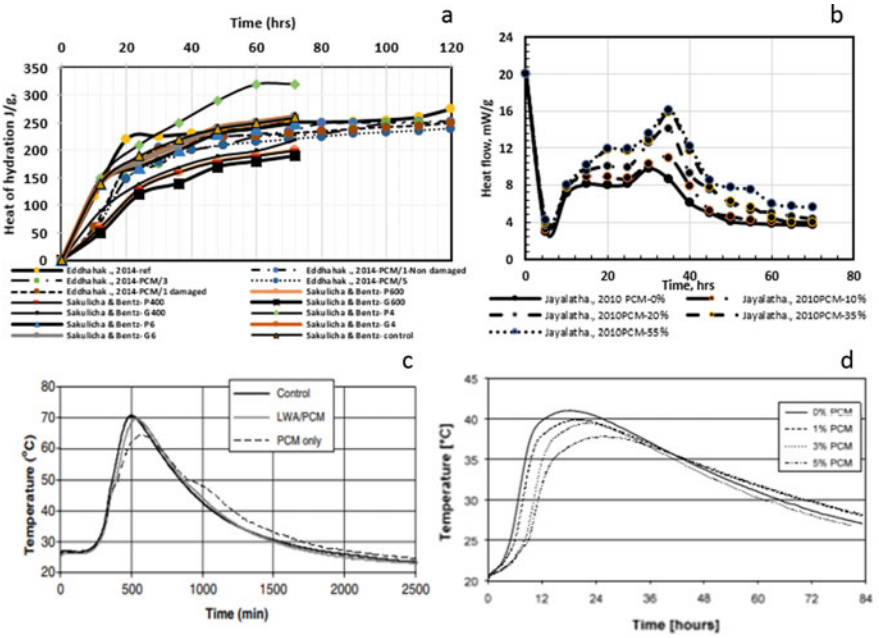

Fig. 10 **a**, **b**, **c** and **d**: Plot representing variation in heat of hydration for PCM modified cementitious system **a** [24, 25], **b** [7], **c** [3] and **d** [19]

5 Effect of PCMs on Fresh Properties of Cementitious System

Data reported by researchers [23, 28, 33, 34] on fresh (subjected to only flow values) properties with the incorporation of PCM are depicted in Fig. 11.

The experimental investigation carried out by Snoeck and Belie [23] on fresh property of cement mortar incorporated with different types of microencapsulated PCMs (water dispersed form: Micronal DS 5039X, Powder form: Micronal DS 5040X, Micrathermeric D18, Micrathermeric D18, Micrathermeric D 24, Micrathermeric D 28) revealed that PCM dosage is inversely proportional to flow diameter. Authors also reported that reduced flow with 5% PCM addition in mortar specimens can be considered as the allowable limit. Researchers noticed that PCM in dispersed form showed lower mortar workability, this was attributed to the reduction of water content in mix so as to balance the water contained within the dispersed solution and also owing to its clogging effect. It has been suggested by the researchers that dry PCM are more advisable considering the better dispersion of PCMs in practical point of view.

Fenollera et al. [33] examined the impact of microencapsulated PCMs (polymethyl methacrylate spheres encompassing high purity paraffin waxes) inclusion on flow property in self compacting concrete (SCC) and reported that there is a drop in flow

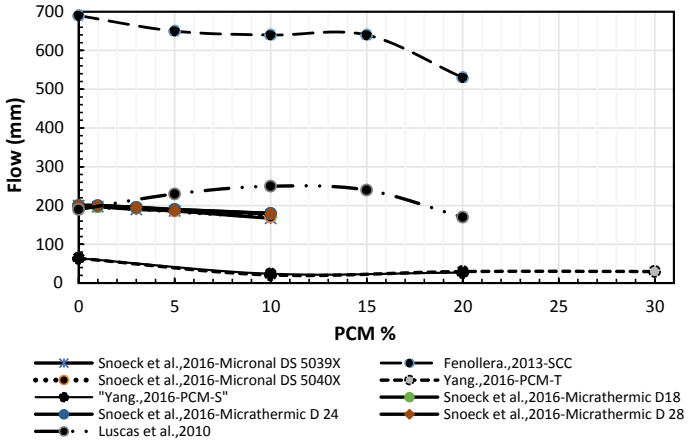

Fig. 11 Flow values in various types of cementitious system contained with phase change materials [23, 28, 33, 34]

diameter with the increase in PCM content. It has also been reported that SCC mix with 20% PCM did not accomplish the permissible range of flow leading to higher viscosity with a reduction in the level of deformability.

Yang et al. [28] carried out an investigation on PCM (PX28) modified concrete by implementing two mix design methods, i.e., by total replacement method and sand replacement method. It has been noted from their experimental data that increased PCM content reduced the flowability of concrete and reported that PCM replaced with respect to sand content lowered the flow more compared with that of total replacement.

The experimental study by Luscas et al. [34] on lime mortar integrated with PCMs revealed that inclusion of greater percentage (20%) of PCMs lowered the workability. However, lower amount of PCM, i.e., 5 and 10% showed good flow value. Therefore, authors have reported that quantity of PCM usage in mortar plays a key role in its lubricating action.

As a whole, it can be observed that with an increase in dosage of PCMs in cementitious system reduced the ability to flow. This may be attributed to its increased viscosity and increased level of water demand [23, 28, 34]. Utilization of appropriate dosage of super plastisizer up-to certain content of PCM may balance the flow/slump [33].

6 Effect of PCMs on Density, Porosity, and Water Absorption of Cementitious System

6.1 Density

Data presented by authors [19, 28–30, 33] on the density variation of PCM included cement mortar/concrete are represented in Fig. 12. It can be noticed from the graph that density reduced step by step with the increase in the inclusion of PCM content.

The study by Hunger et al. [19] emphasized that PCMs (Micronal DS 5008 X) greatly affected the density of concrete by decreasing the unit weight.

The study by Pisello et al. [30] reported that PCMs (organic paraffin based) presence in the concrete lowered the density value in comparison to that of no PCM concrete. Authors also stated that PCM added concrete may possibly act as lightweight concrete and with a thermal energy point of view may aid as thermally effective concrete.

The study on shape stabilized n-octadecane/expanded graphite composite PCM in cement mortar by Zhang et al. [29] revealed that increase in composite PCM content in cement mortar samples linearly reduced its apparent density. However, it is also identified by the researchers that cement mortar with 2.5% PCM composites reduced its density by only 9.5% with respect to the control mortar cube.

The experiments conducted by Fenollera et al. [33] on PCM added concrete samples showed the consistent value of density for concrete mixes with 0–20% PCM and drastically lowered density was observed for concrete mix with 25% PCM. Authors have reported that with reference to the preliminary stipulation of 2400 kg/m^3 as the range of concrete density, PCM admixed concrete (up to 10%)

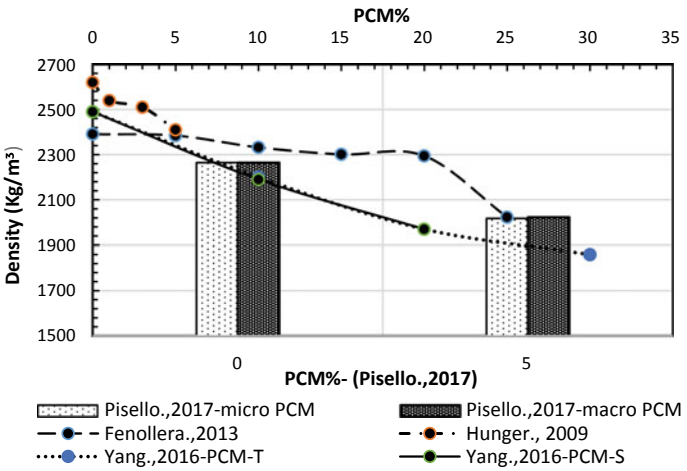

Fig. 12 Representation of density variation in cementitious system with different percentage of phase change materials [19, 28–30, 33]

can be considered for structural panels. However, the concrete with higher dosages of PCM content found to be a density of lower than 2300 kg/m^3.

It has been stated by Yang et al. [28] that PCM PX28 has much lighter weight compared with other ingredients of concrete with specific weight of about 0.694 g/m^3, which acted as key in reducing the total unit weight/density of concrete with increased dosage of PCM.

6.2 Porosity

Data reported by the researchers [19, 34] on the inclusion of PCM in cementitious system state the PCM admixed mix enhanced the percentage of porosity in the system and the compiled one is plotted in Fig. 13.

The experiments by Hunger et al. [19] on porosity of self-compacting concrete (SCC) with PCM resulted higher rate of porosity with increased dosage of PCM compared with the control SCC. Authors have stated that this may be attributed to the change in structural integrity and packing ability owing to the low specific gravity of PCM with respect to other ingredients of concrete.

The investigation by Luscas et al. [34] on mortars integrated with PCMs (Micronal DS5008, BASF) showed higher range of porosity with 10% PCM compared with the reference mortar. It is reported by researchers that mean pore size has been reduced in case of 10% PCM mortar with respect to the reference mortar and this attributed to the contribution of PCM particles in filling up the larger pores. It has also stated by the researchers that 20% PCM content in mortar tends to reduce the total porosity as compared with the reference mortar.

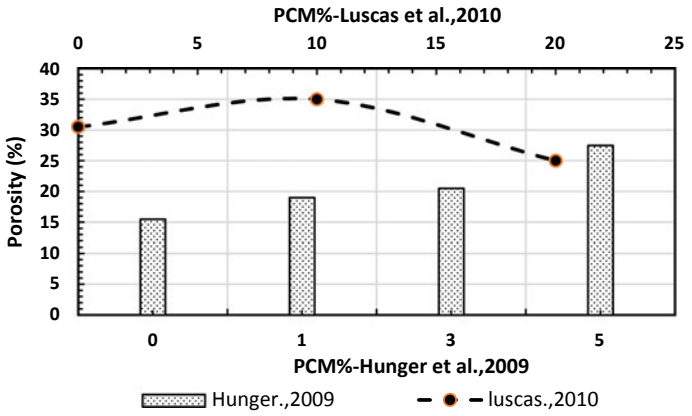

Fig. 13 Representation of porosity in cementitious system with different percentages of phase change materials [19, 34]

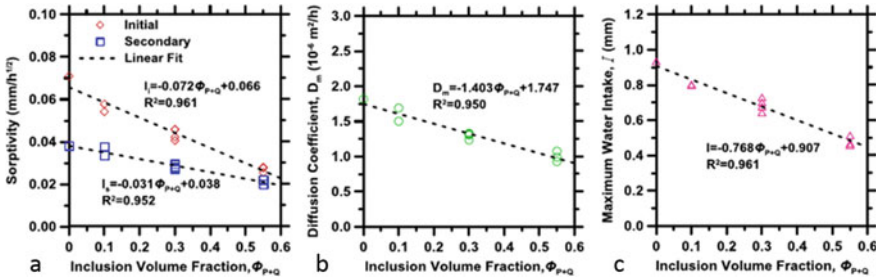

Fig. 14 Plot representing the moisture flow behavior in PCM and quartz admixed cement composites **a** sorptivity, **b** diffusion and **c** cumulative water absorption [41]

6.3 Water Absorption

The experimentation conducted by Wei et al. [41] and the response of PCM and quartz integrated mortars on water absorption by the use of modified ASTM C1585 procedure is plotted in Fig. 14.

Researchers have measured initial (S1) and secondary (S1) sorptivity values, which represent initial 6 h of duration and between 1 and 8 days, respectively (Fig. 14a). From their experimental results, it can be noticed that both the sorptivity (S1 and S2) values decreased linearly with the increase in total volume proportions (PCM + quartz) irrespective of the inclusion nature, thereby weakening the rate of water dissemination. The measure by the researchers on diffusion rate also showed the similar trend like sorptivity and this could be imputed to the nonporous and less permeable nature of PCM/quartz particles compared with cement paste (Fig. 14b). However, the combined effect of sorptivity and diffusivity showed the diminished water absorption (Fig. 14c).

7 Effect of PCMs on Mechanical Properties of Cementitious System

7.1 Compressive Strength

Data reported by several researchers [7, 9, 15, 19, 26, 29–31, 33, 42] on compressive strength of cement mortar/concrete integrated with PCMs were compiled and the plot representing compressive strength versus percentage of PCM mixed with the cementitious system is presented in Fig. 15. It can be understood from the plot that incorporation of PCMs in cement composites drastically reduced the compressive strength. This may be attributed to increase in porosity and decrease in density of PCM modified cement mortar/concrete.

The investigation by Jayalath et al. [7] on mortar and concrete replaced with microencapsulated PCM indicated a reduced trend of compressive strength with the

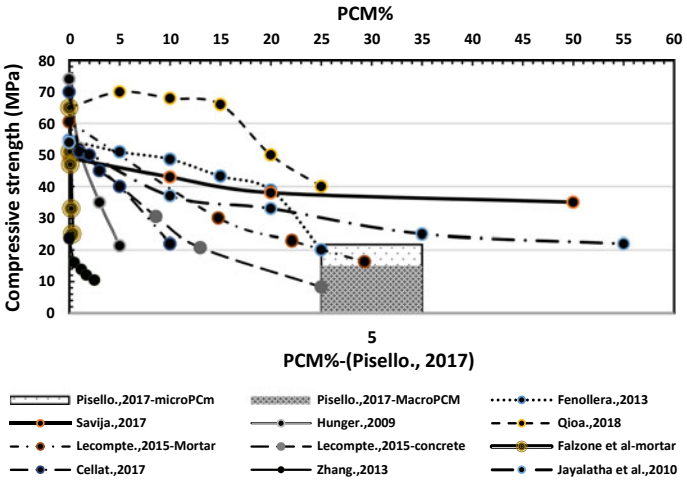

Fig. 15 Variation of compressive strength in cementitious system with different percentage of phase change materials [7, 9, 15, 19, 26, 29–31, 33, 42]

increase in percentage of PCM. Authors also reported that two contrary factors are paying on the way to variation in compressive strength. First is reduction in strength which is due to the replacement of sand (hard particles) by microencapsulated PCMs (soft particles) and second is the smaller particle size of microencapsulated PCM which would assist in improving the compressive strength by the consequence of enhancing the nucleation sites for hydration. Authors have reported that strength loss with 0%–5% amount of PCM replacement owing to the less nucleation sites which is a distant from the ideal level. However, 10%–20% PCM dosage mixes lowered the strength than control mix but were proved to have higher strength comparatively to 5% PCM dosage mixes, the reason could be attributed to formation of sufficient nucleation site. While, higher PCM dosage of 35–55% reported to have dominant "first factor" as reason for drop in strength.

The study by Savija et al. [9] reported a decrement in compressive strength with the incorporation of PCMs and stated that optimum usage of PCM is very much necessary for structural concrete usage.

The experimental investigation by Cellat et al. [15] made use of butyl stearate PCMs in concrete and observed the reduced trend of compressive strength. Authors reported that 5% PCM may be recommended as ideal dosage for building applications.

Hunger et al. [19] noticed the significant drop in the compressive strength of concrete with the increase in PCM content. Authors reported that each increase (1–5%) in percentage of PCM content reduced the concrete strength by 13%.

The study carried out by Falzone et al. [26] also experienced the significant drop in strength and as expected by the researchers in order to compensate this critical effect of PCM mortar quartz particles were supplemented in their experimentation.

The experimental study by Pisello et al. [30] on 5% micro- and macroincorporated paraffin-based PCM showed lower compressive strength compared with the reference concrete. Authors have observed that microencapsulated PCM concrete are more reliable than macroencapsulated PCM concrete with the perspective of compressive strength. Authors reported that this could be due to the breakage and fracture of macro-PCMs, which were observed on fractured surface of tested specimens. However, authors have reported that PCM content lesser than 5% may be attuned for the structural use.

The experimentation conducted by Zhang et al. [29] reported that increased mass percentage of PCM reduced the compressive strength of cement mortar. However, researchers have noticed a sudden drop in strength from 23.7 to 16.1 MPa with 0.5% PCM content and with further increase in PCM content gradual reduction in strength was observed.

The investigation carried out by Fenollera et al. [33] reported that 5% PCM-based concrete showed 7% drop incompressive strength compared with the control mix sample and further increase in PCM content reduced the strength drastically in a linear pattern. Authors have conveyed by their observation that drop in strength may be attributed to increased porosity and aggregation/clustering of PCM particles as well as segregation of PCMs particles on top of the specimens during curing.

The experimental study by Qiao et al. [31] reports that n-octadecane microencapsulated PCM presence in cement mortar showed enhancement in strength for 5% PCM content than control mortar. While, PCM mass fraction of 10 and 15% observed to have marginal increase in compressive strength but further more increase in PCM mass fraction of 20 and 25% showed much lower compressive strength compared to the original mortar.

The study by Lecompte et al. [42] noticed that mechanical strength of microencapsulated PCM modified mortar/concrete reduced significantly. Authors have reported that the drop in strength is owing to the two chief factors that is (a) higher water demand (10% the mass) and (b) rupture of capsules during compression, leading to the formation of voids. Researchers stated that the experimental results are quite adjacent to the values obtained by the use of model [43] proposed by the authors. Authors conveyed that this could be due to the aforementioned factor, i.e., PCM would behave like voids which is an important aspect with respect to the mechanical strength.

7.2 Flexural Strength

The data [31, 34] reported by researchers on flexural strength of cementitious system integrated with PCM are plotted and presented in Fig. 16. It can be noted from the figure that incorporation of PCMs in cementitious system reduced the flexural strength similar to that of compressive strength of PCM modified cementitious system.

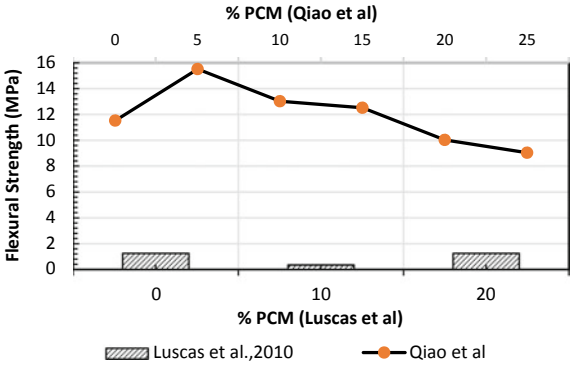

Fig. 16 Variation of flexural strength in cementitious system with percentage of PCM [31, 34]

The experimental study by Luscas et al. [34] reported that 10% PCM in lime mortar lowered the flexural strength due to the reason of enhanced porosity than the control mix. It has also been stated by the authors that 20% PCM content improved the flexural strength along with its compressive strength as a reflex of reduction in the porosity and pore size.

The investigation by Qiao et al. [31] examined that 5% mass fraction of PCM showed highest flexural strength. Authors reported that further increase in mass fraction of PCM from 5 to 15% reduced the flexural strength gradually but it was observed to have higher flexural strength compared with that of control mortar. Further, higher PCM dosage than 20–25% has shown drastic reduction in flexural strength of cement mortar lower than control mortar.

7.3 Modulus of Elasticity

The data reported by the researchers [28, 32] on the influence of PCM incorporation in cement mortar/concrete on modulus of elasticity are compiled and plotted in Fig. 17.

The study conducted by Yang et al. [28] revealed that elastic modulus of concrete reduced with the increase in dosage of PCM with respect to the total replacement method of PCMs. Authors have reported that this is owing to lower strength and stiffness of the soft PCMs. Authors also reported that higher elastic modulus was observed in 23 C curing condition in comparison to that of 40 C curing condition for the specimens prepared by both total replacement method and sand replacement method. Authors have understood that no much significant reduction in elastic moduli was observed in case of sand replacement method than in case of total replacement in arrears to the constant quantity of cement and coarse aggregates.

The experimental investigation by Farnam et al. [32] on mortar specimens integrated with PCMs (paraffin and methyl laurate) embedded in lightweight aggregate (LWA) for pavement applications revealed that LWA containing PCMs in mortar reduced the dynamic elastic modulus. Researchers also reported that cracks were

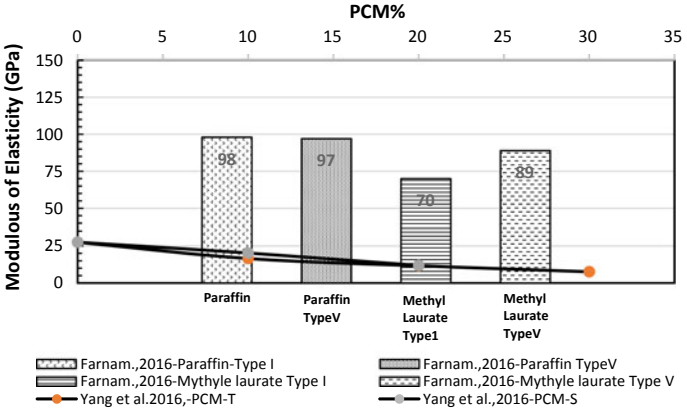

Fig. 17 Variation of modulus of elasticity in cementitious system with percentage of PCM [28, 32]

observed in specimens due to the association of PCMs in cement chemical reaction. Authors have identified that LWA containing paraffin oil PCMs mortar sustained the dynamic elastic modulus for about 95% of control mortar in contrast to that of methyl laurate PCMs.

8 Effect of PCMs on Shrinkage Properties of Cementitious System

The data reported by researchers on shrinkage are plotted and presented in Fig. 18. The experimental study by Yang et al. [28] in regard to shrinkage effect on concrete incorporated with PCM in two ambient curing temperature 23 and 40 °C indicated that higher amount of PCM inclusion enhanced the rate of drying shrinkage irrespective of temperature condition. Authors have reported that this could be attributed to the

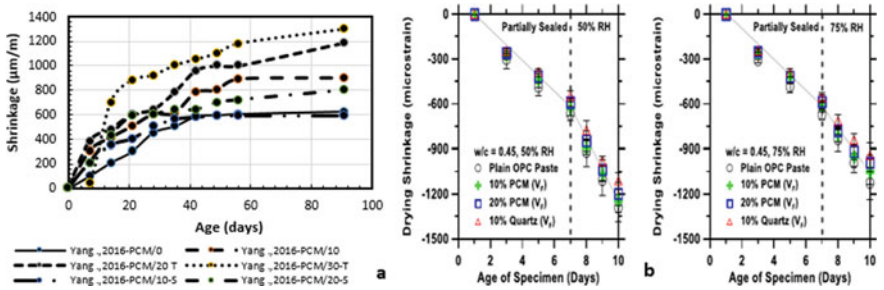

Fig. 18 Plot representing the shrinkage effect in case PCM based cementitious system **a** Yang et al. [28], **b** Wei et al. [37]

low stiffness and strength of PCM material replaced with respect to other ingredients of concrete which hampers the resistance toward volume change thereby instigating drying shrinkage. Other factors affecting the shrinkage noticed by the researchers are with respect to replacement technique. Authors reported that the total replacement method reduced the cement content with an increase in the water cement ratio that deliberately increased the shrinkage rate in concrete. While, in case of sand replacement method, drying shrinkage rate was observed to be lesser compared with the total replacement method as cement and water cement ratio was kept constant (Fig. 18a).

The study by Wei et al. [37] investigated the response of PCM (MPCM24D) inclusion in cementitious matrix on drying shrinkage (as per ASTM C157) for two drying regimes (50% RH and 75%RH) where the specimens were partially sealed up to 7 days. Researcher noticed that as per the anticipation, the specimens in both the drying regime condition showed similar results on drying shrinkage and mass loss over the time of 7 days irrespective of relative humidity (RH). However, it was observed by the researchers that shrinkage and mass loss was found to be greater in the drying regime condition of 50% RH than 75% RH (Fig. 18b). It has been reported by the authors that quartz included paste mixture performed better compared with that of PCM or plain mixtures and this would be due to the stiff property of quartz material in contrary to the soft and complaint nature of PCM that made it incompetent to counterattack the shrinkage effect.

9 Microstructural Studies on Cementitious System with PCMs

The microstructure observation made by previous researchers on PCM integrated cementitious system is presented in this section.

The micrographical characterization carried out by Paksoy et al. [44] on microencapsulated PCM modified concrete by means of scanning electron microscope with different scale of magnification reported that the incorporation of microencapsulated PCM did not disturb the concrete microstructure. The observation found to be prominent CSH and ettringite crystals in scanning electron micrographs (presented in Fig. 19). Authors have also noticed the stable geometry of microencapsulated PCMs (with PCM size ranging from 60 to 160 μm) after subjected to mixing and loading.

Jayalath et al.'s [7] observation made on micrographs of microencapsulated PCM added mortars revealed the good PCM-binder integrity with no obvious damages around the interfacial transition zones of PCMs as well as fine aggregates and also noticed the well dispersion of PCMs in matrix (Fig. 20a) in the cementitious system. Authors stated that spherical geometry of PCMs in the system confirmed no occurrence of any damages in the outer surface of PCM microcapsule during mixing stage and ensured good binder-PCM integrity (Fig. 20a). However, in the course of

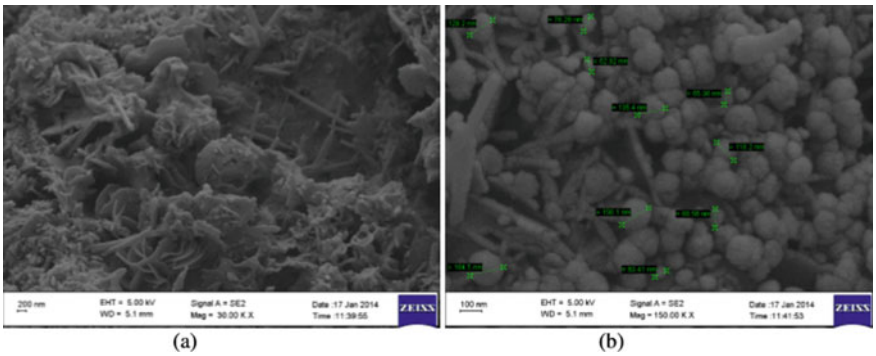

Fig. 19 SEM images of microencapsulated PCM modified concrete specimen **a** 30,000 magnification, **b** 150,000 magnification [44]

postcuring damages of PCMs were observed by the researchers which was supported by the back-scattered image (Fig. 20b) with the broken PCM in the spherical voids and fractured plane zone. Authors reported that this would be attributed to the propagation of fracture plane via spherical voids during loading and due to the soft material of capsules which acted as crack initiating point during the mortar loading. Author had undergone EDS analysis to understand the location area of damaged PCM in the specimen (Fig. 20b) and indicated that damaged PCMs are comprised of shattered particles of polymer shell, paraffin core (center: high carbon—C concentration) and microstructure of mortar (adjacent: high calcium-Ca and silica-Si concentration). EDS report also showed the C/O ratio of paraffin core is high compared with mortar microstructure while contradictory result found in case Ca/O ratio.

The microstructural characterization carried out by Ge et al. [40] on PCM composites by means of SEM analysis depicted that the consumed PCM ($LiNaCO_3$) consists of smooth surface with spherical geometry (Fig. 21a). Authors have reported in aid to the SEM and optical image that when carbon nanotubes (CNTs) are added into the composites it was noticed to be dispersed on the top of the PCM units (Fig. 21b). Researchers also observed an even dispersion of MgO crystals on the sample surface when MgO crystals (0.15–0.6 μm) are added to the composite in the ratio of 1PCM/1MgO/0.0015CNT (Fig. 21c, d). Authors also identified that ample dispersion of CNTs is possible in PCM ($LiNaCO_3$) with the existence of MgO crystals. Authors also justified that this was owing to its good interfacial energies among other composite components (Fig. 21d).

The microstructural analysis (SEM) conducted by Hunger et al. [19] on concrete modified with microencapsulated PCM particles indicated a porous microstructure and probably this could be due to presence of PCM capsules in sphere-shaped voids. Authors have also mentioned that the melting temperature of paraffin varies from soft (melts early) to hard (melts late) type of paraffin. While the mixture containing soft PCM melts fast and seeped paraffin (flaky configuration) enters the pores/cavities of the cementitious system and gets solidified which are not compatible in nature with

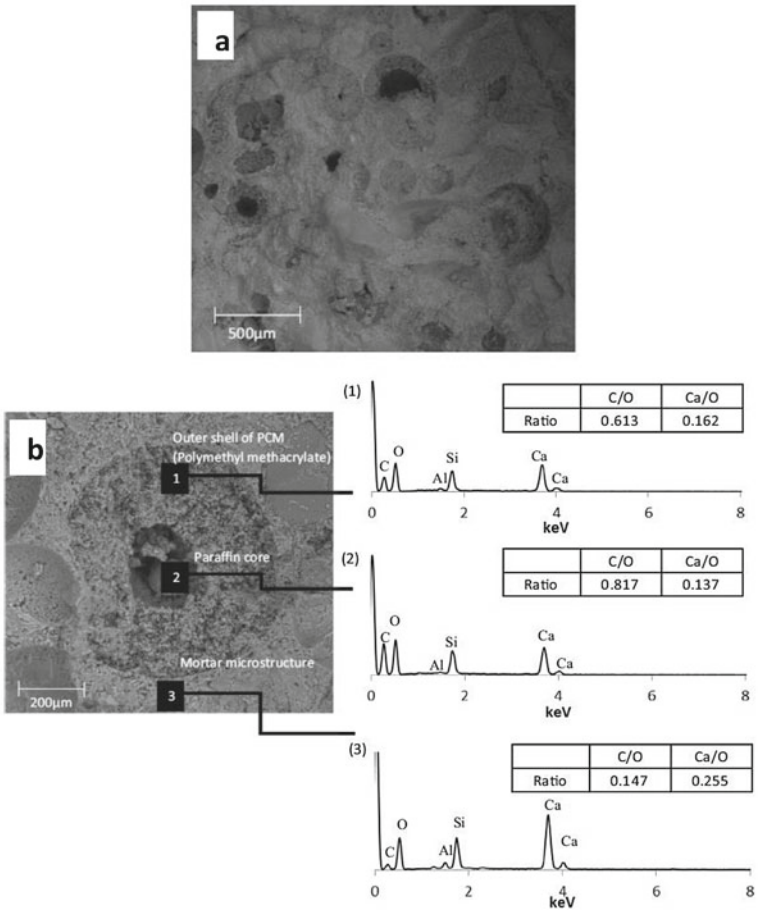

Fig. 20 SEM images of microencapsulated PCM modified concrete specimen **a** fractured mortar surface and **b** damaged PCM with EDS analysis [7]

other constituents of concrete and this evidence can be made from the micrograph (Fig. 22a). Authors also reported that bulk amount of damaged and broken PCM capsules (size: ~6 μm) was observed in adjacent structure (Fig. 22b).

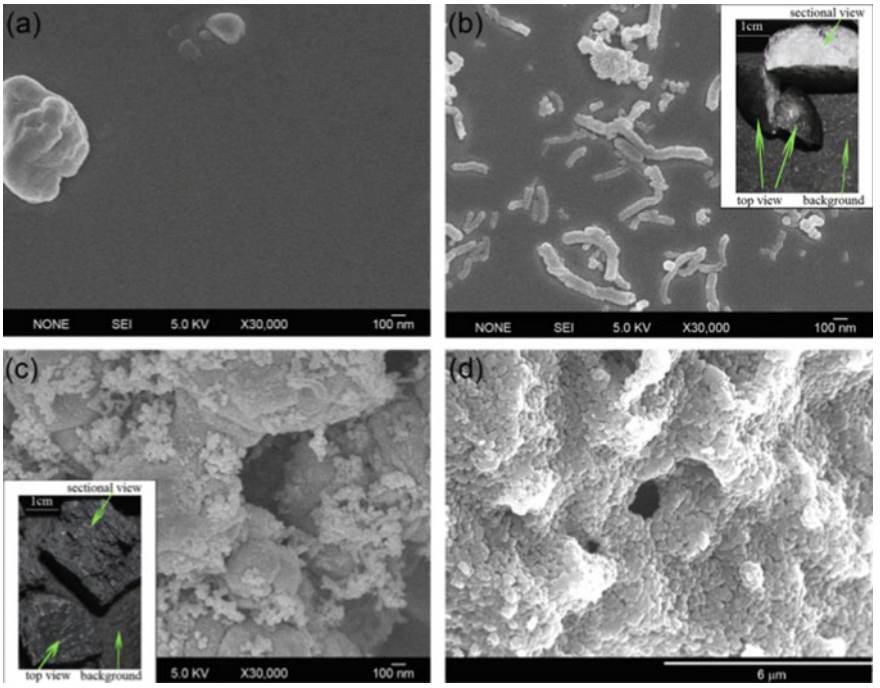

Fig. 21 SEM images of **a** PCM- $LiNaCO_3$, **b** 1PCM/0.01CNT composites, **c** 1PCM/1MgO/0.015CNT composites, **d** 1PCM/1MgO composites, inset images in **b** and **c** are optical images: PCM-white and CNT-black [40]

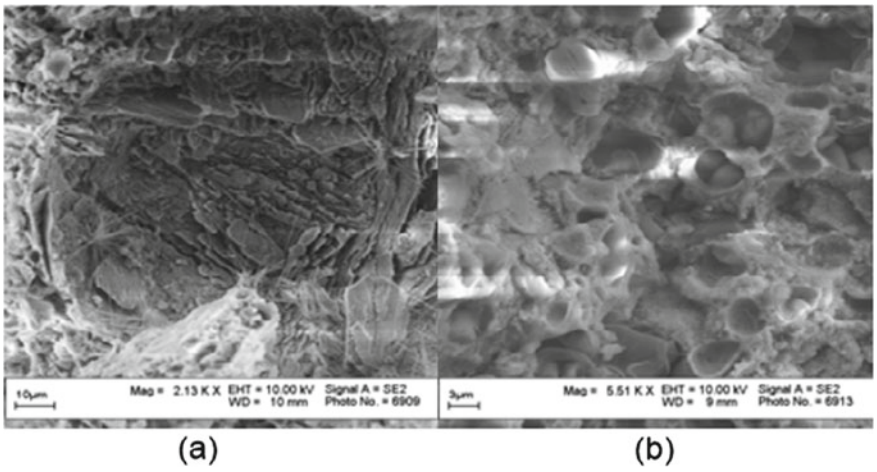

Fig. 22 SEM images of **a** solidified wax-covered open voids, **b** matrix with deformed/broken PCM capsules [19]

10 Categories of Phase Change Materials (PCMs) and Forms of PCM Incorporation into the Cementitious System

The PCMs are classified into three main classes; Table 2 presents the detail of PCM categorization. Organic PCMs provide high-quality feasibility with the conventional construction material, i.e., concrete because of its chemically stable and safe nature compared to any other types of PCMs [8, 9]. Inorganic PCMs may perhaps utilized in some of the construction materials as it processes good thermal conductivity and high volume heat storage in addition it is economical, easily available, and due to its nonflammability [36]. But those are corrosive to metal and endures super cooling effect as well as phase degradation this limits its usage in most of the construction usage. While, eutectic PCMs (combination of organic, inorganic PCMs) are recently explored by researches and are preferred in precise applications with appropriate mixture of organic and inorganic PCMs [45].

Table 2 Classification of PCMs [2, 8, 9, 45]

PCMs	Types	Examples	Remarks
Organic PCMs	1. Paraffin (C_nH_{2n+2})	Paraffin wax	*Merits*: Chemically stable, no super cooling, recyclable, high heat of fusion *Demerits*: low thermal conductivity, volume change, flammable
	2. Non-paraffin (fatty acids $CH_3(CH_2)_2n \cdot COOH$)	Butyl stearate, lauric acid, capric acid, octadecane, glycerol, etc.	
Inorganic PCMs	11. Salt hydrates ($A.nH_2O$; A-salts)	Sodium carbonate, $CaCl_2 \cdot 6H_2O$, $NaCH_3COO \cdot 3H_2O$, $NaCH_3COO \cdot {}_3H_2O$, $CaCl_2 \cdot 6H_2O$	*Merits*: low cost, nonflammable, high thermal conductivity, high heat of fusion *Demerits*: corrosive, super cooling
	12. Metallic	Al, Mg, Zn, etc.	
Eutectic PCMs	1. Organic–organic	Ammonium alum–ammonium nitrate, capric acid–lauric acid, methyl stearate-methyl palmitate, myristic acid–palmitic acid, etc	*Merits*: Properties can be tailored to match specific requirements, high volumetric thermal storage density, and sharp melting point *Demerits*: Less data on thermophysical properties for many combinations, high cost
	2. Inorganic–inorganic	$NaCH_3COO \cdot 3H_2O + NaBr \cdot 2H_2O$, $CaCl_2 \cdot 6H_2O + CaBr_2 \cdot 6H_2O$, $NaCH_3COO \cdot 3H_2O + NaBr \cdot 2H_2O$	
	3. Organic–inorganic	$LiCO_3 + NaCO_3$	

Selection of appropriate way to embed PCMs in cementitious material is very much essential to avoid its adverse effect on these materials. Inclusion of PCMs in concretes can be done by either of the ways mentioned in the following.

(i) Direct addition of PCM: It is an easy practice of employing PCMs [46]. However, major detriment is its leakage effect and alters the material matrix [47].
(ii) Pipes added with PCMs: This approach of incorporating PCMs can be able to resist physical and chemical damage endure during the stage of mixing, casting, and loading. In addition, pipe system avoids the PCM leakage and its negative influence on fresh and hardened concrete properties. But, this approach is complicated and it shows lesser thermal influence due to limited spacing as well as partial melting of PCMs in pipes (low thermal conductivity) leads to the underutilized system [9].
(iii) Surface incorporation of PCMs via pores of concrete: In this method, PCMs in the melted form are allowed to engross into porous concrete and left over for certain time to soak. The major drawback of this technique is leakage of PCM [9, 32].
(iv) Lightweight aggregated impregnated with PCMs: this method adopts evacuation of lightweight aggregates followed by immersing into liquid PCM and kept soaking in precise atmosphere for certain duration [22, 48].
(v) Microencapsulated PCMs with polymeric shell: is a recent technique where base PCM particles are encapsulated within a polymeric shell, which is capable to withstand the outside atmosphere and providing the cyclic stability. It also possess high surface to volume ratio due to its microsizes [9, 32, 48].

11 Conclusions

This review paper gives an insight into the influence of incorporating phase change material in the cementitious system. The following inferences are made based on the reviewed literatures:

1. PCM admixed cementitious composites reduced the peak temperature, thereby acting as a potential media to store thermal energy and manage the energy requirements in buildings and infrastructures.
2. Thermal conductivity of PCM admixed concrete/mortar declined with the increment in PCM content, which could be due to the fact of enhanced porosity or entrapped air content.
3. The inclusion of phase change materials in the cementitious system enhances the thermal mass/heat capacity potential. Higher the dosage of PCM content in the cementitious system showed the prominent increase in specific heat capacity. Latent heat capacity of the cement composites significantly increased in correspondence to the increase in PCM concentration. The existence of PCM in cement composites suppresses the hydration peak by delaying the hydration kinetics and also it can reduce the heat of hydration rate.

4. PCMs incorporation in cementitious system reduces the flow ability of mortar or concrete, which could be attributed to increased viscosity.
5. The low density of PCMs reduced the density when admixed to cementitious system and increased the percentage of porosity.
6. PCM presence in cement composited reduced the sorptivity and diffusivity as a whole combined effect justified the diminished water absorption.
7. The PCM doped cement mortar/concrete drastically reduced the compressive strength and flexural strength. The reason attributed to drop in density, increased porosity and association of PCMs in cement chemical reaction. This can be addressed by adding appropriate type and dosage of PCM which is very much essential for structural concrete usage. Most of the researchers data recommend 5% PCM dosage as an ideal for building applications.
8. The modulus of elasticity reduced in case of PCMs integrated concrete/mortar and increased the shrinkage rate. The reason associated to low stiffness and low strength nature of PCMs.

References

1. Allcott H, Greenstone M (2012) Is there an energy efficiency gap? J Econ Perspect 26:3–28
2. Cao VD, Pilehvar S, Bringas CS, Szczotok AM, Rodriguez JF, Carmona M, Al-Manasir N, Kjoniksen AL (2017) Microencapsulated phase change materials for enhancing the thermal performance of Portland cement concrete and geopolymer concrete for passive building applications. Energy Convers Manage 133:56–66
3. Bentz DP, Turpin R (2007) Potential applications of phase change materials in concrete technology. Cem Concr Compos 29:527–532
4. Cabeza LF, Castell A, Barreneche C, De Gracia A, Fernández AI (2011) Materials used as PCM in thermal energy storage in buildings: a review. Renew Sustain Energy Revol 15:1675–1695
5. Demirbas MF (2006) Thermal energy storage and phase change materials: an overview. Energy Sources Part B 1:85–95
6. Pasupathy A, Velraj R, Seeniraj RV (2008) Phase change material-based building architecture for thermal management in residential and commercial establishments. Renew Sustain Energy Revol 12(1):39–64
7. Jayalath A, Nicolas RS, Sofi M, Shanks R, Ngo T, Ayea L, Mendis P (2016) Properties of cementitious mortar and concrete containing micro-encapsulated phase change materials. Constr Build Mater 120:408–417
8. Fernandes F, Manari S, Aguayo M, Santos K, Oey T, Wei Z, Falzone G, Neithalath N, Sant G (2014) On the feasibility of using phase change materials (PCMs) to mitigate thermal cracking in cementitious materials. Cem Concr Compos 51:14–26
9. Savija B (2018) Smart crack control in concrete through use of phase change materials (PCMs): a review. Materials 11:654
10. Pomianowski M, Heiselberg P, Zhang Y (2013) Review of thermal energy storage technologies based on PCM application in buildings. Energy Build 67:56–69
11. Mankel C, Caggiano A, Ukrainczyka N, Koendersa EAB (2017) Micro-scale thermal analysis of energy storage in cement-based composites containing phase change materials (PCMs). MecanicaComputacional 35:2453–2467
12. Jayalath A, Mendis P, Gammampila R, Aye L (2011) Applications of phase change materials in concrete for sustainable built environment: a review. In: Proceedings of the international conference on structural engineering, construction and management, vol 1, at Kandy, Sri Lanka

13. Norvell C, Sailor DJ, Dusicka P (2013) The effect of microencapsulated phase-change material on the compressive strength of structural concrete. J Green Build 8(3):116–124
14. Cellat K, Beyhan B, Gungor C, Konuklu Y, Karahan O, Dundar C, Paksoy H (2015) Thermal enhancement of concrete by adding bio-based fatty acids as phase change materials. Energy Build 106:156–163
15. Cellat K, Beyhan B, Kazanci B, Konuklu Y, Paksoy H (2017) Direct Incorporation of butyl stearate as phase change material into concrete for energy saving in buildings. J Clean Energy Technol 5(1):64–68
16. Abath (1983) Low temperature latent heat thermal energy storage: heat storage materials. Solar Energy 30(4):313–332
17. Kenisarin MM (2010) High-temperature phase change materials for thermal energy storage. Renew Sustain Energy Rev 14(3):955–970
18. Chang L, Li F, Ma LP, Cheng HM (2010) Advanced materials for energy storage. Adv Mater 22(8)
19. Hunger M, Entrop AG, Mandilaras I, Brouwers HJH, and. Founti, M. (2009) The behavior of self-compacting concrete containing micro-encapsulated phase change materials. Cement Concr Compos 31:731–743
20. Thiele AM, Sant G, Pilon L (2015) Diurnal thermal analysis of microencapsulated PCM-concrete composite walls. Energy Convers Manage 93:215–227
21. Ricklefs A, Thiele AM, Falzone G, Sant G, Pilon L (2017) Thermal conductivity of cementitious composites containing microencapsulated phase change materials. Int J Heat Mass Transf 104:71–82
22. Sahu LK, Mondloe D, Garhewal A (2017) A review on thermal and mechanical properties of concrete containing phase change material. Int Res J Eng Technol 4(5):2154–2165
23. Snoeck D, Belie ND (2017) Reducing the risk of thermal cracking in cementitious materials by means of encapsulated phase-change materials. In: Proceedings of the 1st international conference on construction materials for sustainable Future-Zadar Croatia, pp 170–176
24. Sakulich AR, Bentz D (2012) Incorporation of phase change materials in cementitious systems via fine lightweight aggregate. Constr Build Mater 35:483–490
25. Eddhahak-Ouni A, Drissi S, Colin J, Neji J, Care S (2014) Experimental and multi-scale analysis of the thermal properties of Portland cement concretes embedded with microencapsulated phase change materials (PCMs). Appl Therm Eng 64(1):32–39
26. Falzone G, Falla GP, Wei Z, Zhao M, Kumar A, Bauchy M, Neithalath N, Pilon L, Sant G (2016) The influences of soft and stiff inclusions on the mechanical properties of cementitious composites. Cement Concr Compos 71:153–165
27. Choi WC, Khil BS, Chae YS, Liang QB, Yun HD (2014) Feasibility of Using phase change materials to control the heat of hydration in massive concrete structures. Hindawi Publishing Corp Sci World J 781393:1–6
28. Yang HB, Liu TC, Chern JC, Lee MH (2016) Mechanical properties of concrete containing phase-change material. J Chin Inst Eng 39(5):521–530
29. Zhang Z, Shi G, Wang S, Fang X, Liu X (2013) Thermal energy storage cement mortar containing n-octadecane/expanded graphite composite phase change material. Renew Energy 50:670–675
30. Pisello AL, D'Alessandroc A, Fabianib C, Fiorellic AP, Ubertinic F, Cabezad LF, Materazzic AL, Cotana F (2016) Multifunctional analysis of innovative PCM-filled concretes. Sustain Energy Build Proc 111:81–90
31. Qiao Q, Fang C (1955) Compressive and flexural strength of high strength phase change mortar. In: Advances in materials machinery electronics II AIP conference proceedings, pp 020024-1–020024-4
32. Farnam Y, Krafcik M, Liston L, Washington T, Erk K, Tao B, Weiss WJ (2015) Evaluating the use of phase change materials in concrete pavement to melt ice and snow. J Mater Civ Eng 28
33. Fenollera M, Míguez JL, Goicoechea I, Lorenzo J, ÁngelÁlvarez A (2013) The influence of phase change materials on the properties of self-compacting concrete. Materials 6:3530–3546

34. Lucas S, Senff L, Ferreira VM, Aguiar JLB, Labrincha JA (2010) Fresh state characterization of lime mortars with PCM additions. Appl Rheol 20(6):63166 (1–7)
35. Niall D, West R, McCormack S, Kinnane O (2016) Thermal mass behaviour of concrete panels incorporating phase change materials. In: sustainable built environment conference 2016, Hamburg, German
36. Hawes DW, Feldman D, Banu D (1993) Latent heat storage in building materials. Energy Build 20(1):77–86
37. Wei Z, Falzone G, Das S, Saklani N, Pape YL, Plone L, Neithalath N, Sant G (2017) Restrained shrinkage cracking of cementitious composites containing soft PCM inclusions: A paste (matrix) controlled response. Mater Des 132:367–374
38. Felske JD (2004) Effective thermal conductivity of composite spheres in a continuous medium with contact resistance. Int J Heat Mass Transf 47(14):3453–3461
39. Saeed RMR (2016) Thermal characterization of phase change materials for thermal energy storage. Masters Theses, 7521
40. Ge Z, Ye F, Cao H, Leng G, e Qin Y, Ding Y (2014) Carbonate-salt-based composite materials for medium- and high-temperature thermal energy storage. Particuology 15:77–81
41. Wei Z, Falzone G, Wang B, Thiele A, Puerta-Falla G, Pilon L, Neithalath N, Sant G (2017) The durability of cementitious composites containing microencapsulated phase change materials. Cem Concr Compos 81:66–76
42. Lecompte T, Le Bideau P, Glouannec P, Nortershauser D, Le Masson S (2015) Mechanical and thermo-physical behaviour of concretes and mortars containing phase change material. Energy Build 94:52–60
43. Jegadheeswaran S, Pohekar SD (2009) Performance enhancement in latent heat ther-mal storage system: a review. Renew Sustain Energy Revol 13:2225–2244
44. Paksoy H, Kardas G, Konuklu Y, Cellat K, Tezcan F (2017) Characterization of concrete mixes containing phase change materials. IOP Conf Series Mater Sci Eng 251:012118
45. Kalnaes SE, Jelle BP (2015) Phase change materials and products for building applications: a state-of-the-art review and future research opportunities. Energy Build 94:150–176
46. Lee KO, Medina MA, Raith E, Sun XQ (2015) Assessing the integration of a thin phase change material (PCM) layer in a residential building wall for heat transfer reduction and management. Appl Energy 137:699–706
47. Schossig P, Henning HM, Gschwander S, Haussmann T (2005) Micro-encapsulated phase change materials integrated into construction materials. Solar Energy Mater 89:297–306
48. Ling TC, Poon CS (2013) Use of phase change materials fot thermal energy storage in concrete: an overview. Constr Build Mater 46(99):55–62

Review on Characteristics of Sewage Sludge Ash and Its Partial Replacement as Binder Material in Concrete

Mithesh Kumar, P. Shreelaxmi, and Muralidhar Kamath

Abstract The recent environmental concerns have made the concrete technologists think of alternatives to cement or by partially or completely replacing it with pozolonas. There is developing concern all over the world about the raw materials assets utilized in the creation of concrete, and most of them are limited and exhaustible. Use of recycled solid/liquid waste is in practice from a prolonged period in civil engineering application. The solid waste from wastewater treatment plant can be utilized as fillers or supplementary cementing material for the production of eco-friendly green concrete. Sewage sludge is a by-product of a sewage treatment plant. This paper reviews the properties of, sewage sludge ash and its application as a binder material in concrete. State of the art review on the available literature pertaining to sewage sludge and sewage sludge ash is presented. Since the property of the sludge depends on the source of wastewater, a detailed report on variation in the properties reported in the literature is presented. Particle size analysis, specific surface area, chemical composition of SSA reported in various sources are discussed. Properties are discussed on the probability to be used as a potential binder for concrete making is also discussed. Physical and chemical properties in comparison with that of OPC are discussed.

Keywords Binder · Concrete · Sewage sludge · Sewage sludge ash

M. Kumar (✉) · P. Shreelaxmi · M. Kamath
Civil Engineering Department, MIT, MAHE, Manipal, Karnataka 576104, India
e-mail: mithesh.kumar@learner.manipal.edu

P. Shreelaxmi
e-mail: Shreelaxmi.p@manipal.edu

M. Kamath
e-mail: muralidhar.kamath@learner.manipal.edu

B. B. Das et al. (eds.), *Recent Trends in Civil Engineering*, Lecture Notes in Civil Engineering 105, https://doi.org/10.1007/978-981-15-8293-6_5

1 Introduction

Traditional materials used for making concrete are natural aggregate and the cement. However, the recent environmental concerns have made the concrete technologists think of alternatives to cement or at least reduce its usage. This has provoked the use of various industrial wastes that has cementitious properties. Fly ash is the most popular industrial waste that is siliceous and aluminous.

There is developing concern all over the world that raw material assets utilized in the making of concrete are limited and exhaustible. It should be preserved for the future generation. This has resulted in shifting trends in construction material from being natural to becoming more artificial, and a combination of both and they have their applications. The uses of recycled solid/liquid waste are in practice since a few decades in various civil engineering application. The utilization of fly ash, blast furnace slag, recycled aggregate, plastic waste, E-waste, industrial sludge are some of the successful illustrations of achievement of research carried out on these lines. The solid waste can be utilized as fillers or supplementary cementing material for the production of eco-friendly green concrete.

Sludge is an inevitable residue of the wastewater treatment plant. The treatment process of wastewater and disposal of sludge is expensive. Inefficient treatment and disposal can create environmental problems. With the rapidly growing population and industrialization, wastewater generation has increased, resulting in a massive amount of dry sludge [1]. Sludge is usually in form of slurry is the end product in various water treatment processes. Production of sludge in various treatment processes results in the accumulation of solid and liquid wastes. This if not disposed efficiently results in land pollution. This is usually disposed of in landfills. If this is utilized in concrete, a considerable amount of load on landfills can be reduced. The incineration process of sewage sludge is the most effective way of dispersing the residential sludge. Incineration reduces the waste by about 70% by mass and 90% by volume. Sewage sludge ash (SSA) is what is left at the end of incineration process which can be used as SCM, since it is found to contain silica and alumina in varying proportions.

Researchers have worked on possibilities of utilizing SSA not only as SCM in blend cement but in a wide range of building materials such as bricks, tiles, pavers, light aggregates but also for substitution for cement in concrete and mortar.

This paper is aimed at studying the properties and the use of SSA in binder, mortar, and concrete. A review of published literature is undertaken based on a total of 39 publications, dating from 1995 to 2019.

2 Research Trends

The properties and application of SSA are widely reported in recent years. A breakdown of year wise and region wise publication is presented in Graph 1 and Fig. 1. Significant interest is being taken during the last 5 years to study the properties and

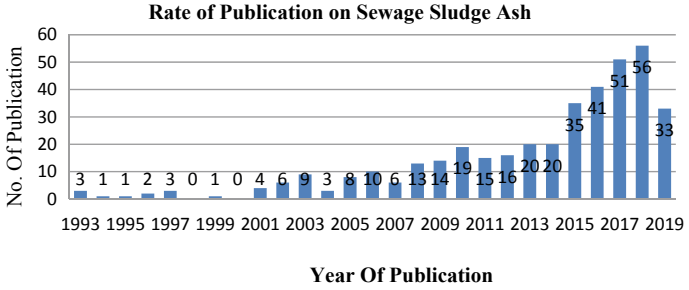

Graph 1 Rate of publication on Sewage Sludge ash. *Source* ("Web Of Science," n.d. [39])

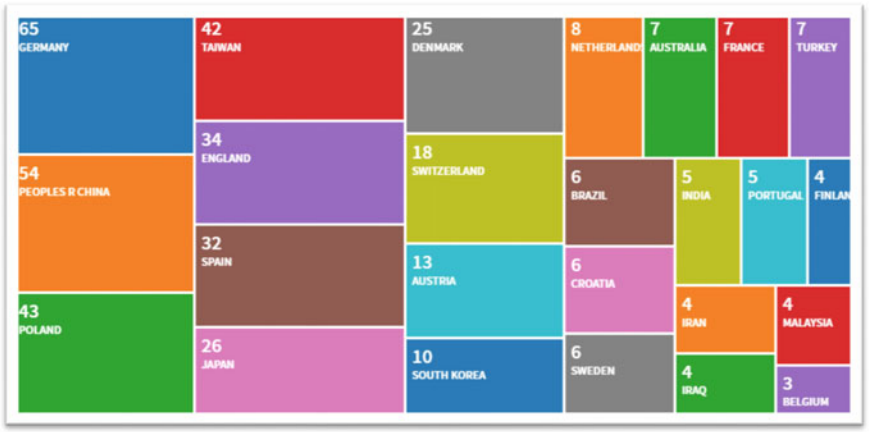

Fig. 1 Region-wise publication on SSA during 1993–2019. *Source* ("Web Of Science," n.d. [39])

application of SSA as a construction material. Germany, China, Poland, Taiwan, and England are the major contributors to publications [39].

3 Characteristics of Sewage Sludge Ash (SSA)

3.1 Density and Specific Gravity

As reported in Wang et al. [2], Pan et al. [3], Pan and Tseng [4], the specific gravity of SSA ranges between 2.29 and 2.99. The mean value of available literature is about 2.55 with standard deviation of 0.15. The material somewhat falls between light sand and Portland cement [2, 3].

It has also been reported that the density of SSA ranges from 2.06 to 2.69 kg/m^3 with a mean value of 2.28 and a standard deviation of 0.24. The variation in density is

due to variation of incineration temperature. Density increases with the temperature of incineration [5].

3.2 Diameter and Particle Size Distribution

The SSA is fine and brown colour with particle diameter in the range 1–250 μm. The percentage by volume of particle diameter greater than 10, 45, and 90 μm were 86.1%, 49.1%, and 25.3%, respectively. Figure 2 shows the granulometric distribution for SSA [6].

Figure 3 shows the comparative analysis of particle size distribution of OPC, PFA, SSA, and FSSA. It is observed that FSSA is finest and SSA is much coarsest

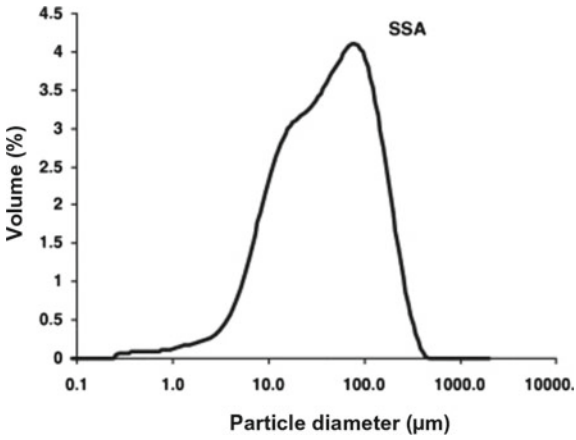

Fig. 2 Granulometric distribution curve for SSA. *Source* Garcés et al. [6]

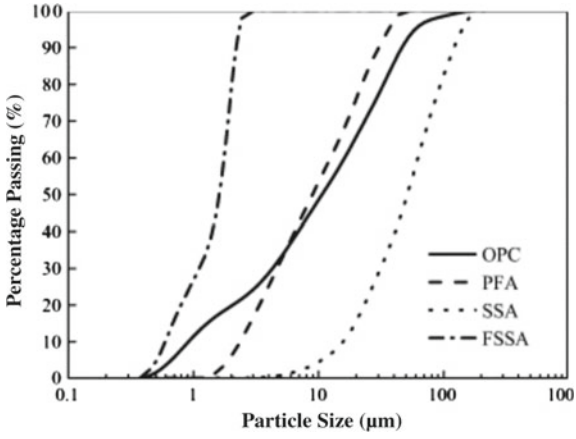

Fig. 3 Particle size distribution of OPC, PFA, SSA, and FSSA. *Source* Chen and Poon [7]

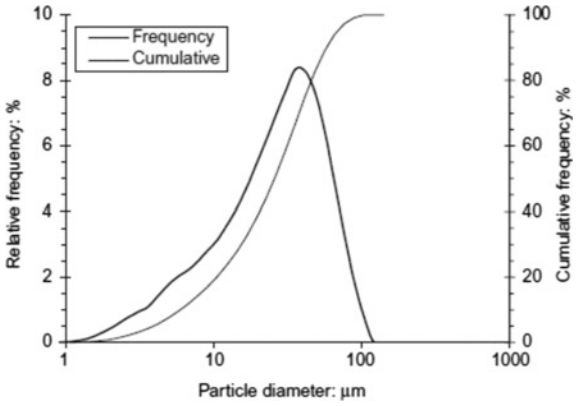

Fig. 4 Particle Size distribution of SSA

among the materials reported. Figure 4 shows the particle size distribution of SSA with respect to relative frequency and cumulative frequency.

3.3 Specific Surface Area

Blaine fineness and BET specific surface area of SSA are found to be in the range 486.1–3900 m^2/kg and 2.5–23.1 m^2/g on analysing the available literature. The values observed in the various literatures are listed in Table 1. The Blaine fineness value of OPC and fly ash is in the range 300–500 m^2/kg and 230–320 m^2/kg [8, 9]. The fineness and specific surface area of SSA are varying due to its irregular particle shape and porous microstructure.

3.4 Loss on Ignition (LOI)

The LOI values obtained through literature are listed in Table 2. A minimum value of zero and the maximum value of 41.8 are observed. LOI value of SSA mainly depends upon the method through which sludge samples are incinerated and the temperature.

3.5 Chemical Composition of SSA

Table 3 presents the composition of SSA observed in the literature. The chemical composition reported in Tables 3 and 4 shows that SSA is mainly composed of SiO_2, Al_2O_3, Fe_2O_3, CaO, and P_2O_5 in the range 14.33–65.00, 2.65–34.20, 2.10–30.00,

Table 1 Blaine fineness and BET specific surface area of SSA

Blaine fineness (m^2/kg)	640	486.1	*	500–3900	*	*	496–993	640	*	*	*	1041
BET specific surface area (m^2/g)	19	*	6.4	2.5–23.1	6.5	6.8	10.9–12.48	19	15.2	17.5–19.9	10.9–12.5	*
References	(Cyr et al. [10]	Lin and Weng [11]	Donatello et al. [12]	Lynn et al. [5]	Gil-Lalaguna et al. [13]	Wang et al. [2]	Pan et al. [3]	Coutandet al. [14]	Pan and Tseng [4]			Liu et al. [15]

Table 2 LOI value of SSA

LOI Value	1.4	5.5	41.8	0.0	5.1	5.1	5.5	23.53
References	AI-Sharif and Attom [16]	Cyr et al. [10]	Al Sayed et al. [17]	Anderson et al. [18]	Monzó et al. [19]	Wang et al. [2]	Coutand et al. [14]	Liu et al. [15]

1.10–40.10, and 0.30–26.70. The graphical representation of chemical composition with minimum, mean, maximum, and average value is shown in Graph 2.

3.6 Microstructure

SEM analysis suggests that SSA particles were less than 600 μm and porous in nature. They were rich in silicon dioxide, calcium oxide, aluminium oxide, and iron oxide. Halliday et al. (2012) [30] observed SEM images of SSA and concluded that it is made up of irregularly shaped particles, onto which smaller particles are fused. They observed that the particle size varies from 200 to 5 μm, this result in porous structure and causes workability problems. The SEM image of SSA is shown in Fig. 5 [30].

4 Application of Sewage Sludge Ash

4.1 Use in Cement Manufacturing

The chemical composition of SSA is found to be similar to those materials, which are used in the production of cement clinker. So SSA can contribute to SiO_2, Al_2O_3, Fe_2O_3, MgO, CaO, K_2O, Na_2O, and SO_3 in the cement production process. SSA, dry sewage sludge, limestone, and gypsum are used in combination to produce cement. Based on an experiment performed by Ryunosuke Kikuchi (2001) [31], one ton of cement can be produced by using 0.5 ton of SSA, 0.3 ton of dry sewage sludge, 0.3 ton of limestone are converted to 0.85 ton of cement clinker and then adding 0.15 ton of gypsum to clinker [31].

Lin et al. [29] in their experimental study, the hydration and engineering properties of eco-cement pastes are studied. They observed that it is feasible to use sludge ash and steel making waste to replace up to 20% of the mineral components of the raw material of cement [32].

Table 3 Chemical Composition of Sewage Sludge Ash

Reference composition	Piasta and Lukawska [20]	Nakic [21]	Krejcirikova [22]		Krejcirikova [22]		Chen et al. [23]	Dyer et al. [24]			Coutand et al. [14]		Garcés et al. [6]	Cyr [25]	Fontes et al. [26]	[27]	Kazberuk [28]	Lin et al. [29]	Wang et al. [2]	Pan et al. [3]
SiO_2	16.60	35.00	14.40	65.00	15.83	14.33	27.91	29.40	35.20	26.40	33.00	34.20	19.20	34.20	39.02	36.00	34.68	63.31	64.95	50.60
Al_2O_3	5.10	7.59	4.40	34.20	4.40	2.65	12.26	10.90	12.40	14.10	24.00	12.60	8.90	12.60	19.09	11.00	6.32	15.38	15.21	12.8
Fe_2O_3	9.10	–	2.10	30.00	16.30	7.15	18.32	13.00	7.30	11.30	6.70	4.70	10.00	4.70	12.48	17.00	10.32	6.81	6.95	7.21
CaO	12.90	34.30	1.10	40.10	23.37	36.38	10.47	14.30	12.40	9.60	5.70	20.60	30.60	20.60	10.12	13.00	15.42	1.8	1.93	1.93
MgO	3.80	4.21	0.02	23.40	1.82	1.99	3.16	1.40	2.20	1.40	1.00	1.90	2.70	1.90	1.89	2.00	2.65	1.03	1.45	1.48
SO_3	2.10	4.56	0.01	12.40	2.00	4.74	6.13	1.30	0.50	0.60	0.20	2.80	11.10	2.80	6.38	3.00	0.60	1.01	*	2.38
Cl^-	0.01	*	*	*	0.01	0.20	*	0.14	0.04	0.01	0.00	*	*	*	*	*	*	*	*	*
P_2O_5	15.00	5.81	0.30	26.70	18.33	10.31	9.77	13.50	12.70	15.70	14.00	14.80	12.30	14.80	4.94	12.00	18.17	7.2	1.51	1.67
Na_2O	3.50	*	0.01	6.80	0.67	0.81	7.32	0.20	0.20	0.40	0.00	1.00	0.80	1.00	1.26		0.70	0.7	0.79	0.32
K_2O	2.80	*	0.10	3.10	1.45	1.81	1.89	1.20	1.80	1.60	1.30	1.70	1.40	1.70	1.76	1.50	1.30	1.51	2.52	1.7
Tio_2	*	*	0.30	1.90	0.83	0.67	0.52	1.30	1.50	1.30	1.20	0.90	1.00	0.90	*	*	0.41	*	*	*
MnO	*	*	0.03	0.90	0.09	0.05	0.24	*	0.20	0.60	0.30	0.06	*	0.06	*	*	*	*	*	*

Note *the values are not represented by author

Table 4 Comparison of chemical composition of SSA

Composition	Cyr et al. [10]			Based on current literature review			
	Mean	Min	Max	Mean	Min	Max	SD
SiO_2	36.10	14.40	65.00	34.46	14.33	65.00	15.93
Al_2O_3	14.20	4.40	34.20	12.30	2.65	34.20	7.35
Fe_2O_3	9.20	2.10	30.00	10.60	2.10	30.00	6.42
CaO	14.80	1.10	40.10	15.83	1.10	40.10	11.94
MgO	2.40	0.02	23.40	3.07	0.02	23.40	4.88
SO_3	2.80	0.01	12.40	3.40	0.01	12.40	3.51
Cl^-	*	*	*	0.06	0.00	0.20	0.08
P_2O_5	11.60	0.30	26.70	11.48	0.30	26.70	6.52
Na_2O	0.90	0.01	6.00	1.47	0.00	7.32	2.17
K_2O	1.30	0.10	3.10	1.69	0.10	3.10	0.64
Tio2	1.10	0.30	1.90	1.06	0.30	1.90	0.46
MnO	0.30	0.03	0.90	0.25	0.03	0.90	0.29

Note *the values are not represented by author

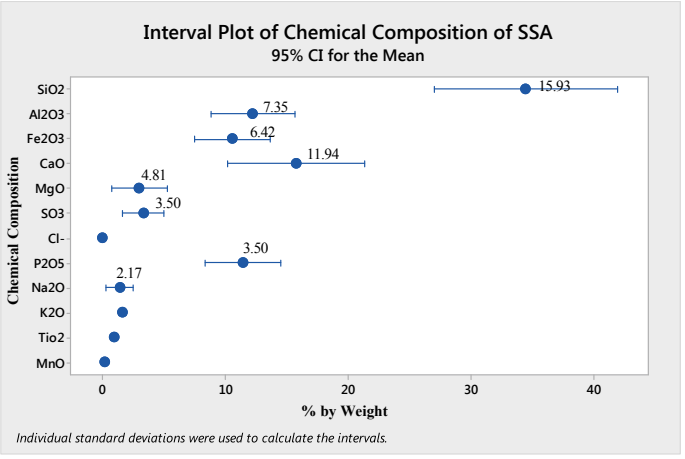

Graph 2 Chemical compositions versus % weight of sewage sludge ash

4.2 Use in Binder Application

SSA has been used as one of the binders in combination with other cementitious material. It is observed that workability of concrete is decreased with an increase in the percentage of replacement. The setting time of the mortars is longer with an increasing percentage of SSA [33]. The addition of 20% SSA resulted in an increase of initial and final setting time by twofold and 2.5-fold [34].

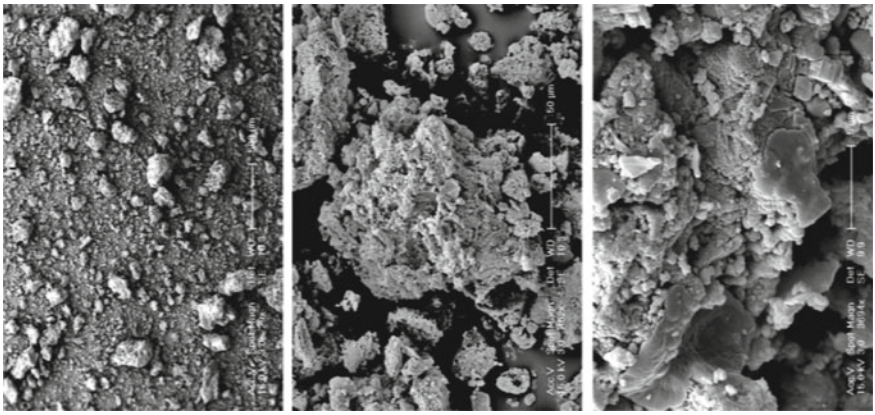

Fig. 5 Microstructure of SSA. *Source* Halliday et al. [30]

Cyr et al. [10] investigated physical, chemical, and mineralogical properties of sewage sludge ash (SSA) and its use as a binder. The binder replacement was done at 25, and 50% and concrete mixtures are prepared according to French standard NF EN 196-1. The compressive strength of the SSA concrete was lower than that of the control mix, but it has long-term positive effect due to pozzolanic activity [10].

Pinarli and Kaymal [34] in their experimental study observed the increase in initial and final setting time of SSA cement paste as the percentage of replacement increases.

Baeza et al. [35] have investigated the properties of cement paste and mortor produced by partial replacement of portland cement with Fly ash, marble dust, sewage sludge ash, and rice husk ash. Water absorptions are higher compared to standard concrete was observed. 9% increase in compressive strength is observed for the 30% blended mix of FA, SSA, and RHA [35].

Pozzolanic activity test conducted on SSA samples shows that the properties are comparable to fly ash [35]. However the influence of SSA on durability, load-dependent, and load-independent deformation is to be studied in order to improve the prospects of material use [5].

Piasta and Lukawska [20] studied the properties of SSA and fly ash and replaced cement by 10 and 20% of SSA. They conclude that SSA can be used as an addition to cement composite at 10%.

From the literature, it is observed that the increase in the percentage of SSA as the binder will affect the compressive strength of concrete. It is observed from the literature that the heat of hydration continues even after 28 days, like in fly ash replacement concrete. The effect of SSA on compressive strength 1, 7, and 28 days is shown in Graph 3.

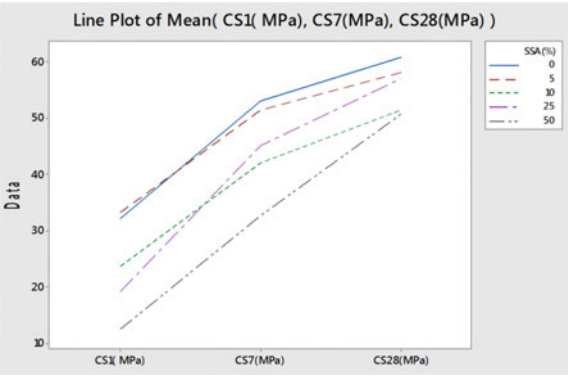

Graph 3 1, 7, and 28 days Compressive strength of SSA replaced concrete [20, 26, 10]

5 Comparison of the Chemical Composition of SSA with Cement and Fly Ash

The comparison of SSA with cement and fly ash is represented in Table 5. It is observed that SSA has similar composition of OPC and Fly ash with varying percentage. The composition of SSA depends upon the source.

Table 5 Comparison of OPC, fly ash, and SSA

Parameter	OPC (Dunuweera and Rajapakse [36])	Fly ash (Gamage et al. [37], Ishwarya et al. [38])		SSA*
		Class F	Class C	
CaO	60–67	8.70	24.30	1.10–40.10
SiO_2	14–25	54.90	39.90	14.33–65.00
Al_2O_3	3.0–8.0	25.80	16.70	2.65–34.20
Fe_2O_3	0.5–6.0	6.90	5.80	2.10–30.0
MgO	0.1–4.0	1.80	4.60	0.02–23.40
Alkalies (K_2O, Na_2O)	0.4–1.3	0.60	1.30	0.10–3.10 0.0–7.32
SO_3	1.3–3.0	0.30	3.30	0.1–12.40

Note *Ranges are observed through a literature survey

6 Research Opportunities to Enhance Sewage Sludge Ash Use in India

It is observed that only 6 articles are published from Indian authors out of 390 articles. There is a huge opportunity to study the characteristics of SSA and its application to Indian scenario.

7 Discussions

It is observed from the literature review that concrete produced by replacing binder by industrial waste products possess superior properties in comparison with normal concrete. Studies are carried out on use of sewage sludge as a filler material. The following gaps are identified from the literature study:

i. There have been a few studies reporting pozzolanic nature of sewage sludge ash and its positive use as a supplementary cementitious material. However, the reactivity of the sewage sludge ash has not been quantified.
ii. The effect of sewage sludge and sewage sludge ash in the presence of other SCM's on the long-term durability has not been reported.

8 Conclusions

- SSA has been proved as an efficient pozzolana with properties similar to that of fly ash.
- Not much research is being carried out in India on SSA. Since India is a populous country with a huge production of sewage waste. If sewage sludge is converted to SSA, it can solve the problem of disposal of sewage to a considerable extent.
- Since the properties and composite of SSA depend upon the source, it is necessary to carry out a detailed characterization study on SSA.

References

1. Mourtada Rabie G (2016) Using of wastewater dry and wet sludge in concrete mix. J Civ Environ Eng 06(01):1–7. https://doi.org/10.4172/2165-784X.1000209
2. Wang KS, Tseng CJ, Chiou IJ, Shih MH (2005) The thermal conductivity mechanism of sewage sludge ash lightweight materials. Cem Concr Res 35(4):803–809. https://doi.org/10.1016/j.cemconres.2004.04.027
3. Pan SC, Tseng DH, Lee CC, Lee C (2003) Influence of the fineness of sewage sludge ash on the mortar properties. Cem Concr Res 33(11):1749–1754. https://doi.org/10.1016/S0008-8846(03)00165-0

4. Pan SC, Tseng DH (2001) Sewage sludge ash characteristics and its potential applications. Water Sci Technol 44(10):261–267
5. Lynn CJ, Dhir RK, Ghataora GS, West RP (2015) Sewage sludge ash characteristics and potential for use in concrete 98:767–779. https://doi.org/10.1016/j.conbuildmat.2015.08.122
6. Garcés P, Pérez Carrión M, García-Alcocel E, Payá J, Monzó J, Borrachero MV (2008) Mechanical and physical properties of cement blended with sewage sludge ash. Waste Manage 28(12):2495–2502. https://doi.org/10.1016/j.wasman.2008.02.019
7. Chen Z, Poon CS (2017) Comparative studies on the effects of sewage sludge ash and fly ash on cement hydration and properties of cement mortars. Constr Build Mater 154:791–803. https://doi.org/10.1016/j.conbuildmat.2017.08.003
8. Yazici Ş, Arel HŞ (2012) Effects of fly ash fineness on the mechanical properties of concrete. Sadhana—Acad Proc Eng Sci 37(3):389–403. https://doi.org/10.1007/s12046-012-0083-3
9. Singh P, Shah ND, Majumdar PK (2018) Influence of flyash on fineness, porosity and permeability of flyash blended cement paste. Int Res J Eng Technol, 1056–1058. Retrieved from www.irjet.net
10. Cyr M, Coutand M, Clastres P (2007) Technological and environmental behavior of sewage sludge ash (SSA) in cement-based materials. Cem Concr Res 37(8):1278–1289. https://doi.org/10.1016/j.cemconres.2007.04.003
11. Lin D, Weng C (2001) Use of Sewage sludge ash as brick material 127:922–927
12. Donatello S, Tyrer M, Cheeseman CR (2010) Comparison of test methods to assess pozzolanic activity. Cement Concr Compos 32(2):121–127. https://doi.org/10.1016/j.cemconcomp.2009.10.008
13. Gil-Lalaguna N, Sánchez JL, Murillo MB, Gea G (2015) Use of sewage sludge combustion ash and gasification ash for high-temperature desulphurization of different gas streams. Fuel, 141:99–108. https://doi.org/10.1016/j.fuel.2014.10.036
14. Coutand M, Cyr M, Clastres P (2006) Use of sewage sludge ash as mineral admixture in mortars. Proc Inst Civ Eng Constr Mater 159(4):153–162. https://doi.org/10.1680/coma.2006.159.4.153
15. Liu M, Zhao Y, Xiao Y, Yu Z (2019) Performance of cement pastes containing sewage sludge ash at elevated temperatures. Constr Build Mater 211:785–795. https://doi.org/10.1016/j.conbuildmat.2019.03.290
16. AI-Sharif MM, Attom MF (2014) A geoenvironmental application of burned wastewater sludge ash in soil stabilization. Environ Earth Sci 71(5):2453–2463. https://doi.org/10.1007/s12665-013-2645-z
17. Al Sayed MH, Madany IM, Buali ARM (1995) Use of sewage sludge ash in asphaltic paving mixes in hot regions. Constr Build Mater 9(1):19–23. https://doi.org/10.1016/0950-0618(95)92856-C
18. Anderson M, Elliott M, Hickson C (2002) Factory-scale proving trials using combined mixtures of three by-product wastes (including incinerated sewage sludge ash) in clay building bricks. J Chem Technol Biotechnol 77(3):345–351. https://doi.org/10.1002/jctb.593
19. Monzó J, Payá J, Borrachero MV, Córcoles A (1996) Use of Sewage sludge ASH(SSA)-cement admixtures in mortars. Cem Concr Res 26(9):1389–1398
20. Piasta W, Lukawska M (2016) The effect of sewage sludge ash on properties of cement composite. In world multidiciplinary civil engineering -architecture-urban planning symposium 2016, WMCAUS 2016 (vol 161, pp. 1018–1024). https://doi.org/10.1016/j.proeng.2016.08.842
21. Nakic D (2018) Environmental evaluation of concrete with sewage sludge ash based on LCA. Sustain Product Consump 16:193–201. https://doi.org/10.1016/j.spc.2018.08.003
22. Krejcirikova B, Ottosen LM, Kirkelund GM, Rode C (2019) Characterization of sewage sludge ash and its e ff ect on moisture physics of mortar. J Build Eng 21:296–403. https://doi.org/10.1016/j.jobe.2018.10.021
23. Chen Z, Li JS, Poon CS (2018) Combined use of sewage sludge ash and recycled glass cullet for the production of concrete blocks. J Cleaner Prod 171:1447–1459. https://doi.org/10.1016/j.jclepro.2017.10.140

24. Dyer TD, Halliday JE, Dhir KR (2011) Hydration chemistry of sewage sludge ash used as a cement component. J Mater Civ Eng 23(5):648–655. https://doi.org/10.1061/(ASCE)MT.1943-5533.0000221
25. Cyr M, Idir R, Escadeillas G (2012) Use of metakaolin to stabilize sewage sludge ash and municipal solid waste incineration fly ash in cement-based materials. J Hazard Mater 243:193–203. https://doi.org/10.1016/j.jhazmat.2012.10.019
26. Fontes CMA, Toledo Filho RD, Barbosa MC (2017) Sewage sludge ash (SSA) in high performance concrete: characterization and application. Revista IBRACON de Estruturas e Mater 9(6):989–1006. https://doi.org/10.1590/s1983-41952016000600009
27. Donatello S, Cheeseman C, Tyrer M, Biggs A (2006) Sustainable construction products containing sewage sludge ash, 33
28. Kazberuk KM (2011) Application of SSA as partial replacement of aggregate in concrete. Pol J Environmen Stud 20(2):365–370
29. Lin KL, Chiang KY, Lin CY (2005) Hydration characteristics of waste sludge ash that is reused in eco-cement clinkers. Cem Concr Res 35(6):1074–1081. https://doi.org/10.1016/j.cemconres.2004.11.014
30. Halliday JE, Jones MR, Dyer TD, Ravindra KD (2012) Potential use of UK sewage sludge ash in cement-based concrete. Proc Inst Civ Eng Waste Resour Manag 165(2):57–66. https://doi.org/10.1680/warm.2012.165.2.57
31. Ryunosuke Kikuchi (2001) Recycling of municipal solid waste for cement production: Pilot-scale test for transforming incineration ash of solid waste into cement clinker. Resour Conserv Recycl 31(2):137–147. https://doi.org/10.1016/S0921-3449(00)00077-X
32. Lin KL, Lin CY (2005) Hydration characteristics of waste sludge ash utilized as raw cement material. Cem Concr Res 35(10):1999–2007. https://doi.org/10.1016/j.cemconres.2005.06.008
33. Lin DF, Lin KL, Chang WC, Luo HL, Cai MQ (2008) Improvements of nano-SiO_2 on sludge/fly ash mortar. Waste Manage 28(6):1081–1087. https://doi.org/10.1016/j.wasman.2007.03.023
34. Pinarli V, Kaymal G (1994) An innovative sludge disposal optionreuse of sludge ash by incorporation in construction materials. Environ Technol (United Kingdom) 15(9):843–852. https://doi.org/10.1080/09593339409385491
35. Baeza F, Payá J, Galao O, Saval JM, Garcés P (2014) Blending of industrial waste from different sources as partial substitution of Portland cement in pastes and mortars. Constr Build Mater 66:645–653. https://doi.org/10.1016/j.conbuildmat.2014.05.089
36. Dunuweera SP, Rajapakse RMG (2018) Cement types, composition, uses and advantages of nanocement, environmental impact on cement production, and possible solutions. Adv Mater Sci Eng. https://doi.org/10.1155/2018/4158682
37. Gamage N, Liyanage K, Fragomeni S, Setunge S (2011) Overview of different types of fly ash and their use as a building and construction material.In: international conference of structure engineering, construction and management. Retrieved from https://www.researchgate.net/publication/264707671
38. Ishwarya G, Singh B, Deshwal S, Bhattacharyya SK (2019) Effect of sodium carbonate/sodium silicate activator on the rheology, geopolymerization and strength of fly ash/slag geopolymer pastes. Cem Concr Compos 97:226–238. https://doi.org/10.1016/j.cemconcomp.2018.12.007
39. Web Of Science. (n.d.). Retrieved August 20, 2019, from https://wcs.webofknowledge.com/RA/analyze.do?product=WOS&SID=C4cj6x41hdmKFAMuz9C&field=PY_PublicationYear_PublicationYear_en&yearSort=true.

Characterization of Rheological and Mechanical Properties of Self-Compacting Concrete with Indian Standard Gradation and Particle Packing Gradations

Adithya Tantri, Adithya Shenoy, and Gopinatha Nayak

Abstract The vast compressive strength of concrete is attributed to its density, which is achieved through rigorous and thorough compaction. Compaction comes into more prominence in Self-Compacting Concrete (SCC), which gets compacted due to its own weight. Generally, aggregates are the major influential factor for concrete properties, because they exist in quantities varying from 85 to 90% of the total mix volume. This paper presents the findings of the study aimed at comparing rheological and mechanical properties of M30 SCC mix with Indian Standard aggregate gradations (IS 383:1970) and particle packing Bailey aggregate gradations. Specific objectives of the study were to assess the effects of aggregate gradation with three different Nominal Maximum Aggregate Sizes (NMAS), namely 20 mm, 16 mm and 12.5 mm. Rheological properties like Slump-flow test, T_{500} Slump-flow test, V-funnel test, L-box test, U-box test, Fill-box test were performed and all prepared concrete mixes fulfilled the requirements of the same successfully. Mechanical properties like compressive strength, split tensile strength and flexural strength were determined for all concrete mixes. Results were statistically analyzed to understand the effect of different NMAS and aggregate gradations. Findings indicate that the rheological and mechanical properties were significantly influenced by the different NMAS and aggregate gradations.

Keywords Self-compacting concrete · Particle packing · Rheological properties · Mechanical properties

A. Tantri (✉) · A. Shenoy · G. Nayak
Department of Civil Engineering, Manipal Institute of Technology, MAHE, Manipal, Karnataka 576104, India
e-mail: aditya.tantry001@gmail.com

A. Shenoy
e-mail: adi4u.vcm@gmail.com

G. Nayak
e-mail: nayak.gopinath@manipal.edu

B. B. Das et al. (eds.), *Recent Trends in Civil Engineering*, Lecture Notes in Civil Engineering 105, https://doi.org/10.1007/978-981-15-8293-6_6

1 Introduction

Historical evidences indicate that particle packing technique of aggregate blend was first introduced by Fuller and Thomson in 1907 [1], which was further developed by Andreasen and Andersen in 1930 [2], but it was not applicable for particle having size less than 250μ. In 1994, Funk and Dinger modified the equations and improved the considerable zone of particles up to 63μ [3]. These approaches form the basic classification of ideal curve mix design. Though these approaches answered the basic questions about constituents of particle packing techniques and their application limitations on concrete studies are being done to optimize the mix design. Optimization can be achieved by studying the ingredients of concrete mixes with an aim to maximize the performance of concrete. Rheological properties of concrete are characterized by workability, which is chiefly influenced by water requirement while being a function of aggregate shape, grading, orientation characteristics and volume fraction. Usually, 85–90% concrete volume is occupied by aggregates and its distribution ratio, i.e., packing density has a major role with regard to the concrete properties [4].

In 2002, a new particle packing technique based on orientation of aggregates was introduced by Mr. Robert Bailey regarding aggregate blending and gradations to achieve aggregate interlock as a stem of the structure and it is a balanced aggregate continuous gradation to complete a void-free blend. This method uses the dry rodded unit weight of aggregates from various chosen stock piles to estimate the void space between the aggregate particles, which is further filled by the finer volume fractions without disrupting the stone on stone contact of coarser particles. This Bailey aggregate grading technique provides an opportunity to develop gradation based on Nominal Maximum Aggregate Size (NMAS)-followed gradation pattern and choosing of unit weight upon bulk and rodded density [5]. So this develops an opportunity to utilize and implement on Self-Compacting Concrete (SCC) mixture where enhanced rheological properties are a major requirement.

Aggregate plays an important role in SCC to achieve the desired rheological properties through aggregate interaction and aggregates orientation factors. In India, IS 383 (1970) [6] represents the guidelines for selection of NMAS-followed gradation pattern. This gradation, although developed for conventional concrete, is utilized for SCC till date. So in this research, a comparative study between particle packing concepts based Bailey aggregate Gradation (BG) and conventionally practiced Indian Standard Gradation (ISG) has been carried out. Importance of research is to understand the influence of gradation and NMAS on rheological and mechanical properties of aggregates in SCC mixture.

2 Materials

In this experiment, natural crushed aggregates are used from three coarse and one fine aggregate stock pile as shown in Table 1. Ordinary Portland Cement of 43 Grade conforming to IS 8112 (1989) [7] was utilized (specific gravity 3.14, normal consistency 32%, initial setting time 63 min and final setting time 163 min). Class F fly ash was utilized as a filler and mineral admixture, along with a PCE-based super plasticizing chemical admixture.

2.1 Theory and Design of Bailey Gradation

Bailey gradation defines coarse aggregates as the particles, which create voids in a unit volume and fine aggregates are ones that fill these voids based on Primary Control Sieve (PCS) which differentiates between the coarse and fine fractions based on NMAS and volume of aggregate blend as represented in Eq. 1.

Table 1 Percentage passing of single sized aggregate stock piles

Sieve Size in mm	CA-1	CA-2	CA-3	FA-1
	First stockpile	Second stockpile	Third stockpile	Fourth stockpile
	% Passing	% Passing	% Passing	% Passing
25	100	100	100	100
20	95–100	100	100	100
16	82–89	82–96	100	100
12.5	55–63	66–73	85–66	100
9.5	22–25	25–32	62–78	100
4.75	0–1	16–18	12–25	95–100
2.36	0–0.5	3–6	0–1	78–93
1.18	0–0.3	1–6	0	45–89
0.6	0–0.3	1–2	0	28–70
0.3	0–0.3	0	0	15–27
0.15	0–0.1	0	0	0–11
0.075	0	0	0	0
Bulk Specific Gravity	2.652	2.634	2.639	2.621
% water Absorption	1.426	1.429	1.326	2.628
Loose Unit Weight (kg/m^3)	1214	1235	1238	1350
Rodded Unit Weight (kg/m^3)	1324	1341	1346	1356

Table 2 Control sieves of respective NMAS

Control Sieves	NMAS		
	20	16	12.5
HS	10	8	6.30
PCS	4.75	3.52	2.36
SCS	1.18	0.77	0.60
TCS	0.3	0.169	0.150

Note The control sieves of 16 mm NMAS are not available for practical aspects, so closest sieve fractions are considered for practice and interpolation procedure is followed for justification of same

$$\text{PCS} = \text{NMAS} \times 0.22 \tag{1}$$

The value of 0.22, used in the control sieve equations was determined from 2 and 3D analyses of packing of different shaped particles. Fine aggregates are further bifurcated by control sieves like Secondary Control Sieve (SCS) and Tertiary Control Sieve (TCS). The SCS is a break point of coarse sand and fine sand and it is a multiple fraction of 0.22 × PCS. Similarly, SCS = PCS × 0.22. The control sieves based on NMAS are as shown in Table 2.

The Bailey method is purely based on volumetric analysis but is represented through weights and percentage passing. Unit weight of each stock piles is to be measured in two phases as loose unit weight and rodded unit weight, because these represent aggregate orientation characteristics and void distribution patterns.

In Bailey gradation, coarse-graded fraction represents aggregate skeleton and fine-graded fraction (lesser than PCS) is the void-filling agents, and therefore load is predominantly carried by fine aggregates. Unit weight is chosen such that it lies between loose and rodded unit weights of the respective stockpiles but a relaxation of ±5% is allowed to ensure interlock. These blends are controlled through Coarse Aggregate Ratio (CA-Ratio), Fine Aggregate Coarser Ratio (F_{AC}-Ratio) and Fine Aggregate Finer Ratio (F_{AF}-Ratio). CA-Ratio represents the gradation pattern of coarse aggregates, F_{AC}-Ratio represents coarse particle distribution of fine aggregates and F_{AF}-Ratio represents fine portion distribution. CA-Ratio is a percentage passing fraction of Half Sieve (HS) & PCS, F_{AC}-Ratio is a percentage passing fraction of PCS & SCS and F_{AF} Ratio is that of SCS & TCS as per Table 3 [5].

Table 3 Recommended ranges of aggregate ratios

	NMAS		
	20	16	12.5
CA-Ratio	0.70–0.85	0.65–0.70	0.50–0.65
F_{AC}-Ratio	0.35–0.50	0.35–0.50	0.35–0.50
F_{AF}-Ratio	0.35–0.50	0.35–0.50	0.35–0.50

Table 4 Bailey gradation (BG)

BG-20		BG-16		BG-12.5	
IS sieve designation (mm)	Dense gradation	IS sieve designation (mm)	Dense gradation	IS Sieve Designation (mm)	Dense Gradation
25	100	25	–	25	–
20	98.53	20	100	20	–
16	92.97	16	94.99	16	100.00
12.5	78.89	12.5	84.99	12.5	91.85
10	57.00	10	65.36	10	78.82
4.75	29.92	4.75	42.78	4.75	37.08
2.36	16.95	2.36	24.30	2.36	15.27
1.18	10.36	1.18	14.81	1.18	9.04
0.6	6.16	0.6	8.73	0.6	5.37
0.3	3.79	0.3	5.19	0.3	3.34
0.15	2.33	0.15	3.17	0.15	2.04
0.075	0	0.075	0	0.075	0
Control sieves					
HS (mm)	10	HS (mm)	8	HS (mm)	6.3
PCS (mm)	4.75	PCS (mm)	3.52	PCS (mm)	2.36
SCS (mm)	1.18	SCS (mm)	0.77	SCS (mm)	0.6
TCS (mm)	0.3	TCS (mm)	0.169	TCS (mm)	0.15
CA-Ratio	0.63	CA-Ratio	0.65	CA-Ratio	0.65
F_{AC}-Ratio	0.35	F_{AC}-Ratio	0.35	F_{AC}-Ratio	0.35
F_{AF}-Ratio	0.37	F_{AF}-Ratio	0.35	F_{AF}-Ratio	0.38

Only such ratios that achieve the density fulfilling, these ranges can be considered as Bailey aggregate gradation. An overview of aggregate gradation process is.

- Chose a unit weight from respective coarse aggregate stock piles, kg/m^3.
- Calculate the created volume of voids by chosen coarse aggregate stock piles.
- Determine quantity of fine aggregate based on rodded unit weight for void fill, kg/m^3.
- Determine the individual volume fractions based on the density of aggregates (kg/m^3).
- Correct the quantities of both coarse and fine aggregates to maintain the desired volume fractions in the final blend.
- Determine the adjusted blend percentage of each aggregate by weight.
- Check the CA-Ratio, F_{AC}-Ratio and F_{AF}-Ratio and confirm that it will fulfill the recommended values to complete the process.

Table 4 represents the arrived Bailey gradation and CA-Ratio, F_{AC}-Ratio and F_{AF}-Ratio which successfully fulfilled the required recommended range.

2.2 Test Methods

M30 grade of self-compacting concrete was designed for NMAS 20 mm of Indian standard gradation conforming to IS 383 (1970) [6], as presented in Table 5, which is abbreviated as ISG-20 mix. Performance of ISG-20 mix is considered as control mix and other Indian standard gradations like ISG-16, ISG-12.5 are compared on the basis of control mix constituents, as presented in Table 6. Bailey aggregate gradation mixes have been indicated as BG-20, BG-16 and BG-12.5.

2.3 Rheological and Mechanical Aspects of Self-Compacting Concrete

Self-Compacting Concrete is characterized by filling ability, passing ability and resistance to segregation measured by Slump Flow, Slump $T_{500,}$ V-funnel, L-Box, U-Box and Fill-Box tests [8].

Mechanical properties of each concrete mixes are decided through three basic tests, compression strength test, split tensile strength test and flexural strength test. Concrete cubes of 150 × 150 × 150 mm, cylinders of 150 mm diameter and 300 mm height and prismatic beams of 150 mm × 150 mm × 700 mm were cast and tested at 7, 14 and 28 days age for compression, split tension and flexure, respectively, as per relevant Indian Standards [9, 10].

2.4 Results and Discussion

Table 7 represents the performance of all rheological tests, conducted as per EFNARC (2005) [8] guidelines. Results indicate that all SCC mixes succeed to fulfill the prescribed standards. It can also be seen that BG exhibits better properties than ISG mixes.

It is evident that BG mixes have more coarse aggregates than ISG mixes as seen in Tables 4 and 5. But contrary to conventional logic, they exhibit better workability than ISG mixes, as seen in Table 7. The findings reveal that increment of fine aggregate is not the only solution for the improvement of workability. The performance of the BG mixes is evidence that the choice of each coarse and fine fraction based on void-filling concepts and particle orientation aspects are influential in the rheological performance of mixes.

Table 5 Indian Standard Gradation (ISG)

IS Sieve designation (mm)	ISG-20		ISG-16		ISG-12.5	
	Recommended gradation (%)	Considered gradation (%)	Recommended gradation (%)	Considered gradation (%)	Recommended gradation (%)	Considered gradation (%)
	Coarse aggregates					
25	100	100	–	–	–	–
20	95–100	98	100	100	–	
16	–	25	90–100	97.5	100	100
12.5	–	25	–	95	90–100	95
10	25–55	25	30–70	70	40–85	59
4.75	0–10	0	0–10	0	0–10	0
Fine Aggregates (Grading Zone-3)						
4.75	90–100	95	90–100	95	90–100	95
2.36	85–100	93	85–100	93	85–100	93
1.18	75–100	88	75–100	88	75–100	88
0.6	60–79	70	60–79	70	60–79	70
0.3	12–40	26	12–40	26	12–40	26
0.15	0–10	0	0–10	0	0–10	0

Table 6 Mix proportions of self-compacting concrete

Gradation	NMAS (mm)	W/C ratio	Cement (kg/m^3)	Water (kg/m^3)	Fly Ash (kg/m^3)	W/Pratio	CA (kg/m^3)	FA (kg/m^3)	SP (%)
ISG	20	0.46	420	192	180	0.32	750	750	0.62
ISG	16	0.46	420	192	180	0.32	750	750	0.62
ISG	12.5	0.46	420	192	180	0.32	750	750	0.62
BG	20	0.46	420	192	180	0.32	1051.2	448.8	0.62
BG	16	0.46	420	192	180	0.32	858.3	641.7	0.62
BG	12.5	0.46	420	192	180	0.32	943.8	556.2	0.62

Note ISG—Indian Standard Gradation, BG—Bailey Gradation

Table 7 Rheological properties of self-compacting concrete

	Gradation						
	Indian Standard Gradation (ISG)			Bailey Gradation (BG)			Criteria
NMAS (mm)	20	16	12.5	20	16	12.5	
Slump Flow (mm)	665	671	682	673	688	700	≥520 to ≤700
Slump T_{500} (sec)	2.56	2.38	2.16	2.43	2.32	1.98	≤5
V-funnel (sec)	7.32	6.36	6.32	7.14	6.25	6.18	≤12
L-Box H2/H1 (mm)	0.71	0.76	0.82	0.81	0.85	0.93	≥0.8
U-Box H2/H1 (mm)	0.2	0	0	0	0	0	≤1
Fill-Box H2/H1 (mm)	95.64	96.92	98.75	97.90	98.35	99.08	–

Note Above mentioned results are average values of three replicates

Mechanical properties are evaluated through compressive strength, flexural strength and split tensile strength of self-compacting concrete with respect to 95% confidence interval for the mean values of three replications. Figure 1 represents the compressive strength of all SCC mixes, which are succeed to gain more than 33 MPa at 28 days. Upon comparison of NMAS like 20 mm, 16 mm and 12.5 mm followed gradation mixes, compression strength for NMAS of 12.5 mm followed gradation mixes of both ISG and BG gradation mixes is higher as compared with higher NMAS. Comparison of gradation parameter of BG mixes and ISG mixes shows that compressive strength is higher for BG mixes at 7, 14 and 28 days. Even interval plot represents that the least variation in strength is for BG mixes, especially

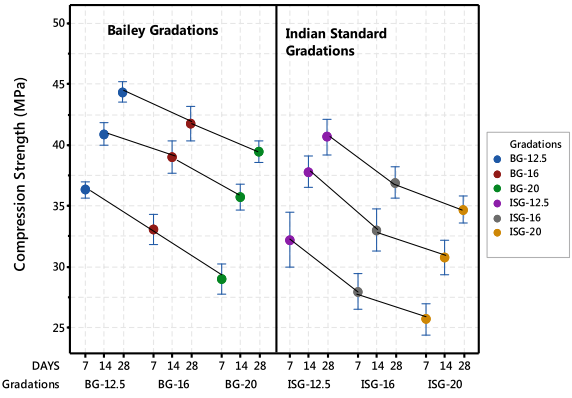

Fig. 1 Interval plot of compressive strength

at 28 days as compared with ISG mixes. Overall highest strength of about 44.74 MPa at 28 days is achieved by BG-12.5 mix as compared with all other SCC mixes.

Through this study, it has been revealed that flexural strength of concrete as a material depends on packing and volume fractions of aggregate as represented in Fig. 2. It was found that flexural strength represented by NMAS of 12.5 mm gradation mixes at 7, 14 and 28 days are the highest among all mixes. It is observed that BG performs better than ISG mixes in flexure irrespective of NMAS.

Split tensile strength is an indicator of interaction in terms of bonding and particle packing efficiency. In this study, it was found that there is no considerable difference of tensile strength observed in ISG-12.5, ISG-16 and ISG-20 mixes at 7, 14, 28 days as in Fig. 3, and all the mixes succeed to get more than 4 MPa at 28 days. It can be noted that tensile strength is a function of the NMAS of aggregates and larger NMAS yielded better tensile strength. It can also be noted that BG mixes had enhanced performance as compared with ISG mixes, which indicates better bonding and particle packing efficiency.

In this research, statistical analysis was carried out using a general linear model with 95% confidence interval (CI) to understand the influence of Gradation (Gd)

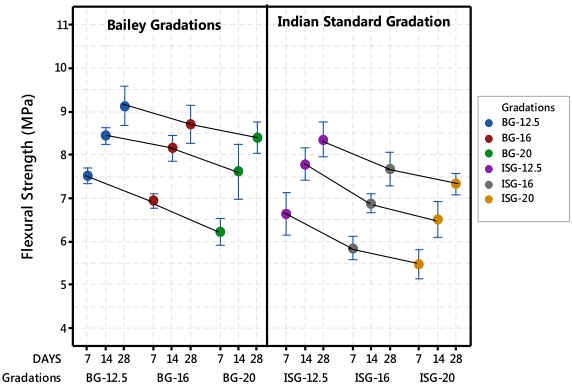

Fig. 2 Interval plot of flexural strength

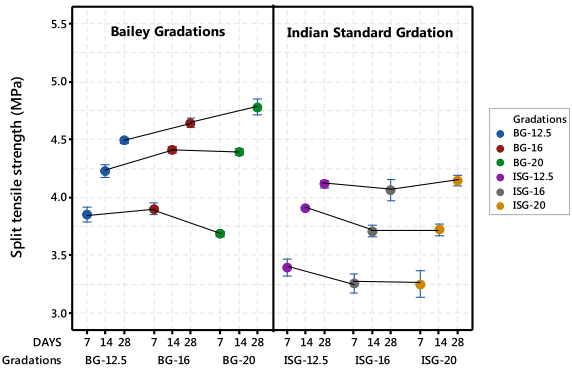

Fig. 3 Interval plot of split tensile strength

Table 8 General linear model results of workability and mechanical properties of self-compacting concrete

RF	Slump flow					Slump T_{500}			
Source	DF	SS	MS	F-value	P-value	SS	MS	F-value	P-value
NMAS	2	1965.44	982.72	47.55	0.000	0.71534	0.35767	128.76	0.000
Gd	1	1283.56	1283.56	62.11	0.000	0.07867	0.07867	28.32	0.000
NMAS*Gd	2	17.44	8.72	0.42	0.665*	0.04861	0.02431	8.75	0.005
Error	12	248.00	20.67	–	–	0.03333	0.00278	–	–
Total	17	3514.44	–	–	–	0.87596	–	–	–

and Nominal Maximum Aggregate Size (NMAS) on rheological and mechanical properties of SCC. In this, primary variables are NMAS, Gd and the interaction of NMAS*Gd. These variables influence rheological and mechanical properties of mixture, which are statistically analyzed and results are presented in Table 8. It is found that all rheological properties and mechanical properties are significantly influenced by gradation and NMAS with regard to all mixes. But interaction effect of NMAS*Gd is insignificant to rheological and mechanical properties excluding the slump T_{500} test property.

RF	V-funnel			
Source	SS	MS	F-value	P-value
NMAS	3.77774	1.88887	839.50	0.000
Gd	0.08681	0.08681	38.58	0.000
NMAS*Gd	0.00781	0.00391	1.74	0.218*
Error	0.02700	0.00225	–	–
Total	3.89936	–	–	–

RF	L-Box					Fill-Box			
Source	DF	SS	MS	F-value	P-value	SS	MS	F-value	P-value
NMAS	2	0.079233	0.039617	33.17	0.000	13.9580	6.9790	19.63	0.000
Gd	1	0.0450000	0.045000	37.67	0.000	8.0267	8.0267	22.58	0.000
NMAS*Gd	2	0.007633	0.003817	3.20	0.077*	2.8220	1.4110	3.97	0.048*
Error	12	0.014333	0.001194	–	–	4.2663	0.3555	–	–
Total	17	0.146200	–	–	–	29.0730		–	–

RF	Compression Strength					Flexural Strength			
Source	DF	SS	MS	F	P	SS	MS	F	P
NMAS	2	89.862	44.931	194.18	0.000	2.4005	1.2027	49.00	0.000
Gd	1	88.711	88.711	383.38	0.000	4.1280	4.1280	168.19	0.000
NMAS*Gd	2	1.255	0.628	2.71	0.107*	0.0797	0.0399	1.62	0.237*
Error	12	2.777	0.231	–	–	0.2945	0.0245	–	–
Total	17	182.606	–	–	–	6.9078	–	–	–

RF	Split tensile strength			
Source	SS	MS	F	P
NMAS	0.08206	0.04103	88.73	0.000
Gd	1.27627	1.27627	2604.63	0.000
NMAS*Gd	0.05561	0.02780	56.74	0.000
Error	0.00588	0.00049	–	–
Total	1.41981	–	–	–

Note F-Value-F-statistic from the adjusted means squares (MS), DF-degrees of freedom
*Not significant.

3 Conclusions

1. It is found that NMAS and gradations affect rheology and mechanical performance of all mixes, with BG-12.5 showing superior performance in most areas.
2. It is found that split tensile strength is significantly influenced by interaction of NMAS and gradation, and BG-20 mix performed better than all other mixes.
3. In the view of overall rheological and mechanical performances, BG-16 mix is preferred for SCC in real-time practice and this study revealed that choosing of aggregate particle fraction for the SCC mix has a significant impact on its rheological and mechanical properties.
4. Gradation comparison revealed that Bailey Gradation (BG) represents superior performance than ISG mixes with regard to all rheological and mechanical properties and hence BG is recommended for real-time practice.

References

1. Fuller WB, Sanford ET (1907) The laws of proportioning concrete (1907): 67–143
2. Andreasen AHM, Andersen J (1930) Relation between grain size and interstitial space in products of unconsolidated granules. Kolloid-Zeitschrift 50.3 (1930): 217–228.
3. Funk JE, Dennis RD (2013) Predictive process control of crowded particulate suspensions: applied to ceramic manufacturing. Springer Science & Business Media
4. Cook MD, Tyler Ley M, Ghaeezadah A (2016) Effects of aggregate concepts on the workability of slip-formed concrete. J Mater Civil Eng 28(10)
5. Vivek SS, Dhinakaran G (2017) Fresh and hardened properties of binary blend high strength self compacting concrete. Eng Sci Technol Int J 20(3):1173–1179
6. IS 383 (1970) Specification for coarse and fine aggregates from natural sources for concrete. Bureau of Indian Standards, New Delhi
7. IS: 8112 (1989) Indian Standard 43 Grade Ordinary Portland Cement—Specification. Bureau of Indian Standards, New Delhi

8. Bibm C, Ermco E (2005) EFNARC. The European Guidelines for Self-Compacting Concrete, Specification, Production and Use
9. IS: 516–1959 (2004) Indian Standard Methods for Test on Concrete. Bureau of Indian Standards, New Delhi
10. IS 5816–1999 Indian Standard Splitting Tensile Strength of Concrete-Method of Test

A Review on Properties of Sustainable Concrete Using Iron and Steel Slag Aggregate as Replacement for Natural Aggregate

Jagadisha, K. Balakrishna Rao, Gopinatha Nayak, and B. Adithya Shenoy

Abstract Generation of industrial byproducts has significantly increased due to the tremendous growth in industrialization. One such industrial waste is steel slag, which is a solid effluent of the steel manufacturing industry. India generates about 12MT of slag annually. However, steel slag is not utilized properly, which leads to severe environmental problems such as groundwater pollution, landfilling issues, etc. Slag is a dense material that is used as an alternative green material and is easily implementable in concrete. The variants in the slag are BF slag (BF), BOF slag (BOF), electrical arc furnace slag (EAF), and others. In last decade, many attempts were made to utilize the slag waste in construction industry, viz., in production of cement, railway, and road aggregate. Recently, researchers have successfully used steel slag as aggregate from various sources in the production of concrete. This review focuses on analyzing the properties of steel slag procured from various sources to understand the effect that it has on the properties of concrete, particularly in its fresh and hardened state while shedding light on the durability aspects. The paper also aims to determine the characteristics for advanced concrete types such as High Performance Concrete, Self-Compacting Concrete and Geopolymer Concrete. The study will help in providing a better understanding of the behavior of iron and steel slag aggregates in concrete and enable the efficient use of the same, reducing the consumption of natural aggregates.

Keywords Steel slag · Utilization · BF slag · BOF slag

Jagadisha (✉) · K. Balakrishna Rao · G. Nayak · B. Adithya Shenoy
Department of Civil Engineering, Manipal Institute of Technology Karnataka, MAHE, Manipal, Karnataka 576104, India
e-mail: jagadisha.achar@learner.manipal.edu

K. Balakrishna Rao
e-mail: kb.rao@manipal.edu

G. Nayak
e-mail: nayak.gopinath@manipal.edu

B. Adithya Shenoy
e-mail: adi4u.vcm@gmail.com

B. B. Das et al. (eds.), *Recent Trends in Civil Engineering*, Lecture Notes in Civil Engineering 105, https://doi.org/10.1007/978-981-15-8293-6_7

1 Introduction

The use of any natural resources in industrial units gives rise to byproducts and waste, and there is no such system that can function without generating waste. The minimization of the waste by finding supplementary use has been a challenge since the industrial revolution. In the manufacture of steel from raw ore using BF, BOF and EAF, the generated wastes have been identified as various forms of coke, slag, sludge, ash and dust. These are dumped and cause severe secondary problems like dust, soil pollution and water contamination by leaching as well as scarcity of dumping lands. An estimated 1.2 tons of solid waste is generated for every 1 ton of steel produced in India. Compared with around 0.55 tons abroad, this vast difference is attributed to inferior raw materials and an absence of proper solid waste management practices. Of these, 63% is being disposed. This can be reintroduced to reduce the waste [44]. India is the fourth largest steel producing nation with 81MT, which causes a proportionately large quantum of waste. Electrical arc furnace slag from steel industry byproduct can be utilized as inert filler material in construction production due to similar performance like natural aggregate, which boosts the sustainability of concrete [2, 17].

Iron and steel manufacturing industries generate slag in three different forms as below:

(i) Iron-making slag (BF slag-BFS).
(ii) Steel furnace slag: BOF(BOF) Slag, Electrical arc furnace (EAF) Slag and Ladle-furnace-slag: (LFS) [42].

Iron making slag is obtained during iron extraction and is rich in limestone or dolomite, which is a feedstock in steel making. BOF (BOF) slag, which is generated during steel manufacture, is added with oxygen and SiO_2 to improve volume solidity and then crushed and sieved to the required specifications. EAF (EAF) slag is a dense, strong material formed during steel manufacture in the EAF. The byproduct of carbon steel manufacture is a steel scrap from the nonalloyed input materials, referred to as EAF C-slag. Stainless steel manufacture gives rise to EAF S-Slag, due to the low or high alloyed manufacturing inputs. Ladle furnace slag (LFS) or secondary refining slag (SRS) is generated during the auxiliary metallurgy method and has a high limestone content, due to which it is extensively used in cement production.

Of the above, EAF C-slag, with the appropriate conditioning, crushing and grading, is suitable for the use as coarse aggregate in concrete [18]. The porous nature of the slag causes dimensional instability and has to be compensated to enable its implementation in concrete. Additionally, the composition of this slag also contains expansive components, as observed during previous use of LD converter steel-making slag (BOF) or Siemens–Martin furnace slag [26].

This technical article reviews the use of various steel slag aggregates from different sources around the world. Few general review articles are available on steel slag aggregate and its use in multiple applications, viz., use in agriculture, production of fertilizer, construction of pavements as road aggregates, production of cement, binder

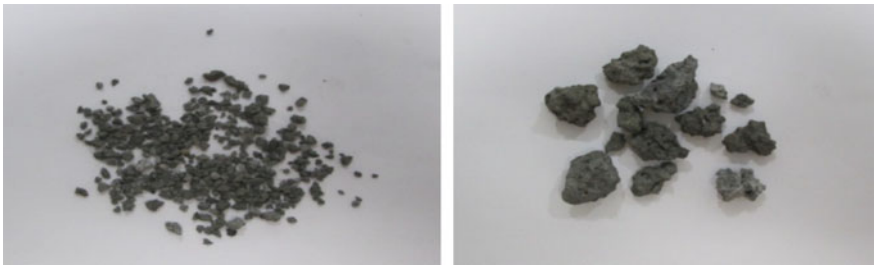

Fine Steel Slag aggregate Coarse steel slag aggregate

Fig. 1 Image of steel slag aggregate [43]

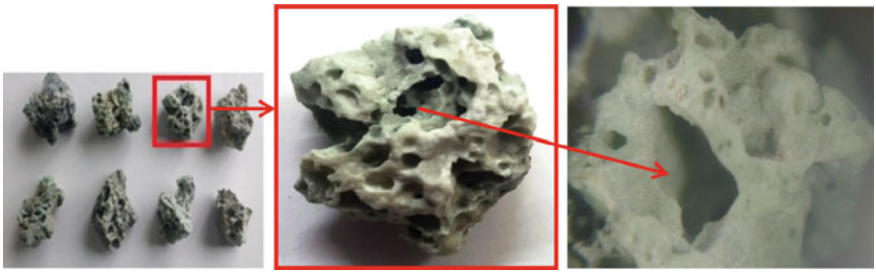

Fig. 2 EAF aggregate and its microscopic view showing pores [36]

in concrete production, aggregate in manufacturing of concrete, etc. The aim of this paper is to highlight the importance of steel slag aggregate in construction industry to reduce the exhaustion of natural assets, thereby producing an environmentally friendly concrete. The paper mainly concentrates on the different forms of steel slag as aggregates in concrete, their physical characteristics of various concrete and chemical characteristics, influence of these aggregates on fresh, mechanical, hardened and durability (Figs. 1, 2 and Table 1).

2 Physical and Chemical Properties of Steel and Iron Byproducts

BOF slag usually angular surface materials, dark color due to high iron content. The specific surface gravity of BOF is usually 30% more than traditional concrete aggregate. It has low crushing value and comparatively porous in structure [1, 30]. BOF has higher content of MgO and CaO due to high fluxes materials to reduce impurities [42]. On the other side compared to BOF slag, EAF slag has been utilized successfully as concrete aggregate in various concrete and it is different compared with BOF slag with lesser MgO and CaO [15]. LF is little different from EAF and

Table 1 Application of steel slag according to its characteristics [14]

Sl. No.	Application	Characteristics
1	Wastewater treatment	Porous, alkaline
2	Aggregates for road and hydraulic construction	Hard, wear-resistant, adhesive, rough
3	Fluxing agent	CaO, MgO, FeO, MgO, MnO components
4	Iron reclamation	FeO_x, Fe components
5	Fertilizer and soil improvement	Fertilizer components (CaO, SiO2, MgO, FeO)
6	Raw material for cement clinker	FeO, CaO, SiO_2 Components
7	CO_2 capture and flue gas desulfurization	CaO, MgO components FeO,
8	Cement and concrete production	Cementitious components (C_3S, C_2S and C_4AF) Cement

BOF with higher content of CaO, i.e., 44.5 and 58.4% [20]. Therefore, it is mainly being used for cement manufacturing and as binder in concrete production rather than substitution for traditional aggregate (Tables 2 and 3).

Table 2 Physical properties of steel slag aggregate

References	Various properties				
	Type	Specific Gravity	Apparent specific gravity (kg/m^3)	Water absorption (%)	Los angeles abrasion (%)
[8]	Medium (2 mm/Coarse 22.4 mm EAF)	–	3640/3970	0.18/0.45	<20
[22]	Aggregate	–	3300–3600		
[21]	Coarse aggregate		3560	1.5	–
[1]	4–20 mm	2.8	–	2.6	23
[26]	EAF aggregate FA and CA	–	3500	0.3–0.9	15–20
[31]	4–22.4 mm	–	2734	0.75	18
[32]	20 mm	3.19	–	0.8	17
[36]	20 mm	2.604	994–1082	0.61	53.7
[43]	Coarse steel	3.51	3268	2.95	–
[43]	Fine steel	3.57	3447	1.31	–

Table 3 Chemical properties of various steels slag aggregate

References	Percentage of oxides												
	CaO	SiO_2	Al_2O_3	MgO	FeO	Fe_2O_3	Fe total	SO_3	MnO	TiO_2	P_2O_5	Free CaO	Free MgO
[8]	24.2-29.5	10.1-14.7	5.7-7.2	1.9-4.6	37.2-44.8	-	-	-	5.1-5.7	-	-	-	-
[22]	60.48	21.44	5.95	3.12	-	-	18	2.12	0.01	$0.87(P_2O_5+TiO_2+Na_2O+K_2O)$ $0.87(P_2O_5+TiO_2+Na_2O+K_2O)$		-	-
[21]	29.99	17.31	4.67	5.39	-	27.33	-	-	5.03	0.78	1.08	-	-
[28]	42.42	11.04	0.42	88.52	-	0.26	-	0.61	-	-	-	8.36/42.42	-
[1]	41.7	34.7	6.3	9.1	0.5	-	-	-	2.1	2.2	-	-	-
[39] BOF1,2,3	35.1-40.6	12.7-18.1	2.4-3.0	8.8-11.3	21.5-28.1	-	-	0.08-0.12	4.0-4.5	-	0.51-0.74	-	-
[26]	25	11	5	5	25	25	-	-	4	-	-	2	-
[31]	27.70	16.61	10.99	4.02	-	-	33.75	-	4.67	-	-	-	-
[32]	29.7	15.5	4.7	6.6	-	37.0	-	0.3	2.9	-	0.4	-	-
[36]	51.43	15.62	18.89	3.89	-	3.75	-	3.12	0.45	0.52	1.42	-	-
[7]	11.0	9.3	2.3	12.7	26.2	-	-	0.1	1.8	0.3	0.3	3.4	2.2
[7]	18.8	9.6	3.9	8.5	23.9	-	-	0.1	3.5pl	0.5	0.2	0.1	0.2
[7]	27.1	1.0	7.1	9.5	25.7	-	-	0.2	1.9	0.4	0.2	0.4	0.3

3 Workability of Concrete Containing Steel Slag Aggregate

Various publications indicate considerable losses in the slump (15–67%) and workability of steel slag incorporation in concrete. The losses occur during the inclusion of slag in both fine and coarse aggregates. The losses are due to the high porosity of the aggregates that lead to higher water absorption. To achieve a constant amount of workability, steel slag aggregates require higher water content and higher water binder ratios [38]. Furthermore, it was also concluded that the consistency in quality of material and its processing play a pivotal role in achieving better workability [33, 38, 43].

4 Density of Steel Slag Aggregate Concrete

The fresh density of steel slag aggregate concrete has been reported to be between 2255 kg/m^3 and 2698 kg/m^3. The density based on the hardening age like 3, 7, 28 days has also been measured and the collective observation was that at all ages, there is an increase of density. Furthermore, it can be observed that concrete becomes denser with an increase of aggregate replacement ratios with densities increasing up to 28.1% in complete replacements. The increase in the density has been attributed to the higher specific gravity of these aggregates as compared with conventional natural aggregates [8, 27, 32, 34, 35, 40, 43].

5 Mechanical Properties of Various Steel Slag Aggregate Concrete

5.1 Effect of Steel Slag Aggregate on Compressive Strength of Concrete

Compressive strength of concrete with EAF slag coarse aggregates was determined and found that there was 30.1% improvement for a 28-day curing period. Also, 7, 28 and 74 days testing revealed similar trends [8]. Another study was both coarse and fine aggregates completely replaced by steel slag aggregates and observed an increase in compressive strength by 31.3% and an insignificant loss in flexural strength by 2.1% [22]. An attempt was done to optimize the replacement of steel slag as both coarse and fine aggregates based on compressive strength and arrived at a conclusion that the most favorable replacement dosage of fine and coarse aggregate is 40 and 30%, respectively, as strength dropped for higher replacements [38]. M30 grade concrete mix designed with construction demolition waste as fine aggregates and steel slag as coarse aggregates wherein the compressive strength performance improved by 15.6%

when steel aggregate was replaced by normal coarse aggregate [4]. An experimental study was taken up to determine the utilization of stainless steel oxidizing slag to produce self-compacting concrete. The 28-day compressive strength of 100 and 50% SSOS concrete was about 4 and 8% higher than the control concrete [37]. Authors successfully implemented EAF slag in concrete up to 40% partial replacement to achieve 25% strength gain [35]. The compressive strength of normal strength concrete was 8.1% higher than the control concrete at 20% steel slag aggregate replaced to fine aggregate and strength gradually decreased till 80% replacement. Further, strength was at its peak 12.3% when fine aggregate replaced at 80% [12]. Authors carried out the experimental assessment of influence of utilization of steel industry slag as aggregate. Coarse aggregates were replaced in various percentages and the 28-day strength gain was 33% for the optimum replacement of 50%, beyond which there was a considerable drop in the strength [36].

5.2 Tensile Strength, Flexural Strength and Modulus of Elasticity of Steel Slag Aggregate Concrete

Mechanical properties were enhanced compared with conventional aggregate concrete. Split tensile strength increased by 22.6% and modulus of elasticity also increased by 7.1% [4]. Concrete mixes designed with EAF slag as coarse aggregates with various dosages and found that split tensile strength and flexural strength improved with improved dosage, with 21.4 and 20.68% gain at the maximum dosage of 25% [23]. Elastic modulus of EAF aggregate concrete improved by 6.8% as compared to standard concrete mixes [35]. Specimens incorporating crystalline slag with GGBS and silica fume exhibited improved modulus of rupture by around 34% and 18%, respectively [6]. Flexural strength of steel slag aggregate concrete optimized at 50% with an increase of 9.8% after 28 days of curing [36].

5.2.1 Durability of Steel Aggregate Concrete

Control lime stone concrete lost strength compared with CEAF steel slag concrete under freeze/thaw test. CEAF concrete was more stable after exposing to higher humidity and temperature than control concrete. Slag mortar has less expansion than reference mix in case of sulfate attack test. Expansion after the alkali-aggregate reaction did not exceed the limit. Performance of CEAF concrete was inferior to the control concrete after exposed to sea tides, chloride penetration and corrosion of steel rebars [5]. The performance of concrete investigated, which consisting of oxidizing EAF slag as coarse and fine aggregate. Durability properties such as soundness, leaching test and accelerated aging of EAF aggregate concrete were acceptable. But lime flakes were observed on the surface in slag aggregate after accelerated aging test. EAF slag concrete enhances the strength while sacrificing durability slightly. The

porosity of slag aggregates triggers increased effects of freeze–thaw cycles and other durability problems. The cloistering effect combined with the toxic products of slag mandate the leaching test of all slag incorporated concrete [18, 26]. The effects of EAF slag aggregate replacement were investigated and concluded that although there is good strength exhibited, the free oxides present and the aggregate-paste interface porosity caused durability concerns. Although air entrainment is a solution for the freeze–thaw action, the material is still vulnerable to wetting and drying cycles [8]. The performance of concrete produced using EAF slag aggregate. EAF slag has high crystalline structure that leads to less hydraulic reactivity and dimensional stability [33]. EAF gives high density, better strength and the durability properties were better with addition of fly ash and micro silica. The durability of stainless steel oxidizing slag concrete increases because of increases CH content after hydration and stated that the optimum replacement reported was 100% [41]. Steel slag aggregate concrete exhibited higher shrinkage due to the presence of CaO and MgO, which also expand up to 0.8% during hydration, leading to durability concerns. It was recommended not to use steel aggregate with high free CaO without pretreatment [3]. Concrete with GGBS as fine aggregates in concrete under marine environment studies conducted and observed that there was strength loss when curing was in a marine environment, which was up to 11.2% in the various mixes [11]. The chelating and attrition processes reduced the reactive CaO, enhancing the properties of concrete, minimizing the associated issues of waste dumping as well as procurement and implementation of natural resources [9].

6 Performance in Geopolymer Concrete and Geopolymer SCC

The performance of steel slag aggregates as fine and coarse aggregates in SCC was observed to have sufficient strength. The higher density and porous nature of the aggregates led to workability loss and higher water demand, as evidenced by various researchers in T-5, L-box, Slump Flow and V-Funnel tests, among others. Under controlled dosages, the loss of workability was within acceptable limits. More than 50% replacement of steel slag reduces workability and demands more cement and mineral admixture in SCC to compensate the same [10, 13, 16, 25, 34]. The use of EAF slag in Geopolymer or alkali-activated concrete showed a slight decrease in strength and durability characteristics, but better performance in ecological studies. The porous and rough nature of the surface combined with the density and free CaO have been attributed to better reactivity and ITZ formation. Authors were successful to design alkali-activated/Geopolymer high performance concrete using GGBS as mineral admixtures [6, 19, 24, 29]. SEM test revealed dense microstructure and ITZ which exhibited better mechanical and durability properties of alkali-activated HPC [24].

7 Conclusion

The replacement of natural/traditional aggregate by steel waste slag aggregate is one initiative toward greening the concrete industry. EAF slag is more suitable for aggregate replacement compared to other forms of steel by product since it has lesser free CaO and MgO. LF slag is more suitable as binder material. Density of steel slag aggregate increases the self-weight of concrete by 10%. Therefore, special attention is required to design suitable workability without segregation and also to adopt in structural concrete. Workability of steel slag aggregate concrete reduces compared to natural aggregate due to its surface characteristics and angular shape. However, it can be managed with suitable chemical admixture. Compressive strength of concrete improves when 30–50% of the aggregates are replaced as evident from a majority of the reported studies. Tensile strength, flexural strength and modulus of elasticity have been found to improve with steel slag aggregates attributed to the surface characteristics, which improve bond between aggregate and paste. Very few studies are available in order to ascertain the effect of free oxide contents of steel slag aggregate. In general with proper gradation, careful inspection and adequate weathering/treatment steel slag aggregate can be successfully used to manufacture required fresh, hardened and durable concrete by substituting natural resources.

References

1. Adegoloye G, Beaucour AL, Ortola S, Noumowé A (2015a) Concretes made of EAF slag and AOD slag aggregates from stainless steel process: Mechanical properties and durability. Constr Build Mater 76:313–321. https://doi.org/10.1016/j.conbuildmat.2014.12.007
2. Adegoloye G, Beaucour A, Ortola S, Noumowé A (2015b) Concretes made of EAF slag and AOD slag aggregates from stainless steel process : Mechanical properties and durability. Construct Build Mater 76:313–321. https://doi.org/10.1016/j.conbuildmat.2014.12.007
3. Alexander, Roesler JR (2015) Steel furnace slag aggregate expansion and hardened concrete properties. Cement Concrete Compos 60:1–9. https://doi.org/10.1016/j.cemconcomp.2015.04.006
4. Anastasiou, Georgiadis Filikas K, Stefanidou M (2014) Utilization of fine recycled aggregates in concrete with fly ash and steel slag. Construct Build Mater 50:154–161. https://doi.org/10.1016/j.conbuildmat.2013.09.037
5. Arribas I, Vegas I, San-josé JT, Manso JM (2014) Durability studies on steelmaking slag concretes. Mater Des 63:168–176. https://doi.org/10.1016/j.matdes.2014.06.002
6. Biskri Y, Achoura D, Chelghoum N, Mouret M (2017) Mechanical and durability characteristics of high performance concrete containing steel slag and crystalized slag as aggregates. Constr Build Mater 150:167–178. https://doi.org/10.1016/j.conbuildmat.2017.05.083
7. Brand AS, Roesler JR (2018) Interfacial transition zone of cement composites with steel furnace slag aggregates. Cement Concr Compos 86:117–129. https://doi.org/10.1016/j.cemconcomp.2017.11.012
8. Carlo, Gaddo V (2009) Mechanical and durability characteristics of concrete containing EAF slag as aggregate. Cement Concrete Compos 31(9):663–671. https://doi.org/10.1016/j.cemconcomp.2009.05.006

9. Ding Y, Cheng T, Liu P, Lee W (2017) Study on the treatment of BOF slag to replace fine aggregate in concrete. Constr Build Mater 146:644–651. https://doi.org/10.1016/j.conbuildmat.2017.04.164
10. Eleftherios, Papayianni I, Papachristoforou M (2014) Behavior of self compacting concrete containing ladle furnace slag and steel fiber reinforcement. Mater Design 59:454–460. https://doi.org/10.1016/j.matdes.2014.03.030
11. Gaurav, Das S, Ahmed AA, Saha S, Karmakar S (2015) Study of granulated blast furnace slag as fine aggregates in concrete for sustainable infrastructure. Procedia Soc Behav Sci 195:2272–2279. https://doi.org/10.1016/j.jhazmat.2017.04.013
12. Guo Y, Xie J, Zhao J, Zuo K (2019) Utilization of unprocessed steel slag as fine aggregate in normal- and high-strength concrete. Constr Build Mater 204:41–49. https://doi.org/10.1016/j.conbuildmat.2019.01.178
13. Gurpreet, Siddique R (2016) Effect of iron slag as partial replacement of fine aggregates on the durability characteristics of self-compacting concrete. Construct Build Mater 128:88–95. https://doi.org/10.1016/j.conbuildmat.2016.10.074
14. Huang, Xu G, Cheng H, Wang J, Wan Y, Chen H (2012) An overview of utilization of steel slag. Proced Environ Sci 16:791–801. https://doi.org/10.1016/j.proenv.2012.10.108
15. Jiang, Ling TC, Shi C, Pan SY (2018) Characteristics of steel slags and their use in cement and concrete—a review. Res Conserv Recycl 136:187–197. https://doi.org/10.1016/j.resconrec.2018.04.023
16. Joao, Tristão FA, Giacometti M, Meneguelli M, Moratti M, Teixeira JESL (2013) Effects of BOF steel slag and other cementitious materials on the rheological properties of self-compacting cement pastes. Construct Build Mater 40:1046–1053. https://doi.org/10.1016/j.conbuildmat.2012.11.039
17. Jose, San-JoseInigo Vegas Idoia I (2014) The performance of steel-making slag concretes in the hardened state. Mater Des 60:612–619. https://doi.org/10.1016/j.matdes.2014.04.030
18. Juan, Polanco JA, Losañez M, González JJ (2006) Durability of concrete made with EAF slag as aggregate. Cement Concrete Compos 28(6):528–534. https://doi.org/10.1016/j.cemconcomp.2006.02.008
19. Khan, Castel A, Akbarnezhad A, Foster SJ, Smith M (2016) Utilisation of steel furnace slag coarse aggregate in a low calcium fly ash geopolymer concrete. Cement Concrete Res 89:220–229. https://doi.org/10.1016/j.cemconres.2016.09.001
20. Kriskova L, Pontikes Y, Cizer Ö, Mertens G, Veulemans W, Geysen D, Blanpain B (2012) Effect of mechanical activation on the hydraulic properties of stainless steel slags. Cem Concr Res 42(6):778–788. https://doi.org/10.1016/j.cemconres.2012.02.016
21. Lim JS, Cheah CB, Ramli MB (2019) The setting behavior, mechanical properties and drying shrinkage of ternary blended concrete containing granite quarry dust and processed steel slag aggregate. Constr Build Mater 215:447–461. https://doi.org/10.1016/j.conbuildmat.2019.04.162
22. Liu, Zha K, Chen D (2011) Possibility of concrete prepared with steel slag as fine and coarse aggregates: a preliminary study. Procedia Eng 24:412–416. https://doi.org/10.1016/j.proeng.2011.11.2667
23. Luigi, Buoso A, Coffetti D, Kara P, Lorenzi S (2016) Electric arc furnace granulated slag for sustainable concrete. Construct Build Mater 123:115–119. https://doi.org/10.1016/j.conbuildmat.2016.06.142
24. Manjunath, Narasimhan MC (2018) An experimental investigation on self-compacting alkali activated slag concrete mixes. J Build Eng 17:1–12. https://doi.org/10.1016/j.jobe.2018.01.009
25. Manjunath, Narasimhan MC, Umesh KM, Shivam K, Bala Bharathi UK (2019) Studies on development of high performance, self-compacting alkali activated slag concrete mixes using industrial wastes. Construct Build Mater 198:133–147. https://doi.org/10.1016/j.conbuildmat.2018.11.242
26. Manso JM, Gonzalez JJ, Polanco JA (2004) Electric arc furnace slag in concrete. J Mater Civ Eng 16(6):639–645. https://doi.org/10.1061/(asce)0899-1561(2004)16:6(639)

27. Maslehuddin, Sharif AM, Shameem M, Ibrahim M, Barry MS (2003) Comparison of properties of steel slag and crushed limestone aggregate concretes. Construct Build Mater 17(2):105–112. https://doi.org/10.1016/S0950-0618(02)00095-8
28. Mo L, Zhang F, Deng M, Jin F, Al-Tabbaa A, Wang A (2017) Accelerated carbonation and performance of concrete made with steel slag as binding materials and aggregates. Cement Concr Compos 83:138–145. https://doi.org/10.1016/j.cemconcomp.2017.07.018
29. Nitendra, Ravi Shankar AU, Mithun BM (2016) Durability studies on eco-friendly concrete mixes incorporating steel slag as coarse aggregates. J Clean Prod 129:437–448. https://doi.org/10.1016/j.jclepro.2016.04.033
30. Pang B, Zhou Z, Xu H (2015) Utilization of carbonated and granulated steel slag aggregate in concrete. Constr Build Mater 84:454–467. https://doi.org/10.1016/j.conbuildmat.2015.03.008
31. Pellegrino C, Faleschini F (2013) Experimental behavior of reinforced concrete beams with electric arc furnace slag as recycled aggregate. ACI Mater J 110(2):197–205. https://doi.org/10.14359/51685534
32. Qasrawi H (2018) Fresh properties of green SCC made with recycled steel slag coarse aggregate under normal and hot weather. J Clean Prod 204:980–991. https://doi.org/10.1016/j.jclepro.2018.09.075
33. Samir, El-Dieb AS, Bedir MS (2012) Performance of concrete mixtures made with electric arc furnace (EAF) steel slag aggregate produced in the Arabian Gulf region. Construct Build Mater 34:249–256. https://doi.org/10.1016/j.conbuildmat.2012.02.012
34. Santamaria, Orbe A, Losañez MM, Skaf M, Ortega-Lopez V, González JJ (2017) Self-compacting concrete incorporating electric arc-furnace steelmaking slag as aggregate. Mater Des 115:179–193. https://doi.org/10.1016/j.matdes.2016.11.048
35. Saveria, Ruello ML, Sani D (2016) Electric arc furnace slag as natural aggregate replacement in concrete production. Cement Concr Compos 66:66–72. https://doi.org/10.1016/j.cemconcomp.2015.10.004
36. Saxena S, Tembhurkar AR (2018) Impact of use of steel slag as coarse aggregate and wastewater on fresh and hardened properties of concrete. Constr Build Mater 165:126–137. https://doi.org/10.1016/j.conbuildmat.2018.01.030
37. Sheen Y, Le D, Sun T (2015) Innovative usages of stainless steel slags in developing self-compacting concrete. Construct Build Mater 101:268–276. https://doi.org/10.1016/j.conbuildmat.2015.10.079
38. Subathra Devi, Gnanavel BK (2014) Properties of concrete manufactured using steel slag. Procedia Engineering 97:95–104. https://doi.org/10.1016/j.proeng.2014.12.229
39. Wang G (2010) Determination of the expansion force of coarse steel slag aggregate. Constr Build Mater 24(10):1961–1966. https://doi.org/10.1016/j.conbuildmat.2010.04.004
40. Yeong, Le DH, Sun TH (2015) Innovative usages of stainless steel slags in developing self-compacting concrete. Construct Build Mater 101:268–276. https://doi.org/10.1016/j.conbuildmat.2015.10.079
41. Yeong, Sun TH (2014) Properties of green concrete containing stainless steel oxidizing slag resource materials. Constr Build Mater 50:22–27. https://doi.org/10.1016/j.conbuildmat.2013.09.017
42. Yildirim IZ, Prezzi M (2011) Chemical, mineralogical, and morphological properties of steel slag. Adv Civil Eng. https://doi.org/10.1155/2011/463638
44. Yüksel İ (2017) A review of steel slag usage in construction industry for sustainable development. Environ Dev Sustain 19(2):369–384. https://doi.org/10.1007/s10668-016-9759-x
43. Yu X, Tao Z, Song T, Pan Z (2016) Performance of concrete made with steel slag and waste glass. Constr Build Mater 114:737–746. https://doi.org/10.1016/j.conbuildmat.2016.03.217

Review of Low to High Strength Alkali-Activated and Geopolymer Concrete

Muralidhar V. Kamath, Shreelaxmi Prashanth, and Mithesh Kumar

Abstract Popular building material has always been improving in the lines of material science developments. In this paper, the no use of Ordinary Portland Cement concrete studied, viz., fly ash-, slag- and meta-kaolin-based concrete, etc., from low to high strengths has been presented. Presently, all researchers and construction industries are working on using waste and energy-efficient material to develop sustainable concrete. This article presents the effects of various variables on the slump properties and mechanical properties, specifically to compressive strength. Recent study results indicated the alkali-activated and geopolymer binders have strong potential to replace conventional binders to a greater extent. Application of this environmentally friendly concrete may be an appropriate alternative to traditional concrete.

Keywords Cement · Alkali-activated · Geopolymer

1 Introduction

Cement is the primary binding material used for concrete making. With the growth in infrastructure, the demand and use of cement are ever increasing. Cement industry causes environmental pollution by emitting CO_2 that is a significant contributor to the carbon footprint around the globe [1]. Ordinary Portland Cement has been the most popular cementitious material for making concrete. OPC performs well and maintains its integrity, chemical stability when it is subjected to extreme conditions from low to high temperatures, various environmental conditions, radiation.

M. V. Kamath (✉) · S. Prashanth · M. Kumar
Department of Civil Engineering, Manipal Institute of Technology Karnataka, MAHE, Manipal, Karnataka 576104, India
e-mail: muralidhar.kamath@learner.manipal.edu

S. Prashanth
e-mail: shreelaxmi.p@manipal.edu

M. Kumar
e-mail: Mithesh.kumar@learner.manipal.edu

B. B. Das et al. (eds.), *Recent Trends in Civil Engineering*, Lecture Notes in Civil Engineering 105, https://doi.org/10.1007/978-981-15-8293-6_8

Environmental issues made the researchers work toward the development of new generation binders, that are eco-friendly and also, cater to the need for special concrete such as high strength concrete, self-compacting concrete [9]. The new generation energy-efficient and sustainable binders, which can produce green concrete is the need of the hour.

Waste disposal is yet another problem faced by mankind. Industrial wastes if not utilized effectively will be dumped in the landfill. To reduce the load on landfill, researchers have been working on zero waste technologies [19]. Alkali-activated cementitious binders utilize industrial waste such as fly ash, GGBS so forth that possess pozzolana properties in significant quantities. The binders activated by using the alkaline solution, which contains sodium hydroxide and sodium silicates.

First research published related to alkaline or alkali-activated cement is a 1908 patent right by the German chemist and engineer Kühl [13]. The process described contains an essential combination of an alkali source, which is rich alumina-silica (pozzolanic) contained solid precursor with combination of alkaline liquid resulting into alkali-activated concrete. Alkali-activated cement seems to have superior performance and durability than the Portland cement.

There have been several studies of alkali-activated binders since the 1940s. Purdon [20] published the study of the interaction of 30 different types of GGBS with various activators in two steps. In the first step, blast furnace slag activated with sodium hydroxide solutions. The second step involves combining calcium hydroxide and different sodium salts. The performance of the resulting paste was found to be comparable to OPC in terms of rate of strength development and ultimate strength [20].

The alkali-activated slag is associated with low water permeability and low heat. Despite excellent mechanical and durability performance, Purdon did mention some issues as potential problems to achieve the desired strength. High activator concentrations are often necessary, and these can lead to prohibitively short setting times. Due to the accelerating effect of highly alkaline activators, it depends on the viscosity of the activating solution as well as the amount of water added [21]. However, all those issues are remedied by understanding the problem at hand.

The alkali-activated binders have been studied in Western Europe by researchers of the former Soviet Union and China. Later by the year of 1957 after several experiences, Victor Glukhovsky a Soviet Union scientist, was the first scientist to discover alkali-carbonate activation of metallurgical slag at the institute in Kiev Ukraine [10].

Subsequently, the effort of Purdon, alkali activation research in the Western world was quite limited until the 1980s, as reviewed by Roy [25]. By the 1980s, Joseph Davidovits from France reinvigorated the area, brought a fresh and scientifically sophisticated way, which was a significant positive step forward from the work of the Glukhovsky. An era that has been developing slowly and on making geopolymer binders Joseph called them “geopolymer” because their microstructure is on polymers [6].

This paper aims to review the hardened properties of alkali-activated and geopolymer concrete. This article presents the silica-alumina abundant particles, sodium hydroxide, sodium silicate, hardening mechanisms, and effects of various

variables on the slump properties and mechanical properties, specifically to compressive strength. An overview of alkali-activated and geopolymer contains various variation of binders, viz., fly ash, GGBS, metakaolin, microsilica, and nanosilica.

2 Prime Material

2.1 Fly Ash

Fly ash is the by-product of the thermal power plant. The flaming of solid, older anthracite coal typically produces low calcium fly ash. Globally, more than 65% of the fly-ash particles are waste product of thermal power stations deposited in ash ponds and landfills. The recycling of fly ash is the major concern to use in geopolymer concrete, which can reduce the consumption of OPC. Generally, fly ash is classified into two grades, i.e., Class C, which contains over 20% lime (Cao) and Class F, which contains under 7% lime (Cao) [16, 29, 30].

2.2 Ground-Granulated Blast-Furnace Slag (GGFS)

Ground-granulated blast-furnace slag (GGFS) is the waste by-product of steel production. GGFS produced by knock downing the molten iron slag with rapid cooling which is then dried and broken down into the glassy and granular particles. GGFS has been found to have a huge potential of being used as a supplementary binder. Typically, it has SiO_2, CaO and Al_2O_3 contain high percentage, which exhibits higher pozzolanic compared with fly ash [3].

2.3 Metakaolin (MK)

Metakaolin is the mineral clay, which is derived from kaolin in the form of the anhydrous compound. The Clay kaolin is calcined at the 600–700 degree Celsius. The metakaolin is finer than the OPC, but not fine as microsilica. The effective use of metakaolin clay tends us to less energy consumption comparing to traditional cement. It majorly consists of SiO_2 and Al_2O_3 above 90% approximately, which is geopolymeric [26].

3 Compressive Strength

3.1 Fly Ash-Based Concrete

Assi Lateef et al. (2018) have elucidated the result of particle size distribution and source on the strength and microstructural properties of pozzolana-based geopolymer concrete. The two pozzolana sources and three different sizes of pozzolana particles, i.e., 38.8, 17.9 and 4.78 μm were studied. Strength (compressive) was found to improve when the distribution of finer particle size used and a different source. Water absorption and the permeable voids proportion after immersion ratio decreased as a fly ash size reduced to the range of 4.78 μm [2]. Gunasekara Chamila et al. (2016) have investigated the durability aspects of various fly ash geopolymer concrete. Fly ash was collected from four different sources, i.e., Collie, Pt. August, Gladstone, and Tarong. Except for the concrete samples prepared from Collie, other all fly ash geopolymer concrete achieved the compressive strength 30 N/mm^2 in 3 days comparable to OPC concrete, 37 N/mm^2 in 90 days and 45 N/mm^2 in 1 year, which shows geopolymerization, which continued after 90 days [10]. Ferdous Wahid et al. (2015) proposed the mix design of geopolymer concrete. Stepwise mix design proposed was evaluated. In this paper, a detailed mix design considered in this experiment is specific gravity, air volume, slump, and lastly density concrete. Geopolymer concrete achieved the compressive strength 40 N/mm^2 in 28 days, modulus of elasticity 190 Gpa and ultimate strain 0.3% [7].

Khoa Tan Nguyen et al. [16] have investigated the properties of marine sand as fine aggregate based on geopolymer concrete and the deterioration of embedded steel reinforcement. The maximum strength (compressive) obtained was 37 N/mm^2 in 28 days when liquid–alkaline to fly ash ratio increased from 0.35 to 0.4 using marine sand as fine aggregate. Then when liquid–alkaline to fly ash ratio increased from 0.4 to 0.65, the compressive strength decreased from 37 to 21 N/mm^2, refer Graph 3. If the Si/Al ratio is increased from 1.16 to 1.67 that resulted in an enhancement of strength (compressive) [16]. Vasquez Alexander et al. (2016) carried out the study on the geopolymer using concrete demolition waste (CDW). In this experiment, OPC was partially replaced with fly ash and metakaolin up to 30% using CDW. Geopolymer concrete based on CDW, fly ash replaced with of 30% OPC and with of 10% metakaolin achieved the highest value of compressive strength of 25 N/mm^2, 33 N/mm^2 and 46.4 N/mm^2 at 28 days with Si to Al ratio of 10.5 without heat curing [28]. From the literature, Graph 1 is plotted between compressive strength (28th day) and fly ash, which showing good fitting value of R^2 equal to 91.5%.

3.2 GGBS-Based Concrete

Rafeet Ali et al. (2017) have compared the aspects of slag-based alkali-activated-concrete (SAAC) and fly ash geopolymer concrete (FGPC) with boron as

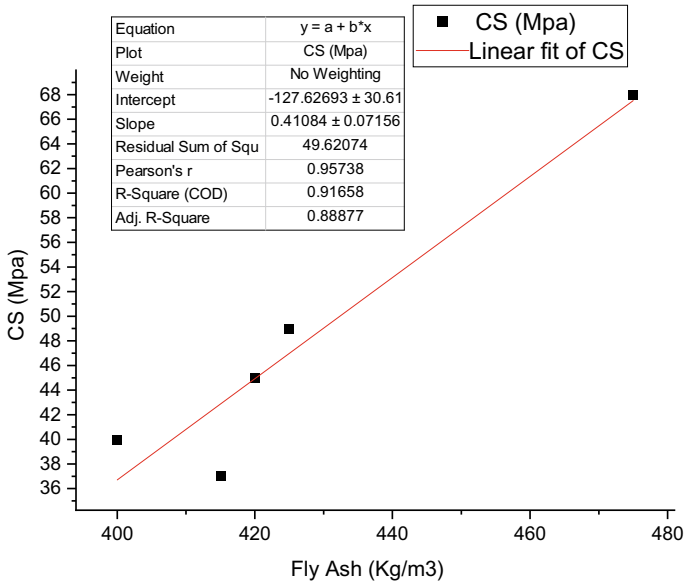

Graph 1 Linear fit of compressive strength (CS) and fly ash

environment-friendly material. The presence of boron results in the improvement of strength (compressive) in both FGPC and SAAC. The enhancement in the quantity of CaO in the binder system produced as a result of reaction compound formed due to product of fly ash and GGFS with the alkaline liquid. The difference between with fly ash-based and GGFS-based concrete is the high content of calcium oxide (almost 45%). In GGFS binder which may direct in forming a calcium–silicate–hydrate paste in the matrix of GGBS concrete. These C–S–H bonds carry a considerable portion in the hardening of the SAAS [22].

Thomas Robert et al. (2015) have investigated on the modulus of elasticity, tensile strength, and the stress–strain correlation of alkali activated-concrete (AAC) with fly ash and slag. The strength (mechanical) of AAC fly ash-based concrete with room temperature curing (28 days @ 22°) which found to have less strength compared with heat curing (48 h @ 50°). There is no difference in AAC slag-based concrete consistently. The strength (tensile) of AAC slag/fly ash both which established to have strength slightly more than OPC-based geopolymer concrete. The Poisson ratio for AAC slag/fly ash is consistently about two-thirds of OPC concrete. The stress–strain relationship showed similar behavior of all AAC concrete [26]. Reddy et al. [23] developed the mix-design for slag/fly ash-based geopolymer concrete under room temperature curing. In this paper, a rational and simple mix design has been explained for developing the slag/fly ash-based geopolymer concrete. One of the main verdicts of the study is that for the development of a well-performing GPC, ACI strength versus the W/B ratio. Alkali activator particle (AAP) to binder particle

(BP) ratio is the parameters to be controlled. Further, the study has found that the medium–high strength is in the range of 32–66 N/mm^2 [23].

4 Metakaolin-Based Concrete

Hadi Muhammad et al. (2017) designed the slag-based geopolymer concrete at room temperature curing by Taguchi approach. In this paper, blend of binder particle-like fly ash, steel slag, metakaolin (MK) and microsilica (MS) to achieve the relative amount of Al to a binder ratio (A/B), SS to SH (SS/SH) with variation SH concentration from 10 to 14 M were studied. Geopolymer concrete with a binder content of 450 kg/m^3, A/B fraction of 0.35, SS/SH fraction of 2.5 and concentration SH of 14 M achieved the maximum strength (compressive) of 60 N/mm^2 in 7 days with normal curing. The combination of fly ash and steel slag found to have increased the setting time under the room curing condition but showed superior compared to a blend of MK and MS [11]. Pouhet et al. [18] developed metakaolin-based geopolymer mortar and concrete. The slump of metakaolin-based geopolymer concrete revealed that with nonporous siliceous aggregate is capable of replacing the conventional cement. The compressive strength of 60 N/mm^2 obtained in 7 days for geopolymer concrete. Geopolymer concrete has shown the refinement of pores compared with normal concrete regardless of pore size [18]. Peem Nuaklong et al. (2018) studied the engineering properties of metakaolin and high-calcium fly ash (Class C) geopolymer concrete incorporating recycled aggregate. The metakaolin replaced 0–30% with Class C fly ash to produce the geopolymer concrete. The partial replacement of metakaolin was found to have improvement of acid attack resistance, transport properties, abrasion and engineering properties. The metakaolin is finer that fly ash refined the pore structure and geopolymerization. 30% metakaolin significantly enhanced the strength (compressive), porosity and absorption (water) with subsequent values of 134%,69% and 89% of geopolymer recycled aggregate concrete compared with concrete without meta-kaolin [17].

5 OPC Based

Yi Fang Cao et al. [4] have investigated the effect of CAC (Calcium–Aluminates–Cement) on geopolymer concrete cured at moist curing. CAC was replaced within the range of 5–20% and NaOH concentration in the range of 10–14 M, while the activator ratio between 35 and 45%. The addition of CAC in the geopolymer concrete found to have strong development at moist curing. The best mix design of geopolymer concrete, which contains 10 M alkali solution, 5% CAC replacement and 45% activator proportion. Again, with the best mix design which found to have the compressive strength of 57 N/mm^2 in 28 days with 14 M alkali solution, 10% CAC and 35% activator [4]. Ankur Mehta et al. (2017) studied the fly ash geopolymer concrete

with various variables on absorption and strength properties. OPC 20% replaced with fly ash with an addition of 15 M solution NaOH cured at 70 degrees for 24 h which found to have the strength (compressive) of 64.39 N/mm^2 in 7 days [14]. Askarian Mahya et al. (2018) have investigated the engineering properties of room temperature cured one-part-hybrid OPC–geopolymer concrete. The one-part geopolymer concrete, which found to have the maximum workability of 120 mm and with 60% OPC, which obtained the lowest workability of 30 mm [1]. Farhan Nabeel et al. (2019) analyzed and compared the OPC concrete with low to high strength fly ash geopolymer concrete (FGPC) and alkali-activated slag concrete (AAC). The direct-tensile strength, flexural strength and indirect-tensile strength of low strength (35 N/mm^2) and high strength (65 N/mm^2) FGPC and AAC concrete were superior to, compared to, OPC concrete [6].

6 Conclusion

On reviewing the available literature on alkali-activated binders and geopolymer binders. Most of the published research attempted to develop the geopolymer concrete as a base binder with fly ash, GGBS, meta-kaolin and so on in conjunction with various curing regimes such as moist curing, steam curing and high-temperature curing. The base binder then activated using alkaline solution with various ratios. Efficient utilization of waste product and alternative binder system to produce green concrete may restrict the consumption of OPC.

In comparison with fly ash based, GGBS-based and metakaolin-based alkali-activated and geopolymer concrete. The early compressive strength development was achieved within 7 days by metakaolin-based concrete. At the same time, GGBS-based alkali-activated concrete highest compressive strength was achieved within 28 days, which is significant compared with OPC concrete.

The present study results indicate that the alkali-activated and geopolymer concrete has exhibited significant feasibility. Application prospect to use as a green building material, which may be an appropriate replacement for the traditional concrete in the future. Studies on long-term performance on alkali-activated and geopolymer for various environmental conditions is not well documented.

References

1. Andrew RM (2017) Global CO_2 emissions from cement production, pp 1–52. https://doi.org/10.5194/essd-2017-77
2. Askarian M, Tao Z, Adam G, Samali B (2018) Mechanical properties of ambient cured one-part hybrid OPC-geopolymer concrete. Constr Build Mater 186:330–337. https://doi.org/10.1016/j.conbuildmat.2018.07.160

3. Assi LN, Eddie Deaver E, Ziehl P (2018) Effect of source and particle size distribution on the mechanical and microstructural properties of fly Ash-Based geopolymer concrete. Construct Build Mater 167:372–380. https://doi.org/10.1016/j.conbuildmat.2018.01.193
4. Bagheri A, Nazari A, Sanjayan JG, Rajeev P (2017) Alkali activated materials vs geopolymers: Role of boron as an eco-friendly replacement. Constr Build Mater 146:297–302. https://doi.org/10.1016/j.conbuildmat.2017.04.137
5. Cao YF, Tao Z, Pan Z, Wuhrer R (2018) Effect of calcium aluminate cement on geopolymer concrete cured at ambient temperature. Constr Build Mater 191:242–252. https://doi.org/10.1016/j.conbuildmat.2018.09.204
6. Davidovits J (1982) Mineral polymers and methods of making them
7. Farhan NA, Sheikh MN, Hadi MNS (2019) Investigation of engineering properties of normal and high strength fly ash based geopolymer and alkali-activated slag concrete compared to ordinary Portland cement concrete. Constr Build Mater 196:26–42. https://doi.org/10.1016/j.conbuildmat.2018.11.083
8. Ferdous W, Manalo A, Khennane A, Kayali O (2015) Geopolymer concrete-filled pultruded composite beams - Concrete mix design and application. Cement Concr Compos 58:1–13. https://doi.org/10.1016/j.cemconcomp.2014.12.012
9. Flatt RJ, Roussel N, Cheeseman CR (2012) Concrete: An eco material that needs to be improved. J Eur Ceram Soc 32(11):2787–2798. https://doi.org/10.1016/j.jeurceramsoc.2011.11.012
10. Glukhovsky V (n.d.) Soil Silicates. Kiev, 1959
11. Gunasekara C, Law DW, Setunge S (2016) Long term permeation properties of different fly ash geopolymer concretes. Constr Build Mater 124:352–362. https://doi.org/10.1016/j.conbuildmat.2016.07.121
12. Hadi MNS, Farhan NA, Sheikh MN (2017) Design of geopolymer concrete with GGBFS at ambient curing condition using Taguchi method. Constr Build Mater 140:424–431. https://doi.org/10.1016/j.conbuildmat.2017.02.131
13. Kühl H (1908) Slag cement and process of making the same. U.S. Patent 900,939
14. Mehta A, Siddique R, Pratap B, Aggoun S, Łagód G, Barnat-hunek D (2017) Influence of various parameters on strength and absorption properties of fly ash based geopolymer concrete designed by Taguchi method. Constr Build Mater 150:817–824. https://doi.org/10.1016/j.conbuildmat.2017.06.066
15. Nath P, Sarker PK (2014) Effect of GGBFS on setting, workability and early strength properties of fly ash geopolymer concrete cured in ambient condition. Constr Build Mater 66:163–171. https://doi.org/10.1016/j.conbuildmat.2014.05.080
16. Nematollahi B, Sanjayan J, Shaikh FUA (2015) Synthesis of heat and ambient cured one-part geopolymer mixes with different grades of sodium silicate. Ceram Int 41(4):5696–5704. https://doi.org/10.1016/j.ceramint.2014.12.154
17. Nguyen KT, Le TA, Lee K (2018) Evaluation of the mechanical properties of sea sand-based geopolymer concrete and the corrosion of embedded steel bar. Constr Build Mater 169:462–472. https://doi.org/10.1016/j.conbuildmat.2018.02.169
18. Nuaklong P, Sata V, Wongsa A, Srinavin K, Chindaprasirt P (2018) Recycled aggregate high calcium fly ash geopolymer concrete with inclusion of OPC and nano-SiO_2. Constr Build Mater 174:244–252. https://doi.org/10.1016/j.conbuildmat.2018.04.123
19. Pouhet R, Cyr M (2016) Formulation and performance of flash metakaolin geopolymer concretes. Constr Build Mater 120:150–160. https://doi.org/10.1016/j.conbuildmat.2016.05.061
20. Provis JL (2018) Alkali-activated materials. Cem Concr Res 114:40–48. https://doi.org/10.1016/j.cemconres.2017.02.009
21. Purdon A (1935) Improvements in processes of manufacturing cement, mortars and concretes
22. Purdon A (1940) The action of alkalis on blast-furnace slag. J Soc Chem Ind Trans Commun 59:191–202
23. Rafeet A, Vinai R, Soutsos M, Sha W (2017) Guidelines for mix proportioning of fly ash/GGBS based alkali activated concretes. Constr Build Mater 147:130–142. https://doi.org/10.1016/j.conbuildmat.2017.04.036

24. Reddy MS, Dinakar P, Rao BH (2018) Mix design development of fly ash and ground granulated blast furnace slag based geopolymer concrete. J Build Eng 20(August):712–722. https://doi.org/10.1016/j.jobe.2018.09.010
25. Roy DM, Gouda GR (1975) Optimization of strength in cement pastes. Cem Concr Res 5(2):153–162. https://doi.org/10.1016/0008-8846(75)90073-3
26. Sun Z, Lin X, Vollpracht A (2018) Pervious concrete made of alkali activated slag and geopolymers. Constr Build Mater 189:797–803. https://doi.org/10.1016/j.conbuildmat.2018.09.067
27. Thomas RJ, Peethamparan S (2015) Alkali-activated concrete: engineering properties and stress-strain behavior. Constr Build Mater 93:49–56. https://doi.org/10.1016/j.conbuildmat.2015.04.039
28. Vásquez A, Cárdenas V, Robayo RA, de Gutiérrez RM (2016) Geopolymer based on concrete demolition waste. Adv Powder Technol 27(4):1173–1179. https://doi.org/10.1016/j.apt.2016.03.029
29. Wang KT, Du LQi, Lv XS, He Y, Cui XM (2017) Preparation of drying powder inorganic polymer cement based on alkali-activated slag technology. Powder Technol 312:204–209. https://doi.org/10.1016/j.powtec.2017.02.036
30. Yang KH, Song JK, Ashour AF, Lee ET (2008) Properties of cementless mortars activated by sodium silicate. Constr Build Mater 22(9):1981–1989. https://doi.org/10.1016/j.conbuildmat.2007.07.003
31. Yaseri S, Hajiaghaei G, Mohammadi F, Mahdikhani M, Farokhzad R (2017) The role of synthesis parameters on the workability, setting and strength properties of binary binder based geopolymer paste. Constr Build Mater 157:534–545. https://doi.org/10.1016/j.conbuildmat.2017.09.102

Hydrodynamic Performance of Spar-Type Wind Turbine Platform Combined with Wave Energy Converter

Ajay H. Patil and D. Karmakar

Abstract In the present study, the numerical investigation of 5 MW spar-type floating offshore wind turbine (FOWT) combined with array of four and six cone–cylindrical shaped heaving type point absorber is performed. Hydrodynamic and multibody analysis is carried out for simple spar, spar combined with circular array of four and six wave energy converters. Individual responses for all wave energy converters are obtained and their effect on spar platform is analyzed. The performance of combined wind and wave energy device is studied on analyzing the motion of platform. The influence of array of wave energy converters on hydrodynamic motion responses on spar platform is analyzed. The Response Amplitude Operator (RAO) for all the three platforms is compared and analyzed for the hydrodynamic stability of platform. The present study will be helpful in the design of novel concept of spar combined with circular array of wave energy converters.

Keywords Wave energy converter · Floating offshore wind turbine · RAO (response amplitude operator) · Combined energy platform

1 Introduction

Due to limitation of nonrenewable energy such as fossil fuels, there is a need of sustainable renewable energy to meet the energy demand. Although wind and wave energy resources in deep water are abundant in nature, but the development of wave and wind energy devices to harness energy from ocean are limited due to high cost of installation and maintenance. Therefore, a lot of studies are being carried out on combined wind and wave energy platforms in order to reduce the cost of the device. The synergies of marine renewable energy devices occupy minimum area

A. H. Patil (✉) · D. Karmakar
Department of Applied Mechanics and Hydraulics, National Institute of Technology Karnataka, Surathkal, Mangalore 575025, India
e-mail: ajaypatil0308@gmail.com

D. Karmakar
e-mail: dkarmakar@nitk.edu.in

B. B. Das et al. (eds.), *Recent Trends in Civil Engineering*, Lecture Notes in Civil Engineering 105, https://doi.org/10.1007/978-981-15-8293-6_9

in ocean and maximize the energy output. Since, the steady and high wind blows in deeper ocean, so the floating foundations are beneficial to support wind turbines in deep water regions because the floating foundation will be more economical as compared to fixed foundation. Further, the individual cost of offshore floating wind turbine and wave energy converter is very high. So to reduce the initial investment and maintenance cost, there is a need of hybrid structures. Since, the wind and waves are closely related in ocean, so there is need for the development of combined wind and wave energy devices to extract maximum energy from ocean. Thus, the hybrid concept for extraction of offshore renewable energy will be more economical and beneficial.

The power extraction from wave energy has been studied by various scientist and researchers experimentally and numerically. Cho et al. [2] studied wave energy device by using relative heave motion between buoy and inner dynamic system. A systematic hydrodynamic theory is developed for the suggested wave energy converter (WEC), for which a cylindrical buoy is adopted. The buoy hydrodynamics motions are verified with experimental results and it is observed that the maximum power can be obtained at the optimal condition of spring and damper, as predicted by the developed WEC theory. Chodnekar et al. [3] analyzed the hydrodynamic performance of TLP-type floating offshore wind turbine and the responses of platform for different diameter, draft and ballast weight of FOWT under operational wave and wind condition. Gobato et al. [4] studied the physical and operational study of Pelamis system to capture energy of ocean waves. The Pelamis WEC is still under development and it has enormous potential to use the tidal waves that can be optimized so that the cost/benefit and production increases exponentially. Sinha et al. [6] studied the numerical modeling of an array of heaving point absorbers in linear and circular arrangements to understand the performance of wave energy absorption of point absorbers in different arrangements. The study suggests that, in the case of 0° wave heading angle, the circular and concentric arrays absorb more power as compared to the linear and grid arrays. Wang et al. [8] studied flexible multibody dynamics modeling of point absorber wave energy converter, FMBD (flexible multibody dynamics) model, which is a combination of multibody dynamics and finite element analysis, developed for point-absorber WECs. The study indicates that the WECs are prone to experience fatigue failure, with the shortest fatigue life of 2 years observed in the floater arm. The FMBD model developed is capable of accurately modeling point-absorber WECs and providing valuable information for designers to further optimize the structure and assess the reliability of WECs.

In recent years, the studies on combined offshore wind and wave energy concept are carried out for more clean energy production from the ocean. Bachynski and Moan [1] investigated the point absorber design for a combined wind and wave energy converter on a tension leg support structure. The combined wave and energy device are observed to have several benefits compared to single TLP-type wind turbine such as reduced surge and pitch motions, reduced tendon tension and tower base bending moment variation and slightly reduced wind turbine power variation. Yde et al. [9] performed both experimental and theoretical study for the combined wave and wind energy conversion platform. The WAMIT code is used for hydrodynamic

analysis and aero–hydro–elastic code based on HAWC2 is used for aero–elastic response of wind turbine. The roll and pitch motions are simulated and compared with measurements, which show that the peak frequencies of the measured and modeled data were almost identical. However, the magnitude of the roll was too small in case of the modeled data. Karimirad and Koushan [5] studied the concept of combining wind and wave energy device inspired by Hywind and Wavestar. The dynamic responses and power production of wave energy device and wind turbine are investigated for different power-take-off systems. The coupled aero–hydro–servo–elastic time-domain numerical simulations are carried out for the combined energy device. The study suggests that on choosing proper power-take-off system, it is likely to minimize effects of wave energy converter on floating wind turbine and hence maintaining the power performance of wind turbine while getting more power through wave energy device.

In the present study, the hydrodynamic performance of the spar-type floating wind turbine platform combined with four- and six-point absorber wave energy converter is performed to analyze the performance of the device in deep water region. The multibody analysis is carried out to analyze the motion characteristics of the combined wave and wind energy device in high waves. Further, the comparative study for the spar-type platform and combined spar-type platform with four and six wave energy converter is performed to analyze the stability of combined wave and wind energy device.

2 Spar with Array of Cone–Cylindrical Point Absorber

In this section, the detailed description of the spar-type platform along with the point absorber WEC is presented. The discretization of the model and the numerical modeling considered to analyze the combined wave and wind energy device is discussed in detail.

2.1 Description of Spar-Type Platform and Point-Absorber WEC

The combined wave and wind energy device considered for study consist of a spar-type platform to support the wind turbine along with the array of four and six cone–cylindrical shape heave buoy-type point absorbers and mooring lines [5]. The spar hull is modeled to support 5 MW NREL wind turbine and array of point absorber wave energy converters. The spar platform is anchored at fair-lead position and seabed by taut leg mooring. The properties of spar platform and wave energy converter are shown in Tables 1 and 2, respectively.

Table 1 Spar hull design

Total draft	120 m
Water depth	320 m
Depth to top of taper below SWL	4 m
Depth to bottom of taper below SWL	12 m
Diameter above taper	6.5 m
Diameter below taper	9.4 m
Spar mass including ballast	8216 E + 3 kg
CM location below SWL along platform center line	-78.5 m
Pitch inertia about CM	69.84 E + 9 kg-m^2
Yaw inertia about center line	16.78 E + 7 kg-m^2

Table 2 Properties of WEC buoy

Diameter	10 m
Draft	3 m
Conic length	1 m
Center of Buoyancy	−1.17 m
Center of Gravity	−1.5 m
Mass	180 E + 3 kg

The workflow involves modeling of the spar-type platform with array of four- and six-point absorber wave energy converters using Rhinoceros 3D to obtain geometric data file (gdf) as an input for WAMIT hydrodynamic analysis and the multibody analysis is carried out for different configuration of platforms.

2.2 Numerical Modeling of Spar with Array of Wave Energy Converter

The modeling of spar-type platform with wave energy converters is performed using a NURBS geometry-based software Rhinoceros. Initially, the heave type cone–cylinder point absorber wave energy converter model is discretized, having 268 panels (Fig. 1).

Then spar-type platform model is designed for different panels to and the convergence of the result is obtained to select the desired panel. The model is observed to converge for 2895 panel onwards. Thus, for the present analysis, the model discretized with 2895 panels is considered, as the model with 2895 panels gives accurate results and takes less simulation time. Figure 2 represents the wetted surface of the discretized combined spar-type platform with four and six wave energy converter.

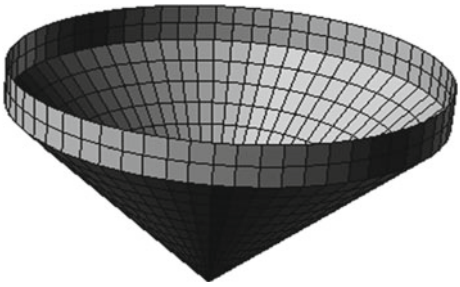

Fig. 1 Discretized model of point absorber WEC

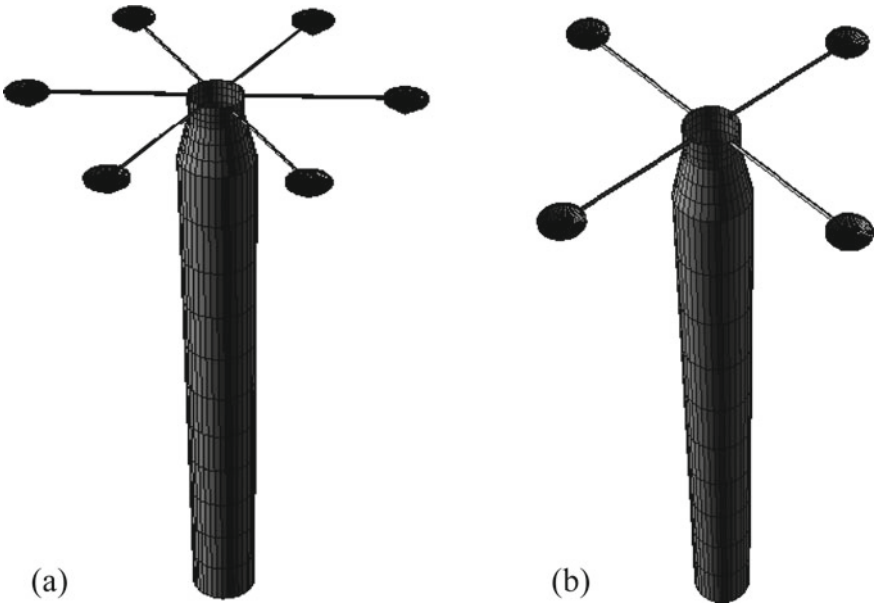

Fig. 2 Spar-type platform with **a** four-point absorber and **b** six-point absorber

2.3 Numerical Analysis

The numerical analysis is performed using the hydrodynamic code WAMIT. The WAMIT is developed for three-dimensional radiation–diffraction problems using panel method by Massachusetts Institute of Technology for wave analysis. The geometric data file (GDF) created from Rhinoceros3D modeling tool is used as an input in WAMIT code. As the total velocity potential in the flow field should include the contribution of incident waves, the contribution of disturbance of floating body to flow field and the contribution of the disturbance of floating body motion to flow field is considered. The velocity potential is expressed as

$$\Phi = \Phi_R + \Phi_D, \tag{1}$$

where, Φ_R is radiation velocity potential and Φ_D is diffraction velocity potential function.

The response amplitude operator (RAO) is obtained by applying the equations of motion for floating body in regular waves are as follows

$$\sum_{j=1}^{6} \xi_j \left\{ -\omega^2 (M_{ij} + a_{ij}) + i\omega b_{ij} + c_{ij} \right\} = AX_i, \tag{2}$$

where, ω is wave angular frequency, ξ_j is the body motion, a_{ij} is added mass,b_{ij} is damping coefficient term, c_{ij} is restoring force term, X_i is wave excitation force per unit wave amplitude and A is the wave amplitude. Equation (2) is solved for the body motion and the complex Response Amplitude Operator for the jth mode is obtained as

$$Z_j(\omega, \theta) = \frac{\xi_j}{A} = \sum_{i=1}^{6} [C_{ij}]^{-1} X_{ij}, \tag{3}$$

where, $[Cij]^{-1}$ indicates the inverse matrix of the member between brackets in the equation of motion.

3 Results and Discussion

The hydrodynamic analysis is carried out for spar-type platform, spar with array of four and six wave energy converters using WAMIT. The comparison of RAO's for simple spar, spar with four and six wave energy converter is presented in the case of 0° wave heading angle. All the six degrees of freedom (DOF) of the combined platform are presented.

In Fig. 3a, b, the surge and sway motion for the spar-type platform and spar platform combined with four and six wave energy converter is plotted and versus wave period. It is observed that, as the wave period increases, the surge motion (Fig. 3a) also increases for all three platforms. In the case of spar-type platform, the surge value attains maximum at 30 s and for spar with four WEC surge value attains peak at 5 s and it decreases further and again increases to maximum value at 30 s. In the case of spar with six WEC, the surge motion attains peak at 6 s and approaches minimum at around 9 s and then increases. In the case of sway response as shown in Fig. 3b, it is observed that as the sway response increases with the increase in the wave period for spar-type platform. In the case of combined spar with array of WEC,

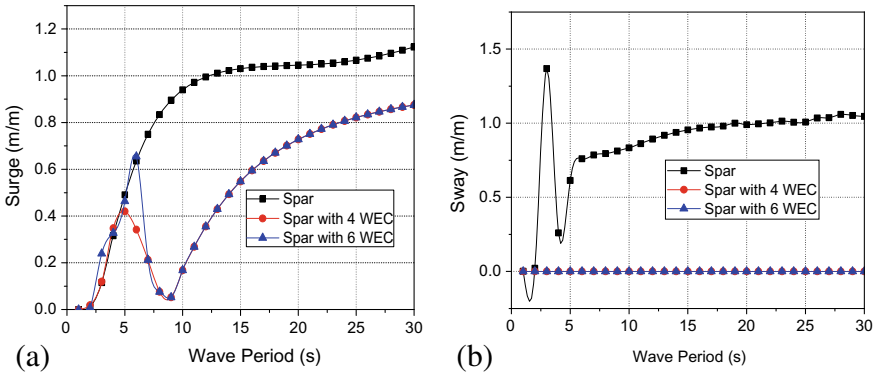

Fig. 3 **a** Surge and **b** sway RAO's of combined spar platform and WEC

sway responses are almost zero but for spar-type platform, the sway responses attain the peak at 4 s then start decreasing.

In Fig. 4a, b, the heave and roll response of the three different spar-type platforms are presented versus wave period. The heave RAO (Fig. 4a) is high for spar-type platform as compared to combined spar platform. In the case of spar-type platform, the heave response attains maximum value for wave period of 11 s and further it decreases. In the case of spar with four and six WEC, the heave motion attains maximum value of 0.2 m and it further decreases with the increase in the wave period. The roll responses (Fig. 4b) for all three platforms are almost zero and it shows that all three platforms are more stable in roll response.

In Fig. 5a, b, the pitch and yaw response for the three different platforms are plotted versus wave period. The pitch response (Fig. 5a) for spar with four WEC is slightly higher than single spar platform and spar with six WEC. The pitch response is showing almost zero values for single spar and spar with six WEC, which suggests

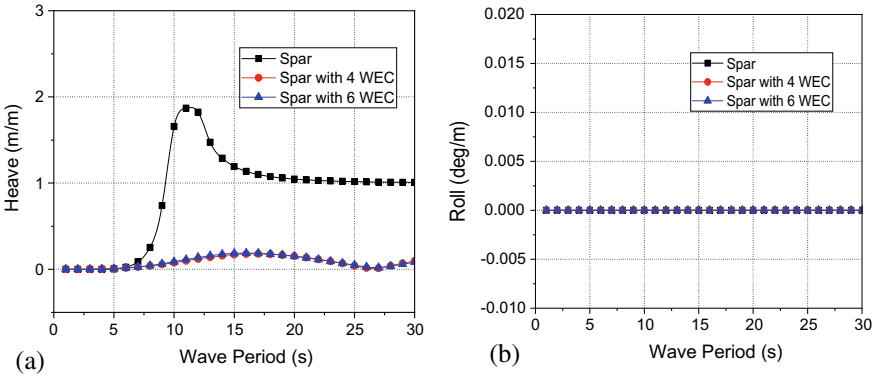

Fig. 4 **a** Heave and **b** roll RAO's of combined spar platform and WEC

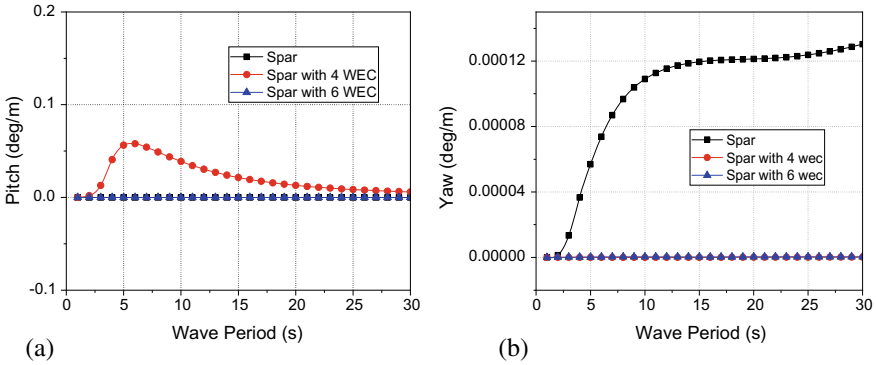

Fig. 5 **a** Pitch and **b** Yaw RAO's of combined spar platform and WEC

that all the three platforms are stable in pitch responses. In Fig. 5b, yaw responses attain maximum value at 30 s for spar-type platform but for spar with four and six WEC, the yaw responses are almost zero.

4 Conclusions

The present study is aimed to analyze the hydrodynamic motion responses for single spar and spar with four and six WEC. All six responses are obtained for the three platforms by using the WAMIT for incident waves. The conclusions drawn from the study are as follows:

- The spar platform combined with array of wave energy converters shows more stability as compared to single spar platform.
- The translational motion shows high responses as compared to rotational motion.
- The platform stability is high in case rotational motion as compared to translational motions.
- The study presents the best combination of spar with array of WEC.

Acknowledgements The authors acknowledge Science and Engineering Research Board (SERB), Department of Science & Technology (DST), Government of India for supporting financially under the Young Scientist research grant number CRG/2018/004184 and DST for India–Portugal Bilateral Scientific Technological Cooperation Project grant number DST/INT/Portugal/P-13/2017.

References

1. Bachynski EE, Moan T (2013) Point absorber design for a combined wind and wave energy converter on a tension-leg support structure. In: International Conference on Ocean, Offshore and Arctic Engineering, Nantes, France
2. Cho IH, Kim MH, Kweon HM (2012) Wave energy converter by using relative heave motion between buoy and inner dynamic system. Ocean Syst Eng 2:297–314
3. Chodnekar YP, Mandal S, Rao KB (2015) Hydrodynamic analysis of floating offshore wind turbine. Procedia Eng 116:4–11
4. Gobata R, Gobato A, Fedrigo DFG (2016) Harnessing the energy of ocean surface waves by Pelamis System. Parana J Sci Educ 1–15
5. Karimirad M, Koushan K (2016) WindWEC: combining wind and wave energy inspired by hywind and wavestar. In: International Conference on Renewable Energy Research and Applications (ICRERA), Birmingham, UK
6. Sinha A, Karmakar D, Guedes SC (2016) Performance of optimally tuned arrays of heaving point absorbers. Renew Energy 92:517–531
7. WAMIT user manual: https://www.wamit.com/manual.htm
8. Wang L, Kolios A, Cui L, Sheng Q (2018) Flexible multi-body dynamics modelling of a point absorber wave energy converters. Renew Energy 127:790–801
9. Yde A, Pedersen MM, Bellew SB, Køhler A, Clausen RS, Wedel Nielsen A (2014) Experimental and theoretical analysis of a combined floating wave and wind energy conversion platform. DTU Wind Energy. E.No. 0044:1–45

Study of Dynamic Characteristics of Circular Liquid Storage Tanks Using Acoustic Principles

P. Nimisha, B. R. Jayalekshmi, and Katta Venkataramana

Abstract Liquid storage tanks are lifeline structures, which should be designed with utmost care. Any damage to a tank, which is used to store hazardous liquid is catastrophic. The estimation of fundamental natural frequencies of liquid storage tanks situated in seismic regions is important for a seismic design. The present study deals with the estimation of natural frequencies of circular steel liquid storage tanks with reference to codal provisions and numerical analysis by using acoustic principles with the aid of FEM software. The study has been carried out for circular tank of diameter 6 m and height 8 m with different liquid depths, viz. 1/3rd, 2/3rd and full tank conditions and stiffness conditions, incorporating the sloshing effect. The natural frequencies obtained by finite element analysis of tanks are compared with those values obtained as per various International codes, viz., IS 1893(part2):2014, API 650 and Eurocode 8. The results show that the convective mode frequencies are matching well whereas, there is slight variation in impulsive mode frequency values obtained as per IS 1893.

Keywords Liquid storage tank · Fluid–structure interaction · Natural frequency · Acoustic modelling · Eigenvalue analysis

1 Introduction

Liquid storage tanks are very essential part of our infrastructure. Its usage varies from the storage of water to the most hazardous liquids. Hence, any damage to the structure will affect the mankind along with the non-living things. Since it is a liquid container, even a small hairline crack can worsen the situation. Hence, the liquid storage tanks should be designed with utmost care giving more importance to the

P. Nimisha (✉)
Research Scholar, Department of Civil Engineering, National Institute of Technology Karnataka, Surathkal, Mangalore, Karnataka 575025, India
e-mail: nimmigouri@gmail.com

B. R. Jayalekshmi · K. Venkataramana
Professor, Department of Civil Engineering, National Institute of Technology Karnataka, Surathkal, Mangalore, Karnataka 575025, India

B. B. Das et al. (eds.), *Recent Trends in Civil Engineering*, Lecture Notes in Civil Engineering 105, https://doi.org/10.1007/978-981-15-8293-6_10

safety factors. Past history witnessed failure of many liquid retaining tanks due to different reasons. During 2011 Tohoku, Japan Earthquake an oil storage tank was damaged, due to the sloshing effects. During seismic excitation, the liquid inside the tank will exert hydrodynamic pressure on the walls of the tank [1] in addition to hydrostatic pressure.

In order to study these structural characteristics, Housner [2] developed a mathematical model for the liquid tanks, which is accepted by most of the International codes [3]. This model considers a liquid tank as a single degree of freedom system if it is full or empty. But if the tank is partially filled, this condition fails and two degree of freedom concept should be used. Under this concept, a liquid mass that is rigidly connected to the tank wall is termed as impulsive liquid mass. It accelerates along with the tank wall. Whereas, the liquid mass in the upper part of the tank, that undergoes movements independently is termed as convective liquid mass [3]. In most of the cases, the tank may not be completely filled. Hence, two degree of freedom idealization of tanks is necessary. The earlier Indian seismic code followed the concept of a single-degree-of-freedom system. But this concept is valid only if the tank is full and for the tank structure with the support of uniform rigidity throughout [4]. Hence the revised Indian seismic code follows the two degree of freedom idealization for liquid storage tanks. Figures 1 and 2 show single degree of freedom and two degree of freedom idealizations, respectively, for the liquid retaining tanks. Where, 'm_i' and 'm_c' are the impulsive mass and convective mass, respectively. 'm_s' is the sum of mass of empty container of elevated tank and one-third mass of staging. 'K_c' and 'K_s' are the spring stiffness in convective mode and lateral stiffness of elevated tank staging, respectively. Later, researchers developed many different ways to model the liquid retaining structures, viz., added mass approach [5], Lagrangian approach [6], Eulerian approach [7], etc.

Recognizing the importance to study the natural frequency of a structure, Gupta and Hutchinson [8] introduced a complimentary Rayleigh's quotient to determine the fundamental frequency of a partially filled cylindrical tank. And they found that the sloshing mode frequencies are independent of the rigidity of the tank wall. Tang [9]

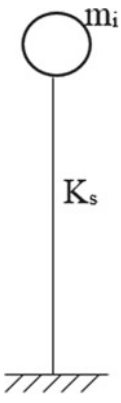

Fig. 1 Single lumped mass model

Fig. 2 Two mass model

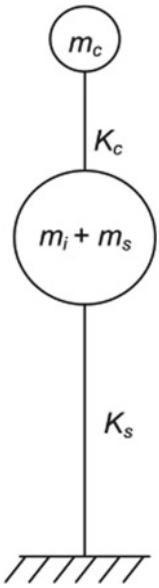

proposed an approximate equation, which is accurate to determine the fundamental frequency of a tank-two liquid system with 'd/R' ratio (ratio of the depth of liquid to the radius of the tank) between 0.25 and 1. With the introduction of liquid, the frequency reduces significantly [10]. Since the dynamic boundary condition makes the problem more complicated, the mathematical computation to obtain the response of the liquid retaining tank under various loading conditions is tedious work. This situation leads to the introduction of software packages in the field of analysis of liquid storage tanks. Many studies have been carried out using LS-DYNA [11], STAAD [12], ANSYS [10, 13, 14], Abaqus [15], etc. Many previous studies have been carried out using ANSYS software since it supports the acoustic modelling of the liquid tanks.

2 Acoustic Modelling

Acoustics is the study of all types of mechanical waves in gases, liquids, and solids. The acoustic modelling technique is an effective means to stimulate the liquid tank system so as to study the structural characteristics. The ANSYS acoustic analysis program, which works on the principles of finite element method (FEM) can be used for this purpose. It helps to simulate the coupled acoustic–structural interaction or the uncoupled pure acoustic wave in the given environment. The acoustic analysis usually involves the modelling of both an acoustic fluid and a structure. The fluid is assumed to be compressible with zero mean flow.

An acoustic Fluid–Structural Interaction (FSI) problem considers the structural dynamics equation along with linearized Navier–Stokes equations of fluid momentum and the flow continuity equation. The programme uses the FSI label to couple the structural motion and fluid pressure at the interface. The incorporation of the free surface boundary condition enables the study of structural characteristics of liquid storage tanks under convective mode [15].

3 Methodology

The acoustic modelling principles were demonstrated numerically by modelling a number of liquid storage tanks using ANSYS mechanical APDL software and studied the dynamic characteristics under both impulsive and convective modes. The details of geometric configurations and material properties considered for the study are given in Tables 1 and 2, respectively.

The bottom plates of the models were assumed to be clamped. The container wall and base were generated with four-noded shell elements and liquid region was modelled with eight-noded fluid elements. In partially filled liquid tanks, the free surface condition was also included to study the sloshing of the liquid in the storage tank.

The study simulated both impulsive and convective modes separately and mode shapes and the frequencies under different modes were evaluated. In the case of acoustic analysis with structural coupling, the ANSYS mechanical APDL software uses unsymmetric mode extraction method to calculate complex eigenvalues and eigenvectors. Hence, in order to study the dynamic characteristics of the liquid tank system, free vibration analysis was carried out using unsymmetric extraction method. Both mode shapes and frequency values were noted for the first three modes.

Table 1 Geometric configuration

Tank	
Size	Height(H) = 8 m Diameter(D) = 6 m
Thickness(t)	5 mm, 10 mm and 20 mm
d/H (where, d = depth of liquid)	1, 0.67 and 0.33

Table 2 Material properties

Tank	Liquid
Material-Steel	Material-Water
Modulus of elasticity = 2.15×10^{11} N/m^2	Sonic velocity = 1500 m/s
Density = 7850 kg/m^3	Density: 1000 kg/m^3
Poisson's ratio = 0.3	

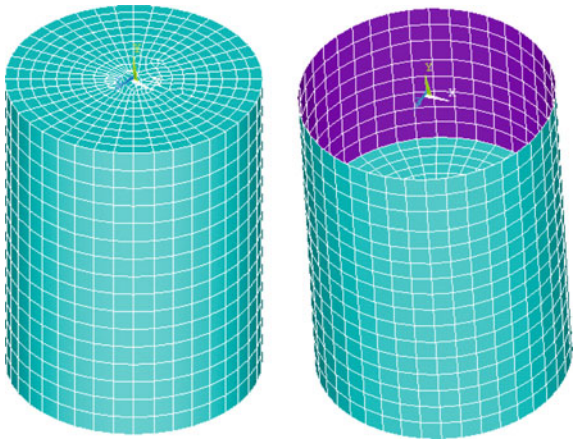

Fig. 3 Full and partially filled tank models using ANSYS

The numerical analysis results in terms of frequency values were compared with various International standards, viz., IS 1893(part2):2014 [16], API 650 [17] and Eurocode 8 [18]. The full tank and partially filled tank models generated in ANSYS mechanical APDL software are given in Fig. 3.

4 Results and Discussion

The free vibration analysis was carried out and the dynamic characteristics of the liquid tank system were noted in terms of frequency and mode shapes under the first three modes. The mode shape indicates a specific pattern of vibration of the mechanical system under consideration, at a particular frequency. It helps to divide the analysis into finite combinations of standard movements, and it aids in arriving a proper solution for the problem.

4.1 Deformed Shapes

The deformed shapes of full tank and partially filled tanks with 2/3rd and 1/3rd liquid for the first three modes are given in Fig. 4. The observed mode shapes indicated a slight translational motion during the initial modes followed by violent rotational and complex mode shapes during the subsequent higher modes. The maximum deformation of the liquid tank model is found to increase with decrease in the liquid depth.

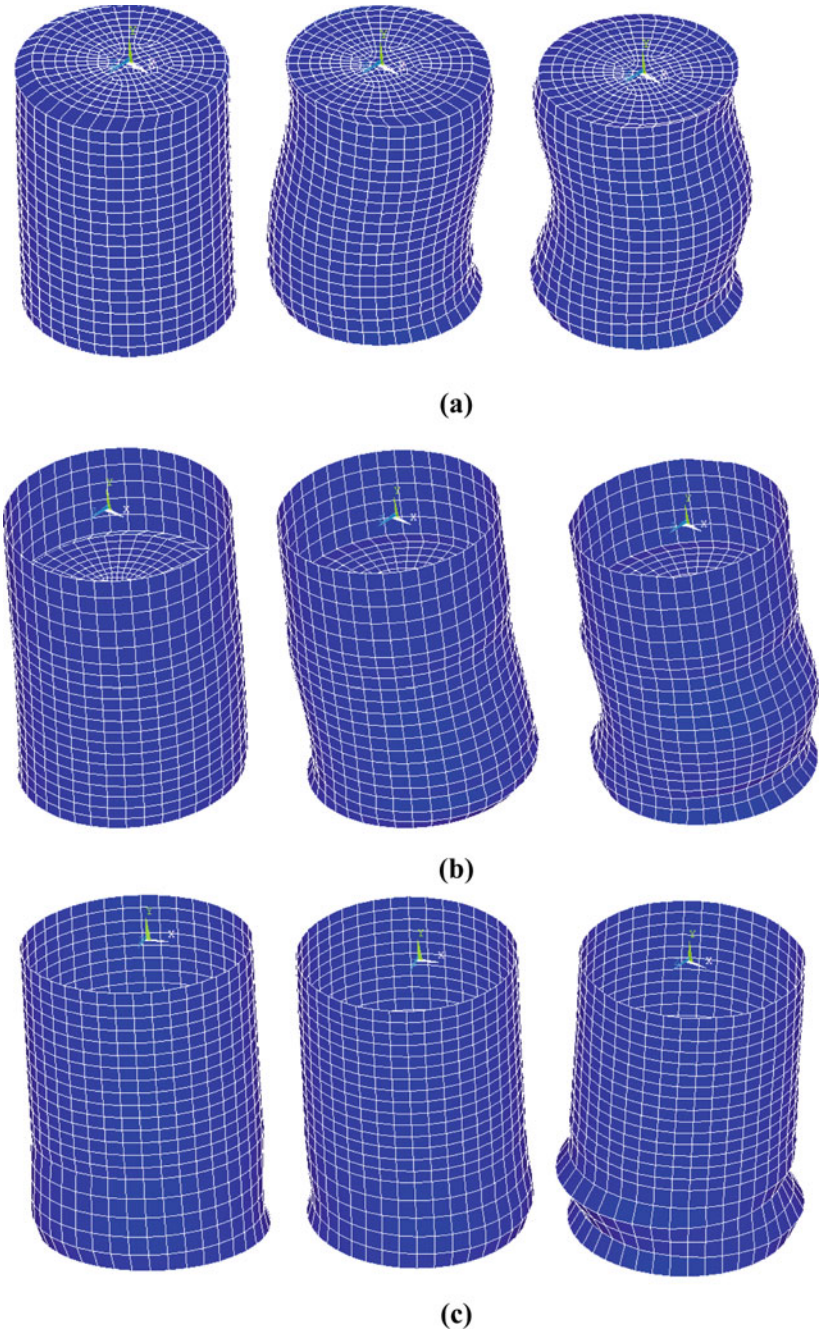

Fig. 4 First three mode shapes for **a** full tank, **b** 2/3rd filled, **c** 1/3rd filled

4.2 Impulsive Frequency

The frequencies under impulsive mode for different d/H ratios are illustrated in Fig. 5. As the depth of liquid increases, the natural frequency of the liquid tank system decreases. This is due to the increase in the impulsive mass of liquid, which will vibrate along with the tank structure. Due to the increase in the impulsive mass, the mass of the system increases causing increased deformation of the tank structure. This will reduce the frequency of the system under impulsive mode. The same trend is observed under higher modes also.

The fundamental impulsive frequencies for different d/H ratios are compared with various International standards as shown in Fig. 6. The observed frequency from the finite element analysis is found to be in good agreement with API 650 and Eurocode 8 as compared to IS1893. There is a variation of around 13% for the fundamental frequency value calculated based on FEM for smaller d/H ratios while comparing with IS1893. This indicates the need for the revision of coefficient of impulsive frequency given in IS 1893 especially for the case of less impulsive mass.

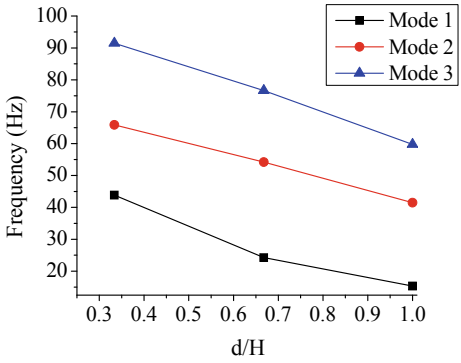

Fig. 5 Variation of impulsive frequency with liquid depth

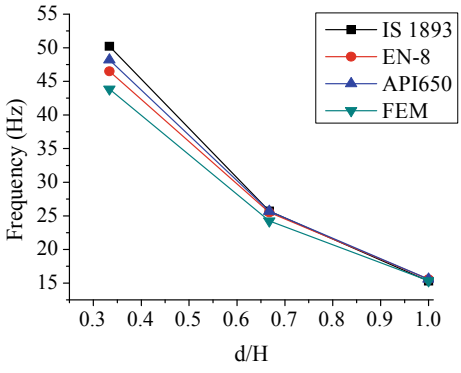

Fig. 6 Comparison of impulsive frequency from FEM and International codes

4.3 Convective Frequency

The convective frequencies for the partially filled conditions under different modes are shown in Fig. 7. The fundamental frequency is found to decrease with a reduction in the depth of liquid in the tank. Whereas, for higher modes, it is observed to be the same for different d/H ratios for a particular mode. This trend of the curves indicates that the convective frequency is independent of the depth of liquid in the tank.

The fundamental frequency under convective mode obtained with finite element analysis is compared with various International standards as shown in Fig. 8. The convective frequency values as per numerical analysis are found to be in good agreement with the frequency values calculated based on different International standards. Only a slight variation of 2.6% is noted for the frequency value calculated based on Eurocode-8 while comparing with numerical model results.

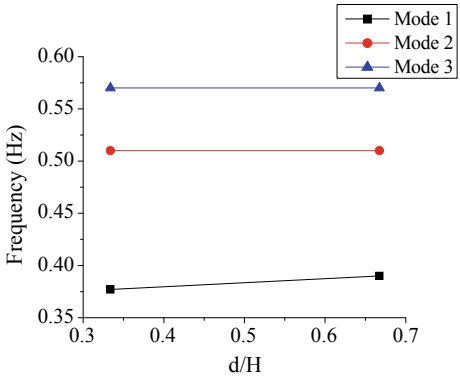

Fig. 7 Variation of convective frequency with liquid depth

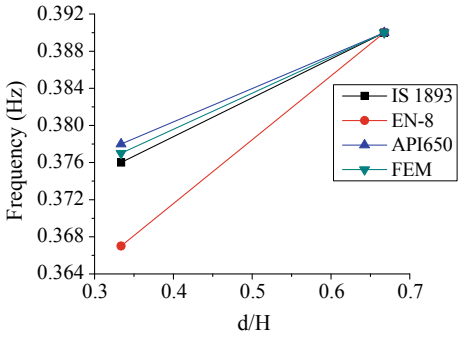

Fig. 8 Comparison of convective frequency from FEM and International codes

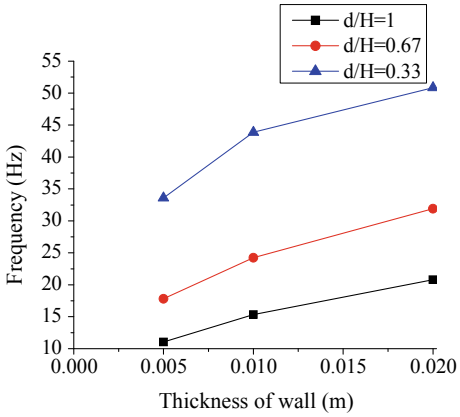

Fig. 9 Variation of impulsive frequency with thickness of tank wall

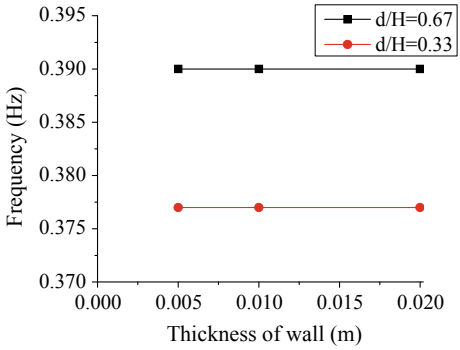

Fig. 10 Variation of convective frequency with thickness of tank wall

4.4 Effect of Thickness of Tank Wall

The variation of impulsive and convective frequencies with the thickness of the tank wall is shown in Figs. 9 and 10, respectively, for different d/H ratios. The impulsive frequency is found to increase with an increase in the thickness of the tank wall. This is due to the increased stiffness of the structure for an increase in the thickness of the tank wall. This increase in the frequency values is more evident for the tank with less impulsive mass of liquid. Whereas, in the case of convective mode, the frequency is found to be independent of the wall thickness. It depends only on the liquid depth.

5 Conclusions

The application of acoustic modelling in fluid–structure interaction problems has been illustrated in this paper by generating circular liquid storage tank models in ANSYS mechanical APDL software. The dynamic characteristics of the liquid tank

model were studied by carrying out the modal analysis. Both mode shapes and the frequency characteristics under impulsive and convective modes were analysed. The mode shapes are observed to be complex for tank with less liquid depth. The impulsive frequency increases with tank wall thickness and it is found to be more evident for the tank with less impulsive mass of liquid. Whereas, the convective frequency is independent of the thickness of the tank wall. The frequency values in the convective mode are found to be in good conformity with the values obtained from the expressions given in the various International codes considered for the study, viz., IS 1893(part 2):2014, API650 and Eurocode-8. Similarly, the impulsive mode frequency values also confirm the values obtained based on International codes, viz., API650 and Eurocode-8 as compared to IS1893. But a variation of 13% was observed for the impulsive mode frequencies obtained based on the IS code results for small d/H ratios. This variation vanishes as the liquid depth increases. Hence, a detailed evaluation is required for the coefficient of impulsive frequency suggested by IS code for small d/H ratios.

References

1. Kumar PD et al (2016) Comparative study of dynamic analysis of rectangular liquid filled containers using codal provisions. Procedia Eng 144:1180–1186
2. Housner GW (1963) Dynamic behavior of water tanks. Bull Seismological Soc America 53:381–387
3. IITK-GSDMA (2005) Guidelines for Seismic Design of Liquid Storage Tanks, Provisions with Commentary on the Indian seismic code, Indian Standard IS 1893 (Part 1): 2002, Indian Institute of Technology Kanpur, Gujarat State Disaster Management Authority
4. Livaoglu R, Dogangun A (2006) Simplified seismic analysis procedures for elevated tanks considering fluid—structure—soil interaction. J Fluids Struct 22:421–439
5. Dogangun A, Durmus A, Ayvaz Y (1996) Static and dynamic analysis of rectangular tanks by using the lagrangian fluid finite element. Comput Strucures 59:547–552
6. Dogangun A, Livaoglu R (2004) Hydrodynamic pressures acting on the walls of rectangular fluid containers. Struct Eng Mech 17:203–214
7. Mandal KK, Maity D (2016) Pressure based Eulerian approach for investigation of sloshing in rectangular water tank. Procedia Eng 144:1187–1194
8. Gupta RK, Hutchinson GL (1988) Free vibration analysis of liquid storage tanks. J Sound Vib 122:491–506
9. Tang Y (1994) Free-vibration analysis of tank containing two liquids. J Eng Mech 120:618–636
10. Kruntcheva MR (2007) Free vibrations of cylindrical storage tanks: finite-element analysis and experiments. J Eng Mech 133:728–733
11. Kilic SA (2009) Simulation of sloshing effects in cylindrical tanks and evaluation of seismic performance. Lifeline Earthquake Eng Multihazard Environ 650:372–381
12. Liu Z (2018) Seismic design and analysis of concrete liquid-containing tanks. Structures Congress 444–454
13. Singal V, Bajaj J, Awalgaonkar N, Tibdewal S (2014) CFD analysis of a kerosene fuel tank to reduce liquid sloshing. Procedia Eng 69:1365–1371
14. Kangda MZ, Sawant SS, Jaiswal OR (2019) Sloshing in liquid storage tanks with internalobstructions. Rec Adv Struct Eng 2:3–12
15. Rawat A et al (2019) Thin-Walled Structures Earthquake induced sloshing and hydrodynamic pressures in rigid liquid storage tanks analyzed by coupled acoustic-structural and Euler-Lagrange methods. Thin Walled Struct 134:333–346

16. IS 1893 (Part 2) (2014) Criteria for Earthquake Resistant Design of Structures-Part 2 Liquid Retaining Tanks. Bureau of Indian Standards
17. API 650 (1998) Welded storage tanks for oil storage. American Petroleum Institute, Washington D. C., USA
18. EN 1998–4: Eurocode 8 (2006) Design provisions for earthquake resistance of structures, Part 1-General rules and Part 4–Silos, tanks and pipelines. European committee for Standardization, Brussels

Repairs and Rehabilitation of Concrete Structures: Case Studies

Shekhar Panandiker, Neena Panandikar, and Celestan Braganza

Abstract Concrete is a very versatile material and the most widely used all over the world. Concrete deteriorates if not handled properly. This deterioration leads to repairs and rehabilitation of concrete structures. This paper makes an attempt to discuss and highlight some of these issues.

Keywords Durability · Repairs · Rebound hammer · UPV test

1 Introduction

Concrete is a very versatile material and the most widely used all over the world. Concrete, as we all know, is a product of four or more materials and thus its quality parameters like its strength, flowability, workability and durability depend upon all its constituent materials.

Concrete as we all know is strong in compression but weak in tension. So concrete needs to be reinforced or embedded with steel reinforcement when it has to resist tensile force. Concrete member with steel embedded inside it is known as reinforced cement concrete. Poorly made concrete with steel embedded inside is an open invite for corrosion-induced distress in concrete. There are other means of concrete deterioration as well. Like poor workmanship, poorly maintained concrete structures, faulty design, change of usage, etc. Thus every year we spend a lot of money in trying to salvage concrete structures, which deteriorate much earlier in their service life.

This paper makes an attempt to look at some of the case studies that were undertaken to salvage the structures which had distress problems much ahead of their intended service life.

S. Panandiker · C. Braganza
Shekhar Panandiker & Associates, Margao, Goa, India
e-mail: shekhar@shekharpanandiker.com

N. Panandikar (✉)
Don Bosco College of Engineering, Margao 403602, Goa, India
e-mail: neena110@rediffmail.com

B. B. Das et al. (eds.), *Recent Trends in Civil Engineering*, Lecture Notes in Civil Engineering 105, https://doi.org/10.1007/978-981-15-8293-6_11

Case (1) Remedial measures for footings due to lesser grade of concrete achieved as against the concrete grade specified:

This happened at one of our project sites. The concrete grade to be used at the site as per the design was M-30. A design mix for the same was carried out. A trial mix as indicated in the design mix was carried out at the site and tested after 3 days and gave satisfactory results. Hence a go head for casting of footings was given to the contractor. As per the standard prevailing practice, random cube samples were taken during the concrete pour. The cube samples obtained were crushed to ascertain the compressive strength of the concrete. The crushing of the cubes was carried out at 3 days, 7 days, 14 days and at 28 days. Total number of footings concreted was 20. Out of 20 footings, for 8 footings, the average compressive strength found was 25 N/SQMM, which indicated a concrete grade of M-25. As per the design and specification, the concrete grade to be achieved was M-30. As the specified grade could not be achieved, initially it was decided to demolish the footings and cast afresh. Since breaking of these footings would be quite a task a decision was taken to salvage the footings, if possible. Also breaking the footings would have taken up the valuable time which would have delayed the project and also probably have a cost over rum.

A methodology had to be adopted to salvage these footings. As the footings cast were more than 28 days old, a digital rebound hammer test was carried out on the footings using a Proceq Digital rebound hammer. The test readings also confirmed that the concrete grade was M-25. The structural design was rechecked with M-25 grade of concrete in place of M-30 as originally designed. There was no change in the size of the footing as the footing size is independent of the grade of concrete and depends upon the load being carried by the column versus safe bearing capacity of the soil. For the given grade of concrete the footing depth had to be increased by 200 mm to satisfy the criteria for punching shear. One of the earlier cast footings had a depth of 450 mm. This was now to be increased to 650 mm for the grade of concrete achieved in the cast footing. Thus fresh concrete of equivalent grade had to be poured on the existing footing to increase its depth by 200 mm. But the real challenge was that both old and new concrete had to act as one pad with total depth of 650 m. In other words, we had to ensure that there was no slip at the interface of the two blocks.

To avoid the slip at interface the surface of the old concrete footing was hacked and made rough as shown, refer Fig. 1. Then just before the pour the surface was once again cleaned of the dust and debris and then the surface was coated with NITOBOND—EP of FOSROC and concrete was poured when the surface was still tacky.

Steel reinforcement was provided in the top layer to take care of reversal of stress due to wind load. Steel rebars were fixed in the column using RE-500 of HILTI, refer Fig. 2. The other reinforcement was tied just like how the reinforcement is tied for the footing mesh. Clause 34.5.2 of IS:456 stipulates to provide @360SQMM per meter length in each direction on each face, when the thickness of footing slab is greater than one meter (Refer IS:456-2000).

Fig. 1 Hacking of the footing top

Fig. 2 Steel Reinforcement at footing top

On completion of the work, the footing was suitably cured. The cubes cast were crushed at 3 days and checked for the strength. The compressive strength was correlated using the formula Ft = (T/(a + bt))x F28 where T = number of days, a = 4.8, b = 0.833 both empirical constants and F28 = strength of the concrete grade at 28 days.(Special Publication—Explanatory Handbook to IS:456).

As mentioned, a design mix was done and the random cubes were crushed at 3 days. The result obtained was corelated using the formula Ft = (t/(a + bt)) x F28.

Where t = no. of days, a and b are empirical constants, where a = 4.7 and b = 0.833 and F28 is the characteristic strength of concrete grade at 28 days. This confirmed the design mix.

The random cube samples taken during the pour were crushed at 3, 7, 14 and 28 days and the strength checked. This was found to be 25 N/SQMM.

IS 13311 (Part 2): 1992 (Reaffirmed 2004) Non-Destructive Testing of Concrete—Method of Test—Rebound Hammer.

A digital rebound Hammer PROCEQ make was used, which directly indicates the grade of concrete. Prior to test, the hammer was used on the concrete cube cast as per the design mix and on achieving 28 days maturity. This also helped in calibration of the hammer. Similarly, the hammer was also used to check the cubes obtained from the site pour and hammer readings were also obtained on the footings cast on completion of 28 days. All these corelations helped to ensure that the strength

Fig. 3 Concreting of the footing

checked from rebound hammer test was similar to that of destructive compressive strength.

Figure 3 shows the concreting of the footing to increase the depth of the footing.

An Ultrasonic Pulse Velocity (UPV) meter (Refer IS 13311 (Part1):1992) was used and UPV test was carried out by indirect way of testing to check the bond between the two faces of the concrete. The test gave a good reading indicating a perfect bond between the surface and no void at the interface. A Proceq Digital Rebound hammer (IS 13311 (Part2): 1992) was also carried out to ascertain the compressive strength. Both results were good.

Finished footings can be seen in Fig. 4. Thus concrete footings were to be demolished for not meeting the design specifications could be salvaged and taken in use.

Case (2): Restoration of damaged RCC structural members:

Concrete, as already mentioned, is a widely used and very versatile material. But most of the problems start with concrete are due to two reasons. First, the shrinkage of concrete that leads to shrinkage cracks and second concrete as a material is very weak in tension. Because of its low tensile strength, we have to embed steel inside concrete as reinforcement and this combination is what we call reinforced cement concrete.

Fig. 4 Finished footings after increase of depth

Steel is the most preferred reinforcement as the coefficient of linear expansion of the two is almost the same and hence it helps in better bond and transfer of stresses.

However, if the concrete surface encasing steel is not meeting the durability requirement like proper cover to the reinforcing bar or if the surrounding concrete is honeycombed or is not impermeable then in presence of moisture and oxygen the steel embedded in the concrete starts to corrode. The corrosion of steel inside concrete is a very dangerous situation and it leads to cracking, lack of bond and in the long run has a drastic effect on the integrity of the structure as a whole.

Most of the concrete structures deteriorate over a period of time for this one simple reason. We will now discuss the restoration measures of how we can rehabilitate the structures affected by corrosion of steel reinforcement.

After we were called to carry out structural audit and to check the status of the structure. There was severe corrosion of the reinforcement bars of the columns. This had resulted in severe cracking of the column concrete. At some places, the steel reinforcement itself had disintegrated over a period of time.

The first step was to immediately prop the structure to ease the structure of its load. Generally, when corrosion is severe and the structural skeleton gets affected, there is a redistribution of the stress and the structure will adjust itself to ease itself of the stress concentrations. So the first and immediate step in such situations is to prop the slabs and ease the structure of some of its loading. After proper propping, the next step is to remove the debonded concrete and clean the affected structural members of loose concrete, debonded plaster, etc.

The severely corroded bars were cleaned of corrosion using wire brush and subsequently were checked for reduction in diameters. Reduction in diameters would drastically reduce the load-carrying capacity of the structural members. After the surface of the structural members was thoroughly cleaned, rebound hammer test [2] was carried out to ascertain the grade of concrete and also UPV test was carried out to ascertain the quality of the concrete used, refer Fig. 5.

The bars were checked and loss of reinforcement was noted. These bars which had reduced in diameter were replaced with new bars. Holes were drilled of size 2 mm more than the existing bar diameter. Rebars were then fixed using chemical anchors and replacement reinforcement was tied to these rebars. The lateral ties of the columns were badly corroded. The lateral ties are important as they help in confinement of concrete and also assist in load-carrying capacity of the column by resisting bursting of the column under compressive load. The lateral ties were also replaced the same way the main reinforcement bars were replaced.

Once the reinforcement was in place the column member was ready for the concrete pour, refer Fig. 6. The bars were then coated with anticorrosive chemical, refer Fig. 6.

After due curing of the chemical, shuttering was fixed and the concreting was carried out. The finished concrete column can be seen in Figs. 7 and 8.

The concrete samples taken during the pour were crushed to check the compressive strength. After 28 days, the concrete was also checked using digital rebound hammer to ascertain the strength. This matched with the results obtained from crushing of the concrete cubes. The UPV test was also carried out to check the concrete quality and

Fig. 5 Proceq digital rebound hammer test

Fig. 6 Tieing of the reinforcement

Fig. 7 Coating of Steel bars

it also gave good results. The contractor was then cleared to carry on with finishing activities.

IS 13311 (Part 1): 1992 (Reaffirmed 2004) Non-Destructive Testing of Concrete—Methods of Test—Ultrasonic Pulse Velocity

The Ultrasonic Pulse Velocity Test was carried out on the hardened concrete using PUNDIT Lab of PROCEQ. Table 2 velocity criterion for concrete quality grading of IS 13311 (Part 1): 1992 [1] gives a clear indication of concrete quality based on pulse velocity readings. As per the code, a reading between 3.5 and 4.5 km/sec indicates good quality concrete. A reading above 4.5 km/sec indicates excellent quality and a reading between 3 and 3.5 km/sec indicates medium quality concrete. And any reading below 3 km/sec indicates concrete of doubtful quality. The reading of PUNDIT Lab obtained at site was in range of 3.5–4.5 km/sec thus indicating good quality concrete.

Fig. 8 Finished column

2 Conclusion

The structures in distress can be repaired using such simple techniques. The main steps can be summarized as carry out rapid visual assessment, propping the structure to relive it of its stresses, cleaning of the members, replacement of damaged reinforcement, and concreting by assuring a proper bond between old and new concrete.

The paper refers to only footing and columns as these two were site-specific problems. The same ideology could be further used for different structural members as recommended.

References

1. SP:24 Explanatory Handbook on Indian Standard Code of Practice For Plain & Reinforced Concrete (IS456-1978)
2. IS 13311 (Part1): 1992—Non destructive testing of concrete—methods of test Part 1 ultrasonic pulse velocity

Strength and Fire Behaviour of Concrete Reinforced with PET Fibres

Shruti K. Chodankar and P. Savoikar

Abstract In the construction industry, the term 'concrete' plays a very significant role. But concrete faces drawbacks such as brittleness, low fatigue, low ductility, low durability. To fix these problems, the concept of using non-biodegradable plastic bottle fibres can stay in the existence for hundreds of years. The best way to handle this waste is to introduce it in a concrete mix to minimize the environmental issues and also to study the plastic characteristics. Not only does non-biodegradable waste cause damage to the environment but it also has serious consequences for human and other things. In the present study, PET fibres were incorporated in the M30 grade of concrete with fibre volume fraction 0.5, 1 and 1.5% and strength was compared with concrete without plastic fibres. Appropriate tests were performed to measure mechanical properties such as compressive strength, flexure strength, split cylinder test and Fire test. Various specimens like cube, beams and cylinders were cast, cured and tested for 7 days strength and 28 days strength. Compression test, flexure test, split cylinder test and Fire test were carried out and then compared to the conventional concrete.

Keywords Plastic bottles · Compression test · Flexure test · Split cylinder test · Fire test

1 Introduction

Concrete is moderately brittle and weak in tension due to its capacity to cast in any shape. Therefore, conventional concrete is usually strengthened with steel reinforcing bars specifically intended and positioned in the concrete member's tensile area. Present work is an attempt of using Polyethylene Terephthalate (PET) fibres

S. K. Chodankar (✉) · P. Savoikar
Department of Civil Engineering, Goa Engineering College, Farmagudi, Veling, Goa 403 401, India
e-mail: chodankar.shruti@yahoo.in

P. Savoikar
e-mail: psavoikar@gmail.com

B. B. Das et al. (eds.), *Recent Trends in Civil Engineering*, Lecture Notes in Civil Engineering 105, https://doi.org/10.1007/978-981-15-8293-6_12

extracted from the unwanted plastic bottles, which is one of the potential wastes which could be used for the various applications. During past 50 years, there has been immense increase in the global plastic production which has become the most essential part of our modern lifestyle. In the present work, attempt was made to make the effective use of domestic PET waste in concrete in order to reduce the environmental issues caused by them and to limit over consumption of natural aggregates. Hence, effect of addition of these wastes on mechanical behaviour of concrete is investigated.

2 Literature Review

Luiz et al. [1] carried out an investigation on Polyethylene terephthalate (PET) fibres that were recycled as fibres reinforced rendered mortar. Various fibre percentages of 0, 0.5, 1.0 and 1.5% were introduced in dry mortar mixes. It showed significant improvement in flexural strength and mortar toughness. Maximum volume of pet fibres is for a desired workability was found to be 1.5%. Bhogayata et al. [2] carried out experimental study on use of polyethylene waste used for food packing and fly ash obtained from thermal power stations in concrete. Many samples were cast for M10 concrete mix with two different water/cement ratios. Plastic waste was converted into fibres with the volume of 0–1.5% and was added in concrete along with the fly ash from 0 to 30% by volume. The effect of chemical attack and corresponding compressive strength of the concrete mix was studied carrying out different curing conditions. Author also focussed on use of plastic waste in concrete in order to reduce environmental issues caused by dumped plastic. The author concluded that plastic bags can be used in shredded form to avoid problems in workability. It was seen that as far as was gain is concerned, plastic fibre along with fly ash showed a good result. The ideal water/cement ratio found was 0.45 with different curing media like water, acid and sulphate. It was reported that fibres in combination with fly ash showed comparatively resistance to chemicals without much reduction in strength. It was understood that for a non-structural concrete, durability aspect can be effectively increased introducing fibre which will not only increase its strength but will be great solution for the environmental issue of waste disposal of non-biodegradable plastics.

Ananthi et al. [3] used plastic cups as a fibre with two aspect ratio and using grade of concrete M20. The result proved that the addition of plastic increases the compressive strength and split strength. Hence plastics can be added as fibre to improve the properties of concrete.

Roohollah et al. [4] evaluated the hardened concrete properties like 7—and 28-day compressive strength, splitting tensile strength, flexural strength, water and air absorption and restrained shrinkage cracking. It was observed that addition of polypropylene (PP) fibres was helpful in the improvement of microstructure and restrained the formation and growth of micro-cracks in concrete. It was understood that aspect ratio of the fibres plays an important role in reinforcing the concrete.

Ruben et al. [5] carried out an investigation on waste PET bottles without processing through plastic melting and fibres spinning. First fibres were obtained by simply and directly shredding the waste plastic bottles with no need for pre-processing the plastic and secondly investigations were carried out to study the properties of the fibres and bond with the matrix. Nine mixes were tested with two different fibres profiles and length with three different volume fraction and using PET fibres as reinforcement in concrete.

3 Methodology

In the present study, PET fibres were obtained from PET bottles with two different widths and four different aspect ratios were used. Behaviour of concrete with PET fibres of different width and aspect ratios was studied by conducting compression tests, split tensile tests, flexure tests and fire tests.

3.1 Material Used

The materials used in the present study include PET bottle fibres, cement, sand, coarse aggregate and plasticizer.

3.1.1 Cement

Cement is the main constituent mixed with water, coarse and fine aggregates to form a concrete. Concrete is by far the most versatile and most extensively used construction material globally. Dalmia OPC 53 grade cement confirming IS 516 & IS 1199:1959 was used in this study. Cement mass was taken 240 kg/m^3 for M30 grade of concrete. GGBS (Ground Granulated blast-furnace slag) was added, which was obtained from CMPPL. The mass was taken 130 kg/m^3 for the respective grade of concrete.

3.1.2 Fine Aggregates

The fine aggregates used for the experimental work were locally available quarry and conformed to Indian Standard Specifications IS: 383-1970, with a specific gravity 2.71 and water absorption 3.46.

3.1.3 Coarse Aggregate

Coarse aggregates were used, which retained on BIS test sieve no. 480. The crushed aggregate was used from local source 20 mm downsize and confirms to (IS 2386:1963 (part I, II and III) with specific gravity 2.83 and water absorption 0.80.

The minimum size of 10 mm aggregate was used in this study having specific gravity 2.81 and water absorption 0.77. The aggregates were tested as per Indian Standard Specifications IS: 383-1970.

3.1.4 Chemical Admixture

D830 Chryso superplasticizer was used to improve workability and reduction in water–cement ratio. Usage of this admixture classically results in impermeable, honeycomb free and high-quality concrete.

3.1.5 PET Fibres

The polyethylene terephthalate (PET) bottles (which are often dumped openly causing environmental concern) were collected with no extra were shredded and added into concrete to understand the strength behaviour of various specimens like beam, cubes and cylinders. These bottles were used from discards of food and preferred beverage and other local industries where they are used for packaging of aerated drinks and water. These bottles used were the ones which are used for packaging of aerated drinks and not the packaging of water as these bottles are much thinner. Bottles used were mostly 1 litre and 2 litres. Some bottles were found with many undulations, which became difficult in shredding whereas plain bottles were comparatively smoother and were easy to cut. Smoother bottles were preferred over undulated ones. The shredding equipment is shown in Fig. 1 was fabricated in the laboratory. The neck and bottom of the bottle were cut into thin fibres of 1 mm and 2 mm width. The aspect ratio of 1:15, 1:25, 1:35, & 1:45 of PET fibres was used in the study. The fibre percentage used was 0.5–1.5% of the weight of cement. Table 1 shows the different combinations of fibres used in the tests.

3.2 Equipment Used

A wooden board of dimension 20 × 25 cm was drilled with two openings at a distance of 2.5 cm centre to centre. Bolts were inserted in through the openings, head of the bolt being at the bottom while tail at top. Washers were inserted to attain the desired height at both the bolts and to maintain the required width of the extracted strand. A blade was put on the washers and was held firmly by tightening of nuts to the respective bolt.

Fig. 1 **a** Strand cutting equipment and **b** PET strands cut to the required length

Table 1 PET fibres combinations

Sr. No.	Aspect ratio	Percentage of fibres (%)	Length × width	
1	1:15	0.5	0.1 × 1.5 cm	0.2 × 3 cm
		1		
		1.5		
2	1: 25	0.5	0.1 × 2.5 cm	0.2 × 5 cm
		1		
		1.5		
3	1:35	0.5	0.1 × 3.5 cm	0.2 × 7 cm
		1		
		1.5		
4	1:45	0.5	0.1 × 4.5 cm	0.2 × 9 cm
		1		
		1.5		

3.2.1 Strand Extracting Equipment

The strand extracting equipment was designed and fabricated to extract the fibres from PET bottles. The fibres obtained were removed from plastic bottles using this equipment. The materials required for this equipment are wooden board, bolt and nut and washer and blade. The bottle is placed over the blades and rotated in clockwise direction and accordingly strands are removed. Figure 1a shows the equipment used for extracting PET strands and Fig. 1b shows the strands cut to the required aspect ratio.

Table 2 Mix design details for M30 grade concrete

Parameters	Details	Parameters	Details
Grade of concrete	M30	Specific gravity of cement	3.15
Max nominal size of aggregate	20 mm	Specific gravity of: Coarse Aggregate 20 mm 10 mm	2.83 2.81
Min cement content	240 kg/m^3	Water absorption: Coarse Aggregate 20 mm 10 mm	0.80 0.77
GGBS	130 kg/m^3	Zone of sand	II
Water:Cement ratio	0.40		
Workability	100 mm slump	*Final mix proportions*	
Exposure conditions	Moderate	Mass of cement	370 kg/m^3
Method of placing	By hand	Mass of water	197 kg/m^3
Type of aggregate	Crushed semi cubical angular	Water cement ratio	0.40
Degree of supervision	Strict	Mass of admixture	2.22 kg/m^3
Maximum cement content	450 kg/m^3	Mass of sand	673 kg/m^3
Chemical admixture used	Chryso (Superplasticizer)	Mass of coarse aggregates (20 mm)	1250 kg/m^3

3.3 Mix Design

Mix design was done as per IS:10262-2019 for M30 grade mix. The detailed proportions are shown below in Table 2.

4 Results and Discussions

In this research work, the polyethylene terephthalate (PET) fibres were used in the concrete and their impact on normal concrete was investigated through experimental analysis. The test such a compressive strength, split tensile strength, flexural test and fire test were conducted. Following are the results obtained are tabulated below.

4.1 Influence of Fibre Percentage on Compressive Strength

The compressive strength of PET fibres concrete was calculated after 7 and 28 days of curing. Concrete cubes of size 150 mm for control mix as well as with PET fibre were cast. The average compressive strength for M30 cubes is shown in Fig. 2. It

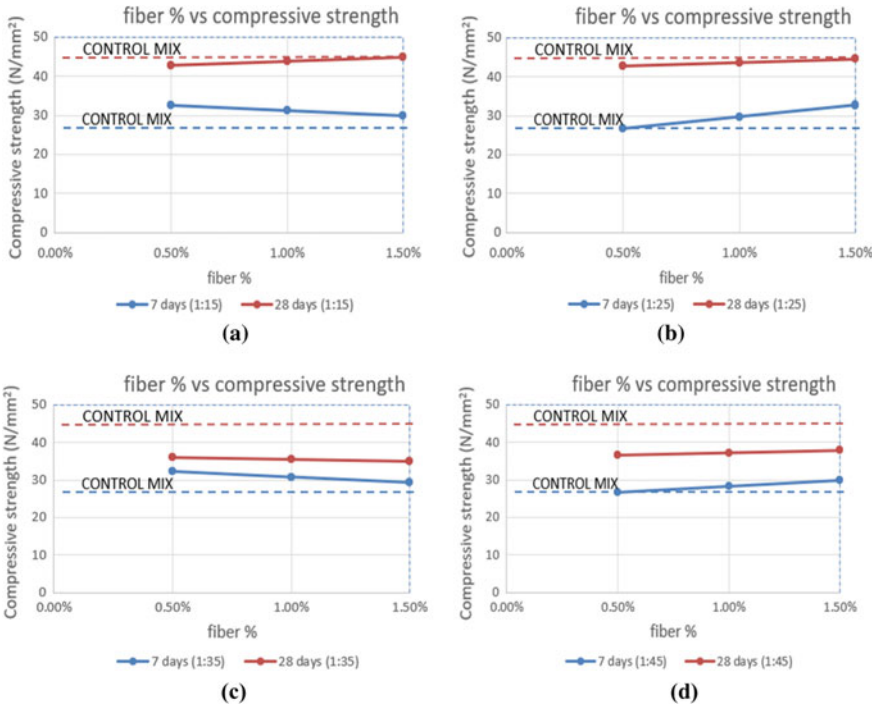

Fig. 2 Fibre content vs. compressive strength for aspect ratios of **a** 1:15, **b** 1:25, **c** 1:35 and **d** 1:45

was observed from Fig. 2a–d, that the seven-day compressive strength is more than the strength of control mix, whereas for fibre percentage of 1.50%, the compressive strength of is almost same as that of control mix for aspect ratios of 1:15 and 1:25. For aspect ratios of 1:35 and 1:45, the compressive strength falls slightly below the control mix strength. Figure 3a–c shows the plot of compressive strength with aspect ratio for different fibre contents.

4.2 Influence of Aspect Ratio and Fibre Content on Split Tensile Strength of Concrete

The behaviour of concrete in splitting tension was studied by conducting this test on cylinders of size 150 diameter × 300 mm height, cured for 28 days as per Indian Standards. The cylinder was kept on the platen of the compression testing machine horizontally. The variation of split tensile strength is plotted against fibre percentage and aspect ratio in Figs. 4 and 5, respectively. It can be seen that as fibre content increases, the split tensile strength also increases for all aspect ratios except for aspect

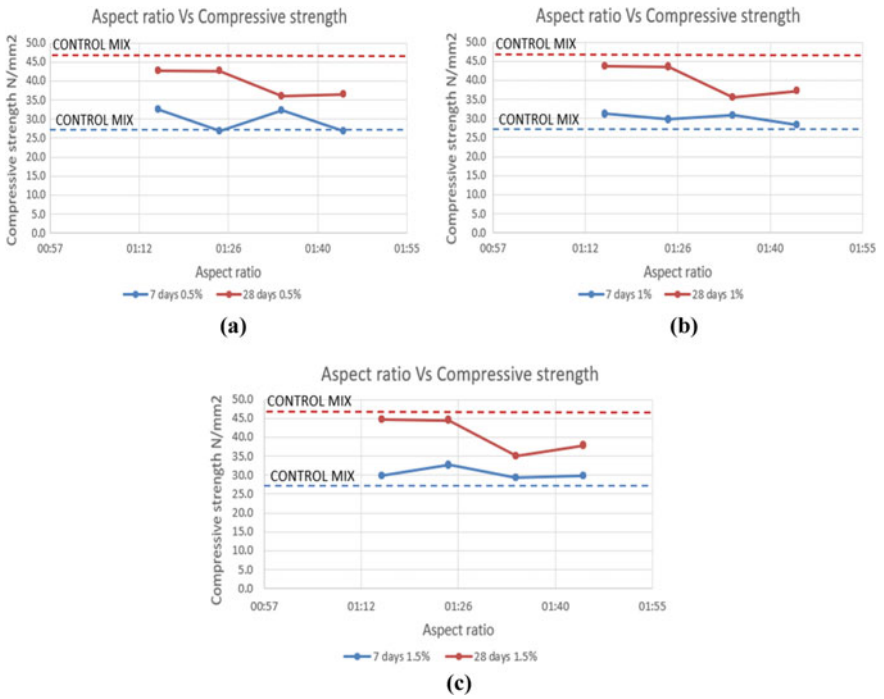

Fig. 3 **a** Aspect ratio versus compressive strength for 0.5% PET fibres to the weight of cement

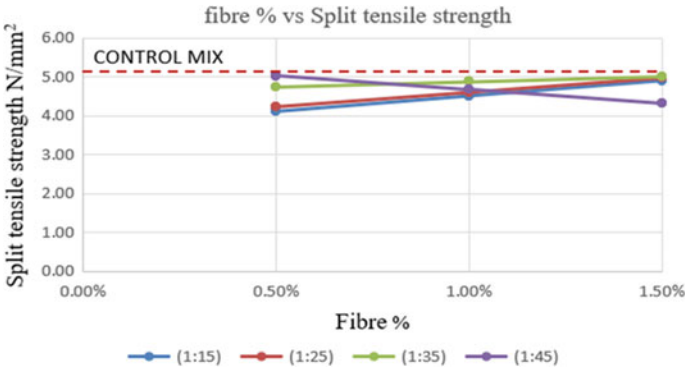

Fig. 4 Variation of split tensile strength at 28 days with fibre percentage

ratio of 1:45. For aspect ratio of 1:35 and fibre content of 1.5%, split tensile strength is maximum, almost same as control mix.

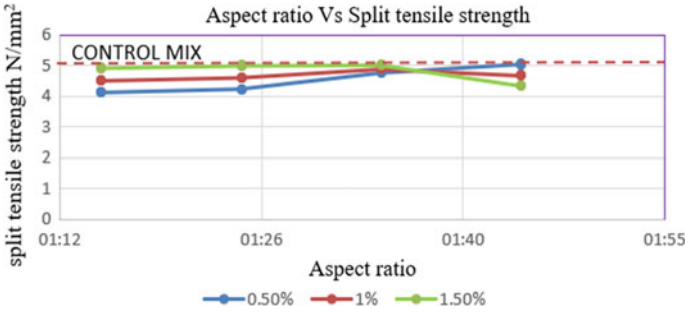

Fig. 5 Variation of split tensile strength at 28 days with aspect ratio

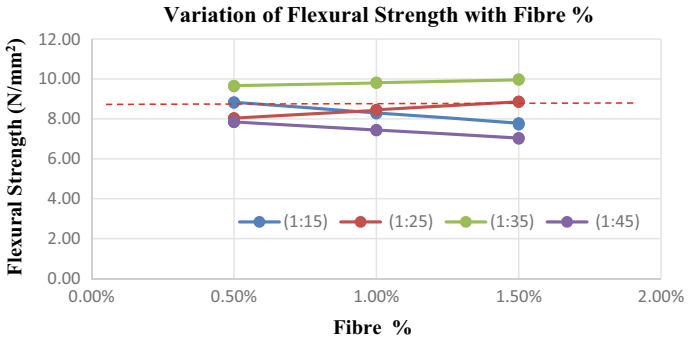

Fig. 6 Variation of flexural strength with fibre percentage

4.3 Influence of Fibre Content on Flexural Strength of Concrete

The flexure test was done on beam specimen of size 100 × 100 × 500 mm cured for 28 days and confirming to IS: 516-1959 to find out the behaviour of beams and other flexural members when cast at different aspect ratios. Figure 6 shows the variation of flexural strength with different fibre content for different aspect ratios. It is observed that there gradual increase in flexural strength with increase in fibre content. Aspect ratio of 1:35 shows increase in flexural strength of 13.2% over flexural strength of control mix.

4.4 Influence of Fire on Compressive Strength of Concrete

Fire testing was done on the concrete specimen of 75 mm × 75 mm × 75 mm for the different temperature variations of 200, 400 and 600 °C for the duration of 1 h, 2 h,

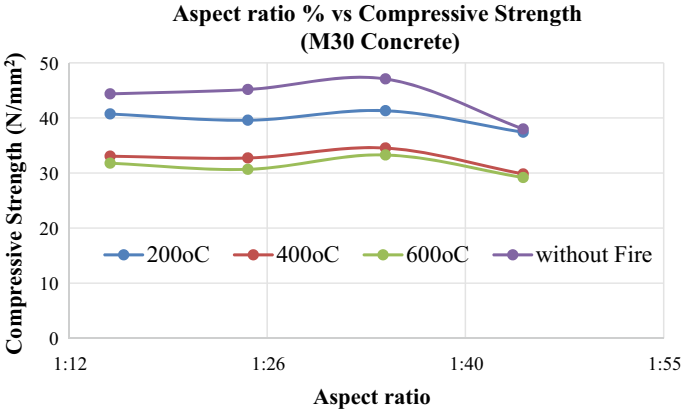

Fig. 7 Variation of compressive strength with aspect ratio after fire test (fibre percentage of 1.50%)

3 h, respectively. Figure 7 shows the variation of the compressive strength with aspect ratio of cubes subjected to fire test, for fibre content of 1%. It was observed that there was 12–29% reduction in strength over the control mix for fibre percentage of 1% and aspect ratio of 1:35 as compared to other aspect ratios for M30 grade concrete.

5 Conclusions

Plastic is one of those group fibres that can improve certain properties of concrete. This study is aimed at utilizing the plastic waste in the construction industry in order to control the environmental pollution and nuisance caused to humans. The objective of the present study is to study the effect of PET fibres in the concrete. From the above study, it is concluded that:

(1) Addition of PET fibres in various percentages increases the strength of concrete.
(2) Higher compressive strength is obtained with 1.50% fibre percentage in concrete.
(3) As aspect ratio increases from 1:15–1:35, compressive strength also increases, thereafter it decreases for aspect ratio of 1:45. Based on these, it is concluded that fibres with aspect ratio of 1:35 and fibre percentage of 1.5% give better results.
(4) Split tensile strength increases with fibre percentage of 0.5–1.50% for all aspect ratios of 1:15–1:35, while for 1:45 aspect ratio, split tensile strength if found to reduce.
(5) There is marginal increase in flexural strength with fibre percentage. Aspect ratio of 1:35 gives higher flexural strength.

(6) Compressive strength decreases with increase in temperature and time of exposure to which cubes are subjected. However, better results are obtained with aspect ratio of 1:35.
(7) Based on the above conclusions, fibre percentage of 1.50% and aspect ratio of 1:35 are found to give better performance in compression, flexure, split tensile strength and fire behaviour.

References

1. Luiz A, Pereira de Oliveira, João Castro-Gomes P (2011) Physical and mechanical behaviour of recycled PET fibre reinforced mortar
2. Bhogayata A, Shah KD, Vyas BA, Arora NK (2012) Feasibility of waste metallised polythene used as concrete constituent. Int J Eng Adv Technol 1
3. Ananthi A, Jay Tamil Eniyan A, Venkatesh S (2017) Utilization of waste plastics as a fibre in concrete. Int J Concrete Technol 3
4. Roohollah B, Hossein Sadeghi A, Masoud L (2011) Utilizing polypropylene fibres to improve physical and mechanical properties of concrete. Text Res J 82(1):88–96
5. Ruben Paul B, Baldacchino O, Liberato F (2016) Early age performance and mechanical characteristics of recycled PET fibre reinforced concrete. Constr Build Mater 108:29–47

Assessment of Construction and Demolition Waste in Goa for Re-use in New Construction

Kohen Duarte, Paraj Fernandes, Nadya Baracho, Roshani Majik, Samantha Dias, and Manisha Dias

Abstract Demolition of old structures to construct new ones leads to a lot of waste generation. This waste is dumped in landfills, open sites or water bodies and is becoming a serious environmental issue. In the state of Goa itself, structures above 50 years are due for demolition and would generate a lot of waste. The construction and demolition (C&D) wastes are widely untapped resources available to the construction industry. It has a large potential to sustainably and economically provide raw materials for new constructions. In this paper, the authors have investigated and proposed, through tests, methods of recycling and re-using construction and demolition waste to make new constructions environment-friendly while being economical.

Keywords Demolition waste · Sustainability · Recycling

1 Introduction

The construction industry has gained very fast growth in recent decades due to the increase in the population, IT sector and introduction of new infrastructure because of which there is demand for construction materials, and these construction activities result in generation of massive amount of construction waste. Construction material wastage results in the huge financial setbacks to builders, contractors, regional authorities and also to the country.

The production of waste due to demolition of structures is more than the wastage which occurs during construction of structures, so there is need of management of C&D wastes as this is a relatively new subject in India.

The state of Goa in India is undergoing massive changes in its infrastructure and construction landscape, changes which are resulting in the demolition of aged government and private buildings and an exponential rise in its new construction industry, and both these processes of demolition and construction are creating a lot

K. Duarte (✉) · P. Fernandes · N. Baracho · R. Majik · S. Dias · M. Dias
Department of Civil Engineering, Don Bosco College of Engineering, Fatorda, Goa, India
e-mail: Kohenduarte1995@gmail.com

B. B. Das et al. (eds.), *Recent Trends in Civil Engineering*, Lecture Notes in Civil Engineering 105, https://doi.org/10.1007/978-981-15-8293-6_13

of waste which the small state of Goa is having to dispose of in its landfills. But with recent disputes over waste management and land allocation for landfill sites, this is becoming a cumbersome task for authorities. As it stands, Goa has a very small reserve of usable sand and other construction material, and the importance of the study into the reuse of its now rapidly growing C&D waste stockpile is at its peak.

The unique climatic conditions of Goa with its high humidity and rainfall interspersed with high saline content of the soil and temperature fluctuations affect the construction and demolition material in many ways, because of which we have to ascertain the quality, strength and usability of these materials for the recycling process.

2 Method of Obtaining Recycled Material

2.1 Concrete and Cement Plaster

Concrete and cement plaster were obtained from various sites in Goa. The source and its age are tabulated in Table 1.

The concrete obtained from these sites (Fig. 1) were made into smaller chunks using sledge hammers. The cement plaster from each of these sites was carefully removed by downward action of chisel breaker. Care was taken not to allow excessive

Table 1 Source of concrete

Material	Location	Used in	Age of material in years
Concrete	Verna, Goa	Beams	8
Concrete	Verna, Goa	Columns	16
Cement plaster	Nuvem, Goa	Cement plaster	12
Cement plaster	Raia, Goa	Cement plaster	18
Concrete	Raia, Goa	Concrete slab	18
Concrete	Mapusa, Goa	Beams	30
Concrete	Mapusa, Goa	Columns	30
Concrete	Mapusa, Goa	Concrete slab	30
Cement plaster	Mapusa, Goa	Plaster	30
Concrete	Verna, Goa	Slab	New construction
Cement plaster	Verna, Goa	Plaster	New construction

Fig. 1 Concrete waste obtained from Verna

laterite particles to stay attached to the cement plaster. After reaching the satisfactory size the chunks were put into Los Angeles abrasion testing machine for further breakdown for approximately 1000 rotations. After 1000 rotations the material was removed from the drum (Fig. 2) and sieved using 4.75 mm sieve. All that is retained

Fig. 2 Chunks of concrete in Los Angeles abrasion testing machine (left). Aggregate obtained after rotations (right)

Fig. 3 Sieving of fine aggregate to adhere to zone II (left). Powder retained on pan (right)

on 4.75 mm is coarse aggregate and all that passes through the sieve is fine aggregate and powder.

2.1.1 Fine Aggregate

The powder obtained or the recycled sand obtained from the breaking was then sieved through 4.75 mm, 2.36 mm, 1.18 mm, 600 μ, 300 μ, 150 μ to adhere to the specifications of zone II sand as per IS 383:1970. Material retained on pan is known as 'powder' and is used for different purposes as fine aggregates (Fig. 3).

2.1.2 Coarse Aggregate

Coarse aggregate obtained from the breaking was sieved through 20 and 10 mm and retained on 4.75 mm. Material passing through 20 mm and retained on 10 mm is known as 20 mm downsize, and material passing through 10 mm and retained on 4.75 mm is known as 10 mm downsize.

2.2 Flooring

Details of flooring from various sites are tabulated in Table 2.

After the materials were obtained from the site (Fig. 4), they were broken down into smaller pieces using a sledge hammer. Processing of tiles obtained from the breaking was sieved through 20 mm, 10 mm and retained on 4.75 mm. Material passing through 20 mm and retained on 10 mm is known as 20 mm downsize, and material passing through 10 mm and retained on 4.75 mm is known as 10 mm downsize.

Table 2 Source of tiles and flooring

Material	Location	Used in	Age of material in years
Khadappa	Fatorda, Goa	Flooring	4
Granite	Fatorda, Goa	Table top	4
Mosaic	Nuvem, Goa	Flooring	16
Khadappa	Nuvem, Goa	Exterior flooring	12
Granite	Mapusa, Goa	Flooring	10
Mosaic	Raia, Goa	Flooring	18
Granite	Verna, Goa	Flooring	New construction

Fig. 4 Mosaic and Khadappa flooring obtained from Nuvem

2.3 Steel

Steel was retrieved from the same sites as those of concrete. The columns and beams were broken with breakers and the steel reinforcement was removed from them. Bars were immediately kept in stable condition so as to avoid reaction with air. Steel was segregated into 8, 10, 12 mm bars. Bars which were previously exposed and now rusted were treated with physical treatment like hammering and scrubbing with sand paper.

2.4 Glass and Plastic

The first step of the demolition process is the removal of glass and plastic materials carefully without causing much damage. These materials have to be stored separately on site which can be reused if in good condition or are send for recycling. There are currently several plants in Goa which recycle these materials.

2.5 Masonry

Masonry is usually destroyed during the demolition process and it is found to be economically viable to crush and dump the broken masonry either in the site of demolition or in landfills. If carefully removed, it can be reused. The broken masonry can be used for rubble soling, decorative purpose.

3 Experimental Programme

Standard IS tests were carried out on the materials obtained. The details of these tests and results are tabulated in Table 3.

4 Methodology

Trials with recycled sand, natural sand, recycled coarse aggregates, natural coarse aggregates and cement were taken. The various trials of mix design carried out are tabulated in Table 4.

Concrete cubes were cast and the compression test was carried out as per IS:516-1959. For testing of mortar, six cubes of cement and recycled sand were cast. The proportion of 1:3, that is 1 part of cement and three parts of recycled sand, was used. These cubes were compared with cubes cast of cement and natural sand for 7 and 28 days strength.

5 Results

5.1 Compression Test on Concrete and Discussion

The compression tests were carried out on compression testing machine (Fig. 5), and the results of these tests on the various mixes are tabulated in Table 5. The results of the construction and demolition waste cubes were found to be on par with the cubes cast with natural materials considering the compressive strength.

As seen in Table 5, the compressive strength of concrete increases with the use of Masterset AC 100 in Trial VI as compared to Trial I. Masterset AC 100 is an admixture used to improve early strength as well as the ultimate strength of concrete, and increase in slump was also observed.

The use of Mastercast 1162 admixture reduces the slump of mixed concrete as it is a no-slump admixture. This was seen by comparing results obtained in Trials II

Table 3 Tests and results on materials

Test	Material	IS code	Result	Remarks
Sieve analysis	Recycled 20 mm coarse aggregates	IS:2386-PART 1	Conforms to IS values	Material made to conform with IS standards[a]
	Recycled 10 mm aggregates		Conforms to IS values	Material made to conform with IS standards[a]
	Recycled tiles		Conforms to IS values	Material made to conform with IS standards[a]
Specific gravity	Coarse aggregates	IS:2386-PART 3	2.876	–
	Recycled coarse aggregates		2.96	–
	Fine aggregates		2.4	–
	Recycled fine aggregates		2.5	–
	Cement	IS:4031-PART 2	2.91	–
Water absorption	Natural coarse aggregates	IS:2386-PART 3	0.40%	–
	Recycled coarse aggregates		0.60%	–
	Natural fine aggregates		0.80%	–
	Recycled fine aggregates		0.80%	–
Abrasion test	Natural coarse aggregates	IS:2386-PART 4	18.30%	–
	Recycled coarse aggregates		20.50%	Within permissible limits
	Tiles (as coarse aggregates)		25.91%	Within permissible limits
Impact value	Natural coarse aggregates	IS:2386-PART 4	10.02%	–
	Recycled coarse aggregates		17.30%	Within permissible limits
	Tiles (as coarse aggregates)		7.60%	Within permissible limits
Flakiness index	20 mm recycled aggregates	IS:2386-PART 1	9.91%	Within permissible limits
Elongation index	20 mm recycled aggregates	IS:2386-PART 1	14.94%	Within permissible limits

(continued)

Table 3 (continued)

Test	Material	IS code	Result	Remarks
Silt content	Recycled fine aggregates	IS:2386-PART 2	3%	Within permissible limits

[a]The material was sieved and sorted into its sieve size categories and then added together to form the IS code required percentages of sieve distribution for the type of aggregate

Table 4 Description of mixed proportions considered in the study

Trial	Description	Remarks
1	Natural sand, natural coarse aggregate, cement	Admixture was added as required
2	Recycled sand, recycled coarse aggregates, cement	
3	Recycled sand, natural coarse aggregates, cement	
4	Natural sand, recycled coarse aggregates, cement	
5	Coarse aggregates (flooring), recycled sand, cement	
6	Recycled sand, recycled coarse aggregates, cement	
7	Recycled sand, coarse aggregates, cement	
8	Natural sand, recycled coarse aggregates, cement	

Fig. 5 Testing of concrete cubes

Table 5 Compressive test results of concrete cube

Trial	Test no	Constituents materials	Grade	Admixtures	Slump	Curing time	Strength (N/mm^2)
I	1	Natural sand, natural coarse aggregate, cement	M25	Nil	100 mm	Accelerated curing	32.87
	2						31.41
	3						31.41
						Average	**31.89**
II	1	Recycled sand, recycled coarse aggregates, cement	M25	Mastercast 1162	25 mm	Immersed curing for 28 days	30.33
	2						29.33
	3						27.11
						Average	**28.92**
	1	Recycled sand, Recycled coarse aggregates, cement	M25	Mastercast 1162	25 mm	Immersed curing for 7 days	17.77
	2						20.00
	3						18.88
						Average	**18.86**
III	1	Recycled sand, natural coarse aggregates, cement	M25	Masterset AC 100	150 mm	Immersed curing for 28 days	33.77
	2						37.33
	3						35.88
						Average	**35.66**
IV	1	Natural sand, recycled coarse aggregates, cement	M25	Masterset AC 100	90 mm	Accelerated curing	27.44
	2						28.22
	3						30.11
						Average	**28.59**
V	1	Coarse aggregate (flooring), recycled sand, cement	M25	Masterset AC 100	25 mm	Accelerated curing	18.60
	2						17.85
	3						18.3
						Average	**18.25**

(continued)

Table 5 (continued)

Trial	Test no	Constituents materials	Grade	Admixtures	Slump	Curing time	Strength (N/mm^2)
VI	1	Recycled sand, recycled coarse aggregates, cement	M25	NIL	75 mm	Accelerated curing	31.55
	2						28.44
	3						30.66
						Average	**30.21**
VII	1	Recycled sand, natural coarse aggregates, cement	M25	NIL	80 mm	Accelerated curing	33.77
	2						35.55
	3						32.22
						Average	**33.84**
VIII	1	Natural sand, recycled coarse aggregates, cement	M25	NIL	130 mm	Accelerated curing	35.11
	2						37.33
	3						34.44
						Average	**34.96**

and VI which had the same combination of recycled sand, recycled coarse aggregate and cement.

It was also observed that the compressive strength of cubes cast with coarse aggregates obtained from tiles and flooring was much lower than any of the other combinations.

Table 6 shows the standard deviations and the coefficients of variation of the results tabulated in Table 5 for 28 days strength. The variation in compressive strength of concrete cubes with varying combinations of material is illustrated in Fig. 6.

Table 6 Standard deviation and coefficient of variation of trials

Trial	Standard deviation (N/mm^2)	Coefficient of variation (%)
I	5.40	17.77
II		
III		
IV		
V		
VI		
VII		
VIII		

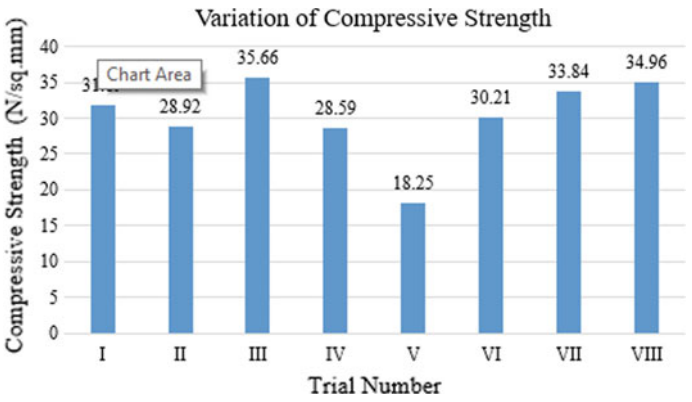

Fig. 6 Graph of variation in compressive strength for different material combinations

5.2 Compression Test on Cubes

The cement-recycled sand cubes were tested for 7 days strength and 28 days strength. The results of the compression tests carried out on the UTM are tabulated in Table 6 and the failure pattern was as seen in Fig. 7. Strength of cement—natural sand cubes casted was 21.77 N/mm^2 for 7 days and 31.1 N/mm^2 for 28 days (Table 7).

Fig. 7 Failure pattern of cement-recycled sand cubes

Table 7 Compression test on cement-recycled sand cubes

For 7 days of curing					
S. no.	Load (N)	Area (mm^2)	Strength (N/mm^2)	Standard deviation (N/mm^2)	Coefficient of variation (%)
1	60×10^3	50×50	24	0.47	1.94
2	65×10^3	50×50	25		
3	60×10^3	50×50	24		
		Average	**24.33**		
For 28 days of curing					
S. no.	Load (N)	Area (mm^2)	Strength (N/mm^2)	**Standard deviation (N/mm^2)**	**Coefficient of variation (%)**
1	75×10^3	50×50	30	0.71	2.28
2	78×10^3	50×50	31.2		
3	79.2×10^3	50×50	31.68		
		Average	**30.96**		

6 Conclusion

Crushing of C&D waste in the Los Angeles abrasion testing machine was done as a trial and it was observed that the recycled material obtained was of satisfactory quality. For actual crushing of C&D waste on site, the existing crushers could be modified to obtain desired grade of aggregates.

The materials retrieved from various sites of different ages, locations and types of construction help us establish a realistic C&D waste material quality, which will be practically retrieved from sites across Goa. Hence it can be assumed that the results of the tests would be similar to those which will be achieved when implementation of this process takes place. However, tests have to be carried out on these materials before being used.

The abrasion value of the recycled aggregate was well below the permissible limit of 40%. The impact value of recycled aggregates indicated that the aggregates were exceptionally strong with values lesser than 30%, the water absorption was less than 1%, the combined value for elongation and flakiness is less than 30% and hence the aggregates can be used in construction of wearing surfaces such as runways and roads [9, 14].

The silt content below 6% indicates that the recycled aggregates could be safely used in concrete. Concrete of mix M25 could be achieved in Trials III, VII and VIII (the strength obtained is above target strength of 31.6 N/mm^2). Recycled materials can be used for the infrastructure development currently being undertaken in Goa. However, the durability of concrete using the recycled aggregates is to be studied.

Very good strength of cement-recycled sand cubes was obtained, indicating that it could be used as mortar or plaster in masonry work.

References

1. Shahidan S et al (2017) Utilising construction and demolition (C&D) waste as recycled aggregates (RA) in concrete. Procedia Eng 174:1028–1035
2. Ulubeyli S, Kazaz A, Arslan Volkan (2017) Construction and demolition waste recycling plants revisited: management issues. Procedia Eng 172:1190–1197
3. Anthony J, Nair DG (2016) Potential of construction and demolished wastes as pozzolana. Procedia Technol 25:194–200
4. Wagih AM, El-Karmoty HZ, Ebid Magda, Okba Samir H (2013) Recycled construction and demolition concrete waste as aggregate for structural concrete. HRBC J 9:193–200
5. Lai Ying-Ying, Yeh Li-Hsu, Chen Ping-Fu, Lee Po-Hsun Sung Yuh-Ming (2016) Management and recycling of construction waste in Taiwan. Procedia Environ Sci 35:723–730
6. Wahi N, Joseph C, Tawaie R, Ikau R (2016) Critical review on construction waste control practices: legislative and waste management perspective. Procedia—Soc Behav Sci 224:276–283
7. Shetty MS (2005) Concrete technology theory and practice. S. Chand and company Ltd., Ramnagar, New Delhi
8. Neville AM (2003) Properties of concrete, 4th edn. Pitman publishing, London
9. IS: 383-1970, "Specification for coarse and fine aggregates from natural sources for concrete", Bureau of Indian Standard, New Delhi
10. IS 456:2000, "Plain and reinforced concrete - Code of practice", Bureau of Indian Standard, New Delhi
11. IS: 2386 – 1963 (Part I, Part II, Part III, and Part IV), "Methods of test for aggregates for concrete", Bureau of Indian Standard, New Delhi
12. IS 4031 (Part 2):1999, "Methods of physical tests for hydraulic cement", Bureau of Indian Standard, New Delhi
13. IS: 10262-1982, "Recommended guidelines for concrete mix design", Bureau of Indian Standard, New Delhi
14. IRC:110-2005, "Standard specifications and code of practice for design and construction of surface dressing", The Indian Road Congress, New Delhi

A Comprehensive Review of Ultra-Fine Materials as Supplementary Cementitious Materials in Cement Concrete

Vinay Mohan Agrawal and Purnanand Savoikar

Abstract The cement consumption worldwide is increasing rapidly with vast development in the construction sector. The cement production emits large amount of hazardous carbon-di-oxide to the atmosphere. So control on consumption of cement is not easy, rather use of any other pozzolanic material as partial replacement of OPC is a solution which can reduce cement production. The pozzolanic materials such as fly ash and slag and fly ash have been used previously in cement concrete as a replacement of cement. These pozzolanic materials give good mechanical strength at later age but not at early age. The strength at early age is important for pre-cast members, to reduce stripping time, slab cycle time and the overall construction time. Early age strength is possible with ultra-fine materials such as ultra-fine fly ash and ultra-fine slag in cement concrete. Due to smaller particle size they react much faster and impart better early strength in cement concrete. This paper critically reviews the feasibility of ultra-fine material usage as supplementary cementitious materials. The paper elaborates the mechanical and durability properties with regards to ultra-fine material in cement concrete.

Keywords Cement · Supplementary cementitious materials · Fly ash · Slag · Ultra-Fine material

1 Introduction

Fly ash and slag are the two main industrial byproducts used in raw as well as processed form as supplementary cementitious materials. The particle size of fly ash and slag are almost the same as that of ordinary Portland cement. Due to similarity in

V. M. Agrawal (✉) · P. Savoikar
Civil Engineering Department, Goa College of Engineering, Farmagudi, Goa, India
e-mail: vmagrawal@yahoo.co.in

P. Savoikar
e-mail: psavoikar@gmail.com

V. M. Agrawal
NICMAR Goa Campus, Ponda, Goa, India

B. B. Das et al. (eds.), *Recent Trends in Civil Engineering*, Lecture Notes in Civil Engineering 105, https://doi.org/10.1007/978-981-15-8293-6_14

particle size, the packing density of the new composite material with either fly ash or slag does not improve significantly if used unprocessed or in raw form. The smaller particle size of fly ash and slag can be achieved by classifying and/or grinding the bigger/coarser fly ash and slag into finer ones. This fine or ultra-fine size of slag and fly ash is observed to significantly improve the particle packing density, microstructure, physical and durability properties of the mortar and/or concrete. This paper reviews research on utilization of two main ultra-fine material, that is, ultra-fine fly ash and slag. The paper discusses the feasibility of ultra-fine material usage as supplementary cementitious material with regards to its mechanical and durability properties in cement concrete.

Deb et al. [1] proposed an efficient way to produce ultra-fine fly ash by air cyclone method and they concluded that flow property and mechanical strength increases by usage of ultra-fine fly ash. Yazici and Hasan [2] have investigated the effect of fineness of ultra-fine material in compressive strength of concrete. Partha and Prabir [3] investigated the setting time and compressive strength of geopolymer made with normal and ultra-fine fly ash. Effect of ultra-fine slag has been studied by [4] by comparing ultra-fine slag for compressive strength estimation.

Studies on the use of ultra-fine fly ash and slag have been investigated by many other researchers as discussed under literature review presented further in this paper.

2 Usage of Ultra-Fine Material as Supplementary Cementitious Material

Grinding of fly ash using grinding aid to ultra-fine size is studied by [5]. They have added 0.05% of organic grinding aid to raw fly ash which is fed in laboratory-scale ball mill. The study is focused on properties of fly ash. Those which are produced with and without the addition of grinding aid for reducing the size of fly ash. The major conclusion drawn was with respect to improvement in specific surface area, which was seen to improve with the grinding aid introduction with respect to that of control sample. They have presented the results pertaining to reduction or narrowness in particle size distribution. Also, the particles less than 16 microns are seen to be in large percentage when grinding aid is used. Ultra-fine fly ash produced by this method have shown improved hydration degree, product quantity, uniformity and compactness. The results were analyzed with microstructure tests such as SEM and XRD to confirm the improvement in microstructural level.

An air cyclone method for the preparation of ultra-fine fly ash is proposed by Deb et al. [1]. Air is used as a fluid medium in an air cyclone method to reduce the size of coarse fly ash to ultra-fine fly ash. They have been able to achieve a particle size of less than 10 microns by using this particular method. The particle size distribution achieved is well distributed, and hence it is capable of imparting better particle packing when used as supplementary cementitious material. The properties such as flow spread and compressive strength are studied, and a significant improvement is

observed in these properties with respect to control concrete. They have used 15 and 30% as the replacement levels for both raw and ultra-fine fly ash. They have observed almost 100% increase in flow properties and significant improvement is observed in compressive strength of mortars with ultra-fine fly ash after 28, 90 and 180 days.

Effect of curing under normal and steam curing condition was studied by [6]. They replaced OPC by 20 and 35% ultra-fine fly ash to achieve high strength concrete. They found reduction in adiabatic temperature rise within early days in concrete with ultra-fine fly ash due to its poor reactivity quotient. They concluded that for 7 and 28 days, the compressive strength is matching with that of control concrete when steam curing is performed. Also, improvement in pore structure is observed which reduces the permeability of concrete. They concluded that due to poor reactivity, ultra-fine fly ash shows slow reactivity in the initial days, but the same can be accelerated by steam curing.

High-volume fly ash mortar is studied by [7]. They have focused on microstructure, compressive strength and workability of the mortar. They replaced OPC by 40, 50, 60 and 70% fly ash. The combination is made ternary by adding 5, 8, 10, 12 and 15% of ultra-fine fly ash. They concluded that with the increase in the percentage of ultra-fine fly ash, the flow properties of the mortar increases. They studied the compressive strength parameter and concluded that the effect of 8% ultra-fine fly ash provides the maximum strength specifically at early age due to high specific area. They confirmed using SEM and XRD results that, due to high silica content in ultra-fine fly ash, mortar could generate additional CSH gel. This is helpful in increasing the consumption of CH in high volume fly ash mortar. They presented the compressive strength values of 7 and 28 days.

Li [8] investigated the ultra-fine fly ash, metakaolin and silica fume usage in different combinations. He concluded that the use of ultra-fine fly ash gives better flow property than with the usage of silica fume or metakaolin. He also investigated the drying shrinkage and found that the addition of ultra-fine fly ash and silica fume increased the drying shrinkage, whereas the addition of metakaolin reduced the drying shrinkage. The ternary blend with OPC, ultra-fine fly ash and metakaolin is recommended to be economically advantageous for production of high strength concrete. Ultra-fine slag as a partial replacement of OPC is studied in terms of mechanical and durability properties by [9]. They concluded that due to large surface area of ultra-fine slag, it is more reactive and hence it enhances the hydration and pozzolanic reactions. They proved that compressive strength at all ages as well as flexural strength is seen to improve with ultra-fine slag addition. The durability properties such as chloride diffusivity are seen to be significantly less in ultra-fine slag as compared to control mix. They have observed significant reduction in pore connectivity, chloride diffusion and penetration in mix containing ultra-fine slag.

Jindal et al. [10] developed a study with fly ash-based geopolymer with ultra-fine slag. They have identified the mechanical and durability properties with three different fly ash content with 0, 5 and 10% of ultra-fine slag. They concluded that

workability increases with the addition of ultra-fine slag. The compressive and flexural strength have also been noted to increase with increase in percentage of ultra-fine slag content. Improvement in microstructure is seen, and hence they concluded improvement in durability properties.

Praveen et al. [11] studied the mechanical and microstructural properties of fly ash-based geopolymer with ultra-fine slag. They concluded that due to polymerization and improved hydration, the mechanical strength improves significantly. The SEM results shows matrix with denser mix, fewer cracks and less voids, hence they conclude this to be better compacted mix. Mechanical and durability properties are investigated by [12] in concrete with 10% replacement of OPC by ultra-fine slag. They concluded that due to improvement in rheology of fresh concrete, the workability and consistency increased with the inclusion of ultra-fine slag. They also concluded that the durability properties such as permeability and chloride penetration are found to reduce with ultra-fine slag.

Kavitha and Kala [13] studied the replacement of OPC by ultra-fine slag in the range of 5–20% with constant GGBS replacement content of 30% in self-compacting concrete. They concluded that compressive strength, flexural strength and split tensile strength improve significantly with 10% replacement of ultra-fine slag. Mechanical strength and durability parameters were examined using ultra-fine slag and silica fume by [14]. They replaced OPC by 5, 10 and 15% of ultra-fine materials. They concluded that with 10% replacement, the maximum compressive strength can be achieved. Void content, water absorption and sorptivity are observed to be reducing with the inclusion of ultra-fine materials. Ultra-fine slag and silica fume both showed remarkable performance in sulphate attack and acid test.

Usage of ultra-fine GGBS is studied by Pradeep et al. [15] as a replacement of OPC in the range of 10% with addition of 2% of calcium nitrate as chemical admixture. They have found that the addition of ultra-fine GGBS enhances the water demand and hence workability is reduced. Compressive strength of concrete and rebar bond strength are found to increase by 18 and 45%, respectively. With the addition of calcium nitrate the increment in compressive strength is seen to enhance by 32% and bond strength by 131%. They also examined the SEM images of corroded rebar and concluded that the addition of calcium nitrate reduced the corrosion in rebar along with increment in mechanical properties. [16] investigated the effect of addition of ultra-fine fly ash in cement paste and concrete. They concluded that setting time gets longer and reduction in slump loss was observed due to ultra-fine fly ash. They also concluded that with higher percentage of ultra-fine fly ash the compressive strength reduction is unavoidable.

Subramanian et al. [17] compared the feasibility of ultra-fine fly ash as cement replacement and compared its properties with that of silica fume. They concluded that with the addition of ultra-fine fly ash shrinkage cracking is reduced and increment in compressive strength is seen as compared with silica fume and control concrete [18] investigated the effect of fineness of ultra-fine fly ash in mechanical properties of concrete. They replaced the fly ash in different percentage and fineness. They concluded that the setting time increases for all 15 and 30% replacement as compared to control mix. The compressive strength of concrete with highest fineness and with

replacement up to 45% is shown to increase as compared to control concrete. Tensile strength is also observed to increase as compared to control mix.

3 Conclusions

Based on the research available in the usage of ultra-fine material as supplementary cementitious materials, it can be concluded that ultra-fine materials are very much suitable in cement mortar and concrete. The replacement level in percentage is not very high (5–20%), but the improvement seen in fresh, mechanical and durability properties is very promising. Each ultra-fine material has its own advantage and limitations, which largely depend on their physical and chemical characteristics.

Ultra-fine fly ash and ultra-fine slag impart good early strength, by improving the microstructure of the cement mortar and concrete which is attributable to large surface area. The reactivity increases due to smaller size particles and hence early strength is enhanced. The improvement in the pore structure and densification of mix imparts better durability properties to the mortar and concrete. The mix with ultra-fine materials shows better resistance against chloride attack, acid attack and reduces permeability and porosity.

It can be concluded from the literature study that ultra-fine material can be used as supplementary cementitious materials which will improve the fresh, mechanical and durability properties of the mix. Usage of these will also save OPC and hence carbon emission can be reduced. The waste utilization as a result of its usage in modified form is an added advantage to the industry.

References

1. Deb JM et al (2006) Characteristics of the ultrafine component of fly ash. Fuel 85(16):2250–2259
2. Yazici Ş, Hasan ŞA (2012) Effects of fly ash fineness on the mechanical properties of concrete. Sadhana 37(3):389–403
3. Partha S, Prabir KS (2017) Effects of ultrafine fly ash on setting, strength, and porosity of geopolymers cured at room temperature. J Mater Civ Eng 29(2):211–216
4. Reddy MVS et al (2016) Studies on eco-friendly concrete by partial replacement of cement with alccofine and fine fly ash. ARPN J Eng Appl Sci 11(5):4–8
5. Zhao J et al (2015) Ultrafine grinding of fly ash with grinding aids: impact on particle characteristics of ultrafine fly ash and properties of blended cement containing ultrafine fly ash. Constr Build Mater 78:250–259
6. Feng J et al (2015) Effects of ultrafine fly ash on the properties of high-strength concrete. J Therm Anal Calorim 121(3):1213–1223
7. Supit SWM et al (2014) Effect of ultrafine fly ash on mechanical properties of high volume fly ash mortar. Constr Build Mater 51:278–286
8. Li Zhengqi (2016) Drying shrinkage prediction of paste containing meta-kaolin and ultrafine fly ash for developing ultra-high performance concrete. Mater Today Commun 6:74–80

9. Teng S et al (2013) Durability and mechanical properties of high strength concrete incorporating ultra fine ground granulated blast-furnace slag. Constr Build Mater 40:875–881
10. Jindal Y et al (2016) Development of high strength fly ash based geopolymer concrete with alccofine. J Mech Civ Eng, Special Issue:54–58
11. Praveen S et al (2018) Mechanical and microstructural properties of fly ash based geopolymer concrete incorporating alccofine at ambient temperature. Constr Build Mater 180:298–307
12. Sivakumar H et al (2015) Durability and mechanical characterization of concrete using alccofines. Int J Appl Eng Res 10(1):178–182
13. Kavitha S, Felix Kale T (2016) Evaluation of strength behaviour of self-compacting concrete using alccofine and GGBS as partial replacement of cement. Indian J Sci Technol 22(9):1–7
14. Mohan A, Mini KM (2018) Strength and durability studies of SCC incorporating silica fume and ultra fine GGBS. Constr Build Mater 171:919–928
15. Pradeep KM et al (2018) Ultrafine GGBS and calcium nitrate as concrete admixtures for improved mechanical properties and corrosion resistance. Constr Build Mater 182:249–257
16. Baoju Y et al (2000) Influence of ultrafine fly ash composite on the fluidity and compressive strength of concrete. Cem Concr Res 30:1489–1493
17. Subramaniam G et al (2005) Influence of ultrafine fly ash on the early age response and the shrinkage cracking potential of concrete. J Mater Civ Eng 17(1):45–53
18. Choi L et al (2012) Effect of fly ash fineness on temperature rise, setting, and strength development of mortar. J Mater Civ Eng 24(5):499–505

Optimization of Infrared Thermography for Damage Detection in Concrete Structures Using Finite Element Modelling

Madhuraj Naik, Ganesh Hegde, and Lalat Indu Giri

Abstract Utilization of infrared thermography for detection of damage in a concrete slab is presented in this paper. Thermal non-destructive testing of concrete structures has many advantages, like rapid scanning of concrete surface, high speed of data collection and non-contact testing. The purpose of this study is optimization of the method to accurately determine damage extent in concrete structures. Active infrared thermography has been utilized to detect sub-surface defect in a concrete slab. Irregularities have been observed in the laboratory results. To collaborate experimental investigations, a model of the concrete slab that can be used in an experiment has been developed using finite element software. In the FEA software concrete slab was subjected to same amount of thermal excitation to simulate laboratory experiment. Transient analysis of concrete slab was done to get thermal images of surface of the slab. The images obtained were further processed by MATLAB program to get area of defect. Temperature readings obtained from model were observed to be much higher. However, defect area obtained from FEM model images was found to be closer to actual defect area than experimental images.

Keywords Infrared thermography · Transient analysis · Finite element model · Thermal image · MATLAB

M. Naik (✉) · G. Hegde
Civil Engineering Department, Goa College of Engineering, Farmagudi, Ponda, Goa 403401, India
e-mail: naikmadhuraj@rediffmail.com

G. Hegde
e-mail: gh@gec.ac.in

L. I. Giri
Electronics and Communication Engineering Department, National Institute of Technology, Farmagudi, Ponda, Goa 403401, India
e-mail: lig@nitgoa.ac.in

B. B. Das et al. (eds.), *Recent Trends in Civil Engineering*, Lecture Notes in Civil Engineering 105, https://doi.org/10.1007/978-981-15-8293-6_15

1 Introduction

Civil structures including critical infrastructure works like bridges deteriorate over time because of fatigue, environmental reasons, corrosion, and so on. If this is left unchecked then it might compromise the integrity of the structure in future. Thus, identifying the location and extent of damage and determining the current health condition of structures are of utmost importance. As a result, numerous studies have been undertaken to develop new and advanced methods for damage detection in structures.

Current damage detection methods are either visual inspection-based or localized experimental methods such as rebound hammer, ultrasonic pulse velocity (UPV) and core cutting [1]. All of these techniques require location of damage to be already known and area of damage to be accessible. Also, these methods can identify damages on or near the surface of structure while damages deep within structure can go unnoticed. These techniques for correct interpretation of damage need experienced inspectors who are in shortage. This has given rise to global techniques which can be applied to complex structures. In these techniques the structure under test is subjected to frequency excitations, and vibration responses, like velocity, displacement and acceleration, are picked up. First few mode shapes and corresponding frequencies are calculated and compared with the data of healthy structure which yields information about damages. However, a basic drawback of this technique is low sensitivity to incipient damage [2].

Infrared thermography is becoming popular as a non-destructive technique (NDT) for industrial processes while it is still in initial stages in civil engineering field. Infrared thermography is the process of detecting electromagnetic energy emitted by an object in the electromagnetic spectrum. Use of infrared thermography for non-destructive testing is called thermal non-destructive testing (TNDT). TNDT is commonly used to do quality testing of metals, ceramics, machineries, and so on in industry. Only until recently, it has been used in concrete structures to detect defects embedded within the body. In TNDT thermal excitation of the object under test is done and its surface temperature variation is monitored over time. The existence of defects in the object interrupts heat flow causing localized changes in temperature distribution on the surface. This is recorded using an infrared camera. Infrared thermography is divided into two types which are passive thermography and active thermography [3]. Active thermography is further divided into stepped thermography, lock-in thermography, pulsed thermography, pulsed phase thermography and frequency-modulated thermal wave imaging depending on the nature of thermal excitation used [4].

TNDT is a whole field technique rather than point by point technique and is relatively cheaper than X-ray imaging [4]. Use of infrared thermography (IRT) as a health monitoring technique in civil structures is growing steadily. IRT has also been used frequently in nuclear, aerospace, food, paper, wood and plastic industries [5]. Infrared thermography can be used to perform inspections relatively quickly without even having to touch the surface of an object. Concrete has low thermal conductivity;

as a result, more thermal excitation is required to induce heat flow in concrete structures to be able to identify all defects. This makes use of IR thermography in concrete structures difficult. Despite these limitations, there has been improvement in use of IRT for concrete structures. The purpose of this study is to collaborate experimental readings obtained with FEM model results. A MATLAB program which uses image processing technique has been used to calculate area of defects from image obtained using FEM model. The objective of this work is to compare the area results obtained from FEM model and experiment.

2 Current Situation and Challenges Regarding IRT

Hiasa et al. (2018) [6] explored favourable time window to perform IRT on a concrete slab using both experimental observations as well as numerical simulations. Effect of debris on the surface of concrete was also investigated. Same authors in 2017 [7] conducted experiments on a concrete slab and used FEA simulations to determine temperature difference between sound and defect areas. They concluded that defects at 1.27 and 2.54 cm could be detected using IRT. Birgul et al. (2017) [8] found sensitive parameters for effective utilization of IRT using heat transfer models of concrete blocks from a previous test. Różański et al. [9] conducted experimental studies on laboratory casted reinforced concrete slab with four embedded damages. Various thermal excitation sources were used and the sensitivity of the slab response was investigated using different infrared cameras along with FEA simulations. Milovanović et al. [10] did thermal excitation for 60 min on a defect embedded concrete slab using a 1000 W halogen lamp. Surface temperature of the slab was monitored during heating as well as 60 min cooling period. The distance of excitation source from the surface was varied. Pulsed phase thermography (PPT) was used by Maldague et al. [11] to process the images.

The importance of cooling time and quantification of defects was established by Huh et al. [12] through experimental studies with defects at varying depths. They concluded that thermal contrast decreases with depth but increases with size of defect. Cotič P et al. [13] conducted experiments on four concrete test specimens containing voids and established relationship between the depth of the defect and $t_{\max}$ or $f_{\max.}$ This was validated with 3D numerical model of the thermal transfer occurring in concrete specimens. Cannas et al. [14] with the aim to evaluate reliability of infrared thermography in building diagnosis developed an experimental program using a concrete wall with different defects. This experiment was successfully replicated numerically using COMSOL multiphysics software. Showunmi [15] used FEM model developed in ABAQUS to establish the effectiveness of infrared thermography for non-destructive testing of steel-concrete composites. It was concluded that the finite element model can predict behaviour of infrared thermography but with less accuracy.

3 Gaps in Research

From the above cited papers, it was found that trial and error approach is adopted by all authors using different excitation times and magnitude of excitation. This needs to be optimized. Apart from thermal excitation, detection of defect depends upon the material properties of the object as well as experimental setup. Existing methods should be revised to take into effect change in thermal properties of concrete, atmospheric conditions and noise due to emissivity changes and reflection from other sources. Defects of different sizes and at different depths and concrete with varying parameters will require different amounts of excitation energy. Using heat equation or FEM simulation, a mathematical formula can be developed to calculate exact amount of heat required for a concrete structure to identify all defects. This will optimize the process and make it more methodological rather than the current practice of experimenting with different heating times and energy fluxes. Use of FEM simulation to validate infrared thermography experiments has been successfully used by many researchers [6–8, 14, 15].

4 Methodology

4.1 Preparation of Concrete Specimen

One concrete slab of size 50 × 50 cm was casted with embedded thermocol defect D1 having size 12.5 × 6.0 × 3.5 cm. The thickness of the slab was 10 cm and it had 4 bars of 8 mm dia. at equal spacing in both the directions. Grade of the concrete slab was M25. Layout of concrete slab S1 with defect D1 is shown in Fig. 1.

Defect D1 was placed at the level of steel reinforcement. Clear cover provided was 2 cm. Figure 2 shows slab S1 before and after concreting.

The slab was demoulded 24 h after casting. Curing was done by submerging the slab in curing tank for 3 days. Experiment on S1 was performed 3 months after curing.

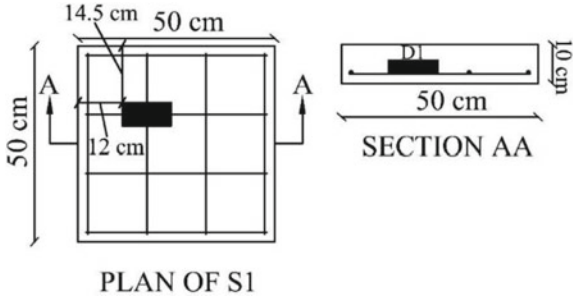

Fig. 1 Layout of slab S1

Fig. 2 Slab S1: **a** before concreting **b** after concreting

4.2 Experimental Procedure

The experiment was carried out in concrete laboratory of civil engineering department of Goa College of Engineering. Room temperature measured at the beginning of the experiment was 27 °C (300.15 K). Concrete slab temperature was assumed to be the same as room temperature.

Slab S1 was subjected to stepped active thermography using one 500 W halogen lamp. The horizontal distance between the surface of the slab and lamp was kept constant at 1 m. The height of the lamp above the ground was 45 cm. This is shown in Fig. 3.

Total duration of thermal excitation was 60 min. Thermal images of the slab surface were taken at four different times after the start of thermal excitation using FLIR E6 hand-held infrared camera.

The sequence of images taken using the camera is shown in Fig. 4.

5 Model Development

5.1 Geometrical Settings and Material Properties

The concrete slab S1 summarized in Sect. 4.1 was modelled using commercial FEA software Ansys Workbench 19.2. The FEM model was developed to simulate and validate the stepped infrared thermography experiment performed on slab S1. The

Fig. 3 Experimental setup for S1

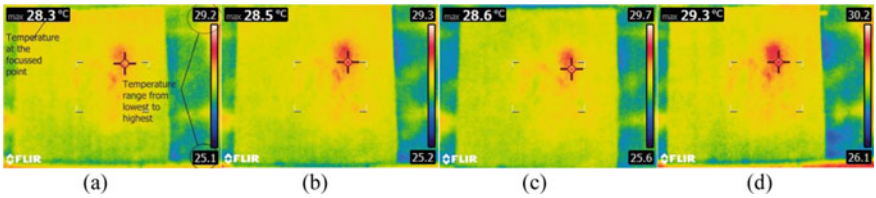

Fig. 4 Series of images taken after **a** 5 min **b** 20 min **c** 30 min **d** 60 min

slab model having dimensions 50 × 50 × 10 cm was modelled as 3D cuboid. Reinforcement was modelled as line bodies in both directions. The slab model developed is shown in Fig. 5.

In the experiment, the concrete slab S1 is seen resting on concrete blocks as seen in Fig. 3. However, this was not shown in the model. Defect D1 was represented as empty space or void within the model at the same location as in experiment with size 12.5 × 6.0 × 3.5 cm. The defect modelled is shown in Fig. 5.

Input material property thermal conductivity was calculated using equation derived by K.- Kook-Han K. et al. [14]. The values are shown in Table 1.

A plot of variation of thermal conductivity with temperature is shown in Fig. 6.

Other properties used are shown in Table 2.

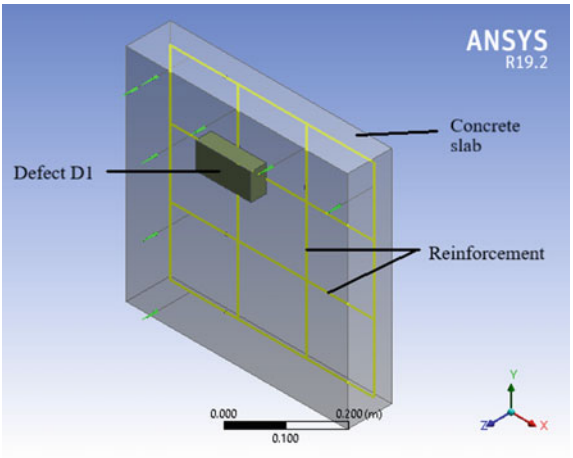

Fig. 5 Model of slab S1

Table 1 Thermal conductivity values of concrete at different temperatures

Temperature (K)	Thermal conductivity (W/m-K)
293.15	1.96
295.15	1.42
297.15	1.41
299.15	1.40
301.15	1.39
303.15	1.39

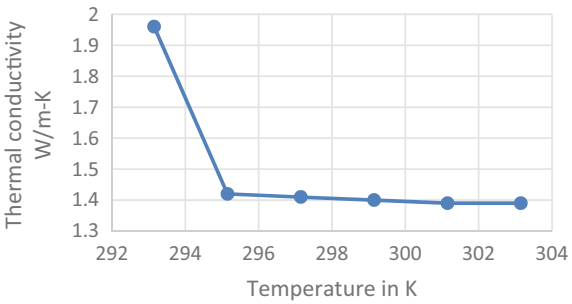

Fig. 6 Variation of thermal conductivity of concrete with temperature

Table 2 Material properties inputted in model

Properties	Concrete slab	Reinforcement
Density (kg/m^3)	2500	7850
Elastic modulus (N/m^2)	2.5E10	2.1E10
Strength (N/m^2)	2.5E07	2.1E11
Thermal conductivity (W/m-K)	As shown in Table 1	60.5
Specific heat (J/Kg-K)	880	434

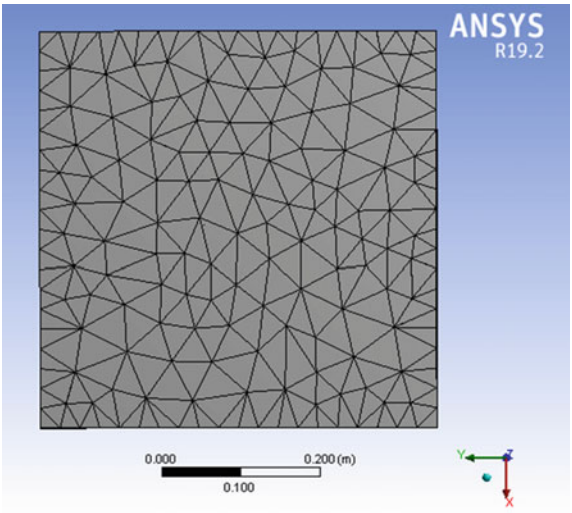

Fig. 7 Meshed model of S1

The FEM model consisted of slab, defect and reinforcement which are modelled as different components. To ensure all these components act as a single body, connections were made between defect, slab and reinforcement by using contact option in Ansys Workbench 19.2. All contacts were chosen as bonded. Meshing done was program-controlled mesh with mesh size as 0.05 m. The meshed model is shown in Fig. 7.

5.2 Loading and Boundary Conditions

For heat loading, stepped heat load of magnitude 500 W to simulate halogen lamp used in the experiment was applied. It was applied on that surface of the slab where reinforcement was closest. Results were obtained for 5, 20, 30 and 60 min duration and were compared with the experimental results. Convection boundary coefficient was applied on all faces of concrete except the one where heat load was applied. Convection coefficient was taken as 12 W/m^2 K.

6 Results and Discussions

6.1 Experimental Results

As seen from Fig. 4, defect D1 is visible (red area) after just 5 min of thermal excitation. It is observed that as heating time increases the temperature over the

Table 3 Error between estimated area and actual area

Defect	Dimension (cm × cm)	Heating time/cooling time (min)	Depth at which D1 is located (cm)	Actual area (cm^2)	Estimated area (cm^2)	Error (%)
D1	12.5 × 6.0	5	2.0	75.00	35.2	−53.1
D1	12.5 × 6.0	20	2.0	75.00	43.7	−41.7
D1	12.5 × 6.0	30	2.0	75.00	44.8	−40.3
D1	12.5 × 6.0	60	2.0	75.00	50.6	−32.5

surface increases non-uniformly. Area of the defect was estimated from the images using MATLAB program. This estimated area was compared with the actual area. These are shown in Table 3.

As heating time is increased, the error between estimated area and actual area decreases. This preliminary experimentation conducted shows successful application of infrared thermography for NDT of concrete structures.

6.2 FEM Model Results

As mentioned earlier, the FEM model of concrete slab was subjected to 5, 20, 30 and 60 min thermal excitation. The resulting images taken from Ansys Workbench are presented in Fig. 8.

From Fig. 8, it is observed that temperature above the defect D1 is higher compared to the surrounding surface which is as per the experiment.

6.3 Comparison Between Experimental and FEM Model Results

The comparison between experimental and FEM model temperature readings are shown in Table 4.

Using the images in Fig. 8, area of the defects was calculated using MATLAB program and compared with the results from experimental images. For 5 min heating the area was not calculated because unlike others maximum temperature is not concentrated over defect region.

Tables 4 and 5 indicate that there is a large difference between experimental and numerical model results. It is observed that the error between actual and calculated area is lesser for FEM model as compared to experimental values. However, in 30 min heating the error was so large because the maximum surface temperature was observed over a larger area and not localized over defect area.

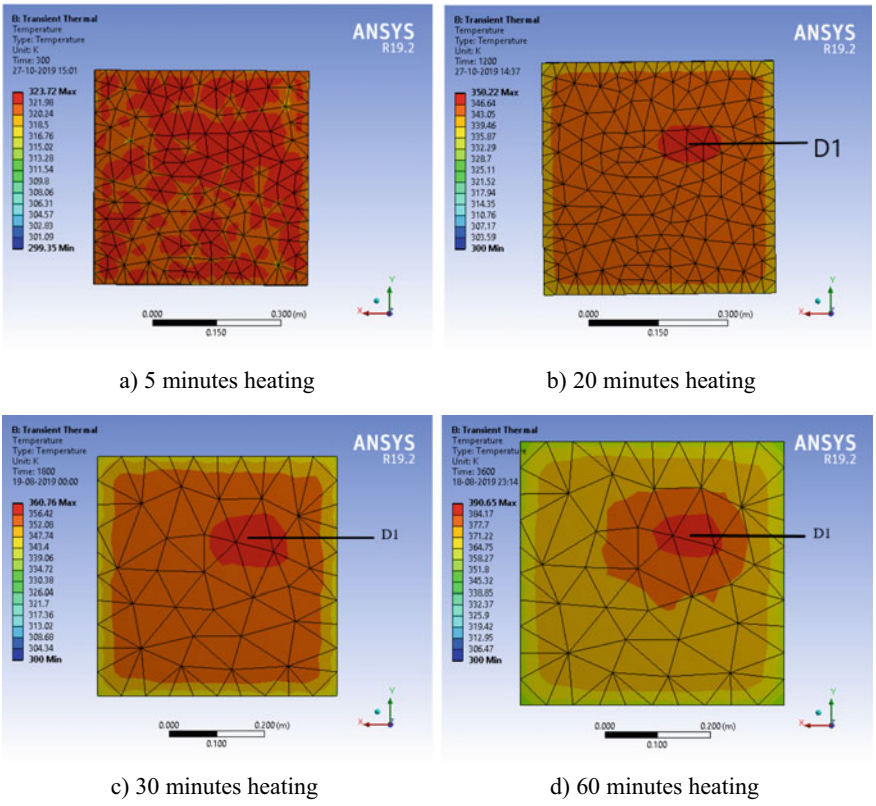

a) 5 minutes heating b) 20 minutes heating

c) 30 minutes heating d) 60 minutes heating

Fig. 8 Model surface temperature for different heating times **a** 5 min **b** 20 min **c** 30 min **d** 60 min

Table 4 Comparison between surface temperature over defect D1 for experiment and FEM model

	Experimental (K)	Model (K)	Difference (K)
5 min heating	301.45	322.41	20.96
20 min heating	301.65	349.98	48.33
30 min heating	301.75	359.34	57.59
60 min heating	302.45	388.60	86.15

7 Conclusions

The preliminary experimentation conducted shows the successful application of infrared thermography for NDT of concrete structures. This method can be used for NDT of concrete structures and can give faster data acquisition rate without having to touch the surface. However, thermal images by themselves do not give any

Table 5 Comparison between areas estimated using experimental and FEM model results

Defect	Heating time	Defect depth (cm)	Actual area (cm^2)	Area estimated using experimental observations (cm^2)	Error (%)	Area estimated using FEM model (cm^2)	Error (%)
D1	20 min	2.0	75.00	43.70	−41.70	90.90	+21.20
D1	30 min	2.0	75.00	44.80	−40.30	151.50	+102.00
D1	60 min	2.0	75.00	50.60	−32.50	84.70	+12.93

information. They have to be subjected to processing to obtain the required information like area and depth of defects. From the above results it is observed that the FEM model is not able to give the required results. This is because in the FEM model the heat load applied is on the slab surface and does not account for non-uniform heating of the surface, reflection of heat and emissivity of concrete.

Future work will focus on removal of these errors in FEM model results. Correction factors for non-uniform heating and emissivity will be derived using experiments. These correction factors will be incorporated in numerical simulations. There is large amount of difference between the actual defect area and calculated defect area for both experiment as well as numerical simulation. This highlights the importance of heat optimization which will be subject of future studies.

References

1. Bungey J, Millard S, Grantham M (2006) Testing of concrete in structures. Book, Fourth edn, Taylor & Francis
2. Ramashanker (2009) An integrated approach for structural health monitoring. Doctoral Thesis, Indian Institute of Technology, New Delhi
3. Milovanović B, Banjad Pečur I (2016) Review of active infrared thermography for detection and characterization of defects in reinforced concrete. J Imaging 2(11):01–27. https://doi.org/10.3390/jimaging2020011
4. Chatterjee K (2011) Development of simulator and image processing tools for multi technique thermography. Doctoral thesis, Indian Institute of Technology, New Delhi
5. Bagavathiappan S, Lahiri BB, Saravanan T, Philip J, Jayakumar T (2013) Infrared thermography for condition monitoring–a review. Infrared Phys Technol 60:35–55. https://doi.org/10.1016/j.infrared.2013.03.006
6. Hiasa S, Birgul R, Matsumoto M, Catbas F (2018) Experimental and numerical studies for suitable Infrared thermography implementation on concrete bridge decks. Measurement. https://doi.org/10.1016/j.measurement.2018.02.019
7. Hiasa S, Birgul R, Catbas F (2017) A data processing methodology for Infrared thermography images of concrete bridges. Int J Comput Struct 190:205–218. https://doi.org/10.1016/j.compstruc.2017.05.011
8. Hiasa S, Birgul R, Catbas F (2017) Investigation of effective utilization of infrared thermography (IRT) through advanced finite element modelling. Int J Constr Build Mater 150:295–309. https://doi.org/10.1016/j.conbuildmat.2017.05.175

9. Różański L (2017) Detection of material defects in reinforced concrete slab using active infrared thermography. 63:82–85
10. Milovanović B, Banjad PI (2014) Detecting defects in reinforced concrete using the method of Infrared thermography. CrSNDT J
11. Maldague X, Galmiche F (2001) Advances in pulsed phase thermography. Infrared Phys Technol 43:175–181. https://doi.org/10.1016/S1350-4495(02)00138-X
12. Huh J, Tran QH, Lee JH, Han DY, Ahn JH, Yim S (2016) Experimental study on detection of deterioration in concrete using Infrared thermography technique. Adv Mater Sci Eng. 01–12. doi:http://dx.doi.org/10.1155/2016/1053856
13. Cotič P, Kolarič D, Bosiljkov VB, Bosiljkov V, Jagličić Z (2015) Determination of applicability and limits of void and delamination detection in concrete structures using infrared thermography. NDT E Int 74:87–93. https://doi.org/10.1016/j.ndteint.2015.05.003
14. Cannas B, Carcangiu S, Concu G, Trulli N (2012) Modelling of Active Infrared thermogarphy for defect detection in Concrete structures. Excerpt from Proceedings of the 2012 Conference in Milan
15. Showunmi T (2013) Finite element infrared thermography study on concrete and steel-concrete composite structures. Master's Thesis. Department of Civil and Environmental Engineering. Lehigh University, Pennsylvania

Evaluation of Pozzolanic Performance of Bagasse Ash and Rice Husk Ash

S. Praveenkumar, G. Sankarasubramanian, and S. Sindhu

Abstract One of the most consumed materials in the world for the development and advancement of humankind is cement. However, the production and consumption of cement has its own disadvantages. The eco-system is affected to a large extent because of the release of toxic gases like CO_2 into the environment during the production of cement. The reaction (exothermic) of cement with water leads to enormous heat production. Hence cement replacements known as supplementary cementing materials (SCMs) with high pozzolanic or hydraulic nature are used. Bagasse ash (BA) and rice husk ash (RHA) are the two commonly used SCMs in India. They are obtained as by-products from burning boilers in industries and for heating purposes in rural homes. The properties of both the ashes vary to a large extent. The source of the ash and the different chemical, mineralogical and morphological characteristics are the main reasons for variation in properties. These properties define their suitability for replacement as a partial binding material. This paper investigates on the performance and microstructure characterization of BA and RHA.

Keywords Supplementary cementing material (SCM) · Pozzolanic activity · RHA · BA · Strength activity index

1 Introduction

The materials which are added partially or completely in place of cement to enhance the cementing properties are known as supplementary cementing materials (SCMs). They are also good alternatives to cement, as the production of cement involves the depletion of natural resources, excess energy consumption and emission of carbon-di-oxide which is a harmful greenhouse gas [1]. The solid by-products from various industries and natural pozzolans are commonly used as SCMs throughout the world pozzolans [2]. A few examples of industrial waste products, which can be used as

S. Praveenkumar (✉) · G. Sankarasubramanian · S. Sindhu
Department of Civil Engineering, PSG College of Technology, Coimbatore, India
e-mail: spk.civil@psgtech.ac.in

B. B. Das et al. (eds.), *Recent Trends in Civil Engineering*, Lecture Notes in Civil Engineering 105, https://doi.org/10.1007/978-981-15-8293-6_16

mineral admixtures in concrete, are RHA and BA. Metakaolin and volcanic ash are the examples of natural.

While BA is added to cement, the silica reacts with free lime. A new compound called calcium silicate hydrate (C–S–H) is formed during the hydration process which improves the mechanical and durability properties of concrete. Also, the smaller particle size of BA helps in increased pozzolanic activity of cement. BA and RHA have a high content of silica (SiO_2) and hence can be used as a pozzolan [3, 4]. BA is obtained from sugarcane industries in huge quantities as a by-product. After extracting the juice from the sugarcane, the fibrous matter that is left behind is known as bagasse [5]. For running the boilers in various industries, bagasse was used as fuel [6]. After combustion of the bagasse, a large quantity of carbon residue is left behind which is dumped over huge landfills. They are collected using a bag-house filter and used as a supplementary cementing material [7]. This offers an environment-friendly and profitable alternative in the disposal of the ash. BA obtained as an industrial by-product can be directly used or is processed as per the standards to obtain the desired properties as a replacement material. These treatment processes increase the pozzolanic properties of the BA by forming siliceous products. It is found that burning the raw BA at 600 °C is the most appropriate temperature to obtain a good pozzolan for the cement replacement [8]. The sieve size normally adopted is 75 μm sieve [9].

RHA is converted to a pozzolanic material by controlled burning, and the same treatment processes are carried out for BA, like grinding, sieving and chemical activation [10].

In this study, the properties and characterization of BA and RHA are studied. Raw bagasse and rice husk collected from landfills have coarse and fine fibrous particles along with a few burnt particles. They are then burned, sieved and pulverized in laboratory to finally obtain the BA and RHA for replacement in cement.

2 Materials

The raw bagasse is collected from a dumping yard of a sugarcane mill at Gobichitti-palayam near Coimbatore. The moisture content in the raw bagasse is removed and burnt to get BA [11]. The raw RHA is collected from a rice mill in Kangayam. The collected ash is already burnt in open fills at the desired temperature and is free from moisture content. Both the raw BA and RHA showed the presence of coarse and fine fibrous particles rich in carbon content.

The fine BA and RHA is obtained in laboratory as shown in Fig. 1 [11]. For finding the properties of the pozzolan, ordinary Portland cement (OPC) of Grade 53 conforming to IS:12269 [12] is used. The properties of cement are enlisted in Table 1.

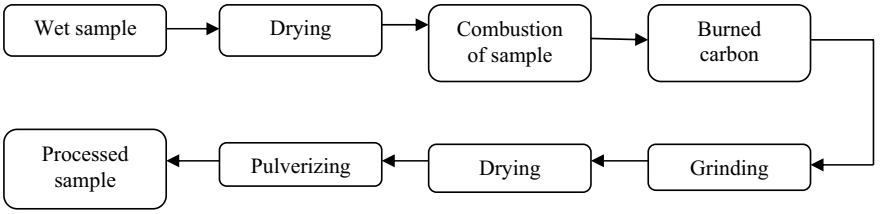

Fig. 1 Processing of sample

Table 1 Properties of cement

Property	Cement (OPC 53 Grade)
Specific gravity	3.2
Standard consistency (%)	30
Initial setting time (IST) (min)	132
Final setting time (FST) (min)	178
Fineness (Blaine's m^2/kg)	310

3 Experimental Methods

The material, mineralogical and microstructure properties of the BA and RHA are found out. As per IS:1727-2004 [13] specific gravity of RHA and BA is determined. The empty weight of the flask is measured (W_1). Around 50 g of ash (RHA and BA) is filled in the flask and is weighed again (W_2). Kerosene is then added up to the top of the flask with the ash and weighed (W_3). The flask is then emptied and filled completely with kerosene and weighed (W_4). The specific gravity is then given by $\left(\frac{W_2-W_1}{(W_2-W_1)-(W_3-W_4)\times 0.75}\right)$. The fineness of RHA and BA is found using Blaine's air permeability test as mentioned in IS:1727-2004 [13].

As per IS:4031 (Part 4) 2005 [14], standard consistency of BA and RHA blended cement is determined. The IST and FST for the blended cements with BA and RHS are determined as per IS:4031 (part 5) 2005 [15].

SAI of the RHA and BA is determined as per ASTM C311-11b [16]. Mortar mix with 1:3 ratio of blended cement to sand is taken. One part of blended cement in the mix has 0.2N:0.8 of ash (RHA and BA) and cement as per IS:1727-2004 [13]. Water of $\left(\frac{P}{4}+3\right)\%$ is required, where P is the standard consistency. Three 70.6 mm cube moulds for each blended cement mortars with RHA and BA are filled with the mix. Control mortar specimens (without RHA and BA) are also prepared. The compressive strength test is conducted on 7th and 28th day, and the result is found out by taking the average of three specimens. The strength activity index is the percentage of the strength of the blended specimen to the strength of the control mix.

Loss in ignition (LOI) test is carried out as per IS:1727-2004 [13]. A platinum crucible of 20 mL capacity containing 1 g of air dried, finely ground sample is placed over a muffle furnace at 1000 °C for about 20 min. It is then cooled and weighed (B).

Again heat for five minutes and check the loss in weight (A). The LOI is then given by $\left(\frac{A}{B} \times 100\right)$.

The mineralogical analysis of the BA and RHA is done by X-ray diffraction (XRD), using Cu Kα radiation. No significant difference in the diffraction patterns was observed in both the BA and RHA as they constitute the same type of minerals [17, 18].

The chemical composition of the BA and RHA is determined using X-ray fluorescence (XRF) and energy dispersive spectroscopy (EDS). The silica content in the RHA is found to be higher than BA. The morphological study of BA and RHA is carried out using scanning electron microscopy (SEM).

4 Results and Discussion

The physical characterization of the BA and RHA is enlisted in Table 2. BA has a specific gravity of 2.21 whereas the specific gravity of RHA has a value of 2.07. The fineness using Blaine's air permeability test is found to be 290 m^2/kg for BA and 267 m^2/kg for RHA. The specific gravity and fineness for RHA and BA are less when compared to that of cement. However, BA has a very close value of specific gravity and fineness with the cement [19]. This shows that the fine fibrous particles are very less in BA than in RHA.

The consistency of the BA and RHA blended cement is 37 and 45%, respectively. The IST and FST of the BA blended cement are 205 and 330 min, respectively [20]. The initial setting time and final setting time of the RHA blended cement are 312 and 510 min, respectively. The standard consistency of IST and FST for the blended cements are higher than that of the OPC 53 Grade used. This is because the SSA of BA and RHA is less than that of cement and hence they require more water to meet the consistency and more time for setting. However, they satisfy the Indian standards for consistency, and IST and FST to be used as a replacement material [21, 22].

Table 2 Physical characteristics of BA and RHA

Material property	Bagasse ash (BA)	Rice husk ash (RHA)
Specific gravity	2.21	2.07
Specific surface area (Blaine, m^2/kg)	290	267
Consistency (%)	37	45
IST (min)	205	312
FST (min)	330	510
Loss on ignition (%)	4	2
SAI at 7 days (%)	109	115
SAI at 28 days (%)	111	134

SAI of the BA at 7 and 28 days is found to be 109 and 111%, respectively, whereas the SAI of the RHA at 7 and 28 days is found to be 115 and 134%, respectively. For a material to be pozzolanic, a minimum value of 75% SAI is required as per ASTM C618-12a. Both BA and RHA satisfy the requirement to be considered a pozzolanic material. The SAI of RHA at 28 days is much higher than that of BA. This is as a consequence of the high silica content present in RHA.

The LOI of BA and RHA is 4 and 2%, respectively. This indicates that the unburnt carbon particles are very less in both the ashes. If the coarse and fine fibrous particles are not removed by sieving, the LOI values will further increase and may have a value of 70–80%, which is highly insignificant for using in blended cements [23, 24].

The XRD diffraction patterns obtained for BA and RHA show the presence of quartz and cystobalite peaks in both. These minerals are a clear indication of high quantity of silica in both the ashes. The amorphous nature of the minerals in rice husk ash is more than that of bagasse ash. This amorphous nature is more suitable for pozzolanic reaction when compared to the crystalline peaks. The optimized burning at 600 °C gives the amorphous peaks of the minerals. Improper burning at a temperature either below or above the optimized temperature gives rise to more crystalline peaks for the ash and hence becomes undesirable to be used as a replacement material.

Electron dispersive spectroscopy results for the elemental composition and X-ray fluorescence analysis for the molecular composition of the BA and RHA are given in Table 3. Both analyses show a higher silica content of 90.47% for rice husk ash when compared to the bagasse ash with silica content of 41.286%. The silica content of BA is almost 50% of RHA. This is because after treatment the chemical alignment of the particles in the ash is modified and it gives rise to formation of more Si–O bonds in RHA. The EDS spectra of the BA and RHA are shown in Fig. 2.

The SEM micrographs of BA and RHA are shown in Figs. 3a–c and 4a–c, respectively. Rod-shaped well-defined particles and tough particles are experiential in BA. The RHA showed clear indication of prismatic quartz minerals and fibrous cystobalite minerals. Hence the network of silicon tubes is more in RHA.

Table 3 Elemental and molecular composition of BA and RHA

Element	BA (%)	RHA (%)	Compound	BA (%)	RHA (%)
O	45.01	44.24	SiO_2	41.286	90.47
Si	22.39	33.97	K_2O	10.985	0.48
Al	11.10	3.9	CaO	9.225	5.92
Ca	5.30	15.21	Fe_2O_3	3.143	Nil
K	4.75	2.68	P_2O_5	2.054	Nil
Mg	3.89	Nil	Na_2O	4.123	Nil
Na	3.39	Nil	Al_2O_3	25.43	3.13
Fe	2.91	Nil	MgO	3.754	Nil
P	1.27	Nil			

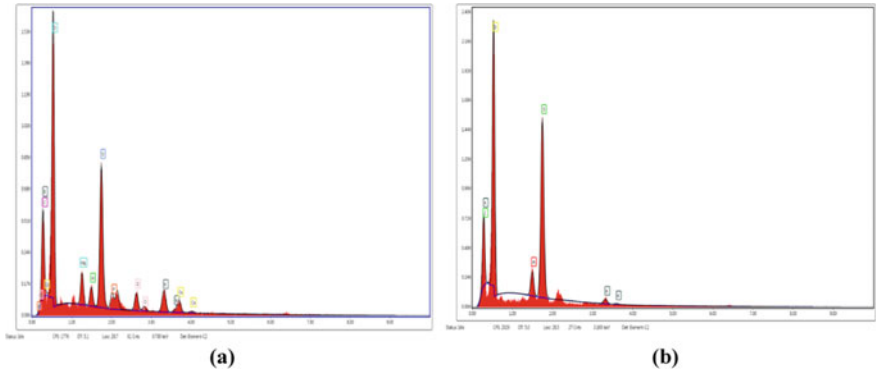

Fig. 2 EDS Spectrum: **a** BA and **b** RHA

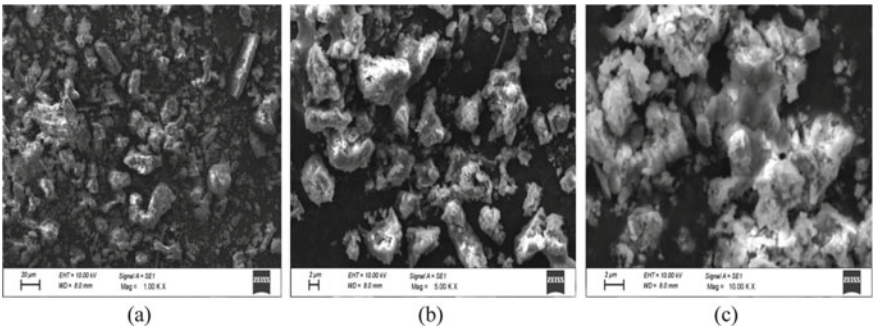

Fig. 3 SEM micrographs of BA: **a** At 1 k magnification; **b** at 5 k magnification showing rod-shaped particles and **c** at 10 k magnification showing fibrous particles

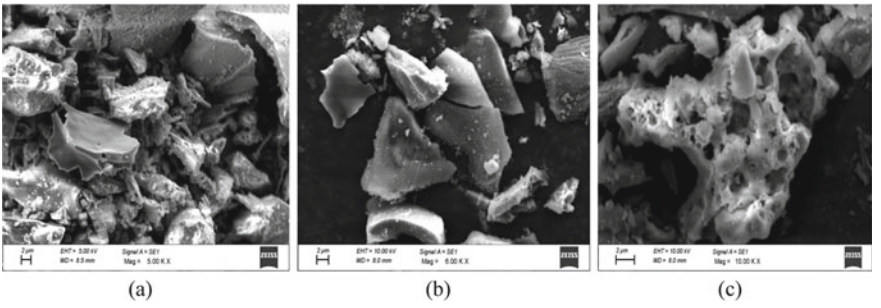

Fig. 4 SEM micrographs of RHA: **a** At 5 k magnification; **b** at 10 k magnification showing prismatic shapes of the quartz mineral and **c** at 10 k magnification showing fibrous forms of cystobalite mineral

5 Conclusion

From the results obtained, it is observed that both BA and RHA are good pozzolanic materials. They have their own advantages and disadvantages.

- The fineness/specific surface area and specific gravity of BA is more than the RHA.
- This leads to increased setting time for RHA when compared to BA and also more water is required to attain consistency for RHA blended cement.
- The higher content of silica in RHA helps in attaining more strength for blended cements as the pozzolanic performance and quantity of hydration products increases.
- The silica minerals are clearly viewed in RHA than in BA.
- The strength activity index of the RHA is much higher than the BA. Hence RHA is a better pozzolan than BA.
- The low value of loss on ignition is obtained for both BA and RHA. This implies that the carbon content is less in both BA and RHA.

Acknowledgements The authors wish to thank UGC, New Delhi, for their financial support under minor research project (MRP-6458/16(SERO/UGC) and Dr. K Prakasan, Principal-in-charge, PSG College of Technology, Coimbatore for the facilities and support provided in carrying out this research work at Advanced Concrete Research Laboratory.

References

1. Mackechnie JR, Alexander MG (2009) Using durability to enhance concrete sustainability. J Green Build 4(3):52–60
2. Bapat JD (2013) Mineral admixtures in cement and concrete. CRC Press, New York
3. Cordeiro GC, Toledo Filho RD, Fairbairn EMR (2009) Effect of calcination temperature on the pozzolanic activity of sugar cane bagasse ash. Constr Build Mater 23(10):3301–3303
4. Cordeiro GC, Toledo Filho RD, Fairbairn EMR (2009) Use of ultrafine rice husk ash with high-carbon content as pozzolan in high performance concrete. Mater Struct 42:983–992
5. Nuntachai C, Chai J, Kraiwood K (2009) Utilization of bagasse ash as a pozzolanic material in concrete. Constr Build Mater 23(11):3352–3358
6. Jagadesh P, Ramachandramurthu A, Murugesan R, Sarayu K (2015) Micro-analytical studies on Bagasse ash, Sadhana. Indian Acad Sci 40(5):1629–1638
7. Bahurudeen A, Santhanam M (2014) Bagasse ash-an alternative supplementary cementitious material. In: International conference on advances in civil engineering and chemistry of innovative materials, India, pp 837–842
8. Ganesan K, Rajagoapl M, Thangavel K (2007) Evaluation of bagasse ash as supplementary cementitious material. Cem Concr Compos 29(6):515–524
9. Venustiano R-P, Víctor Guillermo J-Q, Pedro Leobardo V-T, Pedro M-G (2017) Characterization and use of an untreated Mexican Bagasse ash as supplementary material for the preparation of ternary concretes. Constr Build Mater 157:83–95
10. Siti AS, Nasir Shafiqand MA (2018) Physicochemical properties and pozzolanic performance of ultrafine treated rice husk ash (Uftrha) as additive in concrete. J Malaysian Inst Plan 16(2):314–323

11. Praveenkumar S, Sankarasubramanian G, Sindhu S (2020) Strength, permeability and microstructure characterization of pulverized bagasse ash in cement mortars. Constr Build Mater 238:117691
12. Indian Standard (IS) 12269-2008 Specification for 53 grade ordinary Portland cement
13. Indian Standard (IS) 1727-2004 Indian Standard Methods of Test for pozzolanic materials
14. Indian Standard (IS) 4031 (Part 4)-2005 Methods of physical tests for hydraulic cement: determination of consistency of standard cement paste
15. Indian Standard (IS) 4031 (Part 5)-2005 Methods of physical tests for hydraulic cement: determination of initial and final setting times
16. American Society for Testing and Materials (ASTM) C311-11b-2011 Standard test methods for sampling and testing fly ash or natural pozzolans for use in Portland-cement concrete
17. Praveenkumar S, Sankarasubramanian G, Sindhu S (2019) Selecting optimized mix proportion of bagasse ash blended high performance concrete using analytical hierarchy process (AHP). Comput Concr 23(6):459–470. https://doi.org/10.12989/CAC.2019.23.6.459
18. Krishna RN (2012) Rice husk ash—an ideal admixture for concrete in aggressive environments. In: International conference on our world in concrete and structures, Singapore
19. Praveenkumar S, Sankarasubramanian G (2019) Behavior of high performance fibre reinforced concrete composite beams in flexure. Revista Romana De Materiale-Roman J Mater 49(2):259–266
20. Bahurudeen A, Santhanam M (2015) Influence of different processing methods on the pozzolanic performance of Bagasse ash. Cem Concr Compos 56:32–45
21. Bahurudeen A, Marckson AV, Kishore A, Santhanam M (2014) Development of Bagasse ash based Portland pozzolana cement and evaluation of compatibility with superplasticizers. Constr Build Mater 68:465–475
22. Bahurudeen A, Kanraj D, GokulDev V, Santhanam M (2015) Performance evaluation of Bagasse ash blended cement in concrete. Cem Concr Compos 59:77–88
23. Seyed Alireza Z, Farshad A, Farzan D, Mojtaba A (2017) Rice husk ash as a partial replacement of cement in high strength concrete containing micro silica: evaluating durability and mechanical properties. Case Stud Constr Mater 7:73–81
24. Shanmugam P, Gopalan S (forthcoming) Effect of fibers on strength and elastic properties of bagasse ash blended HPC composites. J Test Eval 48. https://doi.org/10.1520/JTE20170698

An Overview of Indian Steel Industry and Its Impact on Construction Sector

James Mattom, P. Herrick, and Vinay Mohan Agrawal

Abstract In the construction industry, steel is a prime and a rapidly growing sector in our country. India has leapfrogged its position from fourth to the second largest producer in steel sector outdistancing Japan and are using all the state-of-the-art technology for the production. Still the demand of steel tends to increase every year and helps in the overall economic growth in the long term. Industries like automobiles, consumer durables, infrastructure, production and so on are some of the major consumers of the steel sector, among which the construction and infrastructure industry has the maximum utilization of 63% from its total production. There has been observance of exponential increase in demand of steel sector since 1874, when the first steel production began for which new industrial policy is considered to be one of the important catalysts. In the present scenario, the government spends huge amount of funds for the steel and it predicts that the total production of steel is supposed to increase up to 300MT by the financial year 2030–2031 [1]. All the new projects initiated by the government like smart city and other infrastructures could benefit the escalating demand of steel sector in India. The usage of goods that are locally produced would indirectly help in increasing the national revenue and GDP. But there are a lot of problems like uncertainty in the supply of raw materials due to environmental issues and lack of metallurgy engineers. The government is promoting local production of steel by levying a heavy tax of 30% for export of the iron ore. Ministry of Steel (MOS) is also under the purview of establishing SRTMI (Steel Driven and Technology Mission of India), which is a pubic–private partnership and had been allotted Rs. 200 crores for the research and development purpose. It is affirmed that steel sector of China is currently the largest steel producer in recession,

Reviewers Comment: This non-technical article is important for all civil engineers. This article well balances the economic growth with steel industry and thus adds another dimension to civil engineers to think beyond regular design and construction.

J. Mattom (✉) · P. Herrick · V. M. Agrawal
National Institute of Construction Management and Research, Goa Campus, Ponda, India
e-mail: jamestom895@gmail.com

V. M. Agrawal
e-mail: vagrawal@nicmar.ac.in

B. B. Das et al. (eds.), *Recent Trends in Civil Engineering*, Lecture Notes in Civil Engineering 105, https://doi.org/10.1007/978-981-15-8293-6_17

while the country's steel sector is at a steady growth which would help India as a nation to take a bigger leap, and thus incorporating a sustainable growth in the future.

Keywords Steel industry · Construction sector · Indian economy · GDP

1 Introduction

Among all the major manufacturing industries, steel sector is proved to be the backbone for nation's stable economic growth and it plays an important role in boosting most of the developing and under-developing countries (G20). As per the reports of Steel Users Federation of India (SUFI), one of the major achievements is that our country India has surpassed Japan to achieve the feat of being the globe's second largest producer of steel after China having grabbed a biggest milestone for than 50% of the total production worldwide.

In the current stage, the Indian steel industry has better technology and has been always on-looking for continuous upgradation and renovation of archaic plants in such a way that greater energy efficiency levels can be reached. The Indian steel industry is currently operating at 77% capacity utilization with major producers exhibiting capacity utilization of 100%, while small and medium enterprises (SME) producers' capacity utilization is at slightly lower level [2].

Most of the resources which are being un-utilized cater to the demand of many products (TMT, wire rods and structural steel), providing a major demand in the infrastructure building section. On the other hand, with respect to the growth of manufacturing and other processing industries machinery and equipment would be in demand of flat steel products. The stable growth in sectors like architecture, building and construction (ABC) and auto, railway and transport (ART) segments would enhance the need for special and value-added steel that must be made available at indigenously competitive prices which would prove to be one of the key factors to sustain in the mindset of domestic players as shown in Fig. 1.

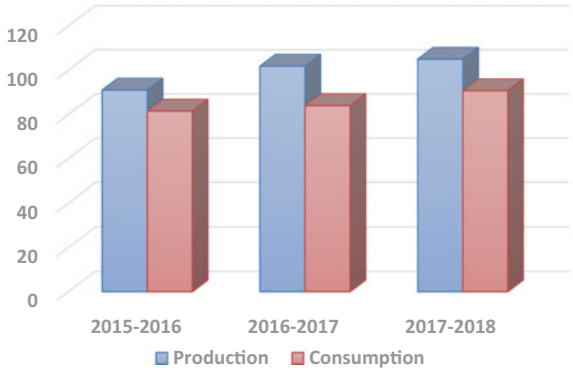

Fig. 1 Rhetoric comparison of steel's production versus consumption from 2015 to 2018

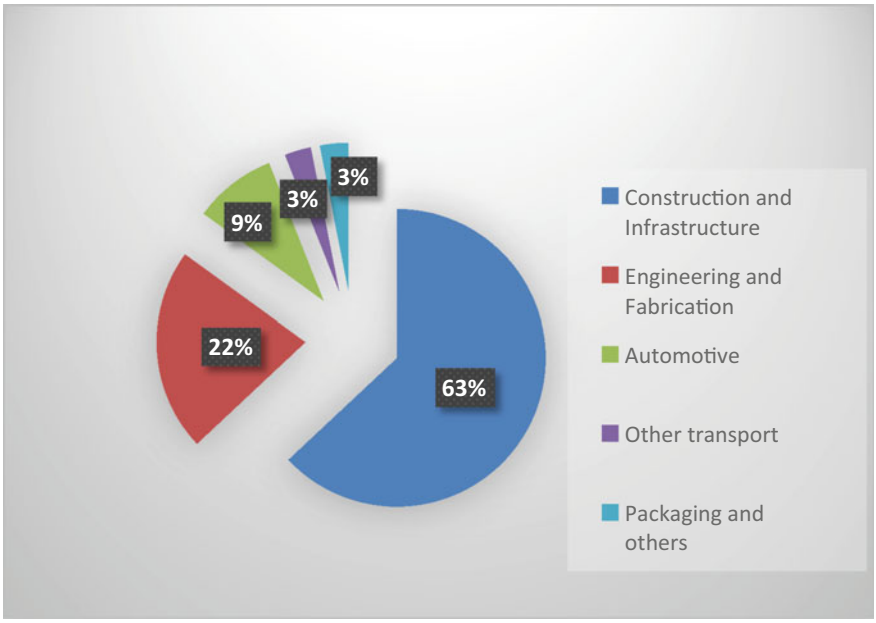

Fig. 2 Percentage proportion of steel in different sectors

In the fiscal year 2018–2019, India's steel production is sustained to remain higher as compared to the growth which is seen due to domestic demand from industries such as automobile, infrastructure and other user-oriented industries.

Figure 2 shows the usage of steel by major sectors in India and it can be seen that the construction and infra sector depicts the highest demand driver of steel, accounting a share of 63% during the fiscal year 2017–2018, then the engineering and fabrication sector of 22.1% of the total finished steel consumed in an year. Thereafter, the automotive sector is the third large steel consumer of 10.1%, and other transport and packaging sector of 2.9%.

2 Literature Review

As per many researchers and industry experts, the steel industry is considered to be the archaic and most prime industry. It is considered as the backbone of our country's economy. Through past records there is a valid proof that the steel manufactured in India in the late 1810s were of much superior in quality to British steel. After India's independence in 1947, a total capacity of 25 lakhs tons was achieved by three major steel companies [3].

In order to achieve an industrial growth in general and also in adherence with the steel industry, the economic reforms commenced by the government since 1991

have added an entirely new definition. This led to oversee, specifically for the steel industry which has been removed from the knowledge of other industries reserved for public sector. Since January 1992, in order to get a long-term vision to make the steel industry more competitive and efficient, certain prices and distribution controls have been eradicated and also relaxation has been observed in an automatic approval of foreign equity investment up to 100% allowed by the Government of India. In the region of both imports and exports, restrictions of external trade have been removed, which gradually led to lower import duty rates. Certain other benefits which have profited the Indian steel industry for a fixed period of time are: allowance to relocate resources from foreign financial markets, convertibility of rupees on trade account and rationalization of current structure of tax [4].

Amidst India replacing Japan as the second largest steel producer, China has profoundly grabbed a share of 51% crude steel production. The global steel body in its latest report noted that China's crude steel output increased in an order as follows:

1. 928.3 MT (million tons) in 2018 from 870.9 MT in 2017 (a rise of 6%).
2. China's share increased in an order to 51.3% in 2018 from 50.3% in 2017.
3. India's crude steel production in 2018 stood at 106.5 MT (rose by 4.9%) from 101.5 MT in 2017.
4. Japan produced 104.3 MT in 2018 (down by 0.3%) from 104.33 MT in 2017 [5].

The demand of steel in China is expected to escalate from 600 MT (in the year 2010) to a peak of 753 MT (until the year 2025), and then gradually decrease to 510 MT in 2050. While the construction industry in the steel sector will gain the highest total share, it will eventually portray a decrease in demand in the future. In the automobile manufacturing, the demand will increase rapidly before 2035 and its share will increase from 6.0% in 2010 to 19.0% in 2050. Over the last few decades, the steel industry in China has geometrically increased at an astonishing rate, which eventually lead to rise in economic development. Amidst this growth, there are many un-toward problems such as excessive environmental pollution and increasing energy consumption [3].

Way back in the year 2008, the steel industry has acquired a massive over-capacity due to a universal slowdown and because of that its demand gradually decreased in major developed countries, like USA, Europe and Japan, and in developing countries, like China, India, Africa and so on. At the current stage, India is climbing up the ladder efficiently to overcome the same in view of steel production. Import of surplus steel from the neighbouring countries in the Indian market would create problems such as reduced profits leading to no jobs, lower prices of the finished products and even to an extent of bankruptcies of domestic firms [3].

3 Growth and Evolution

The first blast furnace in India was constructed at Kulti in the year 1870 and the production of steel in this furnace began in the year 1874. Later, TATA started its steel production TISCO in the year 1907. Later, several different steel production

Table 1 Important steel manufacturing industries and their year of inundation

TISCO	1907
IISCO	1918
MISC	1923
SCB	1939
Hindustan Steel Ltd.	1954
Bokaro Steel Plant	1964

started in the preceding years. Table 1 shows important steel producing industries and their year of establishments; these industries laid the foundation for the present achievements in the steel sector.

Government of India has formed a New Industrial Policy in 1948 according to which the new ventures relating to steel industries was established by Government of India and already existing units were allowed to be managed and developed by private sector. Until 1990, the liberalization reforms of the steel industry were under the government and was completely controlled by the government. For the price regulation and setting up of additional plants, it was mandatory to get approval from the government authorities [6]. In the year 1993, government planned to partially privatize SAIL and also government agreed to the following major aspects in accordance with steel industry:

- Allow foreign players to enter
- Giving license to all the players who are interested to enter
- Permission for the export of iron ore.

After the privatization of steel industry, there has been a lot of developments in the production of steel.

4 Steel Production and Its Type

Steel in India is manufactured by two routes: oxygen route and electric route, as shown in Fig. 3. In oxygen route method of steel production, the metal is melted to the desired temperature and then the oxygen is blown into it. Generally, a blast furnace is used for this purpose. Almost 44% of the steel production in the country uses the blast furnace. Generally, the impurities come and float at the top layer and are to be manually removed. Electric route is a method in which the metal is generally melted with the help of electric power. This method generally contributes to about 56% [2] of the production of steel in the country. In the electric route the production is done by two different furnaces: electric arc furnace and induction furnace.

Electric arc furnace is one of the types of electric route. It is generally considered to be the most efficient way for the production of steel. This method contributes to the production of steel of about 22% [2]. This method is considered to be eco-friendly since it emits a very little quantity of CO_2. When compared to the oxygen route,

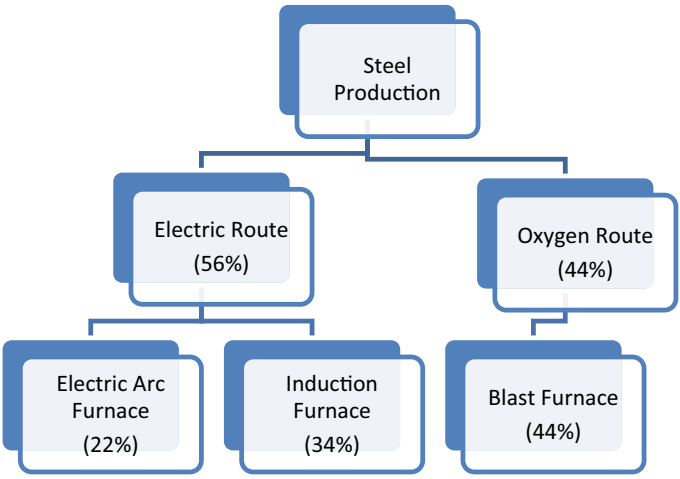

Fig. 3 Types of steel production

the total energy required to produce the steel is about 400–500 kWh/ton. Another advantage of electric arc furnace is that scrap metal can be used for the production of steel in this method which utilizes waste efficiently.

Induction furnace is another type of electric route. This method of production generally contributes to about 34% [2] of the total steel that is produced. It can produce steel from both scrap and direct-reduced iron (DRI). In India the availability of scrap metal is very less but there is a huge abundance of available coal as a natural resource. The availability of coal in abundance could help in the production of DRI at a very low cost. This type of DRI is called as coal-based DRI and is used in the electric route in the process of melting and helps in the production of steel at a very low cost. In India the availability of the scrap metal is very less but there is a huge abundance in the availability of the coal as a natural resource.

In the total production, almost 63% is used in the infrastructure sector which includes both structural steel and reinforcement bars. Reinforcement bars or reinforcing steel are of two types: mild steel bars and deformed steel bars.

The government expects the demand for steel to be in a constant state of increment and to be raised to the level of 230 MT by the FY30-31. In the present condition the infrastructure is holding almost 9% of the total steel that are produced, and the sector seems to be increasing at a constant rate. At this rate it is expected to reach 11% by the FY25-26.

During the twelfth 5-year plan, the government expected the investment to be Rs. 55.74 lakh crores and then later revised to Rs. 37.24 lakh crores for the infrastructure development in the country [7]. It is expected that the government would increase the funds for country's infrastructure development in years to come.

Government of India is planning to create a number of smart cities, and initially government has released about Rs. 9940 crores to the states for the smart city up to 31

March 2018 [8] and it is expected that about 2.04 lakh crores is to be allotted for the development of about 99 smart cities as Finance Minister informed the Parliament. This smart city project will need a huge construction which will increase the demand of steel.

The total steel demand per person in the finance year 2016–2017 is about 9.89 kg/person and it is expected to increase by the end of FY21-22 to 12–14 kg/person. This is mainly due to the different policies and schemes that are made by both the central and the state government like Indra Awaas Yojana, Pradhan Mandhiri Gram Sabha Yojana and Housing for all. These schemes will demand construction activity and will increase in per capita consumption of steel.

In the financial year 2017–2018, the traffic at the airport was around 308.75 million in all the 94 airports throughout the country that are operational for the public use. So the government has planned to create and develop airports in the tier-2 cities to reduce the traffic density. During the financial year 2014–2015 the government proposed for the construction of 16 different sea ports throughout the country. All these infrastructure projects will boost the steel demand in India.

From the Fig. 4 (Steel production growth rate in India) and Fig. 5 (Annual growth rate of steel vs. GDP growth rate), it is evident that during the FY2013 to FY2018 there is a huge variation noted down in the year 2016 because of demonetization which had a mirror effect in the FY2017 and showed the GDP growth declining from 7.11 to 6.68% and also internally there is an astonishing decline in the steel sector showing a negative value of −1.30% in the year 2016 and eventually escalating to 5.6% in FY2017 [9].

It can be inferred that any variation in the objectives of macro-economic variables would have an internal effect in the instruments such as monetary policy. But between the FY2017 and FY2018 we can observe that the annual growth rate of steel is increasing gradually from 5.6 to 6.7% and also the GDP growth rate has increased from 6.68 to 7.3% [10]. By the year 2020 the expected REAL gross domestic product would be figured to 7.75% and four years down the line from 2018 to 2022 the GDP

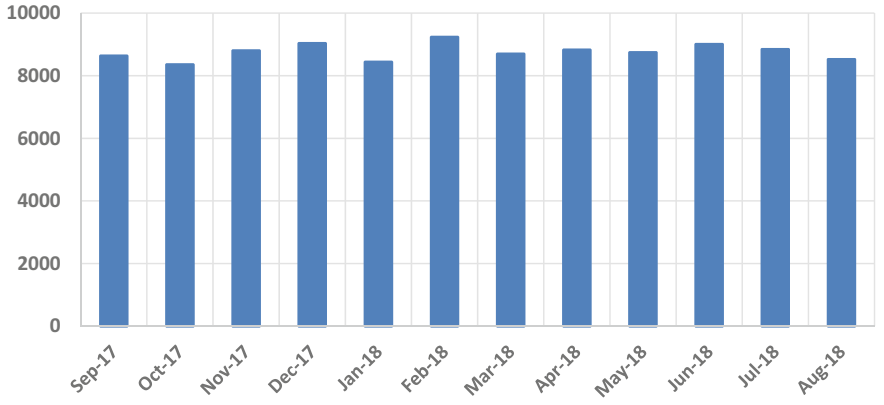

Fig. 4 Production of steel during Sep. 2017 to August 2018

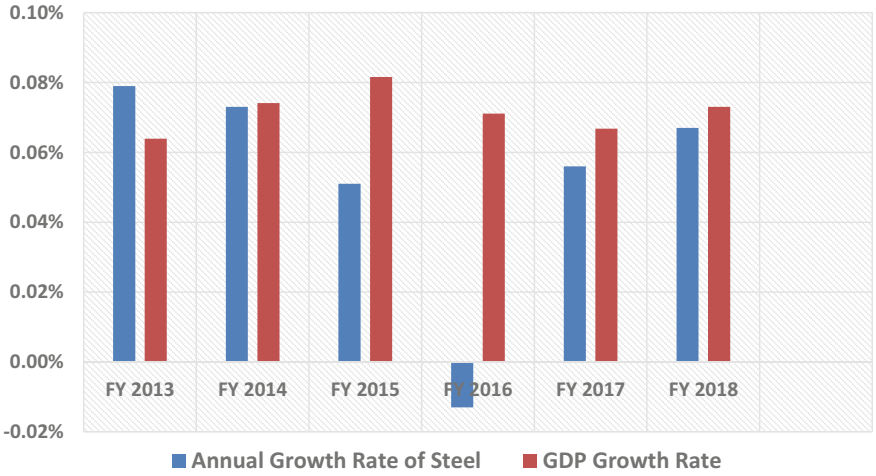

Fig. 5 Annual growth rate of steel versus GDP growth rate

growth rate of India would be 7.73% as per the reports. The future proposed increase in GDP would alternatively boost the Indian steel sector market scenario and would also show less variations in the business cycles [11].

5 Current Scenario and Initiatives by Government

The Indian steel industry tussle with variations leading to uncertainties pertaining to its availability and consistent supply of raw materials, that is, both coal and iron ore still remains a challenge in Western Ghat places like Goa's early mines stoppage: An add-on hassle in the industry. Since the markets shifted its domain from an allocation process to an auction process in order to achieve the mining blocks, it has brought about considerable transparency such as issues related to transport logistics from the mine areas which needs to be differentiated to mitigate lag in evacuation of coal, iron ore and other minerals.

The Indian steel industry has acquired all the required expertise to produce steel at a minimal cost but indeed, the infrastructure is a daunting sector and until it reaches to a saturation point, it will not act as catalyst in order for India to remain as the major steel producer. Another major hurdle is that land acquisition (confidentially Indian steel industry being about 100 years old) has a wide gap in research, development and innovation [12].

According to Joint Plant Committee, the country's production w.r.t steel sector was 8.22 MT in the FY2017, which escalated to 4.4% rise, leading to the production of 8.59 MT during April 2018. Well-known players like SAIL, RINL, JINDAL STEEL and so on, all combinedly produced 5.01 MT during April 2018 as compared to 4.7

MT produced in FY2017. The rest 3.57 MT came from other small players thriving in this industry, portraying a growth of 1.4% over FY April 2017.

During April 2018, the hot metal's output was at 5.8 MT as compared to 5.38 MT in 2017. While 4.38 MT was produced by the major stakes in the sector, the rest 0.96 MT resulted from other big players. Pig iron's output rose from 0.78 MT in FY2017 to 0.8 MT FY2018 (a 1.9% rise). Our country's steel resultant rose to 8.43 MT in Feb 2018 against 8.29 MT as in Feb 2017 [13].

The recent government initiatives in this sector are:

- To ensure the required supply of domestic steel industry, an export duty of 30% has been levied on iron ore.
- Upcoming road and infra projects are considered to be a back-end measure in order to escalate the increasing demand for steel products.
- To have a higher growth rate in the demand of steel, the upgradation of rural economy and its domain in infrastructure proves to be the best approach.
- In order to promote R&D activities in ferrous and steel industry, Ministry of Steel, Govt. of India has put an initial amount of Rs.200 crores in accordance with Steel Driven and Technology Mission of India, combining both private and public sector companies [2].

6 Analysis of Indian Steel Industry

- In the long term, steel sector incorporates the overall economic growth of other major industries whose fortune is directly proportional to the growth of these industries.
- The steel sector indirectly alleviates the overall economy over 2% to the gross domestic product of the nation and helps in providing 20 lakh employment opportunities [14].
- Our country has suffered from prodigious in-flow of imports of steel from other Asian countries like South Korea, Japan and China. South Korea and Japan had a benefit due to India's free-trade agreement [15].
- In order to maintain an equilibrium between imports and domestic demand, there is an observance of aligning of steel prices to global export prices. It poses a major risk in improving the demand for Europe and other Asian countries if there is an increase in resultant growth in exports [16].

7 Conclusions

From the above discussions it can be concluded that the Indian steel industry has all the capabilities in meeting the escalating demand of other important industries.

It runs through the blast furnace process with high consolidation. Due to the difference in the ratio of hot metal to that of crude steel productions, it can be

analysed that the secondary steel producers (non-ISP) are using scrap route to meet the difference created by integrated steel producers (ISP) which could only produce about 60% of the total demand.

With the initiative of the government requiring major infrastructure developments, the demand of steel is increasing rapidly. These initiatives will create a good number of job opportunities to the young population of our country which will definitely help in improving the GDP of the nation.

References

1. Sabnavis M (2018) Steel review and outlook
2. IBEF (2018) 27 Dec 2018. https://www.ibef.org/pages/steel.aspx
3. Singal A (n.d.) An analysis of the impact of imports of steel from China on Indian. J Bus Fin Aff 1–7
4. Development of Indian Steel Sector Since 1991 (2018)
5. India replaces Japan as second top steel producer (2019), 28 Jan 2019. https://economictimes.indiatimes.com/industry/indl-goods/svs/steel/india-replaces-japan-as-second-top-steel-producer-worldsteel/articleshow/67721395.cms
6. Lora Z, Dmitriy K (2017) Overview of steel and iron market
7. Sunny V (2017) Twelfth Five Year Plan: on weak economy, infrastructure investment projected to decline sharply. The Indian Express, India
8. PTI (2018). The Economic Times, 11 Feb 2018. https://smartcitiesmission.com/
9. Sajal G (2006) Steel Consumption and economic growth: Evidence from India. Sci Direct. Management Development Institute (MDI), Gurgaon, India
10. Banerjee S (2018) Current growth cycle in steel sector to last for 24 months, 23 Oct 2018
11. 25 12 2018. https://www.statista.com/statistics/661391/manufacturing-industry-production-growth-rate-india/
12. Bhaskar C (2018) Business today. 21 May 2018. In: Indian steel industry: overcoming challenges and strengthening itself. https://www.businesstoday.in/opinion/columns/indian-steel-industry-overcoming-challenges-and-strengthening-itself/story/277398.html
13. D'Souza N (2018) India steel sector outlook: will metal prices loose their sheen in wake of China slowdown? Dec 27 2018
14. Indian Steel Industry Analysis (2018)
15. Bhatia S (2017) Crisis in Indian steel industry: issues and challenges. Int J Sci Res Publ
16. Master E (2018) https://www.equitymaster.com/research-it/sector-info/steel/Steel-Sector-Analysis-Report.asp

Partial Replacement of Fine Aggregates with Coconut Shell Ash in Concrete

Aditi Lawande, Areeb Ahmed, Laukik Dessai, Rahul Naik, Tanvi Kavlekar, Gauresh Desai, Starina Dias, and Kaushik Pai Fondekar

Abstract Concrete has been continuously used for infrastructural development due to which its demand as a construction material has increased. The depletion of the natural sand has been the major concern in the construction industry, and this makes the need of finding other alternative approaches for this problem. Considering that natural sand has to be saved for the future for sustainable development, there is a need of replacing this sand partially or fully with other suitable materials. Waste materials are also on an increase creating environmental problems, hence if they are incorporated into the concrete construction industry, it will reduce the environmental problems, thus helping in saving natural sand extraction. This paper focuses on using manufactured sand with varying percentages of coconut shell ash as fine aggregate along with two different types of cements (PPC and PSC) and then comparing the 7th and 28th day compressive strength, respectively. The seven days compressive strength of concrete replaced with 0, 5 and 10% of coconut shell ash as fine aggregate along with PPC and PSC was found to be 23.70, 21.33, 18.22, 24.74, 23.70 and 22.22 N/mm^2, respectively. The 28 days compressive strength test of concrete replaced with 0, 5 and 10% coconut shell ash as fine aggregate along with PPC and PSC was found to be 37.33, 28.00, 19.68, 26.37, 24.88 and 19.70 N/mm^2, respectively. As the replacement percentage kept on increasing, it was observed that the compressive strength of concrete decreased.

Keywords CSA (coconut shell ash) · PPC (portland pozzolana cement) · PSC (portland slag cement) · M-sand (manufactured sand) · Compressive strength

1 Introduction

Concrete is a composite material made by mixing cement, sand and aggregates with water in a suitable ratio. Concrete is used extensively in the construction of buildings, dams, roads and other structures and has become an indispensable part of civil

A. Lawande (✉) · A. Ahmed · L. Dessai · R. Naik · T. Kavlekar · G. Desai · S. Dias · K. P. Fondekar
Department of Civil Engineering, Don Bosco College of Engineering, Fatorda, Goa, India
e-mail: aditi.lawande806@gmail.com

B. B. Das et al. (eds.), *Recent Trends in Civil Engineering*, Lecture Notes in Civil Engineering 105, https://doi.org/10.1007/978-981-15-8293-6_18

engineering. Concrete is relatively cheaper and has few maintenance requirements. Apart from being cheap and low maintenance, it has a number of other advantages such as it is strong in compression, can be moulded in any shapes and has good resistance towards weather and fire.

With every second passing, the world is becoming more and more advanced, and to cope up with this advancement the demand for concrete construction is on the rise. The demand for structures, construction materials, aesthetic products and interior decors is also on the rise. In recent years there has been a tremendous increase in construction which has resulted in scarcity of raw materials. Naturally occurring river sand which is a very important ingredient in concrete is decreasing day by day. This problem has made a quest for alternate solutions very essential. Depletion in natural sand has been affecting environment since a long time. A point has reached to treat natural sand like a "RESOURCE" and find other alternative materials available in the environment. Many researches have been carried out using fly ash, siliceous stone powder, copper slag and so on as alternatives to sand in concrete.

The coconut tree is known for its versatility, where all its parts get used in some way or the other. Coconuts are produced almost worldwide in more than 90 countries. In India, the state of Kerala stands first in coconut production, and the other major coconut-growing states are Tamil Nadu, Karnataka, Andhra Pradesh, West Bengal, Orissa, Assam, Goa, Maharashtra, Gujarat, Lakshadweep and so on. The state of Goa stands on the seventh position in producing coconuts products in India. The coconut husk and coconut shells which are present in plenty as agricultural waste can be used in some form or the other. In the construction industry this waste can be utilized as a substitute for either fine or coarse aggregates or cement in the concrete production. In some of the research works carried out, the "Performance of waste coconut shell as partial replacement of natural coarse aggregate in concrete" was used to produce M20 grade concrete by replacing coarse aggregates with coconut shells by 0, 5, 10, 20, 30, 40 and 50% by weight. This research showed that the compressive strength of concrete reduced with percentage increase in replacement. Hence it was concluded that coconut shells can be grouped under lightweight aggregates and can also be used to reduce construction cost as it is considered to be an agricultural waste [1]. In other paper on "Advance concrete-aggregate replaced by coconut shell", replacement of 25 and 50% of aggregates was carried out with coconut shells with production of M20 grade of concrete mix. Tests like compressive test, flexural test and split tensile test were carried. It was concluded from this paper that concrete replaced by coconut shells satisfied the requirements of lightweight concrete [2].

In this study an attempt was made to use the coconut shell ash which is available in the state of Goa as an option for partial replacement of sand along with the use of manufactured sand or M-sand.

2 Materials and Methodology

2.1 Materials

2.1.1 Cement

The cement used was fresh and free from any lumps. All the tests were done as per the specifications given in IS:1489 Part I—1991 [3] for PPC and IS:455-1989 [4] for PSC.

2.1.2 Coarse Aggregates

Coarse aggregates of 20 and 10 mm obtained from a local quarry are used in this experimental investigation. These aggregates were tested as per IS:2386-1963 (Part I, Part III) [5, 6].

2.1.3 Fine Aggregates

Manufactured sand obtained from local sources was used in this experimental work. The required tests were done on sand as per IS:383-1970 specifications and sand confirming to zone II was obtained.

2.1.4 Coconut Shell Ash

Coconut shells were obtained from local sources and coconut shell ash was prepared by burning coconut shells in open air for many hours. Coconut shells were burnt using uncontrolled combustion.

2.1.5 Water

Water used for mixing and curing of concrete during the course of the project was clean, potable water free from all the impurities like oil, grease, salts and others. For mixing and curing of concrete potable water is considered as per IS:456-2000 [7].

2.2 Methodology

2.2.1 Mixing

For this experimental work machine mixing was used for mixing concrete as it was easier, efficient than hand mixing. This produced better quality and quantity of concrete in a shorter period of time.

2.2.2 Casting

Cubes of cast iron having dimensions of 15 cm × 15 cm × 15 cm were used. Concrete cubes were casted varying the percentages of coconut shell ash as a replacement for manufactured sand, and compressive strength test was performed.

2.2.3 Curing

In this experimental work, curing of concrete cubes was done using water curing method for 7 and 28 days.

2.2.4 Mix Design

The design covered was M25 grade concrete. Mix design of concrete was carried out as per IS:10262-2009 [8]. The results of preliminary tests carried out are tablulated from Tables 1, 2, 3, 4, 5 and 6 and the final reults are shown from Figs. 1, 2, 3, 4, 5, 6, 7, 8 and 9.

Table 1 Specific gravity of cement

S. No.	Description	Value
1	Specific gravity of PPC cement	2.50
2	Specific gravity of PSC cement	2.63

Table 2 Specific gravity of aggregates

S. No.	Description	Value
1	Specific gravity of fine aggregates (manufactured sand)	2.560
2	Specific gravity of coarse aggregates	2.860

Table 3 Particle size distribution for fine aggregate

IS sieve	Weight retained (g)	Percentage of weight retained (%)	Cumulative percentage retained (%)	Cumulative percentage finer (%)
4.75 mm	9.0	0.90	0.90	99.10
2.36 mm	133.0	13.30	14.20	85.80
1.18 mm	261.0	26.10	40.30	59.70
600 μ	168.0	16.80	57.10	42.90
300 μ	184.0	18.40	75.50	24.50
150 μ	130.0	13.00	88.50	11.50
Pan	115.0	11.50	100.00	0.00

The sand belongs to Zone II.

Table 4 Silt content of manufactured sand

S. No.	Description	Value
1	Silt content of sand (%)	11.50

Table 5 Compressive strength of concrete cubes with addition of different percentage of coconut shell ash (7 days)

S. No.	Percentage of CSA (%)	Grade of concrete	Age of cubes (days)	Load (N)	Cross-sectional area of cube (mm^2)	Compressive strength (N/mm^2)
PPC						
1	0	M25	7	533,330	22,500	23.70
2	5	M25	7	480,000	22,500	21.33
3	10	M25	7	410,000	22,500	18.22
PSC						
1	0	M25	7	556,670	22,500	24.74
2	5	M25	7	533,330	22,500	23.70
3	10	M25	7	500,000	22,500	22.22

3 Results and Discussions

Based on the experimental work the following can be noted that by using coconut shell ash as a partial replacement to fine aggregates:

1. There was no significant improvement in the compressive strength in the properties of M25 grade concrete using PPC and PSC.

Table 6 Compressive strength of concrete cubes with addition of different percentage of coconut shell ash (28 days)

S. No.	Percentage of CSA (%)	Grade of concrete	Age of cubes (days)	Load (N)	Cross-sectional area of cube (mm^2)	Compressive strength (N/mm^2)
PPC						
1	0	M25	28	840,000	22,500	37.33
2	5	M25	28	630,000	22,500	28.00
3	10	M25	28	443,330	22,500	19.68
PSC						
1	0	M25	28	593,330	22,500	26.37
2	5	M25	28	560,000	22,500	24.88
3	10	M25	28	443,330	22,500	19.70

Fig. 1 Testing of concrete cube in CTM

2. The 7 days compressive strength test of concrete cubes having PSC showed more gain in compressive strength as compared to strength test of concrete cubes having PPC.
3. The 28 days compressive strength test of concrete cubes showed that PPC had gained more compressive strength as compared to PSC.

4 Conclusion

Since there is no significant improvement in the strength of concrete using manufactured sand by partially replacing it with coconut shell ash, ways of strength gain may be achieved by adding more reinforcing materials. Hence it is concluded that

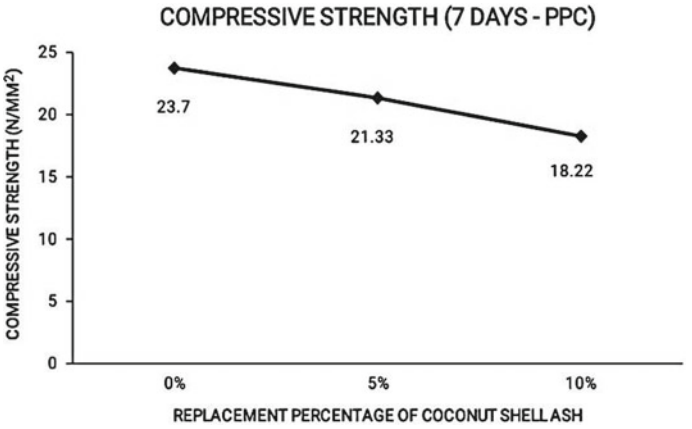

Fig. 2 Compressive strength of concrete cubes (PPC) after 7 days

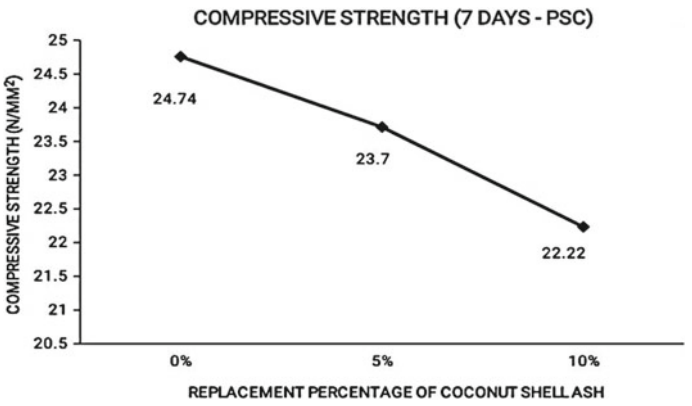

Fig. 3 Compressive strength of concrete cubes (PSC) after 7 days

concrete having manufactured sand when partially replaced with coconut shell ash can be used for lighter works such as PCC. Also, this concrete may help to solve the problem of agricultural waste disposal mostly in rural areas and also help to resolve issues on shortage of natural materials in concrete construction.

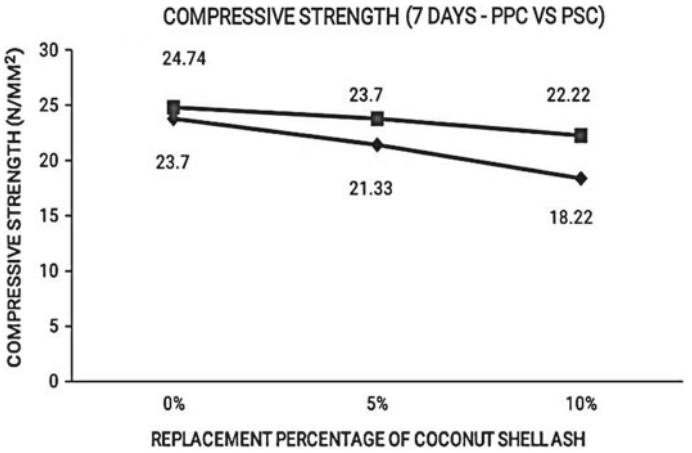

Fig. 4 Compressive strength of concrete cubes (PPC v/s PSC) after 7 days

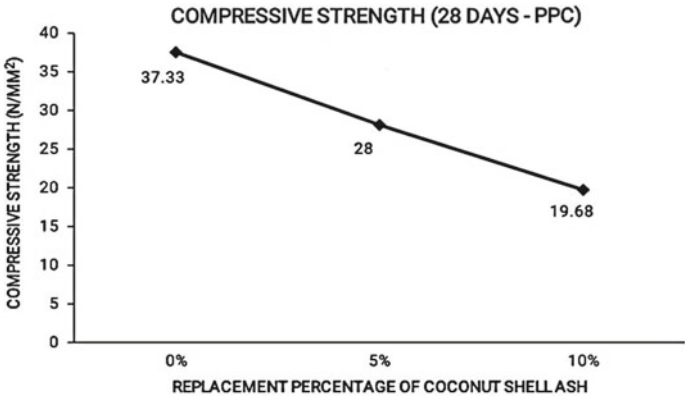

Fig. 5 Compressive strength of concrete cubes (PPC) after 28 days

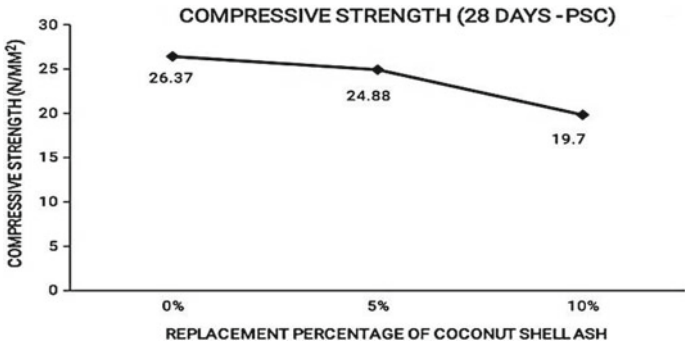

Fig. 6 Compressive strength of concrete cubes (PSC) after 28 days

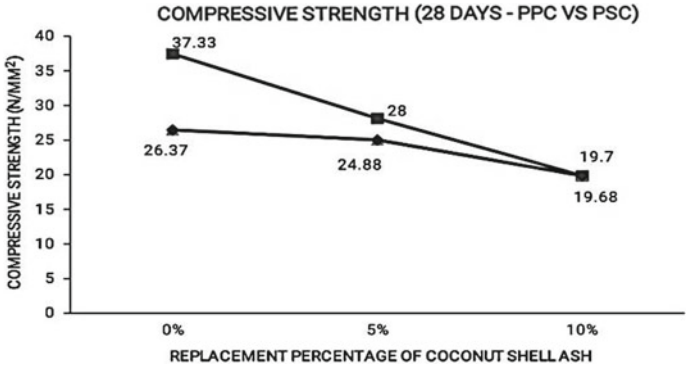

Fig. 7 Compressive strength of concrete cubes (PPC v/s PSC) after 28 days

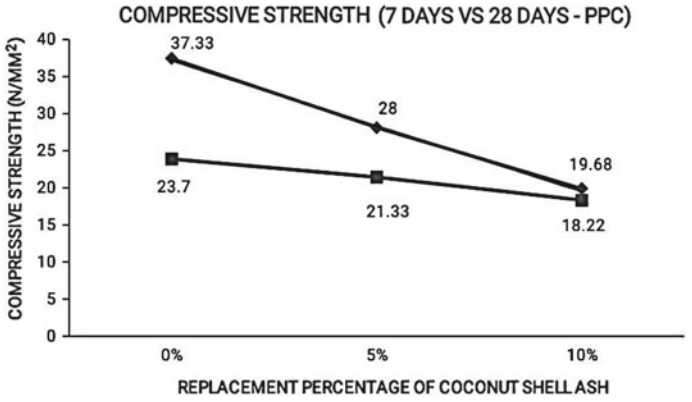

Fig. 8 Compressive strength of concrete cubes (7 days v/s 28 days PPC)

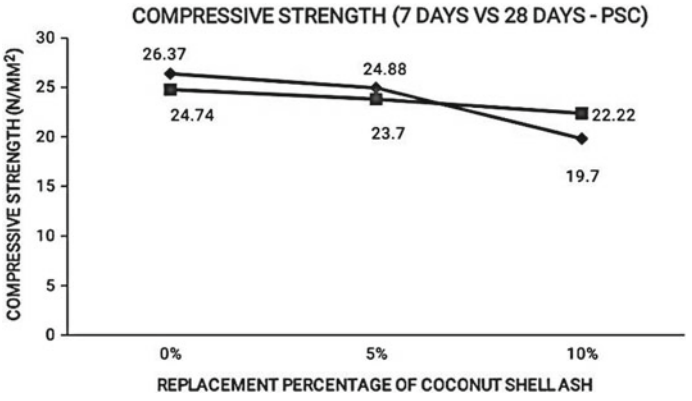

Fig. 9 Compressive strength of concrete cubes (7 days v/s 28 days PSC)

References

1. Abdullah A, Sabih A, Syed AA (2016) Performance of waste coconut shell as partial replacement of natural coarse aggregate in concrete. Int J Sci Eng Res 7(8):1802. ISSN 2229-5518
2. Ajim SS, Sagar BT, Rahul VU, Prasad SS (2015) Advance concrete—aggregate replaced by coconut shell. Int Res J Eng Technol (IRJET) 02(05). e-ISSN: 2395-0056 p-ISSN: 2395-0072 www.irjet.net
3. IS 1489 Part 1 1991 Portland pozzolana cement–specification
4. IS 455-1989 Portland slag cement-specification
5. IS 2386-1963 Methods of tests for aggregates for concrete Part I Particle size and shape
6. IS 2386-1963 Methods of tests for aggregates for concrete Part III Specific gravity, density , voids , absorption and bulking
7. IS 456-2000 Plain and reinforced concrete–code of practice
8. IS 10262-2009 Concrete mix proportioning—guidelines

Brick Manufacturing Using Laterite Soil

Satyesh A. S. Kakodkar, Atish Lolienkar, Sajal Kamat, Shwetang Nadkarni, Gaurai Naik Gaunekar, and Vikesh Malik

Abstract The construction industry is on the forefront for the growth of any nation. In olden days, shelter was merely a means for survival but in the present age infrastructure symbolises a position of power. In order to build infrastructure, there is a need of material, most importantly building material. Building materials make up for 75% of the total cost of construction. As the years go on, there is a need for innovative and sustainable building materials using industrial, agricultural and natural wastes. Bricks are the most frequently used building constituents in the construction world. For lining furnaces in metallurgy and glass industries, bricks are used. Green building material has attracted attention because of sustainability factor. Using the waste as substitute raw material in manufacturing of building products is an innovative way of waste utilisation. A large quantity of waste is produced in every sector of life. In this paper we have given a thrust on the use of waste material such as lateritic soil, human hair along with other raw materials to manufacture a masonry unit. These materials are used in different proportions, and several trials are conducted to obtain a product with better competencies than a traditional brick, creating an alternative and sustainable masonry unit.

Keywords Building material · Waste · Human hair · Sustainability

1 Introduction

Ever since the dawn of humanity, we have left no stone untouched when it comes to innovation, be it the discovery of fire to the invention of the wheel. The apex of human civilisation does not exist as we keep on evolving with the passage of time. Ever since childhood we have learned that humans have three basic needs: the need for food, clothing and shelter.

The need for shelter has changed throughout history, and in the present time we use different materials like wood, bricks, concrete and steel to construct houses and

S. A. S. Kakodkar (✉) · A. Lolienkar · S. Kamat · S. Nadkarni · G. N. Gaunekar · V. Malik
Don Bosco College of Engineering, Margao, India
e-mail: satyesh.kakodkar@dbcegoa.ac.in

B. B. Das et al. (eds.), *Recent Trends in Civil Engineering*, Lecture Notes in Civil Engineering 105, https://doi.org/10.1007/978-981-15-8293-6_19

skyscrapers. Out of these materials our paper focuses on bricks. Bricks, by definition, are small rectangular blocks of clay typically made by firing or sun-drying. Fired bricks are one of the most durable and strongest building materials since 4000 BC and they have been widely known as artificial stones. Our aim is the innovation of processes and materials used in the creation of a brick.

Goa, a state that lies on the western coast of India, has nearly two-thirds of its land mass covered with laterite, which has made it as most popular construction unit.

Clay when heated gains strengths and hardness. Clay in its pure has a mineral composition of quartz, mica, feldspar and so on, while the composition of laterite includes zircon, quartz and oxides of minerals like iron, titanium, aluminium and manganese.

The study is carried out with an objective of using locally available lateritic soil for manufacturing of a brick, thereby creating a construction material that surpasses the traditional brick in properties and which is economically viable.

2 Materials and Equipment

The main focus is on manufacturing an eco-friendly brick using locally available waste materials. The aim is to create a product which will enhance the economic value of waste material. This section highlights the different materials and equipment used. The foremost component used for manufacturing is lateritic powder.

2.1 Lateritic Powder

Laterite is a type of rock as well as soil. This consists of aluminium and iron. It is generally found in hot as well as wet tropical regions. Most of the laterites are rusty-red in colour due to the presence of high iron oxide content. It is the parent rock on which the chemical composition as well as the mineral composition of laterite is dependent. Quartz, manganese, Zircon, iron oxides, tin and aluminium which persist during the process of weathering are the key minerals present in laterite. Quartz is the most lavish antique mineral from the parent rock.

2.2 Lime Powder

Technically, lime is an inorganic mineral composed primarily of oxides and hydroxides of calcium. In early days, lime has been used as building grout and has the ability of adhering or sticking. The rocks that possess calcium or magnesium carbonates in the range of 80% or more, including chalk, marl and marble are termed as limestone. Further classification is by composition as high calcium, argillaceous,

siliceous, magnesium, conglomerate, dolomite and other limestone. Uncommon sources include coral, sea shells, calcite and ankerite. Limestone is digged out from quarries or mines.

2.3 Stone Dust

Stone dust comprises the crushed rocks which are finely crushed and processed by both the natural as well as the mechanical means, and also contains minerals. The igneous rock, that is, basalt and granite, most of the time consists of the maximum mineral content; on the other hand, there is consideration of limestone. Stone powder is a by-product of crushed stones. Therefore, it has similar compositions that are dolomite and limestone.

2.4 Cement

Cement is a widely used ingredient for construction that has the properties of setting, hardening and adhering to other constituents to muddle them together. Cement cannot be used alone and is generally used for binding sand along with aggregate. Cement mortar is produced when cement is mixed with fine aggregates and is used for masonry, or when it is mixed with sand along with gravel produces concrete. One of the most widely used material is cement after water; it is the resource that is most consumed on this planet. Generally, cement which is used for construction is based on lime or calcium silicate and commonly inorganic in nature; and this can be recognised as both the hydraulic as well as non-hydraulic, based on its potential to set with water.

2.5 Human Hair

Hair is a protein tendril that grows within the dermis from the follicles present in it. Hair is one of the most common characteristics of all the mammals. Other than area of glabrous skin, all the parts of human body are being protected by follicles and these help in producing thick terminal and also a fine vellus hair. It is also a critical biomaterial which fundamentally consists of protein, notably alpha-keratin. Medulla, cuticle and cortex are the compositions of every hair strand. The innermost region which is always present, open as well as unstructured region is known as medulla. The one which is highly structural and is also arranged is cortex, the third layer of the hair. This is also a primary mechanical strength uptake source. Cortex also consists of melanin, which also standards the fibre supported number, distribution and kinds of

melanin granules. The outer covering is known as cuticle. There has been a variation ranging from 0.017 to 0.18 mm in regards to the diameter of human hair.

2.6 Rice Husk

The tough coatings of the rice grains are known rice husk. These can be used in many ways, like insulation material, building materials, fertilizers and fuel. This also helps as a protection for rice in growing. Rice husk is itself a part of rice. Husk is made up of tough materials like opaline, silica and lignin.

2.7 Fly Ash

The particulate which has been displaced out of boilers for coal-fired together with the flue gases, when composed for coal combustion is known as fly ash. Bottom ash is particularly the ash which falls on the bottom part of the boiler's combustion chamber. In power plants based on coal-fired and highly based on technology, electrostatic precipitators are used to capture the fly ash and rest of the particles are being filtered before they reach the chimneys. "Together with bottom ash removed from the boiler, it is known as coal ash. Based on the supply and combination of the coal being burned, the components of fly ash differ drastically, but all fly ash contains massive quantities of silicon dioxide (SiO_2) (each amorphous and crystalline), aluminium oxide (Al_2O_3) and calcium oxide (CaO), the main mineral compounds in coal-bearing rock strata.

The minor elements of fly ash rely upon the unique coal bed composition, however, they may also encompass one or more of the following factors or compounds observed in trace concentrations (as much as lots of ppm): arsenic, beryllium, boron, cadmium, chromium, hexavalent chromium, cobalt, lead, manganese, mercury, molybdenum, selenium, strontium, thallium, and vanadium, together with very small concentrations of dioxins and PAH compounds."

2.8 Water

Water is a polar inorganic combination, which at room temperature is an odourless and tasteless fluid, and that is practically colourless aside from a natural inherited link of blue. It is the most analysed chemical compound that has been labelled as the "universal solvent" as well as the "solvent of life".

Water would be the substance material with chemical structure H_2O; one particular particle of moisture has two hydrogen atoms covalently bonded to an individual much needed oxygen atom. Water in liquid form has inadequate absorption rings at wavelengths of 750 nm, which in turn lead it to appear to have a blue colour.

This might be easily experienced inside a water-filled tub or even washbasin whose coating is whitened. Big ice crystal deposits, as within glaciers, additionally appear bluish.

As opposed to additional related hydrides of the much-needed oxygen loved ones, drinking water is essentially a fluid that costs less than regular circumstances as a result of hydrogen bonding. The particles of moisture are continuously shifting inside relation to one another, so the hydrogen bonds are constantly busting just reforming at timescales more quickly than 200 femtoseconds ($2 \times 10'$ 13 s). Nevertheless, the bonds are robust adequate for making a lot of the uncanny qualities of water, several of that make it essential to existence.

2.9 Equipments

2.9.1 Standard Test Sieve

A mesh filter, typically known as sieve, may become a device for separating essential components from undesirable materials or maybe for characterising the particle size distribution of a sample, typically employing a woven display like a mesh or even metal or web. Sieve analysis is vital for analysing components since particle size distribution is able to impact a broad range of properties that includes strength, solubility of mixture, surface area properties. Sieving is a simple method for separating particles of different sizes. Rough dust particles are separated by grinding from one another and also screen openings.

Based on the kinds of particles to be separated, sieves with various forms of openings are used. In the study of ours, we've employed a sieve of dimension 1.18 mm, as the particle under 1.18 mm diameter aids in void compaction, therefore providing excellent compressive strength.

2.10 Trowel

A trowel is a small tool used for applying, smoothing or moving little quantities of viscous or particulate material. Various kinds of trowel are used in masonry, concrete and drywall construction; further it is also used to apply coatings and laying synthetic flooring. Masonry trowel is historically a product of forged carbon steel; however, few latest versions are product of cast stainless steel that has longer wear and is also rustless.

2.11 Weighing Scale

Weight is displayed in the form of number, usually by a liquid crystal display through electronic digital scales. They are multipurpose as they perform calculations on the measurement along with transmitting to other digital devices. We have used two types of weighing machines, one for getting accurate measurements in grams in the case of hair fibres, and the other one is to get weights in kilograms to weigh cement, soil, stone dust and so on. Weighing is very important so as to maintain the proportions as calculated before the casting of bricks.

2.12 Measuring Cylinder

Measuring cylinder is a laboratory equipment used to measure the volume of liquid. It has a narrow cylindrical shape. The amount of liquid to be measured is represented by each line marked on the graduated cylinder.

Polypropylene which possesses excellent chemical resistance or poly-methyl pentene which is known for the transparency, making them lighter as well as less fragile than glass, are majorly used in the manufacturing of cylinders. Graduated cylinders are usually more correct and are also more precise than the laboratory flasks or the beakers; however, they must not be used in order to perform volumetric analysis; volumetric glassware, like a volumetric flask or volumetric pipette, must be used, as it is more correct as well as precise. Graduated cylinders are commonly used to measure the degree of a solid indirectly by measuring the displacement of liquid.

2.13 Vibrating Table

An unbalanced mass which is smaller on a DC motor is used by an eccentric rotating mortar, which when rotates generates a force that translates to vibrations. A force is created when a linear resonant actuator with internal mass attached to a spring is driven. The application of vibration working with the force of gravity can often move materials via a technique more successfully than different methods. Vibration is generally used to place small components in order that they may be gripped mechanically with the aid of automated equipment as needed for assembly and so on. The particular design of this type is capable of holding a load of 140 kg. Size is generally 24 $\times$ 24 inch. The equipment contains a motor fitted with a variable pitch pulley housed in a cabinet. The vibrations are imparted by using off-balance masses rotating on a shaft of a vibrator clamped to the underside of the table top. The vibration helps in giving better compaction of the mixture inside the mould.

2.14 Mould

The mould was designed in such a way that we were able to cast six bricks in a single mould wherein each brick slot was of size 19 cm × 9 cm × 9 cm. The mould was made up of teak wood, which also makes it lighter in weight. The mould was so designed that different parts of the mould could be removed and assembled again which helped in placing the mix and removing off the bricks from the mould after drying comfortably without any damage caused to the bricks.

2.15 Mixing Tray

The tray is made up of stainless steel; hence there is no problem of rusting. It has its edges bent so as to prevent the mix to fall off from the tray. It also helps in proper mixing of the contents with a strong base. It prevents the wastage of the mix and hence maintains proper proportions as calculated.

2.16 Universal Testing Machine

Another name for universal testing machine is a universal tester which is used to perform many standard tensile and compression tests on materials, components and structures. The load begins to apply in increasing order once the machine begins. Throughout the tests the control system along with its associated software record the load as well as extension or compression of the specimen.

3 Methodology

In order to arrive at most economical and efficient brick, different proportions were tried and tested. The methodology involves working out correct proportions and then manufacturing the final product. Initially brick casting was done manually and the proportion that gave satisfactory results was cast using machinery.

Initially cubes of 5 cm × 5 cm × 5 cm, with a sole aim of arriving at the best proportion were cast. After the process of drying and curing, the bricks were tested for compressive strength. The best proportion was then chosen for further study.

3.1 Casting of Bricks: Manual

This method was processed based on the following steps:

1. **Mixing and casting of bricks**: The best proportion was chosen from the results obtained from compressive test of cast cubes. The quantity of material required to cast bricks of size 19 cm × 9 cm × 9 cm was weighed and mixed in required proportions together in dry state. After ensuring proper mix, water was added in parts until a workable mix was formed. Simultaneously human hair was sprinkled over the mix instead of directly adding it at once, as direct adding leads to the formation of lumps. This mix was properly filled into moulds. With the help of tamping rod the laid mix was compacted. Further, the moulds were placed on a vibrator to ensure through compaction.
2. **Drying of Bricks**: Normal sun drying was done for 3 days.
3. **Curing**: Bricks were cured with water for 7 days.

3.2 Casting of Bricks: Machine

After successfully finalising the proportion, casting and testing of manually manufactured brick, it was decided to go for machine-made manufacturing.

The lateritic soil and stone dust was sieved to remove the lumps and bigger size particles. The quantity of material required to cast bricks was weighed in required proportions and mixed together in a mixer in dry state. After having a good blended mix, hair fibre was added in such a way that it mixes evenly and does not form lumps. Water was added in parts. Mixing was done for about 10 min. The mix was then filled into the moulds of the hydraulic compression machine. The moulds had dimensions of 23 cm × 10.5 cm × 7 cm. Curing was done for 7 days.

4 Observation and Results

After the selection of best proportion from the different trials conducted, the final trial mix was then casted on the machine. This section highlights the results of tests performed on final proportion of brick cast.

The following are the different test results conducted on the machine-made bricks.

4.1 Compressive Test on Machine-Made Bricks

See Table 1.

Table 1 Compressive test for machine-made bricks

Brick No.	Weight (kg)	Compressive strength (N/mm^2)	Failure load (kN)
1	3.144	3.913	90.0
2	3.138	4.008	92.2
3	3.148	4.050	93.2

4.2 Flexure Test on Machine-Made Bricks

See Table 2.

4.3 Water Absorption Test on Machine-Made Bricks

See Table 3.

4.4 Alternate Wetting and Drying Method on Machine-Made Bricks

See Table 4.

Table 2 Flexure test on machine-made bricks

Brick No.	Weight (kg)	Longer length (cm)	Failure load (kN)
1	2.756	23	1.8
2	2.802	23	2.4
3	2.700	23	2.2

Table 3 Water absorption test for machine-made bricks

Brick No.	Weight before (kg)	Weight after 24 h (kg)	Water absorption percentage (%)
1	2.965	3.427	15.58
2	3.159	3.580	13.32
3	2.997	3.215	7.273

Table 4 Alternate wetting and drying method

Brick No.	Weight before (kg)	Weight after 24 h (kg)	Dried weight (kg)	Difference (kg)
1	2.965	3.427	2.991	0.026
2	3.159	3.580	3.247	0.088
3	3.115	3.470	3.160	0.045

Table 5 Compressive test of machine-made bricks after alternate wetting and drying method

Brick no.	Weight (kg)	Compressive strength (N/mm^2)	Failure load (kN)
1	2.991	2.965	68.2
2	3.247	2.904	66.8
3	3.148	2.973	68.4

4.5 Compressive Test on Machine-Made Bricks After Alternate Wetting and Drying Method

See Table 5.

5 Conclusion

Based on different trials conducted during the course, we have summarised the following conclusion:

1. Rick husk absorbs most of the water in the laterite–lime mixture and reduces the strength of the brick considerably. We can achieve lightweight brick to a great extent, but the strength produced by the brick is negligible and not practical. Therefore, rick husk is not advised to be added in the brick.
2. Addition of excess lime reduces the compressive strength of the brick and should be added in desired quantity. Addition of desired quantity of lime can result in better bonding of the raw materials and also give a better finished product with sharp and fine edges.
3. Addition of sand is not advised in the bricks as it makes the edges loose and does not give the desired strength. The lime is not a strong binding material like cement and does not provide good binding between the sand and the laterite soil.
4. Hair fibre should be added in desired quantity for better grip and bonding. Addition of excess hair fibre has resulted in weaker bonds.
5. During drop test, when the brick was dropped it didn't break completely due to the presence of hair fibres.
6. Bricks have the compressive strength that satisfies IS code limits.

References

1. Agus SM (2011) Engineering characteristics of the compressed-stabilized earth brick. Constr Build Mater 25:4215–4220
2. Annappa CH (2012) Application of value engineering for cost deductions: a case study on universal testing machines. Int J Adv Eng Technol 4(1):618–629. Retrieved 1 Dec 2017
3. Davis JR (2004) Tensile testing, 2nd ed. ASM International, p 2. ISBN 978-0-87170-806-9
4. Deguchi S, Tsujii K (2007) Supercritical water: a fascinating medium for soft matter. Soft Matter 3(7):797. Bibcode:2007SMat.... 3..797D. https://doi.org/10.1039/b611584e. ISSN 1744-6848
5. Eboziegbe PA, Mizi F (2013) Development of wood-Crete building materials from sawdust and waste paper. Constr Build Mater 40:361–366
6. El-Mahllawy MS, Kandeel AM (2013) Engineering and mineralogical characteristics of stabilized unfired montmorillonite clay bricks, House. Build Natl Res Centre J 10:82–91
7. EPRI (Project Manager K. Ladwig) (2010) Comparison of coal combustion products to other common materials—chemical characteristics. Electric Power Research Institute, Palo Alto, CA
8. Glossary of terms in soil science (PDF) (1976) Agriculture Canada, Ottawa, p 35. ISBN 978-0662015338
9. Gouny F (2013) Mechanical behaviour of an assembly of wood–geopolymer–earth bricks. Constr Build Mater 38:110–118
10. Hill D (1984) A history of engineering in classical and medieval times. Routledge, p 106, ISBN 0415152917
11. Ley B (1999) Diameter of a human hair. Archived from the original on 28 June 2010. Retrieved 28 June 2010
12. Managing Coal Combustion Residues in Mines. Committee on Mine Placement of Coal Combustion Wastes, National Research Council of the National Academies, 2006
13. Pradyot P (2003) Specifications for volumetric ware. In: Dean's handbook of analytical chemistry, 2nd ed. McGraw-Hill. ISBN 978-0071410601
14. Pilegis M, Gardner D, Lark R (2016) An investigation into the use of manufactured sand as a 100% replacement for fine aggregate in concrete. Materials 9(6):440. https://doi.org/10.3390/ma9060440.PMC5456819.PMID28773560
15. Powder Checking—Vibrating sieve—Vibrating sifters. PowderProcess.net
16. Snellings R, Mertens G, Elsen J (2012) Supplementary cementitious materials. Rev Mineral Geochem 74:211–278. https://doi.org/10.2138/rmg.2012.74.6
17. Thakur D (2016) Overview of national and global scenario of construction industries 2(12):13. ISSN: 2454-7875
18. Volume Measurements with a Graduated Cylinder (PDF). Archived from the original (PDF) on 2016–02–16. Retrieved 2016–02–04
19. Which Weighing Scale is More Accurate for Measuring Body Weight? Analog or Digital?.Preeti Thakur, 7 May 2019
20. Alavez-Ramirez R (2012) The use of sugarcane bagasse ash and lime to improve the durability and mechanical properties of compacted soil blocks. Constr Build Mater 34:296–305
21. Wild S (1998) Effect of partial substitution of lime with ground granulated blast furnace slag (GGBS) on the strength properties of lime-stabilized sulphate-bearing clay soils. Eng Geol 51(4):37–53
22. Wild S (1996) Effects of ground granulated blast furnace slag (GGBS) on the strength and swelling properties of lime-stabilized kaolinite in the presence of sulphates. Clay Miner 31(3):423–433
23. Millogo Y (2014) Experimental analysis of pressed adobe blocks reinforced with *Hibiscus cannabinus* fibers. Constr Build Mater 52:71–78

Recent Trends in Geotechnical Engineering

A Numerical Study on Interference Effects of Closely Spaced Strip Footings on Cohesionless Soils

S. Anaswara and R. Shivashankar

Abstract Foundations of buildings often need to be placed at close spacings to meet the various structural or functional requirements. In such cases, the combined action of adjacent footings is different from that of a single foundation. The combined effect causes interference of the stress zones. Numerical analysis is carried out on two closely spaced strip footings on sands, by varying the affecting parameters, to study the interference effects. Interference effects are analysed in terms of bearing pressure, settlement and tilt of foundations. In this study, the interference effects of closely spaced strip footings on the surface of cohesionless soils are being investigated. Parametric studies are done for two foundations by varying the clear spacing between the foundations. The results are presented in terms of interference factors. New structures near to the old construction may alter the settlement, pressure and rotational characteristics of the old footing and could lead to its distress. Above all, the load-carrying capacity of the new foundation will be very different from what it would have carried if it were independent—without the interference of the other footing. First footing representing an already existing footing is loaded with half of the estimated failure load of single independent strip footing and second adjacent footing loaded up to failure. The effect of interference of the old foundation is observed to be particularly significant in terms of the settlement and tilt.

Keywords Interference · Strip footing · Settlement · Bearing capacity · Tilt

1 Introduction

Footings of same buildings or adjacent buildings are often constructed close to each other, and this leads to the phenomenon referred to as ‘interference effect’. Bearing pressures, settlements, rotational characteristics and failure mechanisms of footings may alter due to this interference. Interference effects of strip footings were first studied by Stuart [1]. Kumar and Saran [2] conducted laboratory-scale model

S. Anaswara (✉) · R. Shivashankar
Department of Civil Engineering, National Institute of Technology Karnataka, Surathkal 575025, India
e-mail: anaswaras6@gmail.com

B. B. Das et al. (eds.), *Recent Trends in Civil Engineering*, Lecture Notes in Civil Engineering 105, https://doi.org/10.1007/978-981-15-8293-6_20

tests to study interference effects, including tilts, of the closely spaced square and strip footings resting on geogrid-reinforced sand. According to Lavasan et al. [3], who performed laboratory tests, interference has a significant effect on the ultimate bearing capacities, settlements, tilts and the failure mechanisms of the footings. Experimental studies were made by Salampatoor et al. [4] on unequally loaded and sequentially constructed footings to study interference effect. The study showed that settlement and tilting of old footing increases due to a new footing. It was reported that there would be an inward tilt of the two footings. Anaswara et al. [5] numerically studied the interference effects of strip footings on different loading conditions. Gupta and Sitharam [6] studied the interference effects from increased bearing capacities. They attributed interference to increase in confining pressure due to the interaction between the failure zones of interfering footings. Anaswara et al. [7] conducted laboratory-scale model tests and also conducted numerical (FEM) analysis to study the interference effects, in case of simultaneous loading of two adjacent strip footings. They used the experimental results to validate their numerical results. There found to be a good agreement between the two approaches.

2 Methodology

Two identical strip footings spaced at clear spacing S are assumed to be placed on the surface of the sand. One of the footings representing an old/existing foundation is loaded with half of the estimated failure load of a single strip footing, and adjacent new strip footing is loaded up to failure. The footings are loaded unequally and sequentially to simulate the mechanism of the new and old footings with different construction orders. The settlement at points *a*, *b*, *c*, *d*, *e* and *f* which is at depth 0B, 0.25B, 0.5B, 1B, 1.5B and 2B, respectively, at the mid-region between the interfering footings are noted and analysed (Fig. 1). Numerical investigations are carried out with various sands and mainly focused on bearing pressure, settlement and tilt characteristics. A numerical study is carried out by finite element software PLAXIS

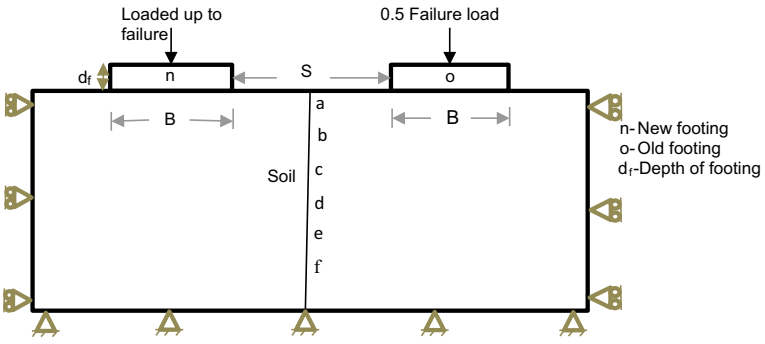

Fig. 1 The geometry of interfering footings

Table 1 Material properties of soils

Parameter	Dense sand	Medium dense sand	Loose sand
Unit weight, γ (kN/m^3)	19.10	18.20	17.4
Young's modulus, E (kN/m^2)	50,000	30,000	15,000
Poisson's ratio, ν	0.25	0.28	0.3
Cohesion, c (kN/m^2)	0	0	0
Angle of internal friction, φ (°)	40	35	30

Table 2 Properties of footing

Parameter	Value
Footing width, B (m)	1
Modulus of elasticity, E (kN/m^2)	25×10^6
Depth of footing, d_f (m)	0.75
Poisson's ratio, ν	0.15

2D. The Mohr–Coulomb failure criterion is selected for soil behaviour. Plane strain condition is used in the modelling. Footings are modelled using plate elements. For the boundary condition, horizontal and vertical displacements are restricted in the bottom boundary. Horizontal movements are restricted in vertical boundaries. Spacing ratio, S/B, is varied from 0.5 to 3. Clear spacing between the foundations divided by the width of the foundations is mentioned as a spacing ratio, S/B. The main objective is to study the interference effects of old and new footings when the spacing between the footings is varied. Properties of soils and footings are tabulated in Tables 1 and 2, respectively.

3 Results and Discussions

3.1 Interference Factor Due to Bearing Capacity ($IF_{(new)}$)

To study the interference effect of old footing on the ultimate bearing capacity of new footing, the interference factor for new footing is determined. Interference factor for new footing $IF_{(new)}$ is defined in Eq. (1).

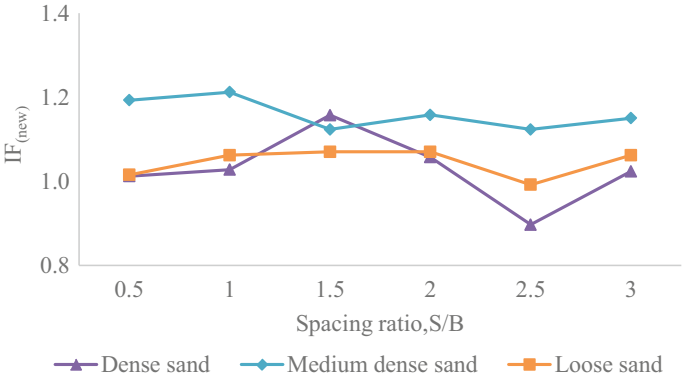

Fig. 2 Variations in efficiency factor (IF (new)) with the spacing ratio, *S*/*B*

$$\mathrm{IF}_{(\mathrm{new})} = \frac{\begin{array}{l}\text{Ultimate load carrying capacity of the new footing in the}\\ \text{presence of old footing}\end{array}}{\begin{array}{l}\text{Ultimate load carrying capacity of single}\\ \text{independent strip footing}\end{array}} \tag{1}$$

Variation in interference factor with spacing ratio plotted for various soils. Maximum improvement of interference is noted for dense sand, medium dense sand and loose sand at the spacing ratio 1.5, 1 and 1.5, respectively. Interference factor with the spacing ratio for footing width, $B = 1$ m is shown in Fig. 2.

3.2 *Interference Factor Due to Settlement (ξ_δ)*

To study the interference effect of settlement, interference factors due to the settlement are determined from the load–settlement plots, where the interference factor due to settlement (ξ_δ) is expressed in Eq. (2).

$$\xi_\delta = \frac{\begin{array}{l}\text{Settlement at the point considered when old footing is loaded}\\ \text{with half of estimated failure load of a single strip footing}\\ \text{and new strip footing is loaded up to failure}\end{array}}{\begin{array}{l}\text{Settlement at the point considered when single footing without}\\ \text{any interference is loaded up to failure}\end{array}} \tag{2}$$

The settlement at predetermined points chosen at the midway between the footing is plotted with spacing ratio. Maximum settlement is reported at the closer spacing for sand. The interference factor recorded highest values at the surface point '*a*' in most of the spacing ratios. Figures 3, 4 and 5 show the variation in the interference

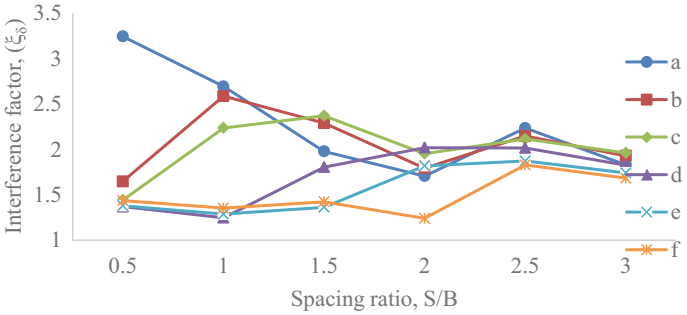

Fig. 3 Variation in interference factor due to settlement (ξ_δ) with the spacing ratio on dense sand

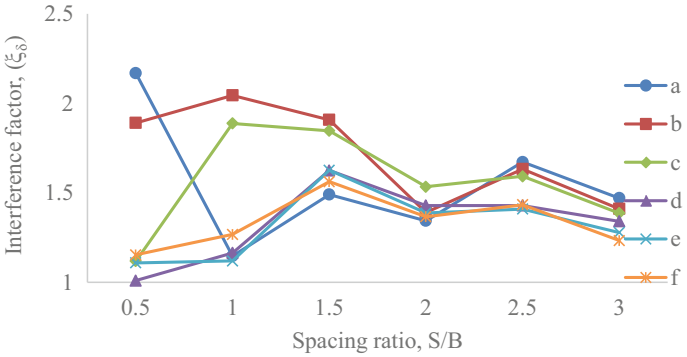

Fig. 4 Variation in interference factor due to settlement (ξ_δ) with the spacing ratio on medium dense sand

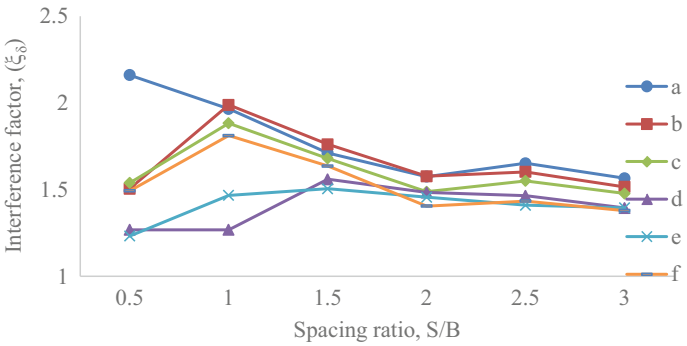

Fig. 5 Variation in interference factor due to settlement (ξ_δ) with the spacing ratio on loose sand

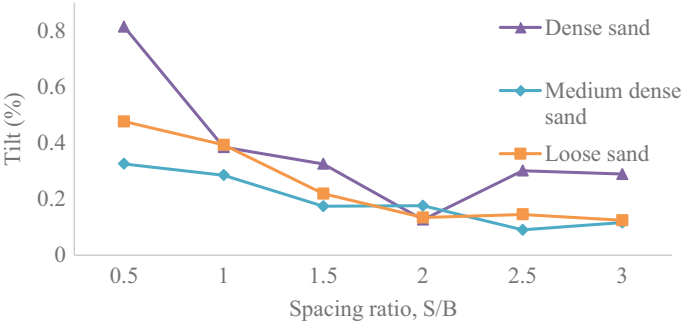

Fig. 6 Variations in tilt of old footing in the presence of newly constructed footing with the spacing ratio

factor due to settlement (ξ_δ) with the spacing ratio for footings width $B = 1$ m for various sands. The interference factor of sands recorded the highest value at closer spacings, and a decreasing trend can be seen as the spacing ratio increases.

3.3 Tilt of Footings

Owing to the increase in confining pressure at any point between the foundations developed due to interference, there is a non-uniform pressure distribution beneath the foundations. Stresses on the inner edge of the footing will be larger than the outer edge, resulting in an inward tilt of the old footings. The tilt of footing is expressed in percentage. Variation in tilt, with the spacing ratio, is plotted for various sands (Fig. 6). In friction soils, the maximum tilt value is observed at the spacing ratio, *S*/*B* 0.5, where footings are very close to each other.

4 Conclusions

Numerical analysis is carried out on two adjacent strip footings on different types of sands, by varying parameters, to study the interference effects. Interference effects are studied in terms of bearing pressure, settlement and tilt of footings. The loading case is considered as (an existing/old footing) loaded with half estimated failure load of single footing condition and then the second (new) footing is loaded up to failure. The analysis yields the following results:

- The cohesionless soils between the footings are subjected to confinement due to the loading on the footings and make the soil in between stiffer and stronger. This is reflected in the case of sands with an interference factor for bearing capacity ($IF_{(new)}$) greater than one in almost all cases studied.

- Interference influences the settlement of adjacent strip footings.
- Maximum tilt in sands occurs at a spacing ratio, S/B of about 0.5.

References

1. Stuart JG (1962) Interference between foundations, with special reference to surface footings in sand. Geotechnique 12(1):15–22
2. Kumar A, Saran S (2003) Closely spaced footings on geogrid-reinforced sand. J Geotech Geoenviron Eng 129(7):660–664
3. Lavasan AA, Mahmoud G, von Achim B, Tom S (2018) Bearing capacity of interfering strip footings. J Geotech Geoenviron Eng 144(3):04018003
4. Salamatpoor S, Jafarian Y, Hajiannia A (2019) Bearing capacity and uneven settlement of consecutively constructed adjacent footings rested on saturated sand using model tests. Int J Civ Eng 17(6):737–749
5. Anaswara S, Shivashankar R, Hridya P (2019) A numerical study on interference effects of closely spaced strip footings on soils. Int J Civ Eng Technol 10:3
6. Gupta A, Sitharam TG (2020) Experimental and numerical investigations on interference of closely spaced square footings on sand. Int J Geotech Eng 14(2):142–150
7. Anaswara S, Lakshmy GS, Shivashankar R (2020) Interference studies of adjacent strip footings on unreinforced and reinforced sands. Transp Infrastruct Geotechnol 1–27

The Need for Unsaturated Soil Mechanics: A Brief Review

K. Ujwala Shenoy, K. S. Babu Narayan, and B. M. Sunil

Abstract Soils exhibit seasonal saturation and desiccation, often resulting in varying degrees of moisture content. In practice, soil is seldom fully saturated. When it is completely dry or wet, it behaves as a two-phase system. Otherwise, the moisture content within the interstices of soil vary, leading to partially saturated conditions. Unsaturated soil condition has significant influence on soil behaviour. This paper presents a brief review of the emergence of unsaturated soil mechanics and its applications.

Keywords Soil · Moisture content · Matric suction · Slope stability

1 Introduction

Soil, in general, is considered to be comprised of soil solids and pore spaces (filled with air and water). Yet, the analysis of geotechnical problems in day-to-day world is often based on a two-phase saturated soil model which assumes the soil to consist of soil solids and a water-filled pore space (saturated condition). In practice though, soil is seldom fully saturated. Seasonal saturation and desiccation, a commonly observed phenomena in soils all over the world, often results in soils that are in a state of varying degrees of saturation. The term 'unsaturated' has been adopted to distinguish soils whose behaviour is influenced by this variable degree of saturation. Since no completely dry or completely saturated soil exist permanently, soils which are partially saturated can be called as 'unsaturated soils' [3, 16, 21, 26].

Expansive soils, remoulded soils, compacted soils, collapsible soils, residual soils—all fall under the purview of unsaturated soils. Unsaturated soil behaviour is prominently seen in dry and arid climates around the world. The influence of highly unpredictable environmental factors has been one of the earliest deterrents to the lack of development of unsaturated soil mechanics on par with that of saturated soil mechanics.

K. Ujwala Shenoy (✉) · K. S. Babu Narayan · B. M. Sunil
Department of Civil Engineering, National Institute of Technology Karnataka, Surathkal, Mangaluru, Karnataka 575025, India
e-mail: ujwala.shenoy12@gmail.com

B. B. Das et al. (eds.), *Recent Trends in Civil Engineering*, Lecture Notes in Civil Engineering 105, https://doi.org/10.1007/978-981-15-8293-6_21

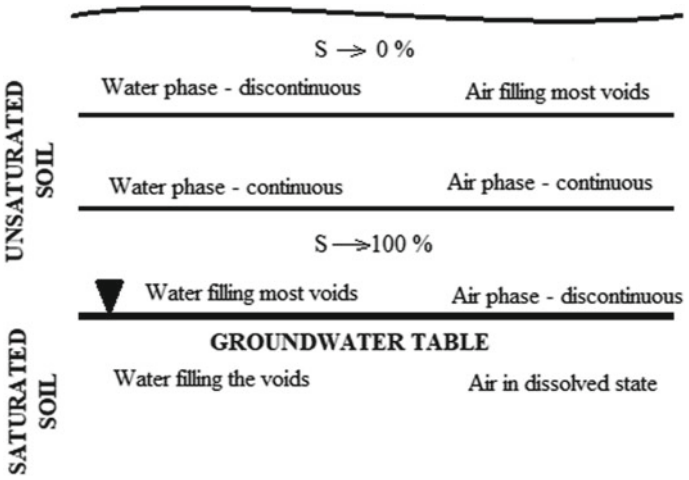

Fig. 1 Soil profile exhibiting varying degree of saturation [10]

The top-most part of the ground surface is often subject to changing environmental and climatic flux, as seen in Fig. 1. Since it is the region which has direct interaction with the surrounding environment, the soil pores are largely filled with air, leading to a discontinuous water phase. But with increasing depth below the ground, as the groundwater table is approached, the water phase tends to be continuous. The soil pores still consist of some air since the soil is above the groundwater table. In the vicinity of the groundwater table, the pores in the soil are filled with water due to capillary action while the pore air is discontinuous. All of these constitute an unsaturated soil, with varying degrees of saturation.

For a realistic description of the observed geotechnical phenomena and to obtain a result that is as close a solution to the problem at hand, it is important to take into account all the soil components. A thorough understanding of the behaviour of unsaturated soils would be highly beneficial in such a study.

2 Historical Developments in Unsaturated Soil Mechanics

Historical records of research on unsaturated soils obtained as conference proceedings and publications show the gradual emergence of the need to focus exclusively on unsaturated soils. The use of capillary theory in the 1950s to account for the behaviour of movement of water from the groundwater table towards the surface, although not successful, can be considered to be one of the earliest attempts made in the field of unsaturated soil research.

The applicability of independent state variables to describe the physical behaviour of any material has been relevant in soil mechanics right from its earliest conception

stage. In the beginning, several effective stress equations were proposed for unsaturated soils (similar to that of saturated soils). However, researchers since then have come to the conclusion that the effective stress ($\sigma - u_w$) alone is not sufficient to holistically describe the processes associated with unsaturated soil mechanics. Gens et al. [16] note that attempts to justify the observed phenomena in unsaturated soils by applying the concept of effective stress, as known in saturated soil study, were not entirely successful.

According to Fredlund [9], the acceptance of the presence of pore air in the voids and the recognition of the pressure this pore air exerts challenge the very concepts of soil mechanics that is often in practice. By the 1960s, the matric suction ($u_a - u_w$) was recognized as an important independent stress state variable that has to be considered to portray the behaviour of an unsaturated soil.

As a modification of Terzaghi's effective stress equation, Bishop [2] proposed the following equation for the effective stress of unsaturated soils, by introducing a parameter χ (related to the degree of saturation):

$$\sigma' = (\sigma - u_a) + \chi(u_a - u_w) \tag{1}$$

in which σ' is the effective stress for unsaturated soils, u_a is the pore air pressure, u_w is the pore water pressure and χ is a function of the degree of saturation (S), with values ranging from 0 (when soil is dry) to 1 (when soil is saturated). However, it has been noted by researchers that the form of the function $\chi(S)$ has been difficult to determine, and Eq. (1) has often been questioned ever since [21].

The 1970s saw further development of the theoretical foundation for the establishment of stress state variables. The 1980s concentrated on solving problems in unsaturated soils by assuming suitable boundary values. The increasing advancements in the computational sciences in the form of computers with superior computational prowess during this period also smoothened the way for the transition of unsaturated soil mechanics from theoretical concepts to problem-solving methods. However, this did not translate into a practicing science, that is, application of unsaturated soil mechanics into practice did not pick up at a pace as expected by the pace of advancements in unsaturated soil science [10].

The 1990s saw the focus shift towards implementation into practice. The major obstructions here were the excessive time and cost involved in experimental determination of the unsaturated soil properties. The move to concentrate the research focus on unsaturated soils from the erstwhile broad spectrum of expansive soils began from 1992 onwards. Till then, soils with a negative pore water pressure (like residual soils and expansive soils) were grouped under expansive soils. Fredlund [9, 10] notes that this shift towards unsaturated soils has paved the way forward for a better understanding and theoretical conception to experimentation and subsequent push towards a practical implementation.

3 Soil–Water Characteristic Curve (SWCC)

Soil–water characteristic curve (SWCC) or soil–water retention curve (SWRC) is the plot of the volumetric water content or gravimetric water content against the matric suction. The SWCC exhibits hysteresis and has drying, wetting and scanning branches. A typical soil–water characteristic curve is presented in Fig. 2. The desorption curve is also known as the drying curve, and the adsorption curve is also known as the wetting curve. The hysteresis results in the adsorption and desorption curves not being a single, unique curve. The air entry value (AEV) of the soil is the matric suction at which air starts to enter the largest pores in the soil. The residual water content is that value of water content for the soil at which a large suction is needed to remove further water from the soil [11]. It mainly describes the interaction of soil air and soil water. SWCCs are useful in the study and analysis of the behaviour of an unsaturated soil. Properties such as shear strength, volume change and permeability are dependent on SWCC.

Rao and Singh [24] and Rostami et al. [25] based on their study concluded that SWCC can be used to determine hydraulic conductivity, shear strength, chemical diffusivity, chemical adsorption, volumetric water content, specific heat, thermal conductivity and volume change of soils. Fredlund [10] opines that it will not be wrong to conclude that the determination of the SWCC is the first and foremost requirement for a study on an unsaturated soil. SWCC is considered one the most important aspect of an unsaturated soil, which, when obtained, can further lead to the determination of many other unsaturated soil parameters.

To plot a SWCC, suction measurement is important. Filter paper, axis translation technique, vapor equilibrium method, osmotic method, pressure plate apparatus, tempe cell, tensiometer, pressure membrane extractor, dew-point potentiometer and so on are used to measure suction. The measurement techniques and procedures have

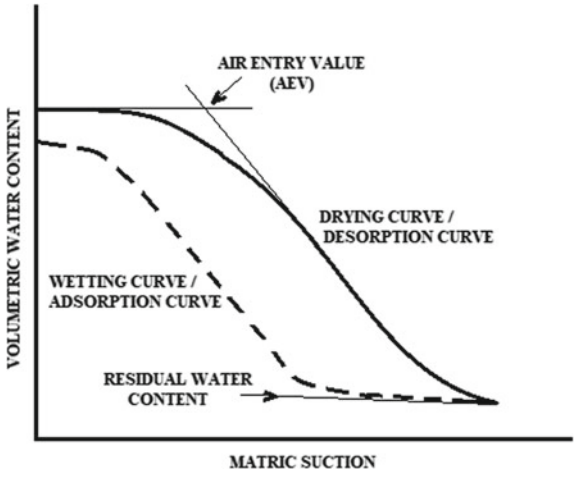

Fig. 2 Typical soil–water characteristic curve

their own limitations. The filter paper method is simple and affordable with its validity over a large suction range. However, its implementation needs extreme caution. The axis translation technique (ATT) also has some disadvantages—equilibration time required for soil with porous plate is lengthy, contact of soil with the plate has to be continuously ensured and the presence of occluded bubbles should be taken into consideration [4]. The insertion tensiometers, geotechnical centrifuges and pressure membrane extractors are valid for suctions between 80 and 1500 kPa while the dew-point potentiometer (WP4) is valid for suctions ranging from 1500 to 80000 kPa. Type of soil, size of soil specimen, applied air pressure and so on also influence the measurement time, as noted by Yang et al. [30]. Malaya and Sreedeep [20] reported that soil aging induces hydration which may in turn affect the SWCC through different suction measurement techniques and internal pore water redistributions over time.

The determination of SWCC by direct measurements is a time-intensive process and considering the economics involved, the search for alternative methods of obtaining an accurate and reliable SWCC in a cost and time-effective manner has been the focal point of many studies. The measurement of the complete SWCC is a difficult process with only a few data points actually measured on the desorption curve. The rest of the data points are plotted by using suitable curve-fitting equations to get the SWCC over the entire soil range. This has often led researchers to find alternative ways of obtaining or estimating the SWCC such as correlating the fitting parameters of SWCC with the plasticity as well as with the grain-size distribution curve. Since the shape of the SWCC resembles the grain-size distribution curve, many researchers have focused on establishing a relationship between these two so as to use the grain-size distribution curve parameters to estimate SWCC [9].

Table 1 gives a few well-known curve-fitting equations for SWCC (θ_w—volumetric water content, θ_s—saturated volumetric water content, θ_r—residual volumetric water content, a, b, c—parameters of the curve-fitting functions). Fredlund and Houston [13] have noted that the Fredlund and Xing [11] and van Genutchen [27] equations yield an accurate SWCC and hence are considered a best fit up to residual soil suction.

Table 1 Soil–water characteristic curve functions

Author	Equation	Remarks
Gardner [14]	$\theta_w = \theta_r + \frac{\theta_s - \theta_r}{1+\left(\frac{\psi}{a}\right)^b}$	Three-parameter equation, Unknowns: θ_r, a, b
Brooks and Corey [5]	$\theta_w = \theta_r + (\theta_s - \theta_r)\left(\frac{a}{\psi}\right)^b$	Three-parameter equation, Unknowns: θ_r, a, b
van Genutchen [27]	$\theta_w = \theta_r + \frac{\theta_s - \theta_r}{\left[1+\left(\frac{\psi}{a}\right)^b\right]^c}$	Four-parameter equation, Unknowns: θ_r, a, b, c
Fredlund and Xing [11]	$\theta_w = \left[1 - \frac{\ln\left(1+\frac{\psi}{\psi_r}\right)}{\ln\left(1+\frac{1{,}000{,}000}{\psi_r}\right)}\right] \frac{\theta_s}{\left\{\ln\left[e+\left(\frac{\psi}{a}\right)^b\right]\right\}^c}$	Four-parameter equation, Unknowns: ψ_r, a, b, c

Although the various methods of indirect measurement of SWCC give an estimation, they can never replace an SWCC obtained by actual measurements. The prediction/estimation of soil suction directly from the SWCC is not encouraged as the hysteretic behaviour of SWCC results in a range of soil suction values rather than a single suction value. The errors involved in the measurement of SWCC may also show up as cumulative and lead to erroneous predicted suction values. Limitations such as these show that the soil suction estimation from SWCC is a potential area for future research.

4 Utility of Unsaturated Soil Mechanics in Prediction–Protection–Prevention of Landslides

The concepts of unsaturated soils can be effectively implemented in addressing a large variety of soil-related problems, especially in a country like India, which has a predominant tropical climate. With a booming population, the strain on our resources is at an all-time high. In such scenarios, the pressure or burden on soils is also heavy. Some of the areas where unsaturated soil mechanics can be successfully applied are in slope stability cases (subject to rainfall), landfill liner systems (mining, natural resources and waste management), nuclear waste disposal through clay barriers, water recharge through deep wells and bore holes, foundations, pavements, retaining walls, buried structures and so on. Issues related to expansive soils such as damage to foundations of buildings, infrastructure like roads and bridges can also be addressed by employing the concept of unsaturated soil mechanics [19].

Slope stability has been a significant issue in the field of soil engineering. From an economic point of view, the losses incurred as a result of slope failures in a variety of domains from road and railway embankments to natural slopes are huge. Hence, the study of stability of slopes is of great economic importance.

It is well known that the stability of a slope is largely due to the shear strength of the soil comprising it, which in turn is dependent on numerous factors. The angle of inclination of the slope, the soil density, surcharge acting on the slope are also influential in the stability. Some of the factors affecting shear strength of unsaturated soils are rate of strain, matric suction, initial water content and so on [28]. The extended Mohr–Coulomb failure envelope, as shown in Fig. 3 (which is a modification of the Mohr-Coulomb failure envelope for saturated soils), is considered for unsaturated soils. The additional cohesion provided by the matric suction contributes to the shear strength of an unsaturated soil. Hence, when the matric suction decreases, the associated cohesion also decreases and the shear strength reduces.

The shear strength of a saturated soil is given by the equation proposed by Terzaghi:

$$\tau = c' + (\sigma - u_{\mathrm{w}}) \tan \phi' \tag{2}$$

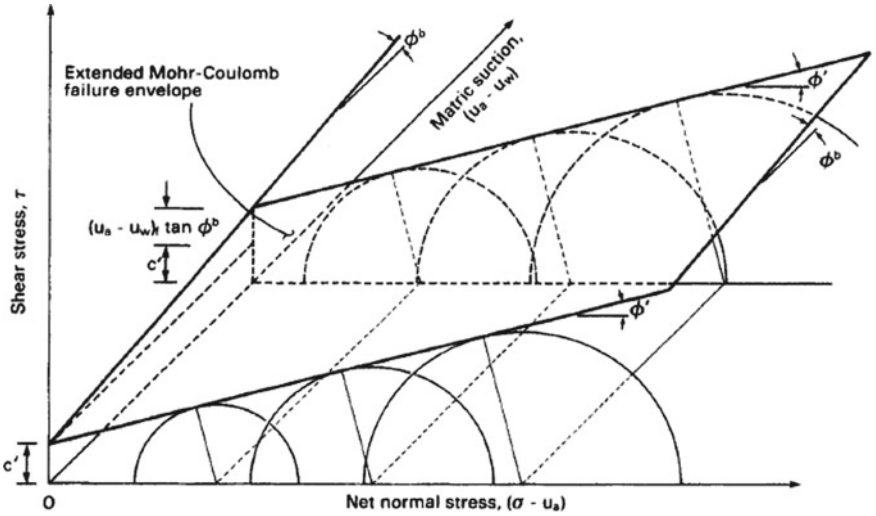

Fig. 3 Mohr–Coulomb failure envelope for an unsaturated soil [12]

where

τ	shear stress at failure
c'	intercept on the shear stress axis for a zero effective normal stress
$(\sigma - u_w)$	effective normal stress at failure
ϕ'	effective angle of internal friction.

To account for the pore air pressure and its effects in an unsaturated soil, the above shear strength equation has been modified as [12]:

$$\tau = c' + (\sigma - u_a) \tan \phi' + (u_a - u_w) \tan \phi^b \tag{3}$$

where

c'	intercept on the shear stress axis of the extended Mohr–Coulomb failure envelope when the net normal stress and the matric suction are equal to zero
$(\sigma - u_a)$	net normal stress at failure
ϕ'	angle of internal friction identified with net normal stress state
$(u_a - u_w)$	matric suction at failure
ϕ^b	angle signifying the rate of increase in shear strength relative to the matric suction.

Similar to the determination of SWCC, the experimental procedures to determine unsaturated shear strength are most often slow and expensive. Alternative procedures for estimating the unsaturated shear strength using various tools like the soil–water characteristic curve, relationship between the air entry value and confining pressure

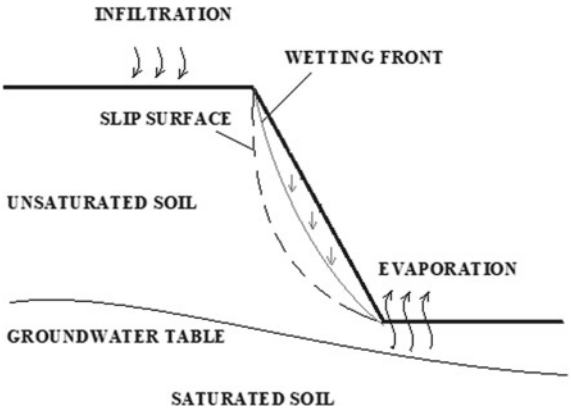

Fig. 4 Slope failure due to rainfall-infiltration [23]

have been reported. The lack of a universal, unique equation that can satisfactorily predict the shear strength of all unsaturated soils has been noted by Garven and Vanapalli [15]. Most of the proposed equations deal with the drying shear strength of the unsaturated soil and do not address wetting shear strength [17]. There is a need for further research to provide more improved and reliable techniques for the estimation of shear strength of soils. More experimental studies are required to be conducted following standard testing procedures to achieve this.

Studies on stability of slopes have been the focal point of many researches worldwide, especially in the areas subjected to rainfall. A typical slope failure due to rainfall-infiltration is exhibited in Fig. 4. Many instances of slopes being stable with a factor of safety less than one (as computed by using saturated concepts) is proof enough that there is a necessity to widen our horizons and look beyond the theories of saturated soils. The inclusion of unsaturated soil properties in a slope stability analysis is important, particularly for slopes in tropical areas where the residual soils are often partially saturated and are highly susceptible to failure under rainwater infiltration [7, 12, 18].

According to Cho [8], the infiltrating rainwater displaces the air from the pores in the soil, causing an increase in the air pressure which results in a delay in the advancement of the wetting front. As the water starts filling the soil pores, the bulk weight (γ) of the soil increases, altering the shear stress distribution along the slope depth. The critical failure surface for a slope under infiltration conditions is not constant and is influenced by the interactions between the air and the infiltrating water. For an accurate slope stability analysis, the influence of hydraulic hysteresis has to be suitably considered to avoid underestimating the safety factor associated with slope stability. Air entrapment is an important factor that has a considerable influence on the suction stress profile and correspondingly on the factor of safety. Thus, the concept of unsaturated soils can also be effectively applied as a slope protection measure [6, 29].

Landslides in tropical regions are often caused due to water seeping into the soil. The introduction of any form of drainage system to expel the excess pore water

pressure makes the negative pore water pressure a permanent fixture, which has to suitably accounted during the modelling and analysis of stability of a slope [1]. Providing surface and sub-surface drainage is important as a preventive action to increase the stability of the landslide-prone slope. Use of unsaturated concepts has also been proven beneficial in cover systems designed to protect slopes. These act as a retaining wall and help to maintain suction values, thereby preserving the shear strength of the slopes [22].

5 Summary and Conclusion

A developing country like India, pushing for a massive overhaul in the infrastructure sector, necessitates the focus to be on the development and maintenance of these infrastructures on a low cost-maximum benefit basis. With natural disasters such as floods and droughts ravaging large parts of the country, a transition towards reliable, robust technologies and monitoring systems for the maintenance of these infrastructures is the need of the hour.

The need for considering multi-phase aspect of soil behaviour for a better engineering judgment is significant for any type of geotechnical problem encountered in the field. These issues can be realistically described by considering soil as a multi-phase material where the presence of pore air influences the behaviour of the soil. A deviation from the two-phase saturated soil behaviour increases the complexity of soil mechanics with the introduction of the suction component. With more and more 'problematic soils' being encountered in the field, the need to understand unsaturated soils has never been as acute and important as in the present.

As interest in unsaturated soil mechanics is gaining momentum and with people realizing that the adoption of unsaturated soil concepts can, in fact, produce better results which are closer to reality, implementation is gaining traction, albeit at a slow pace. It is often opined that a major hindrance to the successful implementation of the principles of unsaturated soil mechanics in routine geotechnical applications is a lack of sufficient technical knowledge in engineers together with the high cost expected in the measurement of unsaturated soil properties such as SWCC.

The estimation and indirect determination methods and techniques become significant as laboratory determination of parameters of unsaturated soils is still considered complex and is not as popular as its saturated counterparts. The search for cost-effective alternatives for the expensive testing procedures is a prime area for research. The theoretical knowledge on unsaturated soils has been developed over the decades into a robust science and the versatility of the applications of unsaturated soil mechanics has opened up a wide range of possibilities for future research.

The ultimate goal of any theoretical formulation or research is a sound practical implementation. The technological advancements in the form of superior instrumentation and computational tools has resulted in further enrichment of our knowledge and comprehension of the behaviour of unsaturated soils. It is high time we apply this

theoretical knowledge to solve and optimize the solutions to a variety of situations often faced in civil engineering practice.

References

1. Batali L, Andreea C (2016) Slope stability analysis using the unsaturated stress analysis. Case study. Proc Eng 143:284–291
2. Bishop AW (1959) The principle of effective stress. Teknisk ukeblad 39, 859–863
3. Blight GE (2013) Unsaturated soil mechanics in geotechnical practice. CRC Press
4. Bonder BH, Miguel MG (2010) Soil-water characteristic curves obtained through the wetting paths for a tropical soil profile. In: Fifth international conference on unsaturated soils, Barcelona. Taylor & Francis Group, London, vol 1, pp 441–446
5. Brooks R, Corey T (1964) Hydraulic properties of porous media. Hydrol Papers, Colorado State Univ 24:37
6. Chen P et al (2017) Effect of hydraulic hysteresis on stability of infinite slopes under steady infiltration. J Geotechn Geoenviron Eng 143(9):04017041
7. Ching RK et al (1984) Increase in factor of safety due to soil suction for two Hong Kong slopes. Proc 4th Int Symp Landslides 617–623
8. Cho SE (2016) Stability analysis of unsaturated soil slopes considering water-air flow caused by rainfall infiltration. Eng Geol 211:184–197
9. Fredlund DG (2000a) Historical developments and milestones in unsaturated soil mechanics. In: Proceedings of the 1st Asian conference on unsaturated soils (UNSAT-ASIA 2000), Singapore, pp 18–19
10. Fredlund DG (2000) The 1999 RM Hardy lecture: the implementation of unsaturated soil mechanics into geotechnical engineering. Can Geotech J 37(5):963–986
11. Fredlund DG, Xing A (1994) Equations for the soil-water characteristic curve. Can Geotech J 31(4):521–532
12. Fredlund DG, Rahardjo H (1993) Soil mechanics for unsaturated soils. Wiley
13. Fredlund DG, Houston SL (2009) Protocol for the assessment of unsaturated soil properties in geotechnical engineering practice. Can Geotech J 46(6):694–707
14. Gardner WR (1958) Some steady-state solutions of the unsaturated moisture flow equation with application to evaporation from a water table. Soil Sci 85(4):228–232
15. Garven EA, Vanapalli SK (2006) Evaluation of empirical procedures for predicting the shear strength of unsaturated soils. Unsaturated Soils 2006:2570–2592
16. Gens A et al (2006) On constitutive modelling of unsaturated soils. Acta Geotechnica 1(3):137
17. Guan GS et al (2009) Shear strength equations for unsaturated soil under drying and wetting. J Geotechn Geoenviron Eng 136(4):594–606
18. Ip SCY et al (2020) Three-dimensional slope stability analysis incorporating unsaturated soil properties in Singapore. Georisk: Assess Manag Risk Eng Syst Geohazards 1–15
19. Likos WJ et al (2019) Fundamental challenges in unsaturated soil mechanics. In: Geotechnical fundamentals for addressing new world challenges. Springer, Cham, pp 209–236
20. Malaya C, Sreedeep S (2012) Critical review on the parameters influencing soil-water characteristic curve. J Irrig Drainage Eng 138(1):55–62
21. Pande GN, Pietruszczak S (2015) On unsaturated soil mechanics–personal views on current research. Stud Geotechn Mech 37(3):73–84
22. Rahardjo H et al (2017) Numerical analyses for assessment of geobarrier system performance. PanAm Unsaturated Soils 2017:132–148
23. Rahardjo H et al (2019) Role of unsaturated soil mechanics in geotechnical engineering. Int J Geo-Eng 10(1):8
24. Rao BH, Singh DN (2009) Establishing soil-water characteristic curve of a fine-grained soil from electrical measurements. J Geotechn Geoenviron Eng 136(5):751–754

25. Rostami A et al (2013) Pore network investigation on hysteresis phenomena and influence of stress state on the SWRC. Int J Geomech 15(5):04014072
26. Sheng D (2011) Review of fundamental principles in modelling unsaturated soil behaviour. Comput Geotech 38(6):757–776
27. van Genuchten MTh (1980) A closed-form equation for predicting the hydraulic conductivity of unsaturated soils 1. Soil Sci Soc Am J 44(5):892–898
28. Vanapalli SK (2009) Shear strength of unsaturated soils and its applications in geotechnical engineering practice. In: Keynote Address. Proceeding of 4th Asia-Pacific Conferennce on Unsaturated Soils. New Castle, Australia, pp 579–598
29. Xie W et al (2020) Influence of the features of the unsaturated zone on the air injection method in a slope. Proc Inst Civil Eng-Geotechn Eng 173(2):115–124
30. Yang H et al (2004) Factors affecting drying and wetting soil-water characteristic curves of sandy soils. Can Geotechn J 41(5):908–920

Seismic Behaviour of Soil Nailed Wall

Amrita, B. R. Jayalekshmi, and R. Shivashankar

Abstract Soil nailing is a technique used to stabilise steep cut slopes and to retain excavations. The method consists of inserting nail bars into the ground either by drilling or by grouting. The present study evaluates the seismic behaviour of a soil nailed wall supporting a vertical cut of height 6 m. The finite element analysis has been carried out to study the stability and performance of the soil nailed wall using ANSYS software. The seismic resistance of the wall is analysed under the El-Centro ground motion. The seismic response variation for different parameters such as angle of inclination of nails and soil strength properties are studied. The maximum lateral displacements and acceleration response of soil nailed wall are evaluated under static as well as dynamic conditions. The results of the study indicate that soil nailed system imparts stability to the retaining system under dynamic conditions.

Keywords Soil nailing · Vertical cut · Finite element analysis · Seismic resistance

1 Introduction

Soil nailing is an earth retention method which is used to retain excavations and stabilise steep slopes. The process involves the passive inclusion of reinforcement bars, known as nails, into the soil mass which are subsequently encased in grout material. The method has top to bottom construction sequence and are provided with either a temporary and/or a permanent facing. The nails are provided at regular horizontal and vertical spacing and can be either placed horizontally or at specific inclination. Generally, they are inclined at 10–20° to the horizontal with their length varying from 50 to 80% of the excavation height.

Amrita (✉)
Research Scholar, Department of Civil Engineering, National Institute of Technology Karnataka, Surathkal, Mangalore, Karnataka 575025, India
e-mail: 23amritar@gmail.com

B. R. Jayalekshmi · R. Shivashankar
Professor, Department of Civil Engineering, National Institute of Technology Karnataka, Surathkal, Mangalore, Karnataka 575025, India

B. B. Das et al. (eds.), *Recent Trends in Civil Engineering*, Lecture Notes in Civil Engineering 105, https://doi.org/10.1007/978-981-15-8293-6_22

The method of soil nailing has been used for various slope stabilising purposes and excavation retention works in various places and has proved to be economical and efficient under both static as well as dynamic conditions. Its application includes roadway widening under an existing bridge, highway embankments, stabilisation of steep cut slopes, tunnel constructions and temporary or permanent excavation works and underground facilities. The method is feasible and cost-effective when compared to conventional ground improvement methods. The literature also reveal that the method has performed well under dynamic condition by withstanding earthquake motion having ground acceleration as high as 0.7 g.

2 Literature Review

In the literature, different research methods have been used to better understand the behaviour and stability of the soil nailed retaining wall under static and seismic conditions. These include field studies, experimental studies of full-scale structures and reduced scale soil nailed models, analytical analysis as well as numerical analysis. The first field study of soil nailed wall was performed by Stocker et al. [11] in cohesionless soil having height of 18 m. Felio et al. [2] performed the field study on nine different soil nailed excavations in San Francisco Bay area under the 1989 Loma Prieta earthquake and found that they performed better under seismic excitation, thus emphasising on the combination of conservative design and construction of the structure. Experimental studies to understand the behaviour of soil nailed retaining wall under static and dynamic conditions were carried out by Li et al. [7], Shen et al. [9], Juran [4], Vucetic et al. [12], Kim et al. [5], Hong et al. [3] and Morgan [8]. To study about the complex soil–structure interaction and to evaluate the characteristics of soil nailed walls, numerical simulations are being performed with rigorous computational codes based on numerical techniques. Various numerical studies on soil nailed retaining wall were carried out by Briaud and Lim [1], Zhang et al. [13], Sivakumar Babu et al. [10] and so on. In this study, a 6 m high vertical soil nailed retaining wall has been analysed using finite element software, ANSYS. The effect of soil property and inclination of nails on the seismic stability of the structure was evaluated by time history analysis.

3 Methodology

The numerical study of a 6 m high soil nailed retaining wall was carried out using finite element software. The wall was assumed as retaining sandy soil which was stabilised using soil nailing. In this study, the soil nailed wall was designed using Federal Highway Administration (FHWA) guidelines provided by Lazarte et al. [6] and was analysed under both static and dynamic conditions. The length of the nail determined for the given structure was 4 m, which was found to satisfy the required

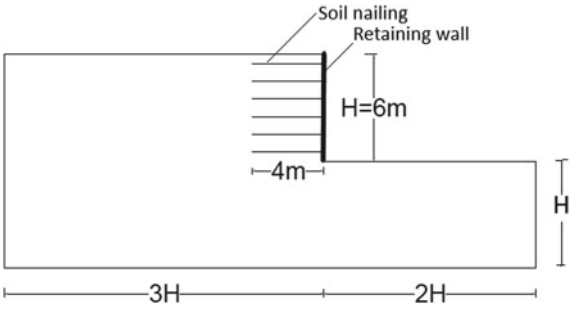

Fig. 1 Schematic illustration of soil nailed retaining wall

Table 1 Material properties

Parameter	Value
Vertical height of the wall (m)	6
Backfill slope angle (degree)	0
Soil type	Sandy
Cohesion (kPa)	1
Friction angle (degree)	30
Unit weight of soil (kN/m^3)	18
Modulus of elasticity of soil (MPa)	30
Poisson's ratio	0.3
Nail type	Grouted
Yield strength of reinforcement (MPa)	415
Elastic modulus of reinforcement (GPa)	200
Elastic modulus of concrete (GPa)	22
Nail diameter (mm)	16
Length of nail (m)	4
Spacing $S_h \times S_v$ (m × m)	1 × 1
Facing thickness (mm)	200

safety factors. ANSYS, a three-dimensional finite element software, was used for the modelling and analysis of the soil nailed retaining wall. The length ratio of soil nails used for the study was $L/H = 0.67$, where L is the length of the nail and H is the height of the wall. The schematic diagram of the proposed model is shown in Fig. 1, and Table 1 presents the material properties used in this study.

3.1 Numerical Modelling

The computer-aided analysis of displacement of soil structures have made remarkable advances. And the finite element method has become a popular tool for the analysis of

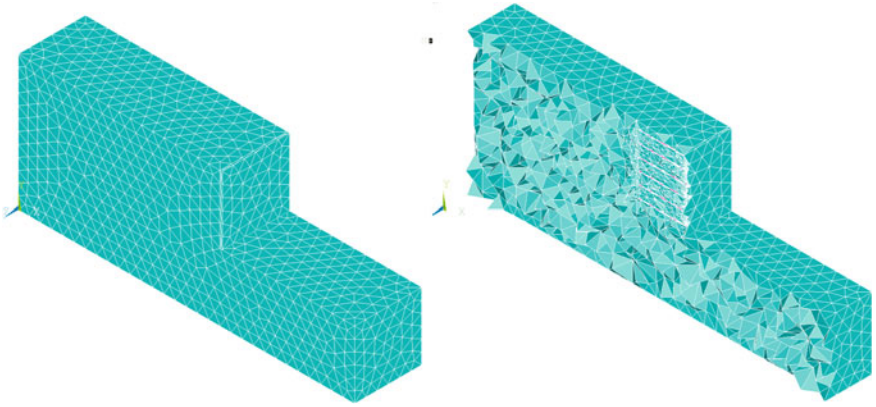

Fig. 2 Isometric view of full model and cross-section of the model showing nails

complex geotechnical engineering structures. The finite element modelling and analysis of soil nailed wall used in the study is described below. The soil was modelled as 3D structural solid elements (SOLID 185) whereas wall and nail were modelled as 3D reinforced concrete solid elements (SOLID 65). In order to model the connection between the various materials of the structure, suitable contact elements were provided between them. The bottom boundary of the model was set fixed and the lateral boundaries were provided with viscous boundaries so as to avoid the reflection of the seismic waves. The numerical modelling of the structure is shown in Fig. 2.

The modelled soil nailed wall was subjected to static and time history analysis. The time history motion of El Centro earthquake was used and was applied at the base of the model. The study was further carried out by evaluating the effect of soil property by varying the Young's modulus of soil. The modulus of elasticity of soil was varied as 10MPa, 30MPa and 50MPa. The effect of inclination of nail was also studied by placing the nails at different angles to the horizontal—0°, 10° and 20° with the horizontal.

4 Results and Discussions

The influence of soil property and inclination of nail on the performance of the soil nailed retaining wall is evaluated under static and dynamic excitation. The model was subjected to 1940 El Centro earthquake time history having the peak ground acceleration of 0.343 g as indicated in Fig. 3. The earthquake data was for 30 s with the seismic magnitude of 6.9. The El Centro data was used as it has the peak frequency range under which the frequency of the structure was found to fall.

The results of the study are presented in terms of the maximum displacement of the structure and maximum acceleration response. It is observed that the maximum horizontal displacement occurs at top of the wall in every analysis. With the increase

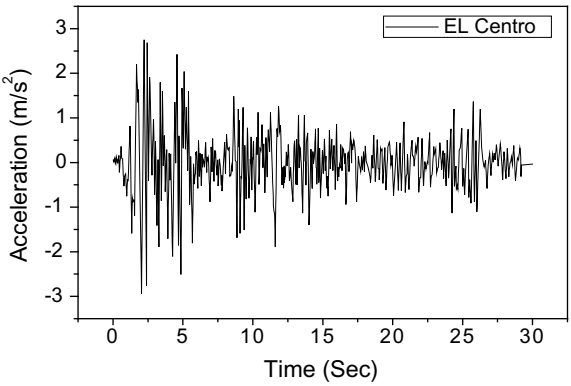

Fig. 3 Time history of input ground motion

of modulus of elasticity of soil from 10 to 50 MPa, it is observed that the horizontal displacement decreased due to the high strength of soil for both static and dynamic condition. And it is observed that under dynamic excitation, the displacement was approximately 70–90% larger than those obtained under static condition. Similar trend is shown by the structure with and without inclusion of the nails. With the use of soil nails the horizontal displacement was found to decrease by 70%. Figures. 4 and 5 show the effect of modulus of elasticity of soil and presence of nails, when they are placed horizontally into the soil mass.

The effect of nail inclination on the performance of the soil nailed structure is shown in Fig. 6 and Fig. 7. It can be seen that with the increase of inclination of the nail with the horizontal the maximum lateral displacement occurring at the top of the wall decreased. However, the acceleration response of the wall shows different trend. It was found to increase with the inclination of nails from 0° to 20°.

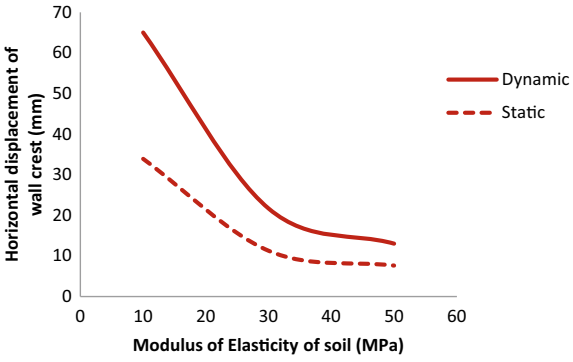

Fig. 4 Horizontal displacement at the top of the wall for different modulus of elasticity of soil under static and dynamic condition

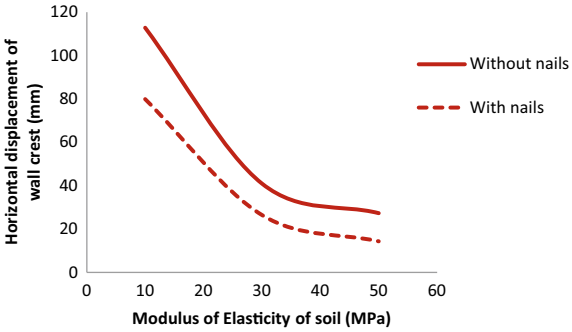

Fig. 5 Horizontal displacement at the top of the wall for different modulus of elasticity of soil with and without nails

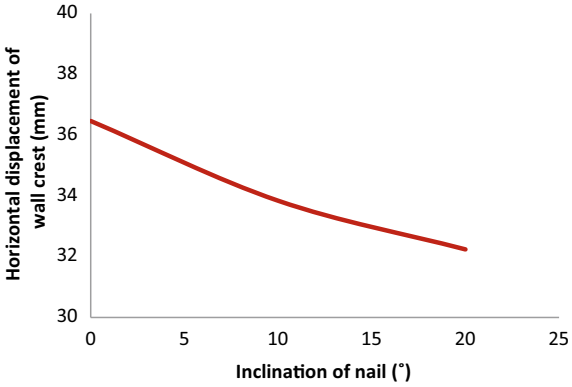

Fig. 6 Horizontal displacement at the top of the wall for different inclination of nail

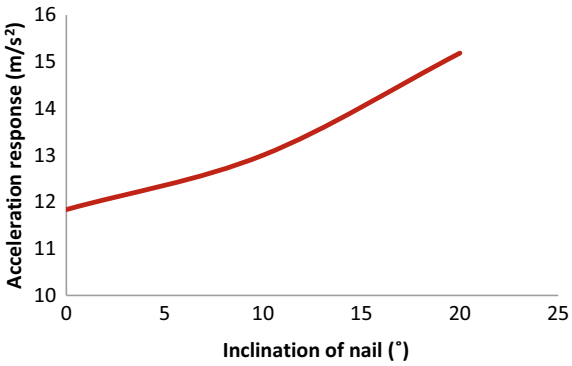

Fig. 7 Acceleration of the wall for different inclination of nail

5 Conclusions

The finite element analysis of a 6 m high vertical soil nailed wall retaining sandy soil was carried out to evaluate the effect of soil property and nail inclination on the

performance of the structure. From the results of the study, the following conclusions are made:

1. With the inclusion of the soil nails, the maximum lateral displacement of the structure decreased and this reduction is about 70%.
2. The maximum horizontal displacement occurred at the top of the wall and with the increase of modulus of elasticity of soil, this displacement of the wall decreased.
3. The inclination of the nail with the horizontal results in reduction of maximum horizontal displacement of the wall.

References

1. Briaud J-L, Lim Y (1997) Soil-nailed wall under piled bridge abutment: simulation and guidelines. J Geotechn Geoenviron Eng 123(11):1043–1050
2. Felio GY et al (1990) Performance of soil nailed walls during the October 17, 1989 Loma Prieta Earthquake. In: Proceedings of the 43rd Canadian geotechnical conference, Quebec, Canada, vol 1
3. Hong Y-S et al (2005) Shaking table tests and stability analysis of steep nailed slopes. Can Geotechn J 42(5): 1264–1279
4. Juran I (1985) Reinforced soil systems-application in retaining structures. Geotech Eng 16(1):39–82
5. Kim JS et al (1996) A large-scale experimental study of soil-nailed structures. Int Symp Earth Reinforcement
6. Lazarte CA et al. (2015) Geotechnical engineering circular No. 7 soil nail walls-reference manual. No. FHWA-NHI-14-007. National Highway Institute, US
7. Li J et al (2008) Loose fill slope stabilization with soil nails: full-scale test. J Geotechn Geoenviron Eng 134(3):277–288
8. Morgan N (2002) The influence of variation in effective stress on the serviceability of soil nailed slopes. Diss. University of Dundee
9. Shen CK et al (1981) An in situ earth reinforcement lateral support system. NASA STI/Recon Technical Report N 82
10. Sivakumar Babu GL et al (2002) Analysis of construction factors influencing the behaviour of soil-nailed earth retaining walls. Proc Inst Civil Eng-Ground Improv 6(3):137–143
11. Stocker MF et al (1979) Soil nailing. Proc Int Conf Reinforcement 469–474
12. Vucetic M et al (1993) Dynamic centrifuge testing of soil-nailed excavations. Geotech Test J 16(2):172–187
13. Zhang M et al (1999) Ground movement analysis of soil nailing construction by three-dimensional (3-D) finite element modeling (FEM). Comput Geotech 25(4):191–204

Design and Development of Efficient Under-Drainage System for Lined Canals

Anuj Sharma and Bibhuti Bhusan Das

Abstract Under-drainage system for lined canal is present beneath the canal bed to drain off the water present over there. It consists of longitudinal and transverse perforated drain pipes along with the arrangement of pressure relief valves. Cases of failure of lining of canal are there due to inconsistency in under-drainage system. Performance of geocell is exceptionally well in soil compaction, slope stabilization, earth retention and as reinforcement in case of retaining structure, road construction and railway embankments. Contrary to other researches, here performance of geocell as reinforcement of buried pipe under canal bed is investigated. Experimental study is carried out on canal model and on an under-drainage system. Strain in the buried pipe is observed due to application of various loading patterns on canal model. For sustained loading, 29% increase in strain is observed in pipe buried in unreinforced soil as compared to 18% in pipe buried in reinforced soil. For maximum loading almost three times more strain is stored in pipe in unreinforced soil. Yield is also observed in pipe without geocell, whereas at same loading no such behaviour is observed in pipe with geocell. It is reported that geocell can act as reinforcement for buried drain pipes under canal bed, and this helps in making under-drainage system efficient.

Keywords Under-drainage system · Geocell · Strain

1 Introduction

Water is the most consumed material on the earth, and survival without it on the planet earth is impossible. It is made available for consumption through a proper distribution system. In context to irrigation a canal is used to convey water to a long stretch by carrying it from a source such as river, lake or reservoir. It is made available to far cultivable areas by a network of pipelines.

A. Sharma (✉) · B. B. Das
National Institute of Technology Karnataka, Surathkal, Mangalore, Karnataka, India
e-mail: sharmaanuj220396@gmail.com

B. B. Das et al. (eds.), *Recent Trends in Civil Engineering*, Lecture Notes in Civil Engineering 105, https://doi.org/10.1007/978-981-15-8293-6_23

Under-drainage system for lined canals is present beneath the canal bed to drain off the water present over there. Canal in terrain with seasonal high ground water level subjected to high seasonal variations or where soil is sufficiently impervious to prevent free drainage of leakage or seepage from canal, excessive hydrostatic pressure sufficient to damage the lining may get generated, and thus there is requirement of under-drainage system. Weep holes of small diameter (50 mm) in lining in canal bed and side slope with suitable spacing, having its bottom open in pockets containing inverted filter can be used as under-drainage system [1]. Haider and Mitchell [2] suggested a flap-valve weep for draining off water but that was not suitable on side slopes of canal. Schultz [3] suggested French drain as under-drainage system which comprises perforated pipe buried under gravel and rock. Tile drains and porous concrete sleepers are also used as under-drainage system. As per Indian standards for under-drainage system in canals, depending upon the position of water table and type of soil subgrade, perforated longitudinal and transverse drain pipes are laid in an inverted filter along with arrangement of pressure relief valves (PRVs) [4]. For canals running in expansive soils like black cotton soil and so on and for under-drainage system along with drain pipes, an additional sandwiching cohesive non-swelling (CNS) soil layer is also placed between expansive soil and canal lining to prevent the lining from any deformation caused due to swelling and shrinkage of expansive soil [5]. As mentioned, under-drainage system comprises system of pipes, and these pipes are subjected to various static and dynamic loads such as dead load of canal lining, backfill of drain, weight of water in the canal, and load due to fluctuations in water level. It is necessary to ensure thorough safety of these pipes, otherwise chances of disruption are there.

In recent times geosynthetics gained significant attention from the geotechnical engineers, as they are economical, reliable and easy to install. Geosynthetics have eight main product categories, namely geonets, geosynthetic clay liners, geotextiles, geomembranes, geogrids, geocomposites, geofoam and geocells. Geogrids and geocells are mostly used as reinforcement for buried pipe. Faheem and Hassan [6] use geogrid as reinforcement to attenuate effective stress and vertical surface settlement in concrete pavement, and findings suggest that geogrid is not that much effective for dynamic loadings. Multiple geogrid layers do not provide any significant improvement in pavement system. Corey et al. [7] used geogrid as reinforcement for buried pipe; 25 and 10% reduction in surface settlement and vertical stress at crown, respectively, is reported but has insignificant effect on pipe's vertical deflection.

The performance of geocell is exceptionally well in soil compaction, slope stabilization, earth retention, as reinforcement and so on, in case of retaining structures, road construction, railway embankments and so forth. Research has been carried out to study the behaviour of pipe in planar reinforced soil, combination of rubber–soil mixture and geocell reinforcement under various loading conditions. Tavakoli Mehrjardi et al. [8] reported that geocell reinforced soil above the buried pipelines or under the footings or pavement surfaces is able to attenuate failure vulnerabilities. The soil surface settlement can be attenuated by 68% and strain in pipe can be reduced by 33%. Almohammed et al. [9] and Fattah and Redha [10] concluded in their paper that reduction in surface settlement and vertical pressure at crown of the pipe is observed

when soil is reinforced with geocell as compared to soil alone. Moreover, geocell also improves performance of embankment over weak soil [11].

Cases of failure of lining of canal have been observed due to inconsistency in under-drainage system. In major canal of Sardar Sarovar project a lot of instances had been observed where embankments and lining fails. After doing analysis the shortcomings reported are: absence of horizontal filter blanket, inadequate compaction of soil, high seepage forces resulting in piping and progressive failure, hydrostatic pressure on lining and so on [12].

The objective of this work is to perform a comparative study of strain in the drainage pipe by applying load on canal model in a normal case (NC), and in case with geocell (GC), attempt is made to monitor the behaviour of pipe in both the cases under various loading conditions using real-time data. Variety of geocell material is available in the market. For this study PMGSY-geocell is selected.

2 Methodology

2.1 Materials

2.1.1 Pipe

The pipe used for test is uPVC class-2 pipe conforming to [13] used for water supply, lift irrigation and so on. The outer diameter (D) of the pipe is 110 mm and wall thickness (t) is 2.5 mm and hence the standard dimension ratio $= D/t = 44$. The working pressure for pipe is 4 kgf/cm^2 and Poisson's ratio is 0.4.

2.1.2 Geocell

Geocell is a three-dimensional cellular confinement system formed from concertina expansion of polymeric geosynthetic strips and looks like honeycomb structure of cells. PMGSY-geocell is used in this case which is made up of polypropylene. The cell depth is chosen as 10 cm instead of smaller sizes because in those cases pocket size will be small and that's why the capacity of attenuating the pipe deflection would be less [14]. The engineering properties of geocell are specified in Table 1.

2.1.3 Concrete

Ordinary Portland cement of 53 grade conforming to [15] is used in casting of canal model. The physical properties of cement are mentioned in Table 2.

For fine aggregate river sand conforming to zone II [16] passing through 4.75 mm sieve was used. The sand was free from organic matter. The specific gravity of sand

Table 1 Properties of Geocell

Description	Value
Cell depth	10 cm
Expanded cell dim	205 × 225 mm
Thickness	200 μ
Mass/unit area (g/m^2)	280
Tensile strength (KN/m)	15.1

Table 2 Properties of cement

S. No.	Properties	Values
1	Specific gravity	3.15
2	Standard consistency	29.5%
3	Initial setting time	61 min
4	Final setting time	300 min
5	Fineness	325 m^2/kg
6	Compressive strength (28 days)	54 N/mm^2

was found to be 2.61 and moisture content was 5%. The fineness modulus of sand was 3.31. For coarse aggregate crushed stone, aggregate of 20 mm down size was used. The pile of aggregate comprises mixture of rounded and angular aggregates. The specific gravity of coarse aggregate was found to be 2.69, and the moisture content is almost nil. The fineness modulus of aggregate was 6.72. Tap water is used for casting.

2.1.4 Strain Gauge and Data Logger

To find strain in the pipe due to loading, 5 mm-350 Ω foil type strain gauge is used, and in order to record that strain automatically, a two-channel strain indicator cum data logger USB/RS232 is used.

2.1.5 Soil

Two types of soil—native soil (shedi soil) and backfill soil (laterite soil)—are used. The soils are classified as CH and SM, respectively, as per Indian standard of soil classification system based on sieve analysis and hydrometer analysis results. Grain size distribution curve for both the soil is shown in Fig. 1, and Table 3 presents the properties of these soils.

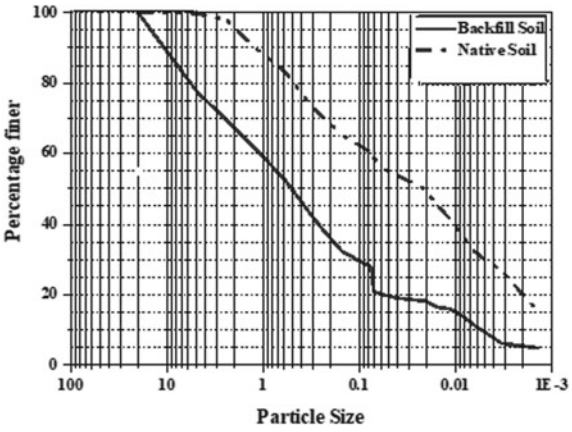

Fig. 1 Grain size distribution curves for both soils

Table 3 Properties of soils

Description	Backfill soil	Native soil
Specific gravity	2.68	2.68
Coefficient of uniformity, C_u	211.53	1.75
Coefficient of curvature, C_c	50	0.31
Effective size, D_{10}, mm Liquid limit (W_L%) Plastic limit (W_P%)	0.0052 36.30% 26.84%	0.001 61.50% 18%

2.2 Method

2.2.1 Test Installations

A canal model of 1 m length is created with M15 grade of concrete and 75 mm lining thickness. The bed width of model is 425 mm and side slope is 285 mm (1.5H:1V). Figure 2 depicts schematic test models. A tank of dimension 1250 × 950 × 950 mm and 40 mm thickness is prepared and it contains shedi soil till bottom 275 mm. Above this tank is filled with laterite soil passing 4.75 mm sieve for next 250 mm, and then for next 260 mm tank is filled with laterite soil retained on 4.75 mm sieve. This is done in order to create an inverted filter. As the length of model is 1 m, bed slope of soil is kept flat. Earth rammer is used to compact the soil and the required cut is made to create proper side slope. The load of canal model helps in maintaining the slope. Pipe of 1 m length is buried at a depth of 150 mm from bottom of canal model [17]. A strain gauge is installed at the centre of the pipe whose lead wire is connected to data logger for recording of strain at the rate of one reading for every 3 s. The soil is compacted in three layers at 0, 120 and 260 from the point where pipe is placed with 1, 1 and 3 rounds of vibrating compactor, respectively. The width of reinforcement is taken equal to width of tank and it is placed 40 mm below the base of canal [18]. Figure 3 presents the test installations at laboratory.

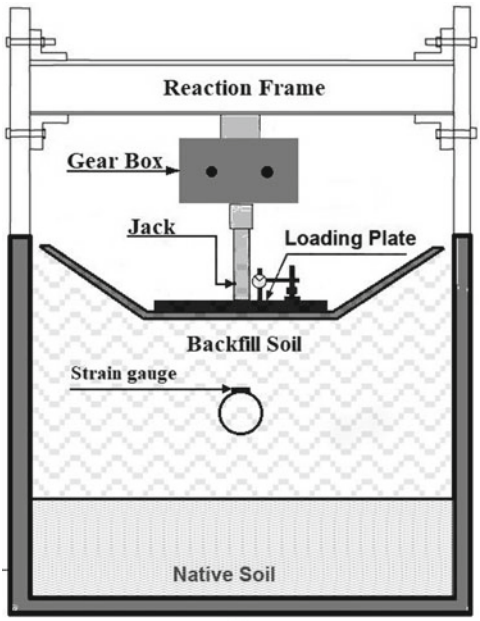

(a)

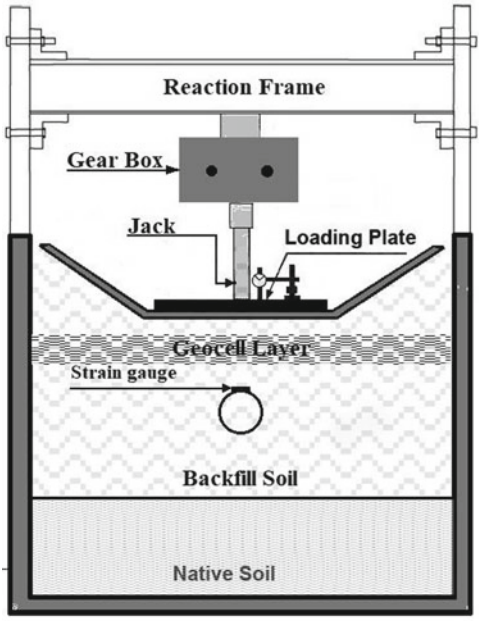

(b)

Fig. 2 Schematic test models, **a** Normal case, and **b** Geocell case

(a)

(b)

Fig. 3 Test installations. **a** Loading arrangements, and **b** geocell installation

2.2.2 Loading Pattern

A hand-operated mechanical jack is used to apply load on a rectangular plate of dimension 1000 × 275 × 16 mm (L × B × T) covering complete base of canal model. Jack is connected to the plate through a precalibrated proving ring to measure the load transferred to the model. Loading on the canal model is applied in three patterns for both normal and geocell case: first is continuous increment in load and this is attributed to the case where there is continuous supply of water to the canal; second is sustained loading at maximum load for 24 h and this is attributed to the case where canal is full; and the third one is loading–unloading–reloading and this is attributed to the case where canal is filled till a particular level only and then after drawdown of water it is again filled at some other level. In first two cases of the loading patterns load applied is till 60 KN, whereas in last case it is till 50 KN only.

3 Results and Discussion

3.1 Continuous Increment in Load

In this case load is increased continuously at a constant rate from 0 to 60 KN. The value of strain at every load is observed in both normal case (NC) and geocell case (GC) and recorded using a digital strain indicator cum data logger.

3.1.1 Load Versus Strain Curve

From Fig. 4, it is clear that the value of strain at all the loading points is more in normal case (without geocell) as compared to geocell case. Initially, the slope of the curve increases, then it remains constant and starts to decrease in the end. Moreover, from 50 to 60 KN in normal case very significant increase in strain is observed due to minor increase in load, which indicates yield point of pipe, whereas no such behaviour is observed in geocell case.

3.1.2 Increase in Strain

Figure 5 clearly indicates that increase in strain at every interval of 10 KN increase in load is more in NC. Major difference in increase in strain is observed at initial and final loading interval and in the middle its more or less the same. This can be possible because load transfer to pipe is more during first loading. After that voids are filled and soil becomes more compacted, so increase in strain decreases. In last (heavy) loading there is yield in pipe of NC, so again higher increase in strain is observed.

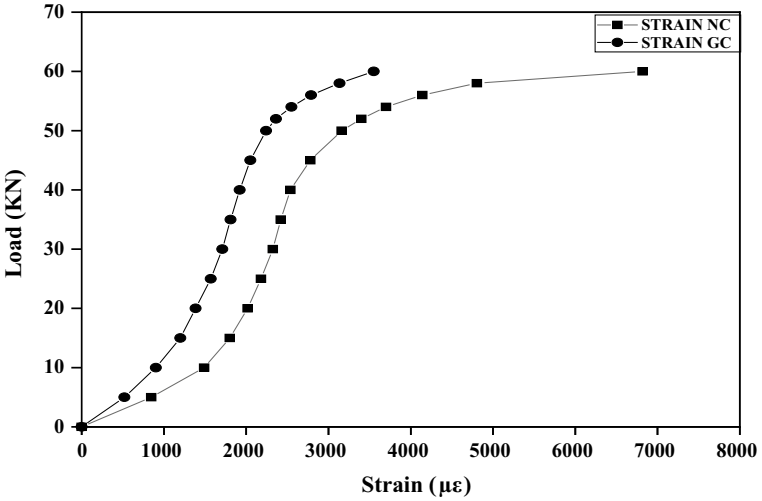

Fig. 4 Load versus strain curve for NC and GC

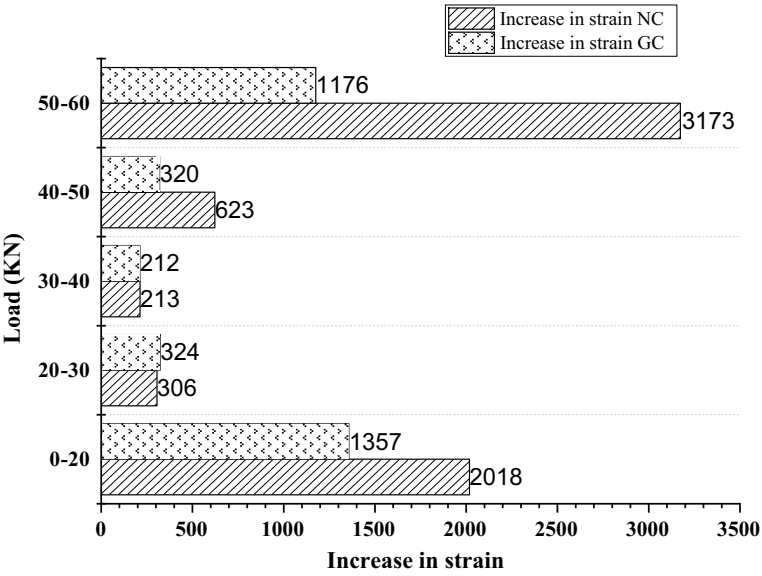

Fig. 5 Comparison of increase in strain between NC and GC

3.2 Sustained Loading

In this case maximum load is applied on the canal and withstands it for a period of 24 h in order to find long-term effect of sustained loading on the pipe. Figure 6

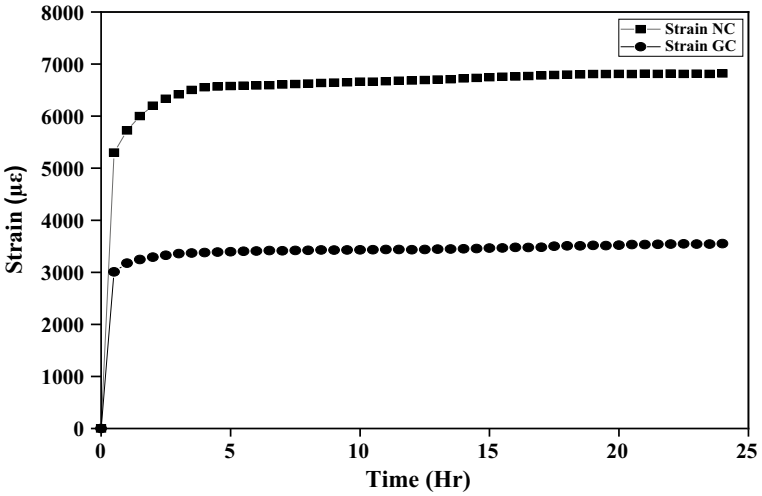

Fig. 6 Sustained loading in NC and GC

indicates strain in NC and GC. The ultimate strain in NC is almost double than that in GC and it is also observed that major changes in strain are for much longer duration in NC as compared to GC. This indicates attenuation of load transferred to the pipe because of the presence of geocell in between canal model and pipe.

3.3 Loading–Unloading–Reloading

In this case we gradually increase the load from zero to a particular level, then unload it and again apply load till next higher level, and so on.

3.3.1 Load Versus Strain Curve

Figure 7a shows load vs strain curve for pipe of unreinforced soil. For every loading–unloading–reloading cycle, the amount of strain stored in the pipe can be easily observed. For final loading almost similar curve is observed as in continuous increment in load case with an offset on horizontal axis.

Figure 7b shows load vs strain curve for pipe of reinforced soil. For every loading–unloading–reloading cycle the amount of strain stored in this pipe is less than that in pipe of unreinforced soil. In the starting range GC pipes almost behave elastically, that is, after unloading all the strain is released and Hooke's law is followed. After unloading the pipe from the peak loading almost three times more strain is stored in the pipe of NC as compared to GC. This can be attributed to the fact that geocell creates a beam effect due to which load is transferred to a wider area, hence the

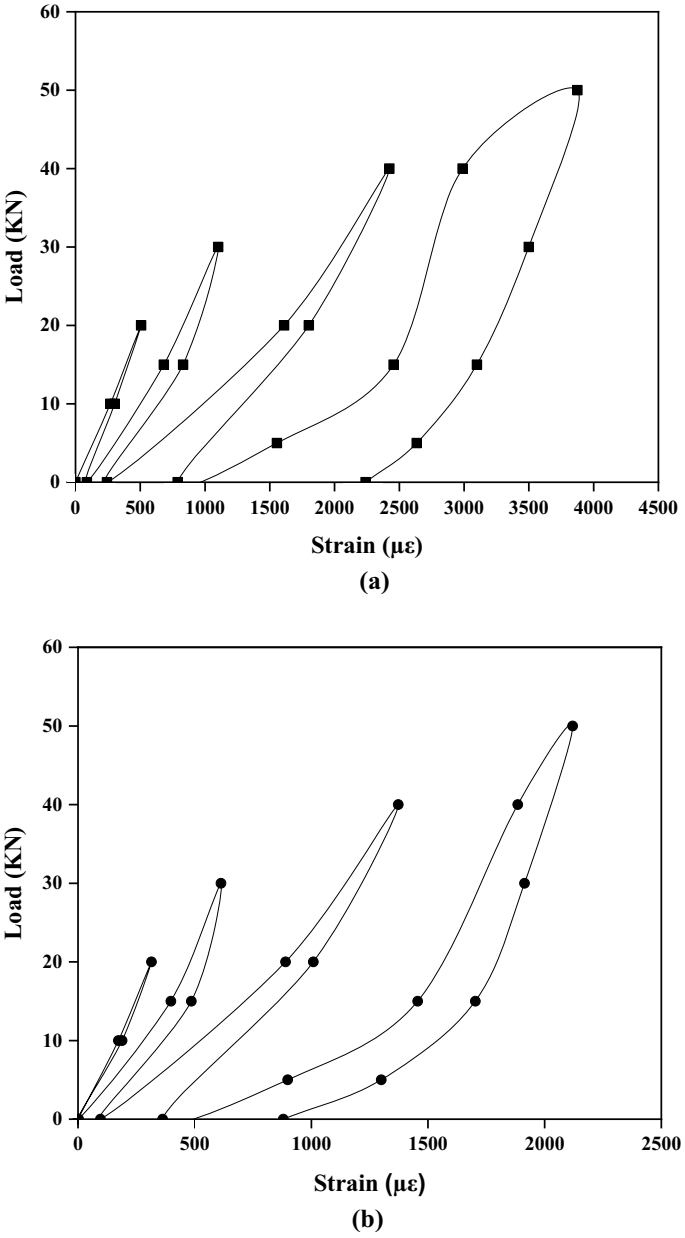

Fig. 7 **a** Load versus strain (NC), **b** Load versus strain (GC)

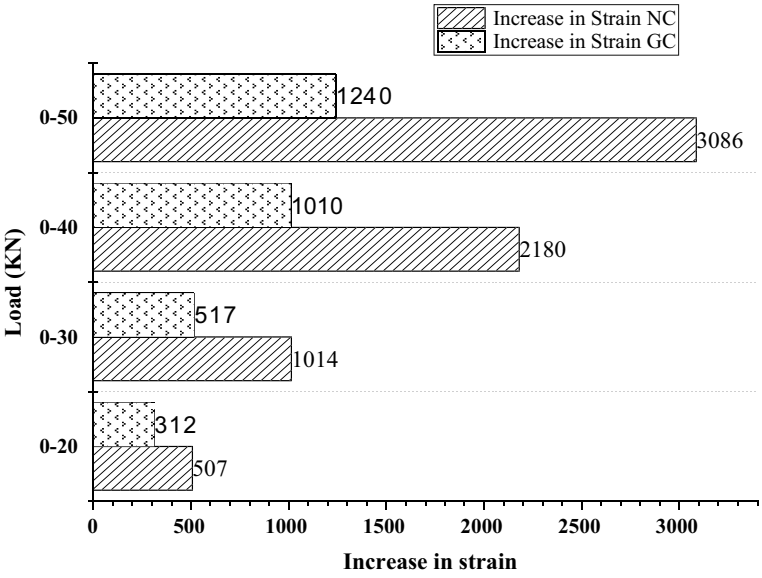

Fig. 8 Comparison of increase in strain between NC and GC

intensity of load on the pipe is reduced and lesser strain is generated and stored in the pipe.

Area under stress–strain curve (hysteresis loop) for loading and unloading at maximum loading for pipe of NC is 159,321 units and for pipe of GC is 93,108 units. This area indicates loss in energy in various forms. Thus, the characteristic properties of material of pipe will remain more intact in geocell case [19].

3.3.2 Increase in Strain

Figure 8 clearly indicates increase in strain for NC and GC. Here increase in strain for all cases of loading from 0 KN is more in NC as compared to GC. For higher loading level, higher variation in increase in strain is observed.

4 Conclusion

The conclusion of the project is as follows:

- On continuous increase of load case, the value of strain at all loading points is more in NC as compared to GC. Yield is observed in pipe of NC but not in that of GC at same loading.

- On continuous increase of load case, variation in increase in strain is more for initial and final loading interval, whereas in the middle it is more or less the same. However, value of increase in strain is more in NC as compared to GC.
- In sustained loading case, 28.66% rise in strain is observed in NC, whereas in GC it is 18.02% only. The ultimate strain in NC (6819με) is almost double than that in GC (3350με). Major changes in strain are observed for much longer period in NC (4.5 h) than in GC (2.5 h).
- In loading–unloading–reloading case, strain in pipe at all the loading stage is more in NC as compared to GC. Almost three times more strain is stored in pipe in NC (2240με) as compared to GC (880με). For initial loading stage, GC pipes almost behave elastically. In final loading stage almost 16% more strain is released in geocell case as compared to normal case.
- In loading–unloading–reloading case, for all the stages increase in strain is more in NC as compared to GC. Variation in increase in strain is higher for higher loading levels.

Evidently, the use of geocell has the potential to absorb more energy compared to soil alone, so it can reduce the energy transferred to the pipe through the soil due to applied loading. Because of this there is decrease in transfer of stress and shocks to the pipe, which as a result limit the strain in the pipe and can prevent its premature cracking, and thus making the under-drainage system more efficient.

References

1. Punmia BC, Lal PBB et al (2009) Irrigation and water power engineering. Laxmi Publications, pp 643–645
2. Haider TR, Mitchell TG (1988) Interim report on canal lining used by the Bureau of Reclamation. Bureau of Reclamation, United states
3. Schultz B (1990) Guidelines on the construction of horizontal sub-surface drainage systems. Int Comm Irrig Drainage 186
4. IS: 4558 (1995) Under-drainage of lined canals—code of practice. Bureau of Indian standards, New Delhi
5. IS: 9451 (1994) Guidelines for lining of canals in expansive soils. Bureau of Indian standards, New Delhi
6. Faheem H, Hassan A (2014) 2D Plaxis finite element modelling of asphalt-concrete pavement reinforced with geogrid. J Eng Sci 42(6):1336–1348
7. Corey R et al (2014) Laboratory study on geosynthetic protection of buried steel-reinforced HDPE pipes from static loading. Int J Geotech Geoenviron Eng 140(6)
8. Tavakoli Mehrjardi Gh, Moghaddas Tafreshi SN, Dawson AR (2015) Numerical analysis on buried pipes protected by combination of geocell reinforcement and rubber-soil mixture. Int J Civil Eng 13(2):90–102
9. Almohammed H, Fattah Y, Rasheed E (2018) Numerical analysis of the effect of geocell reinforcement above buried pipes on surface settlement and vertical pressure. Int J Geotechn Geol Eng 12(3)
10. Fattah Y, Redha B (2016) Effect of geocell reinforcement in the mitigation of traffic loads transmitted to the flexible buried pipe. Global J Eng Sci Res Manag 3(7):118–128
11. Latha GM, Rajagopal K, Krishnaswamy NR (2006) Experimental and theoretical investigations on geocell-supported embankments. Int J Geomech 6(1)

12. Kapadia VP (2016) Applications of geosynthetics in canals: case studies of gujrat. IEI Gujrat State Centre
13. IS: 4985 (2000) Unplasticized PVC pipes for potable water supplies. Bureau of Indian Standards, New Delhi
14. Tavakoli Mehrjardi Gh, Moghaddas Tafreshi SN, Dawson AR (2011) Influence of geocell reinforcement on damping properties of trench with pipe. In: Proceedings of 15th European conference on soil mechanics and geotechnical engineering, vol 1 no 2, pp 1073–1078
15. IS: 12269 (2013) Ordinary portland cement, 53 grade-specification. Bureau of Indian Standards, New Delhi
16. IS: 383 (1970) Specification for coarse and fine aggregates from natural sources for concrete. Bureau of Indian Standards, New Delhi
17. Dash SK, Reddy PD, Raghukant STG (2008) Subgrade modulus of geocell-reinforced sand foundation. Proc Instit Civil Eng-Ground Improv 161(2):79–87
18. Moghaddas Tafreshi SN, Dawson AR (2010) Comparison of bearing capacity of a strip footing on sand with geocell and with planar forms of geotextile reinforcement. Geotext Geomembr 28(1):72–84
19. Ewing JA (1889) On hysteresis in the relation of strain to stress. Br Assoc Rep 502

A Correlation Equation on the Influence of Length to Diameter Ratio on the Unconfined Compressive Strength of Lateritic Rocks in Goa

Mrudula R. Ingale and Purnanand P. Savoikar

Abstract Rock materials with unconfined compressive strength (UCS) less than 20 MPa are termed as soft rocks. The factors on which UCS may depend are shape and size of specimen, rate of loading, degree of saturation and so on, which are termed as external factors, while defects, porosity, mineralogy and degree of weathering are termed as internal factors. One of the parameters which affect the unconfined compressive strength (UCS) of rock materials is length to diameter ratio (L/D) of test cores. In this study, the shape effect on the UCS of lateritic rock was investigated. A number of unconfined compression tests have been conducted onto the lateritic rock samples from Pernem site in Goa with different L/D ratios. An equation is proposed for the correction of unconfined compressive strength test results to a length to diameter ratio. The results obtained by this equation are compared with previously published equations for correction of unconfined compressive strength.

Keywords Lateritic rock · UCS · L/D ratio · Soft rocks · Correlation equation

1 Introduction

The most important geotechnical property of rock is unconfined compressive strength. This property is mainly used for design of structures and characterisation of intact rock material. It is defined as the failure strength of rock specimen. Turk and Dearman [12] proposed equations for normalisation of test results to a L/D ratio of 2:50 mm. Agustawijaya [1] conducted UCS on a number of samples of soft rock considering dry and saturated conditions. Ergun and Nilsun [5] investigated the effect of L/D ratio and shape on UCS for the dry cores of seven rocks samples with L/D ratio of 1:2.5.

M. R. Ingale (✉) · P. P. Savoikar
Civil Engineering Department, Goa Engineering College, Farmagudi, Goa 403401, India
e-mail: mrudulaingale2@gmail.com

P. P. Savoikar
e-mail: psavoikar@gmail.com

B. B. Das et al. (eds.), *Recent Trends in Civil Engineering*, Lecture Notes in Civil Engineering 105, https://doi.org/10.1007/978-981-15-8293-6_24

Table 1 Geotechnical properties of lateritic rocks in Goa

Location	Unit weight (kN/m^3)	UCS (kN/m^2)
Pernem—Goa	**12.72–34.0**	753–8095
Porvorim—Goa	10.5–21.7	295–5481
Dona Paula—Goa	20.7–24.0	1270–6375

Laterite covers the major portion of Goa and typically occurs as plateau landforms. Widdowson [13] reported about geological properties and evolution of laterites in Goa. Geotechnical properties of lateritic rocks in Goa were explored by Ingale and Savoikar [7] for Dona Paula and Porvorim Goa sites. Ingale [8] studied the geotechnical properties and strength behaviour of lateritic rocks in Goa. The geotechnical properties of the lateritic rocks in Goa studied were: UCS, density, water absorption test, and so on. The variation in density and UCS for the lateritic rock in Pernem, Porvorim and Dona Paula in North Goa is shown in Table 1.

The L/D ratio of test specimen is one of the parameters affecting UCS of lateritic rocks in Goa. Mutual relationship between L/D ratio and UCS is developed. Also, the correction equations are discussed and applied to the obtained data to get corrected UCS for L/D ratios other than 2. Relationship between actual UCS/measured UCS is also studied. Based on the data obtained from the tests and previous investigation, a correlation equation is derived using dimensional analysis for lateritic rocks in Goa.

2 Correlation Equation Using Dimensional Analysis

Dimensional analysis [4] is aimed at reducing to the minimum dimension spaces. In this behaviour specific system might be studied by combining and arranging the assumed variables (v) and systematically enclosing m number of primary independent dimensions (D) into N dimensionless groups, where $(v) = (v_1, v_2, v_3, \ldots, v_n)$, $(D) = (D_1, D_2, D_3, \ldots, D_N)$, $N = n - m$ and $D \cdot Gs$ are $(\pi_1, \pi_2, \pi_3, \ldots, \pi_N)$.

Here,

σ Unconfined compressive strength for L/D ratio of 2 in kg/cm^2.
L Length of the specimen in cm.
D Diameter of the specimen in cm.
P_f Failure load in kg

Now, $v = \{\sigma, P_f, L, D\}$ hence $n = 4$

Writing dimensions of variables

$\{v\} = \left[ML^{-1}T^{-2}, MLT^{-2}, M^0LT^0, M^0LT^0\right]$; hence $m = 3$, where m is the number of repeating variables forming set Q.

Let $MLT^{-2} = S$

Therefore, $v = \left\{SL^{-2}, S, L, L\right\}$

Hence number of dimensionless Pi groups is

$$N = (n - m) = 4 - 2 = 2$$

Now R = set of variables in v having totally different dimensions from each other.
Therefore, $R = \{\sigma,\ P_\mathrm{f},\ L\}$
Q should be selected from R; therefore $Q_1 = \{\sigma,\ P_\mathrm{f}\},\ Q_2 = \{\sigma,\ L\},\ Q_3 = \{P_\mathrm{f},\ L\}$
Select any combination of Q. Hence selecting $Q_3 = \{P_\mathrm{f},\ L\}$
Therefore, the dimensionless groups are

$$\pi_1 = \{\sigma,\ P_\mathrm{f},\ L\} \quad \pi_2 = \{P_\mathrm{f},\ L,\ D\}$$

Thus

$$\pi_1 = \{\sigma^a,\ P_\mathrm{f}^b,\ L^c\} \tag{1}$$

Finally, in dimensional form

$$\left[M^0L^0T^0\right] = \left[ML^{-1}T^{-2}\right]^a \times \left[MLT^{-2}\right]^b \times [L]^c$$

Comparing the indices of LHS and RHS for M, L and T.

$$0 = a + b,\ 0 = -a + b + c,\ 0 = -a + (-2b)$$

Therefore, $a = 1,\ b = -1$ and $c = 2$
Substituting the values in Eq. (1)

$$\pi_1 = \{\sigma^1,\ P_\mathrm{f}^{-1},\ L^2\} = \sigma L^2/P_\mathrm{f}$$

Similarly, $\pi_2 = L/D$
Let $\pi_1 = \phi(\pi_2)$ where ϕ is an unknown function.
Therefore, we can write

$$\pi_1 = \beta_1(\pi_2)^{\beta_2}$$

Substituting π values in the above equation

$$\frac{\sigma L^2}{P_\mathrm{f}} = \beta_1\left(\frac{L}{D}\right)^{\beta_2} \tag{2}$$

For finding the values of β_1 and β_2, based on actual test conducted on lateritic rock specimens, guiding point has been selected. The average of UCS of specimens with L/D ratio 2 cored from same depth is taken. Similarly, for L/D ratio other than 2, the average of failure load of the specimen from the same depth is taken [8].

Unconfined compressive strength of specimen with L/D ratio $2(\sigma) = 37.607\,\mathrm{kg/cm^2}$

Length of the specimen (L) = 7.8 cm
Diameter of the specimen (D) = 5.2 cm
Load at failure (P_f) = 801.48 kg
Substituting the above values in Eq. (2)

$$2.8547 = \beta_1 (1.5)^{\beta_2} \tag{3}$$

In logarithmic form

$$1.0489 = \log \beta_1 + 0.4055 \beta_2 \tag{4}$$

Solving Eqs. (3) and (4) by trial and error procedure, we get
$\beta_1 = 1$ and $\beta_2 = 2.4$
Substituting values in Eq. (2)

$$\boldsymbol{\sigma} = \boldsymbol{L}^{0.4} * \boldsymbol{D}^{-2.4} * \boldsymbol{P}_f \tag{5}$$

Using Eq. (5) the corrected unconfined compressive strength of the cylindrical specimen of lateritic rocks in Goa can be found out.

3 Previously Proposed Correlation Equations for Correction of UCS

Various corelation equations have been suggested for correction in UCS values in the case of non-standard L/D ratios (other than 2) as shown in Table 2, where σ_c is the corrected UCS value and σ_m is measured UCS value for non-standard L/D

Table 2 Correlation equations for non-standard L/D ratios

Equation	Applicability	References
$\frac{\sigma_c}{\sigma_m} = \frac{1}{0.778+0.444\frac{D}{L}}$	For non-standard L/D ratios other than 2	IS 9143-1979 [9]
$\frac{\sigma_c}{\sigma_m} = \frac{1}{0.88+0.24\frac{D}{L}}$	For non-standard L/D ratios other than 2	ASTM (D2938-79) [2]
$\frac{\sigma_c}{\sigma_m} = \frac{1}{0.848+0.304\frac{D}{L}}$	Coal measures rocks in UK	Hobbs [6], Szlavin [11]
$\frac{\sigma_c}{\sigma_m} = \frac{1}{0.875+0.25\frac{D}{L}}$	For non-standard L/D ratios other than 2	Protodykonov [10]
$\sigma_c = 1.0234 * H^{0.3} * D^{-2.3} * L_f$	For non-standard L/D ratios other than 2	Birid [3]

ratios. The corrected UCS values with five different correlation equations are shown in Table 2.

4 Results and Discussions

The results obtained above are compared with the available data and correlation equations (Table 2 and Fig. 1) and are tabulated in Table 3. Table 3 comprises the values of compressive load obtained from tests data and corrected UCS using equations mentioned in Table 2 and an equation is derived using dimensional analysis for the same load.

From Table 3, one can see that the values of corrected UCS of L/D ratio 2 using derived equation closely match with the values corrected using previously published equations. The plots of equations mentioned in Table 2 are shown in Fig. 1. As it can be seen, each curve has a different path but are following the same trend. These equations represent experimental results of different countries. Figure 2 shows the mean of all previously proposed correlation equations. It also shows the trend line of all the results obtained from experiments conducted on the samples collected from different places of Goa and corrected using previously proposed correlation equations.

This correction equation is applied to the test data and the correction factor is determined and the plot of L/D ratio versus correction factor is obtained as shown in Fig. 3. It can be seen from the plot that the proposed equation is following the same trend as other equations.

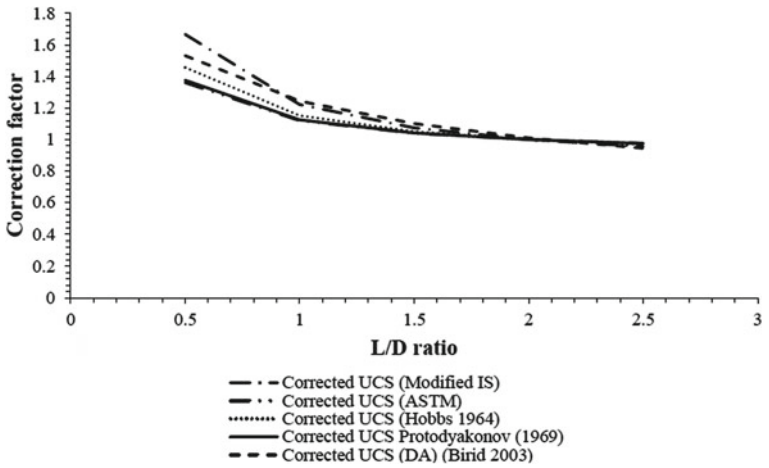

Fig. 1 Comparison of previously proposed correlation equations

Table 3 Comparison of correlation equations

Length (cm)	Diameter (cm)	L/D ratio	Compressive load (kg)	Compressive strength (kg/cm^2)	Corrected UCS (modified IS)	Corrected UCS (ASTM)	Corrected UCS [6]	Corrected UCS Protodyakonov [10]	Corrected UCS (Birid 1999)	Corrected by DA
2.6	5.2	0.5	367.09	17.28	10.37	12.71	11.87	12.57	11.28	10.29
2.6	5.2	0.5	163.15	7.68	4.61	5.65	5.27	5.58	5.02	4.57
2.6	5.2	0.5	1631.52	76.79	46.09	56.46	52.74	55.85	50.16	45.73
2.6	5.2	0.5	1478.56	69.59	41.77	51.17	47.79	50.61	45.45	41.44
2.6	5.2	0.5	1009.50	47.52	28.52	34.94	32.63	34.56	31.03	28.29
2.6	5.2	0.5	652.61	30.72	18.44	22.59	21.09	22.34	20.06	18.29
2.6	5.2	0.5	336.50	15.84	9.51	11.65	10.88	11.52	10.34	9.43
2.6	5.2	0.5	1600.92	75.35	45.23	55.41	51.75	54.80	49.21	44.87
2.6	5.2	0.5	489.46	23.04	13.83	16.94	15.82	16.75	15.05	13.72
2.6	5.2	0.5	448.67	21.12	12.68	15.53	14.50	15.36	13.79	12.57
2.6	5.2	0.5	856.55	40.32	24.19	29.64	27.69	29.32	26.33	24.01
2.6	5.2	0.5	356.89	16.79	10.08	12.35	11.54	12.22	10.97	10.00
2.6	5.2	0.5	662.80	31.19	18.73	22.94	21.43	22.69	20.38	18.58
2.6	5.2	0.5	479.26	22.56	13.54	16.59	15.49	16.41	14.73	13.43
2.6	5.2	0.5	601.62	28.32	16.99	20.82	19.45	20.59	18.49	16.86
2.6	5.2	0.5	407.88	19.19	11.52	14.12	13.19	13.96	12.54	11.43
5.2	5.2	1	662.80	31.19	25.53	27.85	27.08	27.73	25.09	24.51
5.2	5.2	1	356.89	16.79	13.75	14.99	14.58	14.93	13.51	13.19
5.2	5.2	1	1264.43	59.51	48.70	53.12	51.66	52.90	47.86	46.76

(continued)

Table 3 (continued)

Length (cm)	Diameter (cm)	L/D ratio	Compressive load (kg)	Compressive strength (kg/cm^2)	Corrected UCS (modified IS)	Corrected UCS (ASTM)	Corrected UCS [6]	Corrected UCS Protodyakonov [10]	Corrected UCS (Birid 1999)	Corrected by DA
5.2	5.2	1	1060.48	49.91	40.85	44.57	43.33	44.37	40.14	39.22
5.2	5.2	1	1437.78	67.67	55.38	60.42	58.74	60.15	54.42	53.17
5.2	5.2	1	581.23	27.36	22.39	24.43	23.75	24.32	21.99	21.49
5.2	5.2	1	683.19	32.16	26.32	28.71	27.91	28.58	25.86	25.27
5.2	5.2	1	815.76	38.39	31.42	34.28	33.33	34.13	30.87	30.17
5.2	5.2	1	652.61	30.72	25.14	27.43	26.66	27.30	24.70	24.13
5.2	5.2	1	407.88	19.19	15.71	17.14	16.66	17.06	15.44	15.08
5.2	5.2	1	438.47	20.64	16.89	18.43	17.92	18.34	16.59	16.22
5.2	5.2	1	632.21	29.76	24.35	26.57	25.83	26.45	23.93	23.38
5.2	5.2	1	550.64	25.92	21.21	23.14	22.49	23.04	20.84	20.36
5.2	5.2	1	520.05	24.48	20.03	21.85	21.25	21.76	19.68	19.23
5.2	5.2	1	805.56	37.92	31.03	33.85	32.92	33.70	30.49	29.79
5.2	5.2	1	469.06	22.08	18.07	19.71	19.16	19.62	17.75	17.35
7.8	5.2	1.5	734.18	34.56	32.18	33.23	32.89	33.17	31.38	31.93
7.8	5.2	1.5	1080.88	50.87	47.37	48.92	48.42	48.84	46.20	47.01
7.8	5.2	1.5	1029.9	48.48	45.14	46.61	46.14	46.54	44.02	44.79
7.8	5.2	1.5	591.43	27.84	25.92	26.77	26.49	26.72	25.28	25.72
7.8	5.2	1.5	397.68	18.72	17.43	17.99	17.82	17.97	16.99	17.29
7.8	5.2	1.5	1417.38	66.71	62.12	64.15	63.49	64.04	60.58	61.65

(continued)

Table 3 (continued)

Length (cm)	Diameter (cm)	L/D ratio	Compressive load (kg)	Compressive strength (kg/cm^2)	Corrected UCS (modified IS)	Corrected UCS (ASTM)	Corrected UCS [6]	Corrected UCS Protodyakonov [10]	Corrected UCS (Birid 1999)	Corrected by DA
7.8	5.2	1.5	1386.79	65.27	60.78	62.76	62.13	62.66	59.28	60.32
7.8	5.2	1.5	754.58	35.52	33.07	34.15	33.80	34.09	32.25	32.82
7.8	5.2	1.5	927.93	43.68	40.67	41.99	41.57	41.93	39.66	40.35
7.8	5.2	1.5	1386.79	65.27	60.78	62.76	62.13	62.66	59.28	60.32
7.8	5.2	1.5	1213.44	57.11	53.18	54.92	54.36	54.83	51.87	52.78
10.4	5.2	2	1753.88	82.55	82.55	82.55	82.55	82.55	81.72	85.58
10.4	5.2	2	897.34	42.24	42.24	42.24	42.24	42.24	41.81	43.79
10.4	5.2	2	1600.93	75.35	75.35	75.35	75.35	75.35	74.59	78.12
10.4 10.4	5.2 5.2	2 2	989.11 601.62	46.56 28.32	46.56 28.32	46.56 28.32	46.56 28.32	46.56 28.32	46.09 28.03	48.27 29.36
10.4	5.2	2	1019.7	47.99	47.99	47.99	47.99	47.99	47.51	49.76
10.4	5.2	2	774.97	36.48	36.48	36.48	36.48	36.48	36.11	37.82
10.4	5.2	2	1407.19	66.23	66.23	66.23	66.23	66.23	65.57	68.67
10.4	5.2	2	866.74	40.79	40.79	40.79	40.79	40.79	40.39	42.29
10.4	5.2	2	662.80	31.19	31.19	31.19	31.19	31.19	30.88	32.34
10.4	5.2	2	1142.06	53.75	53.75	53.75	53.75	53.75	53.22	55.73
10.4	5.2	2	744.38	35.04	35.04	35.04	35.04	35.04	34.68	36.32
10.4	5.2	2	825.96	38.88	38.88	38.88	38.88	38.88	38.49	40.31
13	5.2	2.5	479.26	22.56	23.61	23.11	23.26	23.14	23.88	25.57

(continued)

Table 3 (continued)

Length (cm)	Diameter (cm)	L/D ratio	Compressive load (kg)	Compressive strength (kg/cm^2)	Corrected UCS (modified IS)	Corrected UCS (ASTM)	Corrected UCS [6]	Corrected UCS Protodyakonov [10]	Corrected UCS (Birid 1999)	Corrected by DA
13	5.2	2.5	1580.53	74.39	77.85	76.22	76.73	76.30	78.74	84.33
13	5.2	2.5	1111.47	52.31	54.75	53.60	53.95	53.66	55.38	59.30
13	5.2	2.5	1111.47	52.31	54.74	53.60	53.95	53.66	55.38	59.30
13	5.2	2.5	1203.25	56.63	59.26	58.03	58.41	58.09	59.95	64.19
13	5.2	2.5	785.17	36.96	38.67	37.86	38.12	37.90	39.12	41.89
13	5.2	2.5	1193.05	56.15	58.76	57.53	57.91	57.59	59.44	63.65
13	5.2	2.5	785.17	36.96	38.67	37.86	38.12	37.90	39.12	41.89
13	5.2	2.5	846.35	39.84	41.69	40.82	41.08	40.86	42.17	45.16
13	5.2	2.5	622.02	29.28	30.63	29.99	30.19	30.03	30.99	33.19

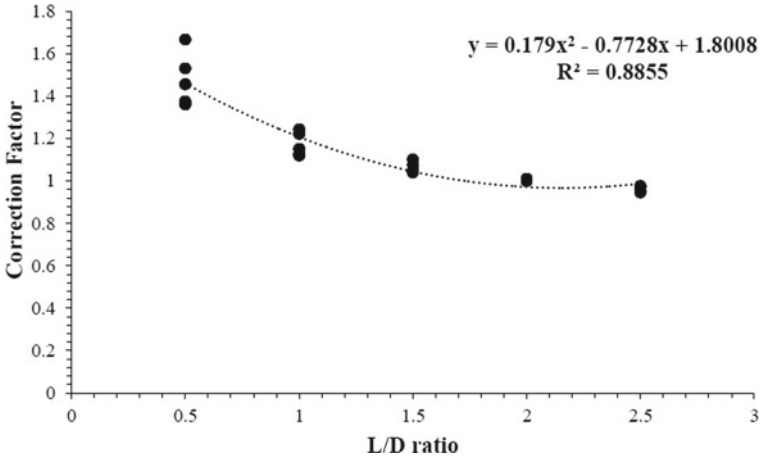

Fig. 2 Variation in correlation factor with L/D ratio for different equations

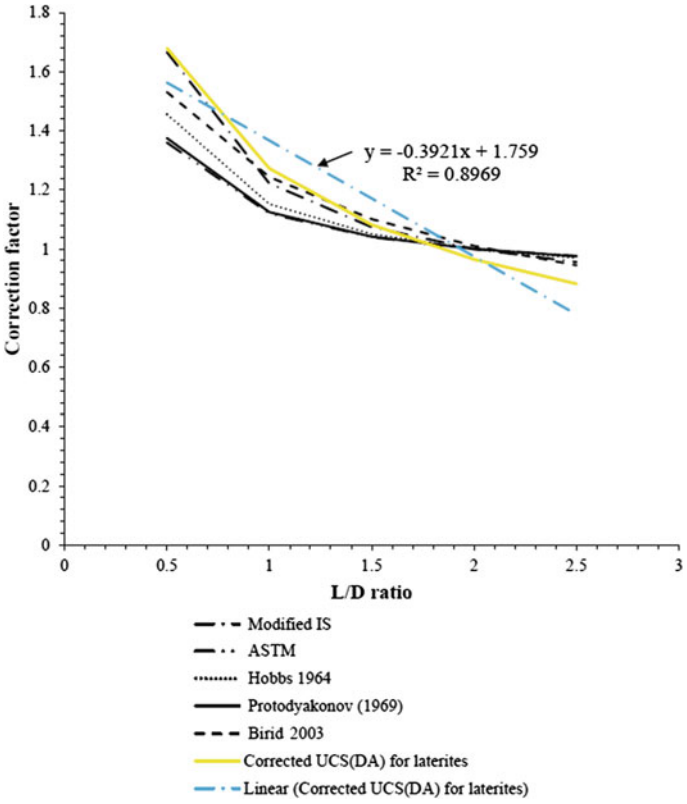

Fig. 3 Variation in correction factor with L/D ratio

5 Conclusions

Based on the above methodology of dimensional analysis and its comparison with the other test results, the following conclusions are drawn.

It is revealed from the comparison of the dimensional analysis with other methods and with that of actual test results that the D.A equation can be applied effectively to determine corrected UCS of lateritic rocks in Goa with L/D ratios other than 2.

It is possible to formulate D.A equation to determine corrected UCS of rock with a requirement that the various parameters involved in the problem should be known either experimentally or assumed using conventional analysis, along with their interrelationships with each other.

The above equation is obtained from the results samples collected from Pernem site. Similarly, an equation for correction of unconfined compressive strength can be obtained by studying other different sites in Goa. An equation derived using dimensional analysis for laterites in Goa can be used as a guide for deriving equation for correction of unconfined compressive strength for other types of rocks as UCS is used in determining safe bearing pressures on rocks.

References

1. Agustawijaya DS (2007) The uniaxial compressive strength of soft rock. Civil Eng Dimension 9(1):9–14
2. ASTM D-2938-79 (1980) Standard method of test for unconfined compressive strength of rock core specimens. Annual Book of ASTM Standards, Part 19, pp 440–443
3. Birid KC (2003) Critical assessment of unconfined compressive strength of rock using modified Buckingham method. Geotechn Eng Infrastructural Develop 529–534
4. Butterfield R (1999) Dimensional analysis for geotechnical engineers. Geotechnique 49(3):357–366
5. Ergun T, Nilsun H (2009) The effect of length to diameter ratio of test specimens on the uniaxial compressive strength of rock. Bull Eng Geol Environ 68(4):491–497
6. Hobbs DW (1964) Rock compressive strength. Colliery Eng 41:287–292
7. Ingale M, Savoikar P (2019) Geotechnical properties of Lateritic rocks in North Goa. In: Proceedings of international conference on recent developments in sustainable infrastructure (ICRDSI2019), KIIT University, Bhubaneswar
8. Ingale M (2019) Strength behaviour of Lateritic rocks in Goa. Masters Dissertation submitted to Goa University
9. ISRM (1979) Suggested methods for determining the uniaxial compressive strength and deformability of rock materials. Int J Rock Mechan Min Sci, Abstract 16:135–140
10. Protodyakonov MM (1969) Method of determining the strength of rocks under uniaxial compression. In: Protodyakonov MM, IKoifman M et al (eds) Mechanical properties of rocks. Translated from Russian, Israel Program for Scientific Translations, Jerusalem, pp 1–8
11. Szlavin J (1974) Relationships between some physical properties of rock determined by laboratory test. Int J Rock Mechan Min Sci Geomechan Abstracts 11:57–66
12. Turk N, Dearman WR (1986) A correction equation on the influence of length to diameter ratio on the uniaxial compressive strength of rocks. Eng Geol 22:293–300
13. Widdowson M (2009) Evolution of laterite in Goa. In: Mascarenhas A, Kalavampara G (eds) Proceedings of natural resources of Goa: a geological perspective. Geological Society of Goa, Miramar Goa, pp 35–68

Is Global Warming Hampering the Stability of Substructure?

K. S. Varun, T. Hari Lokesh, K. Tejas, and S. Shilpa Shet

Abstract In the present environmental situation, the temperature of earth's atmosphere as well as the earth's sub-surficial temperature is increasing at a very tremendous rate. Since 1979, global average land temperatures have increased about twice as fast as global average ocean temperatures (0.25 °C per decade against 0.13 °C per decade). Though the figure seems to be insignificant when considered on a global average, it sounds to be significant when particular regions on earth are considered. This increase in temperature is not only affecting the habitation of living species but also the habitation and stability of structures by affecting their foundations. Hence efforts have been made in this study to interpret and plot the effects of global warming on substructures by provision of mathematical and theoretical proofs. In the study, the phenomena of thermal expansions and thermal contractions of material subjected to temperature variations have been exploited, to attain at the result. This depicts a significant impact of temperature stress on the stability of subsurface structures which are in contact with subsurface geological structures. The principal upon which the study is based is thermal: Different materials expand or contract thermally when subjected to temperature variations; the same material expands or contracts thermally to a different extent at various degree of temperature variations. The study deals with mathematical expressions to plot the effects of global warming on stability of substructures.

Keywords Global warming · Temperature stress · Thermal expansion and contraction · Coefficient of thermal expansion · Volumetric stress and strain

1 Introduction

A gradual increase in the overall temperature of the earth's atmosphere is generally attributed to the greenhouse effect caused by increased levels of carbon dioxide, CFCs, and other pollutants. This phenomenon of global importance has become an

K. S. Varun (✉) · T. Hari Lokesh · K. Tejas · S. Shilpa Shet
Department of Civil Engineering, Acharya Institute of Technology, Bengaluru, India
e-mail: varunsathya123@gmail.com

B. B. Das et al. (eds.), *Recent Trends in Civil Engineering*, Lecture Notes in Civil Engineering 105, https://doi.org/10.1007/978-981-15-8293-6_25

instinct for global rise in temperature both diurnal as well as annual temperature range. Since 1979, global average land temperatures have increased about twice as fast as global average ocean temperatures (0.25 °C per decade against 0.13 °C per decade). Though the figure seems to be insignificant when considered on a global average, it sounds to be significant when particular regions on earth are considered. Temperature changes at the earth's surface propagate downward into the subsurface and impart a thermal signature to the rocks. "The average surface temperature of the continents has increased by about 1.0 K over the past 5 centuries; half of this increase has occurred in the twentieth century alone, where the linear increase of temperature with depth in the deeper sections of the holes was observed with increase in surface hotness" (Henry 2000) [1]. This is a vice versa operation. The change in temperatures of subsurface can be due to fluctuations in water table as well [2].

Now, it is a known fact that materials expand when subjected to higher temperature. Keeping this as the basis, the present study will derive at suitable mathematical expressions on how the expansion in substructures and sub-surficial lithology with which they are in contact due to rise in temperature will result in an unstable substructure. The present study specifies the magnitude of this instability as well. The study has given a vivid insight on different scenarios to be faced in the field while dealing with this issue [3–6].

The principal upon which the study is based is thermal: Different materials expand or contract thermally when subjected to temperature variations; the same material expands or contracts thermally to a different extent at various degree of temperature variations. The study deals with mathematical expressions to plot the effects of global warming on stability of substructures [2, 7, 8].

2 Methodology

The effort is mainly concerned with the effects of temperature stresses on pile foundations, as a result of global warming. So, the temperature change is taken as the difference of annual average temperature in the field for the present year of study and the annual average temperature in the field 100 years ago. When global warming was insignificant and its effect can be eliminated, the procedure followed is as follows:

Most of the material when subjected to variations in temperature either expand or contract. If this expansion or contraction is constrained fully or partially, stresses are induced in them, and these stresses are referred to as temperature stresses.

That is to say

$$\Delta T = T' - T(t) \tag{1}$$

where

T' annual average temperature in the field for the present year of study;

T annual average temperature in the field 100 years ago (when GLOBAL WARMING was insignificant).

Then the effective expansions in both pile and rock strata if found for this corresponding rise in temperature.

Now, both the pile cap and the rock strata are in tight contact with each other. There is no allowance allowed. So, as expressed in point, the resultant stresses (i.e. temperature stresses) induced in the bodies due to these expansions are calculated and hence the resultant forces. Then the line of action of these forces is considered to enumerate the final resultant stress and its line of action.

So, this forms the basic methodology on which the paper is pivoted on. Further, it should be noted that this paper also provides three different variants, in terms of alignment or orientation pattern existing between the pile cap and the strata bearing it.

As rock strata can be considered more compact, homogenous and isotropic in terms of its properties when compared to pile, most of the piles are not designed to carry any kind of lateral stress (i.e. the piles are usually designed to bear axial loads specifically, and in very rare cases they are designed to bear lateral stresses). Hence, it can be concluded that a lateral, volumetric compressive stress is acting upon the pile under consideration. The resulting compression of the pile at its bottom-most part there by induces a settlement.

3 Mathematical Proof to Prove the Effect of Global Warming on Substructures

3.1 Scenario 1

The pile cap and the rock strata bearing it are perpendicular to each other (i.e. they form an angle of 90° with each other), as depicted in the diagram.

Now, consider ΔT as the rise in temperature as an effect of global warming.

Now, expansions in the material due to rise in temperature are:

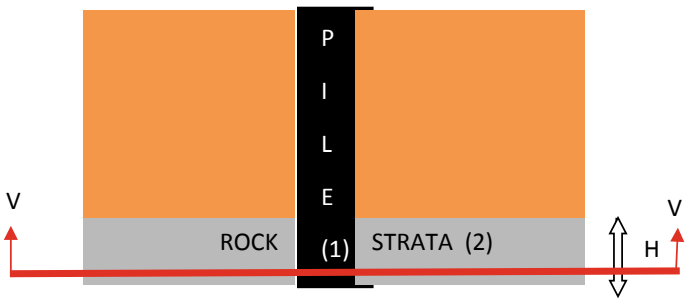

Fig. 1 Horizontal strata scenario

Fig. 2 Cross-section @ V-V

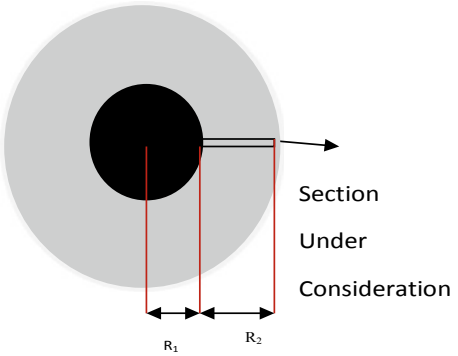

$$\mathrm{dR}_1 = \alpha_1 * \Delta T * R_1 \tag{2}$$

$$\mathrm{dR}_2 = \alpha_2 * \Delta T * R_2 \tag{3}$$

where

dR_1 radial expansion in pile;
dR_2 radial expansion rock strata bearing it.
α_1 coefficient of thermal expansion of pile
α_2 coefficient of thermal expansion of rock strata
R_1 radius of pile
R_2 radius of rock strata.

The corresponding temperature stresses induced in the materials are:

$$\sigma_1 = \frac{E_1 * \mathrm{dR}_1}{R_1} \tag{4}$$

$$\sigma_2 = \frac{E_2 * \mathrm{dR}_2}{R_2} \tag{5}$$

where

σ_1 temperature stress induced in pile;
σ_2 temperature stress induced in rock strata;
E_1 Young's modulus of pile;
E_2 Young's modulus of rock strata;

Here, it can be interpreted that due to increase in temperature, the pile tends to expand radially, and so is the rock strata but in different direction. As a consequence, either the pile might develop a greater force compared to that of rock strata, thereby pushing the rock strata radially, or rock strata might develop a greater force compared to that of pile, thereby crushing the pile.

Let $A_1 = A_2 = A =$ surface area of contact

Now, if the expansion in the pile foundation is greater than that of rock strata:

$$\text{i.e.} \quad (\sigma_1 * A) \geq (\sigma_2 * A) \tag{6}$$

$$A = 2 * \pi * R_1 * H \tag{7}$$

Net force (F) is acting radially outwards from the pile, and is given by

$$F = (\sigma_1 * A) - (\sigma_2 * A) \tag{8}$$

$$\begin{aligned} \text{Corresponding net stress} &= \frac{[(\sigma_1 * A) - (\sigma_2 * A)]}{A} \\ &= \sigma_1 - \sigma_2 \end{aligned} \tag{9}$$

Now, if the expansion in the rock strata is greater than that of pile foundation:

$$\text{i.e.} \quad \text{If}(\sigma_1 * A) \geq (\sigma_2 * A) \tag{10}$$

Then, rock strata is expanding to a greater extent in comparison to the pile.

Also, as per this condition, the net force (F) is acting on the pile in radially inward direction; or in other words, the net force is tending to crush the pile foundation, and is given by:

$$F = (\sigma_2 * A) - (\sigma_1 * A) \tag{11}$$

$$\text{Corresponding net stress} = \frac{[(\sigma_2 * A) - (\sigma_1 * A)]}{A} = \sigma_2 - \sigma_1 \tag{12}$$

Here whatever might be the direction of the net force, irrespective of this factor, the stress is always assumed to accumulate on the pile itself.

3.1.1 An Extended Version of Scenario 1

An extrapolated case of the present scenario is as shown in Fig. 3, wherein the methodology and the formulation remain the same, except for the fact that the pile is acted upon by two or more such lateral, volumetric compressive stresses (i.e. one due to the hard strata and the other due to soft strata as shown in Fig. 3).

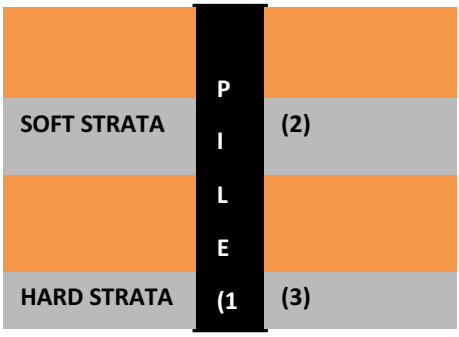

Fig. 3 Extended version of scenario 1

Formulae:

$$\text{Net stress at the interface of soft strata and pile} = \sigma_1 - \sigma_2 \text{ OR } \sigma_2 - \sigma_1 \tag{13}$$

depending on whether σ_1 or σ_2 are greater than the other.

$$\text{Net stress at the interface of hard strata and the pile} = (\sigma_1 - \sigma_3) \text{ OR } (\sigma_3 - \sigma_1) \tag{14}$$

depending on whether σ_1 or σ_3 are greater than each other.

4 Scenario 2

Here the pile is considered to make some angle with the rock strata on which it rests (i.e. in other words, PILE RESTING ON AN INCLINED STRATA).

Considering,

R radius of the pile footing,
R_2 radius of the strata dipping at an angle θ_1 in horizontal plane, and
α_1, α_2 are the coefficient of thermal expansions of pile and rock strata dipping at angles θ_1, respectively.

Now, according to Fig. 4, total surface area of contact between pile and rock strata (A') is obtained. Here the pile considered is of circular cross-section (Fig. 5).

Total surface area of contact (A') = Area of rectangle + Area of triangle (as shown in Fig. 6).

$$A' = (2\pi R * h) + \left[\left(\frac{1}{2}\right)(H - h)2\pi R\right] \tag{15}$$

$$A' = \pi R(H + h) \tag{16}$$

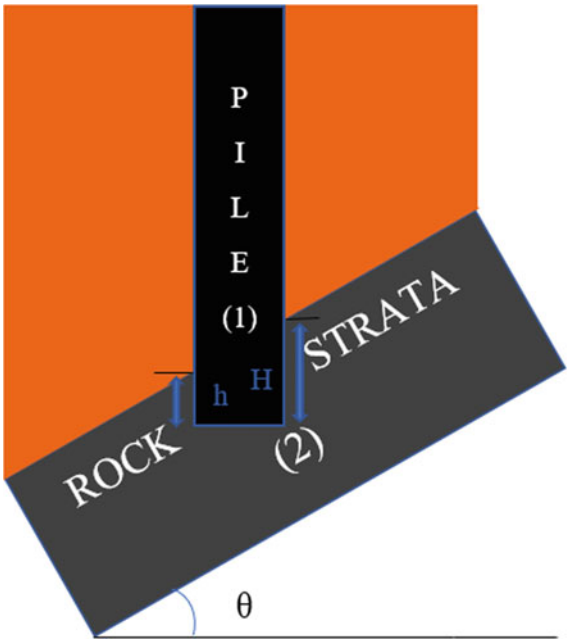

Fig. 4 Pile resting on inclined strata

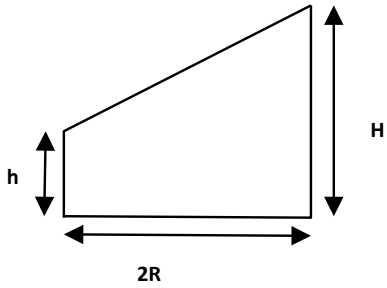

Fig. 5 Elevation of pile overlapped by inclined rock strata

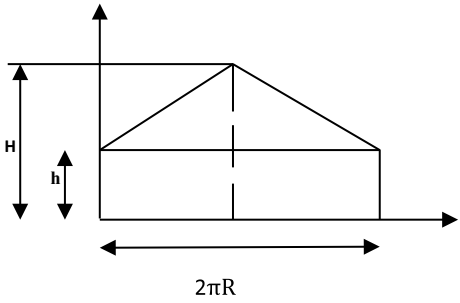

Fig. 6 Total surface area of contact between pile and inclined rock strata

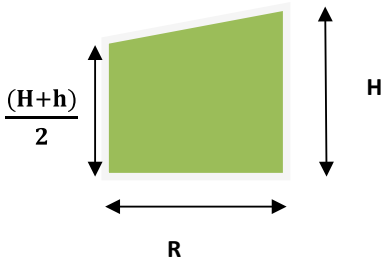

Fig. 7 Elevation of pile overlapped by inclined rock strata on the right half of the pile

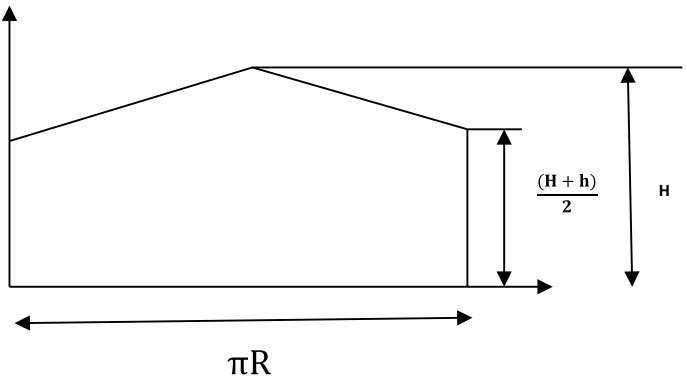

Fig. 8 The area upon which the weight of the inclined rock strata is suspected to be exerted on pile

Now, surface area of pile in contact with rock strata (A''), only to right section of limb for the figure shown above (i.e. the area upon which the weight of the inclined rock strata is suspected to be exerted) is given by the formulae:

$$A'' = \left[\left(\frac{\pi R(H+h)}{2}\right) + \left(\frac{\pi R(H-h)}{4}\right)\right] \tag{17}$$

$$A'' = \frac{\pi R[3H+h]}{4} \tag{18}$$

Now, similar to the previous scenario, to find the expansions in different material, the formulae are:

$$\mathrm{dR}_1 = \alpha_1 * \Delta T * R \tag{19}$$

$$\mathrm{dR}_2 = \alpha_2 * \Delta T * R \tag{19.1}$$

4.1 The Stress on Pile Due to Temperature Variation

Corresponding temperature stresses induced in the materials are:

$$\sigma_1 = \frac{E_1 * \mathrm{dR}_1}{R_1} \tag{20}$$

$$\sigma_2 = \frac{E_2 * \mathrm{dR}_2}{R_2} \tag{21}$$

Now, the net force due to temperature variation acting on the pile foundation may be either radial outwards or inwards and is dependent on the magnitude of force corresponding to temperature stresses σ_1, $\sigma 2$.

That is, if $(\sigma_1 * A) \geq (\sigma_2 * A)$, then the net force is acting radially outwards from the pile.

If $(\sigma_1 * A) \geq (\sigma_2 * A)$, then the net force is acting radially inwards the pile.

Therefore, the net effective temperature stress (σt) acting ultimately on the pile is

$$\mathrm{Ft} = (\sigma_1 * A) \sim (\sigma_2 * A) \tag{21}$$

$$\begin{aligned} \sigma t &= \frac{[(\sigma_1 * A) \sim (\sigma_2 * A)]}{A} \\ &= \sigma_1 \sim \sigma_2 \end{aligned} \tag{22}$$

Now, the stress acting on pile on account of weight of the inclined strata (i.e. to the right of the pile) is:

Weight of the strata on right half of the pile is given by:

W_1 = Density of the strata * Volume * Acceleration due to gravity.

$$W_1 = \rho * V_1 * g \tag{23}$$

Therefore, the net force due to weight of this stratum on the pile (Fw) is:

$$\mathrm{Fw} = W \sin\theta_1 - f_1 \tag{24}$$

where f_1 = frictional resistance opposing the force FW_1, which is given by:

$$f_1 = \mu * W_1 \tag{25}$$

and μ = coefficient of friction between a rock stratum and the subsequent strata bearing the pile, situated above it.

Therefore, the net stress on pile due to weight of the strata is:

$$\sigma w = \frac{\mathrm{Fw}}{A''} \tag{26}$$

5 Scenario 3

Here the pile is considered to be situated such that the bottom-most part of the pile rest on the hinge point or on the hinge line of a synclinal or anticlinal fold (Fig. 9).

5.1 Synclinal Folds

Where

R radius of the pile footing
R_2 radius of the strata dipping at an angle θ_1 in horizontal plane
R_3 radius of the strata dipping at an angle of θ_2 in horizontal plane.

$\alpha_1, \alpha_2, \alpha_3$ are the coefficient of thermal expansions of pile and rock strata dipping at angles θ_1, θ_2, respectively.

Usually, $\alpha_2 = \alpha_3$ (due to homogeneity of strata in terms of its composition).

The procedure for deducing the stress is the same as in other cases:

Initially, the total surface area of contact between pile and rock strata (A) is:

E_1, E_2, E_3 are modulus of elasticity of pile, rock strata titled (2) in the above diagram, rock strata titled (3) in the above diagram.

Usually, $E_2 = E_3$, owing to the homogeneous composition of strata in a fold.

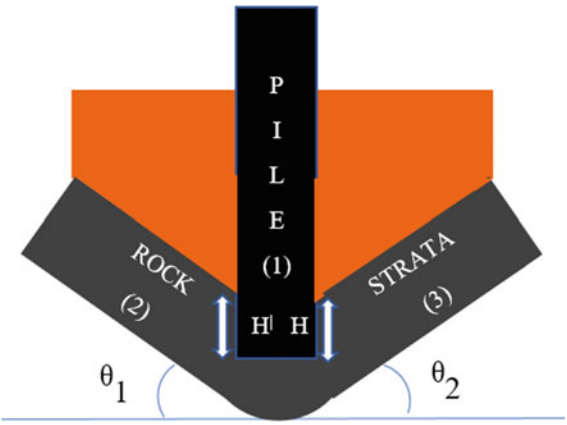

Fig. 9 Pile resting on a synclinal fold

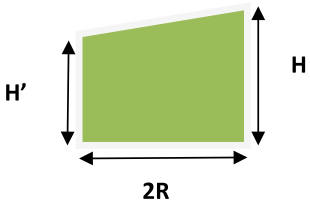

Fig. 10 Elevation of pile overlapped by synclinal rock strata

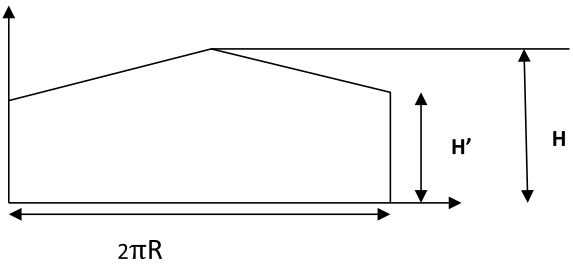

Fig. 11 Total surface area of contact between synclinal rock strata and pile

$$A = \left[2\pi R H^{'}\right] + \left[\left(\frac{1}{2}\right)2\pi R\left(H - H'\right)\right] \tag{27}$$

$$A = \pi R\left(H + H'\right) \tag{27.1}$$

Now, let the surface area between the pile and strata dipping at an angle θ_2 be $A\#$ (i.e. the area of contact between the pile and the rock strata to the right half) (Figs. 12 and 13).

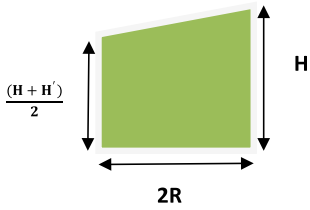

Fig. 12 Elevation of pile overlapped by synclinal rock strata to the right half

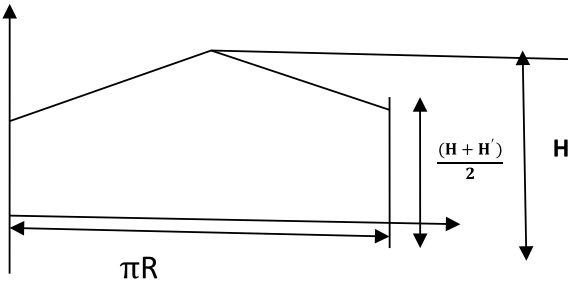

Fig. 13 Total surface area of contact between synclinal rock strata and pile to the right half

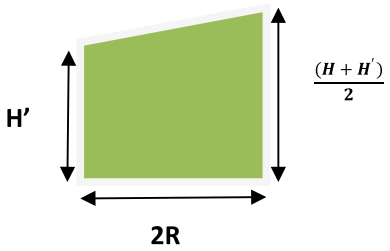

Fig. 14 Elevation of pile overlapped by synclinal rock strata to the left half

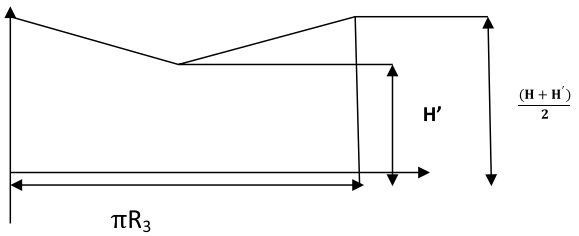

Fig. 15 Total surface area of contact between synclinal rock strata and pile to the left half

$$A\# = \left[\pi R\left(\frac{H + H'}{2}\right)\right] + \left[(1/2)\pi R\frac{(H - H')}{2}\right] \tag{28}$$

$$A\# = \frac{\pi}{4}R\left[3H + H'\right] \tag{28.1}$$

Similarly, surface area between the pile and strata dipping at angle θ_1 be $A\$$ (i.e. the area of contact between the pile and the rock strata to the left half) (Figs. 14 and 15).

$$A\$ = \left(\pi R H'\right) + 2\left[(1/2) * \frac{\pi}{2}R * \frac{(H - H')}{2}\right] \tag{29}$$

$$A\$ = \frac{\pi}{4}R\left[3H' + H\right] \tag{29.1}$$

Reduction of R_2 and R_3, which are in horizontal plane to inclined plane of angles θ_1 and θ_2, respectively:

$$R_2' = (R_2/\cos\theta_1) \tag{30}$$

$$R_3' = (R_3/\cos\theta_2) \tag{31}$$

where

R_2' value of R_2 reduced to inclined plane of angle $\theta 1$
R_3' value of R_3 reduced to inclined plane of angle θ_2.

Considering the stresses enacted on the pile due to temperature variations:
Now, expansions in the members under consideration are given by:

$$\mathrm{dR}_1 = \alpha_1 * \Delta T * R \tag{32}$$

$$\mathrm{dR}_2 = \alpha_2 * \Delta T * R_2' \tag{33}$$

$$\mathrm{dR}_3 = \alpha_3 * \Delta T * R_3' \tag{34}$$

where

$\mathrm{dR}_1, \mathrm{dR}_2, \mathrm{dR}_3$ thermal expansions in the pile, rock strata 1 and rock strata 2, respectively.

Corresponding temperature stresses induced within the elements are:

$$\sigma_1 = \frac{E_1 * \mathrm{dR}_1}{R} \tag{35}$$

$$\sigma_2 = \frac{E_2 * \mathrm{dR}_2}{R_2'} \tag{36}$$

$$\sigma_3 = \frac{E_3 * \mathrm{dR}_3}{R_3'} \tag{37}$$

where

$\sigma_1, \sigma_2, \sigma_3$ are the temperature stresses induced in the pile, rock strata 1 and rock strata 2, respectively.

Therefore, the net effective temperature stress (σt) acting ultimately on the pile is

$$\sigma t = (\sigma_2 \sim \sigma_1) + (\sigma_3 \sim \sigma_1) \tag{38}$$

Therefore, now considering the stress on pile due to weight of the strata:
For strata dipping with an angle of θ_1, W_1 = density of the strata * Volume * Acceleration due to gravity

$$W_1 = \rho * V_1 * g \tag{39}$$

where

$$V_1 = \int_0^{H'} \pi \left(R_2' \wedge 2/2\right) \mathrm{d}H \tag{40}$$

$$V_1 = \frac{\pi}{2}\left(R_2' \wedge 2\right)H' \tag{40.1}$$

Therefore, net force due to weight of this stratum on the pile (Fw_1) is:

$$\mathrm{Fw}_1 = W \sin\theta_1 - f_1 \tag{41}$$

$f1 =$ frictional resistance opposing the force Fw1, which is given by:

$$f_1 = \mu * W_1 \tag{42}$$

where

μ coefficient of friction between a rock stratum and the subsequent strata bearing the pile, situated above it.

For strata dipping with an angle of θ_2:
$W_2 =$ Density of the strata * Volume * Acceleration due to gravity

$$W_2 = \rho * V_2 * g \tag{43}$$

where

$$V_2 = \int_0^H \pi\left(R_3' \wedge 2/2\right)\mathrm{d}H \tag{44}$$

$$V_2 = \frac{\pi}{2}\left(R_2' \wedge 2\right)H \tag{44}$$

Therefore, net force due to weight of this stratum on the pile (Fw_1) is:

$$\mathrm{Fw}_2 = W \sin\theta_2 - f_2 \tag{45}$$

$f_2 =$ frictional resistance opposing the force FW_2, which is given by:

$$f_2 = \mu * W_2 \tag{46}$$

where

μ coefficient of friction between a rock stratum and the subsequent strata bearing the pile, situated above it.

Therefore, now the net stress on the pile due to weights of the strata is σw:

$$\sigma w = \left[\mathrm{Fw}_1/A\$\right] + \left[\mathrm{Fw}_2/A\#\right] \tag{47}$$

Now, suppose if $\theta_1 = \theta_2$, it directly implies that $H = H'$.

Then, almost all the formulae remain the same, except for the one mentioned below.

(Denotations remaining the same).

$$
\begin{gathered}
A = 2\pi RH \\
A' = A\# = A\$ = \pi RH \\
R'_o = R'_2 = R'_3 = (R_2/\cos\theta) = (R_3/\cos\theta) \\
\mathrm{dR}_1 = \alpha_1 * \Delta T * R \;;\; \mathrm{dR}_2 = \alpha_2 * \Delta T * \mathrm{R}'_o \\
\mathrm{dR}_3 = \alpha_3 * \Delta T * \mathrm{R}'_o \\
\sigma_1 = \tfrac{E_1 * \mathrm{dR}_1}{R},\ \sigma_2 = \tfrac{E_2 * \mathrm{dR}_2}{\mathrm{R}'_o},\quad \sigma_3 = \tfrac{E_3 * \mathrm{dR}_3}{\mathrm{R}'_o} \\
\sigma t = (\sigma_2 \sim \sigma_1) + (\sigma_3 \sim \sigma_1) \\
V = \pi\left(R' \wedge 2\right)H \\
W = \rho * V * g \\
\mathrm{Fw} = W\sin\theta - f \\
\sigma w = \left(\mathrm{Fw}/2A'\right)
\end{gathered}
\tag{48}
$$

Hence it can be concluded that when the pile is situated on hinge axis of a synclinal fold the resultant stress system which tend to crumble the stability of pile are:

1. Stress due to temperature variation (i.e. due to global warming) (σt).
2. Stress due to weight of the inclined strata (σw).

5.2 Anticlinal Folds

Where

R radius of the pile
R_2 radius of the strata dipping at an angle θ_1 in the horizontal plane
R_3 radius of the strata dipping at an angle of θ_2 in the horizontal plane (Fig. 16).

$\alpha_1, \alpha_2, \alpha_3$ are the coefficient of thermal expansions of pile, rock strata dipping at angles θ_1, θ_2, respectively.

Usually, $\alpha_2 = \alpha_3$ (due to homogeneity of strata in terms of its composition). The procedure for deducing the stress is the same as in other cases. Initially, total surface area of contact between pile and rock strata (A) is :

E_1, E_2, E_3 are modulus of elasticity of pile, rock strata titled (2) and rock strata titled (3) in Fig. 16.

Usually, $E_2 = E_3$, owing to the homogeneous composition of strata in a fold.

$$
A = \left[2\pi RH'\right] + \left[\left(\frac{1}{2}\right)2\pi R\left(H - H'\right)\right] \tag{49}
$$

$$
A = \pi R\left(H + H'\right) \tag{49.1}
$$

Now, reducing the radius R_2, R_3 which are in horizontal plane to inclined plane of inclinations θ_1, θ_2 respectively, we get:

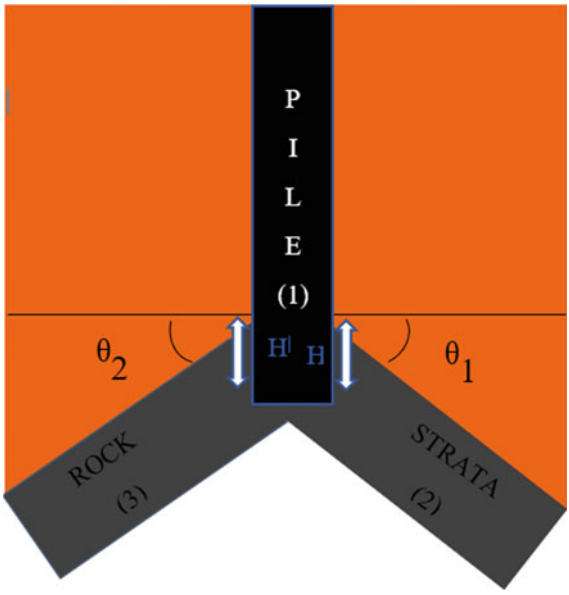

Fig. 16 Pile resting on anticlinal fold

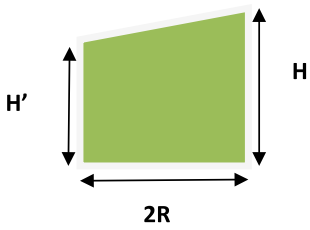

Fig. 17 Elevation of pile overlapped by anticlinal rock strata

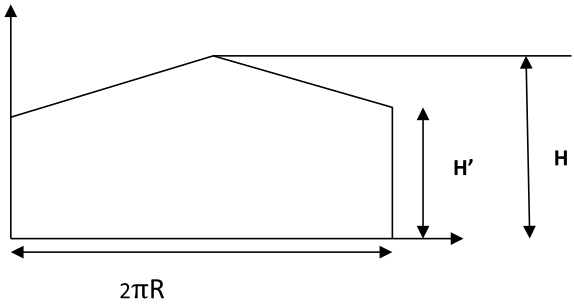

Fig. 18 Total surface area of contact between anticlinal rock strata and pile

$$R_2' = \frac{R_2}{\cos\ \theta_1} \tag{50}$$

$$R_3' = \frac{R_3}{\cos\ \theta_2} \tag{51}$$

Where

R_2' value of R_2 reduced to inclined plane of angle θ_1
R_3' value of R_3 reduced to inclined plane of angle θ_2.

Now, the expansions in all the elements under consideration due to an increment in temperature (i.e. global warming) are given by

$$\mathrm{dR}_1 = \alpha_1 * \Delta T * R \tag{52}$$

$$\mathrm{dR}_2 = \alpha_2 * \Delta T * R_2' \tag{53}$$

$$\mathrm{dR}_3 = \alpha_3 * \Delta T * R_3' \tag{54}$$

where

$\mathrm{dR}_1, \mathrm{dR}_2, \mathrm{dR}_3$ thermal expansions in the pile, rock strata 2, rock strata 3, respectively.

Corresponding temperature stresses induced in the elements are:

$$\sigma_1 = \frac{E_1 * \mathrm{dR}_1}{R} \tag{55}$$

$$\sigma_2 = \frac{E_2 * \mathrm{dR}_2}{R_2'} \tag{56}$$

$$\sigma_3 = \frac{E_3 * \mathrm{dR}_3}{R_3'} \tag{57}$$

where

$\sigma_1, \sigma_2, \sigma_3$ are the temperature stresses induced in the pile, rock strata 2 and rock strata 3, respectively.

Therefore, now the net effective stress acting on pile due to global warming (i.e. increment in temperature) is given by the equation:

$$\sigma t = (\sigma_2 \sim \sigma_1) + (\sigma_3 \sim \sigma_1) \tag{58}$$

Now, if $\theta_1 = \theta_2$, then it directly implies that $H = H'$.

Then almost all the equations remain the same except for few which are being mentioned below (denotations remaining same)

$$
\begin{gathered}
A = 2\pi RH \\
R_2' = R_3' = R_o' = \frac{R_2}{\cos\theta_1} = \frac{R_3}{\cos\theta_2} \\
\mathrm{dR}_1 = \alpha_1 * \Delta T^* R; \quad \mathrm{dR}_2 = \alpha_2 * \Delta T^* R_o'; \qquad \mathrm{dR}_3 = \alpha_3^* \Delta T^* R_o' \\
\sigma_1 = \frac{E_1 * \mathrm{dR}_1}{R} \\
\sigma_2 = \frac{E_2 * \mathrm{dR}_2}{R_o'} \\
\sigma_3 = \frac{E_3 * \mathrm{dR}_3}{R_o'} \\
\sigma t = (\sigma_2 \sim \sigma_1) + (\sigma_3 \sim \sigma_1)
\end{gathered}
\tag{59}
$$

6 Conclusion

The paper derives at a relation proving the effect of global warming on subsurface structures such as pile foundation with a precise mathematical equation to determine the stress acting upon the pile foundation due to global warming. Through this we can also provide the magnitude of stress accumulated on the pile foundation due to the weight of the rock strata in case of inclined strata, synclinal fold and anticlinal fold.

This could be inculcated in design of pile footings (which are usually designed to bear axial loads only) to bear lateral stresses too, which are likely to be exerted on them due to global warming (temperature variations). The values of these lateral stresses can be determined using the relations presented by the paper; thereby the design of the pile can be recalibrated to take both axial and lateral/traverse loads efficiently.

7 Further Scope

Throughout the paper, the pile considered is of circular cross-section. Hence further research can be conducted to derive at relations for piles of various cross-sections keeping the present study as a background.

This paper depicts so as to how the temperature variations in the rock strata and the pile tend to develop an unanticipated traverse/lateral stress on the pile. There are cases wherein the pile reaches the strata after encountering a layer of crushed gravels, which also have some thermal expansion behavior, so the paper can be considered as a reference to deduce relations validating the effect of crushed gravels on pile due to global warming.

References

1. Public Perceptions of Global Warming. https://doi.org/10.1007/BF01091637
2. van Roosmalen L, Christensen BSB, Sonnenborg TO (2007) Regional differences in climate change impacts on groundwater and stream discharge in Denmark. Vados Zone J 554–571. https://doi.org/10.2136/vzj2006.0093
3. Babuška V, Plomerová J, Šílený J. Structural Model of the Subcrustal Lithosphere
4. Cook J, Nuccitelli D, Green SA. Quantifying the consensus on anthropogenic global warming in the scientific literature
5. Morscher GN, Hurst J, Brewe D. Intermediate—temperature stress rupture of a woven Hi—nicalon, BN—interphase, SiC—matrix composite in air
6. Gurdak JJ, Hanson RT, McMahon PB, Bruce BW, McCray JE, Thyne GD, Reedy RC. Climate variability controls on unsaturated water and chemical movement, high plains Aquifer, USA. Vados Zone J 533–547. https://doi.org/10.2136/vzj2006.0087
7. Lommens P, Meyer CD, Bruneel E, Buysser KD, Van Driessche I, Hoste S. Synthesis and thermal expansion of ZrO2/ZrW2O8 composites
8. Warpinski NR, Teufel LW. Influence of geologic discontinuities on hydraulic fracture propagation

Estimation of Ultimate Bearing Capacity of Soil for Shallow Foundation

Ajay Gaonkar, Shubham Arondekar, Akshay Mungarwadi, Pritesh Gaude, Vishwesh Gaude, Vedant Haldankar, Swaroopa Sail, and Akshata Kudchadkar

Abstract Evaluation of ultimate bearing capacity is a tedious process, as the determination of shear strength parameters within the underlying soil structure is a difficult task. The purpose of current research work was to arrive at an alternative way for calculating ultimate bearing capacity by thoroughly considering soil properties like density, specific gravity and grain size distribution. Soil samples were collected from different construction sites of South Goa at 1.5 m depth from the ground level. Numerous tests like core cutter, moisture content, specific gravity, direct shear, sieve analysis and pipette analysis were conducted to determine the soil properties. Using the results of direct shear test (c and ϕ values), ultimate bearing capacities were calculated as per Terzaghi, Hansen, Meyerhof, Vesic and code IS: 6403-1981 methods for square footing of 2 m $\times$ 2 m. The softwares like SoFA and OptumG2 were also used to calculate ultimate bearing capacities. Various correlation equations were arrived between different soil properties and ultimate bearing capacity using multiple regression technique. The softwares used to arrive at a regression equation were IBM SPSS Statistics 24 and Minitab. Prediction accuracies were evaluated using coefficient of determination, root mean square error and mean error between the measured and the predicted values.

Keywords Ultimate bearing capacity · Shear strength · Multiple regressions · OptumG2 software · Minitab

1 Introduction

Bearing capacity is the strength of the soil, which absorbs the superstructure effort, without undergoing shear failure or excessive settling. While designing the foundation we consider two main factors, namely the ultimate bearing capacity (UBC) of the soil beneath the foundation and the amount of settlement that is allowed with taking

A. Gaonkar (✉) · S. Arondekar · A. Mungarwadi · P. Gaude · V. Gaude · V. Haldankar · S. Sail · A. Kudchadkar
Don Bosco College of Engineering, Goa, India
e-mail: ajaygaonkar28@gmail.com

B. B. Das et al. (eds.), *Recent Trends in Civil Engineering*, Lecture Notes in Civil Engineering 105, https://doi.org/10.1007/978-981-15-8293-6_26

into consideration that the settlement does not affect the efficiency of soil. The ultimate bearing capacity means the load under the foundation can carry without failing in shear and the settlement consists of approximation of the settlement which is caused by superstructure load [1]. The bearing capacity of foundations depends on some of the mechanical properties of the soil, such as density, shearing strength and deformation characteristics. It also depends on the original stresses and the water conditions inside the ground. The size, shape, depth and roughness are some visible features of the foundation on which bearing capacity depends [2]. Judging of the ultimate bearing capacity is a tough process as it is hard to evaluate the shear strength parameters within the underlying soil structure. To determine the ultimate bearing capacity of soil for shallow foundation, Terzaghi's [3], Meyerhof's [2], Hansen's [4], Vesic's [5], IS 6403: 1981 [6] methods and also softwares such as SoFA [7] and OptumG2 [8] were used. A comparison was made between the values found from methods given by various investigators, SoFA and OptumG2. Manual methods for the estimation of ultimate bearing capacity are based on shear strength parameters. A nonlinear regression is used to model the relationship between bearing capacity and fines contents of soil using square footing [9]. An attempt was made to provide an easier, faster and economical method to determine the ultimate bearing capacity of soil by generating an equation by regression analysis using IBM SPSS Statistics 24 [10] and Minitab [11] softwares. A relationship was derived between ultimate bearing capacity and soil properties such as density, specific gravity and grain size distribution. Based on the coefficient of determination (R^2), the derived equation was validated. The nearer the R^2 is to 1, the accurate is the relationship between the dependent and independent variables [12].

2 Methodology

The present work was carried out for shallow foundation considering a square footing of size 2 m $\times$ 2 m and depth of foundation as 1.5 m.

2.1 Soil Sampling

The soil samples used in the study were collected from different talukas of Goa. The samples were collected using core cutter method from the base of the foundation which were approximately at 1.5 m depth. The location of some of the sites from where the soil samples were collected is as shown in Table 1.

Table 1 Location of sites

Soil sample	Location	Latitude	Longitude
Site 1	Housing Board, Gogol, Curtorim, Margao	15°16′47.0″ N	73°59′35.4″ E
Site 2	Behind Korgaonkar Petrol Pump, Fatorda, Margao	15°17′29.5″ N	73°58′37.3″ E
Site 3	Panjifond, Margao	15°16′31.3″ N	73°57′46.4″ E
Site 4	Borda, Margao	15°16′47.9″ N	73°58′28.4″ E
Site 5	Near GEC campus, Donshiwadi, priol, Ponda	15°25′11.0″ N	73°58′59.5″ E
Site 6	Ponda Tisk, Ponda	15°23′37.7″ N	74°00′07.9″ E
Site 7	Mhalshewada, Margao-Belgaum By pass Road, Ponda	15°24′16.4″ N	74°01′51.8″ E
Site 8	Near Margao-Quepem Road, Paroda, Quepem	15°13′19.5″ N	74°03′29.7″ E
Site 9	Pontemol, kakoda, Quepem	15°15′05.4″N	74°07′28.0″E
Site 10	Margao-Chandor-Curchorem Road, Xelvona, Quepem	15°15′52.5′’N	74°05′02.8′’E
Site 11	Near Sanguem-Calem Road (MDR35), Sanguem	15°14′07.4″ N	74°08′58.2″ E
Site 12	Kharkhate Ghati, Cotarli, Sanguem	15°13′44.5″ N	74°07′60.0″ E
Site 13	Near Tilamol-Rivona-Colomb Road, Rivona, Sanguem	15°09′32.3″ N	74°06′57.1″ E

2.2 Laboratory Analysis

The different tests on soil samples were conducted in laboratory-like core cutter test to find density and moisture content; direct shear test to find cohesion (c) and angle of friction (ϕ); specific gravity test, wet sieve analysis to find percentage of gravel and sand; and pipette analysis to find percentage of silt and clay.

2.3 Data Analysis

The data obtained from the above test results were used to find ultimate bearing capacity of soil at different sites. Using the values of ultimate bearing capacity, regression analysis was done using IBM SPSS Statistics 24 Regression analysis and Minitab software.

3 Results and Discussion

Tests were carried out on the soil samples to determine different properties of soil. The tests like density of soil according to IS:2720 (1975: Part 29) [13], moisture content according to IS:2720 (1973: Part 2) [14], specific gravity according to IS:2720 (1981: Part 3: Sect. 3) [15], shear strength (cohesion and angle of internal friction) according to IS:2720 (1986: Part 13) [16], wet sieve analysis (% gravel and % sand) and pipette analysis (% clay and % silt) according to IS:2720 (1985: Part 4) [17] were conducted. The test results of different soil samples for the above properties are as shown in Table 2.

The inputs required to find the ultimate bearing capacity of soil are cohesion, unit weight of soil, depth of foundation, width of footing and angle of internal friction. A square footing of size 2 m × 2 m was considered. The ultimate bearing capacity for each soil sample was determined using Terzaghi's analysis, Hansen's analysis, Vesic's analysis and IS 6403: 1981 code and also using softwares such as SoFA and OptumG2. The values of ultimate bearing capacity are shown in Table 3.

In statistical modelling, regression analysis is a set of statistical processes for estimating the relationships among variables. It includes many techniques for modelling and analysing several variables, when the focus is on the relationship between a dependent variable and one or more independent variables (or predictors). More specifically, regression analysis helps one understand how the typical value of the dependent variables changes when any one of the independent variables is varied, while the other independent variables are held fixed. Multiple linear regression analysis was carried out between the values of ultimate bearing capacity and the soil properties (such as density, specific gravity and grain size distribution) to form an equation using IBM SPSS Statistics 24 Regression analysis and Minitab software. After the comparison was made between manual methods and softwares, it was found that IS 6403: 1981 code values and OptumG2 softwares values of ultimate bearing capacity are similar. Hence IS 6403: 1981 code values of ultimate bearing capacity were used for regression analysis. The independent variables used in regression were density (kN/m^3), specific gravity, gravel (%), sand (%), silt (%), clay (%) and water content (%). Using different combination of variables, regression analysis was done and the combination which gives greater value of coefficient of determination was considered as perfect combination which relates variables well. Using combination of dependent variable as ultimate bearing capacity and independent variables as specific gravity, density, gravel (%), sand (%) and silt (%) an equation was obtained which gives greater value of coefficient of determination from all other combination which were used for regression analysis in IBM SPSS Statistics 24 Regression analysis software. To check whether there was any multiple relation between the variables selected the simple correlations, variance increase factors (VIFs), tolerance value and the condition index (CI) were examined. The values of VIF are shown in Table 4.

When the simple correlations are examined, if variance increase factors (VIF) is equal to or greater than 10, then there are multiple relations between variables

Table 2 Soil test results

Soil sample	Dry density (g/cm^3)	Water content (%)	Specific gravity	Cohesion (kN/m^2)	Angle of friction (in degrees)	Gravel (%)	Sand (%)	Silt (%)	Clay (%)
Site 1	1.45	31.36	2.69	4.807	12.27	6.6	20.0	73.4	0.00
Site 2	1.75	14.99	2.73	12.753	12.13	39.2	39.2	21.6	0.00
Site 3	1.83	14.24	2.57	1.780	17.87	50.0	13.6	36.4	0.00
Site 4	1.64	12.27	2.89	15.696	14.70	36.4	23.4	40.2	0.00
Site 5	1.63	13.44	2.96	10.100	20.68	43.8	38.6	1.4	0.18
Site 6	1.93	15.81	2.69	5.000	13.22	58.4	12.4	28.5	0.71
Site 7	1.57	14.00	2.61	2.330	11.15	15.4	27.6	57.0	0.00
Site 8	1.80	15.51	2.54	5.200	11.86	21.8	29.2	48.4	0.63
Site 9	1.74	9.07	2.67	9.830	10.24	55.4	30.2	14.4	0.00
Site 10	1.50	6.49	2.51	8.400	5.63	0.2	59.2	40.6	0.00
Site 11	1.80	12.76	2.73	13.160	10.26	33.2	30.0	36.8	0.00
Site 12	1.54	9.07	2.55	7.200	7.69	0.4	23.2	76.4	0.00
Site 13	1.77	11.95	2.87	18.400	10.24	18.1	43.9	38.0	0.00

Table 3 Comparison of ultimate bearing capacity using manual method, SoFA and OptumG2

Soil sample	Theory (kN/m^2)					Software (kN/m^2)		
	Terzaghi	Meyerhof	Hansen	Vesic	IS code	SoFA		OptumG2
						Meyerhof	Hansen	
1	111.85	169.98	185.98	193.29	99.96	165.50	178.64	80.55
2	212.75	303.78	329.36	341.53	174.90	297.81	321.87	184.95
3	138.19	281.02	298.98	319.07	148.52	272.18	292.41	144.74
4	272.62	412.82	438.71	467.81	217.05	413.36	445.48	256.56
5	284.48	570.31	567.94	636.72	244.11	565.17	592.52	314.31
6	140.94	224.04	245.92	250.70	130.55	219.38	237.01	124.27
7	81.81	128.91	138.72	143.39	80.47	122.34	131.36	48.72
8	127.37	192.43	210.53	219.87	116.27	186.76	201.38	100.65
9	161.13	217.95	238.54	246.28	136.72	216.67	233.39	126.16
10	110.64	130.59	150.56	143.13	90.18	118.83	135.61	55.99
11	198.27	263.60	288.43	306.07	163.37	262.93	283.65	163.07
12	112.28	143.07	160.81	158.93	93.09	125.08	148.24	64.42
13	245.39	314.62	344.76	365.24	193.75	290.69	338.42	203.98

Table 4 Multiple relations coefficients

Model		Unstandardized coefficients		Standardized coefficients	*t*	Sig.	Correlations			Collinearity statistics	
		B	Std. Error	Beta			Zero-order	Partial	Part	Tolerance	VIF
1	Specific Gravity	260.176	59.272	4.746	4.390	0.003	0.961	0.856	0.199	0.002	566.793
	Density (kN/m^3)	5.690	7.205	0.658	0.790	0.456	0.956	0.286	0.036	0.003	336.478
	Sand (%)	−6.092	2.152	−1.373	−2.831	0.025	0.900	−0.731	−0.129	0.009	114.140
	Gravel (%)	−6.450	2.413	−1.533	−2.673	0.032	0.871	−0.711	−0.121	0.006	159.367
	Silt (%)	−6.944	1.989	−2.130	−3.492	0.010	0.766	−0.797	−0.159	0.006	180.449

[12] and from Table 4, it can be seen that VIF values for all are greater than 10. In addition to these, if tolerance values are greater than 0.10, no multiple relations between variables are decided [12]. It can be seen from Table 4 that all tolerance values are less than 0.10. The absolute value β (beta) in Table 4 indicates the order of importance of the independent variables. The variable with the highest β value is relatively the most important variable. The CI values are shown in Table 5.

In cases where the CI value is greater than 30, it is regarded that there are multiple relations between variables [12]. Yet, as it is clear from Table 5, the CI values calculated are greater than 30. Thus, it can be concluded that there were multiple relations between the variables. The summary of the model according to ANOVA statistics is shown in Table 6.

In consequence of the standard regression analysis, the model's degree of predicting dependent variable, that is, correlation coefficient was found to be $R = 0.993$. The model's degree of explaining the variance in the dependent variable, that is, coefficient of determination was found to be $R^2 = 0.986$. Hence, the model predicts the dependent variable very well. Based on the regression analysis result, the regression equation was obtained as shown in Eq. 1:

$$\text{UBC} = 260.176X_1 + 5.690X_2 - 6.092X_3 - 6.450X_4 - 6.944X_5 \quad (1)$$

where UBC = ultimate bearing capacity, X_1 = specific gravity, X_2 = density (kN/m^3), X_3 = sand (%), X_4 = gravel (%), X_5 = silt (%).

Values used for regression analysis (observed UBC, that is, values obtained from IS 6403: 1981 code) and values obtained from Eq. 1 of regression analysis (predicated UBC) are tabulated in Table 7 and graph of observed UBC versus predicated UBC is shown in Fig. 1.

To verify the results obtained using IBM SPSS Statistics 24 software, Minitab was used. The test results which were used as input for regression analysis in IBM SPSS Statistics 24 software were used in Minitab software. The result of regression analysis obtained using Minitab software is shown in Table 8.

When the correlations were examined with Minitab software, from Table 8, it can be seen that VIF values for all terms are greater than 10 (Gulden et al. 2013). The result of regression analysis obtained using Minitab software is shown in Table 9.

From Table 9, the coefficient of determination was found to be $R^2 = 98.56\%$. The regression equation was obtained as it is shown in Eq. 2:

$$\begin{aligned}\text{UBC}\left(\text{kN/m}^2\right) &= 5.69\,\text{Density}\left(\text{kN/m}^3\right) + 260.2\,\text{Specific Gravity} \\ &\quad - 6.45\,\text{Gravel}\,(\%) - 6.09\,\text{Sand}\,(\%) - 6.94\,\text{silt}\,(\%)\end{aligned} \quad (2)$$

The regression equations obtained from IBM SPSS Statistics 24 software and Minitab software are the same.

Table 5 Multiple relations between CI values

Model	Dimension	Eigenvalue	Condition index	Variance proportions				
				Density (kN/m^3)	Specific gravity	Gravel (%)	Sand (%)	Silt (%)
1	1	4.336	1.000	0.00	0.00	0.00	0.00	0.00
	2	0.474	3.025	0.00	0.00	0.01	0.00	0.00
	3	0.186	4.826	0.00	0.00	0.00	0.03	0.01
	4	0.003	39.024	0.68	0.19	0.05	0.01	0.02
	5	0.001	65.793	0.32	0.81	0.94	0.96	0.97

Table 6 Model summary

Model	*R*	*R* square	Adjusted *R* square	Std. Error of the estimate
1	0.993	0.986	0.975	23.11

Table 7 Observed and predicated values of ultimate bearing capacity

S. No	Observed UBC (kN/m^2)	Predicted UBC (kN/m^2)	Error
1	99.96	108.28	−8.32
2	174.90	168.22	6.68
3	148.52	114.67	33.86
4	217.05	188.74	28.31
5	244.11	224.24	19.87
6	130.55	159.64	−29.09
7	80.47	105.12	−24.65
8	116.27	108.89	7.38
9	136.72	152.37	−15.65
10	90.18	94.53	−4.35
11	163.37	160.26	3.11
12	93.09	76.64	16.45
13	193.75	199.38	−5.63

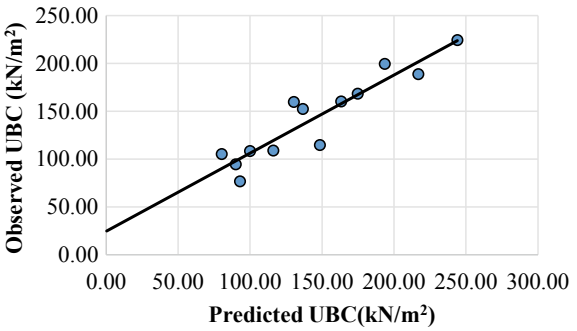

Fig. 1 Graph of observed UBC versus predicated UBC

Table 8 Multiple relations coefficients

Term	Coefficients	SE coefficients	*T*-value	*P*-value	VIF
Density (kN/m^3)	5.69	7.20	0.79	0.456	336.48
Specific gravity	260.2	59.3	4.39	0.003	566.79
Gravel (%)	−6.45	2.41	−2.67	0.032	159.37
Sand (%)	−6.09	2.15	−2.83	0.025	114.14
Silt (%)	−6.94	1.99	−3.49	0.010	180.45

Table 9 Model summary

Std. error of the estimate	*R*-square	*R*-square adjusted	*R*-square predicated
23.1117	98.56%	97.53%	95.63%

4 Conclusion

The ultimate bearing capacity of selected soil samples were determined using Terzaghi, Hansen, Meyerhof, Vesic and IS: 6403-1981 code methods and were compared with OptumG2 and SoFA softwares. The IS 6403:1981 code comparatively matched the software results. The relationship between the soil properties and ultimate bearing capacity of square footing was determined. The regression analysis was performed using values of ultimate bearing capacity obtained using IS 6403: 1981 code and soil properties (specific gravity, density, gravel (%), sand (%) and silt (%)). Regression analysis was done using IBM SPSS Statistics 24 software and was verified using Minitab software. The variance increase factor (VIF) values for all the variables were greater than 10, and also the tolerance values were less than 0.10. The condition index (CI) values obtained were greater than 30. The values of variance increase factor (VIF), tolerance and condition index (CI) state that there are multiple relations between dependent variables and independent variables. The correlation coefficient was found to be $R = 0.993$ and the coefficient of determination was found to be $R^2 = 0.986$. Hence, the model predicts the dependent variable very well. The results obtained from Minitab software and the regression analysis are similar. The relationship between density, specific gravity, grain size distribution and ultimate bearing capacity is valid for locations in the vicinity of the collected soil samples, and for more accuracy data analysis has to be done on more number of soil samples.

References

1. Venkatramaiah C (2006) Geotechnical engineering, 3rd edition. New Age International (P) Limited, Publishers, pp 607–613
2. Meyerhof GG (1951) The ultimate bearing capacity of foundations. Geotechnique 2:301–332
3. Terzaghi K (1928) Theoretical soil mechanics. Wiley, New York
4. Brinch Hansen J (1961) A general formula for bearing capacity. Bulletin No.11, Danish Technical Institute, Copenhagen, Denmark, pp 38–46
5. Vesic AS (1973) Analysis of ultimate loads of shallow foundations. J Soil Mech Found Div (1973)
6. IS: 6403-1981 (1981) Code of practice for determination of bearing capacity of shallow foundation. Bur Indian Stand
7. Nikolaou K (2016) SoFA: a matlab-based educational software for the shallow foundation analysis and design. https://www.sofastatistics.com/
8. OptumG2 (2018) Optum computational engineering. Version 2018.07.28, Denmark. https://www.optumce.com/

9. Adunoye GO, Agbede OA (2013) Statistical modelling of the relationship between bearing capacity and fines content of soil using square footing. Civ Environ Res 3(2):75–81
10. IBM SPSS Statistics 24 (2016) IBM corporation, Version 24. https://www.spss.com/
11. Minitab® 19 (2019) Minitab statistical software, Version 19.1.1. https://www.minitab.com/
12. Uyanik GK, Guler N (2013) A study on multiple linear regression analysis, 4th international conference on new horizons in education. Procedia Soc Behav Sci 106:234–240
13. IS: 2720-29 (1975) Determination of dry density of soils in-place by the core-cutter method. Bur Indian Stand (1st Revision)
14. IS: 2720-2 (1973) Determination of water content. Bur Indian Stand (2nd Revision)
15. IS: 2720-3-1 (1981) Determination of specific gravity. Bur Indian Stand (1st Revision)
16. IS: 2720-13 (1986) Direct shear test. Bur Indian Stand (2nd Revision)
17. IS: 2720-4 (1985) Grain size analysis. Bur Indian Stand (2nd Revision)

Recent Trends in Transportation Engineering

Experimental Investigations on RBI Grade 81 Stabilized Lateritic Soil

B. A. Chethan, Saswati Das, S. Amulya, and A. U. Ravi Shankar

Abstract The effectiveness of the addition of RBI Grade 81 (stabilizer) (dosages of 2, 4, 6, and 8%) to stabilize the largely encountered lateritic soil during construction was investigated. Stabilized lateritic soil mixes were evaluated by conducting a series of experiments, viz., standard and modified compaction, unconfined compressive strength, and California bearing ratio at various curing periods. Mixes under both standard and modified compaction energies have shown the highest density at a 6% stabilizer dosage. A remarkable increase in unconfined compressive strength was observed for the specimens prepared at a 6% stabilizer dosage corresponding to the modified compaction density. An increase in the percentage of stabilizer has increased the California bearing ratio of treated mixes. Exorbitant increase in the soaked California bearing ratio values of the stabilized mixes was observed for higher dosages (6 and 8%). Hence, RBI Grade 81 amended lateritic soil mixes enhance the strength of the subgrade.

Keywords Soil stabilization · RBI grade 81 · Lateritic soil · Unconfined compressive strength · California bearing ratio

1 Introduction

Construction of the highway usually requires the use of in situ or ex situ soil modification techniques to improve its physical and engineering properties. Soil stabilization is a technique that enhances the shear strength and bearing capacity of weak soils [1]. In most cases, in situ soil fails to take the traffic wheel load due to its insufficient capacity. Stabilization can improve the soil to bear extreme weather and traffic conditions in the case of highway pavement. Common additives used to modify the soil from ancient times are lime, cement, and other marginal materials like fly ash, rice husk ash, and so on, with and without cementitious compounds.

B. A. Chethan (✉) · S. Das · S. Amulya · A. U. R. Shankar
Department of Civil Engineering, NITK Surathkal, Mangaluru 575025, India
e-mail: chethanba@gmail.com

B. B. Das et al. (eds.), *Recent Trends in Civil Engineering*, Lecture Notes in Civil Engineering 105, https://doi.org/10.1007/978-981-15-8293-6_27

RBI Grade 81 is an inorganic natural soil stabilizer that can promote the strength properties of weak soil and make it suitable for use in highway pavements. It is a patented product in India. Several naturally occurring compounds are blended to form a powder which can be used for the construction of low-cost roads. Its faster application rate is helpful for opening the stabilized layer to the traffic within a day of compaction. A wide range of soils can be stabilized, which makes it advantageous compared to the other stabilizers. Along with the enormous increase in strength of the pavement, it saves 30–40% of construction cost and 60% of borrow soil transportation cost.

Marginal and natural materials can be blended with RBI Grade 81 to improvise the weak soil. Fair to very good volume stability was observed for stabilizer admixed soil containing the fine silt to coarse sand size particles [2]. It forms a complex framework between soil particles by interconnecting them. The higher the stabilizer dosages, the greater is the California bearing ratio (CBR) and unconfined compressive strength (UCS) of treated and cured soils [3, 4].

Along with the reduction in the plasticity index, beyond a 6% dosage, a fair increase in UCS and a drastic increase in CBR were obtained for treated soil [5]. Along with the increase in density, at 28 days of curing with 5% stabilizer dosage a peak CBR value of 19%, and till 4% stabilizer dosage considerable increase in UCS was observed for expansive soil [6]. However, the highest UCS and CBR values were attained at 6% stabilizer dosage for black cotton (BC) soil [7], plastic clay [8], and highly compressible clay [9].

CBR and UCS of the soil can be effectively increased with the addition of this stabilizer [10]. A significant dosage of 6% stabilizer can effectively increase the UCS and CBR value on 4 days soaking as per recommended IRC limits [5, 11]. Lateritic and BC soil properties were found to improve with the addition of this stabilizer [12]. On curing till 28 days, the UCS and CBR values were increased by 250 and 400% compared to the soil without stabilizer, and this stabilizer application has found to have potential due to its strength improving properties with the increasing dosages [13]. Admixed kaolinite, red soil, and lateritic soil with 2–8% exhibited considerable improvement in CBR strength [14].

The process of stabilization by RBI grade is dominated by CaO, Al_2O_3, and SiO_2 [7]. The CSH and CAH gel formation were observed from the SEM images for cement kiln dust, and RBI Grade 81 treated clayey soil, which resulted in the improvement of UCS and CBR values [15]. Reduced pore spaces due to micro-level structural changes and changes in elemental composition were responsible for the improvement in the strength of the treated soil [9]. The higher the CaO/SiO_2 ratio, the more is the pozzolanic reaction, and hence more effective is the stabilizer [17]. However, in spite of the higher CaO/SiO_2 or $CaO/(SiO_2 + Al_2O_3)$ ratio, the binders can still be ineffective due to lower CaO, SiO_2, and/or Al_2O_3 content available for pozzolanic reactions [16].

From the above-mentioned literature, it is evident that RBI Grade 81 is applied as a stabilizer on different types of soils. But the limited literature is available on the strength and durability of these mixes. In this laboratory study, lateritic soil is admixed with 2% stepped concentrations of stabilizer up to 8% to identify the variations in

chemical and mechanical properties of soil. The following sections include the details of materials used, experiments conducted, and mechanical property variations of treated soil.

2 Materials

2.1 Lateritic Soil

The soil used for the present investigation is procured as a disturbed sample from the borrow pits at Surathkal, India. The collected soil is crushed using the rubber hammer to separate particles from its lump state. Then the soil is oven-dried at 105–115 °C and secured in moisture free containers. The soil sample is then subjected to various tests to evaluate its index properties according to the Indian Standard codes of practice. Test properties are shown in Table 1, according to the Indian Standard soil classification system and this soil belongs to SM (silty sand) group.

2.2 RBI Grade 81

RBI Grade 81 is an odorless powder having a light brown color that can be used for improving properties of lateritic soil. It is a commercial product, which is collected from the local market. It reacts in the presence of soil pore water and forms a rigid mass by binding the particles together. It is having a specific gravity of 2.5, pH of 12.5, with 98% fines (<75 μ IS sieve size, i.e., silt size and clay size range particles). It is inert, chemically stable, insoluble in water, and non-degradable if exposed to UV radiation. Its acceptability in the binding of wide range soils, in addition to its low cost, durability, and simple application procedures, recognize it as a viable option for soil stabilization.

3 Methods

Samples of lateritic soil, RBI Grade 81, and stabilized lateritic soil were subjected to laboratory tests to find the index properties, particle size distribution, soil classification, specific gravity, and compaction characteristics by following the procedures outlined in Indian Standard codes. The UCS tests were carried out following the procedures outlined in IS: 2720 (Part 10), 1991 on desiccator cured samples. The CBR tests were conducted following the procedure outlined in IS: 2720 (Part 16), 1987, which is useful for the design of pavement. The stabilizer is stepped in concentrations of 2%, up to 8% to evaluate the improvement on the strength and durability

Table 1 Lateritic soil properties

Property	Value	Code of practice followed
Specific gravity, G	2.66	IS: 2720 (Part III/Sec- 1), 1985
Gravel size (%) Sand size (%) Silt size (%) Clay size (%)	22 45 31 2	IS: 2720 (Part IV), 1985 (From Wet Sieve analysis)
Liquid limit (%) Plastic limit (%) Plasticity index (%)	36 27 9	IS: 2720 (Part V), 1985
Classification of soil	SM	IS:1498–1970
Standard proctor compaction		
OMC (%) MDD (g/cc)	12.9 1.95	IS: 2720 (Part VII), 1980
Modified proctor compaction		
OMC (%) MDD (g/cc)	13.1 2.09	IS: 2720 (Part VIII), 1983
UCS (kPa)		
@ (OMC-2%) @ OMC @ (OMC + 2%)	227 589 306	IS: 2720 (Part 10), 1991
CBR (@ Modified Proctor compaction)		
Un soaked (%) Soaked (%)	49 18	IS: 2720 (Part 16), 1987
Durability		
Wet-Dry cycle Freeze–Thaw cycle	Failed in 5 h wetting 6.4% weight loss	ASTM D559 ASTM D560

characteristics under wet-dry and freeze–thaw cycles with a hike in dosages. The use of these indices was considered because of their importance for the highway design and construction in India. Mixing of soil and stabilizer is initially carried out in the dry state. To this homogeneous mixture, a known amount of OMC is added, and the mixing is continued until the uniform distribution of moisture is ensured. The resulting homogeneous mixture is then molded into the required specimens.

Table 2 Chemical composition of lateritic soil, 6% treated lateritic soil and RBI Grade 81

Material	SiO_2	Al_2O_3	Fe_2O_3	CaO	MgO	SO_3	pH	Conductivity (ms)
Lateritic soil	65.8	11.9	3.3	5.1	2.2	0.008	10.1	1.2
6% RBI Grade 81 treated Lateritic soil	58.8	16.9	3.8	6.4	3.5	0.28	10.4	1.23
RBI Grade 81	15–19	5–7	0–2	52–56	0–1	9–11	12.5	–

4 Test Results and Discussions

4.1 Chemical Analysis

Soil considered in the investigation contains 76% of silt to coarse sand-size particles; therefore, it can be considered to be suitable for RBI Grade 81 treatment. The chemical constituents of materials used and stabilized mix are presented in Table 2.

The formation of cementitious chemical compounds leading to the development of the crystalline matrix is observed on stabilization. The alkalinity of the soil has increased on stabilizer treatment, which liberated SiO_2 and Al_2O_3 from both soil and stabilizer. Further, Ca ions reacted with this liberated SiO_2 and Al_2O_3, leading to the formation of irreversible calcium aluminum silicate (CAS) compounds. Admixed soil has increased SiO_2 and Al_2O_3 and CaO contents, effectively forming CAS compounds on the chemical reaction. Stabilized soil is found to increase the CaO/SiO_2 ratio from 0.07 to 0.11 at 6% RBI Grade 81 treatment when compared with soil. Similarly, $CaO/(SiO_2 + Al_2O_3)$ ratio has increased from 0.064 to 0.085 at the same dosage.

4.2 Compaction

Standard proctor compaction is used for the design of low volume roads (<1 msa) and modified proctor compaction for high volume roads by the Indian Road Congress. The variation in OMC and MDD under both compaction energies for stabilizer stepped mixes from 0 to 8% with an increment of 2% is presented in Fig. 1a and b. Initially, OMC and MDD were decreased by 2% of stabilizer addition. Above this dosage soil stabilizer, reaction demanded a greater amount of water, leading to an increase in OMC. Void spaces filled by RBI Grade 81 till 6% dosage has increased MDD of soil. But the excess lighter stabilizer particles at 8% dosage after filling up the void spaces reduced MDD. Standard and modified compaction resulted in the highest MDD of 1.99 and 2.13 g/cc, respectively, at 6% stabilizer dosage, hence taken as optimum dosage.

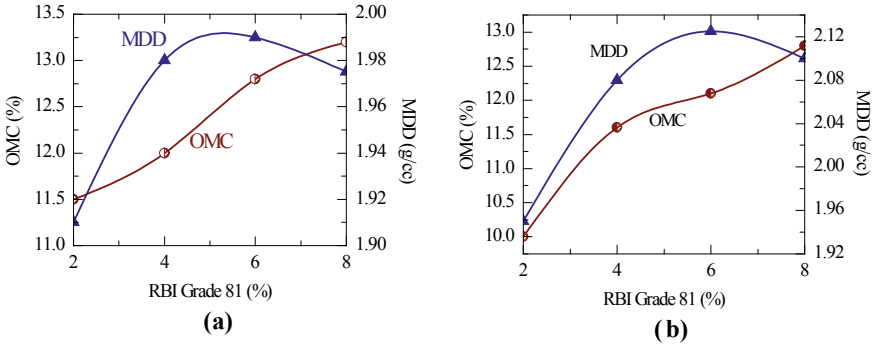

Fig. 1 Variation of **a** standard and **b** modified compaction characteristics of RBI Grade 81 admixed Lateritic soil

4.3 Unconfined Compressive Strength

RBI Grade 81treated soil was tested for UCS as per IS: 4332 (Part 5)-1970 on 7, 14, 28, and 60 days of curing periods only at modified proctor densities. The variations of UCS values at OMC and ± 2% of OMC with different stabilizer dosage and curing periods are represented in Fig. 2a–c. This deviation of ±2% water content may be encountered during construction in the field.

Variation of the water content of desiccator cured specimens due to evaporation or absorption of moisture might have resulted in a slight variation of UCS values of the specimens. Absorption of free moisture during curing might have resulted in the reduction of UCS of samples. Higher UCS values were observed for the samples prepared at OMC compared to those prepared at OMC ± 2%. At 60 days curing a maximum UCS of 4414 kPa was achieved for 6% stabilizer treatment. Similar studies on expansive soil proved that 6% RBI Grade 81 resulted in considerable improvement in UCS [8].

4.4 California Bearing Ratio

Effect of curing period on the strength of the RBI Grade 81 admixed soil samples was analyzed by preparing the CBR specimens. Compacted samples were covered in polythene covers to avoid moisture loss and were cured for 7, 14, and 28 days. Cured samples were then immersed in water for four days to simulate the saturated field condition during the rainy season, and are tested to know the CBR strength.

The soil particles found to aggregate due to the reaction of RBI Grade 81 that happened with the curing period. Hence, even when these mixes were immersed in water, they did not lose the strength and exhibited greater resistance to plunger penetration. The soaked CBR value of stabilizer stepped soil has increased above 90%

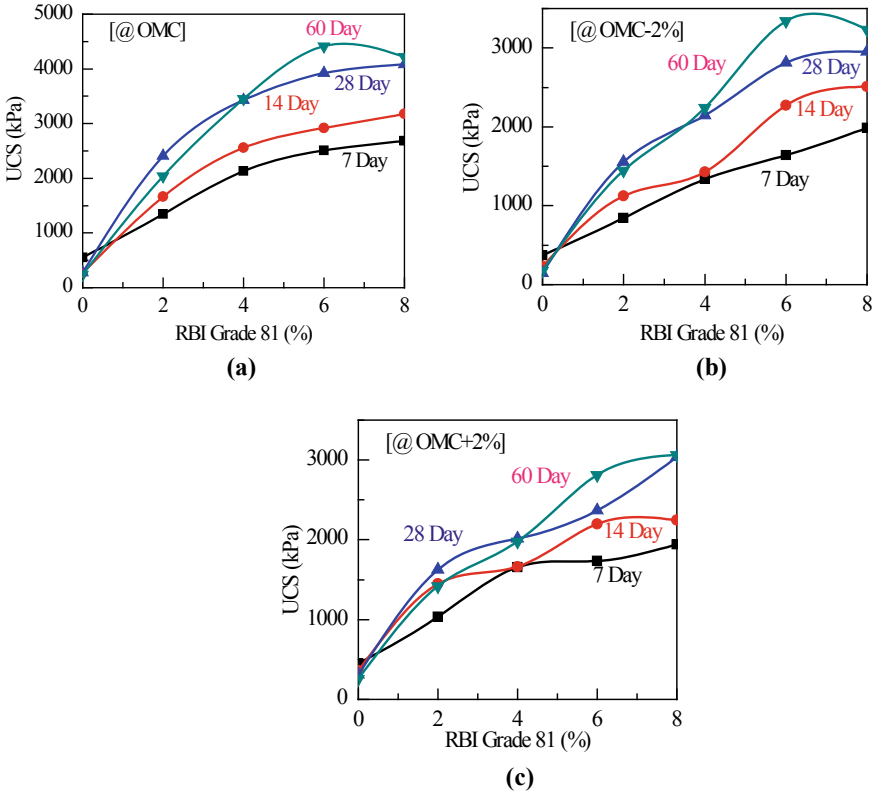

Fig. 2 UCS variation of RBI Grade 81 admixed lateritic soil at **a** OMC **b** OMC-2% **c** OMC + 2%

with an 8% dosage, as shown in Fig. 3, which gives a clear picture of soil binding and lowered void spaces due to cementation. Even though stabilization imparts greater strength improvement to the soil, IRC recommends the use of durability tests for the suitability of the material for the pavements.

4.5 Durability

A soil in its natural state, if not stabilized and compacted, may not be able to withstand the adverse weather conditions like wetting–drying and freezing–thawing during the continuous cyclic natural seasonal changes. Hence, there is a necessity of stabilizing the weak soils to resist these changes. If the stabilized soil can withstand these crucial changes with minimal variation, they can give the best support to the pavement without leading to the deterioration. Hence, 7-day desiccator cured stabilized soil specimens (38 mm diameter and 76 mm height) were subjected to the durability tests.

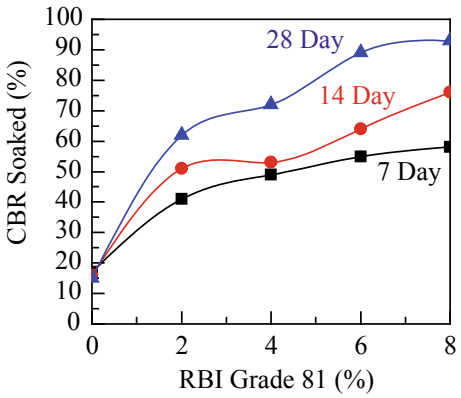

Fig. 3 Variation of CBR of RBI Grade 81 stabilized lateritic soil with curing period

During the wet-dry cycle, the lateritic soil specimen could withstand only 5 h of wetting before failure. However, stepped concentrations of stabilizer has made lateritic soil stronger with the curing period. These samples were failed during the 2nd, 3rd, and 11th cycles at 2, 4, and 6% dosages, respectively. However, the specimen prepared at 8% RBI Grade 81 dosage has shown resistance to the disintegration even after 12 cycles. But soil samples with 6 and 8% stabilizer dosage have exceeded the weight loss limit of 14% (ASTM D559) after the 8th and 9th cycle. Therefore, stabilizer treatment can be given due consideration for improving the lateritic soil in the low rainfall areas. The incremental weight loss with each wet-dry cycle for the soil specimens with stepped concentrations of stabilizer was depicted in Fig. 4a–d. This increase in resistance was offered by the cementation of soil particles with increased RBI Grade 81 dosages, making the mix less susceptible to the changes caused by water.

During the winter season, the subsoil may be subjected to subzero temperatures, leading to the formation of ice crystals from the capillary water, further excreting pressure on the compacted stabilized soil mass. The subsequent increase of the temperature causes these ice crystals to melt to form again pore water. These changes, if repeated in stabilized subgrades, may induce internal stresses leading to the failure. RBI Grade 81 stepped mixes when subjected to these cycles have shown increased resistance with a higher dosage. Cementation of soil particles filled the pore spaces of soil showing the resistance to the capillary rise of water. Hence, all the mixes were found to be resistant against the freeze–thaw cycles with weight loss within the limit of 14% (ASTM D560), as depicted in Fig. 5a–d.

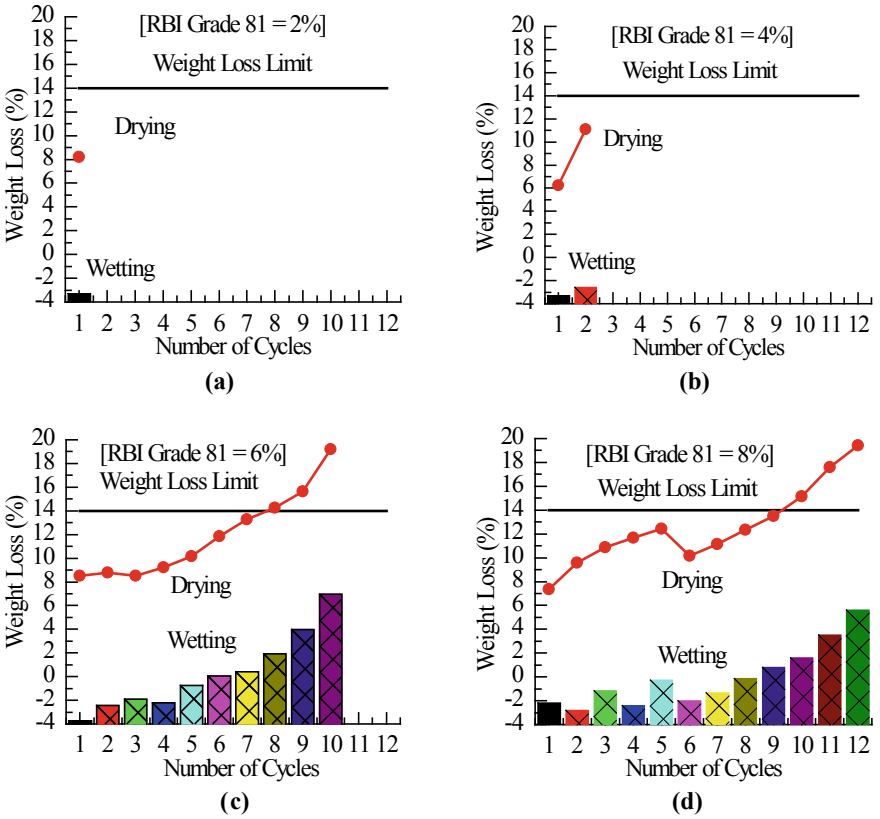

Fig. 4 Weight loss of RBI Grade 81 admixed lateritic soil samples during alternate wet-dry cycles

5 Conclusions

1. The highest density of RBI Grade 81-lateritic soil mix is obtained at 6% dosage due to filling up of void spaces. But, a further increase in dosage resulted in depletion of density due to the replacement of heavier soil particles by lighter stabilizer particles.
2. Even small changes in CaO/SiO_2 and $CaO/(SiO_2 + Al_2O_3)$ dominated the strength improvement of the soil-stabilizer mixes due to the formation of CAS compounds.
3. Soil-stabilizer mixes chemically reacted to form pozzolanic compounds resulting in a considerable increase in UCS value at higher stabilizer dosages. Mixes at OMC have shown higher UCS compared to specimens at ± 2% OMC.
4. RBI Grade 81 stabilization has clearly shown a manifold increase in soaked CBR value with the curing period compared to lateritic soil.

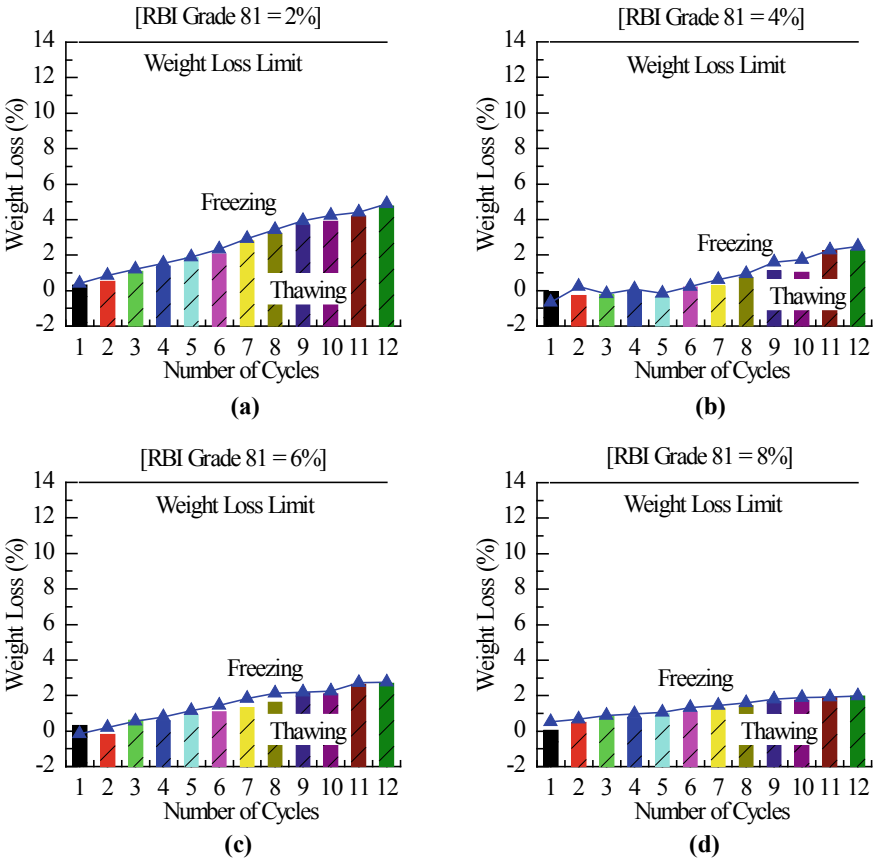

Fig. 5 Weight loss of RBI Grade 81 admixed lateritic soil samples during alternate freeze–thaw cycles

5. At 6% stabilizer dosage durability samples passed 8 wet-dry cycles. Whereas, at 8% dosage samples passed 9 cycles, which clearly indicates increased cementation and bonding of particles leading to lower water susceptibility of stabilized mixes.
6. All samples of soil and soil-stabilizer mixes passed freezing–thawing tests. The higher the dosage, the lower is the observed weight loss.

References

1. Kumar KSP, Ashok Kumar M, Darga Kumar N (2017) Prophecy of plate load test response from theory of elasticity solution and CBR test. Jordan J Civ Eng 11.3
2. Kodicherla SPK, Nandyala DK (2017) Effect of RBI grade 81 on strength characteristics of clayey subgrade. Int J Geo-Eng 8.1(2017):24
3. Madurwar KV, Dahale PP, Burile AN (2013) Comparative study of black cotton soil stabilization with RBI Grade 81 and sodium silicate. Int J Innovative Res Sci Eng Technol 2(2):493–499
4. Muktinutalapati J, Kumar DN, Prashanth SKK (2016) Influence of Zycosoil on consolidation, shear strength characteristics and permeability of clayey subgrade. September, 2016
5. Venugopal G, Chetan Fakkerappa B (2014) Studies on black cotton soil stabilization using RBI Grade-81. Int J Innov Res Sci Eng Technol 3.12 (2014):18205–18210
6. Kumar K, Solanki AJ (2017) Evaluation of RBI grade 81 for stabilization of expansive soil as sub-grade material. Mater Today: Proceedings 4(9):9737–9741
7. Lekha BM, Ravi Shankar AU (2014) Laboratory performance of RBI 81 stabilized soil for pavements. Int J Civ Eng Res 5.2 (2014):105–110
8. Bernadette CJ et al (2017)Laboratory study on subgrade soil stabilization using RBI grade 81. In: IOP conference series: earth and environmental science, vol 80. No. 1. IOP Publishing
9. Gunturi M et al (2014) Effect of RBI-81 on CBR and swell behavior of expansive soil. Int J Eng Res ISSN. pp 2319–6890
10. Jayatheja M, Kumar ND, Kumar SPK (2016) Influence of zycosoil on consolidation, shear strength characteristics and permeability of clayey subgrade. In: 10th international conference on lowland technology, Manglore
11. IRC-37 (2012) Guidelines for the design of flexible pavements (Third Revision)
12. Mamta A, Mallikarjun H (2014) Using RBI Grade 81, a comparative study of black cotton soil and lateritic soil. Int J Res Eng Technol 3(3):613–616
13. Haricharan TS et al (2013) Laboratory investigation of expansive soil stabilized with natural inorganic stabilizer. Int J Res Eng Technol 2(13):201–204
14. Anitha KR, Ashalatha R, Johnson AS (2009) Effects of RBI Grade 81 on different types of subgrade soil. In: Proceeding of 10th national conference of technological trends (NCTT 09)
15. Kumar JS, Janewoo U (2016) Stabilization of expansive soil with cement kiln dust and RBI grade 81 at subgrade level. Geotech Geol Eng 34.4(2016):1037–1046
16. Odadjima H et al (1995) Cement stabilization of peaty ground with consideration of organic matter. In: Proceeding of international workshop on engineering characteristics and behavior of peat
17. Janz M, Johansson SE (2002) The function of different binding agents in deep stabilisation: report 9. Linkoping, Sweden Report 9:44

Effect of Ggbs on Strength of Aluminium Refinery Residue Stabilized by Alkali Solution

Nityanand Kudachimath, H. M. Raviraj, and Bibhuti Bhusan Das

Abstract In the present study aluminium refinery residue (ARR), that is, solid waste generated in the production of alumina also known as red mud, was stabilized with ground granular blast furnace slag (GGBS), silica modulus and Na_2O content. The prime chemical composition of aluminium refinery residue is Fe_2O_3, Al_2O_3, SiO_2 and Na_2O. ARR is a highly alkaline waste. This study describes laboratory study, and the characterization of ARR can be utilized in the materials which are used for road construction. The unconfined compression strength tests were conducted on various proportions of mixes of ARR and GGBS 80% + 20%, 75% + 25% and 70% + 30% and silica modulus (0.5, 1 and 1.5) for different Na_2O content. The UCS specimens were cured for 0, 7 and 28 days to observe the effect of longstanding curing. Based on the laboratory investigations, it was found that 75% ARR + 25% GGBS with 4% Na_2O content increases MDD and decreases OMC content. The most appropriate mix 75% AAR + 25% GGBS with 1 silica modulus was observed with a 308.6% increase in UCS value for 28 days of curing. Higher strength is achieved if longer curing periods allowed.

Keywords Aluminium refinery residue (ARR) · Red mud · GGBS · Silica modulus · UCS test

N. Kudachimath (✉)
Research Scholar, Department of Civil Engineering, National Institute of Technology Karnataka, Surathkal, 575025, Mangaluru, India
e-mail: nskudachimath@gmail.com

H. M. Raviraj
Assistant Professor, Department of Civil Engineering, National Institute of Technology Karnataka, Surathkal, 575025, Mangaluru, India

B. B. Das
Associate Professor, Department of Civil Engineering, National Institute of Technology Karnataka, Surathkal, 575025, Mangaluru, India

B. B. Das et al. (eds.), *Recent Trends in Civil Engineering*, Lecture Notes in Civil Engineering 105, https://doi.org/10.1007/978-981-15-8293-6_28

1 Introduction

Huge quantities of waste materials are generated each and every year due to swift industrialization. One such waste is aluminium refinery residue, which is a byproduct produced at the time of alumina extraction from bauxite ore. More than 1 ton of aluminium refinery residue (ARR) is produced per ton of alumina extraction, and the quantity of ARR depends on the quality of the bauxite ore. Samal et al. [1]. The presence of heavy metals and high alkalinity in ARR make it difficult to dispose it off, as it causes severe environmental issues. Hence, there is a need of safe disposal of aluminium refinery residue. Zhang et al. [2] has described that ground granulated blast furnace slag (GGBS) can be extracted from the blast furance as the byproduct while producing the iron. The byproduct consists of the aluminates of calcium, silicates and other bases. Both ARR and GGBS are rich in chemicals required for alkali activation and Davidovits explained that geopolymerization is obtained from the chemical reaction between the alkali poly-silicates and alumino-silicate oxides. As a result of this reaction, the polymeric Si–O–Al bonds are generated.

The present study states that two major industrial wastes such as aluminium refinery residue and GGBS are used to check their basic chemical and geotechnical properties. Its properties make it extremely difficult to work with and to dispose it off. ARR is a highly alkaline waste. Thus, by adding small amounts of alumino-silicate rich material, it can be solidified. The compaction characteristics were studied for each combination of GGBS, silica modulus and Na_2O content with the ARR. Moreover, the mechanical strength of the same has been studied for different curing periods.

2 Literature Review

Various researches have worked in the area of stabilizing the red mud either by mixing the other wastes generated by the industries or by chemicals. Kusum et al. [3] briefed the strength of the red mud by mixing 1% of gypsum and various percentage of the lime. The test outcomes reveal that 1% of gypsum and 12% of lime has exhibited higher CBR numbers for a curing of 7 days and UCS. Satayanarayana et al. [4] observed that adding 10% lime and curing for 28 days is an effective way of stabilization of red mud. Jian et al. (2013) had invented a new type of geopolymerization by combining the red mud and ash of the rice husk, and concluded by saying that the compressive strength of the mixture varied in the range of 3.2–20.5 MPa. Walid et al. [5] had used the mixtures such as metakaolin, red mud and sodium silicate solution to prepare a new component named geopolymer. This new mixture acts as an alkali activator. It is observed that lesser quanity of the red mud is employed while making mixture and if cured for longer period gives higher values of compression strength. Singh et al. [6] worked on various proportions of red mud and GGBS stabilized with alkali solution (NaOH) and found mechanical strength properties for various curing

days. By adding NaOH, the strength of red mud enhances remarkably after 60 days of curing. Zhang et al. [2] had developed the geopolymer which can be used for fly ash of class F, red mud, and found 28 days UCS of about 11.3–21.3 MPa. Lakshmi et al. [7] has taken attempts to investigate the stabilization process with cement. High strength values are obtained at 28 days for all percentages of cement, that is, at 10% it is 110 kg/cm^2 and at 20% it is 175 kg/cm^2.

Researches have shown that the geotechnical properties of red mud can be increased by stabilizing the mixture with lime, gypsum, flyash, GGBS, cement kiln dust. Slag or any other materials having aluminium oxide and silicon dioxide in their composition can be considered as binders. Sodium silicate and sodium hydroxide are better activators without side effects. Percentage of sodium oxide is important for forming poly-sialate reaction of Al and Si molecules. Considering both red mud and GGBS gives us the information about enhancement of strength. Better mix combination can be selected out of the trials.

3 Materials

The aluminium refinery residue was collected from The Hindustan Aluminum Corporation (HINDALCO Industries Ltd), Belagavi. GGBS was collected from JSW Ltd, Ballary. The materials were oven dried at 105–110 °C to remove the moisture in it. The GGBS has been sieved through 75 μ IS sieve and was used for the project work. By sustaining the purity of 98%, the pellets of sodium hydroxide are prepared. To ensure complete dissolution of NaOH pallets, the solution was prepared before 24 h. And the liquid sodium silicate solution was procured from Shanti Chemical Works, Belagavi.

The properties of the waste materials are determined as per relevant Indian Standard specifications. GGBS is added with different percentages (i.e. 20, 25 and 30%) of the total solid, that is, mixture of ARR and GGBS. The maximum dry densities (MDD) and optimum moisture contents (OMC) for all the mixes are obtained by light and heavy compaction test as per the rules provided in IS (specified in Part VII) in the year 1980. The unconfined compressive strength (UCS) of all the mixes, compacted to their respective MDD at OMC, is determined as per the rules of IS 2720 (Part X) stated in the year 1991. The 38 mm diameter and 76 mm height specimens were collected to perform the cylindrical test. These samples are tested after performing the curing on the 0, 7th and 28th day. Further, the effect of additional alkali on compressive strength of the ARR-GGBS mixture has been studied with various silica modulus, that is, 0.5, 1 and 1.5. Properties of both ARR and GGBS are presented in Table 1 and the composition of ARR is provided in Table 2.

Table 1 Briefs the ARR and GGBS's properties

Properties	ARR	GGBS
Specific gravity	3.1	2.8
Optimum moisture content (%)	30	18
Curvature coefficient (C_c)	1.4	1.2
Maximum dry density (gm/cc)	1.6	1.4
Plastic limit	32	–
Unconfined compression test (MPa)	0.2	0.28
Liquid limit	36	32
Coefficient of uniformity (C_u)	3.2	2.4
Plasticity index	3	–

Table 2 Composition of aluminium refinery residue

Composition	Percentage (%)
Fe_2O_3	36.10
Al_2O_3	22.10
SiO_2	12.20
Na_2O	7.26
CaO	1.30
TiO_2	9.31
V_2O_5	0.31
LOI	10
P_2O_5	0.27

4 Results and Discussions

4.1 Measure of Maximum Dry Density (MDD) and Optimum Moisture Content (OMC)

The MDD and OMC of all the combinations were determined by light compaction test (standard proctor) and heavy compaction (modified proctor) test. The results are presented in the form of a graph. From the compaction test of ARR-GGBS mixture, it is detected that the percentage of GGBS has been increased up to 25%, the maximum dry density increases and further addition of GGBS which resulted in decreased maximum dry density. The highest maximum dry density value is observed in 75% red mud and 25% GGBS with 1 silica modulus at 4% Na_2O content, which is 1.95 g/cc (Graph 1).

For 4% Na_2O, aluminium refinery residue attains maximum dry density for both standard and modified proctor test. Further increase in Na_2O content results in marginal reduction in maximum dry density. As silica modulus increases MDD increased at different GGBS percentages, but the marginal reduction after 25% GGBS

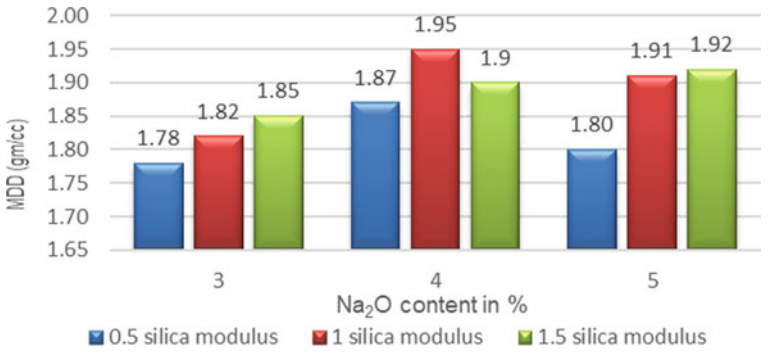

Graph 1 MDD values of ARR:GGBS (75:25) residue with different dosages of silica modulus and Na_2O content

mix. Aluminium refinery residue is devoid of reactive silica and alumina, and an addition of higher alkali to aluminium refinery residue does not bring about any chemical reaction, and hence there is an increase in the maximum dry density.

4.2 Briefs About the Unconfined Compressive Strength (UCS) of ARR

The unconfined compression strength (UCS) of the ARR with various proportions of GGBS, 4% Na_2O dosages and 0.5, 1 and 1.5 silica modulus shown in the graphs, the variations in the UCS values with respect to 20, 25 and 30% GGBS is shown in Graphs 2, 3 and 4, respectively, for different curing periods. It is observed from Graphs 2, 3 and 4 that the UCS values of different mixes have an increasing trend

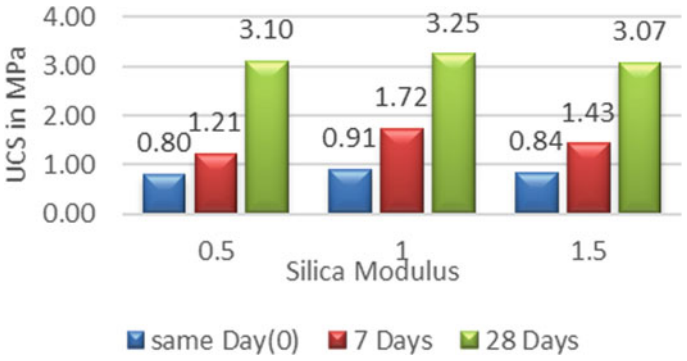

Graph 2 UCS values of ARR:GGBS (80:20) mix with different dosages of silica modulus (standard proctor)

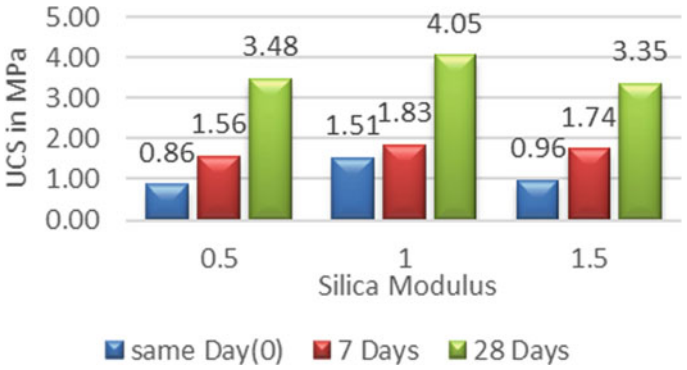

Graph 3 UCS values of ARR:GGBS (75:25) mix with different dosages of silica modulus (Standard Proctor)

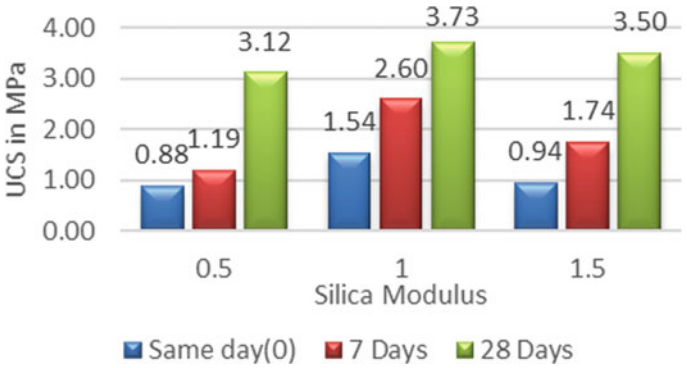

Graph 4 UCS values of ARR:GGBS (70:30) mix with different dosages of silica modulus (Standard Proctor)

with respect to increasing GGBS percentage in the mix, but the UCS decreases for 30% GGBS. When GGBS increases to 30% UCS decreases up to 20%. The curing period influences the strength of the sample, and 28 days of curing has increased UCS values compared to the same day and seventh day test. Comparatively, the silica modulus of 1, with 25% GGBS results in higher UCS values and increased trend of UCS for silica modulus 0.5–1.5 with 30% GGBS.

Similarly, unconfined compression strength (UCS) for modified proctor test of ARR with various proportions of GGBS, 4% Na_2O dosages and 0.5, 1 and 1.5 silica modulus is shown in Graphs 5, 6 and 7.

The aluminium refinery residue without GGBS compressive strength on same(0) day curing is very less, which is 0.2 MPa (Table 1). All the alumino-silicates in aluminium refinery residue may not participate in gepolymer reaction, as some are

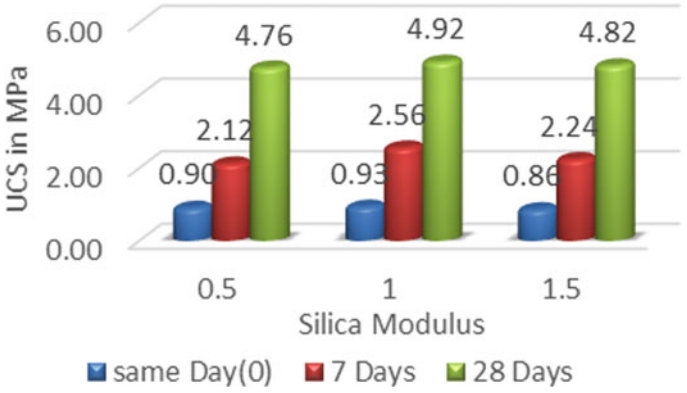

Graph 5 UCS values of ARR:GGBS (80:20) mix with different dosages of silica modulus (modified proctor)

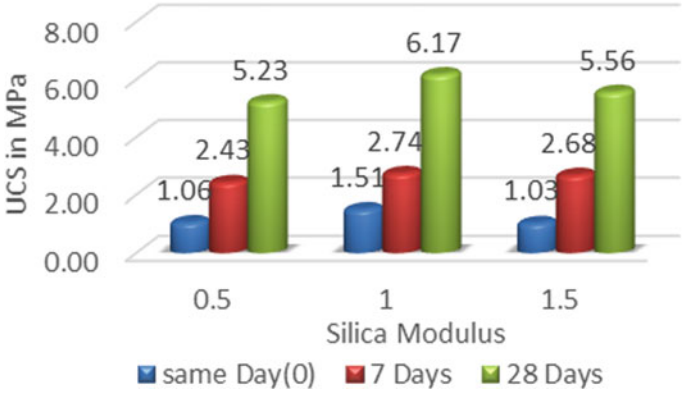

Graph 6 UCS values of ARR:GGBS (75:25) mix with different dosages of silica modulus (modified proctor)

present in crystalline form. So, aluminium refinery residue alone is not able to self-stabilize. The addition of GGBS which is a glassy material produces hydration reaction and forms calcium silicate hydrate gel, hence improves the strength. For the mix 75%ARR + 25%GGBS strength increased about 308.6% for curing from same(0) day to 28 days.

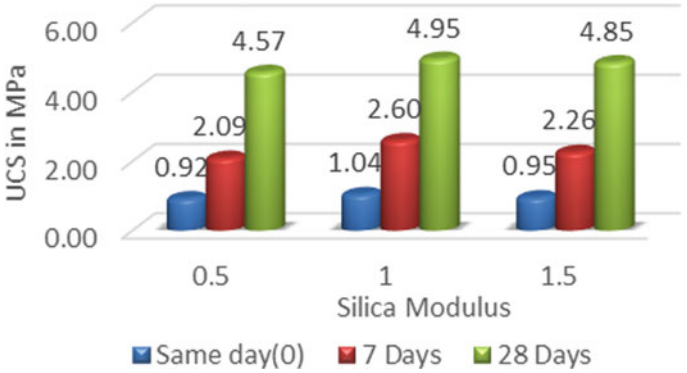

Graph 7 UCS values of ARR:GGBS (70:30) mix with different dosages of silica modulus (modified proctor)

5 Conclusion

This paper provides an experimental analysis to evaluate the importance of the alkali ativators along with the slag which is available in the ground granulated blast furnace to stabilize the ARR as the road construction material. The following conclusion has been summarized based on the laboratory investigation.

1. Aluminium refinery residue is red in colour and possesses higher specific gravity due to the presence of higher percentage of Fe_2O_3 in the mixture. Due to this the specific gravity increases.
2. As the silica modulus increases in ARR-GGBS mixture, the maximum dry density increases with the increase of the GBBS in the mixture.
3. The maximum MDD was achieved for 75%ARR + 25%GGBS with 4% Na_2O both in standard and modified proctor test.
4. Addition of alkali enhances the strength remarkably for aluminium refinery residue-GGBS mixes. With the addition of 25% GGBS and silica modulus of 1, aluminium refinery residue attains a UCS strength of 6.17 MPa for curing of 28 days.
5. Based on the present study, strength achieved is higher for different curing period and it can be used as a road construction material for low-volume roads. As the results are based on laboratory investigation, check for viability and field performance is recommended.

References

1. Samal S, Ray AK, Bandopadhyay A (2013) Proposal for resource, utilization and processes of redmud in India-a review. Int J Miner Process 118:43–55

2. Zhang M, Korchi T, Zhang G, Liang J, Tao M (2014) Synthesis factors affecting mechanical properties, micro structure and chemical composition of red mud—fly as based geopolymers. J Fuel 134:315–325
3. Kusum Deelwal K, Dharavath K, Kulshreshtha M (2014) Stabilization of Redmud by lime, gypsum and investigating its possible use as a geotechnical material in the civil engineering construction. Int J Adv Eng Technol 7(4):1238–1244
4. Satayanarayana PVV, Ganapati Naidu P, Adiseshu S, Hanumanth Rao CHV (2012) Characterization of lime stabilized red mud mix for feasibility in road construction. Int J Eng Res Dev 3(7):20–26
5. Walid H, Andrejkovic S, Zanelli C, Alshaaer M, Dondi M, Labrincha JA, Rocha F (2013) Composition and technological properties of Geopolymers based metakaolin and Red mud. Mater Des 52:648–654
6. Singh SP, Samantasinghar S, Sindhuja D (2016) Influence of GGBS on strenght of redmud satbilized by Alkalination process. In: Indian geotechnical conference IGC 201615-17 Dec 2016, IIT madras, Chennai, India
7. Lakshmi TDV, Prasad DSV, Kumar MA, Raju GP (2015) Stabilization of industrial waste redmud with cement

Laboratory Investigation of Black Cotton Soil Modified with Bioenzyme and Aggregates for Pavement Subgrade

Srinivas F. Chitragar, C. B. Shivayogimath, and Raviraj H. Mulangi

Abstract The major component of the pavement layer is subgrade soil, but the availability of good quality of subgrade soil is not abundantly available in most part of the South India, which includes North Karnataka, Maharashtra, Madhya Pradesh and Gujarat, due to the presence of clayey soil or Black cotton BC soil. This soil is having high plasticity index, high volumetric change behavior and poor load carrying capacity, hence it is not suitable for subgrade layer of the pavement. As there is a shortage of availability of good quality soil so the alternate solution is to stabilize the existing weak soil to meet out the design requirement. There are so many stabilizers available in the market, to overcome this problem. Now a day, nontraditional soil stabilizer called bioenzyme is emerging in the market, which is nontoxic, biodegradable and ecofriendly. In this investigation, attempt had made to study the stabilization of black cotton soil by using bioenzyme with dosages like 0, 50, 100, 150, 200 and 250 ml/m^3 of soil and bioenzyme with 20% of stone aggregates (passing from 6.3 mm and retained on 4.75 mm sieve) are used. Unconfined compressive strength UCS test with different curing periods and California bearing ratio test CBR for unsoaked and soaked conditions was carried out to study the change in strength parameter and to study the reduction in swelling parameter of soil, Free swell index (FSI) was conducted. The experimental results show the increased UCS value from 170 to 435 and 553 kPa for 28 days curing. CBR results are increased from 1.2% to 2.4 and 5.4 for soaked CBR and 4.5 and 8.5% unsoaked CBR. Free swell index (FSI) decreased from 130 to 65%.

Keywords Unconfined compressive strength · Free swell index · California bearing ratio and black cotton soil

S. F. Chitragar (✉) · C. B. Shivayogimath
Basaveshwar Engineering College, Bagalkot, Karnataka 587102, India
e-mail: fc.srinivas@gmail.com

R. H. Mulangi
Department of Civil Engineering, NITK Surathkal, Mangaluru 575025, India

B. B. Das et al. (eds.), *Recent Trends in Civil Engineering*, Lecture Notes in Civil Engineering 105, https://doi.org/10.1007/978-981-15-8293-6_29

1 Introduction

India is a country where population growth is more and where we need strong transportation system for day today serviceability. Black cotton soil is available in India which is not much suitable for road construction, as it is having high shrinkage and swelling properties, high liquid limit and low load bearing capacity [1, 2]. Being an engineer, one must give affordable and easy to construct method to overcome such problems. One of the most adopted methods is stabilization. Soil stabilization is a process where we alter the physical and chemical properties of the soil by the addition of some additives in order to make week and noneconomic soil to economic and good soil in terms of strength. There are many soil stabilization techniques available to improve the soil few of them are lime, fly ash cement, GGBS, and some chemical agents [3]. In many cases, we can replace black cotton soil with good soil but these methods are expensive due to the shortage of good materials. By taking into account of their drawbacks, one can go for the most emerging stabilizer. IRC has accredited several additives for soil stabilization and to use for road construction, one of the upcoming additive is Bio-enzy. Initial cost is high but we can minimize its cost during maintenance time [4, 5]. There are many types of bioenzymes are available in market such as Renolith, Perazyme, Fujibeton, TerraZyme. It is ecofriendly and biodegradable, noninflammable organic liquid, they are available in liquid form they can be used by mixing in water. The mixed solution can be used for soil stabilization process [6–9]. It is a water soluble material and the color is brown which smells like molasses. It is formulated to change the engineering properties of the soil. The TerraZyme should be diluted before its actual use as stabilizer. It is then added to water. The solution is blended with untreated soil. These changes in engineering properties are dependent on the soil type and the dosage of enzyme used. The TerraZyme after application it reduces the voids present in soil, increases the density and strength of the soil which can be checked by UCS CBR tests and reduces the optimum moisture content and free swell index of soil [10].

2 Materials

2.1 Black Cotton Soil

In this present investigation, soil is collected from Gadag District of Karnataka state. This soil is not suitable for road construction due to its more swelling and shrinkage behavior, low-bearing capacity and high plasticity index. Soil had characterized as per IS codes methods. Figure 1 shows the Black cotton soil, which was chosen in this study.

Fig. 1 Black cotton soil

2.2 Bioenzyme

IRC Accredited soil stabilizer Bio-enzyme (TerraZyme), which is commercially available in the market was selected for the study. As per the manufacturer bioenzyme is the extract of vegetable and fruits. TerraZyme is brown in color and smells like molasses. The bioenzyme is nontoxic, biodegradable, noninflammable and organic solution. Properties of the TerraZyme are shown in Table 1.

Table 1 Properties of TerraZyme

Properties	Values
Specific gravity	1.05
pH	3.50
Appearance	Dark brown
Total dissolved solids TDS	9.7 ppm
Hazardous content	None
Cation exchange capacity	3.87%
Boiling point	212 F
Evaporation rate	Same as water
Solubility in water	Complete
Reactivity	Stable

Source http://www.info@avijeetagencies.com

3 Methodology

The Black cotton soil that was collected from Nargund was air and oven dried and tests are conducted on soil as per IS Codes to classify and to characterize the soil. The soil was stabilized with different dosages of bioenzyme (i.e., 0, 50, 100, 150, 200, 250 ml/m^3 of soil). Strength gained by adding bioenzyme was tested by conducting unconfined compressive strength (UCS) for different curing periods and California bearing ratio, (Soaked and Unsoaked CBR) Test. Further, the reduction in swelling behavior was studied by conducting free swell index (FSI) test. To enhance the strength of the soil, an additional 20% of aggregates (passing from 6.3 mm and retained on 4.75 mm sieve) is mixed along with the bioenzyme and the tests were repeated.

4 Result and Discussions

The soil is classified as **A-7–5**. According to the HRB classification which is Inorganic Fat Clay of high plasticity, according to unified soil classification system (USCS), soil is classified as **(CH)**. The physical properties of soil tested are given in Table 2.

4.1 Variation in UCS of Soil

Table 3 shows the change in the UCS of black cotton soil stabilized with the different dosage of TerraZyme. Results show that the optimum dosage of bioenzyme obtained is 200 ml/m^3 of soil, which increase the UCS value from **170 to 432 kPa after 28 days curing** and also we can say that curing period influence the strength gain

Table 2 Physical properties of soil

Test	Result	IS code
Specific gravity [11]	2.07	IS:2720 (PART-III)
OMC [12]	26.5%	IS:2720 (PART-VII)
MDD (gm/cc) [12]	1.35	IS:2720 (PART-VII)
Liuide limit [13]	75.4%	IS:2720 (PART-V)
Plasit limit [13]	32.6%	IS:2720 (PART-V)
CBR (%)	1.2	IS:2720 (PART-16)
UCS (kpa) [14]	170	IS:2720 (PART-10)
Free swell index FSI (%) [15]	130%	IS:2720
pH [16]	8.2	IS:2720

Table 3 Variation of UCS value with different dosage of bioenzyme

Dosage in ml/m^3 of soil	UCS values in kPa according to curing period			
	0 Day	3 Day	7 Day	28 Day
0	170	170	174	176
50	176	190	210	280
100	180	193	289	343
150	190	235	326	386
200	195	276	386	432
250	184	266	380	426

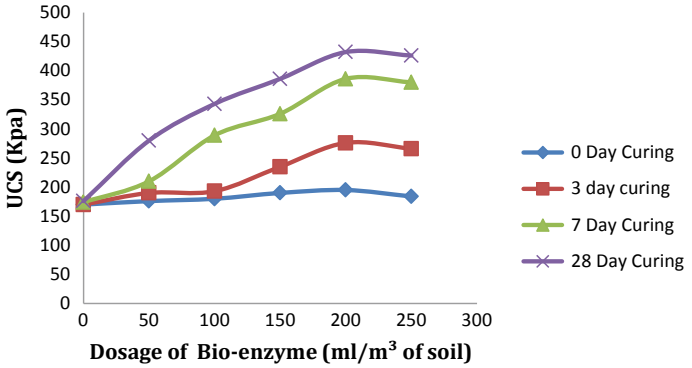

Fig. 2 Variation in the UCS values of soil with different dosage of TerraZyme and for different curing periods

in of soil. Variation in the UCS values for different dosages and for curing period is shown in Fig. 2.

Further, the combination of soil and different percent of **TerraZyme** with 20% of aggregate by weight of soil is taken and subjected for the UCS test and the results were obtained as shown in Table 5. And variation in the UCS values of soil with different dosage of TerraZyme with 20% aggregates and for different curing periods is shown in Fig. 3 and Table 4.

From the above investigation, it is seen that as the curing period increases the UCS value is increasing, the optimum dosage of Bioenzyme 200 ml/m^3 with 20% aggregates is considered as optimum dosage.

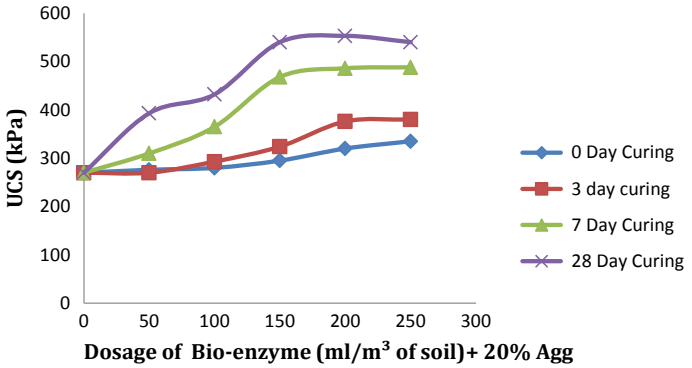

Fig. 3 Variation in the UCS values of soil with different dosage of TerraZyme with 20% Aggregates and for different curing period

Table 4 Variation of UCS values for the combination of different dosage of bioenzyme and 20% of aggregates

Dosage in ml/m^3 of soil + 20% aggregates	UCS values in kpa according to curing period			
	0 Day	3 Day	7 Day	28 Day
0	270	270	270	270
50	276	270	310	393
100	280	293	365	432
150	295	324	468	540
200	320	376	486	553
250	335	380	488	540

4.2 Comparison of UCS Values for Virgin Soil and Stabilized Soil with Different Dosage of Bioenzyme and 20% of Aggregates

Variation in UCS values for the combination of different dosage of bioenzyme and 20% of aggregates for different curing periods (0 Day, 3 Day, 7 Day and 28 Day) are shown in Fig. 4a–d, respectively. Further addition of 20% aggregates with bioenzyme has resulted in increased UCS value, which increased the UCS value from 432 to 553 kPa after 28 days curing. From the graphs, it is seen that addition of 20% aggregates with bioenzyme, the strength has enhanced in all the curing periods with all the dosages.

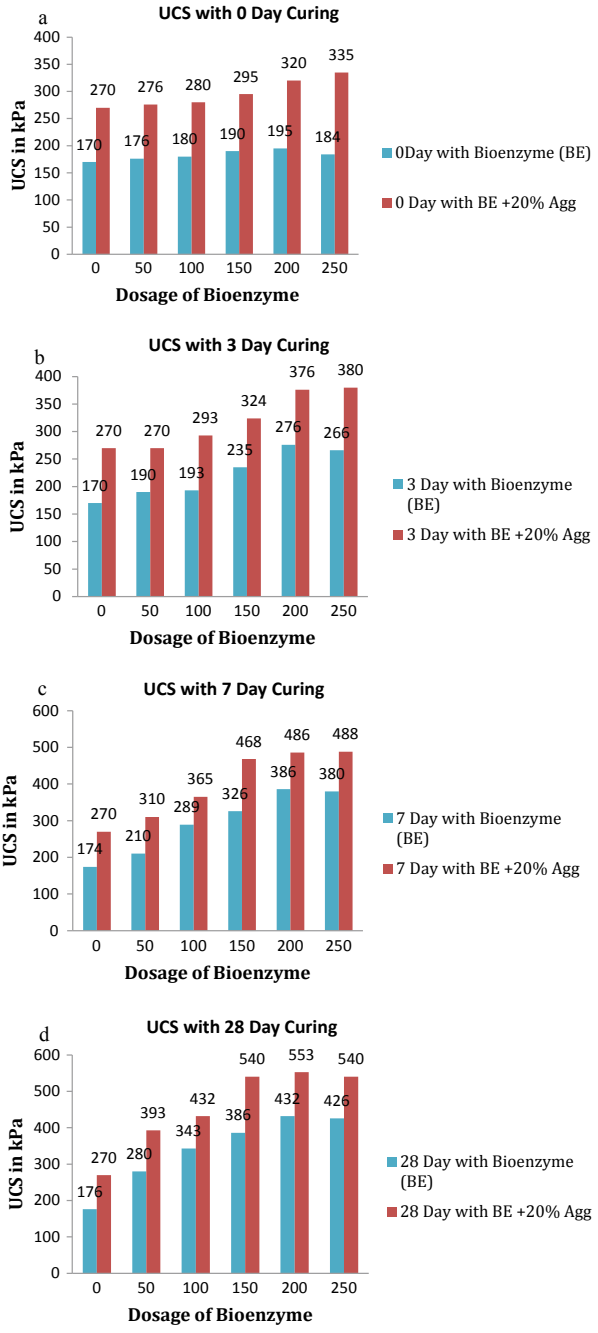

Fig. 4 Variation of UCS values for the combination of different dosage of bioenzyme and 20% of aggregates for different curing periods

4.3 *Variation of Soaked and Unsoaked CBR of Soil for Different Dosage of Bioenzyme*

Table 5 shows the variation in the CBR of black cotton soil stabilized with the different dosage of TerraZyme. From the results, it is observed that optimum dosage of bioenzyme obtained is 200 ml/m^3 of soil, which increase the CBR value from **1.2 to 2.15% for soaked CBR and 6.2% for unsoaked CBR**. Variation in the CBR values of soil with different dosage of terrazyme is shown in Fig. 5.

Table 6 shows the variation in the CBR of black cotton soil stabilized with the different dosage of TerraZyme with addition of 20% aggregates, from the experimental results, it is seen that CBR value increased from **1.2 to 2.4% for soaked CBR and 4.5% for unsoaked** CBR. With optimum dosage of bioenzyme, i.e., **200 ml/m^3** CBR increased from **2.4 to 5.4% for soaked CBR and 8.5% for unsoaked CBR**. Variation in the CBR values of soil with different dosage of terrazyme is shown in Fig. 6.

The soil mixed with bioenzyme of dosage 200 ml/m3 has enhanced CBR increased from 1.2% for virgin soil to 2.15% and 5.4% for soaked CBR and unsoaked CBR,

Table 5 Variation of Soaked and Unsoaked CBR of Soil for different dosage of bioenzyme

Dosage in ml/m^3 of soil + 20% aggregates	CBR Value in %	
	Soaked CBR	Unsoaked CBR
0	1.2	3.5
50	1.3	4.8
100	1.44	5.5
150	2.05	6.0
200	2.15	6.2
250	2.3	6.2

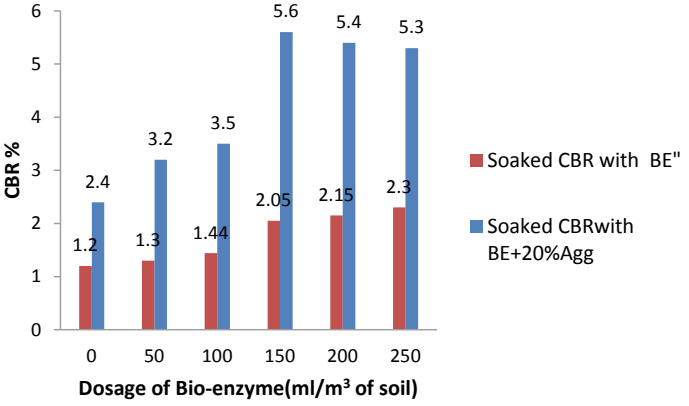

Fig. 5 Variation of CBR for different dosage of bioenzyme

Table 6 Variation of soaked and unsoaked CBR of Soil for different dosage of bioenzyme with 20% aggregates

Dosage in ml/m^3 of soil + 20% aggregates	CBR Value in %	
	Soaked CBR	Unsoaked CBR
0	2.4	4.5
50	3.2	6.0
100	3.5	6.2
150	5.6	7.8
200	5.4	8.4
250	5.3	8.1

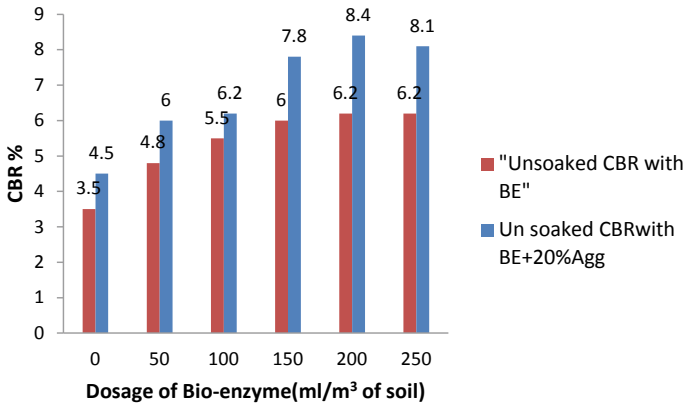

Fig. 6 Variation of CBR for different dosage of bioenzyme with 20% aggregates

respectively. Further to enhance the CBR value, 20% of aggregates are added along with bioenzyme, the results shown are quite satisfactory with the CBR of 4.5 and 8.5% for soaked and unsoaked CBR. This CBR is satisfactory for construction of low volume roads.

4.4 Variation of Free Swell Index of Soil

The free swell index test is performed on the black cotton soil with different dosage of Terrazyme. The free swell index of the soil decreased as the dosage of Terrazyme is increased, which is shown in Fig. 7. The FSI value decreases from 130 to 65%.

From the above FSI test results, it is seen that the FSI value reduced from 130 to 65% but as per MoRTH specification, the subgrade soil FSI value should be less than 50% to use it in subgrade of the pavements, hence care should be taken to reduce FSI further from 65% to less than 50%.

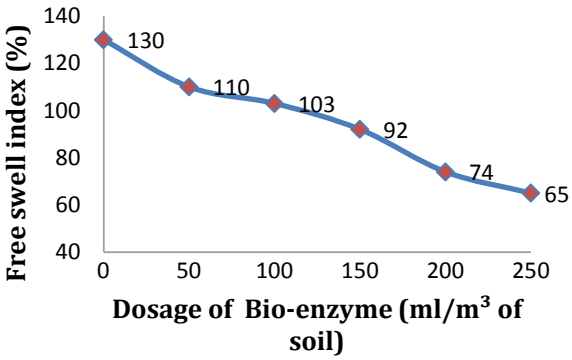

Fig. 7 Variation of FSI of soil with different dosage of bioenzyme

5 Conclusion

Based on the laboratory investigation, the following conclusions are drawn.

The objective of this work is to provide some answers concerning the influence of bioenzyme treatment at variable dosages to investigate the physical and mechanical strength of treated soils and based on result, some conclusions were drawn.

The rate of increase in strength in terms of unconfined compressive strength and also by CBR tests and reduction in swelling or volumetric variation in terms of expansion depending on the bioenzyme percentage and curing period.

We find that enzyme contents of 200 ml/m^3 show that the maximum increment of strength but to enhance further strength 20% aggregates are used to meet out the requirement of stabilized soil to be used for road work. The soil CBR and UCS are an important parameter to decide the suitability of soil for road construction. From the experimental results, it is seen that the UCS value enhanced from 176 to 553 kPa which is around 300% increment.

But stabilized soil is suitable only when it is posses good strength, minimum volumetric change (should, i.e., less than 50% as per MoRTH) and also it should pass durability check. Above investigation shows that the FSI value has reduced from 130 to 65%, which is fairly good but this reduction has to be further reduced to bring below 50% hence care has to be taken to reduce the swelling potential by any other means and also the stabilized soil has to pass durability check, which consists of alternate wetting and drying, the sample has to withstand min 12 cycles.

Future Scope of Work

1. Durability study on stabilized soil
2. Chemical analysis of stabilized soil to know which chemical parameter influence in increasing the strength and reducing the FSI
3. The soil microstructure study and
4. Further reduction of FSI value of the stabilized BC soil using other additive in combination to bioenzyme.

References

1. Ravi Shankar AU, Rai HK, Mithanthaya R (2009) Bio-enzyme stabilized lateritic soil as a highway material. J Indian Road Congr 553:143–151
2. Lekha BM, Sarang G et al (2014) Laboratory investigation on black cotton soil stabilized with non-traditional stabilizer. IOSR J, 7–13. e-ISSN: 2272–1684 p-ISSN:2320–334X
3. Eujine GN, Lamanto T et al (2014) Enzyme stabilization of high liquid limit clay. EJGE: Electron J Geotech Eng 19
4. Rajoria V, Kaur S (2014) A review on stabilization of soil using bio- enzyme. IJRETs eISSM 2319–1163 3:75–78
5. Saini V, Vaishnava P (2015) Soil stabilization by using Terrazyme. Int J Adv Eng Technol 8:566–573
6. Okonta F (2019) Pavement geotechnical properties of polymer modified weathered semi-arid shale subgrade. Int J Pavement Res Technol 12(1):54–63
7. Vardanega PJ, Hickey CL, Laub K, Sarzier HDL, Couturier CM, Martin G (2018) Investigation of the Atterberg limits and undrained fall-cone shear strength variation with water content of some peat soils. Int J Pavement Res Technol. Accepted 18 Nov 2018
8. Chandrakaran S, Sankar N et al (2014) Enzyme stabilization of high liquid limit clay. Electr J Geotech Eng 19:6989–6995
9. Agarwal P, Kaur S (2014) Effect of Bio- enzyme stabilization on unconfined compressive strength of soil. Int J Res Eng Technol 3:30–33
10. Chitragar SF, Shivayogimath CB, Mulangi RH (2019) Study on strength and volume change behavior of expansive soil using non-traditional (Bio-enzyme) and traditional (Lime and Bagasse Ash) Stabilizers. In: Geotechnics for transportation infrastructure, lecture notes in civil engineering, vol 29. Springer, Singapore, pp 587–594. 10.1007/978-981-13-6713-7_46
11. IS 2720 (Part III)-2002 (2002) Determination of specific gravity of soil
12. IS 2720 (Part 7)-2011 (2011) Determination of water content-dry density relation using light compaction
13. IS 2720 (Part 5)-2006 (2006) Determination of liquid and plastic limit (Second Revision)
14. IS 2720 (Part 10) Unconfined compressive strength
15. IS 2720 (Part 40)-1977 (1977) Determination of free swell index of soil
16. IS 2720 (part 26)-1987 (1987) Determination of pH value

Recent Trends in Environmental Engineering

Removal of Pharmaceutical Drug from Water Using Activated Kaolinite–TiO_2 Nanocomposite

Vaibhav R. Chate, Soumya Meti, M. S. Veeresh, M. B. Shivaraj, Utsav Naik, and Raviraj M. Kulkarni

Abstract Pharmaceutical contamination of water has been an emerging environmental area of concern. A large amount of pharmaceuticals is discharged into the nature through human utilization and excretion and is not treated properly by municipal sewage treatment plants. Pharmaceuticals are also disposed into the nature by pharmaceutical industries. Levofloxacin (LVF) is one of them. LVF, a famous fluoroquinolone (FQ) is widely adopted drug owing to its effective activity against microbes. LVF finally enters water environment, because only 15–20% metabolizes in living beings. FQs vary from mg dm^{-3} to ng dm^{-3} in wastewater. Incessant revelation of microorganisms to FQs (2–5 mg dm^{-3}) will help bacterial resistance to FQs. The present investigation focuses on feasibility of using Activated Kaolinite–TiO_2 (AK–TiO_2) nanocomposite for the removal of LVF. In this study, various factors considered for the removal of LVF are the effect of initial LVF concentration, effect of AK–TiO_2 nanocomposite and effect of contact time. The AK–TiO_2 nanocomposite showed boosted photocatalytic activity for the photodegradation of LVF. The photodegradation of LVF improved with an enhancement of AK–TiO_2 nanocomposite dosage and photodegradation time. The maximum LVF removal efficiency of 64% was recorded for AK–TiO_2 dosage of 500 mg/l with photodegradation time of 300 s. With an enhancement in the initial LVF concentration, the photodegradation reduced, this is because enhancement in the LVF increases anions.

Keywords Levofloxacin · Kaolinite · Nanocomposite · TiO_2 · Photodegradation

V. R. Chate (✉) · S. Meti · M. S. Veeresh · M. B. Shivaraj · U. Naik
Civil Engineering Department, K.L.S Gogte Institute of Technology, Udyambag, Belagavi, Karnataka 590008, India
e-mail: chatevaibhav@gmail.com

R. M. Kulkarni
Department of Chemistry and Centre for Nanoscience and Nanotechnology, K.L.S Gogte Institute of Technology, Udyambag, Belagavi, Karnataka 590008, India

B. B. Das et al. (eds.), *Recent Trends in Civil Engineering*, Lecture Notes in Civil Engineering 105, https://doi.org/10.1007/978-981-15-8293-6_30

1 Introduction

Pharmaceuticals in water are considered as emerging environmental contaminants and are of great concern in present scenario. The various pathways of pharmaceuticals into an environment include excretion, improper disposal of wastewater and runoff from sludge. Market share of Fluoroquinolones (FQs) in the total antibiotic market is 17%. Literature reports that antibiotic concentration in water bodies ranges up to 5 μg/l. Discharge of FQs into the environment induces bacterial resistance and causes damage to living organisms. Levofloxacin (LVF), a famous fluoroquinolone (FQ) antibiotic, is widely employed to treat a variety of diseases (chronic prostatitis, pneumonia, acute bacterial sinusitis, urinary tract contagion). Since 80–85% does not metabolize in animal or human bodies, the bulk of LVF ultimately joins the water environment. Moreover, the concentrations of LVF in surface water vary up to 87.4 ng/l. The discharge of LVF in water, even in small quantities causes adverse impact on the ecosystem. The conventional wastewater treatment plants cannot remove LVF efficiently. Degradation of LVF and other FQ by ozonation and H_2O_2/UV process has been reported by researchers ([1–10]; Sheraz et al. 2013).

Researchers have used kaolinite clay and various adsorbents to remove copper, Pb(II), Cd(II) and Ni(II) and fluoride from water [11]. TiO_2 nanoparticles have been extensively employed for photodegradation of dyes and heavy metals [12–20]. There are no reports on the removal of pharmaceutical compounds using Kaolinite–TiO_2 nanocomposite. The present research focuses on the novel application of activated kaolinite–TiO_2 (AK- TiO_2) nanocomposite for the photodegradation of LVF at neutral condition (pH = 7). The results were then discussed in detail and compared with literature for the removal of LVF from water.

2 Materials and Methodology

The raw Kaolinite was collected from Kochi of Kerala state, India. Analytical grade chemicals were used. LVF was purchased from Sigma Aldrich. Double distilled water was employed for preparing synthetic/standard chemical solutions.

2.1 Preparation of Standard LVF Solution

LVF ($C_{18}H_{20}FN_{3O}$. ½ H_2O, molecular weight is 361.368 g/mol) is a pharmaceutical drug. LVF is water soluble, yielding a colourless transparent solution. LVF of 361.368 mg was dissolved in distilled water (total 1 L volume) to prepare stock LVF solution of 1 mmoles/l. Various concentrations of LVF were then prepared by

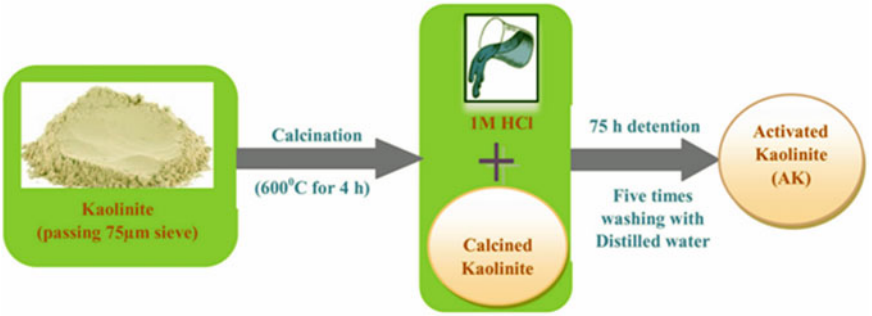

Fig. 1 Synthesis of AK

diluting known quantity of stock LVF solution with distilled water. The various standard LVF solutions used for the study were 10, 30, 50, 70 and 100 µmoles/l. All the photodegradation studies were carried out under neutral condition (pH of 7).

2.2 Preparation of Activated Kaolinite (AK) Nanoparticle

Kaolinite was powdered and the material passing through the 75 µm sieve was selected for the analysis. Fine kaolinite particles were calcined at 600 °C for 4 h to obtain calcined kaolinite. 1 M HCl and calcined kaolinite were added to volumetric flask with liquid to solid (L/S) ratio of 20 ml/g and kept in the shaker for 2 h and further allowed to react with an acid for 75 h without any agitation to yield acid-treated kaolinite. Acid treated kaolinite was then washed with distilled water for five times with L/S ratio of 20 ml/g and dried at 104 °C to get Activated Kaolinite (AK) (Fig. 1).

2.3 Preparation of AK–TiO_2 Nanocomposite

Anatase TiO_2 nanoparticles were prepared by addition of 3 ml of titanium isopropoxide (TTIP) and 1.2 g AK in 25 ml absolute ethanol with constant stirring for 30 min on magnetic stirrer. Distilled water (1.5 ml) and concentrated HCl (0.5 ml) were then added with constant stirring (2 h) and it was undisturbed for 75 h to transform into a gel. Further, the gel was centrifuged for 50 min at 6000 rpm and after that heated at 80 °C for 30 min. It was sintered at 400 °C for 3 h to synthesize AK–TiO_2 nanocomposite by keeping TiO_2 in anatase phase (Fig. 2).

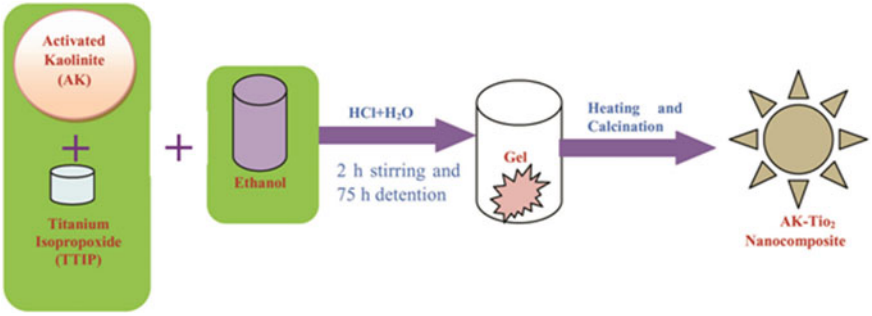

Fig. 2 Synthesis of AK-TiO_2 nanocomposite

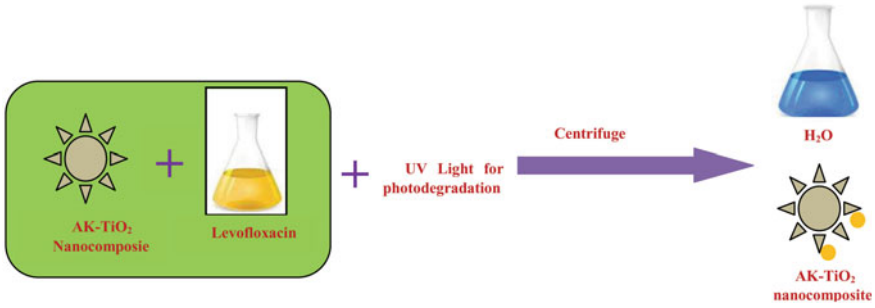

Fig. 3 Photodegradation of LVF by AK–TiO_2

2.4 Experimental Methodology

All the LVF samples with AK-TiO_2 nanocomposite were initially stirred at 700 rpm for 30 min (in absence of sunlight and UV light). The stirred samples were then taken for photodegradation studies (Fig. 3). Investigation was conducted on the effect of AK–TiO_2 dosage, initial LVF concentration and photodegradation time for the removal of LVF from water.XRD and FEG–SEM analysis was carried out for AK–TiO_2 nanocomposite.

3 Characterization of AK–TiO_2

The raw Kaolinite was characterized by powder X-ray diffraction (XRD) to record the parental mineralogical content before activation. The synthesized AK–TiO_2 nanocomposite was characterized by powder XRD and field emission gun (FEG)–scanning electron microscope (SEM) techniques.

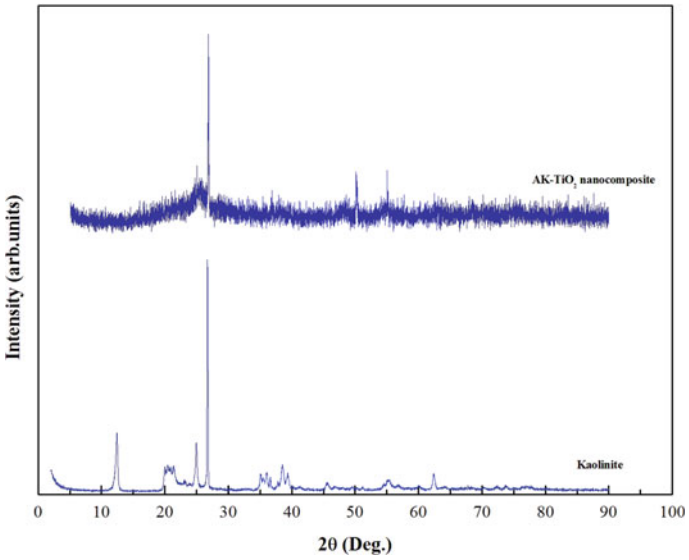

Fig. 4 XRD of Kaolinite and AK–TiO_2 nanocomposite

X-ray diffractometer (Rigaku Ultima IV, Japan) was used to record XRD patterns (with 2θ range of 3–90°). After treating with acid, the kaolinite was converted to an amorphous state, this is due to the dissociation of the water and aluminium. This decreases the peak height of 12.5° (001 plane) reflection by 80%. Kaolinite phase is more ordered in AK-TiO_2. Further, activation does not affect quartz and feldspar. The main peaks showed by TiO_2 are 25.7°, 38.1°, 48.8°, 55.1°, 63.1°, 69.9°, and 75.2°; these corresponds to the (101), (004), (200), (105), (211), (204), (116), and (224) planes of anatase. This is due to conversion of Ti^{4+} ions to anatase [13–15, 17, 21–25] (Fig. 4).

JSM-7600F (JEOL, USA) was used to study the SEM and energy dispersive spectroscopy (EDS). Figure 5 indicates the deposition of TiO_2 nanoparticles on aluminium and silica nanosheets [12, 16–18, 26]. EDS and FEG analyses indicate the presence of silica (15.26%), titanium (32.52%), carbon (3.30%), iron (1.52%), aluminium (5.89%), oxygen (41.15%) and traces of chloride elements.

4 Results and Discussions

To study the effect of initial LVF concentration on photodegradation, initial LVF concentration ranging from 10 to 100 μmoles/l was selected, while keeping AK–TiO_2 nanocomposite dosage of 200 mg/l constant. Results showed that as LVF concentration enhances the removal efficiency reduces (Fig. 6). This can be attributed to the fact that, an enhancement in LVF concentration enhances the anion concentration.

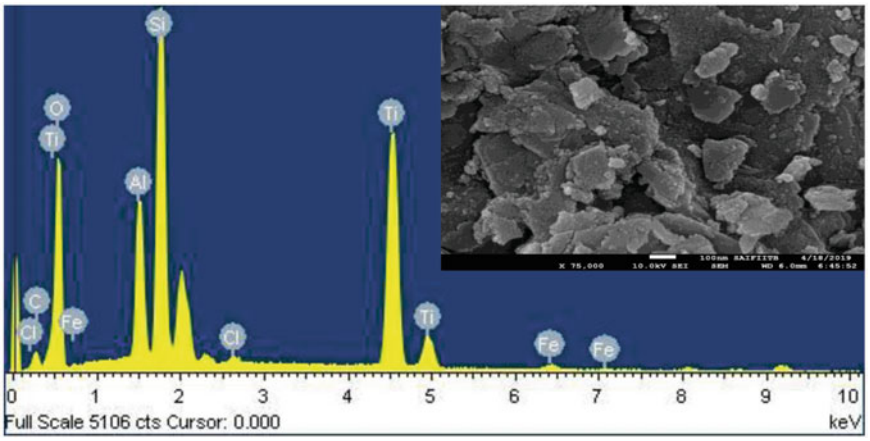

Fig. 5 EDS of AK–TiO_2 (inset image of SEM)

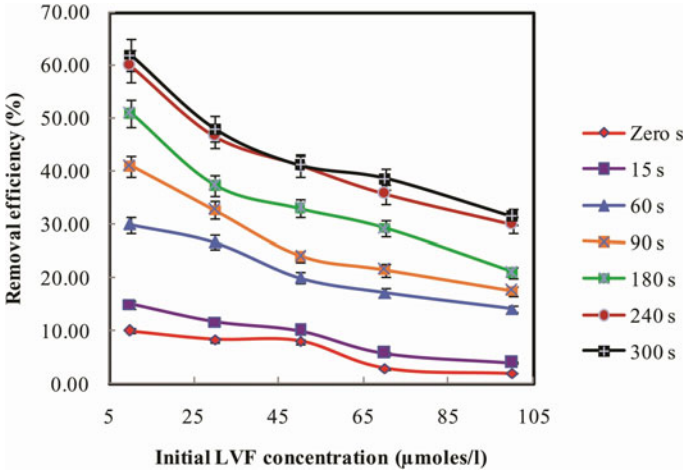

Fig. 6 Effect of initial LVF concentration

Maximum LVF removal efficiency of 62% was observed for initial LVF concentration of 10 µmoles/l.

The effect of AK–TiO_2 nanocomposite (photocatalyst loading) on the photodegradation of LVF was investigated by varying AK–TiO_2 nanocomposite (from 50 to 500 mg/l) while keeping degradation time (300 s) as constant. Figure 7 shows that as AK–TiO_2 nanocomposite dosage increases removal efficiency also increases up to 500 mg/l and thereafter decreases [27–31]. Dosage beyond 500 mg/l causes the solution turbid and masks ultraviolet (UV) light reaching the photocatalyst. Hence, LVF removal efficiency decreases. Maximum efficiency of 64% for AK–TiO_2 nanocomposite dosage of 500 mg/l was obtained at 300 s, which is much higher than activated

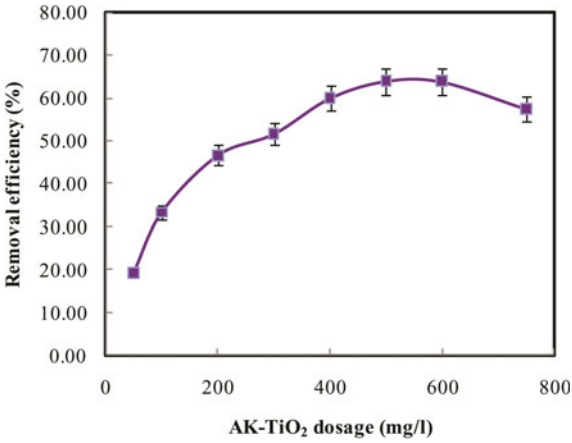

Fig. 7 Effect of AK–TiO_2 dosage

sludge process efficiency of 42% [3]. Turbidity was lowest for 200 mg/l and hence same dosage was considered for further studies.

To study the effect of photodegradation time, AK–TiO_2 nanocomposite dosage of 200 mg/l and initial concentration of 10 μmoles/l were selected and photodegradation time was varied from 0 to 300 s. Figure 8 (representative graph) shows that, as the photodegradation time increases removal efficiency also increases. Highest treatment efficiency of 62% was recorded for photodegradation time of 300 s.

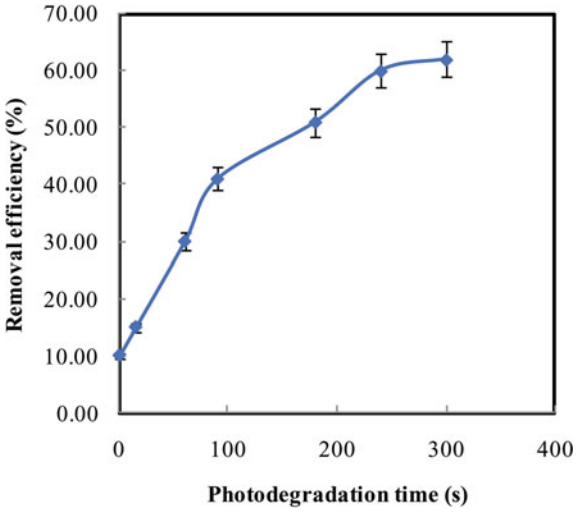

Fig. 8 Effect of photodegradation time

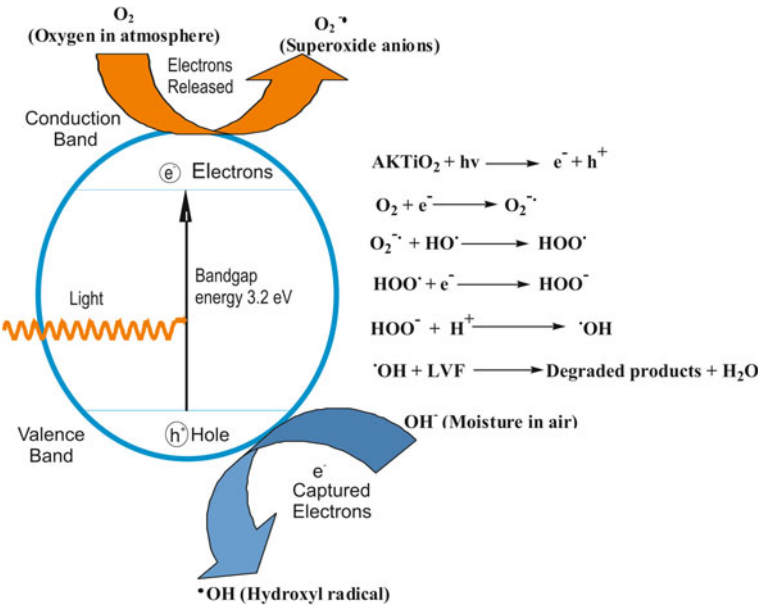

Fig. 9 Degradation mechanism

5 Mechanism

After the incident of UV light on LVF in the presence of AK–TiO_2, the LVF is excited to first singlet state ($^1LVF_1$). The $^1LVF_1$ later goes to the triplet state ($^3LVF_1$) through inter-system-crossing (ISC). $^3LVF_1$ donates electron to AK–TiO_2 and acquires a positive charge. The oxygen present in the solution receives the electron from the conduction band of the AK–TiO_2, leading to production of superoxide anions. The superoxide anions will combine with water to form OH ions and finally to OH radicals. These OH radicals degrade the LVF instantly [30, 32] (Fig. 9).

6 Conclusions

It can be concluded that photodegradation method is more efficient than activated sludge process for the LVF treatment from water. This is because of the reason that when TiO_2 comes in contact with UV light the degradation process starts apart from the adsorption process between activated kaolinite (activated silica, alumina) and LVF. However, prior to photodegradation, adsorption time of 30 min is required so that the nanocomposite (cations) come in contact with LVF.

The maximum LVF removal efficiency was observed at 300 s of photodegradation time and thereafter the equilibrium is reached. With an increase in the AK–TiO_2

dosage, the cation concentration increases which will contribute in the removal of anions from the solution. The decrease in the efficiency due to an increase in the initial LVF concentration is because of increase in anions and lower cations. AK–TiO_2 photocatalyst can be adopted to manage harmful LVF from environment.

Acknowledgements The authors are grateful to thank KSCST for sponsoring the project. They are thankful to SAIF facilities Indian Institute of Technology Bombay and Solapur University, India for providing the XRD and FEG–SEM analysis results.

References

1. Gudaganatti MS, Hanagadakar MS, Kulkarni RM, Malladi RS, Nagarale RK (2012) Transformation of levofloxacin during water chlorination process: kinetics and pathways. Prog React Kinet Mech 37(4):366–382
2. Hirsch R, Ternes T, Haberer K, Kratz KL (1999) Occurrence of antibiotics in the aquatic environment. Sci Total Environ 225(1–2):109–118
3. Kim J-W, Jang H-S, Kim J-G, Ishibashi H, Hirano M, Nasu K, Ichikawa N, Takao Y, Shinohara R, Arizono K (2009) Occurrence of pharmaceutical and personal care products (PPCPs) in surface water from mankyung river, South Korea. J Health Sci 55(2):249–258
4. Langenhove HV, Hemelsoet K (2015) Levofloxacin ozonation in water: rate determining process parameters and reaction pathway elucidation. Chemosphere 76(5):683–689
5. Golet EM, Xifra I, Siegrist H, Alder AC, Giger W (2003) Environmental exposure assessment of fluoroquinolone antibacterial agents from sewage to soil. Science 37(15):3243–3249
6. Marie D, Nathalie K, Vel L (2013) Levofloxacin oxidation by ozone and hydroxyl radicals: kinetic study, transformation products and toxicity. Chemosphere 30:1–8
7. Namieśnik J (2000) Trends in environmental analytics and monitoring. Crit Rev Anal Chem 30(2–3):221–269
8. Nasuhoglu D, Rodayan A, Berk D, Yargeau V (2012) Removal of the antibiotic levofloxacin (LEVO) in water by ozonation and TiO_2 photocatalysis. Chem Eng J 189–190:41–48
9. Virupaxappa BS, Shivaprasad KH, Kulkani RM, Latha MS (2012) Kinetic estimation of antihypertensive drugs in pharmaceutical dosage forms. Res J Pharm Biol Chem Sci 3(3):235–246
10. Yasojima M, Nakada N, Komori K, Suzuki Y, Tanaka H (2006) Occurrence of levofloxacin, clarithromycin and azithromycin in wastewater treatment plant in Japan. Water Sci Technol 53(11):227–233
11. Chate VR, Kulkarni RM, MutalikDesai VG, Kunkangar PB (2018) Seawater-washed activated bauxite residue for fluoride removal: waste utilization technique. J Environ Eng 144 (2018):04018031-1–04018031-11
12. Batistella M, Caro-Bretelle AS, Otazaghine B, Ienny P, Sonnier R, Petter C, Lopez-Cuesta JM (2015) The influence of dispersion and distribution of ultrafine kaolinite in polyamide-6 on the mechanical properties and fire retardancy. Appl Clay Sci 116–117:8–15
13. Bhattacharyya KG, Sen GS (2006) Adsorption of chromium(VI) from water by clays. Ind Eng Chem Res 45(21):7232–7240
14. Bhattacharyya KG, Sen GS (2008) Adsorption of a few heavy metals on natural and modified kaolinite and montmorillonite: a review. Adv Colloid Interface Sci 140(2):114–131
15. Bhattacharyya KG, Sen GS (2011) Removal of Cu(II) by natural and acid-activated clays: an insight of adsorption isotherm, kinetic and thermodynamics. Desalination 272(1–3):66–75. Elsevier B.V

16. Bizaia N, De Faria EH, Ricci GP, Calefi PS, Nassar EJ, Castro KADF, Nakagaki S, Ciuffi KJ, Trujillano R, Vicente MA, Gil A, Korili SA (2009) Porphyrin-kaolinite as efficient catalyst for oxidation reactions. ACS Appl Mater Interfaces 1(11):2667–2678
17. Tang W, Zhang S, Sun J, Li H, Liu X, Gu X (2017) Effects of surface acid-activated kaolinite on the fire performance of polypropylene composite. Thermochim Acta 648:1–12
18. Vahabi H, Batistella MA, Otazaghine B, Longuet C, Ferry L, Sonnier R, Lopez-Cuesta JM (2012) Influence of a treated kaolinite on the thermal degradation and flame retardancy of poly(methyl methacrylate). Appl Clay Sci 70:58–66
19. Yadav VB, Gadi R, Kalra S (2019) Clay based nanocomposites for removal of heavy metals from water: a review. J Environ Manage 232:803–817
20. Zhang X, Lin S, Chen Z, Megharaj M, Naidu R (2011) Kaolinite-supported nanoscale zero-valent iron for removal of Pb^{2+} from aqueous solution: reactivity, characterization and mechanism. Water Res 45(11):3481–3488
21. Gao W, Zhao S, Wu H, Deligeer W, Asuha S (2016) Direct acid activation of kaolinite and its effects on the adsorption of methylene blue. Appl Clay Sci 126:98–106
22. Hidalgo MC, Aguilar M, Maicu M, Navío JA, Colón G (2007) Hydrothermal preparation of highly photoactive TiO_2 nanoparticles. Catal Today 129(1–2):50–58
23. Hirano M, Ota K (2004) Direct formation and photocatalytic performance of anatase (TiO_2)/Silica (SiO_2) composite nanoparticles. J Am Ceram Soc 87(8):1567–1570
24. Zhao L, Xue F, Yu B, Xie J, Zhang X, Wu R, Wang R, Hu Z, Yang ST, Luo J (2015) TiO_2–graphene sponge for the removal of tetracycline. J Nanopart Res 17(1):2–9
25. Zhao Y, Ren W, Cui H (2013) Surfactant-free synthesis of water-soluble anatase nanoparticles and their application in preparation of high optic performance monoliths. J Colloid Interface Sci Acad Press 398:7–12
26. Panda AK, Mishra BG, Mishra DK, Singh RK (2010) Effect of sulphuric acid treatment on the physico-chemical characteristics of kaolin clay. Colloids Surf Physicochemical Eng Aspects 363(1–3):98–104
27. Fan W, Lai Q, Zhang Q, Wang Y (2011) Nanocomposites of TiO_2 and reduced graphene oxide as efficient photocatalysts for hydrogen evolution. J Phys Chem 115(21):10694–10701
28. Huanjing kexue Z (2015) ke xue yuan huan jing ke xue wei yuan hui "Huan. "TiO_2 induced photodegradation of levofloxacin by visible light and its mechanism." Environ Sci 36:1700–1706
29. Kibanova D, Trejo M, Destaillats H, Cervini-Silva J (2009) Synthesis of hectorite-TiO_2 and kaolinite-TiO_2 nanocomposites with photocatalytic activity for the degradation of model air pollutants. Appl Clay Sci 42(3–4):563–568
30. Kulkarni RM, Malladi RS, Hanagadakar MS, Doddamani MR, Bhat UK (2016) Ag-TiO_2 nanoparticles for photocatalytic degradation of lomefloxacin. Desalin Water Treat 57(34):16111–16118
31. Sabry RS, Al-haidarie YK, Kudhier MA (2016) Synthesis and photocatalytic activity of TiO_2 nanoparticles prepared by sol–gel method. J Sol-Gel Sci Technol 78(2):299–306
32. Kulkarni RM, Hanagadakar MS, Malladi RS, Shetti NP (2018) Ag(I)-catalyzed chlorination of linezolid during water treatment: kinetics and mechanism. Int J Chem Kinetics 50(7):495–506

Green Synthesis of Bioleached Flyash Iron Nanoparticles (GBFFeNP) Using *Azadirachta Indica* Leaves and Its Application as Fenton's Catalyst in the Degradation of Dicamba

S. Bhaskar, Basavaraju Manu, and M. Y. Sreenivasa

Abstract Fly ash made its suitable application in the waste management and remediation application. This article presents the synthesis of nanoiron particles using bioleached fly ash iron and its application as Fenton's catalyst in the degradation of an herbicide dicamba. Novel isolated bacterial strain *Acidithiobacillus Ferrooxidans* BMSNITK (MG 271,840) was used to recover iron from fly ash and green synthesis of fly ash iron nanoparticles was successfully carried out using *Azadirachta indica*. Synthesized iron nanoparticles were characterized with X-ray diffraction and electron microscopy and the catalytic role of bioleached fly ash nanoparticles was evaluated based on the degradation of target pollutant. Hydrogen peroxide and COD were considered as the indicating factors for tracing the reaction progress and degradation resulting 97.81% of dicamba degradation within 90 min. Study confirms the green synthesis of bioleached fly ash iron nanoparticle and its application in Fenton's oxidation.

Keywords *Acidithiobacillus Ferrooxidans* · Fenton's process · Jarosite · Herbicide · Ametryn

S. Bhaskar (✉)
Department of Civil Engineering, St. Joseph Engineering College, Vamanjoor, Mangalore 575028, (D.K), India
e-mail: baskarmalwanitk@gmail.com

B. Manu
Department of Civil Engineering, National Institute of Technology Karnataka, Surathkal, P.O. Srinivasnagar, Mangalore 575025, (D.K), India
e-mail: bmanu@nitk.ac.in

M. Y. Sreenivasa
Department of Studies in Microbiology, University of Mysore, Mysuru, Karnataka, India
e-mail: sreenivasamy@gmail.com

B. B. Das et al. (eds.), *Recent Trends in Civil Engineering*, Lecture Notes in Civil Engineering 105, https://doi.org/10.1007/978-981-15-8293-6_31

1 Introduction

Water quality in response to industrialization is degrading in a drastic way. Agriculture industry in this regards accounts a major contribution to water quality deterioration contributing to many hazardous pollutants. Herbicides a key pollutant from agriculture industry is of much concern to environmentalist in this regards. Dicamba, an herbicide belongs to chlorobenzoic group has its profound application in control of woody plants and broadleaf [1]. Most of the aquatic life gets affected by the traces detectable concentration of this herbicide in water (Wauchope. 1978). Many researchers made an attempt to degrade the dicamba using biological methods, which is feasible and costeffective. Unfortunately, the outcomes of the research claim that biological treatment process is inefficient in treating a large group of herbicides [2, 3]. Fenton's oxidation treatment among advanced oxidation process is one of the efficient and fast methods of treating most of the organic pollutants [4, 5]. It is the cost involved in supply of large amount iron catalyst marks its limitations in the application of Fenton's process in large scale. Successful attempts havbe een made by various researchers in substitution of this iron requirement with natural laterite iron which found to be feasible and cost effective [6–10].

Role of nanoparticles in the treatment of nanoparticles has gain much importance in the field of environment because of its efficiency. Pastrana et al. extensively studied the degradation of diphenhydramine by photo-Fenton's reaction examining catalytic activity of broad range of nanoiron oxide particles dosage. Green synthesis of iron nanoparticles and its application in Fenton's oxidation of organic pollutants is proved to be effective and economical by many researchers [8, 11–13]. The present study involves the synthesis and characterization of bioleached fly ash iron nanoparticles using *Azadirachta indica* leaves and evaluation of the catalytic role of these iron particles in the Fenton's degradation of dicamba.

2 Material and Methods

2.1 Green Synthesis of Bioleached Fly Ash Nano Iron Particles (BFFeNP) Using Azadirachta Indica

Extraction of fly ash iron by bioleaching method was carried out using an isolated strain *Acidithiobacillus Ferrooxidans* BMSNITK17 (Accession No. MG271840) [14]. To extract Azardirachta indica solvent for nanoparticle synthesis, 50 g of fresh leaves were collected and rinsed in distilled water for 5 min to remove dust particles washed and dried in oven at 40 °C. Dried leaves were boiled in demineralized water at 80 °C for about 1 h. The solution was filtered with Whatmann's filter paper (No. 42) and stored at 4 °C for further use. For the synthesis of bioflyash nanoparticle leaves extract and leached lateritic solution was mixed in a proportion 1:1 with continuous stirring at room temperature. Formation of thick black precipitates indicates

the synthesis of iron nanoparticles. The solution is then centrifuged at 10,000 rpm to collect the nanoparticle pellets, which is then dried and stored.

2.2 Catalytic Role of Bioleached Flyash Iron Nanoparticles (BFFeNP's) in Fenton's Oxidation of Dicamba

Catalytic role of bioleached flyash iron nanoparticles in Fenton's degradation of dicamba was evaluated with 100 mg/L initial target compound concentration with initial pH adjusted to 3 [10]. Green Bioleached flyash iron nanoparticles (GBFFeNP's) were added to dicamba solution in an incremental rate of 1.25 mg/L, 2.5 mg/L and 5 mg/L. The solution was kept in an incubator shaker at 180 rpm for 5 min for proper mixing. Hydrogen peroxide (30%) solution was added to this solution correspondingly to study the combined effect of nanoiron and hydrogen peroxide in the degradation of dicamba. Samples were drawn at regular intervals for analysis. During sampling, each time 1 ml of sodium thiosulphate was added to halt the reaction [15]. All the experimental analysis was conducted in triplicates.

2.3 Analytical Procedure

High-performance liquid chromatography (HPLC) (Agilent 1200) was used for the measurement of dicamba concentration [13]. Chemical oxygen demand (COD) measurement was by colorimetric method [16]. UV–Vis spectrophotometer method was adopted for the measurement of H_2O_2 consumption [17]. Iron concentration was measured with UV–Vis spectrophotometer (Woods and Mellon, 1941). The pH was monitored by digital pH meter.

3 Results and Discussion

3.1 Characterization of Green Synthesized Bioleached Flyash Iron Nanoparticles (BFFeNP's)

SEM images reveal that the particles formed appear to be irregular globular particles, which are closely agglomerated structure (Fig. 2). The surface of particles is smooth and exhibits flake-like structure [13] (Xu et al., 2010). Figure 1 shows the XRD plot of synthesized nanoiron particles and the analysis dissipates the presence of iron with broad peaks at 2ϴ 22.451, 27.831, 41.285, 48.055 with d-spacing 0.3149, 0.1968, 0.0720, 0.24 ^{o}A, potassium at 2ϴ 22.22 with d-spacing 0.1968 and manganese at 2ϴ 33.27 with d-spacing 0.1968 (PDF No. 01-086-0231; 01-089-1261; 00-041-0183).

Presence of potassium and manganese is attributed to composition of *Azadirachta indica* leaves.

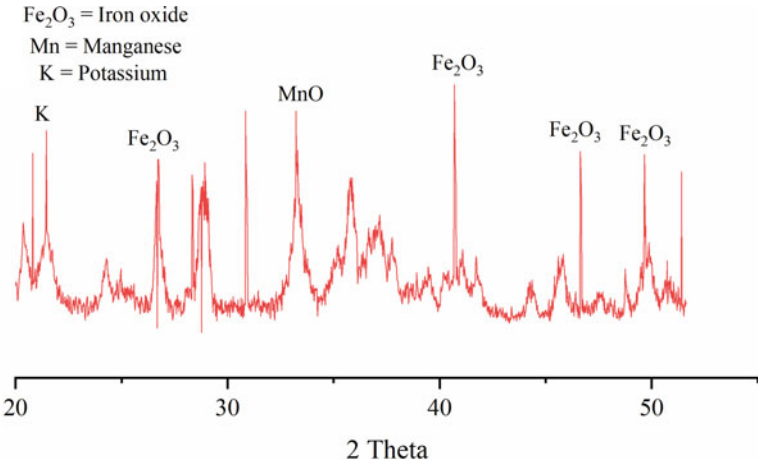

Fig. 1 XRD analysis of bioleached flyash iron nanoparticles (BFFeNP)

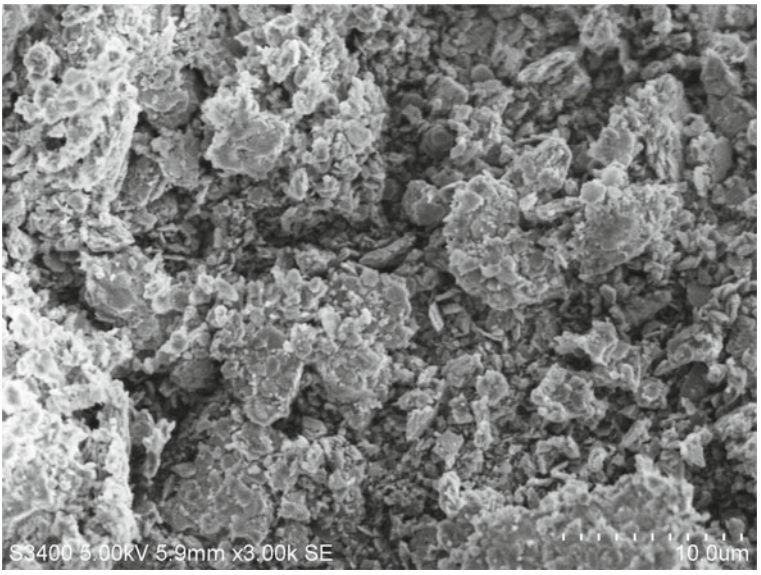

Fig. 2 SEM image of bioleached flyash nanoiron particles (BFFeNP)

3.2 Catalytic Role of Bioleached Flyash Iron Nanoparticles (BLFFeNP's) in Fenton's Oxidation of Dicamba

Initiation of oxidation started on the addition H_2O_2 as no removal of dicamba was found initially without H_2O_2 dosage. Initiation of degradation on H_2O_2 addition confirms the role of H_2O_2 in Fenton's oxidation. Removal of dicamba up to 97.81% was achieved with 20 mg/L of Bioleached Flyash iron nanoparticles and 50 mg/L of corresponding H_2O_2 dosage within 90 min. The observed COD removal was 77.45% during the treatment. Increase in H_2O_2 dosage from 50 mg/L to 100 mg/L to 200 mg/L for 20 mg/L does not increase the removal efficiency but led to drop in the efficiency. On increasing in iron dosage from 5 mg/L to 10 mg/L and 20 mg/L increases the efficiency of dicamba degradation indicating the catalytic role of iron nanoparticles in the Fenton's process. From the graph, it is observed that there is a drastic removal in target compound from 20 to 30 min. The sudden drop in efficiency is attributed to active formation of hydroxyl molecules during this period. Decrease in the efficiency is attributed to the formation of ferric hydroxyl complexes which in turn drops the degradation efficiency [15, 18, 19]. Sangami and Manu [8] successfully synthesized laterite based iron nanoparticles and experimentally claims the catalytic role of laterite-based iron nanoparticles in the degradation of dicamba in which the degradation efficiency was found to be 100%. Catalytic efficiency of iron nanoparticles depends on the process of synthesis of nanoparticles and its size, shape and surface area [13] (Renchao 2014). The catalytic effect of bioleached flyash iron nanoparticles is dissipated in Fig. 3. C/Co being the ratio of final and initial pollution concentration indicates the performance of treatment process at different dosage of bioleached fly ash nanoparticles and hydrogen peroxide. It is observed in Fig. 3a, with 20 mg/L of iron nanoparticles maximum reduction in C/Co has been observed in correspondence with 50 mg/L of H_2O_2 dosage.

4 Conclusions

Nanoiron particles were synthesized using *Azadirachta indica* leaves with iron leached out from flyash by biological means. Synthesized Bioleached Flyash iron nanoparticles (BFFeNP) were characterized with scanning electron microscopy for its surface characterization and X-ray diffraction for its mineralogical composition. Application of synthesized iron nanoparticles as iron catalyst in the Fenton's oxidation of dicamba was evaluated and confirmed. Synthesized iron nanoparticles are confirmed to be low-cost catalyst with dicamba degradation up to 97.81%. Optimum dosage of BFFeNP and hydrogen peroxide was found to be 20 mg/L and 50 mg/L, respectively, with COD removal efficiency of 77.45%. It is observed that there is a reduction in treatment duration in comparison to commercial iron catalyst.

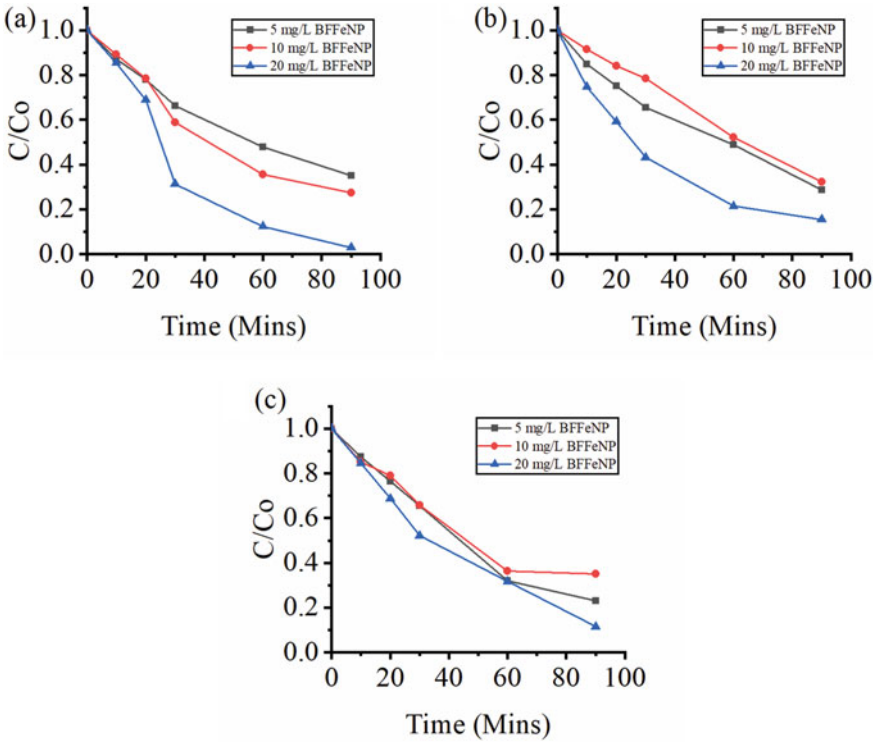

Fig. 3 Degradation of target compound at different nanoiron loadings for **a** 50 mg/L H_2O_2 dosage **b** 100 mg/L H_2O_2 dosage **c** 200 mg/L H_2O_2 dosage

References

1. Caux PY, Kent RA, Tache M, Grande C, Fan GT, MacDonald DD (1993) Environmental fate and effects of dicamba: a Canadian perspective. In Reviews of environmental contamination and toxicology (pp. 1–58). Springer, New York, NY
2. Cheng S, Vidakovic-Cifrek Ž, Grosse W, Karrenbrock F (2002) Xenobiotics removal from polluted water by a multifunctional constructed wetland. Chemosphere 48(4):415–418
3. González-Cuna S, Galíndez-Mayer J, Ruiz-Ordaz N, Murugesan S, Piña-Escobedo A, García-Mena J, Lima-Martínez E, Santoyo-Tepole F (2016) Aerobic biofilm reactor for treating a commercial formulation of the herbicides 2, 4-D and dicamba: Biodegradation kinetics and biofilm bacterial diversity. Int Biodeterior Biodegradation 107:123–131
4. Arnold SM, Hickey WJ, Harris RF (1995) Degradation of atrazine by Fenton's reagent: condition optimization and product quantification. Environ Sci Technol 29(8):2083–2089
5. Gaggi C, Duccini M, Bacci E, Sbrilli G, Bucci M, El Naby AH (1995) Toxicity and hazard ranking of s-triazine herbicides using microtox® two green algal species and a marine crustacean. Environ Toxicol Chem 14(6):1065–1069
6. Karale R, Manu B, Shrihari S (2013) Catalytic use of laterite iron for degradation of 2-aminopyridine using advanced oxidation processes. Contributory Papers, 203
7. Sangami S, Manu B (2017a) Fenton's treatment of actual agriculture runoff water containing herbicides. Water Sci Technol 75(2):451–461

8. Sangami S, Manu B (2018) Catalytic efficiency of laterite-based FeNPs for the mineralization of mixture of herbicides in water. Environmental technology 1–13
9. Amritha AS, Manu B (2018) Degradation of nitroaromatic compounds: a novel approach using iron from laterite soil. Appl Water Sci 8(5):136
10. Manu B, Mahamood S (2019) Photo-fenton degradation of paracetamol—evaluation of iron extracted from laterite soil as catalyst. Adv Sci, Eng Med 11(1–2):127–132
11. Shahwan T, Sirriah SA, Nairat M, Boyacı E, Eroğlu AE, Scott TB, Hallam KR (2011) Green synthesis of iron nanoparticles and their application as a Fenton-like catalyst for the degradation of aqueous cationic and anionic dyes. Chem Eng J 172(1):258–266
12. Xu L, Wang J (2011) A heterogeneous Fenton-like system with nanoparticulate zero-valent iron for removal of 4-chloro-3-methyl phenol. J Hazard Mater 186(1):256–264
13. Kuang Y, Wang Q, Chen Z, Megharaj M, Naidu R (2013) Heterogeneous Fenton-like oxidation of monochlorobenzene using green synthesis of iron nanoparticles. J Colloid Interface Sci 410:67–73
14. Bhaskar S, Manu B, Sreenivasa MY (2019) Bacteriological synthesis of iron hydroxysulfate using an isolated Acidithiobacillus Ferrooxidans strain and its application in ametryn degradation by Fenton's oxidation process. J Environ Manage 232:236–242
15. Khan E, Wirojanagud W, Sermsai N (2009) Effects of iron type in Fenton reaction on mineralization and biodegradability enhancement of hazardous organic compounds. J Hazard Mater 161(2–3):1024–1034
16. Apha A (1995) WPCF. American Public Health Association, Washington, DC, Standard methods for the examination of water and wastewater
17. Eisenberg G (1943) Colorimetric determination of hydrogen peroxide. Ind Eng Chem Anal Ed 15(5):327–328
18. Burbano AA, Dionysiou DD, Suidan MT, Richardson TL (2005) Oxidation kinetics and effect of pH on the degradation of MTBE with Fenton reagent. Water Res 39(1):107–118
19. Kang YW, Hwang KY (2000) Effects of reaction conditions on the oxidation efficiency in the fenton process. Water Res 34(10):2786–2790

River Water Resource Management and Flood Control Using GIS

Jyoti Kumari, Kohima Dessai, Zwegal Wynne Cardozo, Blacinta Pereira, Rhea Fernandes, Annapurna Sakhardande, and Sanford Mascarenhas

Abstract Inappropriate flood mitigation strategies together with uncertainties in monsoon have led to two extremes, namely—droughts and floods in various parts of the globe. Authors of this paper have tried to approach this problem in way, so as to provide a sustainable solution in the domain of flood control system. Low lying areas in Quepem Taluka of South Goa along the bank of River Kushavati get submerged during peak monsoon. This makes it difficult for the locals to commute. The problem here gets magnified annually since silting due to floods makes river shallow. In this paper, authors have carried out studies by understanding the topography and nature of soil. Contours were obtained along with settlement areas to identify areas at lower elevation which would serve as potential relief areas. These areas can be used to detain water near most affected or critical areas. Water harvesting and groundwater recharge methods are proposed along with ponds and trench that will detain excessive downpour.

Keywords Water · Management · GIS · Detention · Flood

1 Introduction

During peak monsoon period, every year, the low lying areas in the heart of Paroda (Goa–India), on the bank of River Kushavati gets submerged. History has it that, 8 h of continuous rain will put some places and roads under water. The Paroda bridge, connecting Avedem, in the North–South direction and the state highway in East–West direction leading to Margao from Quepem gets submerged disrupting the traffic in

J. Kumari (✉) · K. Dessai · Z. W. Cardozo · B. Pereira · R. Fernandes
Don Bosco College of Engineering, Margao, Goa 403602, India
e-mail: virgojyoti02@gmail.com

A. Sakhardande
Department of Civil Engineering, Don Bosco College of Engineering, Margao, Goa 403602, India

S. Mascarenhas
Department of Science and Humanities, Don Bosco College of Engineering, Margao, Goa 403602, India

B. B. Das et al. (eds.), *Recent Trends in Civil Engineering*, Lecture Notes in Civil Engineering 105, https://doi.org/10.1007/978-981-15-8293-6_32

the said area. The meteorological records repeatedly suggest that the duration of the storm, its time of occurrence and intensity is nearly same every year.

This is an age-old problem that is getting worse due to siltation of the river and lack of dredging. Settlements close to the bank of the River and no proper place for disposal makes dredging difficult.

'A flood occurs when the Geomorphic Equilibrium in the river system is disturbed because of internal or external factors or when a system crosses the geomorphic threshold' [1]. Worldwide, floods cause damage to houses, agriculture and public utilities every year in addition to the loss of precious human and cattle lives. Flooding often results from inadequate drainage at rail and road crossings, encroachments in the flood plains, saturation of low lying or flat areas and accumulation of runoff waters. The impact of floods is seen on individuals and communities, thus affecting social and economic environments. The effects of flood can be both positive and negative, and vary depending upon the location and extent of flooding. 'A GIS is a system designed to store, capture, analyse, manipulate, manage, and present spatial or geographic data' [2].

Khanna et al. [3] studied different ways of flood management using structural and non-structural measures and how GIS is helpful in the management of flood hazards. With GIS, geographical information is stored in the database and displayed for analysis. By overlaying different geographic layers, flood-prone area can be identified [3].

Seenirajan et al. [4] performed the study on the causes of Chennai flood 2015. Chennai floods were attributed to poor drainage facilities and excessive silting of Coouam River. With a purpose to analyse potentially affected areas, GIS integrated with multi-criteria decision analysis were employed [4].

Ganova et al. [5] presented the study to analyse the distribution of flood-risk potential at the regional scale. A progressive approach integrating GIS was adopted in the process to find the most causative factors of flooding [5]. Isma'il, Iyorti-mOpeluwaSaanyol [6] studied GIS and remote sensing techniques to produce flood map of the River Kaduna. With high-resolution imagery, a digital elevation model was developed using ArcGIS to identify the flood-prone areas [6]. Orman et al. [7] presented the work, which aimed at using GIS techniques to produce a potential flood hazard map based on geomorphic parameters and to estimate the degree of risk of individual sub-basin by combining normalized values of parameters [7]. In Volkova et al. [8], the purpose of the paper was to developed methods for modelling and analysing of flood situations with the use of GIS [8]. Khan et al. [9] showed that sometimes flood studies are divided into parts and represented using several drawings. The Land Development Division decided to convert them from paper to a digital format so the department could find the information quickly and would make flood studies accessible to a bigger audience [9]. In Kaewboonma et al. [10], the research methods used in this study were document analysis and qualitative method. Liou adopted knowledge acquisition approach for acquiring knowledge from the domain experts [10]. Zhang et al. [11], in this paper, put forward suggestions for design flood calculation with the water surface area taken into consideration.

A watershed was classified into a land watershed and a water surface watershed for flood flow calculation in this study [11].

2 Methodology

The required toposheets were georeferenced by providing the latitude–longitude data for the respective toposheets using ArcGIS software.

Here,

- The topography of the area was studied using digitized maps.
- The lowest contours and non-settlement potential relief areas were found.
- The construction of retention/detention structures was proposed, at places, after visiting sites.
- Various tests were conducted on the soils from the proposed areas.
- Suitable and economical materials were recommended for proposed structures.
- Cost of structures with proposed materials was estimated.

The image below shows digitized map of village Paroda (Fig. 1),
The strategy adopted for the completion of the work.

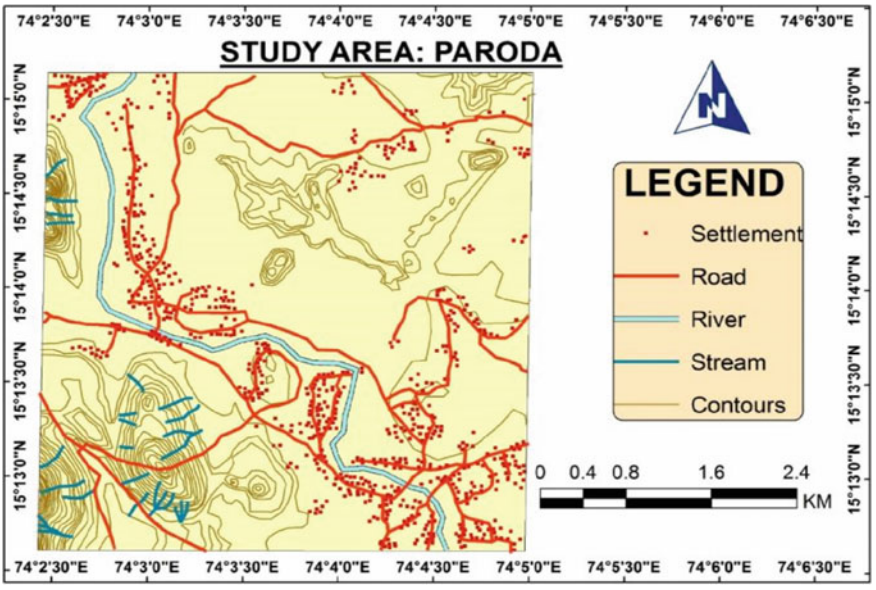

Fig. 1 Digitized contour map of study area using GIS

(a) Collection of data and understanding of topography using GIS
(b) Google maps were used in place of toposheets as base map along with the survey map of the area to digitize the affected area in order to understand the topography.
(c) The data were digitized to prepare the contour map of the area of contour interval 10 m. Also the river and road alignments, the settlement areas and the perennial streams were obtained.
(d) Identifying the critical areas.
(e) Finding the lowest contours and settlements that are very close to the river, critical areas were identified which are most affected by floods. Field visits and guidance from locals further clarified about the criticality of problems.
(f) Identifying the potential relief areas
(g) Potential relief areas were also identified after visiting the village premises, where it is suggested to construct the retention and detention structures.
(h) Ground validation
Different soil tests were performed on the field samples which included liquid limit test, plastic limit test, permeability test and sieve analysis to understand the soil type.
(i) Suggest remedies and offer optimum solutions
It is suggested to construction two ponds and a trench in the low lying areas to reduce the flood effects in the village.

The maximum radius of the ponds which can be fitted in the proposed areas was found out using ArcGIS. The length of the proposed trench along the lowest contour was also got from ArcGIS.

The methodology can be summarized as under (Fig. 2).

3 Proposed Remedies/Structures

Ponds and Trench.

It is proposed to construct two circular ponds in the low lying areas of the village. One pond is of 150 m radius and 86,236.71 m^3 capacity, while other pond is of 100 m radius and 38,327 m^3 capacity. It is also proposed to construct a trench along one of the lowest contours. During floods, the water from the river will be collected in the pond. During rainfall water will be collected along the contour trench. The structures were suggested on the upstream side of the river Kushawati so as to reduce its effects on the downstream side of the river.

The digitized map below shows the proposed ponds at the potential relief areas and the start and endpoint of the proposed trench;

The blue circle shows the 100 m radius pond, while, the green circle shows the 150 m radius pond. The green tracing line shows the proposed trench (Figs. 3 and 4).

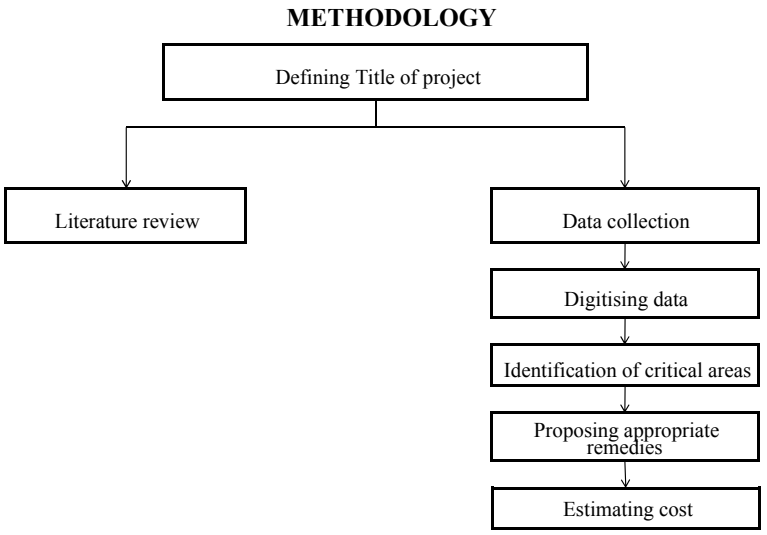

Fig. 2 Flowchart for methodology

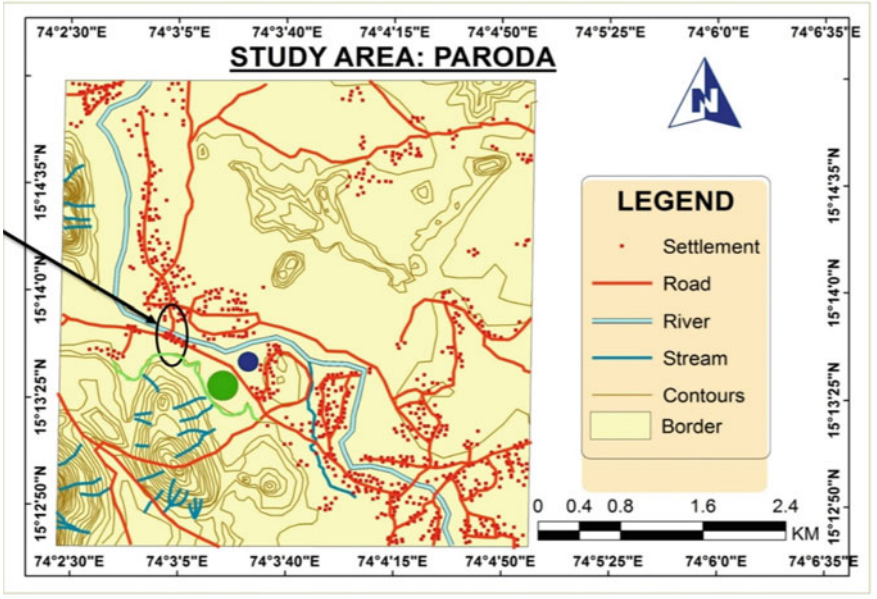

Fig. 3 Digitized image showing detention structures

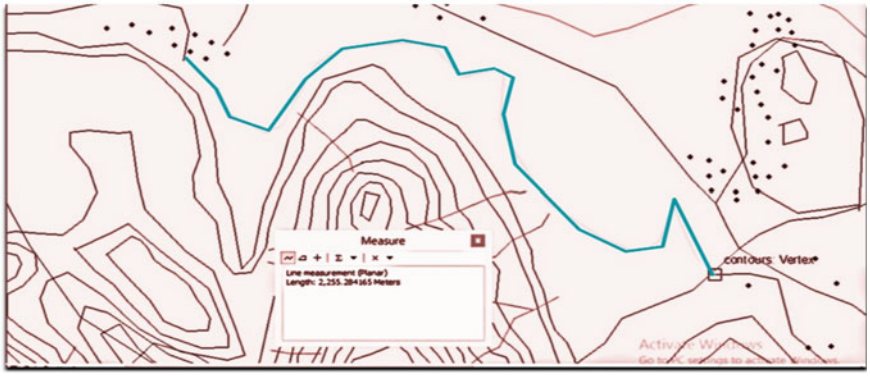

Fig. 4 Enlarged image of proposed trench

3.1 Interpretation of All the Tests Conducted on Soil Samples

Test suggesting the soil classification was conducted, namely Grain size distribution, Atterberg's Limit, Permeability test.

1. Tests were carried out on the soils of proposed detention site. The two tests, namely, Atterberg's limits and permeability test indicate clayey soil of low compressibility.
2. The grain size distribution shows that soil is well-graded sandy soil. Discrepancies could be because of the portion of soil selected for Atterberg's limits were passing through 425 microns.
3. Also, it has been observed from the soil that there is considerable silt content present, which could be the reason of low permeability. Since the percolation expected is less, the soil proves to be useful for intended purpose, i.e. construction of detention structures [12, 13].

4 Conclusions

Methods for harvesting water in the area and recharging the groundwater along with detention structures to store the water during excessive downpour have been proposed.

Sites and materials were so selected that they are economical and environment friendly compared to most other alternatives that will offer a sustainable solution to the long-pending menace in the region.

1. After performing a few studies, remedies are suggested in order to control the flood problem in the said region. Solution to this problem is mainly involved with identifying areas for detaining water nearer to the affected region and at a lower elevation along the downstream. It is suggested to construct two ponds of

86,236.71 m^3 and 38,327.43 m^3, respectively, which can be fitted in the selected potential relief areas. The materials suggested for the construction of ponds are geosynthetic clay liners and asphalt-fabric membrane having approximate cost of Rs. 383 and Rs 162 per square meter. These are more economical and suitable as compared with other alternatives of pond liners [14]. Topography and nature of soil were well understood and used to obtain contours, settlements, river, streams and roads. Using the map, the critical areas and the potential relief areas were identified.

2. It is suggested to construct trench along the lowest contour of depth 1 m. It should be backfilled with gravel layer having thickness of 0.6 m and sand having thickness 0.4 m.

References

1. Raymahashay B, Sinha R Flood disasters and management: Indian scenario. Manual-Bihar state disaster management authority and ministry of earth sciences, Govt. of India
2. Wieczorek WF, Delmrico AM (2009) Geographic information system, WIREs computational statistics. 1(2)
3. Khanna RK, Agarwal CK, Kumar P (2005) Remote sensing and GIS applications in flood management
4. Seenirajan M, Natarajan M, Thangaraj R, Bagyaraj M (2017) Study and analysis of Chennai flood 2015 using GIS and multicriteria technique. J Geogr Inform Sys 9:126–140
5. Ganova L, Zelenakova M, Purcz P, Diaconu DC, Orfanus T, Kuzevicova Z (2017) Identification of urban flood vulnerability in Eastern slovakia by mapping the potential natural sources of flooding
6. Isma'il M (2013) Application of Remote Sensing (RS) and Geographic Information Systems (GIS) in flood Vulnerability Mapping: Case Study of River Kaduna. IyortimOpeluwaSaanyol. 3(3)
7. Orman A, Schroder D, El Rayes A, Geriesh M (2011) Flood hazard assessment in Wadi Dahab, Egypt based on basin morphometry using GIS techniques
8. Volkova Y, Skvortsova O, Nikonova O, Pavlov S, Mirschel W (2016).Use of GIS-environment under the analysis of the managerial solutions for flood Togo. Events protection measures by Aleksandr Nikonorov, Vladimir Badenko, Vitaly Terleev, Issa
9. Khan MM, Vogel R, Edwards RO (2010) Polk county board of county commissioners. GIS-ing flood data
10. Kaewboonma N, Tuamsuk K, Kanarkard W (2013) Knowledge acquisition for the design of flood management information system: Chi River Basin, Thailand
11. Zhang Q, Diao Y, Dong J (2013) Impacts of water surface area of watershed on design flood
12. Bureau of Indian Standards IS code: 2720-5 "Methods of Tests for soils" (1985)
13. Garg SK (2014) Khanna Publications.-Soil mechanics and foundation engineering Edition 11
14. Frasier GW, Myers LE (1983) Handbook of water harvesting. U.S. department of agriculture, Agriculture Handbook No. 600

Recent Trends in Construction Technology and Management

Production of Artificial Aggregates Using Industrial By-Products Admixed with Mine Tailings—A Sustainable Solution

B. P. Sharath and Bibhuti Bhusan Das

Abstract This experimental cum research exploration is focused on the production of artificial aggregates with an adoption of pelletization technique. The influential factors for ascertaining the efficiency of the production process are nature of binding agent, required moisture content, process duration and dosage of alkali binder. Aggregates were produced in various combinations including the industrial by-products replaced partially by mine tailings with the addition of some percentages of lime. These produced aggregates were analysed for their engineering properties. It was observed that with the utilization of these mine tailings in this production of artificial aggregates have given an enhancement in the basic characteristic properties of the produced aggregates which are nearly comparable to that of natural aggregates.

Keywords Pelletization · Fly ash · GGBS · Iron ore tailings · Burnt lime · Alkali binder

1 Introduction

As the definition for artificial aggregates says, these are environmental-friendly materials, which are made out of various industrial by-products which are all considered as contaminants for the environment.

As per the present scenario concerned with respect to the construction industries, the posing concerns reflecting to the world are to find out inventive materials on one hand and on the another, finding out an appropriate solution for the never-ending demand for the naturally available aggregates. In order to compensate both of these things, it is very much essential to come up with these artificial aggregates as these are capable of solving the problem of the disposal of these industrial wastes and also,

B. P. Sharath (✉) · B. B. Das
Department of Civil Engineering, National Institute of Technology Karnataka, Surathkal, Mangalore, Karnataka 575025, India
e-mail: bpsharath1993@gmail.com

B. B. Das
e-mail: bibhutibhusan@gmail.com

B. B. Das et al. (eds.), *Recent Trends in Civil Engineering*, Lecture Notes in Civil Engineering 105, https://doi.org/10.1007/978-981-15-8293-6_33

they can help in preserving the natural resources from getting depleted. In addition to this, the reusage of industrial by-products can lessen the environmental pollution, protecting the natural reserves from deterioration and finally, providing a way for sustainable development in the aggregate industries.

It's a known fact that in this rapidly growing construction world, concrete is the very primary and universal material which is almost used in all types of infrastructures, irrespective of its very specific need in different areas, i.e. from the development of construction blocks till the erection of high-rise buildings. Concrete, which is generally composed of cement, water, aggregates, and admixtures, which undergoes through the process of hydration making it a hardened mass once it has been placed within the forms. For this universal material, there is a never-ending demand for the sources of raw materials (i.e. aggregates) from natural resources, which can be fulfilled only by mining or quarrying of the raw materials. But, in the process of doing this, it has to be ensured that these natural resources can guarantee an adequate and continuous supply only up to certain years or decades until which there will be stepped growth in the construction industries and in turn the economical development of any country. It has to be noted that as the time moves ahead, the impact of the shortage of these construction materials on the construction industries will be very vital such as an increase in the cost of construction and shifting this kind of burden to the end users [1], hence affecting the national development of any nation. Though there is an availability of projected value of the stock of the natural aggregates, which can fulfil the development factor up to some years, but because of the destructive consumption of these aggregates as well as the demand for it, the days are near which will slowly diminish these non-renewable sources of aggregates until and unless an adequate action plan is taken with respect to their conservation. Suitable planning and prevention are very much important for avoiding the impact of shortage and also to solve the issues related to the supply for the future development of any nation. Therefore, it is a need of joining the hands of all the construction industries towards the production methods aimed at sustainability which can maintain the conservation of these natural resources intact. The finest way that can be employed in doing this is to adopt and practise the sustainability concept by reusing the huge rejected materials generated from various industries into the construction or concrete industries.

From the available sources, it is learnt that our country's construction sector has grown at annual average growth rate of 10% compared to the last decade with the simultaneous impact on nation's GDP too, by incrementing ₹1.5 trillion (2001–02) to ₹4 trillion (2011–12), which matches the nation's GDP (viz. 8%). It is also learnt that this construction industry comprises as the second largest part in India's economy with respect to employment, after agriculture, by allocating employment to 35 million people [2]. With respect to the material consumption concerned in India, this construction sector was again the most consumed one, which accounts for almost 20% of all with respect to the demand of materials used [3]. Major materials employed in this sector are sand, stones, soil and limestone. Among all, the cement industries are the most shooters of CO_2 in the open environment, and to the fact that, these accounts for an approximate of 7% of the country's total carbon dioxide emissions. Also, India is the second most happening producer of cement in the world,

producing 210 million tonnes in 2010, which was 6% of global production. In our country, the per capita usage of cement is very low compared to the other developed countries at less than two hundred kg per person, but by observing the present growth rates, it is anticipated that it may go up to four to seven times by 2050 [4]. Since our country has substantial limestone deposits, it is predicated that they may come to an end by 2060 because of the current growing rates.

Therefore, it is very clear from the above context with respect to Indian construction sector that it is most likely going to witness a very serious problem in view of material supplies, if this estimated growth in demand persists. This sector is mainly susceptible to the price escalations, since the material costs itself accounts for 2/3rd of the total cost of a typical building. It's a high time to develop a solid attention on the resource efficiency and to encourage the utilization of secondary and alternate materials for India's construction industries for moving further towards its growth.

Some of the construction industries have already acted upon this alarming situation and they are effectively utilizing the industrial wastes in order to produce value-added materials. To name some of them, first, fly ash, which is a secondary product of coal burning in power plants deployed for production of electricity. It is available in tons together since its dumped in big heaps after the above-mentioned process is over. There are various problems connected to the effective disposal of fly ash and since the construction sector is the only one which is capable of utilizing this huge amount of fly ash lying around. It is mainly composed of aluminous and siliceous contents, which forms cement in the presence of water, and when it is blended with lime and water, FA forms a composite which is similar to Portland cement. Hence, fly ash is being effectively used by many cement industries and also, it is widely accepted as an eco-friendly material because of its less embodied energy, again counting for a step towards sustainable development.

Second, blast furnace slag, which is derived by firing molten iron slag from a blast furnace in water or steam, to make a glassy product which is dried and grounded into fine powder. Its chemical composition is similar to that of an ordinary portland cement and also there are counting benefits, which makes this as an efficient material for reusing in concrete such as it is able to produce a low CO_2 concrete, with low levels of embodied CO_2, more durable as it prevents concrete from being cracked and protecting it from getting damaged from silica-alumina reaction, sulphates and chlorides. It's capable of providing an aesthetic finishing compared to that of done using ordinary Portland cement. Hence, GGBS has found an efficient reusage by various construction industries. Similarly, there are various other alternate materials like Rice Husk Ash, Ferrocement, Plastic wood, Synthetic fibres, recycled aggregates, bamboo, etc., which can be effectively reutilized in the production of value-added materials.

From the last decade, there was an arising curiosity to develop a system for the production of advanced and alternative aggregates also which can aid the several industries in the construction field. The main motivation behind this was to establish and initiate a generation of the production of artificial aggregates which can retort back to the changes posed to them or to the environment in which they are exposed, in a very suitable and controlled manner. There is already a utilization of

these artificial aggregates in the infrastructure development as a substitute for natural aggregates produced by either expansion or sintering of clays, shales, or fly ash, and both lightweight and dense aggregates produced from blast-furnace slag, etc. [5]. Because of their exceptional engineering properties such as absorption, porosity, permeability, strength, density, specific gravity, particle shape, surface texture and also their chemical compositions and possible reactions with systems like cement and concrete, makes them a vital material in various engineering field sciences. Hence, all these are utilized in civil engineering projects so that they can have an impact on improvised performance, comfortability and energy efficiency of structures.

Fly ash, which is a foremost solid waste yielded from the coal incineration in the power plants. The waste generated by a normal 500 MW coal plant comprises of more than 125,000 tons of ash and 193,000 tons of sludge every year. Currently, as per Indian Ministry of Environmental and Forest Figures, only 20–30% of fly ash is being utilized in manufacturing cements, construction, concrete, concrete blocks and tiles and another particular amount is disposed of in landfills and embankments. More than 75% of this waste is not utilized which has led to various environmental problems of air, soil, surface and groundwater pollution. Hence, it needs a suitable disposal and reutilization for the conservation of ecosystem, which is vulnerable to the damages by the incorrect coal plant waste disposal.

It is the chief component, which is being used in the development of artificial aggregates and also, other cementitious materials like slag, metakaolin, lime, silica fume, etc., were also utilized in the development of artificial aggregates [6, 7].

GGBS (Ground Granulated Blast Furnace Slag), or BFS (Blast furnace Slag) or GBS (Granulated Blast Furnace Slag), had found its utilization as industrial by-product from a long history, which was almost 100–150 years. It was utilized in composite cements and as cementitious component of concrete since from years together. The very first marketable usage was (about 1959) for making of bricks with the usage of BFS. In the second half of nineteenth century, there was a finding of its cementitious properties and by the closure of nineteenth century, very first cements consisting of GBS were made. From the late 1950s, the utilization of GGBS was done independently as a pulverized supplement at the concrete mixer together with the portland cement, it attained recognition. It some of the countries, the name ‘slag cement’ is used for GGBS [8]. Hence, it is also an efficient material, which can be utilized for the production of artificial aggregates.

A brief review of literature gives an idea about a number of research investigations that is being carried out on the properties and characteristics of sustainable concrete, such as compressive strength and shrinkage cracking of concrete, influence of finer particles and the binding properties of the binder, porosity of concrete, tensile strength and durability properties, etc., wherein the utilization of aggregates was produced by pelletization with or without the adoption of sintering process. Also, the production of artificial aggregates usually consists of inclusion of rejected materials such as fly ash, bottom ash, volcanic ash along with some other substitutes such as cement, lime, clay binders and glass powder, which are believed to improve the characteristic properties of the aggregates. But, as per the research accomplished

and in view of reported results, it was learnt that the coarse aggregates produced artificially were lightweight which usually are incapable of withstanding the equivalent load alike natural aggregates. Also, there were cases wherein the water absorption values exceeded than the limits set in the Indian Standards [9].

Mine tailings, termed as 'residue' materials, generated after the completion of extraction of any valuable mineral from the invaluable fraction of an ore. The quantity of generation of these tailings differs from a mineral to mineral such as it was 90–98% for copper ores and 20–50% for other minerals [10]. It can be noted that, throughout the process of extraction and processing of mineral resources, the waste generation during this is one of thing which should be taken care of. The enormous quantities of mine tailings from the mining operations have raised concerns on the ecology and environmental entities like land occupation in larger areas, uplift of dusts drawn by wind, adulteration of surface and underground water. At present, the generation of iron ore tailings is estimated to be around 18 million tonnes per year in India [10]. Sustainable solutions for the utilization of such a huge volume of mine tailings in developing a value-added product poses a great challenge to the research fraternity. Hence, there is a huge scope available for the effective production of artificial aggregates with these iron ore tailings admixed with the other industrial by-products, thereby utilizing them effectively in concrete. In total, approximately 290 million tonnes are industrial waste and mine tailing being produced annually of which 18 million tonnes are from the iron ore extraction only [10]. The mine tailings are ultra-fines or slimes, having diameter less than 150 μm, are not useful and hence discarded. The safe disposal or utilization of such vast mineral wealth in the form ultra-fines or slimes has remained a major unsolved and challenging task for the Indian mining industry.

The most common method being used for the production of artificial aggregates from the past literature is by agglomeration. In this process, formation of grains takes place in a mechanized manner such as agitation, granulation and compaction [11]. Among these, in the agitation method, the rotating force is the dominating one. As the addition of moisture on the binding agent continues, the adhesive forces of the particles escalate resulting in the formation of grains. There are various hardening techniques available that can be adopted to harden the fresh pellet and also can aid in attain the required strength within the grains [12]. The much-needed grain size distribution can be attained in the pelletization process by the variation of its basic influential parameters such as speed of the disc, angle of the pelletizer and moisture content required. This pelletization technique is the efficient method that can be employed in the production of artificial aggregates. The disc type pelletizer has more efficiency for aggregate production in comparison with drum type pelletizer or cone type pelletizer [12]. It is learnt that some influential parameters of pelletization should be considered for the efficient production, which are nothing but speed and angle of pelletizing disc, required moisture content and duration of pelletization [11]. The characteristic properties of artificial aggregates after production should be in accordance to acceptance criteria's as per 'Bureau of Indian Standards'. There are various literatures available, which define the different optimum values for these

parameters and among all of them, the best suitable set of optimum values is selected for this research investigation.

In geopolymerization, alkali activator has a major role of initialling the hydrolysis of the entities existing in alumino-silicates which are utilized as raw materials [13]. Its impact is strongly influenced by various affecting aspects involved in it like various kinds of activating agents (mostly alkalis) [13–16], concentration of the alkali solution [16–23] and curing regime [13, 24–28]. Among all, the most influential factors were selected for this research investigation.

There are previous studies wherein the production of artificial aggregates was carried out using different raw materials and binders using this pelletization technology [29, 30], but there are limited studies available, which are aimed at using iron ore tailings as a partial substitute to the industrial by-products. From the previous literature, it was noted that this utilization of iron ore tailings is capable of enhancing the engineering properties of the produced aggregates artificially because of its characteristic properties and hence these produced aggregates can comply to accepting criteria's of Bureau of Indian Standards.

The objective of this stated investigation is focussed on the producing pelletized aggregates using fly ash and GGBS which is partially replaced by iron ore tailings with the addition of some percentages of burnt lime using alkaline solution as a binder. These produced aggregates were evaluated for their basic engineering properties and were compared with that of natural aggregates.

1.1 Significance of the Study

Since there a huge amount of utilization of natural aggregates undergoing because of rapid changes happening in the infrastructure development of country, the days are near when the reserves of these natural aggregates are going to end because of this endless need. Hence, it is very much essential to find alternate materials for various construction works. Along with this urgent need, the aid of the available and emerging technology also plays a very important aspect in the production of aggregates with the local reserves. As it can be reviewed from all the available literature that there is a huge availability of industrial by-products which can be effectively reutilized for the production of these kind of value-added materials, which indeed is an arising challenge for the research fraternity.

2 Sequential Aspects of Experimental Investigation

2.1 Materials

Fly ash (FA) was procured from M/s UPCL, India. It is been identified as 'Class F' type according to Indian standards [31]. The characteristic compositions of fly ash were identified and are tabulated in Table 1.

GGBS (Ground Granulated Blast Furnace Slag) was procured from JSW cement Limited and is located in Toranagallu, Bellary (District), Karnataka. The physical and chemical properties of GGBS were analysed and are tabulated in Table 1.

Iron ore tailings (IOT) and Burnt Lime (BL) were procured from KIOCL Ltd., India. The characteristic properties of IOT were identified and are tabulated below. Potable water was utilized in making the alkali solution for producing the artificial aggregates.

Laboratory scale Na_2SiO_3 solution (8% of Na_2O, 26.5% of SiO_2, 65.5% of H_2O by mass), a constant SiO_2/Na_2O ratio of 3.3 as NaOH flakes (98% purity) was utilized as alkali activator in this investigation. The alkali solution was made by dissolving both Na_2SiO_3 and NaOH in calculated contents for framed experimental trials and the same should be stored in a vacuum-sealed container for 24 h to avoid hardening of the solution.

Table 1 Characteristic properties of materials

Observations	Class—F FA	GGBS	IOT
Specific gravity	2.2	2.9	2.9–3.2
Blaine's fineness (m^2/kg)	240	382	–
Fineness modulus	–	–	2.15
Chemical properties			
SiO_2	60.6	37.7	62.6
Al_2O_3	28.6	14.4	1.3
Fe_2O_3	3.9	1.1	28.1
CaO	1.7	37.3	1.5
MgO	1.8	8.7	0.6
SO_3	1.2	0.2	1.6
Na_2O	0.4	–	0.7
MnO	–	0.02	–
Insoluble residue	–	1.6	–
Glass content	–	92	
K_2O	0.1	–	0.3
LOI	1.6	1.4	2.2

2.2 Aggregate Production

Pelletization of raw materials was done using a pilot-scale disc pelletizer, Fig. 1. The pilot-scale disc pelletizer has disc dia.800–180 mm deep with a constant inclination angle of 45° and speed maintained at 13–15 rotations per minute. A duration of 12–18 min was employed for the pelletization of raw materials. The pelletization process includes: (i) Transferring of all the raw materials that are free from lumps into a Hobart mixer, (ii) Thorough dry mixing of these raw materials in this mixer and then transferring of the mixed raw materials into the pelletizing disc, (iii) Spraying of alkali solution within 3 min on the raw materials which were under rotation in the pelletizing disc, (iv) Scooping out the produced aggregates after 18 min from the pelletizing disc, Fig. 2. These produced aggregates were kept for curing under ambient temperature conditions (28 ± 2 °C with a RH of 80%) by spreading them over a polythene sheet in order to prevent them from sticking with one another. All these produced aggregates were stacked properly and labelled with their respective mix designations in order to avoid confusion.

Fig. 1 Pilot scale disc pelletizer

Fig. 2 Industrial trial production

2.3 Mix Proportions

The raw materials such as FA, GGBS, Burnt Lime and IOT were used for the production of pellets which in turn were termed as 'artificially produced aggregates' in this experimental investigation. Here, the contents of all the raw materials are fixed as percentage by weight of total planned mass of aggregate production in each experimental trial. The pelletization of these artificial aggregates with the incorporation of the above-mentioned raw materials with alkali solution as the binder is tabulated in the following Table 2.

2.4 Testing of Aggregates

2.4.1 Relative Density, Rate of Absorption, Aggregate Impact and Crushing Values (ACV and AIV)

The test for determining relative density and rate of absorption tests were done as per Indian standards [32]. For testing of aggregate impact and crushing values, aggregate samples should be ranging from 12.5 to 10 mm as stated in Indian standards [33].

Table 2 Test matrix of mix proportions for pelletization process

Proportion No	Mix code	IOT content %	FA content %	GGBS content %	BL content %
1	A1	50	50	–	–
2	A2	60	40	–	–
3	A3	70	30	–	–
4	A4	80	20	–	–
1	B1	50	–	50	–
2	B2	60	–	40	–
3	B3	70	–	30	–
4	B4	80	–	20	–
1	AA1	60	20	20	–
2	AA2	70	15	15	–
3	AA3	80	10	10	–
1	AB1	60	10	30	–
2	AB2	70	10	20	
3	AB3	80	5	15	
1	C1	70	30		2
1	C2	75	25	–	1

2.4.2 Individual Pellet Strength of the Pellets

The individual pellet strength of aggregates was measured by utilizing a CCS equipment (cold crushing strength), wherein a sample of pelletized aggregate is placed in between two plates, over which a gradual application of load is made to act, Fig. 3. The individual pellet strength (σ) was calculated using the below Equation [34].

$$\sigma = \frac{2.8 \times P}{\Pi \times X^2}$$

where, P = obtained load recorded from breaking of the sample, X = aggregate size placed for testing. The individual pellet strength was calculated in sequences (usually a count of 20 in numbers) of sizes ranging from 5 to 20 mm.

2.4.3 Experimental Programme

In process of geopolymerization, there are multiple variables that are responsible for it to act as a binder. From the past literature, it can be learnt that there are three factors which are responsible for attaining strength and efficiency within the produced aggregates such as Na_2O content, moisture content and curing regime. An alkali solution with more amounts of Na_2O had imparted higher strength [24]. But, in this

Fig. 3 CCS equipment and the pellet loading arrangement

investigation, less amounts of Na_2O were used for the producing artificial aggregates range from 3.5 to 5% of mass of FA. Moisture content (H_2O) ranging from 13 to 15% of mass of FA, which has shown better values for the desired engineering properties. It was observed that an increase in the moisture content will have a substantial impact on the grain size distribution of the produced aggregates. From process of pelletization, with the adoption of a best set of optimum results of pelletization factors (such as speed and angle of pelletizing disc, required water content and duration of pelletization), has given a better set of values for the desired engineering properties.

3 Results and Discussion

The engineering properties of the produced aggregates such as relative density, rate of absorption, AIV and ACV and individual strength of the samples were adjudged for the adjudgement of the test matrixes. The arising results for particular mixes are presented and discussed below.

3.1 Relative Density and Rate of Absorption

The average relative density of the artificial aggregates cured under ambient temperature conditions was in the range of 2.3–2.5. As per the reported values in the past studies for the relative density of the produced aggregates with different binders ranges from 2.1 to 2.8 [29, 30], but only with the raw materials such a FA, GGBS,

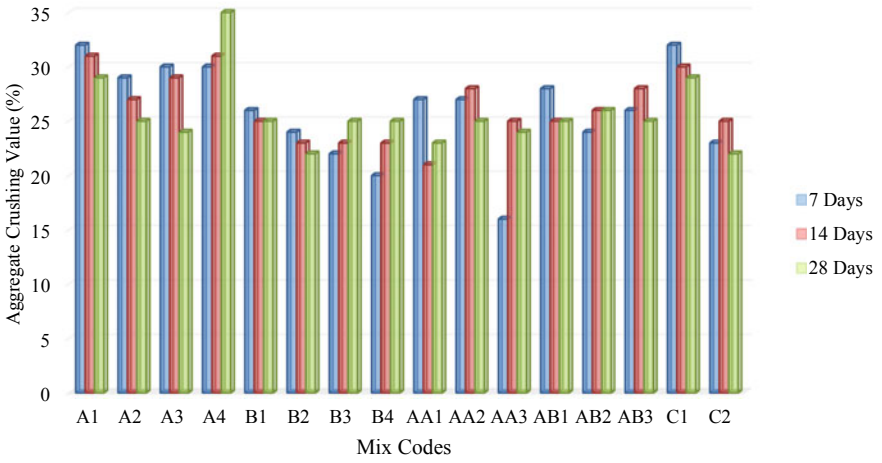

Fig. 4 ACV of the mixes for 7, 14 and 28 days of curing

lime and other cementitious materials. Here, in this experimental investigation, as there is an inclusion of IOT with the other raw materials, an enhancement in the relative density of artificial aggregates is reported in all the mixes. The average rate of absorption found among all the mixes ranges from 9 to 12%, which is still a parameter that needs attention.

3.2 Aggregate Impact and Crushing Value

From the obtained results from this experimental investigation, Figs. 3 and 4, it can be understood that among the mixes A1, A2, A3 and A4, both for impact and crushing values for 7, 14 and 28 days of curing, A2 and A3 have given better results. Similarly, in the case of mixes B1, B2, B3 and B4, the mixes B2 and B3 have given better results among all the other mixes for the three curing periods. However, the mixes B1 and B4 also have shown marginal results. In the cases of AA1, AA2, AA3, the mix AA2 is having better ACV for the three curing periods. In the case of AIV, AA2 is also having better results among all the other mixes. In the cases of AB1, AB2, AB3, almost all the mixes have a marginal ACV and AIV for all the three curing periods. In the case of C1 and C2 mixes, the ACV and AIV are more.

3.3 Individual Pellet Strength

From the obtained values of individual pellet strength chosen from the lot of the produced aggregates, Fig. 5, the mix A3 has the highest one among A series. The

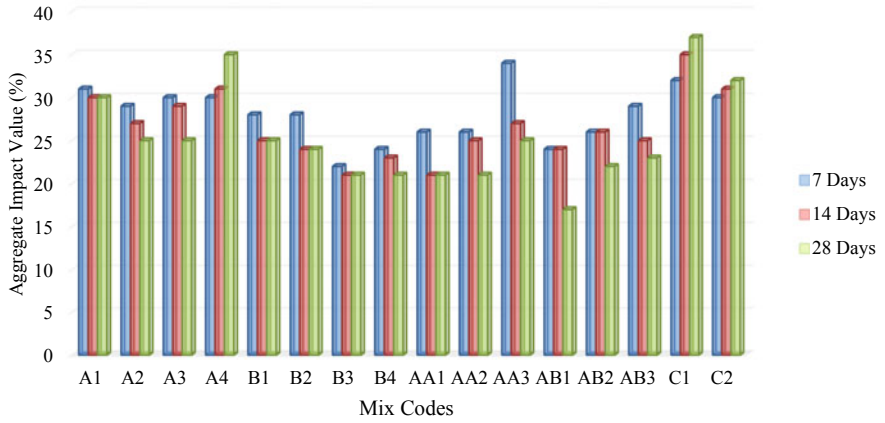

Fig. 5 AIV of the mixes for 7, 14 and 28 days of curing

mix B2 has the highest one among the B series. Mix AA2 and AB2 have the highest ones among AA and AB series, respectively. The mix C2 has better strength than C1 (Fig. 6).

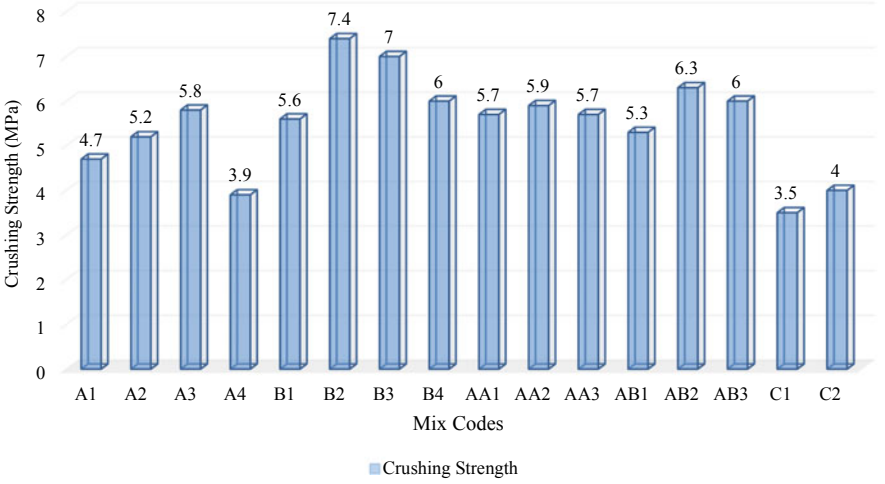

Fig. 6 Crushing strength of individual pellets

4 Conclusion

The present investigation showed the incorporation of industrial by-products such as FA and GGBS, which was replaced partially by mine tailings with the inclusion of some percentages of burnt lime in the mixes. From all the experimental investigations, it can be concluded that there was a less requirement of dosages of alkali binders and even with that so, the required strength and efficiency was achieved in the produced aggregates. The utilization of mine tailings in all the mixes has enhanced the engineering properties, which point out to the fact that it is mainly the proportion that influences the quality of these produced aggregates, all produced with the employment of pellerization process. The inclusion of burnt lime has not shown much influence in the quality of the produced aggregates, but apart from all the mixes, this utilization of mine tailings in the production of such artificial aggregates can surely be a definite step towards sustainable development and unlike this, various other value-added construction products can definitely be produced with the incorporation of these useful mine tailings.

Acknowledgements The authors convey their sincere thanks to Kudremukh Iron Ore Company Ltd., (KIOCL), Mangalore, and DST, India for extending all their laboratory facilities and providing the monetary support, respectively, for this research investigation.

References

1. Pereira JJ, Abd Hamid Z, Ismail S (2006) Minerals security in construction–issues and challenges for sustainable development
2. Banerjee A et al (2016) Material consumption patterns in India: a baseline study of the automotive and construction sectors. GIZ, New Delhi
3. Schandl H et al (2018) Global material flows and resource productivity: forty years of evidence. J Indus Ecol 22(4):827–838
4. Cement Sustainability Initiative. Technology roadmap: Low-carbon technology for the Indian cement industry. World business council for sustainable development and international energy agency
5. Fondriest FF, Snyder MJ (1964) Synthetic aggregates for highway construction. NCHRP Report 8
6. Davies DR, Kitchener JN (1996) Massive use of pulverised fuel ash in concrete for the construction of a UK power station. Waste Manage 16(1–3):169–180
7. Shayan A, Diggins R, Ivanusec I (1996) Effectiveness of fly ash in preventing deleterious expansion due to alkali-aggregate reaction in normal and steam-cured concrete. Cem Concr Res 26(1):153–164
8. Ilyushechkin AY et al (2012) IGCC solids disposal and utilisation, final report for ANLEC project 5-0710-0065: 66–76
9. Priyadharshini P, Mohan Ganesh G, Santhi AS (2011) Experimental study on cold bonded fly ash aggregates. Int J Civil Struct Eng 2(2):507–515
10. Nagaraj DR (2000) Minerals recovery and processing. Kirk-OthmerEncyclopedia of Chemical Technology
11. Harikrishnan KI, Ramamurthy K (2006) Influence of pelletization process on the properties of fly ash aggregates. Waste Manage 26(8):846–852

12. Bijen JMJM (1986) Manufacturing processes of artificial lightweight aggregates from fly ash. Int J Cem Compos Lightweight Concrete 8(3):191–199
13. Rangan BV et al (2005) Studies on fly ash-based geopolymer concrete. Proceedings of the world congress geopolymer, Saint Quentin, France. vol 28
14. Davidovits J (1999) Chemistry of geopolymeric systems, terminology. Geopolymer. 99(292), sn
15. Hardjito D et al (2004) On the development of fly ash-based geopolymer concrete. Mater J 101(6):467–472
16. Khale D, Chaudhary R (2007) Mechanism of geopolymerization and factors influencing its development: a review. J Mater Sci 42(3):729–746
17. Komljenović M, Baščarević Z, Bradić V (2010) Mechanical and microstructural properties of alkali-activated fly ash geopolymers. J Hazard Mater 181(1–3):35–42
18. Hardjito D, Cheak CC, Ing CHL (2008) Strength and setting times of low calcium fly ash-based geopolymer mortar. Mod Appl Sci 2(4):3–11
19. Rattanasak U, Chindaprasirt P (2009) Influence of NaOH solution on the synthesis of fly ash geopolymer. Miner Eng 22(12):1073–1078
20. Al Bakri AMM et al (2012) Effect of Na2SiO3/NaOH Ratios and NaOH molarities on compressive strength of fly-ash-based geopolymer. ACI Mater J 109.5
21. Görhan G, Kürklü G (2014) The influence of the NaOH solution on the properties of the fly ash-based geopolymer mortar cured at different temperatures. Compos part B: Eng 58:371–377
22. Patankar SV, Ghugal YM, Jamkar SS (2014) Effect of concentration of sodium hydroxide and degree of heat curing on fly ash-based geopolymer mortar. Indian J Mater Sci 2014
23. Phoo-ngernkham T et al (2015) Effects of sodium hydroxide and sodium silicate solutions on compressive and shear bond strengths of FA–GBFS geopolymer. Constr Build Mater 91:1–8
24. Fernández-Jiménez A, Palomo A (2005) Composition and microstructure of alkali activated fly ash binder: effect of the activator. Cem Conc Res 35(10):1984–1992
25. Rahim A et al (2014) Effect of solid to liquid ratio on the mechanical and physical properties of fly ash geopolymer without sodium silicate. Applied mechanics and materials. vol 625. Trans Tech Publications Ltd
26. Rahmiati T et al (2015) Effect of solid/liquid ratio during curing time fly ash based geopolymer on mechanical property. Materials science forum. vol 803. Trans Tech Publications Ltd
27. Kong DLY, Sanjayan JG, Sagoe-Crentsil K (2007) Comparative performance of geopolymers made with metakaolin and fly ash after exposure to elevated temperatures. Cem Concr Res 37(12):1583–1589
28. Shinde BH, Kadam KN (2015) Properties of fly ash based geopolymer mortar. Int J Eng Res Technol 4.7
29. Gomathi P, Sivakumar A (2014) Cold bonded fly ash lightweight aggregate containing different binders. Res J Appl Sci Eng Technol 7(6):1101–1106
30. Le Anh-tuan B et al (2012) Manufacture and performance of cold bonded lightweight aggregate using alkaline activators for high performance concrete. Constr Build Mater 35:1056–1062
31. IS 3812—Part 2 (2013) Specification for pulverized fuel ash: For use as admixture in cement mortar and concrete, Bureau of Indian Standards, New Delhi
32. IS 2386—Part 4 (1963) Methods of test for aggregates for concrete: mechanical properties, bureau of Indian standards, New Delhi
33. Gomathi P, Sivakumar A (2012) Characterization on the strength properties of pelletized fly ash aggregate. ARPN J Eng Appl Sci 7(11):1523–1532
34. Shivaprasad KN, Das BB (2017) Influence of alkali binder dosage on the efficiency of pelletization of aggregates from iron ore tailing and fly ash. Int J Eng Res Mechan Civil Eng 2(3):388–392

Predicting the Service Life of Reinforced Concrete by Incorporating the Experimentally Determined Properties of Steel–Concrete Interface and Corrosion

E. P. Sumukh, Sharan Kumar Goudar, and Bibhuti Bhusan Das

Abstract Service life of a reinforced concrete structure depends on its durability in aggressive exposure conditions. In the case of reinforced concrete structures, the phenomenon that directly affects its durability is corrosion of rebar, which has direct influence on the residual service life. Corrosion in reinforced concrete basically initiates at its weakest zone called steel–concrete interface due to its porous nature. The extent of this porous zone is being represented in terms of Porous zone thickness which has been extensively reported by various researchers. This porous zone thickness is one of the key influencing factors in the prediction of residual service life of the reinforced concrete structure. Several mathematical models were proposed by various researchers to estimate the time required for cover cracking of concrete due to rebar corrosion by assuming different values of porous zone thickness (PZT) without any systematic experimental investigation. Assuming a steady value of PZT for all kinds of concrete without any practical justification will misinterpret the predicted residual service life. In the present work, an effort has been made to evaluate an existing analytical model to predict the time to concrete cover cracking by incorporating the experimentally obtained and published data on porous zone thickness. It was found that the porous zone thickness and rate of corrosion have a major role in evaluating the residual service life of reinforced concrete structures.

Keywords Service life prediction · Porous zone thickness · Corrosion · Cover cracking · Durability

E. P. Sumukh (✉) · B. B. Das
Department of Civil Engineering, National Institute of Technology Karnataka, Surathkal, Mangalore 575025, India
e-mail: sumukhgowdaekkeri@gmail.com

B. B. Das
e-mail: bibhutibhusan@gmail.com

S. K. Goudar
Full Time Adjunct Faculty, Department of Civil Engineering, College of Engineering, Pune, Maharashtra 411005, India
e-mail: sgcr17@gmail.com

B. B. Das et al. (eds.), *Recent Trends in Civil Engineering*, Lecture Notes in Civil Engineering 105, https://doi.org/10.1007/978-981-15-8293-6_34

1 Introduction

Steel reinforced concrete is the primary and extensively used material in the present era of construction. This reinforced concrete structure once it is built, it should serve the purpose effectively for which it has been built. Reinforced concrete has become the primary construction material for shelter, pavements, bridges, dams, under water structures, tunnels, etc., irrespective of the type of surrounding exposure and continuously varying climatic conditions. But this surrounding exposure and climatic conditions have a greater tendency to cause deterioration inside the reinforced concrete. Their destructive effect on the durability of reinforced concrete structures will be severe as concrete is having porous structure [1–5]. Hence, determining the life span of reinforced concrete structure during which it could satisfy all its purpose of construction is very much essential for repairs and rehabilitation of the structure.

Reinforced concrete is a hardened mass formed by the fusion of various ingredients such as finer binder material (usually <90 μm in size), medium of hydration, i.e. water, fine aggregates (75 μm to 4.75 mm), coarse aggregates (>4.75 mm), admixtures, reinforcing steel bars, etc., of different physical, morphological and chemical properties. Further the grain size, shape, texture and specific gravities (usually ranges from 1 to 3.15) are also responsible for the development of non-homogeneity inside the reinforced concrete [5–11]. This non-homogeneity leads to the creation of interfaces among the various compositions of reinforced concrete and is being named as interfacial transition zone (ITZ) [5, 10, 12–15]. The interface between binder paste and aggregates and between steel and concrete are the most crucial as well as critical zone of reinforced concrete when durability is taken under consideration because of their permeable and porous nature [5, 7–11, 13, 16, 17]. In addition to these kinds of interfaces some air voids, capillary pores and gel pores are also being exist in the mass of concrete [6]. Owing to all these, concrete has a porous structure that allows harmful agents which are present in the surrounding medium such as chloride, sulphate, carbon environment to pass into its core structure [5, 18, 19]. The ions of these harmful agents alter the inside environment of reinforced concrete and start deterioration mainly in the form of corrosion and carbonation [5, 16].

Among the various types of voids, pores and interfaces in reinforced concrete, the interface between concrete and steel is termed as a weakest zone, which has impact on both mechanical properties and durability of a RC structure [1, 2, 4, 15, 19–29]. The reasons for being a weakest zone are due to weak bonding/adhesion between steel and concrete because of non-homogeneity[1, 5, 10, 30, 31], existence of air voids or defects at steel–concrete interface (SCI) because of excessive compaction and higher w/c ratio[1, 4, 5, 18–21, 27, 32] and also due to occurrence of corrosion initiation point at this zone.

Steel–concrete interface is a region with slightly higher water to cement ratio [4] and higher porosity due to a phenomenon called wall effect [6]. The extent of this porous zone from the surface of rebar is being represented in terms of porous zone thickness [1, 4, 25–28]. It is also surrounded by a irregular layer of $Ca(OH)_2$ which is

responsible for maintaining higher pH (>13.5) that creates alkali environment around the SCI (passive layer) [1, 5, 18, 33, 34]. This alkali environment forms a thin oxide layer that performs as a substantial hurdle for corrosion initiation [1, 4, 5, 12, 19, 21, 25, 28, 35]. This oxide layer degrades with the gradual fall in the pH of pore solution of concrete due to the formation of carbonic acid during carbonation [4, 5, 36, 37]. In case of chloride exposure to reinforced concrete, the ions of chloride migrate into the concrete through cracks, voids, pores, etc., which reduces the pH of the pore solution of concrete that gradually deteriorates the passive layer [1, 5, 18, 33, 34]. Due to the porous structure of SCI, this acidic environment with harmful chloride ions easily ingress the SCI and deposits over there [5, 24, 38, 39]. Once the chloride concentration exceeds the chloride threshold of concrete, activation of corrosion on the exterior rebar surface occurs [5, 19, 36, 37]. Thus the properties of concrete especially the properties of SCI act a fundamental role in the durability and service life of the reinforced concrete structure. Hence, a clear understanding and consideration of the properties of SCI in the service life prediction models are need of the hour.

1.1 Cracking Mechanism of Concrete Cover Due to Reinforcement Bar Corrosion

The service life of a reinforced concrete structure is being described as the prediction of time from initiation of corrosion to corrosion cover cracking of concrete. Service life of a reinforced concrete structure comes to an end upon the formation of corrosion cracking of concrete. Initially, there was a two stage model proposed by Tuutti [40] in 1980 for the prediction of service life. The projected model is as shown in Fig. 1.

This model is mainly composed of two stages of corrosion deterioration namely corrosion initiation period (T_o), followed by corrosion propagation period (T_{cr}). During corrosion initiation period, the aggressive agents in the form of CO_2 or chloride ions from the surrounding exposure tend to ingress inside the reinforced concrete structure through pores, voids, cracks and crevices and ultimately accumulate at the SCI. The corrosion initiation process accelerates at the SCI due to abundance of moisture and oxygen supply [1]. This abundance of moisture and oxygen supply at the SCI is mainly due to the existence of more water to cement ratio than in bulk concrete.

The second stage of corrosion deterioration called propagation period (T_{cr}) commences after the initiation of corrosion. The products of corrosion (rust) start applying expansive stress on the interior walls of concrete once its formation begins. Once the expansive stress on the interior walls of concrete crosses the tensile strength of concrete, radial cracks were developed which is depicted as the termination of service life of structures. The service life of structures predicted with the help of Tuutti's model was found to be lesser than the real service life of that structure. This misinterpretation of service life was due to the impact of ignoring porosity or PZT at

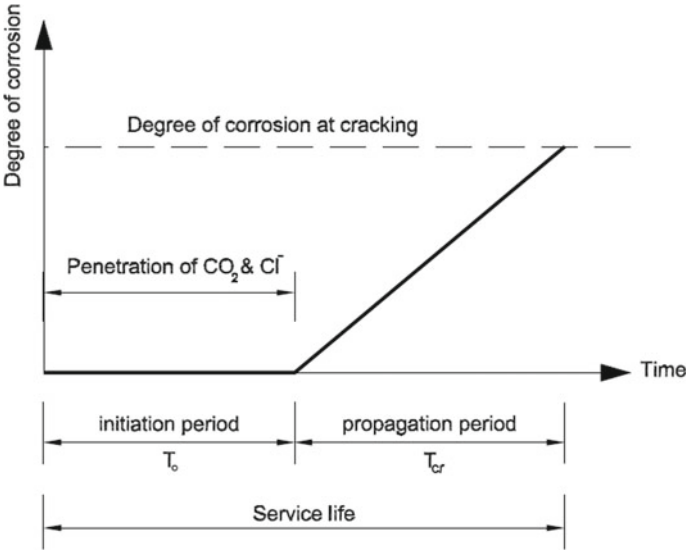

Fig. 1 Service life prediction model proposed by Tuutti [40]

the SCI. This has become a grey area in the field of service life prediction of corroded structures.

Soon after this, the occurrence of porous zone at the SCI was reported by Page and Treadaway [20] in 1982. Later a model by Weyers [41] in 1998 considered PZT at SCI and recommended a three-stage model for the prediction of service life as shown in Fig. 2. In this model, a free expansion zone was introduced in between corrosion initiation and propagation period, which represents the effect of PZT. In this newly developed model, the propagation period, T_{cr} was further subdivided into free expansion period, T_{free} and T_{stress}. The time taken by the rust to accumulate the porous zone outside the periphery of rebar is represented as T_{free} and the time taken by the rust to arrive at maximum tensile strength of concrete on the application of expansive stress before concrete cover cracking was termed as T_{stress}. Few corrosion products that were formed after the initiation of corrosion tends to move away from the SCI through pores, voids and crevices of surrounding concrete and the rest accumulates at the porous zone of SCI. During this period of corrosion, there will be no expansive pressure on the inner walls of concrete surface, but once porous zone was fully occupied by corrosion products, further formation of rust induces expansive stress on the interior faces of concrete [28]. Similarly, carbonation product ($CaCO_3$) also tends to fill pores, voids, etc., during carbonation when the structure is exposed to Co_2 prone environment [42]. This model proposes that the expansive stress on the inner walls of concrete linearly raises with the raise in the volume of rust. When the expansive pressure crosses the tensile stresses of concrete, radial concrete cover cracks were developed. After the generation of cracks, the amount of applied stress by the rust on the adjacent inner walls of concrete was not possible as they may

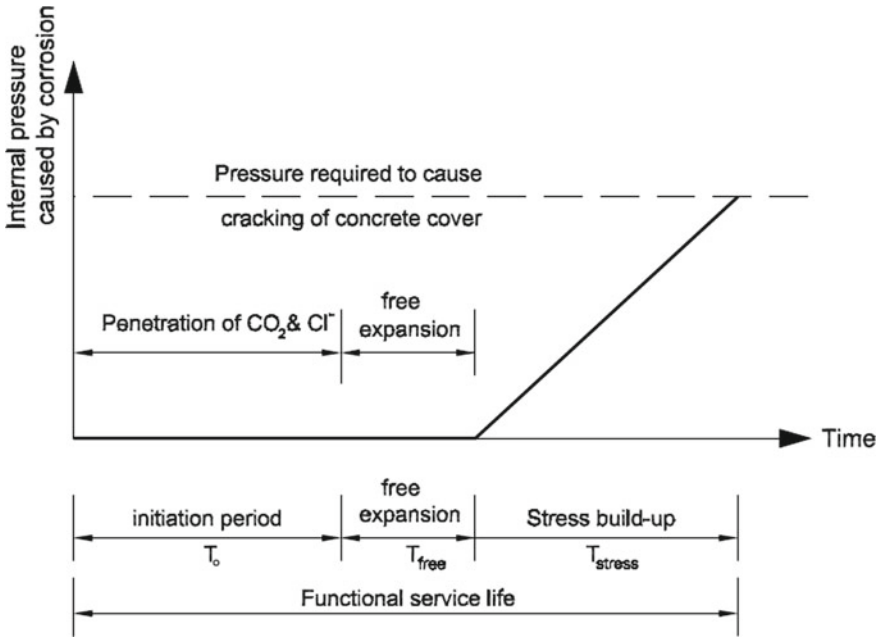

Fig. 2 Weyers three stage service life prediction model [41]

tend to move out from these cracks. Thus the formation of concrete cover crack is considered as the termination of the service life of corroded reinforced concrete structures. Further these cracks will cause the spalling of concrete cover so that the corroding steel surface gets oxygen and moisture in plenty which again triggers the corrosion process.

A typical concrete cracking process due to corrosion process given by Weyers in 1998 is as depicted in Fig. 3. This updated service life prediction model was bound to some assumptions to formulate the internal radial stress due to the expansion of rust. The primary assumption was regarding expansive stresses just about the rebar was because of the uniform formation of corrosion products around the steel reinforcing bar. Many models on volume expansion by corrosion [41, 43, 44] were put forward on the basis of this assumption. But the actual formation of corrosion products around the steel reinforcement bar was not uniform as the degree of corrosion is also not uniform about the steel rebar. This dissimilarity of corrosion is mainly because of non-uniform exposure of steel surface to the corroding environment.

Bazant [43] in 1979 suggested a mathematical model for service life prediction by using corrosion rate, depth of concrete cover, rebar spacing, diameter of the rebar as well as the properties of concrete such as tensile strength, modulus of elasticity, Poisson's ratio, and creep coefficient. Taking this model as base, a mathematical model was introduced by Liu and Weyers [45] in 1998, which considers the rate of

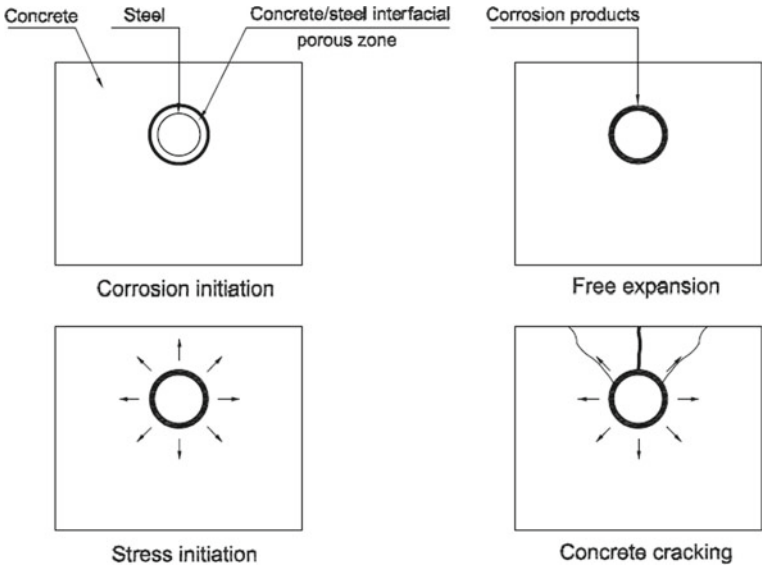

Fig. 3 Corrosion cracking process of reinforced concrete [41]

mass loss of corroding steel and time to fill the porous zone by corrosion products at the SCI before inducing an expansive pressure.

The PZT for the estimation of residual service life of structures was being assumed in several mathematical models without any experimental verification. Liu and Weyers [45] assumed 12.5 μm PZT and Petre-Lazar et al. [46] considered 40 μm PZT at the SCI for modelling. Several researchers considered a PZT of 40 μm too in developing the models [43, 45–49]. It was also found that a homogeneous distribution of PZT around the rebar was assumed in performing the service life prediction models [48]. But the actual distribution of PZT is not uniform and it varies all around the reinforcing steel bar [4, 19, 25, 27].

Thus, considering a constant value of PZT distribution for all types of concrete leads to misinterpretation in service life prediction. Hence a clear understanding about the porosity or PZT at the SCI is very essential in service life prediction. A minor deviation of PZT value in the service life prediction models matters a lot in getting the comparison with real service life of RC structures. Thus measuring the actual PZT at SCI and its consideration in service life prediction models is very much crucial for the accurate prediction of service life.

2 Summary of the Past Researches

Porous zone thickness is an important parameter of steel–concrete interface that is being assumed till date for assessing the residual service life of a reinforced structure [41, 44, 46–48, 50–54]. But several researches have been conducted in order to measure the PZT at the SCI experimentally by using image analysis technique. Some researchers measured the PZT at the SCI in only one or two locations around the SCI (over and beneath the horizontal reinforced steel) [5, 19, 55, 56]. These data are not sufficient to exactly illustrate the entire SCI throughout the steel bar. Thus an accurate measurement with a detailed study has to be done in the area around SCI to understand the deterioration mechanism of reinforced concrete. Only three researchers, Chen et al. [15], Goudar et al. [57] and Kenny and Katz [25] measured the PZT all around the SCI, which helps to understand the variation in PZT around the entire interface. This thickness reported by various researchers found to be uneven and varies from 35 to 85 μm [4], 17 to 69 μm [58], 80 to 103 μm [56] and 60 to 125 μm [59] along the length of reinforcement bars. Goudar et al. [57] measured the PZT at 12 locations around the reinforcement bar at the SCI by performing image analysis of BSE images. According to Goudar et al. [57], PZT at the SCI varies from 1.12 to 30.57 μm around the reinforcement bar.

The present study demonstrated that the PZT is not uniformly distributed around the SCI. The past service life prediction models should be reformed and non-uniform distribution of PZT needs to be considered. There can be two extreme conditions, one with minimum value of PZT and other maximum value of PZT. The corrosion products may fill the smaller porous zone faster and starts exerting the expansive pressure. And in contrary, the larger PZT needs more time to exert the expansive pressure. A detailed and reformed mathematical models need to be developed by considering the non-uniform distribution of porous zone.

3 Research Significance

The primary intention of this work is to validate a service life prediction model by taking experimentally determined published data of porous zone thickness into consideration, which has been neglected in previously developed models. In this paper, the performance of an existing model is presented to report the influence of PZT on the time required for cover cracking of concrete after corrosion initiation. This paper will provide an approximate range of service life of a particular reinforced concrete structure with more precision which is very much essential for repairs and rehabilitation of the structure and also helps in determining the life span of reinforced concrete structure during which it could satisfy all its purpose of its construction.

In this work, an attempt has been made to estimate the time from corrosion initiation to corrosion cracking by considering minimum and maximum values of PZT at the SCI. The two extreme ends that are minimum time with minimum PZT and

maximum time with maximum PZT were studied. The minimum and maximum PZT values were experimentally measured and the same are used to estimate the time from corrosion initiation to corrosion cracking.

4 Model for Service Life Prediction of Corroded Structures

In order to estimate the time from corrosion initiation to concrete cover cracking, several analytical, numerical, and empirical models were proposed. Further, several experimental studies were also conducted to check the results are in line with the proposed model. In the present paper, one such model by El Maaddawy and Khaled Soudki [23] which was proposed in the year 2007 is considered to validate it by introducing some experimental findings and also some experimentally determined published data on the properties of SCI by Goudar et al. [57].

According to El Maaddawy and Khaled Soudki [23], the time from corrosion initiation to concrete cover cracking (T_{cr}) due to corrosion of reinforced steel bar is given by,

$$T_{cr} = \left[\frac{7117.5(D + 2\delta_0)(1 + \vartheta + \Psi)}{i\, E_{ef}}\right]\left[\frac{2C\, f_{ct}}{D} + \frac{2\delta_0 E_{ef}}{(1 + \vartheta + \Psi)(D + 2\delta_0)}\right]$$

where,

D Rebar diameter (mm).
δ_0 Porous zone thickness (mm),
ϑ Poisson's ratio of concrete,

$$\Psi = \frac{D^2}{2C(C + D')}$$

D' $D + 2\delta_0$.
i Current density ($\mu A/cm^2$),
E_{ef} Effective modulus of elasticity of concrete which is given by,

$$Eef = \frac{E_C}{(1 + \emptyset_{cr})}$$

E_c Elastic modulus of concrete [$5000\sqrt{f_{ck}}$],
f_{ck} Characteristic Compressive strength of concrete,
Φ_{cr} Concrete creep coefficient,
C Clear cover of the specimen (mm),
f_{ct} Tensile strength of concrete ($0.7\sqrt{f_{ck}}$).

5 Experimental Results, Analysis and Service Life Prediction

5.1 Experimental Data Collection on the Properties of Steel–Concrete Interface

The extent of permeable space around the reinforcing steel in concrete, i.e. porous zone thickness and the corrosion current density are the most influential factors for the estimation of time from corrosion initiation to corrosion cracking, i.e. service life, of a corroding reinforced concrete structure [41, 44, 46–48, 50–54]. This porous zone thickness is being experimentally measured for different kinds of concrete from image analysis technique by Goudar et al. [57]. The PZT values are taken at 12 spots around the reinforcing steel, attempting to report exact distribution of PZT at their respective spots. At each spot of observation among 12 spots, a minimum of 30 PZT measurements for each sample were taken in order to get more accurate values of PZT. Similar measurements were conducted on three samples; therefore 90 measurements at each spot among 12 were taken for a particular type of concrete. The corresponding results of minimum, maximum and mean of those 90 measurements of PZT are presented in Table 1.

Further, similar concrete samples were subjected to corrosion prone environment for 90, 180, 360 and 720 days. Then the porous zone thickness at these intervals of exposure was measured as mentioned before. In addition to that, corrosion current density that is also a key parameter in estimating time from corrosion initiation to concrete cover cracking was measured for all kinds of concrete at all the exposure intervals. The respective measurements are tabulated in Table 2.

5.2 Analysis of Experimental Data, Discussions and Service Life Prediction

5.2.1 Analysis of Specimens Subjected Only to Curing

The experimental results by Goudar et al. [57] tabulated in Tables 1 and 2 can be summarized as in Table 3. The corrosion current density, I_{corr} (in $\mu A/cm^2$), minimum and maximum values of PZT (μm) among 12 spots and the average of 12 mean values obtained at 12 spots around the reinforcing steel for all kinds of concrete are formulated. Further, by taking these values as input parameters in El Maaddawy and Khaled Soudki model [23], the time needed for cover cracking of concrete after the initiation of corrosion, i.e. service life (years) is predicted and the same is presented in Table 3. Apart from PZT and corrosion current density, the other inputs that are used for calculation of service life by mathematical model are the reinforcing steel bar diameter (10 mm), Poisson's ratio of concrete (0.15), characteristic compressive

Table 1 Porous zone thickness (PZT) of various kinds of concrete [57]

Spots	PZT of OPC concrete (μm)			PZT of PPC concrete (μm)			PZT of PSC concrete (μm)		
	Mean	Min	Max	Mean	Min	Max	Mean	Min	Max
1	6.32	4.02	18.34	5.88	3.76	15.59	5.80	2.36	10.65
2	7.51	2.62	22.31	6.98	2.45	18.96	6.89	3.40	15.32
3	12.05	3.13	20.66	11.21	2.93	30.57	11.05	3.24	25.98
4	13.25	4.12	28.69	12.32	3.86	20.14	12.15	3.66	20.36
5	6.32	2.32	10.63	10.58	2.17	7.62	10.44	2.06	16.31
6	16.79	3.16	20.88	12.35	2.96	17.75	6.34	2.81	15.09
7	7.49	4.18	28.47	6.97	3.91	24.20	6.87	3.72	20.57
8	5.34	3.66	20.26	4.55	3.43	17.22	4.49	1.12	14.64
9	4.07	2.18	9.65	3.79	2.04	8.20	3.73	1.94	6.97
10	5.11	2.66	8.41	10.66	2.49	17.15	10.51	3.34	14.58
11	6.41	3.78	15.36	5.96	3.54	13.06	5.88	3.36	11.10
12	8.69	5.06	25.64	11.34	4.74	21.79	11.18	4.50	18.52
Overall	Average = 8.28	2.18	28.69	Average = 8.55	2.04	30.57	Average = 7.94	1.12	25.98

Table 2 Corrosion current density and porous zone thickness at different exposure periods for different types of concrete

Type	Corrosion current density, I_{corr} ($\mu A/cm^2$)	Porous zone thickness (μm)	
		Minimum	Maximum
OPC 90 days exposure	0.2996	3.65	26.32
OPC 180 days exposure	0.4583	3.11	25.36
OPC 360 days exposure	0.7957	2.35	22.65
OPC 720 days exposure	1.4852	2.66	23.74
PPC 90 days exposure	0.2761	2.88	25.68
PPC 180 days exposure	0.3305	3.32	26.37
PPC 360 days exposure	0.5650	2.88	23.41
PPC 720 days exposure	1.0444	1.89	20.64
PSC 90 days exposure	0.2203	3.54	22.36
PSC 180 days exposure	0.3094	3.68	24.34
PSC 360 days exposure	0.4950	3.44	20.55
PSC 720 days exposure	0.8975	2.22	21.88

Table 3 Prediction of service life for different types of concrete using the experimentally quantified database

Type	Corrosion current density, I_{corr} ($\mu A/cm^2$)	Porous zone thickness (PZT) (μm)			Service life (Years)		
		Min	Average of Mean	Max	Min (1*)	Average (2*)	Max (3*)
OPC	0.0989	2.18	8.28	28.69	15.01	25.14	58.72
PPC	0.0891	2.04	8.55	30.57	16.50	28.39	68.61
PSC	0.0869	1.12	7.94	25.98	15.20	27.97	61.75

1*—Prediction of service life with minimum PZT values
2*—Prediction of service life with Average of Mean values of PZT
3*—Prediction of service life with maximum PZT values

strength of concrete (f_{ck} = 40 MPa), concrete creep coefficient (1.6 for 28 days as per IS 1343:1980[60]; Sect. 5.2.5) and clear cover of the specimen (15 mm). The minimum and maximum values of PZT will give an appropriate prediction about two extreme time bound for service life of reinforced concrete structures when the corrosion current density values are constant. The findings mentioned in Table 3 can also be represented in the form of chart as shown in Fig. 4.

From the findings presented in Table 3, it can be seen that, either PZT or corrosion current density alone could not affect the service life of a structure. The service life of structure is having combined influence of PZT and corrosion current density. But in particular, it can be noted that the service life of structure increases with the increase in the thickness of porous zone which can also be observed through Fig. 4. This is mainly due to the provision of higher free expansion stage, i.e. when the PZT of

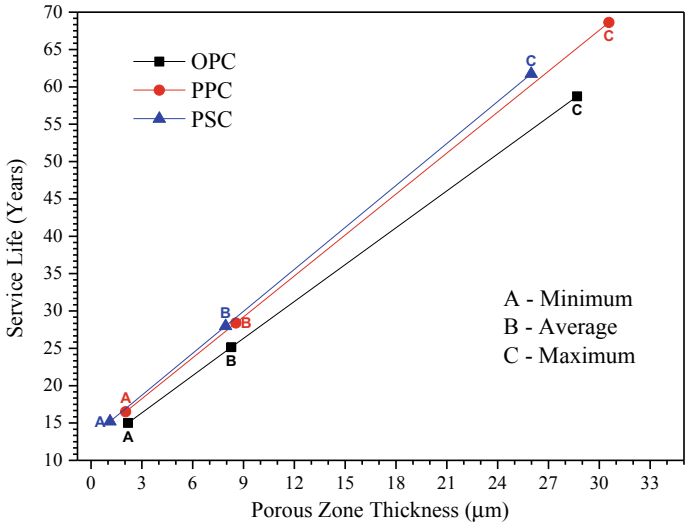

Fig. 4 Influence of porous zone thickness on the service life of different types of reinforced concrete

a concrete is higher, the space availability for accumulation of corrosion product before inducing expansive stress on the inner walls of concrete is higher, which leads to prolonged free expansion stage. This ultimately results in increased service life of a structure. The points A, B and C represent minimum, average and maximum values of PZT and their corresponding service life values, respectively.

PSC concrete is having more resistance to corrosion as we can observe its corrosion current density is lesser when compared to that of other type of concrete. It can also be noted that the PZT of PPC concrete is higher than other types of concrete which leads to the enhanced service life. Even though the corrosion current density of PPC concrete is greater than that of PSC concrete, the service life of PPC concrete is greater as it is having higher PZT, i.e. the effect of increased free expansion stage due to higher PZT is dominant over the effect of having higher corrosion current density than PSC concrete. PPC concrete also has lesser corrosion current density than OPC concrete, thus better resistance to corrosion. So PPC is more preferable than OPC and PSC in mild to moderate exposure condition. Whereas, in case of exposure to aggressive environmental condition such as marine exposure, PSC performs better as it is having less PZT along with greater corrosion resistance than OPC and PPC concrete.

5.2.2 Analysis of Specimens Subjected to Curing and Exposure to Corrosion Prone Environment

Similarly, the essential properties for the prediction of service life such as PZT and corrosion current density are measured for all kinds of concrete after exposing them

to a corrosion prone environment for an interval of 90, 180, 360 and 720 days. Their respective service life values based on the minimum and maximum values od PZT are presented in Table 4.

Influence of Corrosion Exposure Period on the PZT for Different Types of Concrete

The variation in the minimum values and maximum values of PZT for different concrete types with respect to exposure duration is presented in Fig. 5. A decreasing trend for both minimum and maximum values of PZT is observed with the increase

Table 4 Service life prediction under different exposure periods considering minimum and maximum values of PZT

Type	Corrosion current density, I_{corr} ($\mu A/cm^2$)	Porous zone thickness (μm)		Service life (Years)	
		Min	Max	Min (1*)	Max (2*)
OPC 90 days exposure	0.2996	3.65	26.32	5.78	18.1
OPC 180 days exposure	0.4583	3.11	25.36	3.59	11.49
OPC 360 days exposure	0.7957	2.35	22.65	1.91	6.06
OPC 720 days exposure	1.4852	2.66	23.74	1.06	3.37
PPC 90 days exposure	0.2761	2.88	25.68	5.82	19.26
PPC 180 days exposure	0.3305	3.32	26.37	5.08	16.43
PPC 360 days exposure	0.5650	2.88	23.41	2.84	8.76
PPC 720 days exposure	1.0444	1.89	20.64	1.38	4.31
PSC 90 days exposure	0.2203	3.54	22.36	7.78	21.68
PSC 180 days exposure	0.3094	3.68	24.34	5.62	16.48
PSC 360 days exposure	0.4950	3.44	20.55	3.43	9.06
PSC 720 days exposure	0.8975	2.22	21.88	1.67	5.24

1*—Prediction of service life with minimum PZT values
2*—Prediction of service life with maximum PZT values

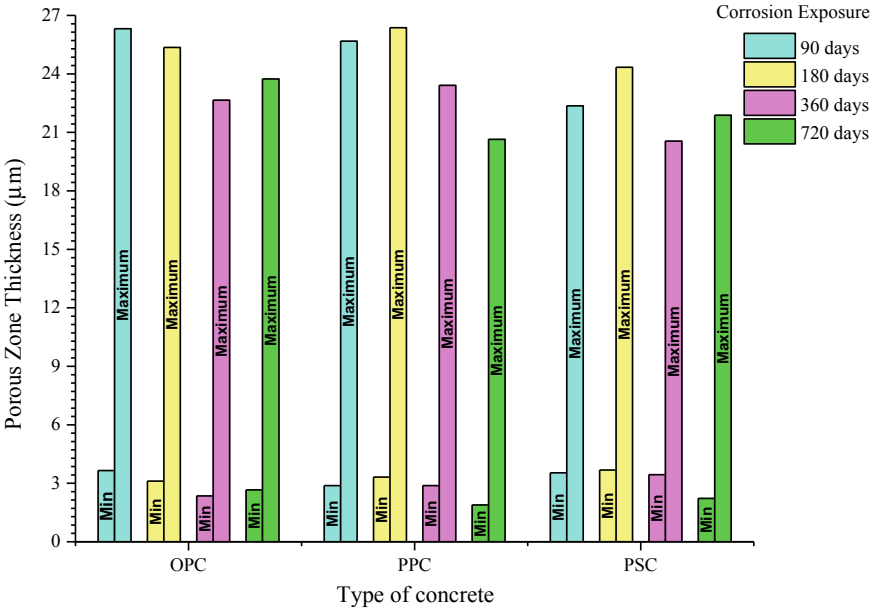

Fig. 5 Influence of corrosion exposure period on the PZT for different concrete types

in the duration of exposure. This happens mainly due to the filling of porous zone with rust around the rebar with the progress of corrosion. As the corrosion exposure duration increases, the corrosion current density also increases, which triggers the generation of corrosion products. This corrosion product (rust) tends to fill the porous zone and ultimately reduces the porous zone thickness with exposure duration. It can also observed from the above chart that the PSC concrete has lesser PZT when compared with OPC and PPC which made them the best ones to use in aggressive environments such as marine environment, etc.

Influence of Corrosion Exposure Period on the Corrosion Current Density for Different Types of Concrete

The variation in the corrosion current density upon the duration of corrosion environment exposure for different types of concrete is shown in Fig. 6. It can be seen that with the increase in the duration of exposure to corrosive environment, the corrosion current density also increases gradually. It is also observed that PSC concrete has lesser corrosion current density than OPC and PPC concrete, which shows that the PSC concrete has higher resistance to corrosive environment. Whereas, OPC concrete has corrosion current density values that made them to not preferable for the usage in aggressive environments such as marine environment, etc.

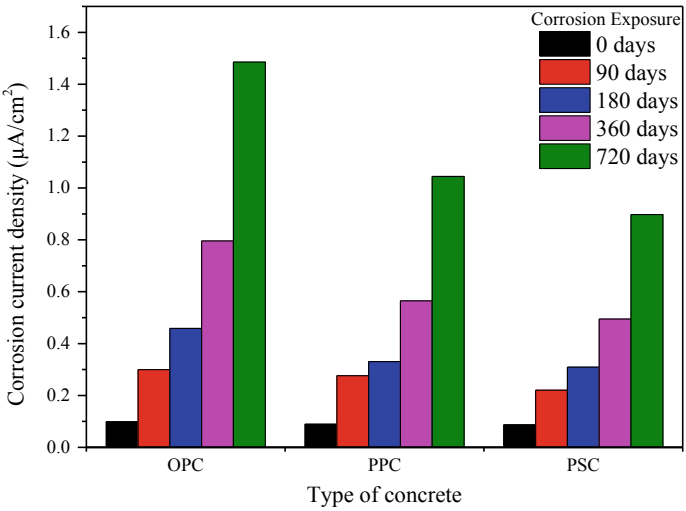

Fig. 6 Influence of corrosion exposure period on the corrosion current density for different types of concrete

Influence of Corrosion Current Density on the Service Life of Different Concrete Types

The influence of corrosion current density upon the two extreme time bound like initiation of corrosion to concrete cover cracking, i.e. minimum and maximum service life considering minimum values and maximum values of PZT for different concrete types are presented in Fig. 7. It is clearly visible that the both minimum and maximum time from initiation of corrosion to concrete cover cracking, i.e. minimum and maximum service life, gradually reduces with the increase in corrosion current density upon exposure to corrosive environment. The service life range of PSC concrete is observed to be higher than PPC and OPC as it is having lesser values of corrosion current density, i.e. more resistance to corrosion. Thus the usage of PSC concrete is recommended in case of aggressive environments such as marine environment, etc. Whereas, OPC concrete is having lesser service life than PPC because of its higher values of corrosion current density, i.e. lesser resistance to corrosion. Thus OPC concrete is recommended to use in mild exposure conditions and PPC concrete is more suitable for mild to moderate exposure conditions.

6 Conclusions

The present paper gives a brief idea about how the inclusion of properties of steel–concrete interface in the service life prediction models plays a major role in forecasting the accurate prediction of service life. The influences of corrosion current

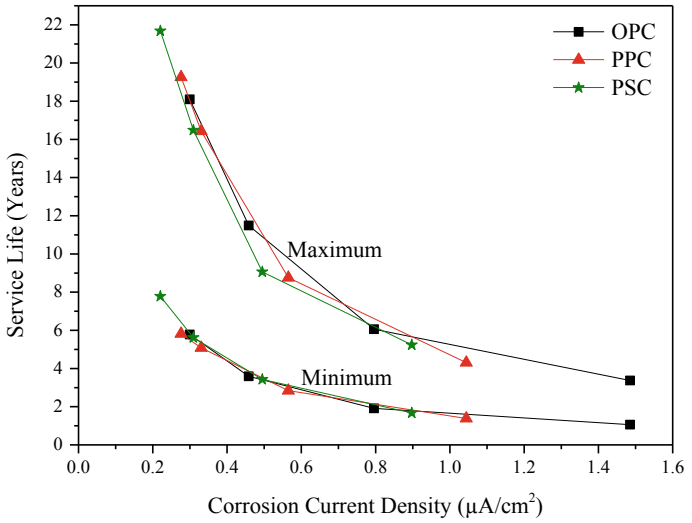

Fig. 7 Influence of corrosion current density on the service life of different concrete types

density, corrosion exposure period and porous zone thickness on the service life of different types of concrete were systematically discussed. Following are the key conclusions from the present study.

- The PZT is not uniformly distributed around the SCI and the inclusion of its exact distribution around the reinforcing steel bar is required for the accurate measurement of service life.
- The service life of a structure has to report in two values, i.e. minimum and maximum, one by considering minimum value of PZT and other maximum value of PZT. The consideration of minimum and maximum values of PZT will give an idea about the two extreme time bound for service life of structures that helps in predicting the left out time for necessary repairs and rehabilitation of the structure.
- It is concluded that the service life of structure increases with the increase in the thickness of porous zone due to the prolonged free expansion stage.
- PZT of PSC concrete is lesser when compared to OPC and PPC concrete, which helps in reducing corrosion-induced problems at aggressive environmental exposure.
- PZT of PPC concrete is higher than OPC and PSC concrete, which helps in increasing service life. PPC concrete also has lesser corrosion current density than OPC concrete and higher corrosion current density than PSC concrete. Thus PPC can be more preferable than OPC and PSC is more corrosion resistant when compared to PPC.
- PZT decreases with the increase in exposure duration for all types of concrete which is mainly due to the filling of porous zone with rust around the rebar with the progress of corrosion.

- Corrosion current density increases gradually with the increase in the duration of exposure to corrosive environment for all types of concrete.
- Both minimum and maximum time from the initiation of corrosion to concrete cover cracking, i.e. minimum and maximum service life, gradually reduces with the increase in corrosion current density upon exposure to corrosive environment.
- The service life range of PSC concrete is observed to be higher than PPC and OPC as it is having lesser values of corrosion current density, i.e. more resistance to corrosion. Thus the usage of PSC concrete is recommended in case of aggressive environments such as marine environment, etc.
- OPC concrete is having lesser service life than PPC and PSC concrete due to its higher values of corrosion current density, i.e. lesser resistance to corrosion. Thus OPC concrete is recommended to use in mild exposure conditions.

References

1. Page CL (1975) Mechanism of corrosion protection in reinforced concrete marine structures. Nature 258:514
2. Al Khalaf MN, Page CL (1979) Steel/mortar interfaces: Microstructural features and mode of failure. Cem Concr Res 9:197–207. https://doi.org/10.1016/0008-8846(79)90026-7
3. Gjorv OE, Monteiro PJM, Mehta PK (1990) Effect of condensed silica fume on the steel-concrete bond. Mater J 87:573–580
4. Horne AT, Richardson IG, Brydson RMD (2007) Quantitative analysis of the microstructure of interfaces in steel reinforced concrete. Cem Concr Res 37:1613–1623. https://doi.org/10.1016/j.cemconres.2007.08.026
5. Angst UM, Geiker MR, Michel A, Gehlen C, Wong H, Isgor OB, Elsener B, Hansson CM, François R, Hornbostel K, Polder R, Alonso MC, Sanchez M, Correia MJ, Criado M, Sagüés A, Buenfeld N (2017) The steel–concrete interface. Mater Struct Constr 50. https://doi.org/10.1617/s11527-017-1010-1
6. Scrivener KL, Crumbie AK, Laugesen P (2004) The interfacial transition zone (ITZ) between cement paste and aggregate in concrete. Interface Sci 12:411–421. https://doi.org/10.1023/B:INTS.0000042339.92990.4c
7. Ollivier JP, Maso JC, Bourdette B (1995) Interfacial transition zone in concrete. Adv Cem Based Mater 2:30–38
8. Moreau M (1973) Contribution to the study of adhesion between the hydrated constituents of artificial Portland cement and embedded steel. Revenue Mater 674:4–17
9. Glass GK, Yang R, Dickhaus T, Buenfeld NR (2001) Backscattered electron imaging of the steel–concrete interface. Corros Sci 43:605–610
10. Elsharief A, Cohen MD, Olek J (2003) Influence of aggregate size, water cement ratio and age on the microstructure of the interfacial transition zone. Cem Concr Res 33:1837–1849
11. Brough AR, Atkinson A (2000) Automated identification of the aggregate–paste interfacial transition zone in mortars of silica sand with Portland or alkali-activated slag cement paste. Cem Concr Res 30:849–854
12. Scrivener KL, Pratt PL (1996) Characterization of interfacial microstructure. Interfacial Transit Zo Concr 2:3–18
13. Prokopski G, Halbiniak J (2000) Interfacial transition zone in cementitious materials. Cem Concr Res 30:579–583
14. Richardson IG (2000) The nature of the hydration products in hardened cement pastes. Cem Concr Compos 22:97–113

15. Chen F, Li CQ, Baji H, Ma B (2018) Quantification of steel-concrete interface in reinforced concrete using backscattered electron imaging technique. Constr Build Mater 179:420–429. https://doi.org/10.1016/j.conbuildmat.2018.05.246
16. Shen Q, Pan G, Zhan H (2017) Effect of interfacial transition zone on the carbonation of cement-based materials. J Mater Civ Eng 29:04017020. https://doi.org/10.1061/(asce)mt.1943-5533.0001860
17. Liao K-Y, Chang P-K, Peng Y-N, Yang C-C (2004) A study on characteristics of interfacial transition zone in concrete. Cem Concr Res 34:977–989
18. Page CL (2009) Initiation of chloride-induced corrosion of steel in concrete: role of the interfacial zone. Mater Corros 60:586–592. https://doi.org/10.1002/maco.200905278
19. Soylev TA, François R (2003) Quality of steel-concrete interface and corrosion of reinforcing steel. Cem Concr Res 33:1407–1415. https://doi.org/10.1016/S0008-8846(03)00087-5
20. Page CL, Treadaway KWJ (1982) Aspects of the electrochemistry of steel in concrete. Nature 297:109–115. https://doi.org/10.1038/297109a0
21. Yonezawa T, Ashworth V, Procter RPM (1988) Pore solution composition and chloride effects on the corrosion of steel in concrete. Corrosion 44:489–499
22. Fu X, Chung DDL (1997) Effect of corrosion on the bond between concrete and steel rebar. Cem Concr Res 27:1811–1815
23. El Maaddawy T, Soudki K (2007) A model for prediction of time from corrosion initiation to corrosion cracking. Cem Concr Compos 29:168–175. https://doi.org/10.1016/j.cemconcomp.2006.11.004
24. Mohammed TU, Hamada H (2001) A discussion of the paper chloride threshold values to depassivate reinforcing bars embedded in a standardized OPC mortar by Alonso C, Andrade C, Castellote M, Castro P. Cem Concr Res 5, 835–838
25. Kenny A, Katz A (2015) Statistical relationship between mix properties and the interfacial transition zone around embedded rebar. Cem Concr Compos 60:82–91. https://doi.org/10.1016/j.cemconcomp.2015.04.002
26. 山口悠, 口田圭吾: No title消費者型官能評価による食味との関連性. 日本畜産学会報. 84, 487–492 (2013)
27. Yu L, François R, Gagné R (2016) Influence of steel–concrete interface defects induced by top-casting on development of chloride-induced corrosion in RC beams under sustained loading. Mater Struct Constr 49:5169–5181. https://doi.org/10.1617/s11527-016-0852-2
28. Wong HS, Zhao YX, Karimi AR, Buenfeld NR, Jin WL (2010) On the penetration of corrosion products from reinforcing steel into concrete due to chloride-induced corrosion. Corros Sci 52:2469–2480. https://doi.org/10.1016/j.corsci.2010.03.025
29. Ryou JS, Ann KY (2008) Variation in the chloride threshold level for steel corrosion in concrete arising from different chloride sources. Mag Concr Res 60:177–187. https://doi.org/10.1680/macr.2008.60.3.177
30. Glass GK, Buenfeld NR (1997) 43 Chloride Threshold Levels for corrosion induced deterioration of steel in concrete. In: PRO 2: International RILEM workshop on chloride penetration into concrete. p. 429. Rilem Publications
31. Castel A, Vidal T, Francois R, Arliguie G (2003) Influence of steel–concrete interface quality on reinforcement corrosion induced by chlorides. Mag Concr Res 55:151–159
32. Hartt WH, Nam J (2008) Effect of cement alkalinity on chloride threshold and time-to-corrosion of reinforcing steel in C. Corrosion 64:671–680
33. Bäumel A (1959) Die auswirkung von betonzusatzmitteln auf das korrosionsverhalten von stahl in beton. Zement-Kalk-Gips 7:294–305
34. Bentz D, Stutzman P (2009) SEM analysis and computer modelling of hydration of portland cement particles. Petrogr Cem Mater 60-60–14. https://doi.org/10.1520/stp12645s
35. Glass GK, Buenfeld NR (2000) The inhibitive effects of electrochemical treatment applied to steel in concrete. Corros Sci 42:923–927
36. Hussain S, Bhunia D, Singh SB (2017) Comparative study of accelerated carbonation of plain cement and fly-ash concrete. J Build Eng 10:26–31

37. Liu W, Cui H, Dong Z, Xing F, Zhang H, Lo TY (2016) Carbonation of concrete made with dredged marine sand and its effect on chloride binding. Constr Build Mater 120:1–9. https://doi.org/10.1016/j.conbuildmat.2016.05.011
38. Ann KY, Song H-W (2007) Chloride threshold level for corrosion of steel in concrete. Corros Sci 49:4113–4133
39. Castel A, Vidal T, François R, Arliguie G (2004) Influence of steel? Concrete interface quality on reinforcement corrosion induced by chlorides. Mag Concr Res 55:151–159. https://doi.org/10.1680/macr.55.2.151.37568
40. Tuutti K (1980) Service life of structures with regard to corrosion of embedded steel. Spec Publ 65:223–236
41. Weyers RE (1998) Service life model for concrete structures in chloride laden environments. Mater J 95:445–453
42. Feng X, Tang Y, Zuo Y (2011) Influence of stress on passive behaviour of steel bars in concrete pore solution. Corros Sci 53:1304–1311
43. Bazant ZP (1979) Physical model for steel corrosion in concrete sea structures—application. J Struct Div 105
44. Morinaga S (1988) Prediction of service lives of reinforced concrete buildings based on rate of corrosion of reinforcing steel. Spec Rep Inst Technol Shimizu Corp 23
45. Liu Y (1996) Modeling the time-to-corrosion cracking of the cover concrete in chloride contaminated reinforced concrete structures. Dissertation
46. Petre-Lazar I, Gérard B (2000) Mechanical behaviour of corrosion products formed at the steel-concrete interface. Testing and modelling. Cond Monit Mater Struct
47. Thoft-Christensen P (2000) Stochastic modeling of the crack initiation time for reinforced concrete structures. In Advanced technology in structural engineering. pp 1–8
48. Bhargava K, Ghosh AK, Mori Y, Ramanujam S (2005) Modeling of time to corrosion-induced cover cracking in reinforced concrete structures. Cem Concr Res 35:2203–2218
49. Chen D, Mahadevan S (2008) Chloride-induced reinforcement corrosion and concrete cracking simulation. Cem Concr Compos 30:227–238. https://doi.org/10.1016/j.cemconcomp.2006.10.007
50. (2001) Scanning electron microscopy and X-ray microanalysis of concretes, with Sarkar SL, Xu Aimin.pdf
51. Bhargava K, Ghosh AK, Mori Y, Ramanujam S (2006) Analytical model for time to cover cracking in RC structures due to rebar corrosion. Nucl Eng Des 236:1123–1139. https://doi.org/10.1016/j.nucengdes.2005.10.011
52. Chen F, Li C-Q, Baji H, Ma B (2019) Effect of design parameters on microstructure of steel-concrete interface in reinforced concrete. Cem Concr Res 119:1–10
53. Chernin L, Val DV, Volokh KY (2010) Analytical modelling of concrete cover cracking caused by corrosion of reinforcement. Mater Struct 43:543–556
54. Morinaga S (2018) 13 Remaining life of reinforced concrete structures after corrosion cracking. Durab Build Mater Components 7. 1, 127
55. Zayed, A.M.: The Nature of the Concrete-Steel Rebar Interface in Plain and Silica Fume Concrete. MRS Online Proc. Libr. Arch. 245, (1991)
56. Yuan Y, Ji Y (2009) Modeling corroded section configuration of steel bar in concrete structure. Constr Build Mater 23:2461–2466. https://doi.org/10.1016/j.conbuildmat.2008.09.026
57. Goudar S, Das B, Arya S (2019) Microstructural study of steel-concrete interface and its influence on bond strength of reinforced concrete BT—microstructural study of steel-concrete interface and its influence on bond strength of reinforced concrete. Adv Civ Eng Mater 8, https://doi.org/10.1520/ACEM20180133
58. Biniam_Thesis_Nov_30 (44)
59. Jacobsen S, Lein HL, Zhang ZL, Lee SF, Wang XH, He JY (2009) Application of nanoindentation testing to study of the interfacial transition zone in steel fiber reinforced mortar. Cem Concr Res 39:701–715. https://doi.org/10.1016/j.cemconres.2009.05.002
60. Of C, For P, Concrete P (2003) Indian standard code of practice for prestressed concrete Indian standard code of practice for prestressed concrete. 1980

Automation of Curing Using Prefabricated Sensors

Akash Agarwalla and Bibhuti Bhusan Das

Abstract Curing is one of the universal phenomena followed after casting and finishing of concrete over an extended period of time, which helps to develop the compressive strength and durability by maintaining an optimum moisture and temperature condition. It keeps the concrete hydrated, restricts volumetric shrinkage, provides resistance to abrasion, freezing and thawing. There are many ways to cure concrete but, in this article, discussion will be on automation of curing using IoT and moisture sensors and relays which will likely replicate the lab condition on site by maintaining constant moisture content in concrete by supplying required amount of water. Generally, on site the curing process is carried out for 6–7 days once or twice a day at a large interval as a result of which the free moisture content falls and the rate of hydration decreases. It results in poor compressive strength and durability compared with laboratory samples because the 7 days compressive strength is not achieved which is more important than that of 28 days compressive strength which is successfully achieved in the lab. Various technologies used in this article will help in real-time monitoring of concrete condition with ease which will further be beneficial for the construction industry. This paper will cover how these technologies are integrated to automate the whole process, and its effect on compressive strength of concrete for which a consistent mix of M20, M25, M30 was prepared to compare the result of strength of concrete at 3, 7 and 28 days of curing in three different conditions, giving the strength of in-situ automatically cured concrete sample similar to that of laboratory cured concrete sample and an increase in **16.09%** of compressive strength was observed with respect to concrete cured manually in site conditions.

Keywords Curing · Automation · IoT · Real-time monitoring

A. Agarwalla (✉) · B. B. Das (✉)
Department of Civil Engineering, National Institute of Technology Karnataka, Surathkal, Mangalore, Karnataka 575025, India
e-mail: akashagarwalla3@gmail.com

B. B. Das
e-mail: bibhutibhusan@gmail.com

B. B. Das et al. (eds.), *Recent Trends in Civil Engineering*, Lecture Notes in Civil Engineering 105, https://doi.org/10.1007/978-981-15-8293-6_35

1 Introduction

Concrete is the most widely used material in construction industry thus it acts as a backbone of worlds infrastructure as it can be moulded into any desired shape. Modern day technology is developing and changing the way industries operate by increasing the production along with its productivity with economy, but the construction industry has been very slow to adapt to any changes in its process. Automation is not the solution to all our problems but eliminating the repetitive task in design, construction and prefabrication will lead us to an efficient and effective industry to meet the future growth demand. It is easier to automate a process rather than automating a project, therefore a project should be broken down to smaller work packages to identify the processes involved, which can be automated to make our work easier as we can learn and implement changes from the past experiences. In order to meet the future expectations of the client and to optimise their resource utilization, we need to understand the benefits of adapting and adopting automation technologies which can prove to be a valuable asset for the industry to sustain in this competitive world.

It's been more than few centuries, modern concrete has evolved since then it has been improving with passage of time. It has been used in the construction of bridges, roads, dams, buildings and other structures. But there are quite a few structures, which have lasted more than a century hence there lacks a consistency in its performance. This does not indicate the failure of code of standards but this failure occurs due to the improper practices involved while concreting which can be due to reasons like improper mixing and curing. Curing is one of the important part of processes that requires equal importance, just the way every living being requires water to survive and stay healthy similarly concrete needs curing to control the rate of moisture loss during hydration, since the process of hydration takes time hence curing must be done for a reasonable period of time and at a controlled temperature as it affects different physical properties of concrete.

ASTM C 150 [1] defines, five different types of Portland cement based on its compound composition and its minimum curing periods to obtain 70% of desired compressive strength. Type I being the most commonly used product with a minimum curing period of 7 days. CCA Australia [2] published a data sheet on curing of concrete, which describes the importance of concrete curing on the basis of the concrete compressive strength. By comparing the compressive strength of sample cured for 180 days to the samples that were cured for 0, 3, 7, 14 and 28 days and then in air till 180th day. They found that the concrete that was allowed to dry after casting achieved only 40% strength as compared to the sample cured for 180 days continuously, similarly the 3 days cured sample achieved only 60%, while the 28 cured sample achieved 95%. Power [3] described the interlinkage of w/c and curing, in developing the micro-structure of hardened concrete. They stated that concrete with low w/c ratio will minimize the pore space between the cement particle. On the other hand, the hardened concrete requires sufficient water to keep it pores filled with hydration product as the crucial aspect to growth of strength and durability is

not dependent upon the degree to which cement has hydrated but upon the degree to which the pores between the cement particle is filled with water which fills the interlayer gel spaces and assures that the reaction area remains hydrated until all the available pore spaces is filled with hydration product. This can be achieved by continuous curing resulting a denser, stronger and less permeable concrete, but the degree to which the pores have filled does not depend only upon the degree to which the cement has hydrated, but also on the initial volume of pores which is achieved by low w/c. While concrete with high w/c will provide enough water to promote high degree of hydration but this leads to a low degree of pore filling because of high degree of porosity. Burg and Ronald [4] studied the influence of casting and curing temperature on the properties of fresh and hardened concrete, which concluded that, when concrete is exposed to higher initial temperature it will obtain early initial compressive strength but its 28 days compressive strength might be lesser when compared to concrete cured at controlled lower temperature. Powers and Neville [5] stated that the process of hydration only proceeds in a saturated condition and the water required for the hydration of each gram of cement is equal to 0.44 g, as the volume of capillary pores in the concrete(i.e., 160 to 180 mm^3 for 0.4 w/c Dhir et al. [6]) is much smaller compared to the total volume of water required for hydration of all cement particle, so continuous curing is needed to keep the capillary pores of the concrete hydrated until the concrete has attained the desired characteristics. ACI 308R-01 2008 [7] studied the effect of curing on the permeability of concrete having a w/c ratio of 0.51 for 90 days, which concluded that the coefficient of permeability varied linearly from 10^{-8} m/s to $10^{-11.5}$ m/s for the first 7 days of curing and then from $10^{-11.5}$ m/s to 10^{-16} m/s till the 90th day as the curing period increases, as a result the concrete durability improves as the period of curing increases. Dhir et al. [6] defined durability as 'the ability to withstand for a longer period without showing significant deterioration when exposed to the natural environment' and studied the effect on depth of abrasion due to continuous moist curing, they found that the depth of abrasion decreases almost to its half on continuously curing it for 3 days only.

There are three basic ways to cure concrete, which includes water curing, sheet curing and member curing but none of them is capable of finding the real-time concrete moisture value which is required to find the correct time to cure concrete. With the objective of eradicating the above limitation led to the research aiming to develop the automation system for curing, which will be helpful in real-time monitoring of concrete moisture value and will simultaneously provide the required moisture content to the concrete to attain the desired characteristics.

2 Methodology

2.1 Materials

2.1.1 Moisture Sensors

The moisture sensor consists of two conducting plates, which measures the volumetric content of water inside the concrete and gives us the moisture level as output. The two probes allow the current to pass through the concrete and then it gets the resistance value to measure the moisture content was used which operated at an input voltage of 3.3 to 5 v DC.

2.1.2 NodeMCU 1.0 ESP8266

NodeMCU is an open source IoT platform, which includes firmware which runs on the ESP8266 and is a Wi-Fi enabled Module from Espressif Systems, and hardware which is based on the ESP-12 module. It uses Lua scripting making the task of developers easier. It is a low-cost Wi-Fi transceiver and receiver that can be used for endpoint IoT developments with full TCP/IP (Transmission control protocol/Internet protocol) stack and microcontroller capability used for connecting network devices to the internet.

2.1.3 Single Channel Relay Module

A relay is an electrically operated device. It has a control system called input circuit or input contactor and a controlled system called output circuit or output contactor. It is commonly used in automatic control circuit. In simple words, it is an automatic switch which controls a high-current circuit with a low-current signal.

2.1.4 Submersible Water Pump

A brushless, permanent magnetic rotor pump which operates at a voltage range of 12–24 V was used which had a super long working life and a higher degree of performance ceramic life whose axis where enclosed with static sealing preventing water leakage and making it completely waterproof ensuring high degree of safety while using this as a submersible pump having a maximum rate of discharge of 4 L/min.

Table1 Properties of cement

S.No.	Properties	Values
1	Specific gravity	3.15
2	Standard consistency	29.5%
3	Initial setting time	61 min
4	Final setting time	300 min
5	Fineness	325 m2/Kg
6	Compressive strength (28 days)	54 N/mm2

2.1.5 Concrete

Ordinary Portland cement of 53 grade conforming to IS 12,269:2013 [8] is used in casting of canal model. The physical properties of cement are mentioned in Table 1. For fine aggregate river sand conforming to zone II (IS 383:1970) [9] passing through 4.75 mm sieve was used. The sand was free from organic matter. The specific gravity of sand was found to be 2.61 and moisture content was 5%. The fineness modulus of sand was 3.31. For coarse aggregate, crushed stone aggregates of 20 mm downsize were used. The pile of aggregate comprises of mixture of rounded and angular aggregates. The specific gravity of coarse aggregate was found to be 2.69 and moisture content is almost nil. The fineness modulus of aggregate was 6.72. Tap water is used for casting.

2.2 Mix Design

To create a foundation of sound infrastructure a good mix design is required. This process involves the preparation of mixing ingredients in a desired ratio to get the desired strength and durability of the structure. Concrete mix of M20, M25, M30 grade was designed following the guidelines in IS 10,262:2009 [10] as shown in Table 2. A total of 81 samples were cast out of which 9 samples of each mix design were normally cured in the laboratory, 9 were auto cured under site condition and 9 were hand cured under site condition. The following samples are denoted as NC1, NC2, and NC3 for sample normally cured in the laboratory; AC1, AC2, and AC3 for samples auto cured under site condition, and HC1, HC2, and HC3 for samples hand cured under site condition.

Table 2 Mix proportion of concrete for 1m3

	M20	M25	M30
Cement (kg)	394	448	492
Fine aggregate (kg)	675	640	627
Coarse aggregate (kg)	1151	1140	1115
Water (kg)	197	197	197

2.3 Method

a. Installation and setup of Arduino IDE:—The latest version of Arduino IDE was downloaded from 'https://www.arduino.cc/en/Main/Software' and installed successfully. The NodeMCU 1.0 ESP8266 was connected using a micro USB port to the computer. As soon as the computer detected the NodeMCU 1.0 ESP826 board, a blue led light started flashing in the board and if the computer failed to detect the board then a USB to UART bridge VCP driver can be installed from 'https://www.silabs.com/products/development-tools/software/usbtouar tbridgevcp drivers'. The Arduino IDE was opened, goto file in the menu bar, select preferences or press 'Ctrl + comma'. In the 'Additional Boards Manager URLs:' Field, type https://arduino.esp8266.com/stable/package_esp8266.com_index.json and then select ok.
Then goto tools in the menu bar and select boards and then select boards, a Board manager dialog box appears, in the search bar type 'esp8266′ and wait for the search to complete. Esp8266 by ESP8266 Community was selected and make sure that the computer is connected to the internet and then click on install. This process may take a few minutes to successfully install the board to the software. Then goto tools in the menu bar and select boards and move the mouse cursor over the down arrow key in the list to search for 'NodeMCU 1.0 (ESP - 12E module)'. Then goto tools in the menu bar and select upload speed and select '115,200′. Then goto tools in the menu bar and select manage libraries or press 'Ctrl + Shift + I' a dialog box appears, wait for the library manager dialog box to install update, then type 'Arduino http' in the search bar and select 'Arduinohttpclient by Arduino' and click on install. Then search for 'Arduinojson' in the search bar and select 'ArduinoJson by Benoit Blanchon' and click on install and then close the library manager dialog box.

b. Setting up the google sheet:—a web browser was opened and Google account was logged in and then Google sheets were opened. A new blank spreadsheet was created. The URL in the address bar of the browser was copied and saved in a notepad for later use. Then goto tools in the menu bar and select Script editor, a new tab opens up and then the code was typed in it. The sheet id was typed, which is the 'https://script.google.com/macros/s/AK**********bwgkxi0fo*********3zWqnaO4/exec' underlined portion of URL copied earlier to the notepad within a single inverted quote. The rest of the program was then typed as per the requirement of the project.
After the code was successfully typed, it was deployed as a web app by going to 'Publish' in the menu bar and selecting 'Deploy as web app…'. A new 'Edit project name' dialog box appears on the screen; the project name was set to 'moisture data' and then select ok (The name of the project can be given anything). A new 'Deploy as web app' dialog box appears on the screen. The 'Project version:' was selected as new and the changes in the program were described in the textbox given below (It is not compulsory to describe what has changed in the project). The owner of the web app was selected from the

'Execute the app as:' dropdown combobox. Further 'who has access to the app:' was set to 'Anyone, even anonymous' from the dropdown combobox list, then select 'Deploy'. A new dialog box appears. The underlined portion of the 'current web app URL:' was copied 'https://script.google.com/macros/s/AK**********bwgkxi0fo***3zWqnaO4/exec' (some portion of the URL is hidden due to privacy concern) and saved in a notepad for future use and then select ok. The process of deploy as web app was repeated every time some changes were made in the program to get the desired output and some changes were observed in the 'Deploy as web app' dialog box. Now The 'project version:' was changed from new to the latest project version number available from the dropdown combobox and then select 'Update'. The current web app URL remains the same throughout the project hence need not to be copied again and again.

c. Programming the NodeMCU 1.0 ESP8266:—Arduino IDE was opened and the code was designed in it. The current web app URL was copied to Gscriptid, to interlink both the programs. The program was successfully compiled and uploaded making sure that the NodeMcu 1.0 ESP8266 was connected via a Micro USB to the computer and the correct port was select in the Arduino IDE by going to tools in the menu bar then selecting ports. Now the NodeMCU 1.0 ESP8266 started working as a receiver which will be able to collect data from the google sheets and will be able to control the submersible water pump. The NodeMCU 1.0 ESP8266 was then disconnected from the computer and was now connected to the relay module which was further connected to the water pump and an external power source to run as shown in Fig. 2 (on the right). The on off stated of the motor is controlled by the upper limit and lower limit data present in google sheets which is set by the user. This upper limit and lower limit value present in the google sheets increases the flexibility of the program as the user gets freedom to change this value to desired range without making any changes to the program, thus the need of compiling and uploading the program to NodeMCU 1.0 ESP8266 is reduced greatly every time user makes any changes to these limits.

Another NodeMCU 1.0 ESP8266 was connected to the computer and another code was designed and similar changes were made as compared with the previous code to interlink the programs with google sheets. The code was successfully complied and uploaded keeping in mind the steps done while uploading code in first NodeMCU 1.0 ESP8266. The second NodeMCU 1.0 ESP8266 was then disconnected from the computer and was connected to the moisture sensor and an external power source as shown in Fig. 1 (on the left). The second NodeMCU 1.0 ESP8266 acts as a transmitter which sends the real-time moisture value of the concrete to the Google sheet interlinked; completing the whole cycle of automation curing. The program is designed in such a way that the transmitting NodeMCU 1.0 ESP8266 will send the moisture value at an interval of every 10 min when the moisture value is greater than the upper limit and when the moisture value is less than the lower limit it will send the moisture value at an internal of 1 min. It will be able to know the limits by reading the upper limit and lower limit data present in Google sheets.

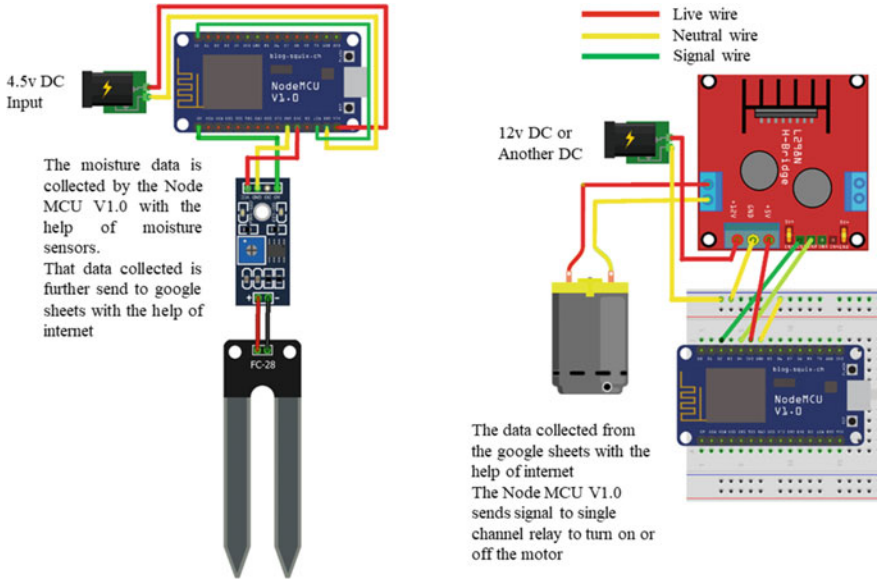

Fig. 1 Schematic circuit diagram of the transmitting and receiving NodeMCU 1.0 ESP8266 used in the laboratory

Figure 1 shows the schematic connection diagram of all the components used for developing the automated curing system, which was used in the laboratory setup, while Fig. 2 shows the schematic connection diagram of all the components used for developing the automated curing system which was used in the construction site setup. The basic difference between the two setups is the that in laboratory setup a 12v dc motor was used to pump the water and it was controlled by a L298N H-bridge motor driver which can operate at a maximum of 25volt dc only, but in construction sites a high-power motor is required which can be controlled by a single channel relay because it can operate in a wide range of power supply.

3 Results

After successful uploading of the compiled program, the following results were observed as shown in Fig. 3 It can be seen that the NodeMCU 1.0 ESP8266 connected successfully to the 'NITK-NET' with a network strength of -70 which falls under very good network coverage area. The moisture sensors start sending data to NodeMCU 1.0 ESP8266 and it receives the data and finds the average of data received before sending it to the Google sheets. After the data are processed it now tries to connect to the online Google script portal and if the connection is successful then it writes the data into Google sheets. A confirmation message is sent back by the Google sheets

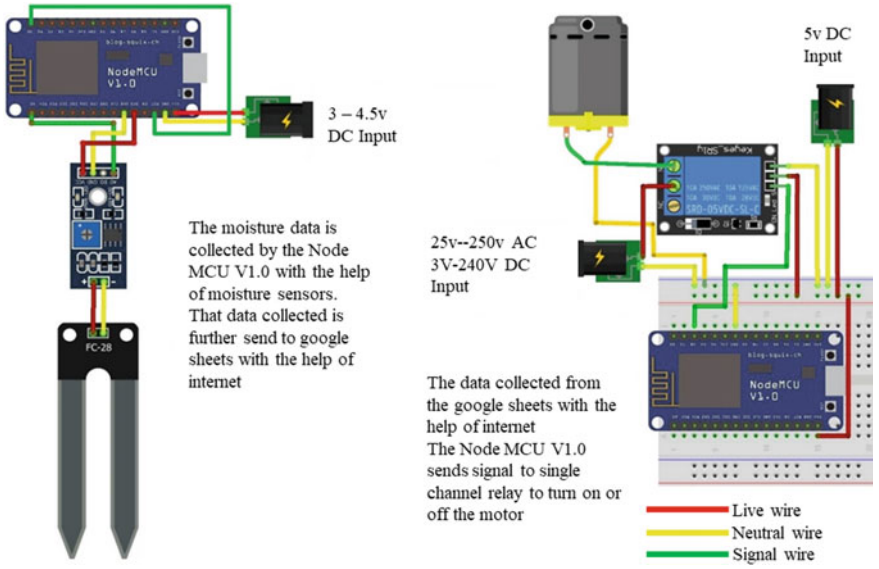

Fig. 2 Schematic circuit diagram of the transmitting and receiving NodeMCU 1.0 ESP8266 used in the construction site

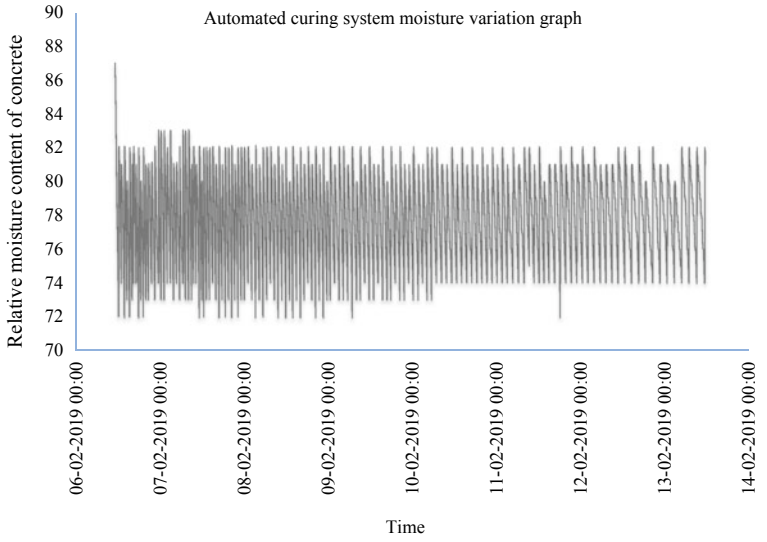

Fig. 3 The variation in relative moisture content of concrete cured using automation system

notifying that the data have been written in the desired row and column. After which the NodeMCU 1.0 ESP8266 goes to sleep depending upon the moisture value it recorded and comparing it with the required moisture percentage value, if the motor state is off it goes to sleep for 10 min or else it goes to sleep for 1 min.

3.1 Test Results of Automation System

The automated curing system was designed to provide water to the concrete cubes when the relative moisture percentage was less than 75% and it continued to water the cubes until the relative moisture percentage of cubes were greater than 80%. The cycle may be defined as the period of curing and retention of moisture content by the concrete sample using the automated curing system. Figure 4 shows the variation of relative moisture content of a M20 concrete cube sample with respect to time in which the moisture sensor was embedded, similar graphs were observed in case of M25 and M30 concrete cube sample. It can be observed that the moisture content of sample continued to increase until it reached above 80% and then it tends to fall as the water supply was stopped and as soon as it falls less than 75% the pump again starts to supply water, this cycle continued till the cubes were cured. During the initial curing period, it can be observed that, the variation in moisture percentage with respect to time was faster as compared to the variation in the later stages. To understand the results better a detailed analysis was done as discussed below with the help of data saved in the Google sheets.

A. Average duration of water flow:—Fig. 5 shows the average duration of water discharged by the pump during a cycle. It can be observed that the duration taken by the M20 concrete blocks to attain the required moisture content is

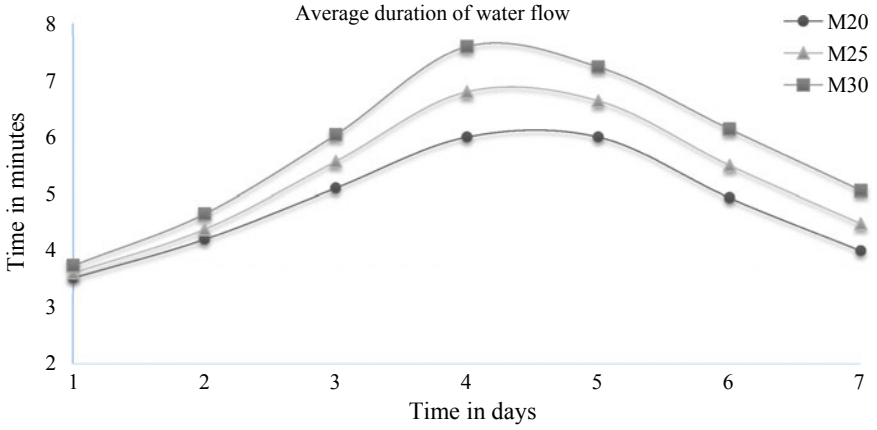

Fig. 4 Average duration of time taken by concrete to attain the required moisture content

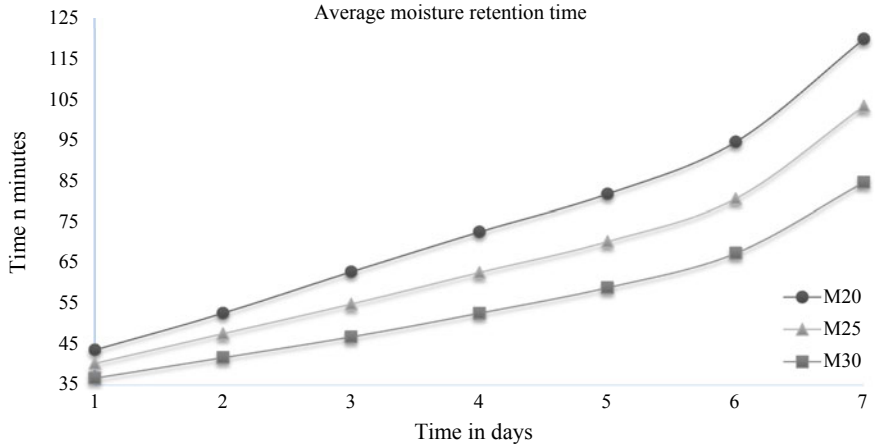

Fig. 5 Average moisture retention time by concrete

less than the time taken by the M25 concrete sample and which further takes less time than the M30 concrete sample. The variation in time is due to the difference in the amount of heat liberated by the different samples, hence it can be concluded that the heat liberated by the M30 concrete sample was greater than the M25 concrete sample, which is greater than the M20 concrete sample. The temperature difference between the internal and external surface of concrete blocks is maximum between 3 and 5 days of curing, hence the average duration of water discharged by the pump during a cycle also increases till this period and then falls as the temperature starts falling. During the later stages even if the temperature of the concrete blocks falls drastically the duration of water discharged by the pump during a cycle does not fall so rapidly because during this time the permeability of the concrete also decreases hence it becomes difficult for the concrete to absorb the water quickly to attain the required moisture content.

B. Average moisture retention time:—Fig. 6 shows the average moisture retention time during a cycle. It can be observed that the duration of moisture retention by the M30 concrete blocks is less than the duration of the M25 concrete sample which is less than the duration of M20 concrete sample. The variation in time is due to the difference in the amount of heat liberated by the different samples as mentioned in the earliest result and as the permeability of the concrete reduces in the later period along with temperature it can be observed that the average moisture retention time increases drastically.

C. Statistical data analysis:—Some inferences where drawn from the observed readings which are mentioned in Table 3. The total water used was calculated assuming that the rate of discharge from the pump was 4 L/min and remained constant throughout the experiment. The average total cycle time was calculated by adding the time taken by the concrete to attain the required moisture and time it retained the moisture. The total water used during the whole process can be

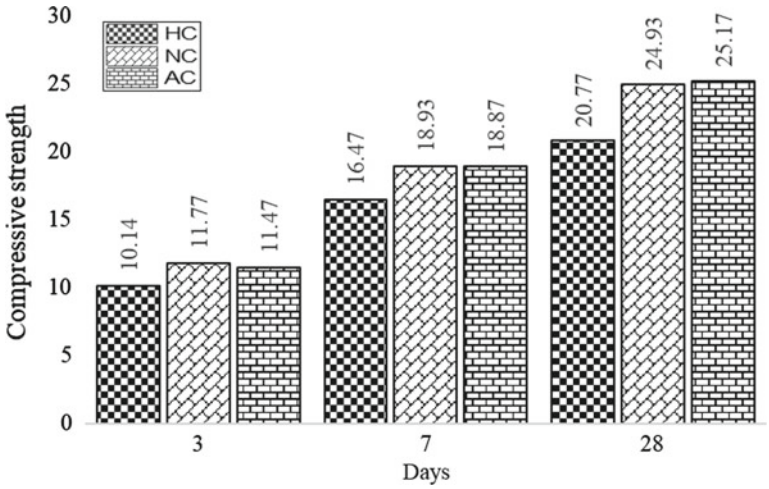

Fig. 6 The compressive strength of M20 concrete sample

Table 3 Statistical data of the automation system

Descriptions	M20	M25	M30
Total pump operating time (min)	607	752	950
Total water used (litres)	2428	3008	3800
Average total cycle time (min)	80	71	61
No. of cycle	126	142	164

reduced by controlling the rate of discharge by the pump which will reduce the water wasted in runoff. The rate of discharge can be matched to the rate of water absorption by the concrete block during curing, which will help in making the system more efficient and effective.

3.2 Test Results of Concrete Compressive Strength

The 3, 7 and 28 days compressive strength of M20, M25, M30 concrete specimen which were cured under three different conditions are shown in Figs. 7, 8, and 9. Where NC refers to sample which was continuously moist cured in the sump tank for 7 days and then was kept to dry for the rest of the days. AC refers to the samples which were cured using the Automated curing system for 7 days and then kept to dry for the rest of the days. HC refers to the samples which were cured twice a day manually for 7 days and then kept to dry. All the samples were cured for 7 days only to match the site conditions.

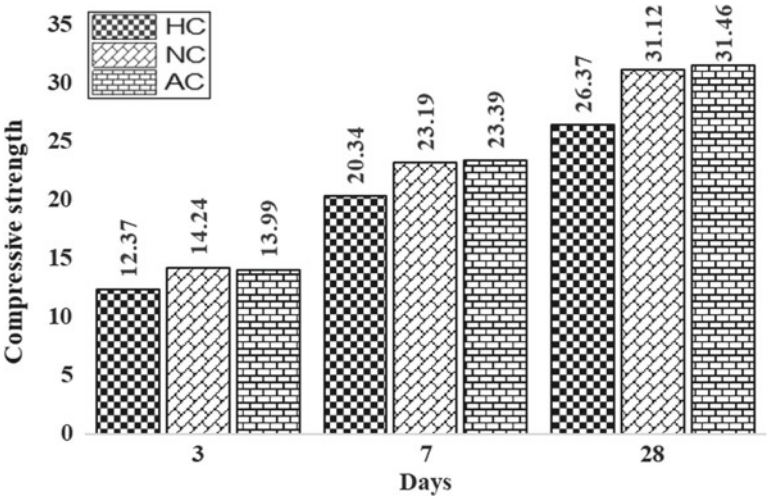

Fig. 7 The compressive strength of M25 concrete sample

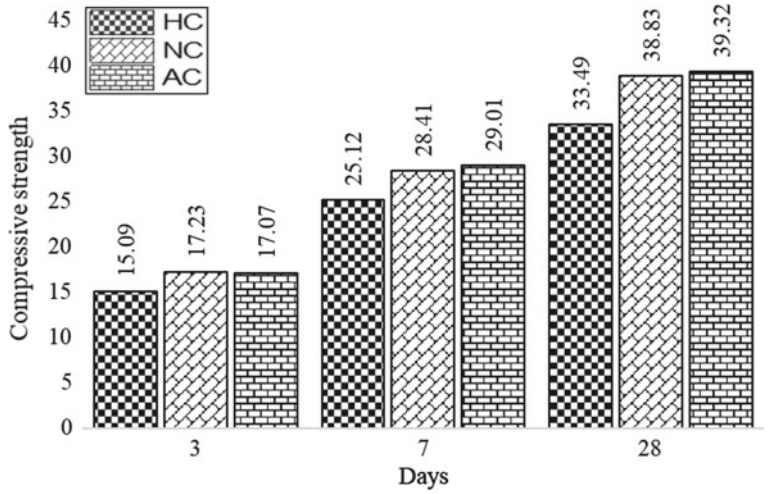

Fig. 8 The compressive strength of M30 concrete sample

It can be observed that the auto cured samples were able to attain a similar compressive strength at the end of 28 days as compared to NC samples, but the HC samples were not able to attain a similar compressive strength. Hence it can be concluded that by using automated curing system in site the quality of concrete can be improved and the risk associated with the quality of concrete decreases. The average increase in compressive strength for the AC sample was found to be 16.6% when compared

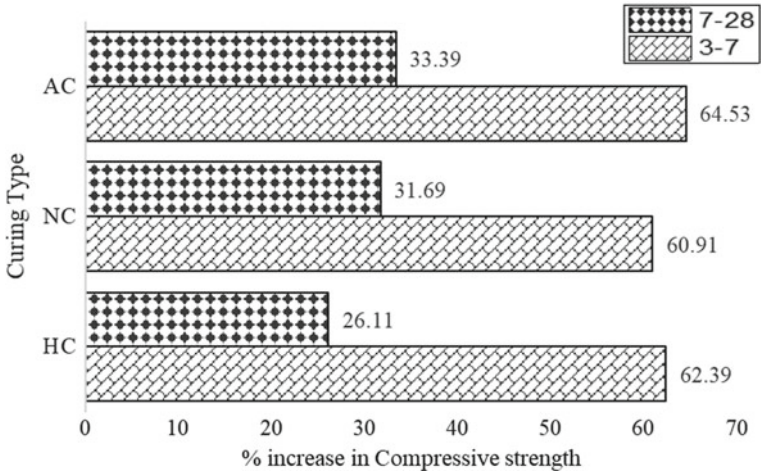

Fig. 9 Percentage increase in compressive strength for M20 concrete

with the HC samples at the end of 28 days, whereas a 1.09% increase in compressive strength was observed when compared to NC samples at the end of 28 days.

A. Percentage increase in compressive strength:—The rate of gain of concrete compressive strength of concrete is higher during the first 28 days of casting and then it slows down. It can be seen in Figs. 10, 11 and 12 that the rate of growth was greater for the AC samples for the initial 3–7 days, than the HC samples, which were higher than the NC samples. These results were obtained because the AC and HC samples were exposed to the atmosphere directly and

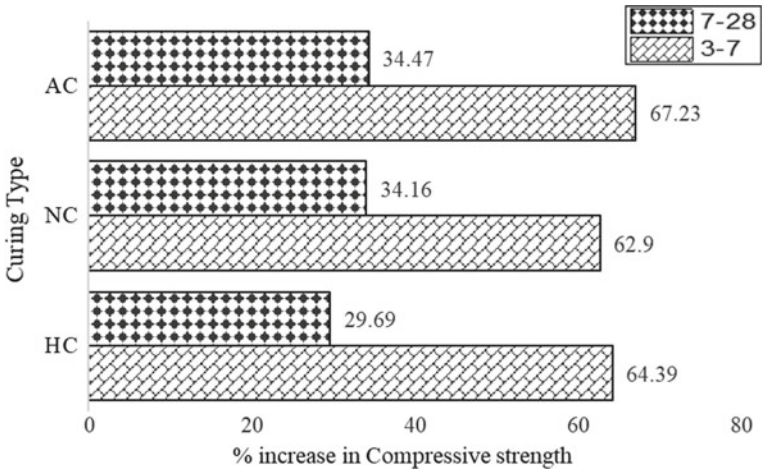

Fig. 10 Percentage increase in compressive strength for M25 concrete

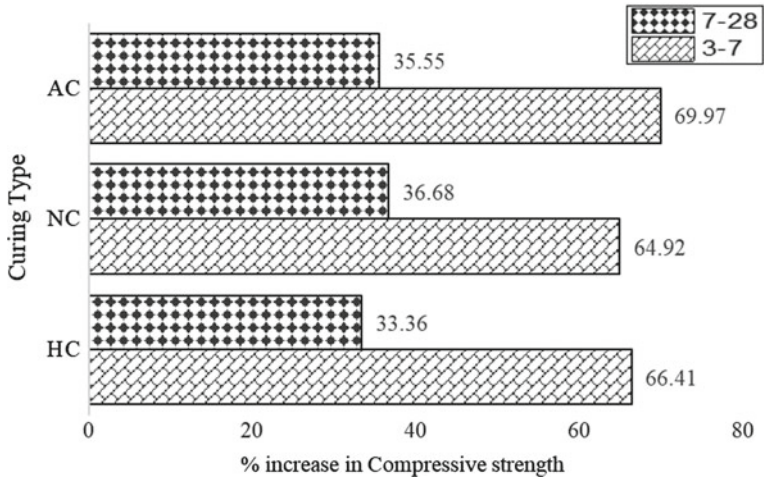

Fig. 11 Percentage increase in compressive strength for M30 concrete

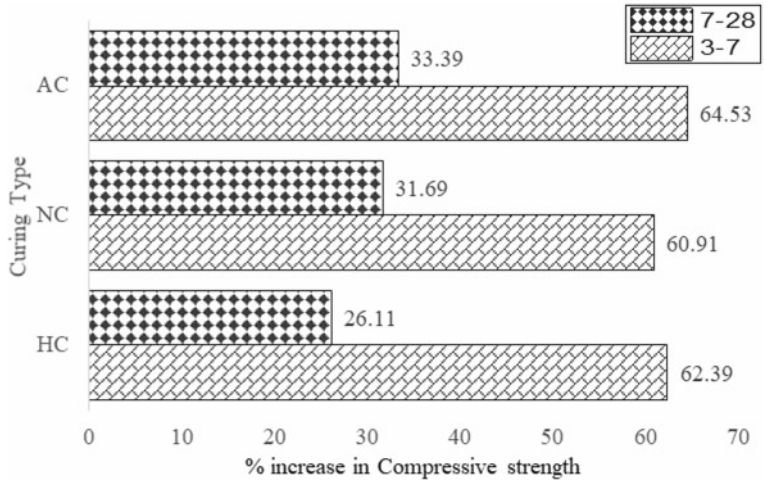

Fig. 12 Percentage increase in compressive strength for M20 concrete

due to the higher initial temperature compared to the NC samples the HC and AC samples gained a faster growth rate during the initial period and AC samples acquired even more strength due to consistent curing which prevented it from thermal expansion and contraction. The rate of growth was greater for the AC samples during the latter 7–28 days, then the NC samples, which were greater than the HC samples. The rate of growth of HC samples decreases during the latter period due to higher initial temperature which reduces the growth rate at the latter stage. This graphs also shows us the percentage increase in strength

after the curing procedure was stopped and, on an average, a 34.57% increase was observed in case of auto cured (AC) samples.

4 Conclusion

The conclusion of the project is as follows:

- As the concrete is cured manually at site the hydration of cement decreases as less water is available to react with the cement. This leads to decrease in the compressive strength of concrete compared to a normal cured and auto cured concrete.
- The automated curing system helped in real-time monitoring of concrete moisture data.
- The automatic curing system increased the concrete compressive strength by **16.09%** when compared to the HC samples, which is a significant increase in the compressive strength and it also prevented the concrete from thermal cracks during the initial stage as it prevented a large variation in temperature of concrete by providing the required moisture at the correct time.
- A **34.57%** increase in compressive strength was found at the end of 28 days when compared to 7th day strength in case of concrete cured under automation system after the curing procedure was stopped at 7th day.
- From the above results, it can be concluded that, the overall efficiency of the system when compared to the NC samples stand at **99 Percentile** as the strength obtained after 28 days of curing in NC and AC samples are within a variation of $\pm 1\%$ when an uninterrupted supply of power is ensured.

References

1. ASTM C 150-11 Standard specification for portland cement. In 2007 Annual book of ASTM Standards, ASTM, Vol. 04.01, Philadelphia, USA
2. Cement, concrete and aggregates Australia (CCA) (Apr 2006) Data sheet, pp 1–7
3. Power TC (1948) A discussion of cement hydration in relation to the curing of concrete. Proceedings, highway research board. vol 27, pp 178–188
4. Burg RG (1996) The influence of casting and curing temperature on the properties of fresh and hardened. P.C.A, Skokie, Illlinois, U.S.A
5. Neville AM (1996) Properties of concrete, 4th edn, Wiley, pp 844 and Power TC, Brownyard TL (1947) Studies of the physical properties of hardened Portland cement paste. Research laboratories of the Portland cement association, Bulletin 22, Mar, pp 992
6. Dhir RK, Hewlett PC, Chan YN (1986) Near surface characteristics and durability of concrete an Initial appraisal, magazine of concrete research, vol 38, pp 54–56
7. ACI committee 308 R-01 R08 (2007) Guide to curing concrete American concrete Institute, Detriot, Michigan, p 30
8. IS 12269:2013, Indian standard—Specification for 53 grade ordinary Portland cement. Bureau of Indian standards, New Delhi, pp 4

9. IS 383:1970 Specification for coarse and fine aggregates from natural sources for concrete, Bureau of Indian standards, New Delhi, p 18
10. IS 10262:2009 Indian standard—concrete mix proportioning—guidelines 1st revision, Bureau of Indian standards, New Delhi, p 14

Inventory Management for Transmission Line Projects

Chandra Kant Singh, Apurva Naik, and Bibhuti Bhusan Das

Abstract In the developing countries, the industrial development plays the key role for enhancing growth of the nation and the industries have basic necessity of continuous and day by day increasing demand for electricity. The transmission lines have the most important responsibility for the effective transmission of electricity, i.e. to transmit the electricity from the generating station to the load centres. In the recent days, the physical storage and distribution have vital roles to play for the organization. The importance of the management of stores for inventory management is related to eradicate the unused, surplus or leftover materials that add cost to the supply chain so as to cultivating the efficiency and the effectiveness of the store functions at the same time intends to maximize those areas, which can add value. Inventory management is complex and crucial task of any transmission line project. At present, the organisations normally set inventory targets using thumb rules or single-stage calculations. Thumb rules involve to set the number of days for supply as the coverage target. Single-stage calculations include the single item in the single location and thereby calculating the amount of inventory needed to satisfy or fulfil the demand. This study is trying to implement statistical inventory management model in the construction of transmission line projects. In this study, we will try to optimize the inventory level of a transmission line project to reduce the overall cost of project by reducing the excess cost associated with excess inventory. This paper is anticipated to help the decision-makers by enhancing the current performance of the store management in the construction projects by finding the economic order quantity to minimize the total inventory cost.

Keywords Inventory management · Economic order quantity · Holding cost · Ordering cost

C. K. Singh · A. Naik · B. B. Das (✉)
Department of Civil Engineering, National Institute of Technology Karnataka, Surathkal, Mangalore, Karnataka, India
e-mail: bibhutibhusan@gmail.com

B. B. Das et al. (eds.), *Recent Trends in Civil Engineering*, Lecture Notes in Civil Engineering 105, https://doi.org/10.1007/978-981-15-8293-6_36

1 Introduction

Power transmission line is the bridge that connects the generating stations such as the thermal power station or hydropower station and the load centres, which are the consumers of electricity. These consumers can be of commercial, industrial or the domestic type.

In the real-life practice, managing the resources used in transmission line are tremendously risky, expensive and needs focussed care. As it includes structural steels, which are prefabricated and have huge shape and size are very bulky, construction materials used for concrete foundations, reels of conductor cables, transmission line accessories and fittings and stringing machineries such as tensioner and puller, which are of huge masses, have to be transported from warehouses to extreme ground level like hills or muddy areas [13].

There are a lot of material inventories used at the construction site. There are advantages of stocking extra inventories than the average utilization, it can encounter unanticipated demands and it also provides an economical advantage by evading the material escalation price. Whereas, on the contrary side, stocking more than average have some disadvantages also. The main reason being it decreases the construction productivity by incurring high cost by storing redundant inventory. Thus an appropriate model for calculating an optimal level of material inventories to be ordered and stocked plays a significant role in the construction projects for economic efficiency.

The objective of the study is to suggest a statistical inventory management model, which can be applied in the store yard of TL construction projects so that all the items meet its expected demand at right time and at the minimum total cost.

1.1 Inventory Management

Inventory that is commonly known as the stock implies to the goods, resources or the materials that the company holds for the eventual objective of consumption or resale. The inventory management is defined as the science that generally specifies the shape and placement of stocked goods. Throughout the project life cycle, it is essential at different period and locations to optimize the supply chain management and to plan and schedule the optimum quantity for the materials required to complete the project in due time [12].

The optimal inventory management model is devised to support purchase decisions where users can make timely actions on how much to order and when to buy raw materials.

1.2 Costs Related to Inventory

There are few costs related to inventory which are as follows:

1.2.1 The Ordering Cost

The ordering costs refer to the expenditures to generate and process the order to the material supplier. These costs are involved in finding the economic order quantity as it affects the inventory cost of the material.

Ordering costs includes:

- Expense incurred to place the purchase requisition.
- Expense incurred to place the purchase order.
- Expense incurred to process the bill of the supplier for the delivered order.
- Expense incurred to process the payment to the supplier.

1.2.2 The Holding Cost

This is the total carrying cost of inventory also denoted as the total cost of holding the inventory, for example costs like the rent, the insurance costs, the utilities, the salaries, etc.

1.3 Cost-Trade Off Curve

Cost-trade off curve is used to find out the optimum economic order quantity at which the cost of inventory/storage is minimum. Economic order quantity is the quantity of order at which the sum of the holding costs and the ordering costs will be the least or economical.

The cost-trade off curve consists of three different curves representing different cost associated with inventory and there variation with amount of order quantity. The intersection of holding cost and ordering cost gives the value of most optimum economic order quantity. At economic order quantity point, the total cost of inventory is minimum. So economic order quantity meets all the demand requirement and at the same time with minimum cost.

Cost-trade off curve is shown in Fig. 1.

Inventory carrying or holding cost is increasing as we are increasing the order quantity. This is because as soon as order quantity will increase we have to put more extra resource to keep the inventory item in store yard.

Initially, total cost curve goes downwards, i.e. as we are increasing the order quantity total cost is decreasing. This is because initially procurement cost dominates the inventory holding cost. The point of intersection of two cost curve, i.e. inventory

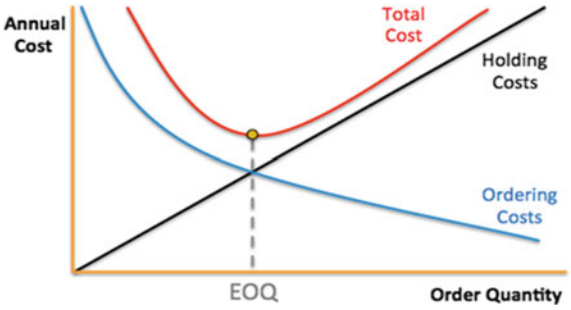

Fig. 1 Cost-trade off curve

carrying cost curve and procurement and stock out cost curve gives the value of economic order quantity value where the total cost is minimum.

2 Methodology

We use the Harris–Wilson Economic Order Quantity Model for optimizing the inventory for the resources utilized at the construction site. However, there are many assumptions in this model, still, in many real-life scenarios, it has been of utmost importance. There have been some scenarios where this model gives cost-saving options. As such is the case where this model is utilized immensely in the automobile and pharma sectors by reducing the costs incurred [11]. The objective of this model is to answer the common problem faced in the inventory management, i.e. at what time the order should be regularly purchased (the reordering point) and what should be the quantity for every order [7].

2.1 Assumptions

The demand arises uninterruptedly at the fixed and known rate of Q per unit time. As it arrives at the continuous rate, it is known that the optimal order quantity may not be an integer. Unless the optimal order quantity is really small in numbers, the fraction part of the order quantity will not be of much significance. In reality if such scenario occurs, we can round off to the nearest integer of the order quantity [14].

Also, the demand that is assumed to arise at the fixed and known rate is hardly satisfied in reality. But, when this model is applied where demand is comparatively stagnant with time, it gives decent results. Let us denote the following variables as follows:

- D is annual or yearly demand (units/year)
- Q is quantity to be ordered at each order point (units/order)
- N is the no of order to be placed in a year (order/year)

- T is the time length of one inventory cycle or time gap between two successive order (year/order)
- C = The purchasing cost a unit of inventory item (Rs. per unit)
- C_o = The placing cost of particular order (Rs./order)
- C_h = The holding cost of one unit of inventory item for one complete year
- The order arrives LT time after the order is placed. We assume that lead time LT is deterministic.
- The model parameters are constant and not changing with time.
- All demand is satisfied on time.

2.2 Objective of Economic Order Quantity Model

The goal is to find the order quantity with the lowest possible cost of inventory and the reorder interval to make sure the resources are available with just in time deliveries.

As the parameters are considered stationary and uniform over time, the quantity of order which is assigned as Q, will be also stationary as well. The reordering interval is at what time the order should be placed, since the reordering interval is the time between two successive epochs when the order should be placed and is known as the cycle length. The cycle is the time between placing of two successive orders [7] (Fig. 2).

The problem to determine at what time to place the order has solution with respect to this model. Since it is assumed that the demand would arise at deterministic and constant rate while the order which is placed takes LT time to be delivered and the

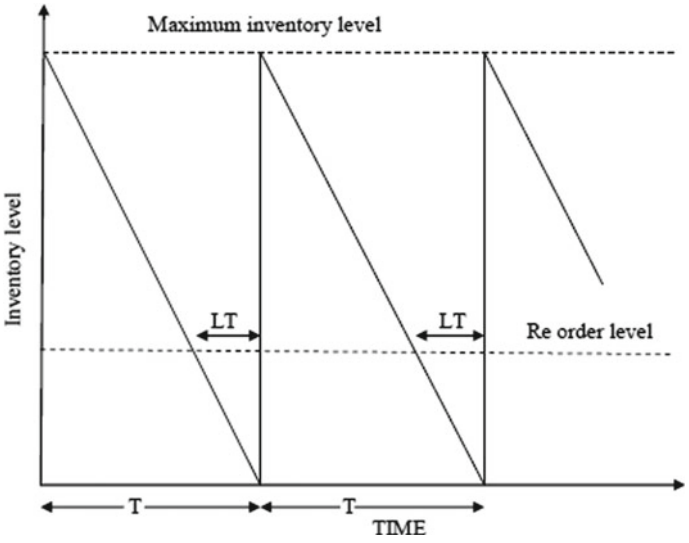

Fig. 2 Change in inventory level with respect to time

order should be reached exactly when the last unit of that quantity is being consumed. So, the order needs to be placed LT time before the exhaustion of inventory.

2.3 Cost Calculation

$$\text{Total annual cost} = \text{Purchase cost} + \text{Ordering cost} + \text{Holding cost} \tag{1}$$

$$\begin{aligned}\text{Purchase cost(PC)} &= \text{Demand per unit time} \\ &\quad \times \text{cost of purchasing one unit of inventory item} \\ &= \text{D} \times \text{C}\end{aligned}$$

$$\begin{aligned}\text{Ordering cost(OC)} &= \text{No. of order to be placed per unit timecost of placing one order} \\ &= \frac{\text{Demand for given period of time}}{\text{Quantity to be ordered at each order point}} \text{ cost of one order}\end{aligned}$$

$$\textbf{Ordering cost (OC)} = \frac{\mathbf{D}}{\mathbf{Q}} \times \mathbf{C_o} \tag{2}$$

$$\begin{aligned}\text{Holding cost for one cycle time} &= \text{Average inventory for one complete cycle} \\ &\quad \times \text{holding Cost} \times \text{time of one cycle} \\ &= \frac{\text{Q}}{2} \times \text{C}_\text{h} \times \text{T}\end{aligned}$$

So annual holding cost $= \frac{Q}{2} \times C_h \times T \times N$

$$\textbf{Holding Cost (HC)} = \frac{\boldsymbol{Q}}{2} \times \boldsymbol{C_h} \tag{3}$$

$$\text{Total annual cost} = \text{Direct cost} + \left[\frac{D}{Q} \times C_o\right] + \left[\frac{Q}{2} \times C_h\right]$$

So substituting Eqs. (2) and (3) in Eq. (1), we get

$$\text{total variable cost or total inventory cost} = \text{Ordering cost} + \text{Holding cost}$$

$$\text{So, } \textbf{Total Inventory Cost} = \left[\frac{\boldsymbol{D}}{\boldsymbol{Q}} \times \boldsymbol{C_o}\right] + \left[\frac{\boldsymbol{Q}}{2} \times \boldsymbol{C_h}\right] \tag{4}$$

2.3.1 Economic Order Quantity Calculation

From the cost-trade off curve, it is evident that order quantity at which holding cost becomes equal to ordering cost, at that point total inventory cost is minimum and

hence this quantity of order will be Economic order quantity (EOQ) which is denoted by Q'.

At EOQ, Ordering cost = holding cost

$$\left[\frac{D}{Q'} \times C_o\right] = \left[\frac{Q'}{2} \times C_h\right]$$

$$\boldsymbol{Q' = \sqrt{\left[\frac{2 \times D \times C_o}{C_h}\right]}} \tag{5}$$

2.3.2 Total Inventory Cost Calculation at EOQ

It is denoted by TIC' and is shown below:

$$\text{TIC}' = (\text{Ordering Cost})_{\text{EOQ}} + (\text{Inventory Holding Cost})_{\text{EOQ}}$$

$$\text{TIC}' = \left[\frac{D}{Q'} \times C_o\right] + \left[\frac{Q'}{2} \times C_h\right] \tag{6}$$

But at economic order quantity-

$$\text{Ordering cost} = \text{Holding cost}$$

$$\left[\frac{D}{Q'} \times C_o\right] = \left[\frac{Q'}{2} \times C_h\right] \quad \left[\text{From Eqs. (2) and (3)}\right] \tag{7}$$

$$\text{TIC}' = 2 \times \left[\frac{Q'}{2} \times C_h\right] \quad \left[\text{Substituting Eq. (7) in Eq.(6)}\right] \tag{8}$$

$$\boldsymbol{\text{TIC}' = \sqrt{[2 \times D \times C_o \times C_h]}} \quad \left[\text{Substituting Eq. (5) in Eq. (8)}\right] \tag{9}$$

And total inventory cost at any order quantity Q can be calculated as given below:

$$\boldsymbol{\text{TIC}(Q) = \left[\frac{D}{Q} \times C_o\right] + \left[\frac{Q}{2} \times C_h\right]}$$

2.3.3 Determination of Reordering Level

$$\text{Reordering level} = \text{Lead time} \times \text{Rate of consumption of given inventory} \tag{10}$$

2.4 Order Detail and Data Collection

Following are the order details of inventory item and other important data regarding inventory of a transmission line project executed by Larsen and Toubro (source of data is from L&T Construction) (Table 1).

All the above cost which is given in the table is the cost per year. Other inventory-related costs are as follows:

- Store rent per year = ₹12.24 Lakh
- Inventory cost (other utilities) for 12 months = ₹26.6 Lakh
- Staff expenses for 12 month = ₹9 Lakh
- Security expense for 12 month = ₹6.4 Lakh.

2.4.1 Inventory Cost Calculation and Comparison for Cement Bags

Demand for the cement bags = 169,566 bags/year.

Ordering cost for cement bags = ₹15,000 per order.

Calculation of Holding Cost Per Bag for One Year

- Inspection cost for one unit cement bag for one complete year

$$= \frac{\text{Inspection Cost per year}}{\text{No of bags}}$$

$$= \frac{75000}{169566} = \mathbf{₹0.44\ per\ bag\ per\ year}$$

- Unloading cost for one unit of cement bag for one complete year

$$= \frac{\text{Unloading Cost per year}}{\text{No of bags}}$$

$$= \frac{508698}{169566} = \mathbf{₹3.00\ per\ bag\ per\ year}$$

- Assuming there are total 15 major component and thus area occupancy ratio by cement bags is (1/15) of total area of store.
- Store rent for one unit of cement for one complete year

Table 1 Order detail of a transmission line project

S. No.	Particular	Unit	Qty.	Rate (₹)	Amount (₹)	No. of PO	Cost per order (₹)	Inspection cost (₹)	Unloading cost (₹)
1	Cement	Bag	169,566	268	45,443,688	18	15,000	75,000	508,698
2	Disc insulator	No	22,950	582.7	13,374,801	1	50,000	9000	68,850
3	Hand gloves	No	2752	10.5	27,846	7	1000	450	450

Source L&T Construction

$$= \frac{\text{Store rent for one year}}{\text{No of bags}} \times \frac{1}{15}$$

$$= \frac{12.24 \times 10^5}{169566} \times \frac{1}{15}$$

$$= \textbf{₹0.48 per bag per year}$$

- Other utilities cost for one unit of cement for one complete one year

$$= \frac{\text{Other Utility Cost for one year}}{\text{No of bags}} \times \frac{1}{15}$$

$$= \frac{26.60 \times 10^5}{169566} \times \frac{1}{15} = \textbf{₹1.05 per bag per year}$$

- Staff expenses for one unit of cement for one complete year

$$= \frac{\text{Total staff expense for one year}}{\text{No of bags}} \times \frac{1}{15}$$

$$= \frac{9 \times 10^5}{169566} \times \frac{1}{15} = \textbf{₹0.35 per bag per year}$$

- Security expenses for one unit of cement for one complete year

$$= \frac{\text{Total security expense for one year}}{\text{No of bags}} \times \frac{1}{15}$$

$$= \frac{6.40 \times 10^5}{169566} \times \frac{1}{15} = \textbf{₹0.25 per bag per year}$$

So Overall Inventory Holding Cost per unit bag for one complete year.
$= (₹0.44) + (₹3.00) + (₹0.48) + (₹1.05) + (₹0.35) + (₹0.25) =$ **₹5.57 per bag per year**.

Actual Order Quantity

Actual order quantity for 18 no. of PO $= \frac{\text{Total Number of Bags}}{\text{Number of PO}} = \frac{169{,}566}{18} =$ 9421 **bags per order**.

TIC at Actual Order Quantity

Using the principle given by Harris–Wilson EOQ model, total inventory cost (from Eq. (4)) at order quantity of 9421 bag per order $= \left[\frac{169,566}{9421} \times 15,000\right] + \left[\frac{9421}{2} \times 5.57\right]$ $=$ **₹296,218.38**.

Calculation of EOQ

Using the Harris–Wilson Economic Order Quantity model, EOQ will be calculated.

using Eq. (5), EOQ $= \sqrt{\left[\frac{2 \times D \times C_o}{C_h}\right]} = \sqrt{\left[\frac{2 \times 169,566 \times 15,000}{5.57}\right]} =$ **30,221 bags per order.**

No. of PO $= \left[\frac{169,566}{30,221}\right] = 5.6 \sim 6.$

Thus, Quantity of Cement Bags per order $= \left[\frac{169,566}{6}\right] =$ **28,261 bags per order**.

TIC at Economic Order Quantity

Using the principle given by Harris–Wilson EOQ model, TIC at economic order quantity [from Eq. (4)]

$$= [6 \times 15,000] + \left[\frac{28,261}{2} \times 5.57\right] = \textbf{₹1,68,706.89}$$

Cost Saving

$$\text{Total amount of cost saving} = (\text{TIC at actual order quantity}) - (\text{TIC at EOQ})$$

$$= (2,96,218.38) - (1,68,706.89) = \textbf{₹1,27,511.49 per year for cement}$$

$$\text{Percentage cost saving} = \left[\frac{127511.49}{296218.38} \times 100\right] = \textbf{43.05}\%$$

3 Results and Discussions

The comparison of the results of actual order to that of the Economic Order Quantity in Table 2 (Fig. 3).

This clearly depicts that Rs. 1.88 lakhs (32.73% Savings) of money can be saved in one year on Cement, Disc Insulator and Hand Gloves procurement only if the inventory management is done. This amount can play a huge factor as the other

Table 2 Comparison of resulting inventory cost

S. No.	Particulars	Actual inventory cost incurred (₹)	Cost wrt economic order quantity (₹)	Cost saving (₹)	% of savings
1	Cement	2,96,218	1,68,707	1,27,511	43.05
2	Disc insulator	2,69,746	2,09,873	59,873	22.20
3	Hand gloves	9,647	8,633	1,013	10.51
		5,75,611	**3,87,213**	**1,88,398**	**32.73**

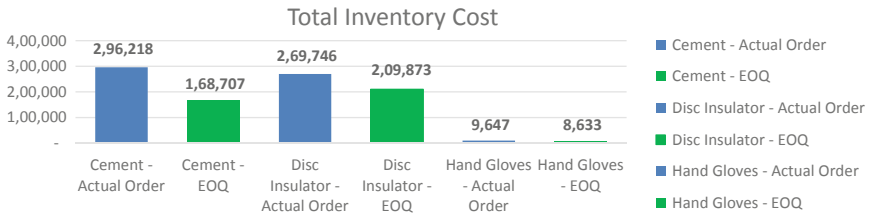

Fig. 3 Graphical representation of cost comparison

materials can also be evaluated for the economic order quantity. The Steel Structures are required in huge quantity in the transmission line projects and thus should be ordered as per the statistical inventory management to increase the savings.

4 Conclusions

Lot of money is being wasted by having the wrong amount of inventory and for wrong duration in the construction industry. This not only adds unnecessary cost to the contractor, but also affects the quality of the work as the contractor's profit margin is directly affected. It may also lead to the increased project time if the reorder is not made on suitable time. Poor planning and poor execution of inventory management can affect the project performance and may lead to major loss to the stakeholders. The importance of inventory management in construction is increasing day by day as it is closely related to the project performance and especially to the cost in the construction industry. The statistical inventory management model has been widely used in manufacturing industry and huge amount of cost is being saved by having the order quantity equal to the Economic Order Quantity. This method if applied in managing inventory of transmission line construction projects, considerable amount of money can be saved by avoiding the excess inventory and hence by avoiding the excess inventory ordering and inventory holding or carrying cost.

References

1. Adams CM (2004) Inventory optimization techniques, system vs. item level inventory analysis. In: Annual symposium reliability and maintainability, 2004—RAMS
2. Arrow K, Karlin J, Scarf H (1958) Studies in the Mathematical theory of inventory and production, vol 44(348). Stanford University Press
3. Bemelmans R (1968) The capacity aspect of inventories. Lecture Notes in Economics and Mathematical Systems, Berlin
4. Buchan J, Koenigsberg E (1963) Scientific inventory management. Prentice-Hall, Englewood Cliff, New Jersey
5. Hanssmann F (1962) Operations research in production and inventory control, vol 12. Wiley, New York, London, pp 254–264
6. Hadely G, Whitin TM (1963) Analysis of inventory systems. Prentice-Hall, New Jersey
7. Muckstadt JA, Sapra A (2010) EOQ model. Principles of Inventory Management, pp 17–45
8. Peter M, Karoly N (2006) A new inventory control method for supply chain management. In: The 12th international conference on machine design and production
9. Kasim N (2011) ICT implementation for materials management in construction projects: case studies. KICEM J Constr Eng Proj Manag 6
10. Patel KV, Vyas CM (2011) Construction materials management on project sites. In: National conference on recent trends in engineering & technology, Gujarat
11. Agarwal S (2014) Economic order quantity model: a review. VSRD Int J Mech Civ Autom Prod Eng 6(12):233–236
12. More S (2016) The study of efficiency and effectiveness of warehouse management in the context of supply chain management. Int J Eng Technol Manag Appl Sci 4(8):160–169
13. Yusof ZM, Sivadass T (2006) Construction management of power transmission lines—logistics and challenges. In: 6th Asia-Pacific structural engineering and construction conference, Malaysia (APSEC 2006), C-60–67
14. Alema-Mensah E (2011) Managing inventory systems using optimization. Department of Mathematics, Kwame Nkrumah University, Ghana

Resource Buffers in Construction Projects

Arun L. Hegde, Aman Jain, and Bibhuti Bhusan Das

Abstract Critical Chain Project Management (CCPM) is created on techniques and procedures taken from the Theory of Constraints (TOC). CCPM was presented in late 90s (1997) in a book named Critical Chain from several studies by Standish Group and others for customary project management methods, only half of the projects normally finish on time, projects generally take twice the duration originally planned, twice of the original planned cost, around 70% of projects fall short of their planned scope, and round about 30% of the projects are shut down in midway. CCPM can be used to avoid these customary statistics. Usually, CCPM case studies report greater than 95% on-time and on-budget completion when CCPM is applied in the approved manner. Initially, the CCPM guidelines and prescriptions and discovers its differences with customary project scheduling methods like Program Evaluation and Review Technique (PERT) and Critical Path Method (CPM). Then the Critical Chain Project Management solution has been outlined, which covers all the proposed steps—the elements of the Critical Chain Project Management solution. Thereafter, the methodology used for data collection and analysis has been explained. Further, it explains the application of CCPM in a Transmission Line Project undertaken by Larsen and Toubro Power Transmission and Distribution. Further, the results of the analysis and discussions about the same have been written.

Keywords Critical Chain Project Management (CCPM) · Resource Buffer Consumption (RBC) · Theory of Constraints (TOC) · Critical Chain Complete (CCC) · Program Evaluation and Review Technique (PERT)

1 Introduction

Critical Chain Project Management (CCPM) is a method of planning and handling projects that can decrease the delivery time of the project and it is becoming the new standard for project success. It was introduced in late 90s to plan and execute

A. L. Hegde · A. Jain · B. B. Das (✉)
Department of Civil Engineering, National Institute of Technology Karnataka, Surathkal, Mangalore, Karnataka, India
e-mail: bibhutibhusan@gmail.com

B. B. Das et al. (eds.), *Recent Trends in Civil Engineering*, Lecture Notes in Civil Engineering 105, https://doi.org/10.1007/978-981-15-8293-6_37

projects in a better way 'in half the time, all the time'. CCPM was developed so that projects can be completed within the budgets and to monitor the progress on regular basis to complete given time period as there are many projects in the past which have missed their deadlines and have overrun their budget. It also gives the detail of the project work schedule and the organization of the project report [1–4] (Lawrence P. Leach). The term 'critical chain' means the longest path in the network diagram that satisfies both task dependency and how easily the resources are available.

CCPM is an innovative process with emphasis on aggressive timelines for tasks, management of project buffer instead of task buffer and stresses on resources to execute them [5–7]. CCPM is the extension and the application of the Theory of Constraints to the practice of project management. Key idea behind CCPM is to gather the protection time from total time assigned to the individual activities or tasks and combined it into different types of strategically allocated buffers (PB, FB). Project buffer helps in protecting the completion date of a project from delays; feeding buffers allows to take advantage of the early finishes of activities and protect the critical chain from delays in non-critical chains, whereas resource buffers make sure of resources availability at a particular time.

CCPM will not only improve adherence to specification but will also reduce cost and enhance time-related order winning criteria. The important aspects of CCPM are mentioned below such as planning, execution and continuous improvement process.

1.1 Planning of a Project with CCPM

In determining the project duration, CCPM methodology considers for resources as well as priority dependences which are labelled as critical chain. In Fig. 1, the critical path could be named by activities 1,3,4 whereas using CCPM, it is termed by 1,3,2,4 because of shared resource B. In these type of cases, the critical chain is generally larger than the critical path due to which management of all the four activities should be done accordingly.

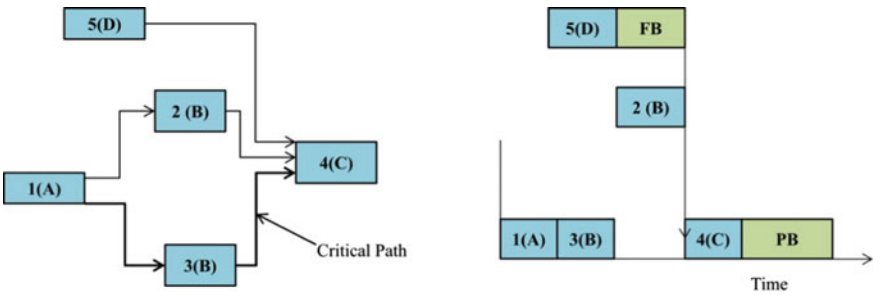

Fig. 1 Network diagram and critical chain schedule showing buffers

To effectively manage the buffer time, CCPM acquaints with the concept of project and feeder time buffers, which is generally unexploited while managing at the task stage. Feeder buffers separate task sequences with a float from the critical chain whereas the project buffer is positioned at project end to protect the critical chain. Thus, such buffers allow the combination of the buffer time and give greater stability, permitting both controllable and shorter lead times. In forming such buffers, the initial phase is to halve the existing activity times and assign other half of activity time into the aggregated buffer. Combination is shown in Fig. 1 for explanation.

While planning for a multi-project environment, CCPM advocates staggering the release of projects for a selected resource which behaves as a drum. This can be used to ensure flow and to shun those projects, which results in doing too many tasks in a single period, which leads to overlooked completion dates (Oded Cohen).

1.2 Execution of a Project and Its Improvement Process

Whenever the activity is in progress, it should be reported with its balance time so that it can be noted down on regular basis which gives an idea about the projects progress but in the case of CCPM reporting of the balance time of an activity is done ideally on daily basis. It provides the information about the upcoming tasks, as it does not have any in-between information about the task dates in the scheduling model, the tasks remaining time data alert you with an advanced notice of approaching tasks (also mentioned as resource buffer earlier).

Most of the undergoing activities are contending for a resource provider's time in this complex multi-project environment. In CCPM, they are listed in terms of the ratio of critical chain completion and buffer consumption, generally using red, yellow and green priority colour codes. Forthcoming activities are shown with their priority order as well as the likely time when these activities can be available to that resource.

Project manager monitors the buffer consumption on daily basis and takes corrective actions where ever required. Consumption of the buffer specifies that an activity is taking more time than the determined period and may need assistance. Managers or executives look after the progress of all undergoing assignments and take required actions. The timely review of the progress of undergoing projects is done on a regular basis. By extracting significant causes of delay project managers should focus on improvement activity (Oded Cohen).

1.3 Review of the Previous Work

The Critical Chain methodology exploits the statistical law of aggregation by protecting the project from common-cause uncertainty of the individual tasks in a task path with time buffers at the end of a path in the project network [4]. The

term CCPM that stands for the Critical Chain Project Management is assigned to TOC solution to denote withdrawal from the conservative methods of critical path. It is holistic, as it does not focus on every single activity or task in spite it looks at the project as a whole. It is analytical, as the conceptual base of the solution can be given by the TOC thinking processes. CCPM can help in defending the project completion date which is guaranteed to the client or customer by transferring the buffer times connected with the critical chain activities to the end in the form of a Project Buffer (PB). It is a win-win situation as it considers the essential requirements of the major stakeholders (Oded Cohen). The shift from handling projects with their locals (tasks) to the global (project as a whole) requires an alteration in the mind-set of employees. They need to pledge to carry out the project on the assured due date. Thus, while designing the CCPM solution, we have to think through these three important characteristics which are mind-set/Human elements, planning and control of execution.

2 Methodology

All projects have an approved starting date, which is basically termed as project kick-off. It suggests that the particular time or period at which the activities should be taken and executed. It permits to take out the resource materials and capital from the project budget. Once a project has been started, the project drives from the planning stage to the execution stage. The harsh truth about most of the execution of the project is the delay and this is triggered mainly by the activities which take more time than allotted time and activities that do not start on time. The delays are the likely outcomes of the inherent nature of carrying out activities in ambiguous surroundings. Through the usage of buffers, Theory of Constraints (TOC) handles the uncertainty in the initial stage of planning and the later stages of execution.

2.1 Project Execution Phase Using Buffer

The CCPM solution tool is used for compensating the delays by shielding them with time from the corresponding buffer. Any sort of delay in Critical Chain munches time from the Project Completion Buffer (PB). Project Completion Buffer (PB) acts as a reservoir helping the higher authorities such as project manager to secure the well-timed delivery and it is the total protecting time of the project. The project manager needs to be acquainted with the amount of the buffer left at every point of time and to attain that buffer penetration should be known.

The buffer status in a project is determined by the level of penetration, which helps in identifying the amount of time disbursed from the buffer. There is zero consumption of the buffers at starting of project. As the project advances, some of the activities are likely to take more time than planned. All the deviations from the original time path

are balanced by taking the time from buffer. Buffer Status is that buffer level which indicates the risk of completing the project on-time to project manager. To get quick response and prompt attention from the management, TOC uses the colour system in which each colour has its own significance. As Green indicates, that the project is on right path and do not call for any interference. Whereas, Yellow signals to 'get ready' as the situation is becoming risky which requires to take additional actions to make sure that the critical path should not deviate from its original path. But when it signals RED—managers must act quickly to take remedial actions to bring back the level of protection the project needs. Restoring some of the buffers and reducing the level of penetration is possible and can be executed by adding time to the project buffer due to the activities which are finished earlier than allotted time by providing float in a critical path [8–11].

2.2 Steps Implemented in the Project

The planned schedule and the As-Built Schedule of a project are obtained from Planning Team. The obtained schedule is rescheduled with CCPM Methodology/Cut & Paste Method. Following steps describe the implementation of TOC to a construction project (Fig. 2).

The schedule obtained with the above description is compared with the As Built or Updated Schedule from which the percentage of the critical path completed is obtained. The allocated quantity of resources for each activity is obtained from the Bill of Quantity submitted to the client at the beginning of the project. The actual quantity of resources consumed is obtained by summation of resources consumed on daily basis (Daily Progress Reports).

2.3 Calculating Percentage Chain Completion for Critical Chain

$$\%\ \text{Chain Complete} = \frac{(\text{original critical chain duration} - \text{remaining duration of longest chain})}{\text{original critical chain duration}}$$

Calculating Percentage Chain Completion for Feeding Chains (FC)

$$\%\ \text{Chain Complete} = \frac{(\text{original duration of longest FC} - \text{remaining duration of longest chain})}{\text{original duration of longest FC}}$$

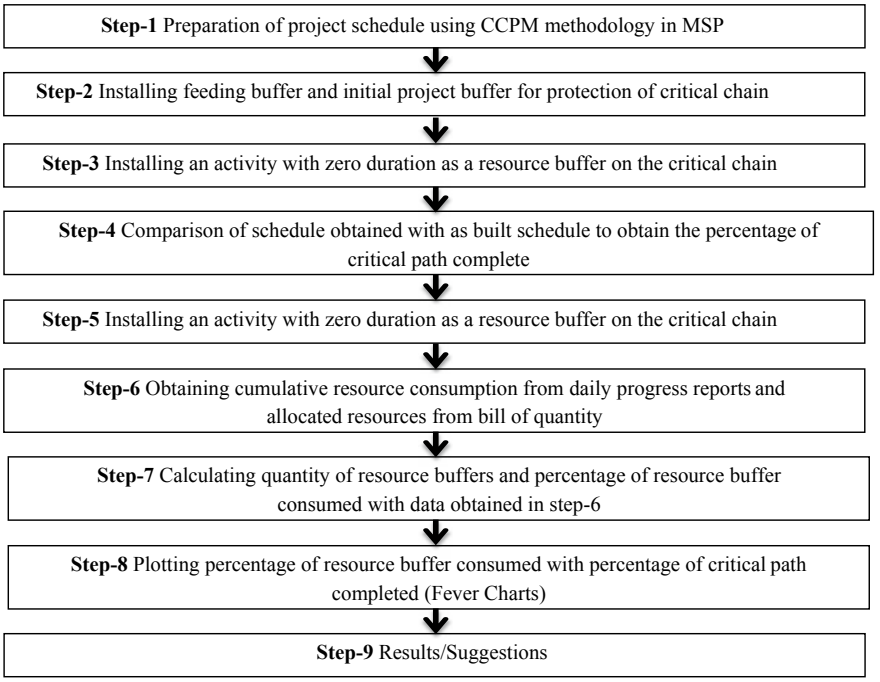

Fig. 2 Flowchart showing steps implemented in the project

Calculating Percentage of Buffer Consumption

$$\%\ \text{Resource buffer consumed} = \frac{(\text{original buffer quantity} - \text{remaining quantity})}{\text{original buffer quantity}}$$

The worst value must be taken, if numerous chains are present in the network [12]. The cumulative value of the resource safety buffer consumed is plotted (along *y*-axis) against the percentage of the critical path complete (along *x*-axis). Markings are provided on the graph, which indicate the actions to be taken in case of particular cases.

2.4 Instantaneous Burn Rate

Instantaneous Burn rate is the slope of the plotted graph that is calculated at each stage which is the ratio of Percentage of Resource Buffer depleted to the percentage of the critical path complete. A ratio of 0.5–1.5 is considered optimum for any project which is being supported by the literature. Any deviation from the optimum burn

rates triggers a warning. Burn rate is a numeric representation of the project status as it is instantaneous value. The above method is applied for the project, which is being used as a case study to give a warning in case of abnormal variations at any stage of the project.

3 Results and Discussions

For the purpose of narrowing down the study to Transmission Line construction projects, a case study was undertaken. It helped to gather in depth information about the existing practices in Resource Allocation, Project Monitoring and Control. Critical resources for the Transmission Line Project were identified and total amount of individual resources necessary for the project are taken from the bill of materials. The quantity of resource buffers considered at the beginning of the project was as follows (Table 1):

The limits for the different zones in the % Resource Buffer Consumption versus the % Critical Chain Complete graphs were also decided after consultation with the project and planning manager.

The actual duration of the project is 365 days as available in the initial schedule. The duration of the project using CCPM Methodology/Cut & Paste Method is found to be 350.5 days as available in the new schedule. The remaining 14.5 days serve as an initial Project Buffer, which serves as a protection to the project from delays.

From Table 2, it is clear that the instantaneous burn rate for the month of November 2016, January and February 2017 are found to be greater than 1.5, which indicate

Table 1 Table showing quantity of buffer considered

Structural steel	11.5 T (4%)
Workmen	5400 h (12%)

Table 2 Instantaneous burn rate calculation for structural steel

Date	Original quantity of buffer	Remaining quantity of buffer	Percentage of resource buffer consumed	Remaining duration of longest chain	Percentage of critical chain complete	Instantaneous burn rate
	Ton	Ton	%	Days	%	
02-09-2016	11.5	11.5	0.0	350.5	0.0	NA
01-10-2016	11.5	10.0	13.0	320.5	8.6	1.5
01-11-2016	11.5	8.5	26.1	289.5	17.4	1.5
01-12-2016	11.5	6.5	43.5	259.5	26.0	2.0
01-01-2017	11.5	5.0	56.5	228.5	34.8	1.5
01-02-2017	11.5	3.2	72.2	197.5	43.7	1.8
01-03-2017	11.5	1.1	90.4	169.5	51.6	2.3
01-04-2017	11.5	0	100.0	138.5	60.5	1.1

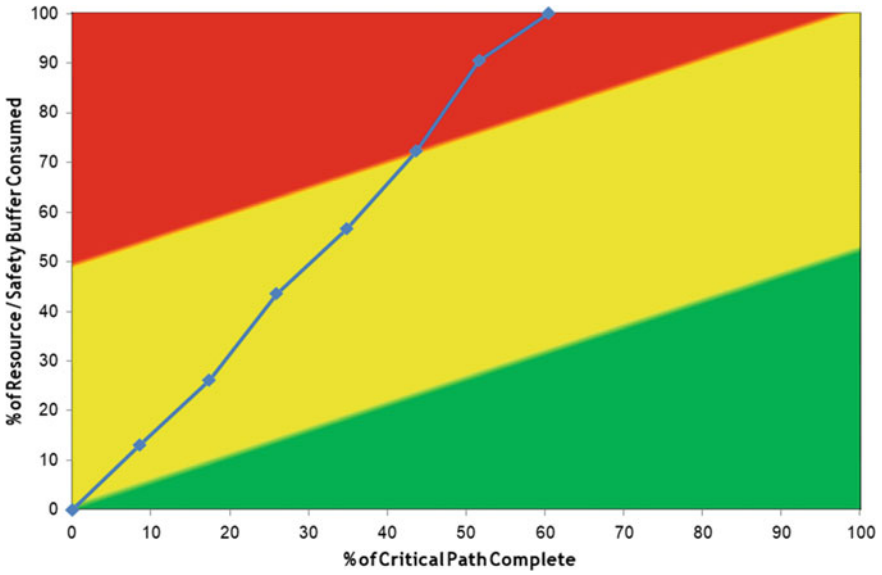

Fig. 3 % Resource buffer consumed versus % critical chain complete for structural steel

that the consumption traits are beyond the optimum. From Fig. 3, it is found that the rate of consumption has exceeded the permissible limit (Yellow Zone) when the critical chain is completed by 45%. From the as-built schedule, it was found that the erection works were incomplete and the buffer was depleted. There had been a delay in supply of structural steel by the supplier (Subsidiary of the Contractor) and hence the buffer quantity was completely exhausted. An alternative source for supply of Structural steel had to be found as a precautionary measure to respond to this threat.

From Table 3, it is found that the instantaneous Burn rate for the month of February 2017 is greater than 1.5, which indicates that the consumption traits are beyond the optimum. From Fig. 4, it is found that the rate of consumption has not exceeded the permissible limit (Yellow Zone) even when the critical chain is the 60% complete. From Table 3, it is found that the critical chain is 60% complete around the first of April 2017. From the as-built schedule, it was found that the erection works were incomplete and 28% of the buffer was remaining. Since the plot is in the yellow zone and the trend doesn't show any erroneous burn rates, not much attention is necessary for this resource.

The case studied does not contain any non-critical activities hence the risks involved in non-critical activities turning into critical activities are absent. The risks or the uncertainties in the non-critical activities can be neglected. The Initial Project Buffer provided in the schedule developed by CCPM Methodology takes into account the uncertainties involved in the execution of critical path activities. Had the project contained non-critical activities, the uncertainties present in such activities would

Table 3 Instantaneous burn rate calculation for workmen

Date	Original quantity of buffer	Remaining quantity of buffer	Percentage of resource buffer consumed	Remaining duration of longest chain	Percentage of critical chain complete	Instantaneous burn rate
	Hours	Hours	%	Days	%	
02-09-2016	5400	5400	0.0	350.5	0.0	NA
01-10-2016	5400	5050	6.5	320.5	8.6	0.8
01-11-2016	5400	4620	14.4	289.5	17.4	0.9
01-12-2016	5400	3950	26.9	259.5	26.0	1.4
01-01-2017	5400	3210	40.6	228.5	34.8	1.5
01-02-2017	5400	2520	53.3	197.5	43.7	1.4
01-03-2017	5400	1803	66.6	169.5	51.6	1.7
01-04-2017	5400	1540	71.5	138.5	60.5	0.6

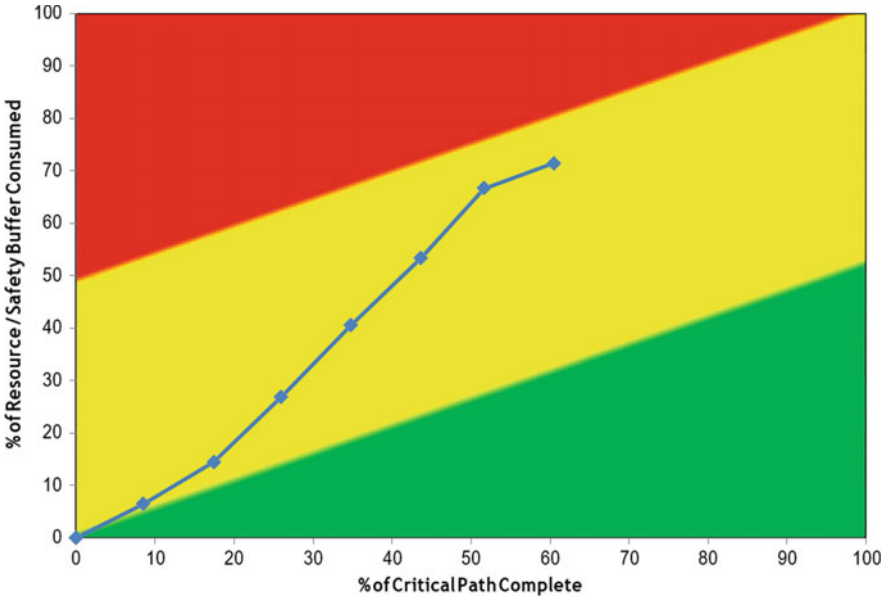

Fig. 4 % Resource buffer consumed versus % critical chain complete for workmen

be taken care of by Feeding Buffers present at intersection of critical path with the non-critical path.

4 Conclusions

The conclusion from this study is that the use of CCPM helps in detecting the problems which can affect project progress. The Cut and Paste method of scheduling ensures that the project duration is protected from delays through the initial Project Buffer & the Feeding Buffers. Also, the delays due to resource constraints are taken care of by resource buffers. Fever charts plotted for the case show the trends in resource buffer consumption and helps in warning the project managers to address in case of unfavourable consumption rates. Using this warning system back-up, plans or alternatives can be generated to cope up with such crisis. Even the progress of the project can be tracked using the fever charts.

References

1. Deming WE (1982) Out of the crisis. MIT
2. Goldratt E (1997) Critical chain. North River Press, Massachusetts
3. Herroelen W, Leus R (2001) On the merits and pitfalls of critical chain scheduling. J Oper Manag 19(5):559–577
4. Leach LP (2005) Lean project management: eight principles for success. Idaho, Advanced Projects, Inc., Boise, Idaho
5. Lechler TG, Ronen B, Stohr EA (2005) Critical chain: a new project management paradigm or old wine in new bottles? Eng Manag J 17(4):45–58
6. Parkinson CN, Osborn RC (1957) Parkinson's law and other studies in administration. Houghton Mifflin, Boston
7. Cohen O, CCPM—The TOC solution for improving the management of single projects and the use of the "U" shape for structuring TOC knowledge and developing TOC logistical applications
8. Masterson P (2005) The Advantages and Disadvantages of Critical Chain Project Management (CCPM) versus Traditional Critical Path (CPM) based project management
9. Sciforma Corporation (2004) Critical chain concepts
10. Simpson III WP, Lynch W (1999) Critical success factors in critical chain project management. In: Proceedings of the 30th annual project management institute 1999 seminars & symposium, Philadelphia
11. Leach LP (2000) Critical chain project management. Library of Congress Cataloging-in-Publication Data. ISBN 1-58053-074-5
12. Dilmaghani F (2008) Critical Chain Project Management (CCPM) at Bosch Security Systems (CCTV) Eindhoven. A Survey to explore improvement opportunities in the scheduling and monitoring of product development projects

Productivity Analysis of Shuttering Works for Sewage Treatment Plant

Abhilash Pandey, Praveen Kumar Chaudhary, and Bibhuti Bhusan Das

Abstract Formwork is considered as important element of construction projects like in traditional reinforced concrete infrastructure projects. It is labor-intensive work that requires highly skilled workers such as carpenters, bar benders, etc., to execute the work more accurately and efficiently. In view of the fact that it is difficult to find high-skilled workers for formwork process and hence it is important to find the ways or methods of formwork construction that is less labor dependent or in other words methods that are highly productive with minimum number of workers. The quality of formwork exerts a direct influence on the surface of concrete and on its dimensions. Since reinforced concrete work is involved in majority of the buildings, the level of workmanship of the construction project can be identified by seeing the quality of formwork. In order to improve the productivity of the formwork process and its quality then it is necessary to improve its working methodology by identifying the bottlenecks using scientific management. And as we very well know that money is always the center of discussion in our construction projects. To complete the project within its expected, designed cost of the project is one of the major requirements of the project to become a successful project. That's why the topic '**Productivity analysis in shuttering for Sewer Treatment Plant Project**' is a great tool to analyze the shortcomings in the present methodology of formwork erection and to mechanize a highly effective model for formwork and this can be achieved by the productivity analysis.

Keywords Formwork · Shuttering · Productivity · Delay · Sewage treatment plant

1 Introduction

Construction of wastewater treatment plant includes the construction of sedimentation tanks, bioreactor tanks, grit chambers, etc. The sewage entering these plants is of the order of million liters per day. Generally for a whole town or suburbs, one

A. Pandey · P. K. Chaudhary · B. B. Das (✉)
Department of Civil Engineering, National Institute of Technology Karnataka, Surathkal, Mangalore, Karnataka, India
e-mail: bibhutibhusan@gmail.com

B. B. Das et al. (eds.), *Recent Trends in Civil Engineering*, Lecture Notes in Civil Engineering 105, https://doi.org/10.1007/978-981-15-8293-6_38

treatment plant is constructed that's why these treatment plants being executed are large in terms of both quantity and cost. Large projects like construction of wastewater treatment plant require proper planning and execution for successful completion of work on time with safety and quality. At the same, various factors affect the productivity of wastewater treatment plant [2, 4, 5, 8, 9]. A successful construction project is one that is completed on time, within budget, meets specified standards of quality, and strictly conforms to safety policies and precautions [10]. Wastewater treatment plant construction requires highly repetitive work sequence throughout the construction areas [11]. The work sequence consists of a series of operations on the critical path, any type of delays on those operations may cause delays of the project delivery. The first step in improving construction productivity is to identify the influencing factors [13–20]. After productivity factors are identified management can take actions to mitigate these issues. We also have to consider the fact that major productivity factors vary from country to country, place to place and project to project.

Productivity is nothing but the efficiency of the process. In simple terms, it can be defined as the ratio of output and input. With respect to construction industry, it can be specifically defined as measure of the end product per unit input of resources (labor and capital) [21]. As we very well know that a firm's success depends on how efficiently it uses its resources, nowadays, it is becoming very important aspect in any project and different firms are investing these days to make there processes more effective. The main idea to implement the productivity is to develop a cost-effective process, which helps us in completion of the project in the prespecified time with the prespecified budget.

Formwork is one of the important aspects in the construction world, which focuses on the traditional reinforced concrete work. Erecting a formwork for any construction is a highly tedious and resource and time consuming [7]. A major chunk of the project cost is being spent on the formwork erection and its assembling. Moreover, it requires skilled formwork carpenters whose availability in the need of hour is always questioned. Formwork is becoming a serious point of discussion in the planning rooms. That is why it is becoming increasingly necessary to devote some time and resources in improving the efficiency of the formworks and shuttering, and in order to do so we need to improve our work processes and work methods and also should use technological advancements to aim for higher productivity.

The significance of productivity is very large in any industry, as described earlier to derive a cost-effective process, which utilizes the minimum of resources and gives optimum of output is desired [24]. We can expect a lot of construction of sewage treatment plant in our country in near future. Its construction or any construction for that matter is very costly projects. Even the smallest of treatment plants would easily cost crores of rupees. With such amount of revenue involved a cost effective process is required. Moreover as already discussed the formwork and scaffoldings take a major chunk of project cost and to make this process cost-effective would save us lots of resources which would help our country in the longer run.

In construction, higher productivity means the process flow is free from the bottlenecks, which in turn makes the process productive. Job dissatisfaction can cause high

cost to the project and introduce time delays that will reduce the productivity of the project [1]. Management can influence the productivity is by checking how smooth the work will flow from one activity to another and how many activities can be accomplished. Management can influence the workers by improving their skills and motivate them toward work by giving rewards to complete the milestones within given time period [12].

Now analyzing productivity and making a certain process to follow is relatively easier in manufacturing and production industry. There is a fixed type of good, is manufactured with same level of tolerances and same level of standard deviation, but that is not the case with construction industry. Construction is a labor-dependent industry, and in most countries, labor costs comprise half of the overall cost of the project and moreover no two construction projects can be touted as similar [6]. Every single construction project is different, they have different budgets, different clients, different contractors, etc. The lack of unpredictability is the main problem in the construction industry. Moreover environment is also not same everywhere. In some places, the temperature might be in high 40 s and somewhere it might be freezing cold. In some places, the labor would be easily available and cheap where as in some places the labor is hard to find and costly [22, 23, 25]. The cost of materials also varies from place to place. Keeping all these factors in mind-predicting productivity is very difficult in construction industry. We cannot do the productivity analysis as a whole for all the projects happening in the country or world. The most we can do is to do a region-specific productivity analysis, for example in hotter climates, colder regions, coastal regions, etc. [3].

2 Methodology

This study investigates and analyses different factors affecting productivity in shuttering in a sewage treatment plant project. Collecting data regarding various factors that affects productivity in sewage treatment plant was the first step of this analysis. The respondents are well aware by the process that is used in this analysis. The data were stored in excel sheets and the output was formulated in excel sheets too. The project site from where data were collected was 318 MLD (70 MGD) Wastewater treatment plant, Coronation pillar, New Delhi. The scope of the project was Construction of 318 MLD WWTP, trial run of WWTP, Operation & maintenance of WWTP and Demolition of old WWTP. The deadline to complete the project was 162 months by Delhi Jal Board.

2.1 Method Productivity Delay Model

The method productivity delay model (MPDM), basically, a tool to combine both time study and productivity measurement. It is an algorithm that depends on the

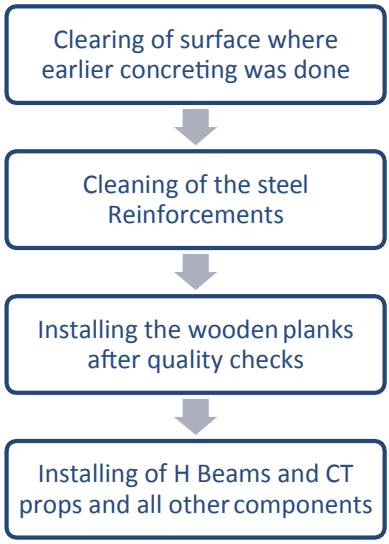

Fig. 1 Flow chart of the process cycle

observer to collect data in a special predefined form and through it a unit cycle is defined. The observer will also note down the type of delay and the visible cause of it. Once the data collection is over, a set of calculations is carried out that determines the productivity of the process and indicates the major factors responsible for delay and gives other important parameters related to productivity.

The cycle that is defined in the above-said model starts with the cleaning of surface where the shuttering is supposed to be done, usually after the installing of steel reinforcement. The wooden planks along with all its components are erected and when the system is ready and when the concrete can be poured in the cycle finishes. The unit of measurement of the cycle is in man-hours, and this unit is defined on the assumption that a labor or worker works 8 h a day. This process cycle is clearly defined in the below-stated flowchart (Fig. 1).

Three structures were observed for data collection in the 'Coronation pillar site', i.e. **Chlorination contact tank**, **Secondary clarifier** and **Primary clarifier**. The data for the first two structures were observed in the month of May–June and the data for the third structure were observed in the month of November.

2.2 Data Collection Sheet

For the collection of data, a data collection sheet was prepared, in which the cycle time for all the process cycles was noted. A process cycle (as discussed above in the flow chart) is measured in man-hours. Since any structure is not constructed at once, but it is made by parts and in stages one after another. That is why we are getting multiple process cycles in the construction of a single structure.

Table 1 Data collection sheet of chlorination contact tank

Data collection sheet							
Date							
Operation: construction of CCT (Chlorine contact tank)							
Production unit: Erection of formwork (per m^2)				Unit of time: Man-Hours			
Cycle process	Cycle time	Environment delay	Equipment delay	Labor delay	Material delay	Management delay	Processing column
	1	2	3	4	5	6	7
1	5.51				x		0.595
2	6.8	x		x			1.885
3	6.93	x	x				2.015
4	5.72	x					0.805
5	4.94						0.025
6	5.82			x			0.905
7	4.89						−0.025
8	6.52	x			x		1.605

The time required from cleaning of the surface to the fastening of final bolt and quality check is noted, which is entered as cycle time. Then the observer is supposed to compare all the cycle times and try to allot the delays in different cycles, he should also note that whether that delay was removable, i.e. was that delay preventable with better management, e.g. Material delay, etc., or not removable like environmental delays. Whatever delay he/she thinks should mark 'x' sign on the data collection sheet. Similar data collection sheets should be filled for different structures simultaneously assigning the delays to the cycles.

Now after the data collection sheet is full, the process is noted where no delay is observed, i.e. no 'x' mark is observed in that process and the cycle time of that process is taken as reference time (man-hours) and in structures where one or more process is there where no 'x' mark then averages of them is taken (Table 1).

2.3 Productivity Analysis

As discussed above that the cycle is defined as the time from which the cleaning of the surface starts till the final bolt is fastened. By using cycle time, the productivity of the Structures such as chlorination contact tank, secondary clarifier and primary clarifier of STP project.

2.3.1 Structure 1: Chlorination Contact Tank

Total cycles observed in this structure are eight and the two cycles in which no delay was observed was cycle number 5 and 7 (Table 2). As stated above if more than one cycle is observed in which no delay is occurred then the average of the two cycles is taken

$$\text{Average cycle time where no delay is observed} = \frac{4.89 + 4.94}{2}$$
$$= 4.915\,\text{man} - \text{hours per m}^2$$

$$\text{Mean Cycle time} = \frac{\text{Total Cycle time}}{\text{Number of cycles}}$$
$$\text{Mean Cycle time} = \frac{47.13}{8} = 5.891\,\text{man} - \text{hours per m}^2$$

After calculating mean cycle time and filling all those columns, we now find out which cause of delay occurs how many time, for example in chlorination tank structure the number of occurrences of environment delay is four and so on. And further the total time in all those delays is calculated and noted in the next row. After that the probability of occurrence is determined by the below stated formula.

$$\text{Probability of occurrence} = (\text{Total } \text{“}x\text{”} \text{ in the delayed row})/(\text{number of cycles})$$

After that relative severity is calculated,

$$\text{Relative severity} = \frac{\text{Total added time}}{(\text{Probability of occurrence}) \times (\text{mean cycle time for overall cycles})}$$

Table 2 Effective cycle time of chlorination contact tank

Cycle No.	Total shuttering area achieved (m^2)	Total time taken (man-hours)	Number of labors used	Total time (in terms of man-hours) per unit m^2 of shuttering
1	11.61	64	8	5.51
2	7.05	48	6	6.80
3	8.08	56	7	6.93
4	11.18	64	8	5.72
5	11.33	56	7	4.94
6	8.24	48	6	5.82
7	11.45	56	7	4.89
8	9.81	64	8	6.52

Table 3 Effective cycle time of secondary clarifier

Cycle No.	Total shuttering area achieved (m^2)	Total time taken (man-hours)	Number of labors used	Total time (in terms of man-hours) per unit m^2 of shuttering
1	5.807	64	8	11.02
2	5.32	56	7	10.52
3	5.65	56	7	9.91
4	5.51	56	7	10.15
5	6.412	64	8	9.98
6	5.56	56	7	9.89
7	5.44	56	7	10.29

After calculating the probability of occurrence and total added man hours we calculate expected percentage of delay time.

After calculating the relative severity we find out expected percentage of delay time Expected % of delay time = (Probability of occurrence) × (relative severity) × 100

Total expected percentage of delay time is find out by adding the expected percentages of all the delays. Total expected percentage of delay time = Σ Expected % of delay time of all delays = 28.25%.

2.3.2 Structure 2: Secondary Clarifier

All the calculations are done similarly as calculated in the structure 1 (Table 3),

$$\text{Average cycle time where no delay is observed} = \frac{9.89 + 9.91}{2} = 9.9 \text{ man-hours per m}^2$$

$$\text{Mean Cycle time} = \frac{\text{Total Cycle time}}{\text{Number of cycles}} = \frac{47.13}{8} = 5.89 \text{ man-hours per m}^2$$

$$\text{Total expected percentage of delay time} = \Sigma \text{Expected \% of delay time of all delays} = 6.304\%$$

2.3.3 Structure 3: Primary Clarifier

See Table 4.

Table 4 Effective cycle time of secondary clarifier

Cycle No.	Total shuttering area achieved (m^2)	Total time taken (man-hours)	Number of labors used	Total time (in terms of man-hours) per unit m^2 of shuttering
1	6.52	64	8	9.81
2	5.74	56	7	9.75
3	6.33	56	7	8.84
4	6.30	64	8	10.15
5	5.86	56	7	9.55
6	5.55	48	6	8.64
7	6.91	64	8	9.25

$$\text{Average cycle time where no delay is observed} = \frac{8.64 + 8.84}{2} = 8.74 \text{ man-hours per m}^2$$

$$\text{Mean Cycle time} = \frac{\text{Total Cycle time}}{\text{Number of cycles}} = \frac{65.99}{8} = 9.427 \text{ man-hours per m}^2$$

$$\text{Total expected percentage of delay time} = \Sigma\text{Expected \% of delay time of all delays} = 14.41\%$$

After calculating the expected percentage of delay time we find out the overall productivity and ideal productivity by using the following two formulae,

$$\text{Ideal Productivity} = \frac{1}{\text{mean cycle time for non delayed cycle}}$$

$$\text{Overall method Productivity} = (\text{Ideal productivity}) \times (1 - \Sigma\text{Expected \% of delay time})$$

3 Results and Discussions

The results of the modeling of the productivity are shown in Table 5.

As we can see that ideal productivity is little more than the overall productivity and total productivity achieved would be ideally 100% if there were no delays in the site.

Table 5 Productivity results

Structure	→ Productivity	Ideal productivity (m^2/man-hour)	Overall method productivity (m^2/man-hour)	Total productivity achieved in percentage (%)
Chlorination contact tank		0.2034	0.1459	71.73
Secondary clarifier		0.1010	0.0946	93.66
Primary clarifier		0.1144	0.0979	85.57

Table 6 Types of delay

Types of delay	Chlorination contact tank	Secondary clarifier	Primary clarifier
Environment delay	4	1	3
Equipment delay	1	2	3
Labor delay	2	2	1
Material delay	2	3	2
Management delay	0	0	0

We can also observe that the productivity of secondary clarifier is slightly more than the other two structures, one reason that can be given is that the data collection of secondary clarifier was done in the month of November and the data collection of the other two structures were collected in the months of May–June and we all know that the temperature in New Delhi remains in high 40 s and that is why is very unsuitable for working for labors but this problem was not observed in November as the temperatures are relatively cooler, thus making it easier to work.

The number of delays observed during the erection can be summarized below in the tabular form (Table 6).

Based on the above result, we can clearly conclude that the most major factor that influenced the productivity in the site conditions is environmental factor. One another factor that is majorly influencing the productivity outcome is equipment delay. As observed by me in the site during internship and also through the above study, there were lots of shortages of equipment's in the site area. Majority of the equipment's were not there on time and the ones which were present there were not working properly so this aspect when improved will definitely improve the productivity.

4 Conclusion

Construction industry is rated as one of the primary industries. The growth of the developing countries is dependent on its construction industries with this regard construction productivity plays a major role because they can cause delay in the

growth of economics of the country. During the execution of the construction project, the knowledge about construction productivity can yield substantial saving in time and money. This research work is designed to identify the causes that affect productivity of formwork in sewage treatment plants.

This research showing the factors affecting the productivity of formwork in sewage treatment plant. This research highlighted the problem of productivity loss resulting from various factors incorporated in the typical construction site. The model provides casual logic to why delay occurs during the erection of formwork in the execution phase of the construction site. The model accounts for a realistic behavior of the productivity being dependent on the various factors.

Most of the delays encountered were due to environmental issues and the unavailability of the equipments. The major conclusion derived was that during planning phase what will be the environmental condition should be the area of focus. The planning should be done according to that only.

A proper inventory management system should be implied such that the equipment and material delays can be avoided. Proper management of these factors discussed above can improve the productivity output substantially.

References

1. AbouRizk S, Knowles P, Hermann UR (2001) Estimating labor productivity rates for industrial construction activities. J Constr Eng Manag 127(6):502–511
2. Aftab HM, Ismail AR (2011) Identifying construction resource factors affecting construction cost. Malaysian Technical Universities international conference on engineering & technology
3. Alaghbari W, Kadir MRA et al (2007) The significant factors causing delay of building construction projects in Malaysia. Eng Constr Archit Manag 14(2):192–206
4. Attar AA, Gupta AK, Desai DB (2012) A study of various factors affecting labour productivity and methods to improve it. IOSR J Mech Civ Eng (IOSR-JMCE), 11–14. ISSN: 2278-1684
5. El-Rayes K, Moselhi O (2001) Impact of rainfall on the productivity of highway construction. J Constr Eng Manag ASCE
6. Harrmon KM, Cole B (2006) Loss of productivity studies—current uses and misuses. Constr Briefings 8(1):1–19
7. Randolph Thomas H, Sanvido VE (2000) Role of the fabricator in labour productivity. J Constr Eng Manag 6(5)
8. Park H-S (2006) Conceptual framework of construction productivity estimation. KSCE J Civ Eng 10(5):311–317
9. Park H-S, Thomas SR et al (2005) Benchmarking of construction productivity. J Constr Eng Manag 131(7)
10. Kazaz A, Ulubeyli S (2007) Drivers of productivity among construction workers. A study in developing Country. Build Environ 42(5):2132–2140
11. El-Gohary KM et al (2013) Factors influencing construction labor productivity in Egypt. J ManagEng
12. Kumar A, Dijkman D, Song M (2013) Optimal resource assignment in workflows for maximizing cooperation. Business process management. Lecture Notes in Computer Science, vol 8094, pp 235–250
13. Lee D (2005) Probability of project completion using stochastic project scheduling simulation. J Constr Eng Manag 131(3):310–318

14. Song L, AbouRizk SM (2008) Measuring and modeling labor productivity using historical data. J Constr Eng Manag 134(10)
15. Loeraa I, Espinosab G et al (2013) Productivity in construction and industrial maintenance. In: Manufacturing engineering society international conference, MESIC, pp 947–955
16. Dissanayake M, Fayek AR et al (2005) A hybrid neural network for predicting construction labour productivity. In: International conference on computing in civil engineering
17. Meepol S, Ogunlana SO (2006) Factors affecting cost and time performance on highway construction projects: evidence from Thailand. J Finan Manag Property Constr
18. Ngowtanasuwan G (2013) Mathematical model for optimization of construction contracting in housing development project. Procedia Soc Behav Sci 105:94–105
19. Vijay Antony RB, Kothai PS (2014) Improving the labour productivity through other resources in construction field. Int J Eng Res Gen Sci 2(2):205–213
20. Shashank K, Hazra S et al (2014) Analysis of key factors affecting the variation of labour productivity in construction projects. Int J Emerg Technol Adv Eng 4(5):152–160
21. Talhouni BT (1990) Measurement and analysis of construction labour productivity. Ph.D Thesis, Dept. of Civil Engineering, Univ. of Dundee, Dundee, UK
22. Zayed TM, Halpin DW (2004) Simulation as a tool for pile productivity assessment. J Constr Eng Manag 130(3)
23. Yi W, Chan APC (2013) Critical review of labour productivity research in construction journals. J Manag Eng
24. Xue X, Shen Q, Wang Y, Lu J (2008) Measuring the productivity of the construction industry in China by using DEA-based Malmquist productivity indices. J Constr Eng Manag-ASCE 134(1):64–71
25. Zhou J, Wang X (2013) Review of methods for optimizing construction scheduling. J Oper Res Soc 64(8):1091–1105

Pre-Engineered Building Design of Gas-Insulated Substation Housed Under Pressurized Ventilation

N. Roopesh, K. A. Swamy, and Bibhuti Bhusan Das

Abstract Building construction in India is carried out using conventional materials like concrete but it has limitation of span and size of components. As a result, large span areas that are essentially required for housing Electrical Extra High Voltage Gas Insulated Switchgears could not be covered by simple frames and required complex frame arrangements thereby increasing the required completion time. For design, steel has been the preferred material because of its ductile, strength, flexible, recyclability nature and low cost. With technology transfers, entrepreneurs had established steel centres where entire design to production is carried under one roof and the product is erected at site. These factories had given advantage of fabricating components either ahead or parallel to the civil works at site, thus saving time. Introducing the concept of Pre-Engineered building (PEB) into structural design resulted in design optimization and many advantages, including economy and easier fabrication when compared with the Conventional Steel building (CSB). PEB construction is widely gaining popularity over regular conventional buildings in India due to its sheer advantage in time saving. However, there is a challenge of proper and optimized design suiting to the Electrical Substation requirements such as pressurized atmospheric environment, Maintenance walkways, entry of electrical Bus ducts at various levels and locations. Any overlooking of the above may lead to overall failure of the electrical system. This would make it unique from the normal conventional PEB buildings done for Ware houses, Factories, etc.

Keywords Pre-engineered building · Conventional steel building · Gas insulated sub-station · Load

N. Roopesh · K. A. Swamy · B. B. Das (✉)
Department of Civil Engineering, N.I.T.K, Surathkal 575 025, India
e-mail: bibhutibhusan@gmail.com

B. B. Das et al. (eds.), *Recent Trends in Civil Engineering*, Lecture Notes in Civil Engineering 105, https://doi.org/10.1007/978-981-15-8293-6_39

1 Introduction

In almost every part of the world steel industry is growing rapidly. With more emphasis on global warming, steel which is eco-friendly is being preferred. Strength to weight ratio is considerably superior in steel structures compared with RCC. They can also be dismantled without much effort and are also economical considering cost and time of construction [1, 2]. Since time is a valuable asset, steel structures (Pre-fabricated) are constructed in a very short time and one such instance is Pre-Engineered Building (PEB).

Pre-Engineered Buildings (PEB) after design are completely manufactured in plant and later shipped/transported to site in CKD (completely knocked down) condition. All parts are assembled and then erected with nut-bolts at the site, thus decreasing the completion time. In PEB, frame geometry is matched with the bending moment shape (internal stress diagram) thereby optimizing the structure's material use and complete weight [3]. While they give advantage of quality control, architectural versatility, large spans, lowered cost and time, few areas of concerns exist like low thermal resistivity, fire resistance, availability of skilled labour, transportation costs, etc. The main objective is to design tapered sections for Gas Insulated Sub-Station (GIS) structure by considering interlinked activities with GIS equipment like bracing position, column spacing and crane system and compare the reduction in weight of the structure in reference to conventional steel building (CSB).

2 Methodology

Allowable stress design (ASD) as per the American Institute of Steel Construction or the IS 800: [4] is used for design purpose. To attain an acceptable design, the program is operated through the specified maximum number of cycles. Stiffness matrix method is used to calculate forces and displacements [5]. Carry over factors, fixed end moments, and stiffness are computed by strain energy method.

2.1 Technical Parameters of PEB

The basic parameters that can define a PEB are:

2.1.1 Width or Span of Building

Span can be measured as the width between two columns. The span length varies for different buildings. The design is done based on span length specified by customer.

The basic span length starts from around 10–150 meters or above with intermediate columns.

2.1.2 Length of Building

The total length ranging from one front end to the building's rear end is taken as the length of PEB. The same can be extended in future.

2.1.3 Building Height

Distance to eave struts outer point from the bottom of base plate of the main frame columns. It is the distance from the finished floor level to the top of eave strut when columns are recessed or elevated from the finished floor.

2.1.4 Roof Slope

Roof slope is the angle of the building's roof with respect to the horizontal. In tropical countries like India, the most common roof slopes are 1/10 and 1/20. In snow fall regions, roof slope can range from 1/30 to 1/60. Any practical roof slope is possible as required by customer.

2.1.5 Bay Spacing

Bay spacing can be defined as the distance between the two consecutive frames of a structure. Bay spacing of 7.5–8.0 m is considered most economical. However, bay spacing up to 10 m is possible.

2.2 Design Process

1. Calculating loads acting on structure.
2. Modelling the structure in STAAD pro V8i
3. Assuming the sections initially
4. Applying the loads on the structure at respective points
5. Define the required commands from the code and assigning to the structure
6. Run the analysis and based on output repeating the iterations till we get optimized sections satisfying limit state of collapse and serviceability criteria (Fig. 1).

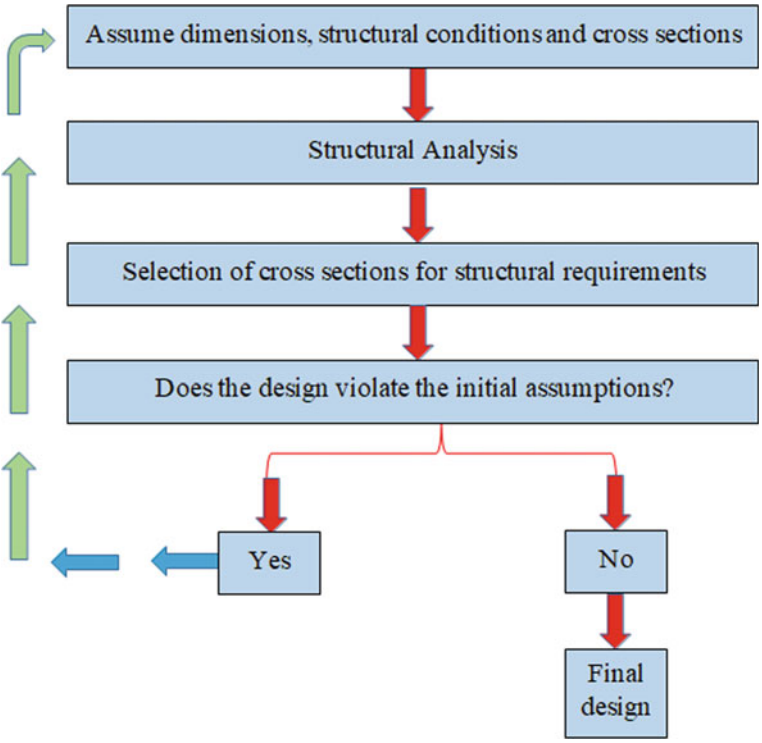

Fig. 1 Design methodology

Nature of the loads acting on a structure differs based on the location, materials, and the architectural design of the structure, which makes it a complex problem. For the same structure, loading conditions can vary (Table 1).

In STAAD Pro, as per code, utilization ratio is considered as the critical value that specifies the suitability of the structural member.

- Value >1.0 indicates the degree to which the element is over stressed,
- Value <1.0 indicates the elements available reserve capacity.

Table 1 Load considered

Type of Load	Reference
Dead load	IS: 875 (Part 1)—[6]
Live load	IS: 875 (Part 2)—[7]
Wind load	IS: 875 (Part 3)—[8]
Seismic load	IS: 1893–2002 (Part 1) & IS: 1893–2005 (Part 4).

Axial tension and bending, slenderness limits, Maximum w/t ratios and shear, Axial Compression and Bending, are used as conditions to determine Pass/Fail status of the member.

2.3 Load Combinations

As per IS 875 (Part 5), load combinations are to be considered.

3 Case Study: Design of 765 KV GIS Sub-station in Nizamabad

The design under discussion is a 114.28 meters length sub-station. The loads are calculated similar to a regular frame. Generally, in PEB, slopes are minor (around 1in 10). Hence the critical conditions governing the design would be (DL + WL) or (DL + LL). The support conditions are given as partial fixed supports and moment releases are selected at certain nodes. Project details are given as below (Table 2).

3.1 Description of the Structure and Geometry

- Structure shall be an enclosed type structure housing the 765 kV GIS building with length of 114.28 meters, height of 16.458 meters and 25.16 meters width.
- Basically structure is pitch slope with 1:10 slope.

Table 2 Project details

Scope	Loads & Load Combinations adopted for design of main structure (sub-station).
Units of measurement	The International System of units (SI)
Codes, standards and references	a)IS: 800-2007—Limit state design for the design of members. b)IS: 800-2007—for Serviceability Criteria. (For Rafters = Span/180; Crane Beams = span/750) c)IS: 1893–2002 (Part-1) d)IS: 875–[6] (Part-1) e)IS: 875–[7] (Part-2) f)IS: 875–[8] (Part-3)
Material properties	Grade of steel (fy): 345 N/mm2 Grade of steel (fy): 250 N/mm2
Plant site information	Basic wind speed: 44.00 m/s Seismic zone: Zone II

- The building is closed on all four sides, frame type is with steel rafters, columns and crane girder and walkway beams. Rafters are in moment connections with columns at top.
- Bracings are provided in the longitudinal direction.

3.2 Structural System Configuration

- The structural system comprises of braced frame in the longitudinal direction and moment resistant frames in the transverse direction.
- The lateral stability in the structure is through moment resistant frame in transverse direction.
- Providing cross bracings at selected bays accounts to the longitudinal stability of the building.

3.3 Load Calculations

DL on roof	= 0.20 kN/sqm (for inaccessible roof)	
Tributary Length	= 7.3 m	
D.L per m on roof	= 0.20 kN/sqm * 7.3 m	= 1.46 kN/m
DL per m LCR	= 0.50 kN/sqm * 7.3 m	= 3.65 kN/m
DL on walkway beam	= 1.54 kN/sqm * 1.1 m	= 0.847 kN/m

3.3.1 Dead Load

Dead load (DL) considerations are as per the IS: 875 (part 1).

Super Imposed Dead Load:

DL on roof	= 0.20 kN/sqm (for inaccessible roof)	
Tributary Length	= 7.3 m	
D.L per m on roof	= 0.20 kN/sqm * 7.3 m	= 1.46 kN/m
DL per m LCR	= 0.50 kN/sqm * 7.3 m	= 3.65 kN/m
DL on walkway beam	= 1.54 kN/sqm * 1.1 m	= 0.847 kN/m

This dead load on walkway beam is applied as point load = 0.847 * 7.3 = 6.2 kN.

Self-Weight: Individual Structural element weights are considered directly in the STAAD as self-weight.

3.3.2 Live Load

Live load is considered as per IS: 875 (Part-2) and as per code the live load of a non-accessible roof will be 75 kg/sqm, i.e. 0.75kN/sqm. Live load (as per IS 875 pt.3) = 0.75 kN/sqm*7.1 m (Table 2, in-accessible roof and roof angle of 2.86 deg).

3.3.3 Collateral Load

Additional load due to Services = 0.150 kN/sqm (as per IS 800: [4].

3.3.4 Wind Load

The wind load on structure shall be calculated for individual structural, cladding (including glazing and fittings) elements and also building as a whole. Wind pressure calculation is done as per IS: 875 (part-3). Once we arrive at the wind pressure then pressure coefficients of roof and wall are taken from Table 4 and Table 5 of IS 875 (part 3).

Calculation of wind pressure:

Basic Wind Speed (Vb) is taken from Fig. 1 of IS 875 (part 3). It gives basic wind speed map of India which has computed for a return period of 50 years.

Basic wind speed	(Vb) = 44.000 m/s	(Nizamabad zone)
Risk coefficient	(K1) = 1.070	(As per table-1 for life of 50 years, clause 5.3.1 of IS 875 Part III)
Probability factor	(K2) = 0.980	(As per clause 5.3.2.2 of IS: 875 Part III)
Topography factor	(K3) = 1.000	(As per clause 5.3.3.1 of IS 875 Part III)
Design Wind Pressure	(Pz) = Vb x K1 x K2 x K3 = 44.00 × 1.070 × 0.980 × 1.00 = 1.277 kN/sqm	

From IS: 875(Part 3)-[6]: Table 7, overall Pressure coefficients for pitched roof are considered. The percentage of openings is between 0–5% (as per clause 6.2.3.2 of IS- 875 part3).

Roof angle (1 in 10)	= 5.710 degrees	
Internal pressure coefficient	= ± 0.200	
Length of the building (L)	= 114.28 m	
Width of the building (W)	= 25.16 m	
Height of the building (H)	=16.458 m	

From the dimensions of the structure it is observed as given below:

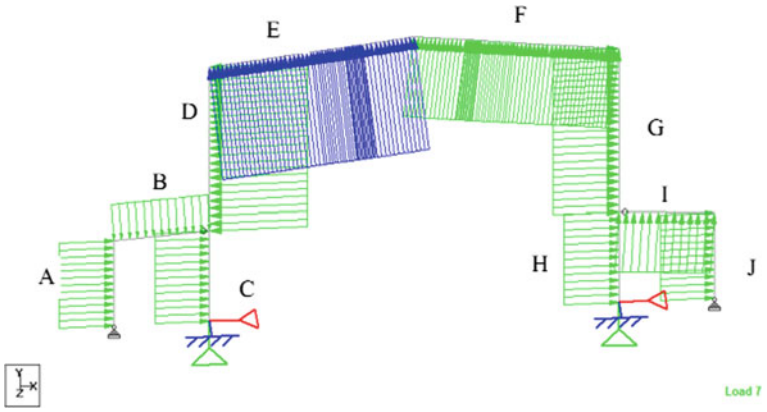

Fig. 2 Wind load (pressure left to right)

- Building Height Ratio (H/W) = 0.66 i.e. 0.5 < (H/W) <1.5
- Building Plan ratio (L/W) = 4.5 i.e. 3/2 < (L/W) <4

Wind Load is calculated by (F) = (Cpe-Cpi)*A* Pz (As per IS 875 (Part 3))
Where,

A = Area on which wind is acting
Pz = design wind pressure
Cpe = External pressure co-efficient (from Table 4 of IS: 875 Part-3)
Cpi = Internal pressure Co-efficient

Generally we consider two values of Cpi. One represents pressure and other represents suction. Pressure indicates force is acting towards the structure while suction indicates force acting away from the structure. Pressure is taken as positive value of Cpi and suction is negative value of Cpi.

Wind Load (Pressure—Left to Right)

As per IS: 875 (Part 3)—2007 Table 4(clause 6.2.2.1), Table 5(Clause 6.2.2.2), Table 28(Clause 6.2.2.10) Cpe values are taken and wind load is calculated as shown below:

For Pressure (Cpi) of +0.20

$$\begin{aligned}\text{Wind Load} &= (\text{Cpe} - \text{Cpi}) * \text{A} * \text{Pz} \\ &= (+0.70 - (+0.20)) * 7.3 * 1.277 = 4.66\,\text{KN/m}\end{aligned}$$

Similarly, forces are calculated and tabulated as shown below (Figs. 2, 3 and Tables 3, 4):

Similarly, values are to be calculated and tabulated for various cases.

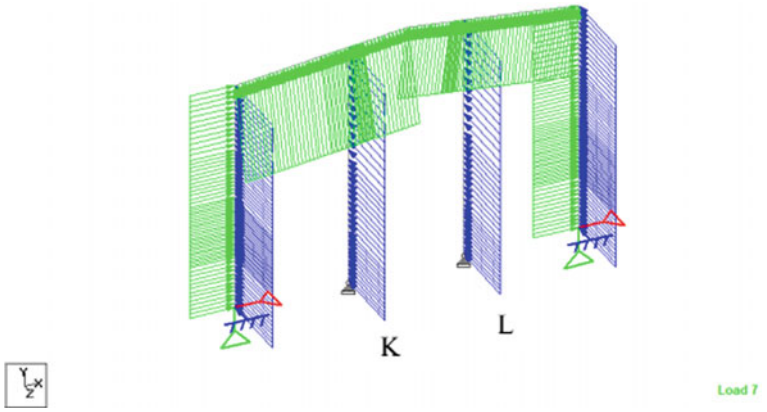

Fig. 3 Wind ward columns (pressure left to right)

Table 3 Wind load, (pressure left to right)

Face	Cpe	Cpi	Cpe-Cpi	(Cpe-Cpi)*A*Pz	Force (KN/m)
A	+0.70	+0.20	+0.50	(+0.50)*7.3*1.277	4.66
B	+0.56	+0.20	+0.36	(+0.36)*7.3*1.277	3.36
C	+0.70	+0.20	+0.50	(+0.50)*7.3*1.277	4.66
D	-0.70	+0.20	−0.90	(−0.90)*7.3*1.277	8.39
E	-0.94	+0.20	−1.14	(−1.14)*7.3*1.277	10.63
F	-0.60	+0.20	−0.80	(−0.80)*7.3*1.277	7.46
G	-0.40	+0.20	−0.60	(−0.60)*7.3*1.277	5.59
H	-0.30	+0.20	−0.50	(−0.50)*7.3*1.277	4.66
I	−0.40	+0.20	−0.60	(-0.60)*7.3*1.277	5.59
J	−0.30	+0.20	−0.50	(-0.50)*7.3*1.277	4.66

Table 4 Wind ward columns, (pressure left to right)

Face	Cpe	Cpi	Cpe-Cpi	(Cpe-Cpi)*A*Pz	Net Force
K	−0.60	+0.2	−0.8	(−0.80)*7.91*1.27	8.09
L	−0.60	+0.20	−0.80	(−0.80)*7.91*1.27	8.09

3.3.5 Earthquake Load Calculations

Seismic Zone of structure	= II	(From Fig. 10.1)
Zone Factor	= 0.10	(Table 2, clause 6.4.2)
Response reduction factor	= 4.00	(Table 7, clause 6.4.2)

(continued)

(continued)

Seismic Zone of structure	= II	(From Fig. 10.1)
Importance factor	= 1.50	(Table 6, clause 6.4.2)
Rock and soil site factor (SS)	= 2	(Figure 2.0, IS 1893(part-1)
Type of structure (ST)	= 2	
Damping ratio	= 0.02	(Table 3, clause 6.4.2)

3.3.6 Crane Load

Client crane data-Critical support reactions:

Maximum vertical reaction RVx	= 170.4 kN
Reaction on other side RVn	= 61.0 kN
Horizontal reaction RH	= 9.6 kN
Longitudinal surge	= 10% of Wheel loads = 1 * 114.66 kn * 0.10 * 2 wheels = 22.932 kN

3.3.7 Load Combinations

All the possible load combinations as per IS 800: [4] are auto generated in STAAD Pro and the same are applied on the structure during design. The software checks for both Limit State of Serviceability and Collapse.

3.3.8 Parameters

Necessary parameters are defined before performing the analysis as mentioned below:

- Code: Here IS 800: [4] is assigned to the structure.
- Lx is the length used for computing slenderness ratio for buckling about local X-axis. Similarly Ly in local Y-axis and Lz in local Z-axis. The program considers the respective member lengths as default values for Lx, Ly and Lz.
- Effective length factor in Y and Z direction are Ky and Kz respectively.

4 Results

The obtained results are tabulated and shown below (Table 5).

Table 5 Results from analysis in STAAD Pro

Description	Conventional I-section		Tapered I-section	
	Rafter	Column	Rafter	Column
Max. shear force (in KN)	149.56	93.147	149.20	81.45
Max. Bending moment (in KN-m)	236.121	570.162	277.61	544.499
Max. deflection (in mm)	91.139	14.55	114.595	20.110
Weight of the structure (in KN)	1311641		1213609	

5 Conclusion

Comparative analysis of the structure based on conventional I sections and tapered I sections with special reference to the case study, the following inferences can be drawn:

- Maximum shear force of rafter and column comes out to be 149.56 KN & 93.147 KN for I section, whereas in tapered section, it was found to be 149.20 KN &81.45 KN.
- Maximum bending moment of rafter and column comes out to be 236.121 KN-m & 570.162 KN-m for I section, whereas in tapered section, it was found to be 277.16 KN-m & 544.499 KN-m.
- It is seen that conventional sections are being heavier when compared to the tapered I sections. The difference in the weight of the structure was approximately 8% (Fig. 4).

The utilization of the sections in tapered case was much better than compared with conventional I sections. As the weight and quantity of the steel used in tapered I sections are reduced hence in-turn it helps in cost reduction and time saving. Also using tapered sections leads to reduction in the dead load of structure thereby reducing the size of foundation.

Fig. 4 Weight comparison

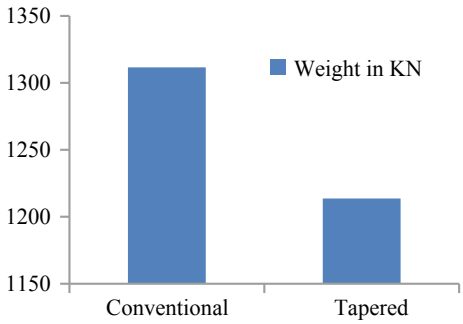

References

1. Jatin DT, Patel PG (2013) Comparative study of pre engineered steel structure by varying width of structure. Int J Adv Eng Technology 4(3):56–62
2. Sai KG, Kailasa RA, Pradeep Kumar R (2014) Comparison of design procedures for pre engineering buildings (PEB): a case study. Int J Civ Architect Struct Construct Eng 8(4):480–484
3. Jayavelmurugan J, Thirumal JR, Padmanabhan H (2015) A study on pre engineered steel building structures. Int J Innov Res Sci Eng Techno1 4(1)
4. IS 800 (2007) Bureau of Indian standards , New Delhi. "Indian standard—general construction in steel—code of practice, IS 800: 2007"
5. Bhavikatti SS (2010) Design of steel structures by limit state method as per IS 800–2007. I.K.International publishing house Pvt. Ltd., New Delhi
6. IS 875 (Part 1) (1987) Bureau of Indian standards, New Delhi. "Indian standard—code of practice for deign loads (other than earthquake) for building and structures: Part 1—Dead loads, IS 875 (Part 1): 1987"
7. IS 875 (Part 2) (1987) Bureau of Indian standards, New Delhi. "Indian standard—code of practice for deign loads (other than earthquake) for building and structures: Part 2—Live loads, IS 875 (Part 2): 1987"
8. IS 875 (Part 3) (1987) Bureau of Indian standards New Delhi. "Indian standard——code of practice for deign loads (other than earthquake) for building and structures: Part 3—Wind loads, IS 875 (Part 3): 1987"

Developing a Standard Template for Activity Linkage and Resource Estimation of MEP Works

Sushant Shekhar, Prince Shukla, and Bibhuti Bhusan Das

Abstract Project planning is the most essential part of project management. It plays a vital role in effective completion of a project. A well-developed project plan and schedule are very helpful in managing project costs more efficiently and can preclude time overruns. Mechanical, Electrical and Plumbing (MEP) works being one of the key parts of construction project also require detailed and specific attention in terms of planning. Planning of these works in terms of activity linkage and resource identification is not properly emphasized leading to loop holes in their execution which further is responsible for cost and time overruns. The current study helps in understanding various activities involved in MEP works, how they are related to each other, what are the civil constraints that affect these activities, how their concurrent occurrence can lead to development of complexity which forces one to properly identify and estimate the resources required for their smooth execution. Productivity Rate Method is one of the estimating tools that is used and compared to the actual resource requirement. A template is developed, conceptually based on the activity linkage, which can be directly implemented in a project with similar services. In addition, this template contains the resources required for execution of enlisted activities. Hence, it can be used as a technical tool for efficient planning of MEP works, which further leads to successful accomplishment of project's goals and objectives.

Keywords Planning · MEP · Productivity rate method

1 Introduction

Construction project generally comprises of civil and MEP works. MEP is the acronym of Mechanical, Electrical and Plumbing works which generally carried out at any construction site. Projects nowadays consist of much more than the old traditional electrical, mechanical and plumbing systems, this can be attributed to

S. Shekhar · P. Shukla · B. B. Das (✉)
Department of Civil Engineering, National Institute of Technology Karnataka, Surathkal, Mangalore, India
e-mail: bibhutibhusan@gmail.com

B. B. Das et al. (eds.), *Recent Trends in Civil Engineering*, Lecture Notes in Civil Engineering 105, https://doi.org/10.1007/978-981-15-8293-6_40

the increase in the complex functions and systems used. Additional systems such as CCTV (Closed-circuit television) surveillance system, PAS (Public address system), FPS (Fire protection system), FAS (Fire alarm system), BMS (Building management system), controls, telephone/Datacom system, etc., have now been included in the scope of MEP Works. Therefore during the initial planning of a project, these MEP works are also put into schedule and need to be planned perfectly for successful completion of project [1–3]. The current study provides a wide range of MEP activities and resources required for those activities which could be taken and implemented in any project planning.

1.1 Construction Planning

Management of construction projects is not possible without proper Construction Planning as it has become central and challenging aspect of Modern Construction Management. It involves the use of technology such as which software to be used, the description and definition of work packages up to the lowest level, the identification and documentation of various resources required and durations for individual activities, and the assigning proper relationships and interactions between the work packages and activities [4–8]. An efficient construction scheme is the foundation for developing the accurate budget and schedule for work. In addition to the technical aspects, organizational judgements and important decisions regarding the project are also part of construction planning. For example, the degree of involvement of different shareholders in the project like subcontractors is decided in the construction planning stage.

Identification and listing of activities, and their further consequences on the succeeding activities are the most important part of Planning. Next step involves decision regarding choosing the most efficient process between two alternate processes to achieve the same result. Scheduling in Construction planning is the most important and is most often done over time. Scheduling ensures proper precedence in the activity order is kept and the resources enlisted are assigned appropriately and used efficiently.

1.2 Scheduling

A schedule is an effort to model activities, their durations and their relations with other activities. These activities take time to complete and use resources such as people, materials, equipment and money that have restricted availability. Actual total program planning cannot be completed unless all of the necessary facts become available at project commencement. Project is broken down into activities that are then input into the software under the Work Breakdown Structure (WBS). Activity duration, predecessor and successor are then assigned to various activities. Estimation of start

and end dates of each activity is then carried out manually or by the software. Roles and resources for activities and the planned project resource budget and costs are then determined [9–12].

As we attain the activity level of a work package, the next task to do is make an activity list. The activity list provides a comprehensive list of tasks to be completed in order to achieve project completion, including the activities to be completed to deliver individual work packages. Next is defining the activity elements, where the description of the activity is done. The attributes of an activity includes all the respective relationships and constraints with the activity and also includes information regarding resources and duration required. Activity sequencing is governed by several factors. They include code regulations, physical relationship among building elements, trade interaction and path interference. By keeping those factors in mind, one can assign predecessor and successor to an activity.

To perform all the activities planned resources are needed, resources include people, equipment, machinery, money or anything else that are needed to complete the project. Resources could be estimated using experts' opinion with ample experience in this sort of work. Otherwise, we have other tools like by using published estimating data or alternative analysis or by using some project management software.

1.3 Resource Estimation

Resources include people, equipment, land, money, or any other material that is required to complete the activities that are planned. Resources must be assigned to each activity in the activity list. Before assigning resources to the project, their availability must be checked.

From the management perception, the important decision in estimating resource requirements is to choose the technology and equipment to be employed and the number of crews to be allocated to each task. For example, assigning more number of crew for a particular task will result in earlier completion. However, additional crews can result in crowding and coordination problems, which would affect the work productivity and it might decline. Further, important point to note is that only completion of activities on the critical path will result in earlier completion of the entire project and not any particular activity.

The types and quantities of resources needed for every activity in a work package are identified through the output of the Estimate Activity Resources process. The estimate for resource required for each work package is then calculated by aggregating the quantities for each activity in the work package. A basic estimate for each resource and activity must be documented at the start. The assumptions that are made in determining resource categories that are applied and their availability must also be mentioned (Table 1).

Table 1 List of abbreviations used

S. No.	Description	Abbreviation
1	Mechanical, electrical and plumbing	MEP
2	Heating, ventilation, and air conditioning	HVAC
3	Extra low voltage system	ELV
4	Public address system	PAS
5	Fire protection system	FPS
6	Fire alarm system	FAS
7	Building management system	BMS
8	Closed-circuit television	CCTV
9	Volatile organic compounds	VOC
10	Diesel generator	DG
11	Automatic transfer switch	ATS
12	Access control system	ACS
13	Galvanized iron	GI
14	Main distribution board	MDB
15	Sub distribution board	SDB
16	Air handling unit	AHU
17	Power distribution board	PDB
18	Light distribution board	LDB
19	Essential light distribution board	ELDB

1.4 MEP Works

Mechanical, electrical and plumbing (MEP) work is one of the important components of construction work. Mechanical works basically involve installation of heating, ventilation, air conditioning system and also Fire Protection System. HVAC equipment as the name suggests, is responsible heating and/or cooling for various kinds of buildings like residential, commercial or industrial buildings. The HVAC system provides fresh outdoor air, which helps to dilute pollutants and toxins present indoor such as odours, VOCs emitted from interior furnishings, chemicals, etc. The FPS is responsible to make the building fire resistant and to ease the speedy evacuation of people present in the event of a fire. A fire sprinkler system is an active fire protection measure. It requires a water supply system, with adequate pressure and flow rate to a water distribution piping system, to which fire sprinklers are connected. Electrical services comprising of transformers, compact substations, high tension and low tension panels, cabling, diesel generator sets, automatic transfer switch, UPS systems, static transfer switches, earthing, internal and external electrification. Other systems like fire alarm system, surveillance system, BMS, ACS and PAS also fall

under electrical services. Plumbing services involve the installation of pipes and sanitary ware. Different pipe systems are gravity-driven and pump-driven waste system, and pressure driven water system.

2 Methodology

The study basically involves close monitoring different MEP works performed at site. An activity list has been created by categorizing different MEP works into subparts known as activity. These activities have then been linked based on constraints associated to them and assigned attributes. Each activity has been assigned labour, equipment and material as resources. A method has been proposed for estimating labour or man-hours using productivity rate. The results of the above study have been used as input to create a standard template using Primavera methodology management module.

2.1 Case Study

To track the MEP activities office building, which is in initial construction stage has been chosen. Office building is a G + 8 structure with approximately 39,820 Sqm of built-up area. The project site is the Shell-NTCB project. The scope of the project is development of a state of the art Research & Development (R&D) Centre and an Engineering Centre. Forty acres of land had been acquired in the KIADB Hardware Park near the BIAL airport to house the campus. Different MEP services have been running through the entire building. The MEP works have been divided into three parts—First Fix, Second Fix, and Final or Third Fix.

2.2 Parameters for Template Development

MEP First Fix involves activities before slab casting and on the block work before plastering. Such activities are pipework, conducting, galvanized iron box fixing, and making sleeves for plumbing purpose, drainage works in toilet and kitchen, etc. The plastering is done only after performing these activities.

MEP Second Fix involves such activities, which have to be done before the false ceiling—like wire pulling; support work for pipe laying, and ducting; pipe for water, drainage, chilled water, with pressure test; galvanized iron conducting; water heater installation; cable tray installation; fan coil unit fixing; cable pulling; fire-fighting pipe work; ducting; main distribution board and sub-distribution board wiring and termination.

MEP Third Fix includes activities that could be done after false ceiling. The final fix activities involve light fixture installation, fire fighter sprinklers, grills and diffusers for HVAC, switch board, toilet fixtures and all other finishing works.

Major Parameters are discussed in this section.

2.2.1 Heating, Ventilating and Air Conditioning

HVAC system has two mechanical units working as the core of the system—AHU and Chiller system. AHU stands for air handling unit. It is used for conditioning and circulating fresh air. Its size can vary depending upon the space to be filled with air. AHU has blower, filter, damper, heating/cooling coil, mixing chamber, vibrational isolator, and controls as components. Chiller is another mechanical component of HVAC system, which removes heat from a liquid through a vapour compression or absorption refrigeration cycle. Water chiller is a refrigeration machine that produces chilled water. The Chiller lowers the temperature of water so that it can be used for producing the cooling effect in integration with AHU. So the works involve in the HVAC installation process are AHU and chiller fixing, pipes and ducts connection. These works further bring into some other activities in connection with them.

2.2.2 Electrical System

The electrical system consists of HV, LV and ELV system. The basic outline of the electrical system is that the power supply from the external permanent power supply (here BESCOM) comes to the substation and from there it is distributed to different buildings. Each building has a dry-type transformer. Transformer is meant for stepping down the voltage to the required level. From the transformer, power is sent to the LT panels from where we have cables transmitting out of panel to the respective power distribution boards, lighting distribution boards and equipment if any in the project. From the distribution boards, we have the wiring done to different light fixtures.

Different control panels are there to control and monitor all the equipment connected. From the main LV panel, cables come out and are connected to distribution boards. Here we have four DBs—PDB, LDB, ELDB, and UPSDB. PDB stands for power distribution board from which different receptacles are connected. Light fixtures are connected to light distribution board.

The scheme of Electrical distribution system is shown below in Fig. 1.

Coming to the construction part, the electrical activity starts from conduits laying in slab prior to concreting and putting them in walls after block work is done. Conduits are those that are used to enclose copper wiring and protect from damage. Cable trays are the ones that carry cables from transformer to panels and panels to distribution board. Diesel generators are also installed in site depending on the requirement. Earth pits are dug and earth strips from the building are connected to these earth pits.

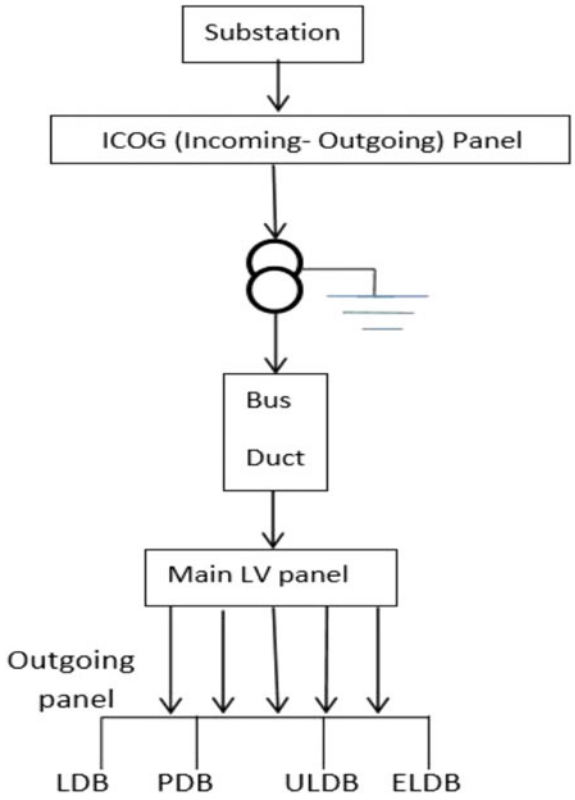

Fig. 1 Scheme of electrical distribution system

2.2.3 Extra Low Voltage System

ELV system consists of different system such as PAS, A/V system, ACS, FAS, BMS, CCTV surveillance system, etc. All these systems use very less power (less than equal to 24 W) that's why falls under ELV category. The cable used to supply power for ELV systems can be differentiated from each other by using different colour cables for different systems. Such as for Fire alarm system, red colour cable is used. Similarly, for Building management system, blue colour cable is used.

Extra low voltage works are similar to electrical works in terms of activities and their sequencing. ELV works are much smaller works when compared with electrical works. Public Address System needs its conduits and cable tray to be laid initially as per design. Cable is then laid from voice alarm controller to amplifier and amplifier to speaker. Access control system also has the same kind of activities as that of public address system. Here we have an access control panel to which the cable is drawn to and from the doors.

2.2.4 Fire Protection System

The Fire Protection System (FPS) makes the building fire resistant. It also enables quick evacuation of the people present inside the building in case of a fire. There are two types of system—active and passive. Active Fire Protection System requires action in order to work as intended in case of a fire. For example, fire extinguisher that is operated manually and sprinkler which is automatic come under this system. Passive Fire Protection divides a building through the use of fire-resistance rated walls and floors, which helps in preventing the fire from spreading fast and offers time to escape for the people present in the building.

Fire sprinkler system consists of a water supply system and water distribution piping system. The water supply system has several pumps that provide adequate pressure and flow rate to the water distribution piping system. Fire sprinklers are connected to the piping system. There is a main pipe known as header that is directly connected through pump. The water first comes to the header pipe and from there it is distributed to different connected pipes of smaller diameter called branches. The sprinkler system has its sprinklers to the branch piping of the main line in all the rooms as per design. The design will be such that the header pipe from pump room will have tapping to the various buildings and to different floors via other header and riser pipe. Riser pipe generally runs in parallel with drain pipe in shafts.

2.2.5 Plumbing System

Plumbing works in a construction project can be classified as domestic water supply and sewage piping. Domestic water piping is a power driven system. Sewage piping is gravity-based system. There is also flush pipeline that is used for sending water to toilet flush. Effluent pipe line is also laid in some projects, which could be power driven or gravity based.

Domestic water from municipality or bore well is fed to a water tank from where it is pumped to the desired locations with the help of a pump. The water pumped is sent to a tank at a higher elevation. From there, the water is tapped to different locations such as toilets, kitchens, wash areas, etc.

Plumbing system basically has pump installation and piping as work packages. Both the activities are independent and can be executed in parallel. Pump is fixed at the place of installation as per shop drawings. The pump and the other associated accessories including the piping manifold are pre-assembled on a base frame. For piping in plumbing system commonly used pipe material is chlorinated polyvinyl chloride. The entire piping system can be divided into two parts—concealed piping above ground piping. Concealed water piping only can happen during the first fix and above ground piping can happen during the second fix. After fixing all the pipes and before sanitary wares, fixing hydraulic testing is done to check the leakage in the pipe system.

2.3 Resource Estimation

Materials and equipment used in performing different MEP works have been identified by tracking involved activity, using shop drawings, BOQs, and taking opinion of different experts. Afterwards, a resource list has been made in which materials, equipment and labours used in completing each activity have been assigned correspondingly. For example, if we consider HVAC piping, the materials required are GI or MS pipes; different valves for controlling flow rate through the pipes; flanges to connect two pipes or to close the end of a pipe; unions, elbows, tees, couplers as pipe fittings; nut and bolts for fastening purposes. Equipment required are welding machines, pliers, and wrenches. Among other accessories, we have strainers, thermometer, and pressure gauge. Labours required are fitter, welder, and helper. Similarly, for other activities resources have been identified and assigned.

Now, for estimating labour, productivity norm approach has been used. Productivity norm is defined as the man-hour requirements per unit of the executed work. So, if the scope of the work is defined and each activity has its duration assigned, labour can be easily estimated.

A simple case of wiring has been taken for the aforesaid purpose. Productivity rate has been taken from central public works department guidelines. Now, the total man-hours required for completing the activity have been calculated.

$$\text{Productivity rate for wiring} = 0.229\ \text{man} - \text{hours/R} - \text{m}$$

$$\text{Total scope of wiring for office building} = 209,180\ \text{R} - \text{m}$$

$$\text{Total man} - \text{hours required} = 0.229 \times 209,180 = 47812.57\ \text{man} - \text{hours}$$

Actual total man-hours for wiring at site were 41,836 man-hours as per their daily and monthly progress report. This is comparable to the estimated figure of 47,812.57 man-hours calculated using the Productivity rate method previously presented.

During the commencement and feasibility stages (when only the scope of work is known), only rough estimations are necessary due to many uncertainties. It is anticipated that such estimates be within $\pm 20\%$. The percentage difference between the figures is 14.29%. Thus this is within $\pm 20\%$ (original parameter). Hence based on the productivity rate, the total man-hour requirements can be estimated at the project inception stage.

3 Result and Discussions

Based on the study so far, all the activities and resources are used as input as part of making a standard template. The template is developed using project management software PRIMAVERA version 6.0. It uses methodology management module for developing template. So based on the case study done, a work breakdown structure has been developed for the entire MEP package. The top-down approach has been followed where the main project is broken down into various works. Each work package has been subdivided into different components. Each of these components has been subdivided into manageable activities. The WBS so developed in hierarchical form is shown in the figure.

As mentioned earlier, each MEP work packages has been divided into three fixes. HVAC works started with marking and fixing of supports and hangers for ducts and pipes. This is the only work in HVAC, which is conducted during the first fix. After that in the second fix, piping and ducting work has been started along with their accessories fixing.

During the initial stage of a construction project, the planning manager schedules the project as per the client's specifications and requirements. MEP works for a project will be limited to certain services depending on the requirement of client and the kind of project. The template shown in the appendix details various MEP works and activities involved in a project. Depending on the type of project, this template can be cut short and trimmed to the project's requirement (Fig. 2).

4 Conclusion

Management and execution of Construction Projects are not possible without proper construction planning as it has become a fundamental process in the modern age. Budget and schedule for a project cannot be completed and determined without a proper construction plan. Successful conclusion of the project is only possible if the project plan is efficient and complete.

With the current study, a list of activities for various MEP works (service wise) has been described and their predecessors have been provided. A simple approach to estimate man-hours at the project inception stage has been proposed. A template has been developed in Primavera methodology management module giving the details of various services of MEP works, their activities, relationship between activities and resources that are necessary for those activities. This template can be saved and used for the project planning just by importing it as the current project baseline. The template can also be edited if necessary in future to make it more general and standard. This kind of template is very useful in improving organisation process assets.

To control the costs and complete the project in time, resource estimation is important. Productivity rate method for estimating labour uses productivity as the

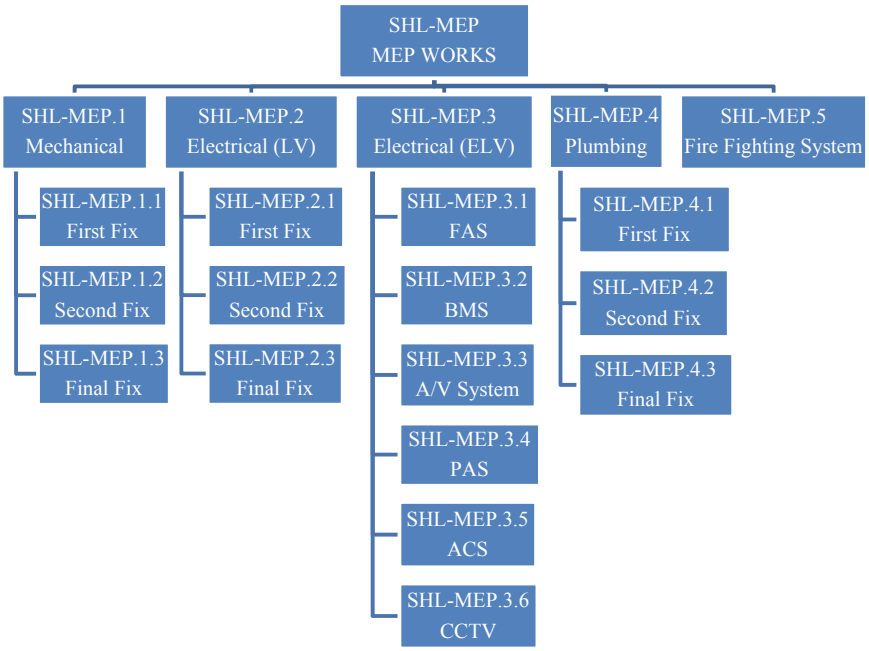

Fig. 2 Work breakdown structure in chart form

basis of analysis. So, by standardizing productivity rate for every work element, entire work force can be estimated at the project inception stage. Also it will be helpful for an organisation in selecting a sub-contractor based on the fact that whether or not he is performing the assigned task at the standard rate.

References

1. Aras R, Surkis J (1964) PERT and CPM techniques in project management. ASCE J Constr Div 90(CO1)
2. Baker KR (2011) Introduction to sequencing and scheduling. Wiley, New York
3. Chadderton DV (2013) Building services engineering, 6th edn. Routledge, Abingdon, Oxon and New York, NY
4. CPWD Works Manual (2014) Central Public Works Department, Government of India
5. Echeverry D, Ibbs CW, Kim S (1991) Sequencing knowledge for construction scheduling. ASCE J Constr Eng Manag 117(1):118–130
6. Proverbs DG (1999) A method for estimating labour requirements and costs for international construction projects at inception. Build Environ 34:43–48
7. Hall F, Greeno R (2013) Building services handbook, 7th edn. Routledge, London
8. Hastings P (2005) The illustrated guide to electrical building services, 2nd edn. Building Services Research and Information Association, Bracknell, Berkshire, England
9. Schwalbe K (2012) Information technology project management, 7th edn. Thomson Course Technology, USA

10. Kerzner H (2010) Project management: a systems approach to planning, scheduling, and controlling. Wiley, New York, NY
11. Heldman K, Baca C (2007) Project management professional exam study guide. Wiley, Hoboken, NJ
12. Kelly JE, Walker MR (2009) Critical path planning and scheduling. Mauchly Associates, Ambler, PA

Multi-criteria Decision-making Approach for Selecting a Bridge Superstructure Construction Method

Prabhath R. Upadhya, Mriganka Shekhar Das, and Bibhuti Bhusan Das

Abstract Selection of an effective construction method of bridge superstructure is critical to the success of the bridge project. Multiple criteria and the relative importance among them are involved in the process of decision-making. These criteria and their relative importance lead to vague and complex situation in the selection process. In order to tackle this complex situation, a mathematical methodology is required. Analytical Hierarchy Process (AHP) is a popular method that is used for solving Multi-Criteria Decision-Making (MCDM) problems. Every construction method of bridge superstructure has its own advantages and disadvantages. The challenge is to select the correct one for the prevailing circumstances. In this paper, the different methods of bridge construction are explained and are compared using their advantages, disadvantages and their suitability to different criteria and constraints associated with a bridge construction. The criteria weights and priorities are collected from experienced professionals of different point of view, i.e. Client, Designer and Contractor using questionnaire survey. Using this comparison, a decision support model is developed along with suitability ranking using AHP in order to simplify the process of selection of the appropriate method of bridge superstructure construction.

Keywords Bridge · Superstructure · Pairwise comparisons · AHP · MCDM

1 Introduction

Continuous progress in materials technology and calculation methods have led to the development and usage of prestressed, precast concrete and continuous beam structural systems. These methods have given rise to new forms of erection like span by span erection, balanced cantilever erection, full span erection, etc. Each method has its own advantages and disadvantages. This means that older form of construction like cast in-situ still exists.

P. R. Upadhya · M. S. Das · B. B. Das (✉)
Department of Civil Engineering, National Institute of Technology, Surathkal, 575025 Mangalore, Karnataka, India
e-mail: bibhutibhusan@gmail.com

B. B. Das et al. (eds.), *Recent Trends in Civil Engineering*, Lecture Notes in Civil Engineering 105, https://doi.org/10.1007/978-981-15-8293-6_41

Currently, bridges have evolved into segmental construction, use newer technologies like precasting, prestressing and continuous spans have been adopted. Erection is useful in negating the topographical conditions, in increasing mechanization, decreasing time required and flow disruption and for bringing better economy into construction. Precasting is useful in maintaining good quality of concrete, increasing speed of construction, negating weather conditions, reducing labour requirement, etc. While precasting has gained lot of prominences, it still cannot match the versatility of in-situ construction. Cast in-situ methods are generally simpler, cost-effective and can be adjusted to suit any circumstances and technical requirements [1, 2].

2 Need of This Study, Scope and Objectives

Selection of methods currently is done by designers using some predominant characteristics of the bridge and the site conditions and based on experience. This may lead to vague and complex situations due to clashing of the deciding criteria. Based on factors such as application conditions, construction surroundings, project driving factor and other requirements the correct method of construction should be chosen to bring upon economic benefits into bridge construction.

Every construction method has its own advantages and challenges. The evaluation of the best possible alternative construction method is a difficult task when we lack the list of particular requirements that make one solution immediately preferable to the others. Comparisons based on the quantities of materials are the most common practice, which consider only one of the various components of the construction method of a bridge. There are various other factors involved and should be considered.

The aim of this study is to compare the different methods of superstructure construction across different criteria and to prepare a decision support model using a multi-criteria decision-making method so as to be able to use the most appropriate one at the right place and right time for a given set of circumstances [4–8].

To achieve the scope of the study, the following objectives have been set up:

- Comparing the construction methods across multiple criteria using a multi-criteria decision-making approach for different parties involved in bridge construction.
- Developing a model in order to facilitate the selection process.

3 Correlation Among the Bridge Types and Construction Methods

Bridges can be classified into various categories based on different parameters. It can be classified as precast and cast in-situ based on the construction and concrete casting technique. To suit the various types of bridges listed above, there are a variety of machines and equipment which are falsework, launching girders,

Table 1 Correlating various bridge classifications to methods of construction

	Construction Methods	Cast in-situ	Precast	Span by span	Full span	Balanced cantilever	Long span	Short span
Machine/Equipment	Launching girder		✓	✓	✓	✓	✓	✓
	Lifting frames		✓			✓	✓	✓
	Movable scaffolding system	✓			✓			✓
	Form traveller	✓				✓	✓	✓
	Falsework	✓	✓	✓				✓
	Push launching		✓		✓		✓	✓
	Stay supported launching		✓			✓	✓	✓
	Crane		✓	✓	✓	✓	✓	✓

movable scaffolding systems, form travellers, lifting frames, incremental launching, cable/stay supported launching etc. The bridge classifications have been correlated to construction methods and summarized in the Table 1.

The highlighted boxes that correspond to the five different methods are used in our Questionnaire Survey.

4 Research Methodology

In this research, we have considered Qualitative comparison using AHP from the various MCDM techniques. The details of the methodology have been discussed thoroughly.

4.1 Qualitative Comparison

While comparing different methods, a quantitative approach is generally preferred as it gives better insights, relative differences among methods and clarity. But in the case of bridge construction, there are a lot of factors which affect the final delivery. These factors cannot always be compared quantitatively directly for a universal comparison.

The numbers fluctuate a lot based on the design conditions due to the methods having limits in both their advantages and disadvantages.

The problems with quantitative comparison of cost and time of bridge construction:

- Current data available for methods (Example from L&T Project) are data for a predefined and predesigned setup—load, span, width, design strategy, etc. Getting data for similar setups but using different methods will be a problem.
- A real comparison would require us to design all the methods for a similar setup then simulating it. But this would require extensive design background and is out of scope of this research.
- Absence of any data to normalize or model different superstructures.
- A method can be designed for different performance and efficiency levels based on the availability of technology and capital.

Due to these problems, we will adopt a qualitative approach which would not need raw numbers and is not very data intensive.

4.2 Multi-Criteria Decision-Making (MCDM)

'Multi criteria decision making is an umbrella term used to describe a collection of formal approaches which seek to take explicit account of multiple criteria in helping individuals or groups explore decisions that matter' (Valerie and Theodor, 2003).

Numerical scores are calculated to represent degree of preference for decision options in value measurement methods. This includes methods like AHP (Analytical Hierarchy Process), MAUT (Multi-Attribute Utility Theory), weighted sum and product model.

Both value measurement models and outranking models can be used in our case. But the easy to use and lesser data-intensive AHP are preferred to the more complex methods (Fig. 1).

4.3 Analytic Hierarchy Process (AHP)

The Analytic Hierarchy Process (AHP) is an approach for multi-criteria decision-making, which was introduced by Saaty (1977 and 1994). The AHP is a supporting tool for decision-making, which can be used to reduce the complexity of the decision-making problems and solve it. A multi-level hierarchical structure of objectives is used. Also, different criteria, sub-criteria, and alternatives are incorporated in that structure. We used a set of pair-wise comparisons for deriving the pertinent data. To calculate the weights of importance of the decision criteria, these comparisons are

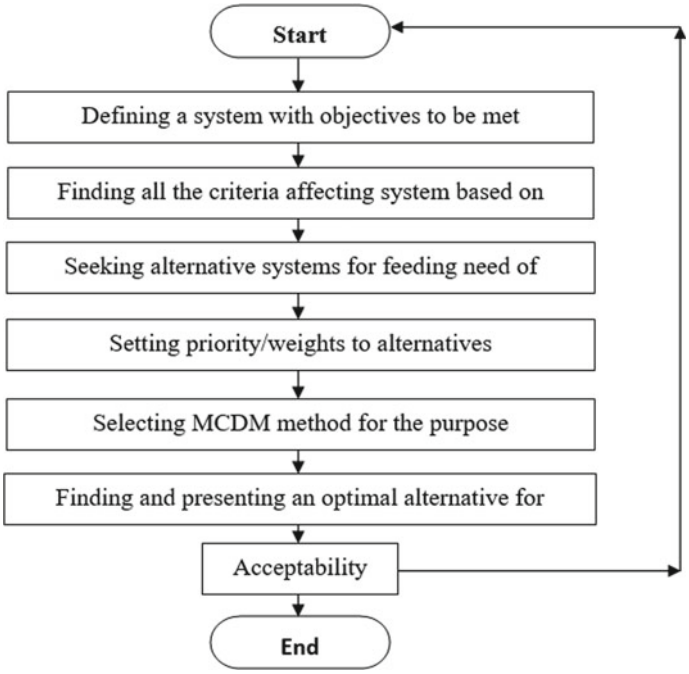

Fig. 1 Procedure for MCDM analysis

used. Moreover, in terms of each individual decision criterion, the relative performance measures of the alternatives are obtained. It has proved its usefulness in various areas of construction management.

For the pair-wise comparisons, we formed a scale of numbers that indicates how good or important one element is over another. The following exhibits the scale generally used for all process using AHP Table 2.

Table 2 Rating scale to compute criteria weights and compare alternatives

Rating	Meaning
1	Equally good
3	Moderately preferred
5	Strongly preferred
7	Very strongly preferred
9	Extremely preferred
2,4,6,8	In between values

Table 3 Random matrix consistency index

n	1	2	3	4	5	6	8	7	9	10
RI	0.00	0.00	0.58	0.9	1.12	1.24	1.32	1.41	1.45	1.49

4.3.1 Consistency

The judgements need to be checked for consistency. In order to limit the inconsistency AHP, concepts of consistency ratio (CR), consistency index (CI) and random matrix consistency index (RI) were presented by Saaty. Saaty [3] has provided the calculated RI for different matrix sizes and has been shown in the Table 3.

The consistency ratio is calculated using the formula $CR = CI/RI$. CI is calculated using

$$CI = \frac{Amax^{-n}}{n-1} \tag{1}$$

where A is the max eigenvalue of the matrix and n is the dimension of the matrix. Saaty [3] has shown that a consistency ratio of 0.10 is acceptable for analysis. If the consistency ratio is more than 0.1 then the judgements must be revised.

4.3.2 Aggregating Judgements

Since there are multiple individual participants in the judgement process, we need to aggregate the information. The two most commonly used methods are aggregation of individual judgements (AIJ) and aggregation of individual priorities (AIP). In this research, the responses have already been divided into different homogeneous groups (clients, contractors and designers). This along with the need for getting consistent responses without too much rework led to the selection of AIJ using the geometric mean of a small group of experts as the preferred method of analysis of the judgements.

4.3.3 Calculation of Priority

Alessio and Markus (2006) found out that when the matrix size is relatively small, and the inconsistency is low then there is very less difference between the methods. The number of rank contradictions was low between the eigenvalue method and mean of normalized and geometric mean method. The eigenvalue method is difficult to execute on a simple excel worksheet. So, for this research mean of normalized method and geometric mean will be selected as the methods to derive priority.

Table 4 List of constraints used for the different parties

Client	Contractor	Designer
Initial cost	Initial cost	Cost efficiency
Erection and indirect cost	Erection and indirect cost	Rate of construction
Rate of construction	Rate of construction	Safety
Safety	Weather susceptibility	Quality
Quality	Safety	Topography
Process efficiency	Quality	Curve
Maintenance efficiency	Topography	Process efficiency
	Curve	Maintenance
	Manpower	
	Process efficiency	

4.4 The Criteria

For an overall comparison of the methods, they will be compared across multiple criteria. Different parties have different preferences and requirements. In order to satisfy all the parties (contractor, client and designer) involved in the construction, different criteria are selected. These criteria may have different meaning for different parties and not all criteria will be used for the three parties. These criteria will be divided into sub-criteria in order to make it easier to give a clear rating to each. The criteria used here are not exhaustive and there are other ones which have not been considered here Table 4.

4.5 The Constraints

The criteria alone cannot decide on the appropriate method. A method can be very good in most criteria but can be severely lacking in one or two criteria. If those criteria turn out to be basic constraints, then the method should not be considered. In order to take this into consideration, some basic conditions are taken as constraint inputs during the analysis. The constraints are selected and rated for each bridge using a basic understanding of the construction method Table 5.

The Y stands for the method being able to work despite the constraint and N stands for the methods inability to contend with the constraint.

Table 5 Relation between different methods and constraints

Construction Method	Weather	Ground	Water	Curves	Span length
Balanced cantilever	Y	Y	Y	Y	Y
Crane and falsework	Y	N	N	Y	Y
Cast in-situ with falsework	N	N	N	Y	Y
Span by span using overhead LG	Y	Y	Y	N	N
Span by span using underslung LG	Y	Y	Y	Y	N

4.6 Questionnaire Survey

The methods will be compared by collecting data of pair-wise comparisons using questionnaire survey in the construction industry.

Design of survey—Questionnaire surveys will be used to obtain ratings for the methods. The rating can be based on ranking or rating (ordinal scales i.e. it will measure a variable in terms of rank). Using pairwise comparisons, we can get a more accurate picture about the methods. But the pair-wise comparisons themselves suffer from a disadvantage.

- As the number of alternatives and criteria increase the total number of pairwise comparisons gets too heavy and cumbersome. For our case of five alternative methods and 10 criteria, it will lead to 100 pair-wise comparisons ('$n * (n - 1) * m/2'$, where n is the number of alternatives available and m is the no of criteria) and 45 pair-wise comparisons for the criteria importance. For our objective to be achieved, a ranking system is too inadequate hence we will go with pair-wise comparisons and AHP.
- Getting responses—Responses will be received from small groups of clients, designers and contractors. In order to get homogeneous replies, the groups are instructed to work together to agree on a rough common hierarchy before they can work on aggregating their responses. For this research, we have collected five responses from the Client, five responses from the Contractor and six responses from the Designer.
- Analysing the results—The results are analysed using AHP. The judgements are aggregated using geometric method and priority will be derived by mean of normalized values and geometric mean method.

4.7 Analysing Survey Responses and Calculations

Responses were taken from engineers with experience as either a client or designer or a contractor in the bridge construction industry. The aggregation of results is done by taking geometric mean of product of all the responses. The MNV method utilizes normalizing the column first. Then the mean of the row is taken to obtain the priority values. The lambda value is obtained by using eigenvalue and vector equation. In

the geometric mean method, all the judgements across a row are multiplied and their geometric mean is taken. The geometric mean values are then normalized.

The consistency check is done to ensure the judgements have not exceeded the allowable levels of inconsistency. Consistency index is calculated using the formula.

$$CI = (A - n)/(n - 1) \tag{2}$$

Where lambda is the eigenvalue calculated in the previous step and n is the matrix size. The random average index is obtained from the table illustrated before. The consistency ratio is obtained by dividing the consistency index by the random average index,

$$CR = CI/RI \tag{3}$$

5 Decision-Making Model

The next step in the AHP decision-making process is obtaining the relative priorities for different criteria. The priorities keep changing with place, preferences, driving goals, etc. Thus, the priorities will be taken as an input in order to get the method more suitable for those conditions. A pair-wise comparison criteria are created similar to previous matrices but for the different criteria. The user will input the pair-wise preferences. The priority and lambda values will be calculated as done in the previous chapters using MNV and GM method. Consistency check is done in order to obtain consistent preferences. Then constraints will be taken in as input in order to filter methods further. Overall priority is calculated as a sum of product of the criteria priority and method priority for those criteria.

5.1 Client's Selection Model

A hypothetical case is taken in order to illustrate the model. In our example, we assume bridge construction in a busy city. The general order of preference of criteria is assumed as safety/quality, time/initial cost followed by maintenance/erection cost and process efficiency. The overall priorities for each criterion are calculated and the sum of the priorities across criteria gives the methods final priority.

The methods are given an initial ranking based on their priorities. Then the constraints are used to filter methods feasibility. And based on the criteria method, a method either passes or gets disqualified. A final ranking is generated where the disqualified method does not feature Table 6.

For the given set of preferences and constraints, the model concludes that erection using crane and falsework is the most suitable method.

Table 6 Ranking table of client's selection model

Type	Initial ranking		Final ranking	
	WSM	GMM	Qualified	Final
Balanced cantilever erection	5	5	5	4
Cast in-situ construction	4	4	NA	NA
Crane and falsework	1	1	1	1
Overhead LG	3	3	3	3
Underslung LG	2	2	2	2

Table 7 Ranking table of contactor's selection model

Type	Initial ranking		Final ranking	
	WSM	GMM	Qualified	Final
Balanced cantilever erection	3	3	3	2
Cast in-situ construction	5	5	5	3
Crane and falsework	1	1	1	1
Overhead LG	2	2	NA	NA
Underslung LG	4	4	NA	NA

5.2 Contractor's Selection Model

A similar case is taken for contractor's selection model and similar calculations are done for the initial and final ranking according to the priorities Table 7.

For the given set of preferences and constraints, the model concludes that erection using crane and falsework is the most suitable method.

6 Designer's Selection Model

A similar case is taken for contractor's selection model and similar calculations are done for the initial and final ranking according to the priorities Table 8.

For the given set of preferences and constraints, the model concludes that erection using underslung LG is the most suitable method.

Table 8 Ranking Table of Designer's Selection Model

Type	Initial ranking		Final ranking	
	WSM	GMM	Qualified	Final
Balanced cantilever erection	5	5	5	2
Cast in-situ construction	2	2	NA	NA
Crane and falsework	1	1	NA	NA
Overhead LG	3	3	NA	NA
Underslung LG	4	4	4	1

7 Conclusion

Accurately choosing a bridge construction method is vital for the success of the bridge project. With multiple factors and interested parties at play, we need a robust mathematical and analytical system to arrive at a suitable choice. Multi-criteria decision-making methods are an elegant way to solve this problem. This project work presents an AHP-based model in order to simplify the process of method selection.

The model is divided into three models based on the different parties involved in the construction process. Each model considers the same alternatives across different relevant criteria. The model takes in expert opinions as the major input in form of pair-wise comparisons. The comparisons also tend to be lengthy and repetitive. Due to this, it is crucial that the expert has enough knowledge and expertise.

Hypothetical cases were considered, and they were analysed using the developed model to illustrate the model's capability and effectiveness. This shows the steps involved and explains the process so that by using that the parties can evaluate their options better.

The proposed model is not restricted to either the five methods used, or the different criteria used for different parties. The methods were selected just based on being the commonly used methods in the Indian construction industry. The list of criteria is also not exhaustive. In future studies, more construction methods may be considered along with changing the criteria in order to introduce newer and different methods into the Indian construction industry.

A qualitative comparison does not always convey the same information which is conveyed by raw numbers. A quantitative comparison is arguably more helpful in deciding. The lack of data availability with respect to simulating the methods is across a given set. Future studies can look into simulating design and construction for different methods in order to make better decisions.

References

1. Saaty TL (2008) Decision making with the analytic hierarchy process. Int J Serv Sci 1(1)
2. Ishizaka A, Lusti M (2006)How to derive priorities in AHP: a comparative study. CEJOR 14(4):387–400
3. Saaty TL (2012) A new approach to the middle east conflict: the analytic hierarchy process. J Multi-Criteria Decis Anal 19(5–6), 201–225
4. Valerie B, Theodor SJ (2003) Multiple criteria decision analysis: an integrated approach
5. Forman E, Peniwati K (1998) Aggregating individual judgments and priorities with the analytic hierarchy process. Eur J Oper Res 108:165–169
6. Triantaphyllou E, Mann SH (1995) Using the analytic hierarchy process for decision making in engineering applications: some challenges. Int J Ind Eng: Appl Pract 2(1):35–44
7. Chaphalkar NB, Shirke PP (2013) Application of multi criteria decision making techniques for bridge construction. Int J Innovative Res Sci Eng Technol 2(8)
8. Hwang C-L, Yoon K (1981) Multiple attribute decision making. Springer.

Safety Stock in Inventory Management and Wastage Analysis at Construction Sites

Bishal Paul, Santosh Tondihal, and Bibhuti Bushan Das

Abstract Inventory control in construction projects is a key function to the project success. Inventory serves as a link between planning and execution of a project. In construction industry, majority of the cost is involved in inventories so it is important to keep the inventories under strict control otherwise it may lead to cost and time overrun. As construction industry consumes large part of inventories, so it produces huge amount of wastes. It is established that the wastages have a significant negative impact on cost and time of a project. So, it is of utmost importance to know the impact of these causes of wastages on cost and time so that a proper mitigation plan can be prepared and impact of these causes of wastage be reduced or eliminated. This paper mainly put emphasis on safety stock analysis aiming to determine the safety stock of inventories after calculation of average lead time, actual lead time, average demand per day, standard deviation and service factor from the set of data obtained from the site. It also aims to provide a model for automation of safety stocks to prevent stock-outs using PYTHON software. Apart from that, it involves a questionnaire survey to analyze the impact of various causes of wastage in construction on the basis of cost and time.

Keywords Inventory · Safety stock · PYTHON · Automation · Wastage

1 Introduction

Inventory is the raw materials, work-in-process products and finished goods that are considered to be the portion of a business's assets that are ready or will be ready for sale [1]. The problem of inventory control is one of the most important in organizational management. As a rule, there is no standard solution—the conditions at each company or firm are unique and include many different features and limitations. For years, companies have been relying on experience and intuition, without regard to optimum need for inventory control [2]. For smaller projects, inventories can be

B. Paul · S. Tondihal · B. B. Das (✉)
National Institute of Technology Karnataka, Surathkal, Mangalore, India
e-mail: bibhutibhusan@gmail.com

B. B. Das et al. (eds.), *Recent Trends in Civil Engineering*, Lecture Notes in Civil Engineering 105, https://doi.org/10.1007/978-981-15-8293-6_42

controlled by experience but for bigger projects, which involves a lot of investment and risks, proper inventory control technologies and methods need to be adopted otherwise it may lead to increase in cost of the project. Inventory control is a very broad topic, and so in this paper, we are mainly concentrating on the safety stock analysis and then to automate the process [3]. At first, data from the site are analyzed and actual lead time, service factor, average demand per day is found out and then finally the safety stock is calculated. Along with that a framework is proposed to automate the safety stock analysis of various inventories and a code is written in PYTHON software in order to validate the framework.

In construction industry, inventories are involved in a large scale and so it produces a huge amount of wastage. Nowadays, the industry faces many challenges with issues related to construction waste [4–6]. Construction waste has become a serious problem in many countries. Waste has negative impact on the environment, cost, productivity, time, social and economy. This waste generation activities consume time and effort without adding values to the client thus resulting losses in material, delay in meeting the stipulated time and execution of unnecessary work [7, 8, 10]. Therefore, to avoid overrun of cost and time of the project it is necessary to get an idea about the causes of wastage and understand the impact of these on cost and time so that a proper mitigation plan can be developed to reduce or eliminate the impact [9, 11, 12].

This paper focuses on finding the various causes of wastage in construction sites. After that a questionnaire survey is prepared which will give an idea about the impact of causes of wastage on cost and time. Then the causes are arranged in the decreasing order of their impact on the cost and time separately on the basis of the responses which will give an idea to the project people about the causes that should be given more importance, along with that some mitigation measures have also been suggested.

2 Methodology

In order to calculate the safety stock, firstly the service level on the basis of the importance of the inventory has to be decided. Then it is required to calculate the actual lead time and the average demand per day of that particular inventory.

2.1 Safety Stock Calculation

The data from the site were collected, and the safety stock of seven important inventories was calculated. Apart that framework has been formulated to automate the process using python so that the safety stock can be used in practical construction world. A code has been written to validate the framework (Fig. 1).

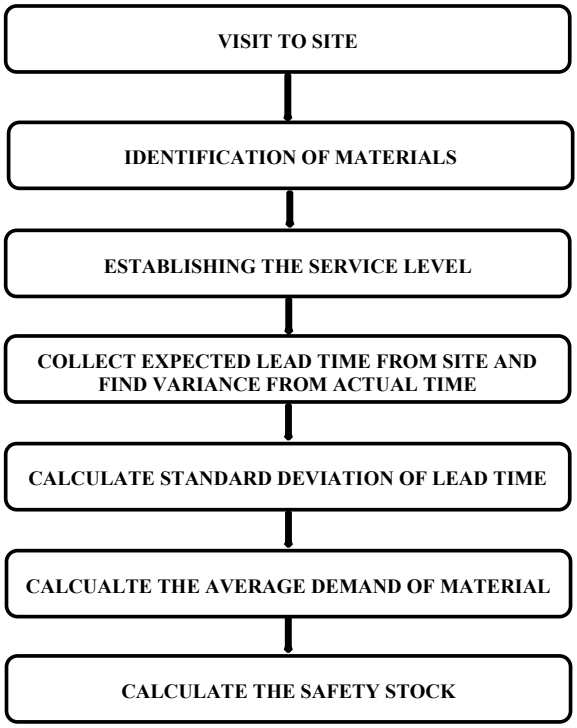

Fig. 1 Flowchart for calculation of safety stock

2.2 Safety Stock Automation

The automation of safety stock can be done using PYTHON software by writing a code with the following algorithm. The code is written in such a way that as soon as the online stock comes near the safety stock an email will be generated to planning in charge and store in charge, letting them to know about the item that may go out of stock (Fig. 2).

2.3 Impact of Causes of Wastage on Cost and Time

In order to assess the impact of wastage on cost and time, the total 20 causes of wastage has been identified on the basis of previous studies and suggestions of project manager, site engineers, architects, considering the impact of the 20 causes on the cost and time being important and critical in the wastewater projects. In this study measurement skill of 1–5 was used to determine the effect level. Participants were asked to indicate to what extent the causes of wastage had impact on cost and time separately. The Questionnaire prepared was distributed amongst respondents. Respondents were required to rate using their experience how all factors affect labour

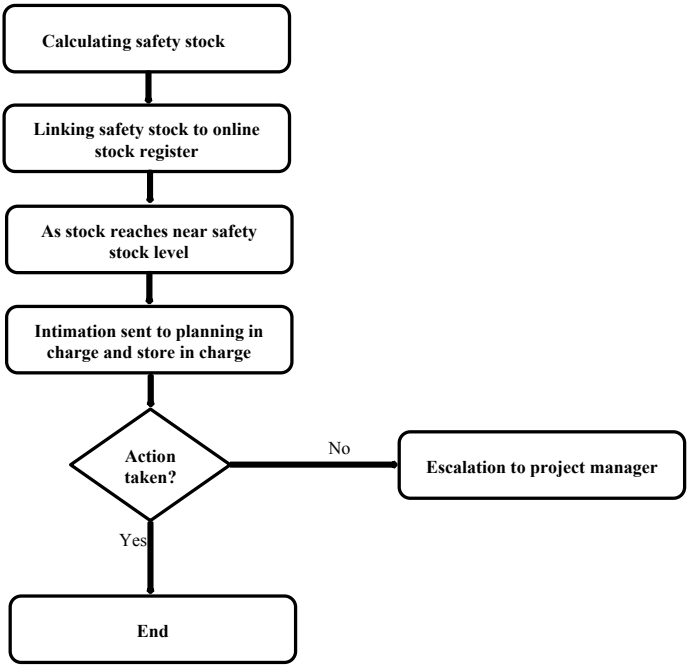

Fig. 2 Flowchart for automation of safety stock

productivity. Most targeted respondents were employees of L&T Constructions. On the basis of survey, Relative Importance Index (Fig. 3)

Fig. 3 Flowchart for analyzing impact of wastage

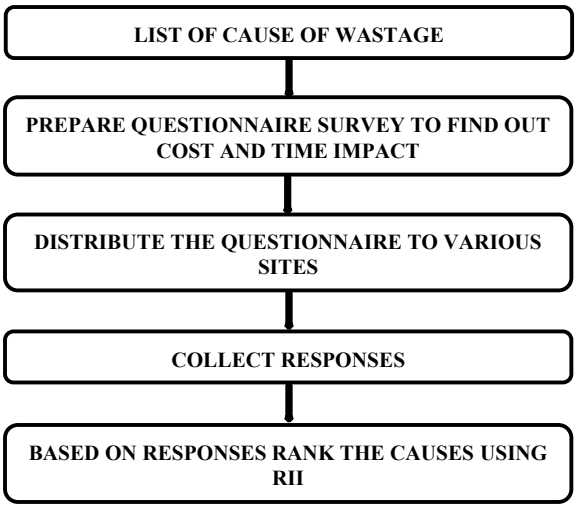

$$\text{Relative Importance Index (RII)} = (5n1 + 4n2 + 3n3 + 2n4 + n5) / \left\{ \begin{pmatrix} n1 + n2 + n3 \\ + n4 + n5 \end{pmatrix} \right\}$$

where n1 represents number of respondents who answered "very high impact", n2 represents number of respondents who answered "high impact", n3 represents number of respondents who answered "medium impact", n4 represents number of respondents who answered "low impact" and n5 represents number of respondents who answered "very low impact". Higher the ranking, greater will be the impact of that cause on cost and time.

3 Results and Discussions

The Material Receipt Note (MRN) and Material Receipt (MR) report have been collected from the site. The reports were analyzed and seven important inventories (Cement, SFRC Manhole, 500 mm RCC pipe, 150 mm DWC pipe, Steel-8 mm, Steel 10 mm, Manufactured Sand) were selected for calculating the safety stock. After that a table was formulated which consisted of the following entities: EMR date, MRN data, EMR Number, Material description, Unit of measurement, Received Quantity, Days between EMR and MRN, actual lead time for calculation, expected lead time and finally the variance. The average demand per day is calculated, expected time is collected from the site and then the variances were calculated and finally the standard deviation for lead time is obtained. In this study, service level of 95% is considered which corresponds to a service factor value of 1.64. Now all the data pertaining to the seven inventories were formulated in the table and the safety stock was calculated as shown in Table 1.

Using PYTHON software the auto-generated intimation mail has been generated if there is any inventory reaching its safety limit (Tables 2 and 3) (Fig. 4).

Some mitigation plans were suggested to reduce the impact of the causes of wastage which are as follows:

- Planning engineer should have good experience in planning as well as execution works and should be well versed with software like Primavera, MS Project, etc.
- The site engineers and supervisors should be given proper training so that they efficiently manage the sites as well as the labourers.
- The managers should properly communicate with the site managers what exactly the work should be done so that there is no requirement of rework.
- Proper training should be given to the labourers so that they can do the work properly with safety.
- Daily meetings should be held between the planning and execution team

Table 1 Safety stock analysis

Safety stock analysis								
Considering 95% service level								
Item no.	Items	UOM	Service factor	Excepted lead time	Sum of Variances/no of entities	Standard deviation of lead time	Average demand/day	Safety stock
a	b		c	d	e	f = d + e	g	h = c*f*g
1	OPC cement	mt	1.64	22	15.71	37.71	5.09	314.79
2	150 mm DWC pipe	m	1.64	260	0	260	21.1	8997.04
3	steel-8 mm	mt	1.64	25	4.11	29.11	0.3	14.32
4	steel-10 mm	mt	1.64	25	21.67	46.67	0.32	24.49
5	SFRC manhole	Nos	1.64	30	10.33	40.33	4.66	308.22
6	500 mm RCC pipe	m	1.64	160	0	160	1.37	359.49
7	manufactured sand	ft^3	1.64	7	18.17	25.17	194.06	8010.56

4 Conclusion

This research is intended to move towards a step of automation which is highly required for Indian Construction Industry to complete the project on time. Stock-outs can have a high impact on time which will lead to delay in project. The study is conducted to give a detailed idea about the calculation of safety stock and them to automate it through PYTHON software so that a better control over the inventories is achieved and thereby stock-outs can be prevented. Along with it, study has been conducted through questionnaire survey to understand the impact of wastage on cost and time of the project. From the analysis done through RII method, it was found that inadequate planning and scheduling has the highest impact on both cost and time of the project. Along with it, poor site management and supervision and rework also have high on cost and time. On the basis of cost, losses due to cutting material and losses during transportation have very less effect and on the basis of time, theft and losses due to cutting material has very less effect and accordingly some mitigation plans have been suggested.

Table 2 Ranking of impact of causes of wastage on the basis of time

Cause no.	Impact of causes of wastage on the basis of time	No. of people responding					RII index
		Very low	Low	Medium	High	Very high	
C-1	Inadequate planning and scheduling	0	0	8	26	42	0.889
C-2	Poor site supervision and management	0	0	14	44	18	0.811
C-3	Rework	0	4	18	32	22	0.789
C-4	Mistake and error in design	0	6	14	42	14	0.768
C-5	Poor coordination between staff and supervisor	0	4	16	38	18	0.784
C-6	Labour productivity	0	2	26	36	12	0.753
C-7	Incompetent subcontractor	0	6	20	36	14	0.753
C-8	Contractor negligence	0	4	32	32	8	0.716
C-9	Poor storage condition	2	8	36	28	2	0.653
C-10	Poor quality control	2	14	22	34	4	0.663
C-11	Lack of experience	2	8	24	32	10	0.705
C-12	Equipment failure	0	10	30	30	6	0.684
C-13	Less skilled labour	0	10	30	30	6	0.684
C-14	Wrong selection of materials	2	14	26	30	2	0.643
C-15	Effect of weather	0	6	36	24	10	0.700
C-16	Equipment availability	0	10	30	30	6	0.684
C-17	Less site worker	0	12	20	34	10	0.711
C-18	Theft	2	30	32	10	2	0.547
C-19	Losses due to cutting material	4	30	32	10	2	0.538
C-20	Losses during transportation	4	26	16	26	2	0.589

Table 3 Ranking of impact of causes of wastage on the basis of cost

Cause no.	Impact of causes of wastage on the basis of cost	No. of people responding					RII index
		Very low	Low	Medium	High	Very high	
C-1	Inadequate planning and scheduling	2	0	12	38	24	0.816
C-2	Poor site supervision and management	0	6	10	48	12	0.774
C-3	Rework	0	2	26	28	20	0.774
C-4	Mistake and error in design	0	8	12	42	14	0.763
C-5	Poor coordination between staff and supervisor	0	6	20	24	16	0.752
C-6	Labour productivity	2	4	22	36	12	0.737
C-7	Incompetent subcontractor	0	12	26	20	18	0.716
C-8	Contractor negligence	0	4	32	32	8	0.716
C-9	Poor storage condition	0	12	26	26	12	0.700
C-10	Poor quality control	0	4	38	30	4	0.689
C-11	Lack of experience	2	12	26	28	8	0.674
C-12	Equipment failure	0	18	24	28	6	0.658
C-13	Less skilled labour	0	18	26	24	8	0.658
C-14	Wrong selection of materials	2	14	26	28	6	0.658
C-15	Effect of weather	2	12	40	10	12	0.647
C-16	Equipment availability	0	18	36	20	2	0.616
C-17	Less site worker	4	14	32	24	2	0.616
C-18	Theft	0	26	32	14	4	0.589
C-19	Losses due to cutting material	2	28	24	18	4	0.584
C-20	Losses during transportation	0	30	26	18	2	0.579

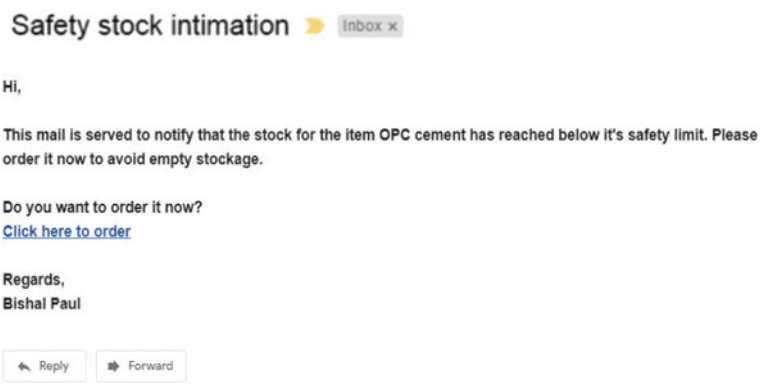

Fig. 4 Automatic generated safety stock intimation mail

References

1. Serhii Z (2015) A literature review on models of inventory management under uncertainty. Bus Syst Econ 5(1)
2. Lewis C (2012) Chapter 1: Demand forecasting and inventory control. In: Demand forecasting and inventory control. Routledge, pp 3–20. ISBN 9781136346835
3. Kumar Y, Kharpade R, Dewangan K, Dhiwar J (2017) FSN analysis for inventory management. Int J Res Appl Sci Eng Technol (IJRASET) 5(II), ISSN: 2321-9653
4. Meghani MD, Vyas CM, Bhavsar JJ, Hingu RJ (2011) A study on basic material waste in building industry. In: National conference on recent trends in engineering and technology, 13–14 May, 2011
5. Nagapan S, Rahman IA, Asmi A, Memon AH, Zin RM (2012) Identifying Causes of Construction Waste. Int J Integr Eng 4(2):22–28
6. Adewuyi TO, Otali M (2013) Evaluation of causes of construction material waste. Ethiop J Environ Stud Manag 6
7. Kasim N, Latiffi A, Mohamad S (2013) RFID technology for materials management in construction projects—a review. Int J Constr Eng Manag 2(4A):7–12
8. William George Grip. Applications of bar code technology in the construction industry. AD-A240 578, Georgia Institute of Technology, Atlanta
9. Xu Y, Chen M (2016) Improving Just-in-time manufacturing operations by using Internet of things based solutions. In: 9th international conference on digital enterprise technology, vol 56. Procedia CIRP, pp 326–331.
10. Subramani T, Bhaskarannair V, Mohammad Ghouse AB, Siva Kumar N (2017) A study of inventory management system in construction industry. Int J Appl or Inno Eng Manag (IJAIEM) 6(5)
11. Mincks WR (1994) The construction contractor's waste management plan. CIB TG 16, Sustainable Construction, Tampa, Florida, USA, November 6–9, 1994
12. Arshad H, Qasim M, Thaheem MJ (2017) Quantification of Material Wastage in Construction Industry of Pakistan. J Constr Develop Countries 22(2):19–34

A Multi-dimensional Study on Impact of Energy Efficiency on Life Cycle Cost of a Single-Family Residential Building

S. Shifad, Pratikshya Pati, and Bibhuti Bhusan Das

Abstract A sustainable building is the one which causes least impact on the environment by appropriate selection of construction materials, appliances and other practices. Many rating systems have been put forward in the recent years to provide guidelines for constructing and accessing the performance of green buildings. Indian Green Building Council (IGBC) rating system is one such guideline available in India. eQUEST has been proved to be powerful tool for analysing the projected energy efficiency of buildings in the initial design phase. This particular study aims to identify effectiveness of higher green certification towards energy savings. Building simulation was done for a double-storey residential building situated in western coast city of Mangalore, India for each certification level namely, certified, silver, gold and platinum. The results obtained from the simulation were analysed to quantify the energy-saving potential and energy efficiency of higher green certification of IGBC green homes. Life cycle costs of single-family green residential buildings of similar type and function rated by IGBC rating systems for buildings was evaluated and compared in terms of savings to investment ratio, net saving and payback period.

Keywords Energy efficiency · Life cycle cost · Sustainable building

1 Introduction

At present, construction is one of the major economic sectors in India. Buildings in India currently consume almost 41% of the total final energy consumption in the country, continue to have increased accumulation because of population growth and urbanisation necessitates the utilisation of green buildings concept to reduce the energy consumption and CO_2 emissions [1]. Environmental Protection Agency (EPA) of USA defines green building as a practice of creating structures and using processes that are environmentally responsible and resource-efficient throughout a

S. Shifad · P. Pati · B. B. Das (✉)
National Institute of Technology Karnataka, Surathkal, Mangalore, India
e-mail: bibhutibhusan@gmail.com

B. B. Das et al. (eds.), *Recent Trends in Civil Engineering*, Lecture Notes in Civil Engineering 105, https://doi.org/10.1007/978-981-15-8293-6_43

Table 1 IGBC green home certification criteria

Certification level	Individual residential unit	Multi-dwelling residential units
Certified	38–44	50–59
Silver	45–51	60–69
Gold	52–59	70–79
Platinum	60–75	80–100

building's life cycle from siting to design, construction, operation, maintenance, renovation and deconstruction [2]. Optimised building orientation, passive solar design techniques, proper insulation and glazing of building envelope, in addition to more efficient electrical appliances and devices constitute the major design strategies to justify the context of the green building [3]. In a typical building, space cooling consumes highest energy followed by lighting and other miscellaneous equipment. Therefore, if the initial design takes into consideration energy efficiency measures focusing on operational energy, significant energy savings can be achieved according to CAMTECH handbook on green buildings [4].

Single family as well as multi-family households have been expected to have higher growth rates between 2005 and 2050. Central European Union has predicted growth in India's residential building energy consumption from 1.9 EJ in 2005 to 8.12 EJ in 2030, which is about a 450% increase [5]. Hence, the requirement of a structured approach towards addressing the need for incorporating appropriate building design impacting life cycle costing continues to be the most viable solution towards achieving the targets of sustainability.

The performance of green buildings is evaluated and rated by the use of building environmental assessment methods, one of them being IGBC in India. The latest version 2.0 of IGBC Green Homes launched in March 2012 is framed for suiting Indian climate and construction codes [6]. The criteria for certification levels are as shown in Table 1.

2 Methodology

For the purpose of analysing the impact of improvement in energy efficiency on life cycle costing of residential homes with corresponding to increased IGBC certifications, baseline model study was undertaken in the building energy simulation tool eQUEST (Version 3.64). It is a public domain software developed by James Hirsch and Associates for Southern California Edition and is based on DOE-2.2. It provides user interfaces for inputting the building-specific data including weather file, orientation, location, construction materials used, occupancy and equipment schedules, lighting power density and properties of HVAC equipments. A residential building of 2604sq. ft. plan area with two storeys was fixed with the required data and specification as per IGBC Green Home guidelines separately for each design case and

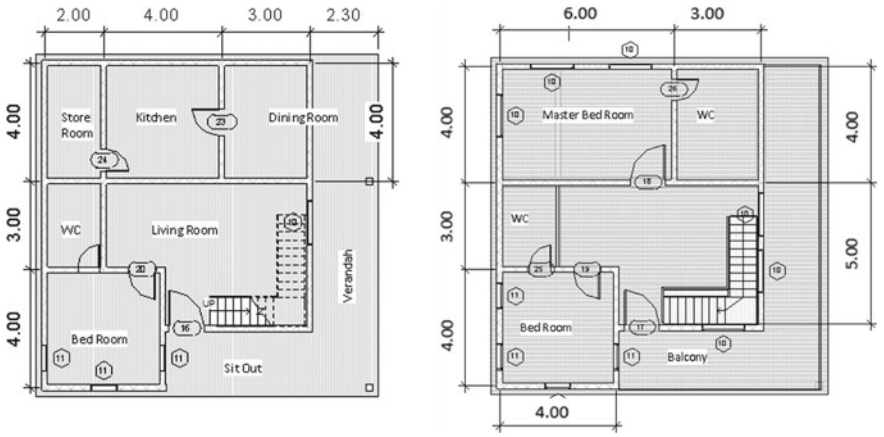

(a) Ground floor plan **(b) First floor plan**

Fig. 1 Floor plans of simulated building

simulated to obtain annual energy consumption, floor plan of the same as shown in Fig. 1.

Then the life cycle cost analysis was undertaken considering construction cost, operating cost and maintainance and repair cost taking into account the present value method for one-time cost or annually recurring energy cost whichever applicable for individual design cases. The life cycle costs were compared with the certified home as base case for both construction as well as use phase. Savings to investment ratio, net savings and payback period were evaluated against base case which gives indications regarding the associated cost advantage of using better energy efficient measures with increasing certification level.

2.1 Model Development

The proposed building situated in Surathkal, Mangalore lies in the warm and humid climate zone of western India. The long walls of the proposed two-storey residential building of 2604 sq. ft (approx. 242 m^2) have been oriented in the North–South direction and short walls in the East–West direction in order to reduce overall heat gain. The roof used is a flat roof, in order to find additional space for the placement of solar PV panel as well as the solar water heater. The height of floor was fixed as 3 m. The HVAC system used was a DX coil-split type unitary AC for all the buildings for 12 h. The values of ventilation are taken as per ASHRAE 60.1 and equipment schedule was taken as 8 h for all the building type. The simulation was carried for one-year duration.

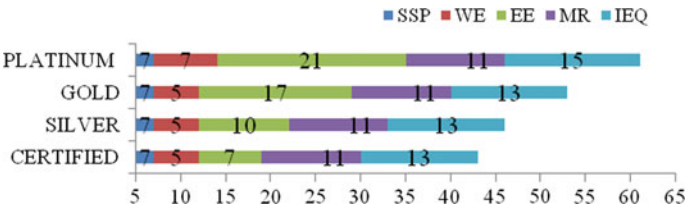

Fig. 2 Target Credit Points along with contribution of various criteria

For the present model study, the target rating points for each certification level after following the credit guidelines of IGBC Green Homes Rating System 2.0 along with contribution from criteria like Energy Efficiency (EE), Indoor Air Quality (IEQ) are given in Fig. 2.

2.2 Selection of Materials and Equipments

Building envelope: Building envelope refers to the external facade and consists of walls, windows, roof, skylights and other openings. Building envelope has been a major factor in heat gain and hence proper insulation of building envelope proves an effective way to manage the heat present in a building [7]. The materials of building envelope primarily involved in energy efficiency criterion have been tabulated in Table 2.

Electrical Appliances: The electrical appliances considered for the purpose of simulation includes fans, 123 cm inch television, frost-free refrigerators of 250 l capacity, split AC units and water heaters as per detailed description in Table 3. Lighting has been chosen in such a way that the lighting density never exceeded 3.5 W/m^2, thus satisfying EE credit 1 and making all the homes eligible for 2 credit points. The lux requirements of a room have been calculated as per the guidelines of

Table 2 Materials for building envelope

Certification level	Roof	Wall	Window glazing
Certified	Coat of cool roof paint 4 cm thick cement screed 4 cm thick Polyurethane Foam (PUF) 15 cm thick RCC slab 12 mm thick cement plaster U value of the roof assembly = 0.46 W/m^{2}K	• 12 mm cement plaster 19 cm × 9 cm × 9 cm burnt clay brick • U value = 2.385 W/m^{2}K	Graphite cool lite ST 136
Silver			Graphite cool lite ST 136
Gold		• 12 mm cement plaster • 60 cm × 20 cm × 7.5 cm AAC blocks • U value = 0.696 W/m^{2}K	Neutral Evolite ET 150 II
Platinum			SKN Envision SKN 165II

Table 3 Electrical appliances specification

Certification level	BEE rating of Appliances	Lighting	Ceiling Fans	AC
Certified	BEE 4	15 W(10), 10 W(6) 27 W(3) CFL bulbs	CROMPTON GREAVES SCORPIO PLUS, 1200 mm for living room(2) SUPER VI, 1400 mm for master bed room(1)	3 Star Split type
Silver	BEE 4	15 W(10), 10 W(6) 27 W(3) CFL bulbs	CROMPTON GREAVES SCORPIO PLUS,1200 mm for living room(2) SUPER VI, 1400 mm for master bed room(1)	3 Star Split type
Gold	BEE 5	15 W(1), 10 W(4), 7 W(10), 5 W(10) LED bulbs	HAVELLS E55, 1200 mm for living room(2) SUPER VI,1400 mm for master bed room(1)	5 Star Split type
Platinum	BEE 5	15 W(1), 10 W(4), 7 W(10), 5 W(10) LED bulbs	HAVELLS E55, 1200 mm for living room(2) SUPER VI,1400 mm for master bed room(1)	5 Star Split type

IS 3646 (1966) [8]. The size of ceiling fans was fixed based on the room size, as per IS 374 (1999) [9].

Renewable energy: Renewable energy is an important characteristic of green building. For the undergone study renewable energy was mainly used in two forms: solar photovoltaic cells and solar water heater, the details of which have been detailed in Table 4 and Table 5, respectively.

Table 4 Solar photovoltaic cell specification

Certification level	Solar panel rating (kW)	Solar panel specification	Inverter rating(kW)	Inverter specification
Certified	–	–	–	–
Silver	0.7	Su kam silicon polycrystalline solar cells at 12 V, 125 Wp	1	Power one Microsystems 1 kW
Gold	1		1.5	Su kam SRS 1.5 kW
Platinum	1.3		1.8	Su kam SRS 2 kW

Table 5 Solar water heater specification

Certification level	Solar water heater specification
Certified	100 l (Orb Sunstream GV 100 l)
Silver	100 l (Orb Sunstream GV 100 l)
Gold	200 l (Orb Sunstream GV 200 l)
Platinum	200 l (Orb Sunstream GV 200 l)

2.3 Life Cycle Cost Analysis

The life cycle cost analysis is carried in this paper in accordance with the procedure prescribed by Fuller and Petersen [10] which considers LCC to address the various projected cost of a project taken over the lifetime of the same adjusted to include the present value of money [11]. Financial advantage of future savings achieved due to the improvement measures adopted for improving building energy efficiency helps in an informed decision-making. The life cycle costing was calculated for construction and operating phase.

The first step was to collect construction cost data for different homes. The components of cost which are common to all the four houses were taken as a percentage of the total construction cost based on various guidelines proposed by the government of India and other literatures. For the purpose of estimation CPWD Schedule of Rates was followed [12]. For the materials not available in the Delhi schedule of rates, market rates were adopted.

The next step was to obtain the energy consumed by the four homes by performing eQUEST building simulation where the energy demand (w/ft^2) for appliances, air delivery, domestic hot water, lighting, cooling and other equipment loads [13]. The per unit electricity cost was obtained from the local electricity body and total energy cost was evaluated.

The repair and maintenance cost were assumed as to be same for the four homes due to the similarity in material properties and equipments used and were not taken into account [14]. However, the replacement cost of CFL and LED varies widely due to the large difference in life hours of both. So, this was also taken into account

separately. Solar grid tie inverters have a lifetime of 10 years and these were also taken into account. The replacement costs of electrical equipments were also considered. The escalation rates for the electrical equipments were assumed to be zero as per NIST Handbook 135 [10]. Most of the operating, repair and maintenance costs are recurring costs, whereas replacement costs are one-time costs.

In order to compare the different options from a life cycle viewpoint, the cost data had to be discounted presented in a net present value context. A high discount rate indicates the near future while a low discount rate indicates the distant future [15]. Inflation rate of 7.3%, interest rate of 10.6% and real escalation rate of energy of 4% were chosen for cost calculations over a period of 25 years [16, 17].

3 Results and Discussions

The annual energy consumption output obtained from the eQUEST simulation model for the four certification levels simulated separately can be in the form of load breakup, annual electricity consumption and breakdown of electricity consumption, either zone-wise, system-wise or equipment-wise.

The total annual electrical energy consumption of certified, silver, gold and platinum rated IGBC Green homes was found to be 14,990 kWh, 14,610 kWh, 12,640 kWh and 12,150 kWh, respectively. Thus, the platinum building consumes 19% less energy than the certified building without considering renewable source of energy. The breakdown of monthly electricity consumption for various appliances as per the usage namely space cooling, ventilation fans, task lighting, area lighting for IGBC certified, silver, gold and platinum green homes have been tabulated in Fig. 3, Fig. 4, Fig. 5, Fig. 6, respectively.

The energy breakdown for various operations in the buildings reveals that almost half of the energy is consumed for space cooling for all the design cases with the peak usage in the summer months of April and May, followed by ventilation fans, miscellaneous equipments and lighting.

The space cooling requirements were reduced by 12.8% and 18.7% in gold and platinum building, respectively, as compared to certified building by use of higher

Electric Consumption (kWh x000)

	Jan	Feb	Mar	Apr	May	Jun	Jul	Aug	Sep	Oct	Nov	Dec	Total
Space Cool	0.66	0.64	0.78	0.85	0.91	0.69	0.66	0.65	0.67	0.71	0.69	0.68	8.57
Heat Reject.	-	-	-	-	-	-	-	-	-	-	-	-	-
Refrigeration	-	-	-	-	-	-	-	-	-	-	-	-	-
Space Heat	-	-	-	-	-	-	-	-	-	-	-	-	-
HP Supp.	-	-	-	-	-	-	-	-	-	-	-	-	-
Hot Water	0.04	0.04	0.04	0.04	0.04	0.04	0.04	0.04	0.04	0.04	0.04	0.04	0.48
Vent. Fans	0.23	0.20	0.23	0.22	0.23	0.22	0.23	0.23	0.22	0.23	0.22	0.23	2.67
Pumps & Aux.	-	-	-	-	-	-	-	-	-	-	-	-	-
Ext. Usage	-	-	-	-	-	-	-	-	-	-	-	-	-
Misc. Equip.	0.18	0.17	0.18	0.18	0.18	0.18	0.18	0.18	0.18	0.18	0.18	0.18	2.15
Task Lights	-	-	-	-	-	-	-	-	-	-	-	-	-
Area Lights	0.10	0.09	0.09	0.09	0.10	0.09	0.09	0.09	0.09	0.10	0.09	0.09	1.11
Total	1.21	1.13	1.32	1.38	1.45	1.21	1.20	1.19	1.19	1.26	1.22	1.22	14.99

Fig. 3 Monthly split up of electricity consumption of IGBC Certified Green Home

Electric Consumption (kWh x000)

	Jan	Feb	Mar	Apr	May	Jun	Jul	Aug	Sep	Oct	Nov	Dec	Total
Space Cool	0.64	0.60	0.73	0.78	0.83	0.67	0.65	0.65	0.65	0.69	0.66	0.65	8.19
Heat Reject.	-	-	-	-	-	-	-	-	-	-	-	-	-
Refrigeration	-	-	-	-	-	-	-	-	-	-	-	-	-
Space Heat	-	-	-	-	-	-	-	-	-	-	-	-	-
HP Supp.	-	-	-	-	-	-	-	-	-	-	-	-	-
Hot Water	0.04	0.04	0.04	0.04	0.04	0.04	0.04	0.04	0.04	0.04	0.04	0.04	0.48
Vent. Fans	0.23	0.20	0.23	0.22	0.23	0.22	0.23	0.23	0.22	0.23	0.22	0.23	2.66
Pumps & Aux.	-	-	-	-	-	-	-	-	-	-	-	-	-
Ext. Usage	-	-	-	-	-	-	-	-	-	-	-	-	-
Misc. Equip.	0.18	0.17	0.18	0.18	0.18	0.18	0.18	0.18	0.18	0.18	0.18	0.18	2.15
Task Lights	-	-	-	-	-	-	-	-	-	-	-	-	-
Area Lights	0.10	0.09	0.09	0.09	0.10	0.09	0.09	0.09	0.09	0.10	0.09	0.09	1.11
Total	1.18	1.10	1.27	1.31	1.38	1.19	1.20	1.19	1.18	1.23	1.18	1.19	14.61

Fig. 4 Monthly split up of electricity consumption of IGBC Silver Green Home

Electric Consumption (kWh x000)

	Jan	Feb	Mar	Apr	May	Jun	Jul	Aug	Sep	Oct	Nov	Dec	Total
Space Cool	0.58	0.55	0.65	0.70	0.75	0.62	0.60	0.60	0.60	0.63	0.60	0.59	7.47
Heat Reject.	-	-	-	-	-	-	-	-	-	-	-	-	-
Refrigeration	-	-	-	-	-	-	-	-	-	-	-	-	-
Space Heat	-	-	-	-	-	-	-	-	-	-	-	-	-
HP Supp.	-	-	-	-	-	-	-	-	-	-	-	-	-
Hot Water	-	-	-	-	-	-	-	-	-	-	-	-	-
Vent. Fans	0.22	0.20	0.22	0.22	0.22	0.22	0.22	0.22	0.22	0.22	0.22	0.22	2.63
Pumps & Aux.	-	-	-	-	-	-	-	-	-	-	-	-	-
Ext. Usage	-	-	-	-	-	-	-	-	-	-	-	-	-
Misc. Equip.	0.16	0.15	0.16	0.16	0.16	0.16	0.16	0.16	0.16	0.16	0.16	0.16	1.91
Task Lights	-	-	-	-	-	-	-	-	-	-	-	-	-
Area Lights	0.05	0.05	0.05	0.05	0.05	0.05	0.05	0.05	0.05	0.05	0.05	0.05	0.63
Total	1.02	0.95	1.09	1.12	1.19	1.04	1.04	1.04	1.02	1.07	1.03	1.03	12.64

Fig. 5 Monthly split up of electricity consumption of IGBC Gold Green Home

Electric Consumption (kWh x000)

	Jan	Feb	Mar	Apr	May	Jun	Jul	Aug	Sep	Oct	Nov	Dec	Total
Space Cool	0.54	0.51	0.61	0.65	0.69	0.57	0.56	0.55	0.56	0.58	0.56	0.55	6.96
Heat Reject.	-	-	-	-	-	-	-	-	-	-	-	-	-
Refrigeration	-	-	-	-	-	-	-	-	-	-	-	-	-
Space Heat	-	-	-	-	-	-	-	-	-	-	-	-	-
HP Supp.	-	-	-	-	-	-	-	-	-	-	-	-	-
Hot Water	-	-	-	-	-	-	-	-	-	-	-	-	-
Vent. Fans	0.23	0.20	0.23	0.22	0.23	0.22	0.23	0.23	0.22	0.23	0.22	0.23	2.66
Pumps & Aux.	-	-	-	-	-	-	-	-	-	-	-	-	-
Ext. Usage	-	-	-	-	-	-	-	-	-	-	-	-	-
Misc. Equip.	0.16	0.15	0.16	0.16	0.16	0.16	0.16	0.16	0.16	0.16	0.16	0.16	1.91
Task Lights	-	-	-	-	-	-	-	-	-	-	-	-	-
Area Lights	0.05	0.05	0.05	0.05	0.05	0.05	0.05	0.05	0.05	0.05	0.05	0.05	0.63
Total	0.99	0.91	1.05	1.08	1.14	1.00	1.00	1.00	0.99	1.03	0.99	1.00	12.15

Fig. 6 Monthly split up of electricity consumption of IGBC Platinum Green Home

star rated equipments, area lighting energy consumption has been reduced by 43.2% in gold and platinum building by the use.

of LED lamps instead of CFL lamps.

Since eQUEST cannot quantify the energy saved by solar photovoltaic cells, the energy obtained from the same was deducted from the final value obtained through simulation, which has been depicted in Fig. 7. The solar photovoltaic cells were designed assuming an average of 300 sunny days and insolation level of 5.6kWh/m^2/day for Mangalore location.

As we go from lower to higher green certification, the electrical energy consumption is reduced by almost 30%. Use of renewable energy bought an additional savings

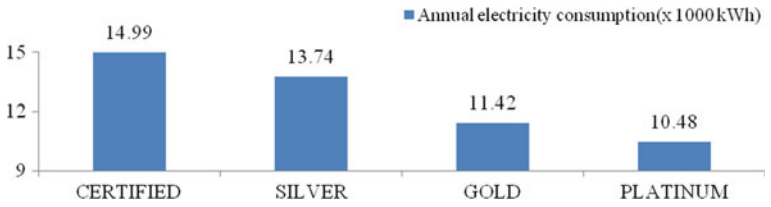

Fig. 7 Comparison of energy consumption after considering renewable source of energy

of 11%. This is in agreement with the fact that higher certification levels lead to higher energy savings.

Initial construction cost showed an increase of 3.5% as the building changed from certified to silver; 3.08% increase for the change from silver to gold and 1.03% increase from gold to platinum as shown in Fig. 8. The increase in cost was mainly due to adoption of energy-efficient measures. The annual electricity costs of the homes obtained have been tabulated in Fig. 9.

Considering energy savings and cost increment, we can see that for every unit of energy savings we spent Rs.105 for certified to silver. Similarly, the savings were Rs.69.75/kWh and Rs.64.24/kWh for gold and platinum buildings, respectively. As rating changes from silver to gold, cost per energy saving is Rs.51/kWh and from gold to platinum is Rs.43.30/kWh. It was observed that with higher certification, cost required for additional savings in energy was reduced.

Life cycle cost calculations of all the 4 buildings are shown in Table 6 with a time interval of 5 years for a lifetime of 25 years and breakdown of the same is featured in Fig. 10.

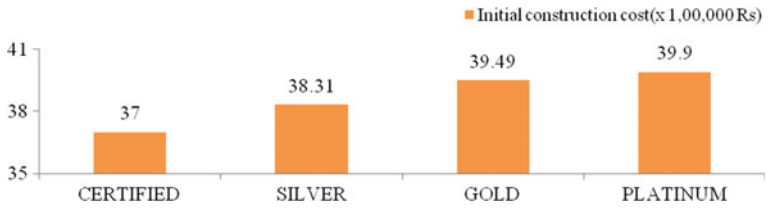

Fig. 8 Comparison of initial construction cost of buildings

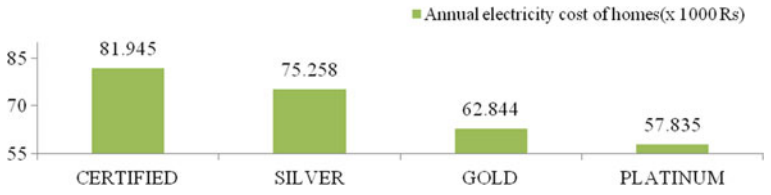

Fig. 9 Annual electricity cost of buildings

Table 6 Life cycle cost of buildings in every 5 years

Green rating	Life cycle cost after 5 years (Rs)	Life cycle cost after 10 years (RS)	Life cycle cost after 15 years (Rs)	Life cycle cost after 20 years (Rs)	Life cycle cost after 25 years (Rs)
Certified	41,23,812	48,72,338	53,36,255	60,43,606	65,49,618
Silver	42,20,421	49,58,886	53,85,250	60,72,430	65,37,380
Gold	42,81,067	49,90,564	53,50,059	59,93,867	63,84,608
Platinum	42,96,050	49,82,339	53,13,704	59,30,826	62,90,810

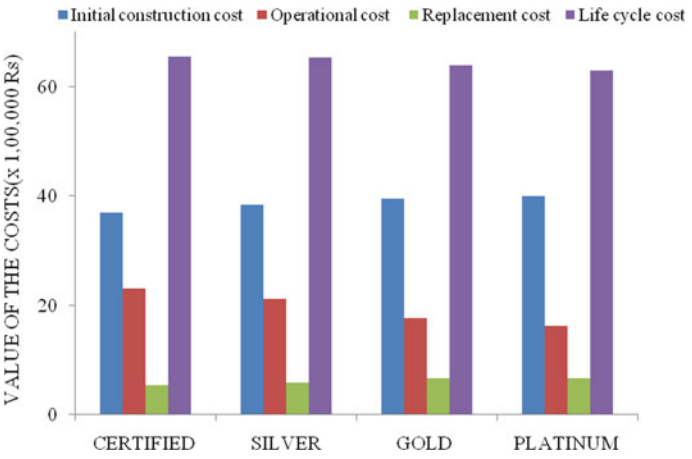

Fig. 10 Life cycle cost construction break up of different homes after 25 years

By comparing the values of life cycle cost after 25 years, it can be seen that platinum homes have the least life cycle cost, which can be attributed to the effective decrease of operational energy by the use of energy efficiency measures. It can be seen that higher certification leads to lower life cycle costs.

Savings to Investment Ratio (SIR) computed for different homes considering certified as the base case have been found to be valued at 1.049, 1.4, 1.6 as shown in Fig. 11. This implies platinum homes will accumulate an average return of Rs. 1.6 for every Re. 1 invested over the minimum required rate of return levied by the discount rate.

The net savings calculated considering life cycle cost at the end of 25 years with certified green home as base case is shown in Fig. 12. As long as the net savings are positive, the alternatives are cost effective. It was found that silver, gold and platinum buildings were cost effective. It shows that the operational savings were sufficient to justify additional investment costs for silver, gold and platinum building. Net savings of Rs. 1069.45/m^2 was found to be seen as the certification changes from certified to platinum.

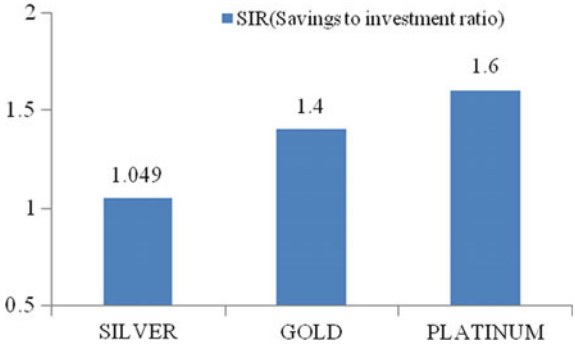

Fig. 11 SIR comparison with Certified home as the base case

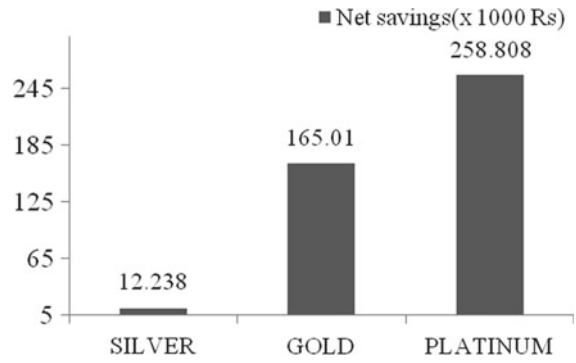

Fig. 12 Net Savings

Payback period, which is the time required for reaching the life cycle cost same as the base case can be used to quantitatively justify the investments at the initial stage. The same can be estimated by intersection of each design case and base case cost over a given period of time [18]. The payback period of silver, gold and platinum home with certified as the base case were 24, 18 and 16 years as shown in Fig. 13, Fig. 14, Fig. 15, respectively.

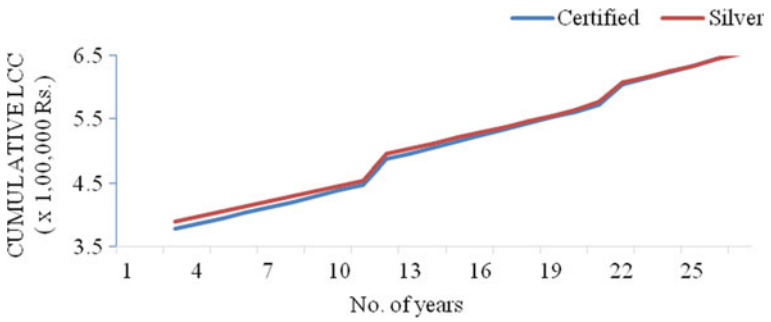

Fig. 13 Payback period of silver home

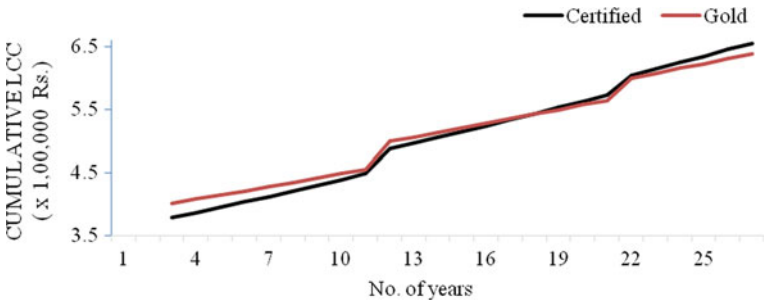

Fig. 14 Payback period of gold home

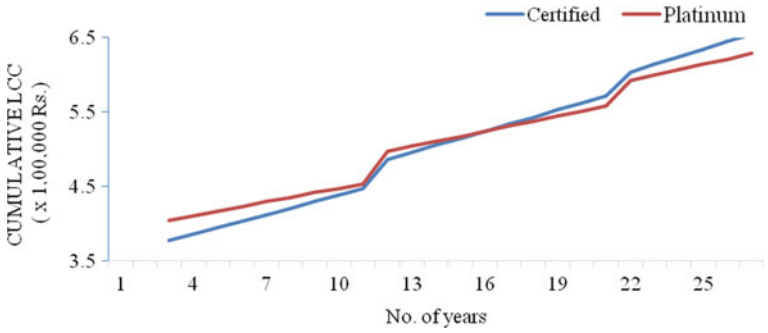

Fig. 15 Payback period of platinum home

4 Conclusions

The present study learns to identify how higher green rating of homes affects the various components of life cycle cost in relation to the increased energy efficiency.

With credit points of 22 out of a total of 75, energy efficiency criteria form the crux of the IGBC Green Homes Version 2.0. The energy efficient measures decrease the operational energy and thus life cycle cost with improved thermal comfort as they use materials with higher U value for the construction.

Renewable energy is a vital part of energy efficiency. Savings in operational energy are significant by the use of renewable energy which acts as an added advantage for stakeholders for investing in the same in addition to financial benefits. Significant initiatives have been undertaken by the government for providing renewable energy services at subsidised rates which can be exploited to the maximum. Grid-connected solar power systems should be encouraged, thereby avoiding cost of batteries. A reduction in discount rates to increase energy rates can also be adopted to incentivize the deployment of onsite renewable energy.

Although higher certifications lead to higher initial construction cost it was observed that with higher certification, costs required for additional savings in

energy were reduced. Operational energy use can be addressed by proper selection of building parameters at the design stage. The incentive for the construction of residential buildings with higher green certification is the higher net savings and lower life cycle costs. Moreover, the payback period for the platinum home is smaller when compared to others, which ensures that the occupants of platinum homes are able to reap financial benefits much earlier compared to other homes. All these advocate the construction of homes of higher green certification. This study can act as a baseline for the energy reduction measures to be adopted in a residential building.

References

1. Lasse R (2019) Tine Steen Larsen, Rasmus Lund Jensen, Olena Kalyanova Larsen, Kim Trangbaek Jønsson, Evangelia Loukou. Determining indoor environmental criteria weights through expert panels and surveys. Building Res Inf 47:1–14
2. Sustainable Design and Green Building Toolkit United States Environmental Protection Agency. Green Building Home (2016)
3. Dwaikata LN, Alib KN (2016) Green buildings cost premium: a review of empirical evidence. J Energy Build 110:396–403
4. Anon (2009) Handbook on Green Building, Center for Advanced Maintenance Technology, Ministry of Railways, Government of India, pp 7–9
5. Rawal R, Shukla Y (2014) Residential buildings in India: energy use projections and savings potentials, technical report, centre for environmental planning and technology. CEPT, India
6. IGBC Green Homes (2012) IGBC green homes rating system version 2.0 published by CII Hyderabad, India
7. IS 3792 (2014) Guide for heat insulation of non-industrial buildings. Bureau of Indian Standards, New Delhi, India
8. IS 3646, Part-II (1992) Code of practice for interior illumination. Bureau of Indian Standards, New Delhi, India
9. IS 374, Part-II (1999) Specification for electric ceiling type fans and regulators. Bureau of Indian Standards
10. Fuller SK, Petersen SR (1995) Life cycle costing manual for the federal energy management Program. NIST Handbook 135, National Institute of Standards and Technology, Gaithersburg
11. Joanna Marszal A, et al (2011) Life cycle cost analysis of a multi-storey residential net zero energy building in Denmark. J Energy 36(9):5600–569
12. CPWD (2014) "Delhi schedule of rates", Central Public Works Department, New Delhi, India. Tempe, "user-friendly life cycle costing: the BLCC Procedure in an easy to use spread sheet". In: Proceeding of the pollution prevention conference, US D.O.E, Albuquerque 2002
13. Bogenstatter U (2000) Prediction and optimization of life-cycle costs in early design. Int J Build Res Inf 28 (5):376–386
14. Dilara Mangana S, Koclar Oral G (2016) Assessment of residential building performances for the different climate zones of Turkey in terms of life cycle energy and cost efficiency. Int J Energy Build 110:362–376
15. Kale N, Joshi A, Menon R (2016) Life cycle cost analysis of commercial buildings with energy efficient approach. Perspect Sci 7:85–91
16. Mahajan SR, Pataskar SV, Jain NS (2015) Life cycle cost analysis of multi storied residential buildings. In: Proceedings of the IRF International Conference, Pune, pp 116–119
17. Kale N, Joshi A (2015) Life Cycle Cost Analysis of Buildings. Int J Eng Comput Sci 4(4):11313–11314
18. Davis M, Coony R, Gould S, Daly A (2005) Guidelines for life cycle cost analysis. Stanford University Land and Buildings, 1–28

Influence of Particle Size of Bottom Ash on Mechanical Properties of M30 Grade Concrete

Sharan Kumar Goudar and Bibhuti Bhusan Das

Abstract Thermal power plants produce fly ash and bottom ash as by-products. A total of 70% of by-product from thermal power plants accounts for fly ash and remaining 30% is bottom ash. One of the most common uses of bottom ash at the present scenario is structural fill in its coarser form only, and it is reported that the disposal leads to leaching of heavy metals to the groundwater table. These disposal problems and potential health hazards can be reduced by large usage of bottom ash in construction industry. A larger percentage of usage of the bottom ash in concrete will significantly reduce the potential health hazards and will give solution to disposal problems. With this in view, bottom ash collected from the Udupi thermal power plant was classified into two different levels according to their particle size and replaced against fine aggregates for different replacement levels, in producing M30 grade concrete. The raw bottom ash was coarse and classified as Zone-I after sieve analysis. The classification of bottom ash according to the particle size was carried out into different zones such as Zone-II and Zone-III, according to the specifications from IS 383–1970. The attainment of required compressive strength is directly correlated to particle size of bottom ash. Results show 47% reduction in compressive strength of concrete when raw bottom ash was (Zone-I) was replaced by 50% in place of natural river sand (NRS). A little effort in grading the bottom ash and converting coarser raw bottom ash from Zone-I to finer Zone-II bottom ash has proved beneficial in improving the compressive strength of concrete. It was observed that lower specific gravity of bottom ash directly influences density of concrete, which intern has adverse effect on compressive strength. The bottom graded as Zone-II can be replaced to NRS by 15–20%, with little compromise in compressive strength. Through value addition of 5% extra cement content, there is a possibility to increase the replacement level of Zone-II bottom ash to 30% with similar compressive strength as that of control concrete. Through cost analysis, it was found that 30% replacement of Zone-II bottom

S. K. Goudar (✉)
Department of Civil Engineering, College of Engineering Pune, Maharashtra 411005, India
e-mail: sgcr17@gmail.com

B. B. Das
Department of Civil Engineering, National Institute of Technology Karnataka, Surathkal, Mangalore, Karnataka 575025, India

B. B. Das et al. (eds.), *Recent Trends in Civil Engineering*, Lecture Notes in Civil Engineering 105, https://doi.org/10.1007/978-981-15-8293-6_44

ash in place of NRS with 5% extra cement content as value addition was found to be economical.

Keywords Bottom ash · Particle size · Compressive strength · Specific gravity · Mechanical properties

1 Introduction

The usage of the primary construction materials is getting depleted gradually due to their high demand and rise in prices. In most of the states in India, mining of river sand is banned with some exceptions in the private land. NRS is depleting very fast and the necessity of protecting natural resources is increasing every day [1–5]. The need of finding the replacement for NRS is increasing drastically as there are restrictions for mining of river sand. There are quite a lot of industrial by-products available which seem to have the potential to replace NRS partially or completely. One such industrial by-product is bottom ash from thermal power plants. A total of 70% of by-product from thermal power plants is fly ash and remaining 30% is bottom ash. Fly ash is being used in many industries such as cement production, brick industry, geopolymer concrete, and many more. However, the use of bottom ash in concrete production as a partial replacement of NRS caught the attention of researchers. Accumulation of bottom ash in landfills pose a potential environmental threat and also there are growing concerns of leaching of some harmful elements into the soil as well as water bodies [3–6]. There is an ever-growing need for the utilization of bottom ash in construction industry.

Bottom ash appears as coarse granular material and the particles almost resemble grains of NRS. The chemical composition of bottom ash mainly consists of Si, Al, Fe, Ca, Mg, SO_4, and few traces of other elements. The bottom ash has specific gravity ranging from 1.8–2.3 depending upon the locality and coal burning process [7]. The porous nature of bottom ash particles significantly affects specific gravity as well as water absorption capacity. From experimental research papers, it was noticed that higher water absorption and lesser specific gravity are the two hindering factors of bottom ash for utilization in concrete production [8–10]. These two drawbacks significantly affect the compressive strength and density of bottom ash replaced concrete. It was noticed that raw bottom ash which generally available in the top layer of landfills is coarser and generally graded as Zone-I. There is a high chance that these coarse bottom ash particles are more porous and lead to higher water absorption. In many research articles, researches have used raw bottom ash which might be of Zone-I grading [4–8]. However, no authors have reported the grading data of bottom ash utilized in their study. Ideally, NRS will qualify Zone-II grading, and it is necessary that bottom ash should also be of Zone-II grading for better results. A little effort is required to process the raw bottom ash of Zone-I grading to Zone-II. Influence of compressive strength development with the classification of bottom ash into different zones that suits the Indian code of practice is not being explored much.

With this in view, an attempt has been made to study the particle size effect on compressive strength of concrete by processing coarse raw bottom ash of Zone-I grading to zone-II and zone-III as partial replacement for NRS. From literature, it was understood that higher levels of replacement of bottom ash result in reduction in mechanical properties of concrete. To recover the compressive strength loss due to higher replacement levels of bottom ash, little extra amount of cement was used in the mix design. A cost analysis was performed to study whether addition of extra amount of cement to recover the compressive strength loss due to higher replacement levels of bottom ash is an economical solution or not.

2 Experimental Details

2.1 Materials and Their Characterization

In the present study, bottom ash collected from Udupi thermal power plant, Karnataka, India was used. Tables 1 and 2 shows the chemical and physical properties of materials used in the present study [11, 12].

2.2 Bottom Ash Characterization

The bottom ash collected from the dumping yard was in wet form. The material was air dried and then taken for sieve analysis. The raw bottom ash collected from the landfill was coarser and hence, the sieve analysis was carried out to characterize the bottom ash. Table 3 and 4 show the sieve analysis of bottom ash and NRS, respectively. The raw bottom ash was classified as Zone-I grade according to IS:

Table 1 Chemical analysis of cement and bottom ash

Content (%)	Chemical analysis	
	Cement	Bottom ash
SiO_2	20.5	7.17
Al_2O_3	4.00	7.01
Fe_2O_3	4.02	72.73
K_2O	0.80	0.30
CaO	64.00	1.03
TiO_2	–	0.17
SO_3	1.80	6.15
MgO	1.20	0.85
Na_2O	0.71	4.29

Table 2 Physical tests on cement, bottom ash, and aggregates

Physical tests	Cement	Raw bottom ash	Sand	Coarse aggregates
Initial setting time (min)	42	–	–	–
Final setting time (min)	362	–	–	–
Specific gravity	3.11	2.12	2.56	2.63
Fineness modulus	–	3.07	2.50	6.80
Zone of aggregate	–	Z-I	Z-II	–
Bulk density (kg/m^3)	–	1070	1700	–
Percentage of voids (%)	–	41.20	33.59	–
Water absorption (%)	–	6.5	1.0	0.5

Table 3 Sieve analysis of bottom ash

IS Sieve	Weight retained on sieve (in gm)	Percentage weight retained (in %)		% Passing
		Absolute	Cumulative	
10 mm	–	–	–	100
4.75 mm	95	9.5	9.5	90.5
2.36 mm	246	24.6	34.1	65.9
1.18 mm	184	18.4	52.5	47.5
600μ	131	13.1	65.6	34.4
300μ	155	15.5	81.1	18.9
150μ	132	13.2	94.3	5.7
Pan	54	5.4	–	–

Table 4 Sieve analysis of NRS

IS Sieve	Weight retained on sieve (in gm)	Percentage weight retained (in %)		% Passing
		Absolute	Cumulative	
10 mm	–	–	–	100
4.75 mm	–	–	–	100
2.36 mm	27	2.7	2.7	97.3
1.18 mm	180	18.0	20.7	79.3
600μ	250	25.0	45.7	54.3
300μ	381	38.1	83.8	16.2
150μ	135	13.5	97.3	1.6
Pan	22	2.2	–	–

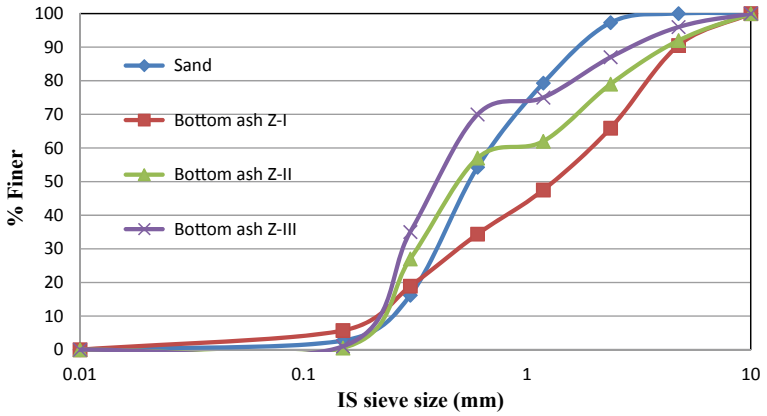

Fig. 1 Particle size distribution of NRS and bottom ash

383–1970 specifications. However, the NRS was classified as Zone-II grade. In order to replace the Zone-II NRS, bottom ash should also be of same grade.

The bottom ash was sieved and particles retained on each sieve size was collected individually. The coarser particles retained on 4.75 mm sieve were collected and stored in a separate container and the same procedure was followed for all the remaining sieve sizes. With the help of reverse calculation, the precise amount of particles was added to each sieve size and bottom ash was graded to Zone-II and Zone-III according to IS: 383–1970 specifications. The grading curve of fine aggregate, Zone-I, Zone-II, and Zone-III bottom ash is presented in Fig. 1.

3 Mix Proportion of Concrete

IS: 10,262–2009 specifications were used for concrete mix proportion. The details of the concrete mix proportions for producing M30 grade concrete are given in Table 5. In the present study, volumetric replacement of bottom ash was considered against NRS up to 50% in the interval of 10%. It is to be noted that the addition of plasticizers is avoided in the concrete mix design. It was aimed to get the workability in the range of 40–50 mm.

4 Results and Discussion

The raw bottom ash collected from landfills was directly replaced in place of NRS. The Compressive strength of raw bottom ash (without grading) replaced concrete is presented in Fig. 2. It can be observed that compressive strength reduced significantly

Table 5 Mix design details of control and bottom ash replaced concrete

Zone	Zone-II						Zone-III					
Mix details (kg/m^3)	CC2	Z2: 10%	Z2: 20%	Z2: 30%	Z2: 40%	Z2: 50%	CC3	Z3: 10%	Z3: 20%	Z3: 30%	Z3: 40%	Z3: 50%
Cement	380	380	380	380	380	380	380	380	380	380	380	380
Sand	736	663	588	515	441	368	712	641	570	499	428	356
Bottom ash	–	65	130	194	259	323	–	61	122	184	245	306
Coarse aggregate	1170	1170	1170	1170	1170	1170	1207	1207	1207	1207	1207	1207
Water	171	171	171	171	171	171	171	171	171	171	171	171

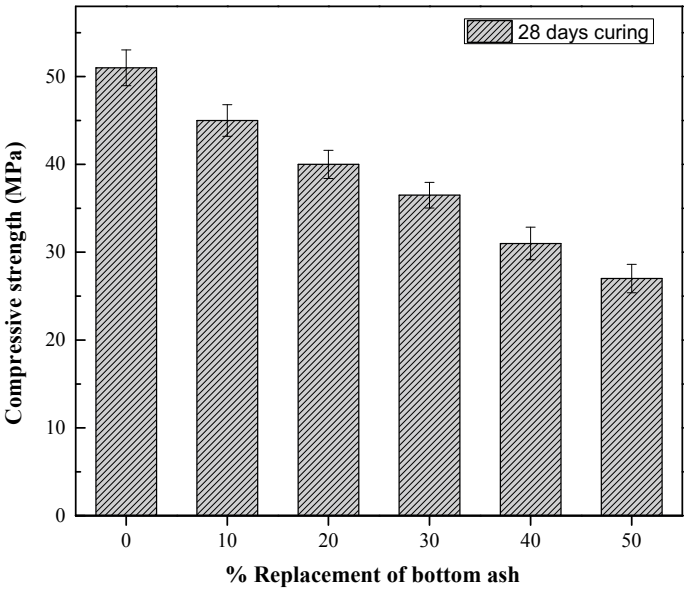

Fig. 2 Compressive strength of raw bottom ash (without grading) replaced concrete at different replacement levels with respect to NRS at 28 days curing

as the replacement level of bottom ash increased from 10–50%. There is nearly 12, 21.5, 28.5, 39.2, and 47% reduction in compressive strength for 10–50% replacement of NRS by raw bottom ash. This significant reduction in compressive strength might be due to the coarse nature of raw bottom ash. Hence, it was decided to properly grade the bottom ash and then replaced with NRS. The bottom ash was graded into Zone-II and Zone-III according to IS: 383–1970 specifications and then replaced with NRS.

Figure 3 shows compressive strength results of Zone-II and Zone-III bottom ash replacement by NRS in production of concrete. The reduction in compressive strength can still be noticed, but the reduction rate improved when compared to raw bottom ash replacement. There is nearly 4, 11.7, 21.5, 37.2, and 43.1% reduction in compressive strength for 10–50% replacement of NRS by Zone-II bottom ash. When compared to raw bottom ash, Zone-II graded bottom ash performed better which may be attributed to better packing and dense microstructure. It is also observed that there is a slight reduction in compressive strength values of zone-III bottom ash replaced concrete mixes when compared to zone-II bottom ash replaced concrete mixes. This may be attributed to the fineness of Zone-III bottom ash particles which might increase the water demand. This behavior is noticed in the workability of concrete, where Zone-II replaced concrete mixes showed 45 mm slump and at the same time Zone-III replaced bottom ash concrete mixes showed a slump value of 34 mm. Another reason for reduction in compressive strength of Zone-III replaced bottom ash concrete mixes might be due to reduced unit weight of concrete [13]. The variation in unit weight of

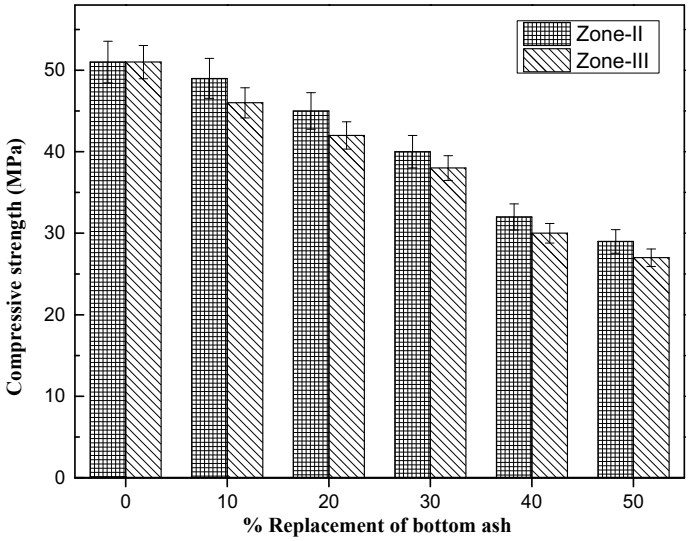

Fig. 3 Compressive strength results of Zone-II and Zone-III bottom ash replaced concrete at different replacement levels with respect to NRS at 28 days curing

Zone-II and Zone-III replaced bottom ash concrete mixes at different replacement levels with respect to NRS is presented in Fig. 4. Overall, the grading of raw bottom ash improves the compressive strength. Hence, it is recommended to properly grade the bottom ash before using as replacement to NRS and Zone-II grading may be preferred. A 20% replacement of Zone-II bottom ash was found to be the optimum level of replacement for NRS.

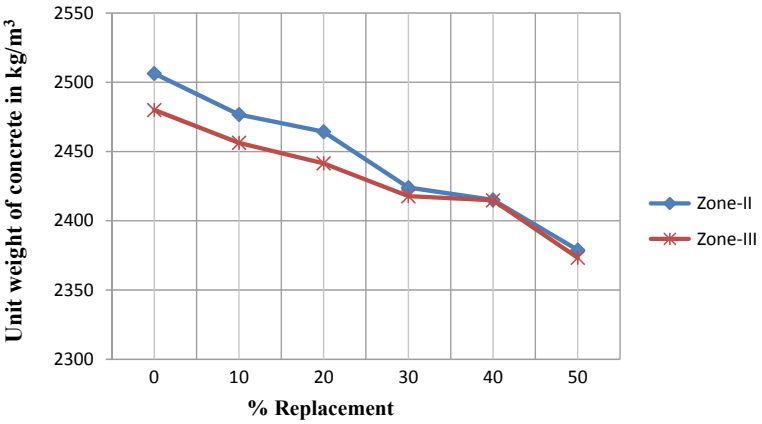

Fig. 4 Variation of unit weight of concrete with different zones at the age of 28 days curing

Most of the researchers reported 30% replacement of bottom ash as optimum level of replacement [4–7]. However, in the present study, there was 21.5% reduction in compressive strength for 30% bottom ash (Zone-II) replacement with NRS. In order to close the compressive strength gap, a new strategy is employed. It was planned to increase the cement content by 20 kg/m^3 (from 380–400 kg/m^3) in the mix design by keeping all other ingredients content at the same level. This value addition nearly accounts for 5% of total cement content which was added during mixing process. This value addition of little extra cement is being followed in the site for gaining little extra strength.

Figure 5 shows the compressive strength of bottom ash (Zone-II) replaced concrete at 10–50% replacement levels when 20 kg/m^3 of extra cement is added to the concrete mix. It is obvious that addition of extra 20 kg/m^3 of cement improved the compressive strength of all the bottom ash replaced concrete mixes when compared to 380 kg/m^3 bottom ash replaced concrete mixes. There is nearly 8.16%, 11.1%, 20%, 21.8%, and 13.8% improvement in compressive strength of 20 kg/m^3 of extra cement added concrete mixes for 10–50% replacement, when compared to 380 kg/m^3 bottom ash replaced concrete mixes. It was aimed to produce a concrete without much compromise in compressive strength for control concrete and 30% bottom ash (Zone-II) replaced concrete. Even after value addition of 20 kg/m^3 of cement to 30% bottom ash replaced concrete there is nearly 4% shortage in compressive strength when

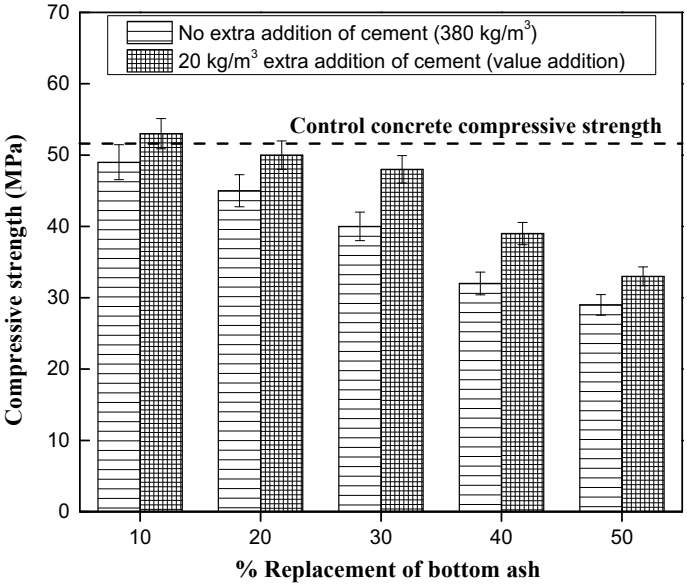

Fig. 5 Compressive strength of bottom ash (Zone-II) replaced concrete at different replacement levels when 20 kg/m^3 of extra cement is added to the concrete mix

compared to control concrete. In other words, there is 20% improvement in compressive strength by extra addition of 20 kg/m^3 of cement to 30% bottom ash replaced concrete.

It is questionable that addition of 5% extra cement to improve the compressive strength of 30% bottom ash replaced concrete is economical or not. A simple cost analysis was performed by considering the cost of individual items as per local schedule rates (SR/DSR). Cement costs around 8 rupees per kg and NRS costs around 25–30 rupees per kg. The value addition of 20 kg/m^3 cement costs 160 rupees extra for producing one-meter cube of concrete. When 30% of NRS (194 kg) was replaced by bottom ash, there is an approximate saving of 4,800 rupees for producing one-meter cube of concrete. Through cost analysis, it was observed that 30% replacement of Zone-II bottom ash in place of NRS with 5% extra cement content was found to be economical.

5 Conclusions

- There was 47% reduction in compressive strength of concrete when raw bottom ash was (Zone-I) was replaced by 50% in place of natural river sand.
- It is recommended to properly grade raw bottom ash before using as direct replacement to natural river sand and Zone-II grading may be preferred for best results.
- It was found that lower specific gravity of bottom ash directly influenced density of concrete, which intern has adverse effect on compressive strength.
- It is observed that 15–20% replacement level of bottom ash with natural river sand is found to be an optimum level of replacement.
- For higher levels of bottom ash replacement (up to 30%), little extra amount of cement may be added during mixing as value addition to improve the compressive strength.
- Through cost analysis, it was found that 30% replacement of Zone-II bottom ash in place of natural river sand with 5% extra cement content as value addition was found to be economical.

References

1. Mandal AK, Sinha OP (2014) Review on current research status on bottom ash: an Indian prospective. J Inst Eng (India): Ser A95(4):277–297.
2. Bhangale PP, Nemade PM (2013) Study of pond ash (BTPS) use as a fine aggregate in cement concrete—case study. Int J Latest Trends Eng Technol 2:292–297
3. Haldive SA, Kambekar DA (2013) Experimental study on combined effect of fly ash and pond ash on strength and durability of concrete. Int J Sci Eng Res 4(5):81–86
4. Ghafoori N, Bucholc J (1996) Investigation of lignite-based bottom ash for structural concrete. J Mater Civ Eng 8(3):128–137

5. Cheriaf M, Rocha JC, Pera J (1999) Pozzolanic properties of pulverized coal combustion bottom ash. Cem Concr Res 29(9):1387–1391
6. Singh M, Siddique R (2013) Effect of coal bottom ash as partial replacement of sand on properties of concrete. Resour Conserv Recycl 72:20–32
7. Andrade L, Rocha JC, Cheriaf M (2007) Evaluation of concrete incorporating bottom ash as a natural aggregates replacement. Waste Manage 27(9):1190–1199
8. Goudar SK, Shivaprasad KN, Das BB (2019) Mechanical properties of fiber-reinforced concrete using coal-bottom ash as replacement of fine aggregate. Sustainable construction and building materials. Springer, Singapore, pp 863–872
9. Hiremath PN, Thanu HP, Basavana Gowda SN, Goudar SK (2019) Early-strength development of blended concrete under different curing conditions. Emerg Mater Res 9(1):1–6
10. Yadav S, Das BB, Goudar SK (2019) Durability studies of steel fibre reinforced concrete. In: Sustainable construction and building materials. Springer, Singapore, pp 737–745
11. Goudar SK, Das BB, Arya SB (2019) Microstructural study of steel-concrete interface and Its influence on bond strength of reinforced concrete. Adv Civ Eng Mater 8(1):20180133
12. Goudar SK, Das BB, Arya SB, Shivaprasad KN (2020) Influence of sample preparation techniques on microstructure and nano-mechanical properties of steel-concrete interface. Constr Build Mater 256:119242
13. Goudar SK, Gedela SK, Das BB A review on mechanical and microstructure properties of reinforced concrete exposed to high temperatures. Recent Developments in Sustainable Infrastructure. Springer, Singapore, pp 719–728

Experimental Studies on Concrete Using the Partial Replacement of Cement by Glass Powder and Fine Aggregate as Manufactured Sand

Y. Pierce, Sumit Kumar B. Kanaka, and B. Niteen

Abstract Cement manufacturing industries are one of the industries that are affecting the environment by contributing to a total of 8% of greenhouse gas emissions to the Earth's surface. Carbon dioxide is the main emitting source that contributes about 65% of global warming, among them. Consequently, the river sand in some regions of our nation which is being used as fine aggregate is an expensive investment and its leading to a shortage on the earth's surface. To overcome these problems, the waste materials have been partially replaced in the construction field is being carried. This study is about the usage of finely grounded glass waste in concrete as replacement material to cement in of 5, 10, 15 and 20%, and manufactured sand had been used as fine aggregate fully. Compressive and Split Tensile strength tests for the hardbitten concrete were done at the time period intervals of (7–14–28) days. At 15% of adding waste glass into the concrete mix by replacing the cement and complete usage of M-Sand instead of river sand is noted as a high asset. Glass powder of the size of less than 90 μm is used throughout this experiment to prevent the alkali-silica reaction. Hence, by outcome results, it is observed that the WGP can be used as partial replacement material to cement and M-sand can be used as a fine aggregate.

Keywords Waste glass powder (WGP) · Manufactured sand (m-sand) · Workability · Strength tests · Ordinary portland cement

1 Introduction

Among the manmade materials, concrete is one of the materials used more on this planet that to more overly in construction fields due to its flexibility, durability and frugality [11]. Because in making a concrete cement, water, fine and coarse aggregates are the main ingredients. In these, cement is the most expensive ingredient that is present. Currently, the cement production rate of the world is approximately 502 million tons for each year in that India stands the second position in the production.

Y. Pierce (✉) · S. K. B. Kanaka · B. Niteen
Department of Civil Engineering, Central University of Karnataka, Gulbarga, India
e-mail: yandrapatipierce@gmail.com

B. B. Das et al. (eds.), *Recent Trends in Civil Engineering*, Lecture Notes in Civil Engineering 105, https://doi.org/10.1007/978-981-15-8293-6_45

By the manufacturing of the cement, CO_2 gas was a majorly emitting source from the industries to the world [12, 13]. Approximately 8% of the world's CO_2 emanation is occurring from the cement industries. Using river sand has fine aggregate in the concrete has become extremely classy, and it is leading the exploitation of natural assets like getting lower of the water table, shrinking of the bridge piers and it's leading to a shortage on the earth's surface [4, 10]. So, there is a need to economize cement and river sand in concrete making. To the reduction of waste materials on earth land fields and in the search for alternative blinders that WGP is replaced partially by cement in concrete and M-sand is used in full replacement of river sand as fine aggregate.

Glass is an associate vague material with the content of great silica which the size of the particle less than 90 μm making probably pozzolanic. Using glass in concrete that makes a chemical antiphon called Alkali–silicate antiphon. This reaction is because of the presence of silica in ground glass and alkali in concrete [9]. As a part of greenhouse management, the researchers have been concluded that ground glass can be used in concrete production by replacement method with various ingredients. Due to high industrialization and non-recycling, the waste glass is increasing rapidly in recent decades. Its inflicting bound certain serious issues.

To overcome the pollution and to reduce the cost expensive and to make eco-friendly concrete, these materials have been used in the concrete making.

2 Objective

The objective of the experiment is to examine the workability and forte of the concrete by victimization materials like WGP and M-sand in the concrete and to understand up to what extent the waste glass powder can be replaced in cement.

3 Experimental Study

In this experimental work, concrete is by part substitution cement with WGP and M-sand is completely used throughout the experiment with no replacement. 5, 10, 15, 20% of WGP is deputized by cement in concrete and also mix design was prepared for the M20 grade concrete. The properties like chemical, physical were studied and chemical components that are present in a glass were also determined in this experiment.

Table 1 Cement parameters

Properties	Results
Normal consistency	30.5%
Initial setting time	54
Specific gravity	3.15
Final setting time	310

*Setting time is in minutes

Table 2 Manufactured sand parameters

Parameters	Results
Zone	II
Water absorption	1%
Specific gravity	2.64

3.1 Materials

3.1.1 Cement, Coarse and Fine Aggregates

Generally, concrete is made by mixing of varied ingredients like cement, water and aggregates and in some cases admixtures. In concrete, cement could be a binding material with having adhesive and robust properties because of the material is in the form of fine grounded. Confirming to IS 12,269–2013 [1] Ordinary Portland 53 grade of cement is used throughout the project. Water is a decisive part of concrete because it could be a reason to occur the chemical reaction and hydration. Portable water as compliance to IS 456:2000 was used for the preparation of concrete, the water–cement ratio chooses the quality of the concrete production [3]. In the making of concrete, up to 70–80% volume is constituted by the aggregates that help in hardening. M-sand was used in this project as a fine aggregate with an all-out size of 4.75 μm is confirming to zone II grade. Graded crushed rock is used as a coarse aggregate throughout this project. As per IS 2386:1963 [5, 6] and IS 383:2016 [7], two sizes of coarse aggregate were used. First, the 25 mm passing through 20 mm retained and 16 mm passing through 12.5 mm retained were collected as coarse aggregate in this project. Blue granite crushed stone by machines that were in angular size type of aggregate is used in this project. In this experiment, admixture has not been used. Table 1 exhibits the possessions of cement and Tables 2 and 3 exhibits the possessions of aggregates.

3.1.2 Glass Powder

The experiment was conducted by using finely grounded powder waste glass in the concrete making by swapping the cement with partially. Waste glass has been collected near the surroundings of Gulbarga shops, after the collection of the material

Table 3 Coarse aggregate parameters

Parameters	Results
Elongation index	12.47%
Grade	I
Water absorption	1.5
Flakiness index	19.17%
Moisture content	Nil
Specific gravity	2.75
Impact value	16.46

the glass has been made into finely powdered with the help of crushing machines. Figure 1 shows the finely powdered waste glass made into a desired size to be partially replaced with the cement in the experiment. In this experiment, particle size is less than the size of 150 μm and it was passed through 90 μm. The retained material is collected and the material is used in the concrete mixing as finely WGP [9, 12, 13]. The collected WGP was tested in the labs and conducted the experiments on it to

Fig. 1 Fine grounded waste glass powder

Table 4 Various parameters of glass powder

Physical properties	Results
Shape	Spherical
Fineness passing 90 μm	99
Normal Consistency	30%
pH	10.25
colour	Greyish white
Specific gravity	2.45

Table 5 Chemical composition of glass powder

Chemical compositions	Glass powder
SiO_2	67.43
MgO	2.71
K_2O	0.74
Na_2O	12.73
CaO	12.41
Al_2O_3	2.56
Fe_2O_3	1.42

know the various properties and chemicals present in it. Table 4 displays the various properties of the glass powder, and Table 5 shows the chemical composition.

3.2 Preparation of Waste Grounded Glass Powder

The collected waste glass sample is broken into particles and created to be finely pulverized and it's sieved through 90 μm sieve and glass powder passing through a 150 μm sieve is taken into account for the experiment.

3.3 Mix Proportion, Casting of Specimens

3.3.1 Mix Design

Via using Indian standard for control concrete mix design was proposed. M20 grade concrete with a target strength of 20 N/mm^2 is designed for this entire experimental work. The concrete mixture is ready with having cement pleased of 394 kg/m^3, and W/C ratio of 0.50. As per IS 10,262–2009 [8], the mix proportion of the material is done. Table 6 shows five different mix samples of (MS 1, MS 2, MS 3, MS 4 and MS

Table 6 Overall mix details

Mix identity	Mix proportions
MS 1	100% cement
MS 2	95% cement + 05%WGP
MS 3	90% cement + 10%WGP
MS 4	85% cement + 15% WGP
MS 5	80% cement + 20% WGP

Table 7 Mix design details of M20 grade concrete

% of WGP replacement	Mix proportion in (Kg/m^3)				W/C ratio
	cement	WGP	M-sand	CA	
0%	394	0	680	1156	0.5
5%	374.3	19.7	680	1156	0.5
10%	354.6	39.4	680	1156	0.5
15%	334.9	59.1	680	1156	0.5
20%	315.2	78.8	680	1156	0.5

5) were prepared by replacing cement with glass powder at levels of (0, 5, 10, 15 and 20%) in concrete and river sand is fully replaced with M-sand. Chemical admixture is not used in this experiment. Table 7 shows the complete details of the M20 Grade concrete mix.

3.3.2 Specimens Casting Procedure

There five types of the concrete mix were considered of which Mix sample 1 (MS 1) is prepared without adding WGP and M-sand in the concrete, of having (1:1.5:3, W/C ratio of 0.50) to achieve 28 days strength of 20 Mpa. Concrete cube size of 150 × 150 mm of total of 45 cubes was cast and cylindrical specimen size of 150 × 300 mm size of a total of 45 cylinders were cast throughout the experiment. The casting of specimens was done as per compliance with 516:1959 [2]. Freshly prepared casted cubes and cylinders were placed for 24 h to complete the hydration process. The samples were detached from moulds after completion of 24 h and placed in a curing tank. These samples were alleviated for 7, 14 and 28 days.

4 Tests on Specimen

4.1 Workability Test

Compliance to IS 1199:1959 slump test is accompanied on fresh concrete to determine its workability. The slump value of contemporary concrete was restrained exploitation slump cone before the concrete was cast into moulds. The core objective of the workability test was to find out the reliability of the samples and it determines the way of concrete mixed properly and consolidated. It depends on water content, aggregates and cementitious content. In this experiment, the range of the slump value on the fresh concrete was 80–100 mm was maintained.

4.2 Alkalinity Test

After 28 days of curing the samples were taken out from the curing tank and sited in an oven for 24 h with keeping the temperature of 105 °C. Then the samples were chilled to room temperature. From concrete the mortar was detached by breaking the specimen and grinded into powder form. The 10 gm of mortar powder was taken from 150 μm sieve by sieving and it is diluted in 50 ml distilled water. Finally, the pH value is noted by immersing the electronic rod into the prepared solution.

4.3 Strength Test

By using CMT machine, the samples were undergone for compressive testing at the ages of 7, 14 and 28 days. Similarly in the same way tensile test was done on samples by using UTM machine at the same specified above ages.

5 Results and Discussions

5.1 Discussion on Workability Outcome Values

Figure 2 exhibits the outcome values of workability for five different mixes which are partially replaced by cement with WGP and fully replaced river sand with M-sand in various percentages vacillating from 0 to 20% in augmentations of 5%. The values were logged as 100 mm for 0%, 96 mm for 5%, 90 mm for 10%, 87 mm for 15% and 82 mm for 20% replacement. This shows that as WGP content increases the workability of concrete is getting decreased because of the quantity of cement fixative is getting fewer for providing emollient consequence per unit surface area of aggregate.

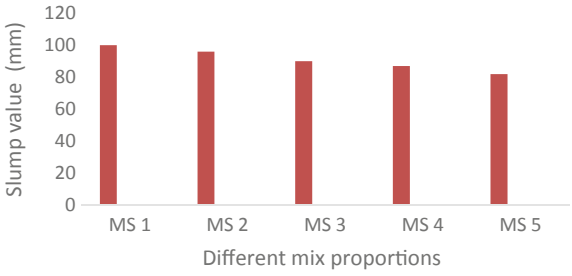

Fig. 2 Slump of concrete values represented in graphically

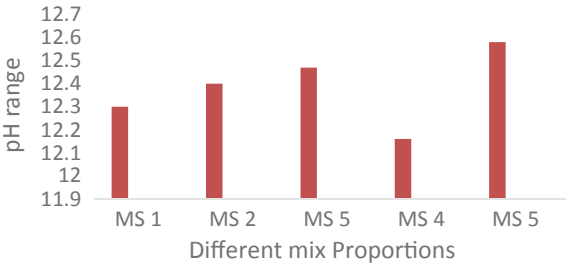

Fig. 3 Alkalinity test values of the concrete specimens

5.2 Discussion on Alkalinity Test Results

Figure 3 exhibits the outcome values of pH for five different mixes which are partially replaced with cement by WGP and fully substituted the river sand by M-sand in various percentages vacillating from 0 to 20% in augmentations of 5%. The values were logged as 12.3 for 0%, 12.4 for 5%, 12.47 for 10%, 12.16 for 15% and 12.58 for 20% replacement.

From alkalinity test, it is detected that the pH values of the samples found to be more alkaline in nature. So, it is said to be more resistant to corrosion.

5.3 Discussion on Strength Tests

5.3.1 Compressive and Tensile Strength

The investigational results of compressive and split tensile strength tests at 7, 14 and 28 days exhibit the effect of usage in concrete by substituting the cement with WGP and M-sand. Tables 8 and 9 exhibit the outcome values of tests conducted on hardened concrete specimens and reported values corresponded to an average of three test results. From the obtained values, it exhibits that the compressive and tensile strength increased with curing time. MS 1 results belong to nominal concrete

Table 8 Compressive strength results

Mix samples	Compressive Strength at days (N/mm^2)		
	7	14	28
MS 1	18.85	23.50	29.40
MS 2	21.30	25.28	31.29
MS 3	23.42	27.01	33.05
MS 4	26.83	30.08	37.02
MS 5	24.48	28.90	35.02

Table 9 Tensile strength test results

Mix samples	Tensile Strength at days in (N/mm^2)		
	7	14	28
MS 1	1.62	1.88	2.06
MS 2	2.04	2.31	2.73
MS 3	2.21	2.34	2.86
MS 4	2.51	2.68	3.05
MS 5	2.26	2.41	2.54

and MS 2 to MS 5 results belong to concrete which is replaced the cement with glass powder and M-sand.

By the outcome values, it seems that compressive strength at 15% replacement (MS 4) showed a higher value compared to MS 1, MS 2, MS 3 and MS 5 concrete specimens for 7, 14 and 28 days correspondingly. Figure 4 represents the values graphically.

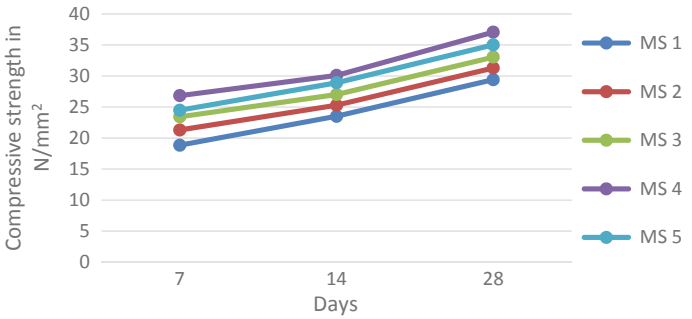

Fig. 4 Variant of Compressive strength progress of concrete

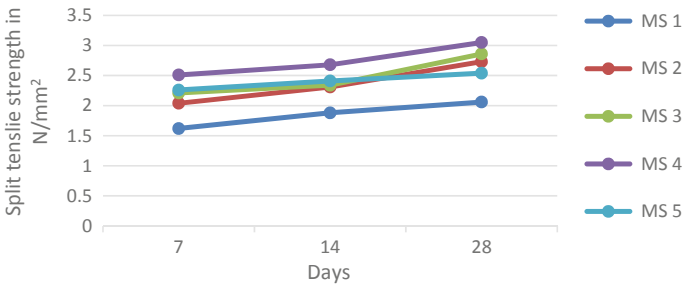

Fig. 5 Variant of tensile strength progress of concrete

Table 9 and Fig. 5 exhibit the outcome values of the tensile strength of concrete specimens. The tests conducted for 7, 14 and 28 days and reported values corresponded to an average of three test results.

By the outcome values, it seems that split tensile strength at 15% replacement (M-4) showed a higher value compared to M-1, M-2, M-3 and M-5 concrete specimens for 7, 14 and 28 days, respectively. Figure 4 represents the values graphically.

The strength of the concrete is been increased by replacing of WGP with cement in concrete from 5 to 15% and beyond that declines at 20% replacement. While compared with nominal concrete results, a 15% replacement level about 22.94% of compressive and 38.74% of tensile strength is noted as the highest incremented percentage. The increment of the strength in concrete which replaced the cement with WGP from 5 to 15% is observed may be due to the content of silica in high, the pozzolanic reaction takes place. More overly it efficiently plugs the voids and gives a thick concrete microstructure. By angular shape and rough surface texture of the M-sand may also be contributing to the high strength for concrete. However, afar 15% the strength gets dropped because of the dilution effect taking place. Thus, it can be concluded that usage of M-sand and glass powder of 15% cement replaced is recommended to use by this experimental work.

6 Conclusion

The subsequent conclusions are noted below based on experimental results:

- The research work evaluates that comparing with nominal concrete the compressive and tensile strengths are found to be increased at 15% substitution of cement by WGP and 100% substitution of river sand by M-sand in a concrete mix.
- 39.85 Mpa compressive strength and 3.05 Mpa tensile strength were noted for M20 grade concrete as maximum in this experimental work.
- The strength is gained by using glass powder and M-sand is because of having their properties like fineness and greater surface area to glass powder and angular shape and surface texture for M-sand.
- Using of WGP in concrete as cement auxiliary helps the environment by plummeting the percent of CO_2. Because cement industries are one of the main sources for CO_2 emission.
- By using WGP in a concrete mix, the amount of waste can be decremented in Earth landfills and the cost of cement production up to 18% can reduce by replacing cement and river sand.
- The replacement examination method in this experiment of using WGP and M-sand in concrete is said to be feasible based upon the overall outcome experimental results. Therefore, we can state that cement can be partially substituted with WGP and river sand by M-sand fully.

References

1. Bhavan M, et al (2013) Bureau of Indian Satandards, pp 1–10
2. Bureau of Indian Standards (2004) Method of tests for strength of concrete. IS : 516 - 1959 (Reaffirmed 2004) p. New Delhi,India. https://doi.org/10.3403/02128947
3. Bureau of Indian Standards (2007) Plain and reinforced concrete code of practice-4th Revision. (Indian Standard, 2007), pp 1–114. https://www.iitk.ac.in/ce/test/IS-codes/is.456.2000.pdf
4. Donza H et al (2002) High-strength concrete with different fine aggregate. Cem Concr Res. https://doi.org/10.1016/S0008-8846(02)00860-8
5. IS 2386- Part I (1963) Method of test for aggregate for concrete. part I—particle size and shape. Bureau of Indian Standards, New Delhi, India (Reaffirmed 2002)
6. IS 2386- Part III (1963) Method of test for aggregate for concrete. part III-specific gravity, density, voids, absorption and bulking. Bureau of Indian Standards, New Delhi, (Reaffirmed 2002)
7. IS 383 (2016) Coarse and fine aggregate for concrete - specification (Third Revision). Indian Standard, vol 3 Jan 2016
8. IS10262 (2009) Guidelines for concrete mix design proportioning. Indian Standard, New Delhi,India
9. Meena MK, Gupta J, Nagar B (2018) Performance of concrete by using glass powder, an experimental study. no. 9, pp 840–44
10. Saji MS, Leema Rose A (2015) Using glass waste as a partial replacement for fine aggregate on the strength of the concrete. Int J Eng Res Online 3(1): 96–99
11. Shanmugapriya T et al (2014) Influence of manufactured sand as fine aggregate on strength properties of high performance concrete. Int J Earth Sci Eng
12. Vandhiyan R et al (2013) Experimental study on replacement of cement by glass powder. Int J Eng Res Technol
13. Vijayakumar G et al (2013) Studies on glass powder as partial replacement of cement in concrete production. Int J Emerg Technol Adv Eng

Experimental Investigation of Using Eggshell Powder as Partial Replacement of Cement in Fiber Reinforced Concrete

Evetta Raneyia Cardoso, Neena Panandikar, and Kaushik V. Pai Fondekar

Abstract Fibers in concrete are one such advancement which offers a convenient, practical and economical method of overcoming many deficiencies in the properties of plain concrete. Fibers used in concrete help in reducing the crack formation and its propagation thereby increasing its toughness. Eggshell has the main component as Calcium Carbonate which is used as one of the main ingredients of Cement. So the use of eggshell instead of natural lime to replace cement in concrete can have benefits like minimizing the use of cement, conserving natural lime, and utilizing waste material. Carbon dioxide gets evolved during manufacturing of cement which is the main contributor of greenhouse effect that leads to global warming. So attempts are made by researchers to partially replace cement with other strength waste materials. The present study has been undertaken to analyze the effect of addition of glass fibers and eggshell powder in plain cement concrete and study its effect on the compressive of concrete. Experiments have been conducted on concrete cubes with partial replacement of cement with eggshell powder and also with addition of glass fibers. The testing has been done using varying percentage of eggshell powder by weight of cement. The first set of experiment was carried out by replacing 5, 10, and 15% of cement with eggshell powder. The compressive strength at 28 days was found out and compared with the conventional concrete. Further, the effect of addition of 0.025, 0.03, and 1% of glass fibers in combination with varying percentage of eggshell powder viz 5, 10, and 15% was assessed. The compressive strength at 28 days with addition of eggshell powder in combination with glass fibers was found out and compared with the conventional concrete.

Keywords Fibers · Eggshell powder · AR glass fiber

E. R. Cardoso (✉) · K. V. P. Fondekar
Department of Civil Engineering, Don Bosco College of Engineering, Fatorda, Goa, India
e-mail: raneyia1603@gmail.com

N. Panandikar
Don Bosco College of Engineering, Fatorda, Goa, India

B. B. Das et al. (eds.), *Recent Trends in Civil Engineering*, Lecture Notes in Civil Engineering 105, https://doi.org/10.1007/978-981-15-8293-6_46

1 Introduction

Concrete is widely used material for infrastructure development. Cement being the major element of concrete and its manufacturing process contributes to greenhouse effects, research is going on so as to find alternate material which can be used for partial replacement for cement. At present for various reasons the concrete construction is not sustainable. Carbon dioxide gets evolved during manufacturing of cement which is the main contributor of greenhouse effect that leads to global warming. Emission of carbon dioxide leads to global warming and directly depends on the cement content used in concrete mix. Our project attempts to study the effect of Replace cement partially with other waste material by eggshell powder and also effect of addition of 1% glass fibers in combination with 0, 5, 10, and 15% on compressive strength.

2 Materials

2.1 Eggshell Powder

Eggshells are rich in calcium and its composition is similar to limestone. Research is going on to replace natural lime with eggshell. This can then minimize use of cement and also serves two purposes viz conserving natural lime and waste utilization. Eggshell waste in land attracts vermin due to attached membrane and causes problems associated with human health and environment. Usage of eggshell waste in civil engineering application has been investigated by a few researchers. Amu et al. [1] studied eggshell powder as a stabilizing material for improving soil properties. Olarewaju et al. [2] studied suitability of eggshell stabilized soil as subgrade material for road construction. Very few researchers have worked on feasibility of using eggshell powder as partial replacement of cement which is presented in the literature review.

2.2 Manufactured Sand

For the present project work, we have used manufactured sand as fine aggregate. Manufactured sand is a substitute of river sand for concrete construction. Hard granite stone is crushed to produce manufactured sand. The crushed sand is of cubical shape with grounded edges, washed and graded to be used as a construction material. The size of manufactured sand (M-Sand) is less than 4.75 mm.

Fig. 1 AR anti crack glass fiber

2.3 Glass Fibers

Glass fiber is a material consisting of numerous extremely fine fibers of glass. AR anti-crack glass fibers are used in this experiment. Diameter of the glass fibers is 10–13 μm and length of glass fibers is 12–17 mm (Fig. 1).

2.4 Cement

Of all the materials that influence the behavior of concrete, cement is the most important constituent, as it is used to bind cement and aggregate. Portland pozzolana cement which satisfies the requirement of IS: 1489–1991 specification has been used in the present experimentation work. 2.72 is the specific gravity of cement.

2.5 Water

Water used for mixing and for curing of concrete throughout that may be deleterious to concrete. As per IS 456:2000, portable water is generally considered satisfactory for mixing and for curing of concrete. Hence, portable tap water is used in the preparation of all concrete specimens mixes.

2.6 Coarse Aggregates

Crushed angular stone aggregate obtained from local quarry has been used. In this experimental work, coarse aggregate used is of 20 mm and 10 mm downsize, tested as per IS:2386–1963 specification and mixed in the ratio of 60:40.

2.7 SP430 Fosroc

It is a chloride free, super plasticizing admixture based on selected sulphated naphthalene polymers. It is supplied as a brown solution which instantly disperses in water. Its addition results in excellent acceleration of strength gain at early ages. It can be particularly used in pre-cast concrete and other high early strength requirements. Major increase in strength at early ages without increased cement contents are of particular benefit in pre-cast concrete allowing earlier stripping times. It makes possible major reductions in water:cement ratio thus producing high strength concrete without excessive cement contents.

3 Methodology

3.1 Mix Design

For any civil engineering project, for quality control of concrete work, it is very essential to perform mix design of concrete. The quantities obtained after performing mix design for the experimental study is shown in Table 1.

3.2 Compressive Strength Test of Concrete Cubes

Many factors such as water–cement ratio, cement strength, quality of concrete material, and quality control during production of concrete influence the compressive strength of concrete. Test for compressive strength is carried out on cube. Compressive strength is the ability of material or structure to carry the loads on its surface

Table 1 Mix design table

Cement (kg/m^3)	Fine aggregate (kg/m^3)	Coarse aggregate (kg/m^3)	Water (kg/m^3)	Water–cement ratio	Chemical admixture
433	631.11	1196.352	205.538	0.4	4.76

Fig. 2 Compression testing machine

without any crack or deflection. Compressive strength of cube is been found out by load divided by area of the cube (N/mm^2) for normal curing. For accelerated curing predicted compressive strength at 28 days of cube is found out by using a formula $R = 8.09 + 1.64 \times Ra$, where Ra is accelerated compressive strength (N/mm^2) (as per IS: 9013–1978) (Fig. 2).

4 Results

Eggshell powder obtained from wastes is added in various ratios for cement replacement and we conclude that with this experiment the 10% of eggshell powder with cement attained maximum compressive strength. So, the eggshell powder is used as a partial replacement with cement in concrete. Replacement of eggshell powder and an admixture in cement yields similar flexural strength as in commonplace concrete. With addition from combination of both eggshell powder and glass fiber, we concluded that with this experiment the 0% eggshell powder and 1% of glass fiber by volume of concrete attained maximum compressive strength.

4.1 Results for 0% Glass Fiber

See Fig. 3 and Table 2.

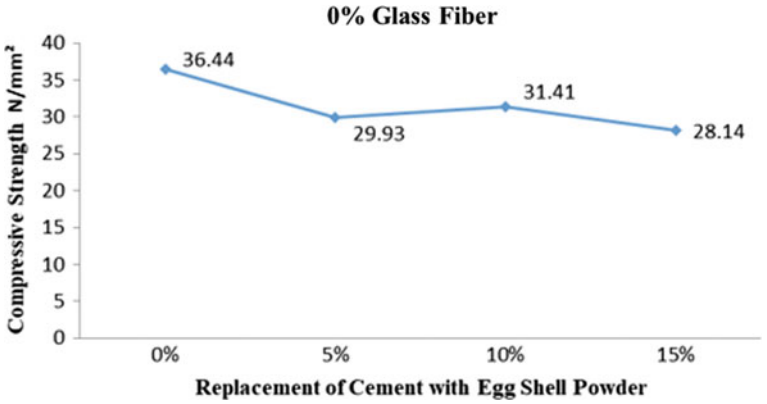

Fig. 3 Variation of compressive strength of concrete cubes at 28 days with varying percentage of ESP

Table 2 Compressive strength of concrete cubes for 0% of glass fiber

Sr. No	Eggshell powder (%)	Grade of concrete	Age of cubes (days)	Load N	Cross-sectional area of cube mm^2	Compressive strength N/mm^2
1	0	M30	28	820,000	22,500	36.44
2	5	M30	28	673,000	22,500	29.93
3	10	M30	28	707,000	22,500	31.41
4	15	M30	28	633,000	22,500	28.14

4.2 Results for 0.025% Glass Fiber

See Fig. 4 and Table 3.

4.3 Results for 0.03% Glass Fiber

See Fig. 5 and Table 4.

4.4 Results for 1% Glass Fiber

Fig. 6 and Table 5.

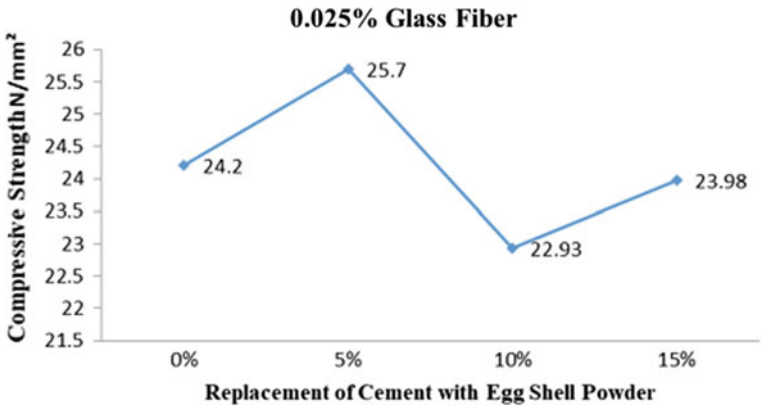

Fig. 4 Variation of compressive strength of concrete cubes at 28 days with varying percentage of ESP and 0.025% of glass fiber

Table 3 Compressive strength of concrete cubes for 0.025% of glass fiber

Sr. No	Eggshell Powder (%)	Grade of concrete	Age of cubes (days)	Load N	Cross-sectional area of cube mm^2	Compressive strength N/mm^2
1	0	M30	28	545,000	22,500	24.2
2	5	M30	28	578,000	22,500	25.7
3	10	M30	28	516,000	22,500	22.93
4	15	M30	28	539,000	22,500	23.98

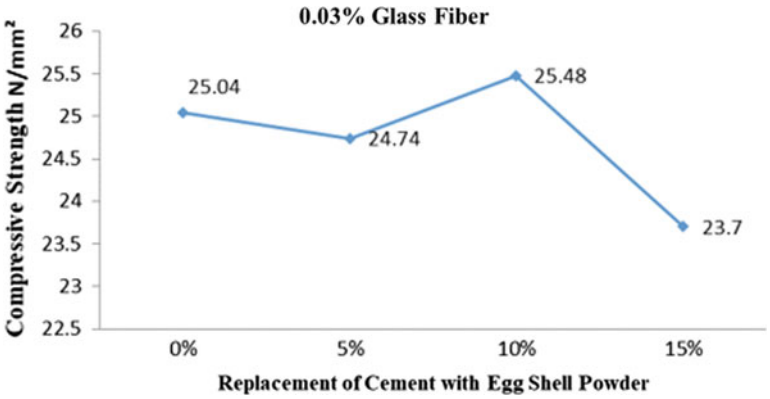

Fig. 5 Variation of compressive strength of concrete cubes at 28 days with varying percentage of ESP and 0.03% of glass fiber

Table 4 Compressive strength of concrete cubes for 0.03% of glass fiber

Sr. No	Eggshell Powder (%)	Grade of concrete	Age of cubes (days)	Load N	Cross-sectional area of cube mm^2	Compressive strength N/mm^2
1	0	M30	28	563,333.33	22,500	25.04
2	5	M30	28	556,666.67	22,500	24.74
3	10	M30	28	580,000	22,500	25.78
4	15	M30	28	533,333.33	22,500	23.7

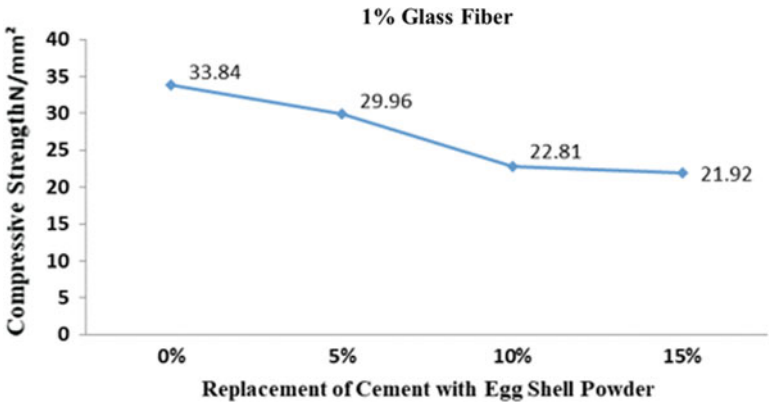

Fig. 6 Variation of compressive strength of concrete cubes at 28 days with varying percentage of ESP and 1% of glass fiber

Table 5 Compressive strength of concrete cubes for 1% of glass fiber

Sr. No	Eggshell Powder (%)	Grade of concrete	Age of cubes (days)	Load N	Cross-sectional area of cube mm^2	Compressive strength N/mm^2
1	0	M30	28	579,474.76	22,500	33.84
2	5	M30	28	492,008.09	22,500	29.64
3	10	M30	28	513,333.33	22,500	22.81
4	15	M30	28	493,333.33	22,500	21.92

4.5 Comparison of Compressive Strength for Different Percentages of Glass Fiber

See Fig. 7.

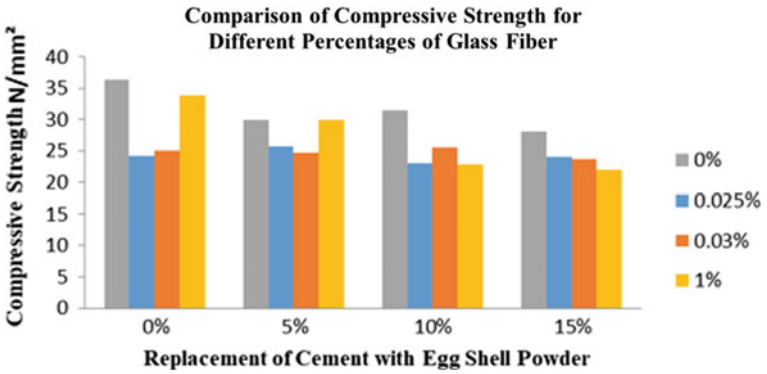

Fig. 7 Comparison of compressive strength of concrete cubes at 28 days

5 Conclusion

The present study was carried out to analyze the effect of addition of glass fibers and eggshell powder in plain cement concrete and study its effects on compressive strength of concrete. From the experimental study carried out by the authors it has been found that when cement is replaced by 5, 10 and 15% of egg shell powder, the maximum compressive strength is obtained for 10% addition of egg shell powder. The maximum compressive strength obtained is for 10% addition of eggshell powder. It is found that with additional of 10% eggshell powder there is minimal decrease in compressive strength of concrete when compared with conventional concrete. With addition of 0.025% of glass fibers in combination with varying percentage of eggshell powder viz 5, 10, and 15%, it was observed that maximum compressive strength was obtained for 5% addition of eggshell powder. With addition of 0.03% of glass fiber in combination with varying percentage of eggshell powder viz 5, 10, and 15%, it was observed that maximum compressive strength was obtained for 10% addition of eggshell powder. With addition of 1% of glass fiber in combination with varying percentage of eggshell powder viz 5, 10, and 15%, it was observed that maximum compressive strength was obtained when there was no addition of eggshell powder. It was also observed that the strength decreased with increase of eggshell powder for 1% addition of glass fiber. From the above study carried, it can be concluded that 10% of eggshell powder can be used as partial replacement of cement in concrete matrix for usage in nonstructural works. If durability and permeability of concrete can be ascertained on additional of eggshell powder, it could be used for structural works and more study needs to be carried out.

References

1. Amu OO, Fajobi AB, Oke BO (2005) Effect of egg shell powder on the stabilizing potential of lime on an expansive clay soil. 5:1474–1478
2. Olarewaju AJ, Balogun MO, Akinlolu SO (2011) Suitability of egg shell stabilized lateritic soil for road construction. Electr J Geotech Eng